The PDQ Two Zone Model

Nuclear Analysis and
Fuel Department
Nuclear Engineering Services

VEP-NAF-1
July, 1990

VIRGINIA POWER

9010090077 901001
PDR ADOCK 05000280
P PDC

VEP-NAF-1

THE PDQ TWO ZONE MODEL

BY

R. A. HALL

NUCLEAR ANALYSIS AND FUEL DEPARTMENT
NUCLEAR ENGINEERING SERVICES

VIRGINIA ELECTRIC AND POWER COMPANY
RICHMOND, VIRGINIA

July, 1990

Recommended for Approval:

D. Dziadosz
Supervisor, Nuclear Core Design

Approved:

R. M. Berryman
Manager, Nuclear Analysis and Fuel

CLASSIFICATION/DISCLAIMER

The data and analytical techniques described in this report have been prepared specifically for application by the Virginia Electric and Power Company. The Virginia Electric and Power Company makes no claim as to the accuracy of the data or techniques contained in this report if used by other organizations. Any use of this report or any part thereof must have the prior written approval of the ginia Electric and Power Company.

ABSTRACT

The Virginia Electric and Power Company (Virginia Power) has developed a coarse mesh (i.e., five non-uniform mesh per assembly), three dimensional, two neutron energy group diffusion-depletion calculational model designated as the PDQ two zone model.

The model uses the Virginia Power computer codes SHUFL, PDQV2, RECON, and PCF codes, as well as input from the EPRI ARMP-02 CELL2 and NUPUNCHER codes, the EPRI ESCORE code, and the SCALE3 package from ORNL (including KENO-V.a). The purpose of the model is to provide power distribution data for axially dependent vessel fluence calculations and to predict physics characteristics of the Virginia Power Surry and North Anna nuclear reactors. The accuracy of the two zone model is demonstrated through comparisons with measurements taken at the Surry and North Anna Nuclear Power Stations.

ACKNOWLEDGMENTS

The author would like to thank Mr. D. Dziadosz who conceived and supported this project, and Mr. Ali Abbasi, Mr. Walter Peterson and Mr. Jeff McElroy for assistance in performing the computer calculations and data preparation required for this report. The author also wishes to express his appreciation to the people who reviewed and provided comments on this report.

TABLE OF CONTENTS

	Page
CLASSIFICATION/DISCLAIMER	i
ABSTRACT	ii
ACKNOWLEDGMENTS	iii
TABLE OF CONTENTS	iv
LIST OF TABLES	v
LIST OF FIGURES	vi
SECTION 1 - INTRODUCTION	1-1
SECTION 2 - MODEL DESCRIPTION	2-1
2.1 Introduction	2-1
2.2 Model Geometry	2-7
2.3 Cross Section Generation	2-17
2.4 PDQ Quarter Core Cycle Calculations	2-26
2.5 Pin Power Reconstruction	2-31
SECTION 3 - RESULTS	3-1
3.1 Introduction	3-1
3.2 Analytical Calculations	3-1
3.3 Measurement Data	3-4
3.4 Results	3-10
SECTION 4 - SUMMARY AND CONCLUSIONS	4-1
SECTION 5 - REFERENCES	5-1

LIST OF TABLES

Table	Title	Page
1-1	Surry Nuclear Power Station Operating History	1-6
1-2	North Anna Nuclear Power Station Operating History	1-7
2-1	Nuclides Included in the PDQ Two Zone Depletion Chains	2-28
3-1	Axial Geometry For Power Distribution Comparisons	3-7
3-2	Summary of Nuclear Reliability Factors	3-18
3-3	Power Distribution Statistics	3-19
3-4	Flux Map Database Listing	3-21
3-5	Reactivity Parameter Statistics	3-24
3-6	Reactivity Computer Induced Bias Error Estimate	3-25

LIST OF FIGURES

Figure	Title	Page
2-1	PDQ Two Zone Model Flowchart	2-5
2-2	Pin Power Reconstruction Flow Chart	2-6
2-3	PDQ Two Zone Axial Mesh Structure	2-10
2-4	Surry Fuel 15 x 15 X-Y Pin Orientation	2-11
2-5	Surry Fuel Two Zone X-Y Mesh Structure	2-12
2-6	North Anna Fuel 17 x 17 X-Y Pin Orientation	2-13
2-7	North Anna Fuel Two Zone X-Y Mesh Structure	2-14
2-8	IAEA 2-D Benchmark Problem PDQ 6 X 6 Uniform Mesh Results	2-15
2-9	IAEA 2-D Benchmark Problem PDQ Two Zone 5 X 5 Non-uniform Mesh Results	2-16
3-1	FULL CORE MONITORED ASSEMBLY LOCATIONS	3-8
3-2	CONTROL ROD BANK LOCATIONS	3-9
3-3	N1C1 P(Z) COMPARISON HZP, 0 MWD/T CYCLE BURNUP	3-26
3-4	N1C1 P(Z) COMPARISON HFP, 881 MWD/T CYCLE BURNUP	3-27
3-5	N1C1 P(Z) COMPARISON HFP, 8405 MWD/T CYCLE BURNUP	3-28
3-6	N1C1 P(Z) COMPARISON HFP, 14070 MWD/T CYCLE BURNUP	3-29
3-7	N1C2 P(Z) COMPARISON HZP, 0 MWD/T CYCLE BURNUP	3-30
3-8	N1C2 P(Z) COMPARISON HFP, 305 MWD/T CYCLE BURNUP	3-31
3-9	N1C2 P(Z) COMPARISON HFP, 3277 MWD/T CYCLE BURNUP	3-32
3-10	N1C2 P(Z) COMPARISON HFP, 8109 MWD/T CYCLE BURNUP	3-33
3-11	N1C3 P(Z) COMPARISON HZP, 0 MWD/T CYCLE BURNUP	3-34
3-12	N1C3 P(Z) COMPARISON HFP, 487 MWD/T CYCLE BURNUP	3-35
3-13	N1C3 P(Z) COMPARISON HFP, 6883 MWD/T CYCLE BURNUP	3-36

LIST OF FIGURES

Figure	Title	Page
3-14	N1C3 P(Z) COMPARISON HFP, 11434 MWD/T CYCLE BURNUP . . .	3-37
3-15	N1C4 P(Z) COMPARISON HZP, 0 MWD/T CYCLE BURNUP . . .	3-38
3-16	N1C4 P(Z) COMPARISON HFP, 305 MWD/T CYCLE BURNUP . . .	3-39
3-17	N1C4 P(Z) COMPARISON HFP, 5521 MWD/T CYCLE BURNUP . . .	3-40
3-18	N1C4 P(Z) COMPARISON HFP, 10170 MWD/T CYCLE BURNUP . . .	3-41
3-19	N1C5 P(Z) COMPARISON HZP, 0 MWD/T CYCLE BURNUP . . .	3-42
3-20	N1C5 P(Z) COMPARISON HFP, 225 MWD/T CYCLE BURNUP . . .	3-43
3-21	N1C5 P(Z) COMPARISON HFP, 6831 MWD/T CYCLE BURNUP . . .	3-44
3-22	N1C5 P(Z) COMPARISON HFP, 12983 MWD/T CYCLE BURNUP . . .	3-45
3-23	N1C6 P(Z) COMPARISON HFP, 379 MWD/T CYCLE BURNUP . . .	3-46
3-24	N1C6 P(Z) COMPARISON HFP, 6690 MWD/T CYCLE BURNUP . . .	3-47
3-25	N1C6 P(Z) COMPARISON HFP, 14340 MWD/T CYCLE BURNUP . . .	3-48
3-26	N1C7 P(Z) COMPARISON HFP, 1062 MWD/T CYCLE BURNUP . . .	3-49
3-27	N1C7 P(Z) COMPARISON HFP, 4995 MWD/T CYCLE BURNUP . . .	3-50
3-28	N2C1 P(Z) COMPARISON HZP, 0 MWD/T CYCLE BURNUP . . .	3-51
3-29	N2C2 P(Z) COMPARISON HZP, 0 MWD/T CYCLE BURNUP . . .	3-52
3-30	N2C2 P(Z) COMPARISON HFP, 3225 MWD/T CYCLE BURNUP . . .	3-53
3-31	N2C2 P(Z) COMPARISON HFP, 6751 MWD/T CYCLE BURNUP . . .	3-54
3-32	N2C3 P(Z) COMPARISON HZP, 0 MWD/T CYCLE BURNUP . . .	3-55
3-33	N2C3 P(Z) COMPARISON HFP, 1566 MWD/T CYCLE BURNUP . . .	3-56
3-34	N2C3 P(Z) COMPARISON HFP, 7674 MWD/T CYCLE BURNUP . . .	3-57
3-35	N2C3 P(Z) COMPARISON HFP, 13040 MWD/T CYCLE BURNUP . . .	3-58
3-36	N2C4 P(Z) COMPARISON HZP, 0 MWD/T CYCLE BURNUP . . .	3-59

LIST OF FIGURES

Fig.	Title	Page
3-37	N2C4 P(Z) COMPARISON HFP, 1060 MWD/T CYCLE BURNUP	3-60
3-38	N2C4 P(Z) COMPARISON HFP, 6610 MWD/T CYCLE BURNUP	3-61
3-39	N2C4 P(Z) COMPARISON HFP, 11267 MWD/T CYCLE BURNUP	3-62
3-40	N2C5 P(Z) COMPARISON HFP, 250 MWD/T CYCLE BURNUP	3-63
3-41	N2C5 P(Z) COMPARISON HFP, 6075 MWD/T CYCLE BURNUP	3-64
3-42	N2C5 P(Z) COMPARISON HFP, 13671 MWD/T CYCLE BURNUP	3-65
3-43	S1C1 P(Z) COMPARISON HZP, 0 MWD/T CYCLE BURNUP	3-66
3-44	S1C2 P(Z) COMPARISON HZP, 0 MWD/T CYCLE BURNUP	3-67
3-45	S1C2 P(Z) COMPARISON HFP, 1100 MWD/T CYCLE BURNUP	3-68
3-46	S1C2 P(Z) COMPARISON HFP, 4050 MWD/T CYCLE BURNUP	3-69
3-47	S1C3 P(Z) COMPARISON HZP, 0 MWD/T CYCLE BURNUP	3-70
3-48	S1C3 P(Z) COMPARISON HFP, 250 MWD/T CYCLE BURNUP	3-71
3-49	S1C3 P(Z) COMPARISON HFP, 7175 MWD/T CYCLE BURNUP	3-72
3-50	S1C4 P(Z) COMPARISON HZP, 0 MWD/T CYCLE BURNUP	3-73
3-51	S1C4 P(Z) COMPARISON HFP, 930 MWD/T CYCLE BURNUP	3-74
3-52	S1C4 P(Z) COMPARISON HFP, 8400 MWD/T CYCLE BURNUP	3-75
3-53	S1C5 P(Z) COMPARISON HZP, 0 MWD/T CYCLE BURNUP	3-76
3-54	S1C5 P(Z) COMPARISON HFP, 1300 MWD/T CYCLE BURNUP	3-77
3-55	S1C5 P(Z) COMPARISON HFP, 7411 MWD/T CYCLE BURNUP	3-78
3-56	S1C5 P(Z) COMPARISON HFP, 10758 MWD/T CYCLE BURNUP	3-79
3-57	S1C6 P(Z) COMPARISON HZP, 0 MWD/T CYCLE BURNUP	3-80
3-58	S1C6 P(Z) COMPARISON HFP, 973 MWD/T CYCLE BURNUP	3-81
3-59	S1C6 P(Z) COMPARISON HFP, 7518 MWD/T CYCLE BURNUP	3-82

LIST OF FIGURES

Figure	Title	Page
3-60	S1C6 P(Z) COMPARISON HFP, 13207 MWD/T CYCLE BURNUP . . .	3-83
3-61	S1C7 P(Z) COMPARISON HZP, 0 MWD/T CYCLE BURNUP . . .	3-84
3-62	S1C7 P(Z) COMPARISON HFP, 807 MWD/T CYCLE BURNUP . . .	3-85
3-63	S1C7 P(Z) COMPARISON HFP, 4329 MWD/T CYCLE BURNUP . . .	3-86
3-64	S1C7 P(Z) COMPARISON HFP, 7630 MWD/T CYCLE BURNUP . . .	3-87
3-65	S1C8 P(Z) COMPARISON HZP, 0 MWD/T CYCLE BURNUP . . .	3-88
3-66	S1C8 P(Z) COMPARISON HFP, 925 MWD/T CYCLE BURNUP . . .	3-89
3-67	S1C8 P(Z) COMPARISON HFP, 3737 MWD/T CYCLE BURNUP . . .	3-90
3-68	S1C8 P(Z) COMPARISON HFP, 8081 MWD/T CYCLE BURNUP . . .	3-91
3-69	S1C9 P(Z) COMPARISON HFP, 240 MWD/T CYCLE BURNUP . . .	3-92
3-70	S1C9 P(Z) COMPARISON HFP, 8460 MWD/T CYCLE BURNUP . . .	3-93
3-71	S1C9 P(Z) COMPARISON HFP, 14606 MWD/T CYCLE BURNUP . . .	3-94
3-72	S2C1 P(Z) COMPARISON HZP, 0 MWD/T CYCLE BURNUP . . .	3-95
3-73	S2C1 P(Z) COMPARISON HFP, 2030 MWD/T CYCLE BURNUP . . .	3-96
3-74	S2C1 P(Z) COMPARISON HFP, 7310 MWD/T CYCLE BURNUP . . .	3-97
3-75	S2C1 P(Z) COMPARISON HFP, 12770 MWD/T CYCLE BURNUP . . .	3-98
3-76	S2C2 P(Z) COMPARISON HZP, 0 MWD/T CYCLE BURNUP . . .	3-99
3-77	S2C2 P(Z) COMPARISON HFP, 730 MWD/T CYCLE BURNUP . . .	3-100
3-78	S2C2 P(Z) COMPARISON HFP, 3750 MWD/T CYCLE BURNUP . . .	3-101
3-79	S2C3 P(Z) COMPARISON HZP, 0 MWD/T CYCLE BURNUP . . .	3-102
3-80	S2C3 P(Z) COMPARISON HFP, 3127 MWD/T CYCLE BURNUP . . .	3-103
3-81	S2C3 P(Z) COMPARISON HFP, 9025 MWD/T CYCLE BURNUP . . .	3-104
3-82	S2C4 P(Z) COMPARISON HZP, 0 MWD/T CYCLE BURNUP . . .	3-105

LIST OF FIGURES

Figure	Title	Page
3-83	S2C4 P(Z) COMPARISON HFP, 1186 MWD/T CYCLE BURNUP . . .	3-106
3-84	S2C4 P(Z) COMPARISON HFP, 8250 MWD/T CYCLE BURNUP . . .	3-107
3-85	S2C5 P(Z) COMPARISON HZP, 0 MWD/T CYCLE BURNUP . . .	3-108
3-86	S2C5 P(Z) COMPARISON HFP, 1830 MWD/T CYCLE BURNUP . . .	3-109
3-87	S2C5 P(Z) COMPARISON HFP, 11320 MWD/T CYCLE BURNUP . . .	3-110
3-88	S2C6 P(Z) COMPARISON HZP, 0 MWD/T CYCLE BURNUP . . .	3-111
3-89	S2C6 P(Z) COMPARISON HFP, 1116 MWD/T CYCLE BURNUP . . .	3-112
3-90	S2C6 P(Z) COMPARISON HFP, 7390 MWD/T CYCLE BURNUP . . .	3-113
3-91	S2C6 P(Z) COMPARISON HFP, 13900 MWD/T CYCLE BURNUP . . .	3-114
3-92	S2C7 P(Z) COMPARISON HZP, 0 MWD/T CYCLE BURNUP . . .	3-115
3-93	S2C7 P(Z) COMPARISON HFP, 1647 MWD/T CYCLE BURNUP . . .	3-116
3-94	S2C7 P(Z) COMPARISON HFP, 5781 MWD/T CYCLE BURNUP . . .	3-117
3-95	S2C7 P(Z) COMPARISON HFP, 13122 MWD/T CYCLE BURNUP . . .	3-118
3-96	S2C8 P(Z) COMPARISON HZP, 0 MWD/T CYCLE BURNUP . . .	3-119
3-97	S2C8 P(Z) COMPARISON HFP, 2423 MWD/T CYCLE BURNUP . . .	3-120
3-98	S2C8 P(Z) COMPARISON HFP, 6525 MWD/T CYCLE BURNUP . . .	3-121
3-99	S2C8 P(Z) COMPARISON HFP, 12391 MWD/T CYCLE BURNUP . . .	3-122
3-100	S2C9 P(Z) COMPARISON HFP, 1072 MWD/T CYCLE BURNUP . . .	3-123
3-101	S2C9 P(Z) COMPARISON HFP, 6887 MWD/T CYCLE BURNUP . . .	3-124
3-102	N1C1 RPD COMPARISON HZP, 0 MWD/T BURNUP D-228 . . .	3-125
3-103	N1C1 RPD COMPARISON HFP, 14070 MWD/T BURNUP D-220 . . .	3-126
3-104	N1C2 RPD COMPARISON HZP, 0 MWD/T BURNUP D-228 . . .	3-127
3-105	N1C2 RPD COMPARISON HFP, 300 MWD/T BURNUP D-228 . . .	3-128

LIST OF FIGURES

Figure	Title	Page
3-106	N1C2 RPD COMPARISON HFP, 3277 MWD/T BURNUP D-222 . . .	3-129
3-107	N1C2 RPD COMPARISON HFP, 8109 MWD/T BURNUP D-210 . . .	3-130
3-108	N1C3 RPD COMPARISON HZP, 0 MWD/T BURNUP D-220 . . .	3-131
3-109	N1C3 RPD COMPARISON HFP, 6883 MWD/T BURNUP D-213 . . .	3-132
3-110	N1C3 RPD COMPARISON HFP, 11434 MWD/T BURNUP D-216 . . .	3-133
3-111	N1C4 RPD COMPARISON HZP, 0 MWD/T BURNUP D-228 . . .	3-134
3-112	N1C4 RPD COMPARISON HFP, 305 MWD/T BURNUP D-221 . . .	3-135
3-113	N1C4 RPD COMPARISON HFP, 5520 MWD/T BURNUP D-216 . . .	3-136
3-114	N1C4 RPD COMPARISON HFP, 10170 MWD/T BURNUP D-226 . . .	3-137
3-115	N1C5 RPD COMPARISON HZP, 0 MWD/T BURNUP D-228 . . .	3-138
3-116	N1C5 RPD COMPARISON HFP, 225 MWD/T BURNUP D-224 . . .	3-139
3-117	N1C5 RPD COMPARISON HFP, 6831 MWD/T BURNUP D-224 . . .	3-140
3-118	N1C5 RPD COMPARISON HFP, 12983 MWD/T BURNUP D-228 . . .	3-141
3-119	N1C6 RPD COMPARISON HFP, 378 MWD/T BURNUP D-219 . . .	3-142
3-120	N1C6 RPD COMPARISON HFP, 6690 MWD/T BURNUP D-228 . . .	3-143
3-121	N1C6 RPD COMPARISON HFP, 14340 MWD/T BURNUP D-228 . . .	3-144
3-122	N2C2 RPD COMPARISON HZP, 0 MWD/T BURNUP D-228 . . .	3-145
3-123	N2C2 RPD COMPARISON HFP, 3225 MWD/T BURNUP D-224 . . .	3-146
3-124	N2C2 RPD COMPARISON HFP, 6751 MWD/T BURNUP D-218 . . .	3-147
3-125	N2C3 RPD COMPARISON HZP, 0 MWD/T BURNUP D-211 . . .	3-148
3-126	N2C3 RPD COMPARISON HFP, 1566 MWD/T BURNUP D-212 . . .	3-149
3-127	N2C3 RPD COMPARISON HFP, 7647 MWD/T BURNUP D-217 . . .	3-150
3-128	N2C3 RPD COMPARISON HFP, 13040 MWD/T BURNUP D-221 . . .	3-151

LIST OF FIGURES

Figure	Title	Page
3-129	N2C4 RPD COMPARISON HZP, 0 MWD/T BURNUP D-211 . . .	3-152
3-130	N2C4 RPD COMPARISON HFP, 6610 MWD/T BURNUP D-220 . . .	3-153
3-131	N2C4 RPD COMPARISON HFP, 11267 MWD/T BURNUP D-228 . . .	3-154
3-132	N2C5 RPD COMPARISON HFP, 250 MWD/T BURNUP D-228 . . .	3-155
3-133	N2C5 RPD COMPARISON HFP, 6075 MWD/T BURNUP D-228 . . .	3-156
3-134	N2C5 RPD COMPARISON HFP, 13671 MWD/T BURNUP D-228 . . .	3-157
3-135	S1C2 RPD COMPARISON HZP, 0 MWD/T BURNUP D-214 . . .	3-158
3-136	S1C2 RPD COMPARISON HFP, 1100 MWD/T BURNUP D-222 . . .	3-159
3-137	S1C2 RPD COMPARISON HFP, 4050 MWD/T BURNUP D-223 . . .	3-160
3-138	S1C3 RPD COMPARISON HFP, 250 MWD/T BURNUP D-212 . . .	3-161
3-139	S1C3 RPD COMPARISON HFP, 7175 MWD/T BURNUP D-225 . . .	3-162
3-140	S1C4 RPD COMPARISON HZP, 0 MWD/T BURNUP D-220 . . .	3-163
3-141	S1C4 RPD COMPARISON HFP, 930 MWD/T BURNUP D-215 . . .	3-16-
3-142	S1C4 RPD COMPARISON HFP, 8400 MWD/T BURNUP D-206 . . .	3-165
3-143	S1C5 RPD COMPARISON HZP, 0 MWD/T BURNUP D-218 . . .	3-166
3-144	S1C5 RPD COMPARISON HFP, 1300 MWD/T BURNUP D-220 . . .	3-167
3-145	S1C5 RPD COMPARISON HFP, 7411 MWD/T BURNUP D-224 . . .	3-168
3-146	S1C5 RPD COMPARISON HFP, 10758 MWD/T BURNUP D-226 . . .	3-169
3-147	S1C6 RPD COMPARISON HZP, 0 MWD/T BURNUP D-201 . . .	3-170
3-148	S1C6 RPD COMPARISON HFP, 973 MWD/T BURNUP D-217 . . .	3-171
3-149	S1C6 RPD COMPARISON HFP, 7518 MWD/T BURNUP D-228 . . .	3-172
3-150	S1C6 RPD COMPARISON HFP, 13207 MWD/T BURNUP D-222 . . .	3-173

LIST OF FIGURES

Figure	Title	Page
3-151	S1C7 RPD COMPARISON HZP, 0 MWD/T BURNUP D-221 . . .	3-174
3-152	S1C7 RPD COMPARISON HFP, 807 MWD/T BURNUP D-228 . . .	3-175
3-153	S1C7 RPD COMPARISON HFP, 4329 MWD/T BURNUP D-228 . . .	3-176
3-154	S1C7 RPD COMPARISON HFP, 7630 MWD/T BURNUP D-228 . . .	3-177
3-155	S1C8 RPD COMPARISON HZP, 0 MWD/T BURNUP D-212 . . .	3-178
3-156	S1C8 RPD COMPARISON HFP, 900 MWD/T BURNUP D-228 . . .	3-179
3-157	S1C8 RPD COMPARISON HFP, 8081 MWD/T BURNUP D-227 . . .	3-180
3-158	S1C8 RPD COMPARISON HFP, 13212 MWD/T BURNUP D-212 . . .	3-181
3-159	S1C9 RPD COMPARISON HFP, 240 MWD/T BURNUP D-220 . . .	3-182
3-160	S1C9 RPD COMPARISON HFP, 7295 MWD/T BURNUP D-222 . . .	3-183
3-161	S1C9 RPD COMPARISON HFP, 14606 MWD/T BURNUP D-217 . . .	3-184
3-162	S2C1 RPD COMPARISON HZP, 0 MWD/T BURNUP D-200 . . .	3-185
3-163	S2C1 RPD COMPARISON HFP, 2030 MWD/T BURNUP D-203 . . .	3-186
3-164	S2C1 RPD COMPARISON HFP, 7310 MWD/T BURNUP D-215 . . .	3-187
3-165	S2C2 RPD COMPARISON HZP, 0 MWD/T BURNUP D-199 . . .	3-188
3-166	S2C2 RPD COMPARISON HFP, 730 MWD/T BURNUP D-210 . . .	3-189
3-167	S2C2 RPD COMPARISON HFP, 3750 MWD/T BURNUP D-216 . . .	3-190
3-168	S2C3 RPD COMPARISON HFP, 3127 MWD/T BURNUP D-221 . . .	3-191
3-169	S2C3 RPD COMPARISON HFP, 8688 MWD/T BURNUP D-224 . . .	3-192
3-170	S2C4 RPD COMPARISON HZP, 0 MWD/T BURNUP D-228 . . .	3-193
3-171	S2C4 RPD COMPARISON HFP, 1186 MWD/T BURNUP D-223 . . .	3-194
3-172	S2C4 RPD COMPARISON HFP, 8250 MWD/T BURNUP D-201 . . .	3-195
3-173	S2C5 RPD COMPARISON HZP, 0 MWD/T BURNUP D-216 . . .	3-196

LIST OF FIGURES

Figure	Title	Page
3-174	S2C5 RPD COMPARISON HFP, 1690 MWD/T BURNUP D-217 . . .	3-197
3-175	S2C5 RPD COMPARISON HFP, 11320 MWD/T BURNUP D-220 . . .	3-198
3-176	S2C6 RPD COMPARISON HZP, 0 MWD/T BURNUP D-223 . . .	3-199
3-177	S2C6 RPD COMPARISON HFP, 1116 MWD/T BURNUP D-228 . . .	3-200
3-178	S2C6 RPD COMPARISON HFP, 7390 MWD/T BURNUP D-228 . . .	3-201
3-179	S2C6 RPD COMPARISON HFP, 13900 MWD/T BURNUP D-227 . . .	3-202
3-180	S2C7 RPD COMPARISON HZP, 0 MWD/T BURNUP D-211 . . .	3-203
3-181	S2C7 RPD COMPARISON HFP, 1647 MWD/T BURNUP D-226 . . .	3-204
3-182	S2C7 RPD COMPARISON HFP, 5781 MWD/T BURNUP D-226 . . .	3-205
3-183	S2C7 RPD COMPARISON HFP, 13122 MWD/T BURNUP D-223 . . .	3-206
3-184	S2C8 RPD COMPARISON HZP, 0 MWD/T BURNUP D-228 . . .	3-207
3-185	S2C8 RPD COMPARISON HFP, 2423 MWD/T BURNUP D-228 . . .	3-208
3-186	S2C8 RPD COMPARISON HFP, 6525 MWD/T BURNUP D-218 . . .	3-209
3-187	S2C8 RPD COMPARISON HFP, 12391 MWD/T BURNUP D-221 . . .	3-210
3-188	S2C9 RPD COMPARISON HFP, 1072 MWD/T BURNUP D-208 . . .	3-211
3-189	S2C9 RPD COMPARISON HFP, 6887 MWD/T BURNUP D-223 . . .	3-212
3-190	N1C3 RPD COMPARISON HZP, 0 MWD/T BURNUP, D-2, C-130 . .	3-213
3-191	N1C6 RPD COMPARISON HZP, 0 MWD/T BURNUP, D-25, ...	3-214
3-192	S1C5 RPD COMPARISON HZP, 0 MWD/T BURNUP, D-0, C-219 . .	3-215
3-193	S2C4 RPD COMPARISON HZP, 0 MWD/T BURNUP, D-0, ...	3-216
3-194	S2C5 RPD COMPARISON HZP, 0 MWD/T BURNUP, D-228, B-33 . .	3-217
3-195	HZP CRITICAL BORON CONCENTRATION DIFFERENCES	3-218
3-196	INTEGRAL CONTROL ROD WORTH DIFFERENCES	3-219

LIST OF FIGURES

Figure	Title	Page
3-197	N1C5 B-BANK INTEGRAL WORTH COMPARISON VS. POSITION . . .	3-220
3-198	N1C5 B-BANK DIFFERENTIAL WORTH COMPARISON VS. POSITION .	3-221
3-199	N1C6 B-BANK INTEGRAL WORTH COMPARISON VS. POSITION . . .	3-222
3-200	N1C6 B-BANK DIFFERENTIAL WORTH COMPARISON VS. POSITION .	3-223
3-201	N1C7 B-BANK INTEGRAL WORTH COMPARISON VS. POSITION . . .	3-224
3-202	N1C7 B-BANK DIFFERENTIAL WORTH COMPARISON VS. POSITION .	3-225
3-203	N2C2 B-BANK INTEGRAL WORTH COMPARISON VS. POSITION . . .	3-226
3-204	N2C2 B-BANK DIFFERENTIAL WORTH COMPARISON VS. POSITION .	3-227
3-205	N2C5 B-BANK INTEGRAL WORTH COMPARISON VS. POSITION . . .	3-228
3-206	N2C5 B-BANK DIFFERENTIAL WORTH COMPARISON VS. POSITION .	3-229
3-207	N2C6 B-BANK INTEGRAL WORTH COMPARISON VS. POSITION . . .	3-230
3-208	N2C6 B-BANK DIFFERENTIAL WORTH COMPARISON VS. POSITION .	3-231
3-209	S1C2 D-BANK INTEGRAL WORTH COMPARISON VS. POSITION . . .	3-232
3-210	S1C2 D-BANK DIFFERENTIAL WORTH COMPARISON VS. POSITION .	3-233
3-211	S1C2 C-BANK INTEGRAL WORTH COMPARISON VS. POSITION . . .	3-234
3-212	S1C2 C-BANK DIFFERENTIAL WORTH COMPARISON VS. POSITION .	3-235
3-213	S1C3 D-BANK INTEGRAL WORTH COMPARISON VS. POSITION . . .	3-236
3-214	S1C3 D-BANK DIFFERENTIAL WORTH COMPARISON VS. POSITION .	3-237
3-215	S1C3 C-BANK INTEGRAL WORTH COMPARISON VS. POSITION . . .	3-238
3-216	S1C3 C-BANK DIFFERENTIAL WORTH COMPARISON VS. POSITION .	3-239
3-217	S1C4 D-BANK INTEGRAL WORTH COMPARISON VS. POSITION . . .	3-240
3-218	S1C4 D-BANK DIFFERENTIAL WORTH COMPARISON VS. POSITION .	3-241
3-219	S1C4 A-BANK INTEGRAL WORTH COMPARISON VS. POSITION . . .	3-242

LIST OF FIGURES

Figure	Title	Page
3-220	S1C4 A-BANK DIFFERENTIAL WORTH COMPARISON VS. POSITION .	3-243
3-221	S2C8 B-BANK INTEGRAL WORTH COMPARISON VS. POSITION . . .	3-244
3-222	S2C8 B-BANK DIFFERENTIAL WORTH COMPARISON VS. POSITION .	3-245
3-223	S2C9 B-BANK INTEGRAL WORTH COMPARISON VS. POSITION . . .	3-246
3-224	S2C9 B-BANK DIFFERENTIAL WORTH COMPARISON VS. POSITION .	3-247
3-225	PREDICTED VERSUS MEASURED DIFFERENTIAL BORON WORTH . . .	3-248
3-226	HFP ARO BORON LETDOWN CURVES FOR N1C1 AND N2C1	3-249
3-227	HFP ARO BORON LETDOWN CURVES FOR N1C2	3-250
3-228	HFP ARO BORON LETDOWN CURVES FOR N1C3	3-251
3-229	HFP ARO BORON LETDOWN CURVES FOR N1C4	3-252
3-230	HFP ARO BORON LETDOWN CURVES FOR N1C5	3-253
3-231	HFP ARO BORON LETDOWN CURVES FOR N1C6	3-254
3-232	HFP ARO BORON LETDOWN CURVES FOR N1C7	3-255
3-233	HFP ARO BORON LETDOWN CURVES FOR N2C2	3-256
3-234	HFP ARO BORON LETDOWN CURVES FOR N2C3	3-257
3-235	HFP ARO BORON LETDOWN CURVES FOR N2C4	3-258
3-236	HFP ARO BORON LETDOWN CURVES FOR N2C5	3-259
3-237	HFP ARO BORON LETDOWN CURVES FOR N2C6	3-260
3-238	HFP ARO BORON LETDOWN CURVES FOR S1C2	3-261
3-239	HFP ARO BORON LETDOWN CURVES FOR S1C3	3-262
3-240	HFP ARO BORON LETDOWN CURVES FOR S1C4	3-263
3-241	HFP ARO BORON LETDOWN CURVES FOR S1C5	3-264
3-242	HFP ARO BORON LETDOWN CURVES FOR S1C6	3-265

LIST OF FIGURES

Figure	Title	Page
3-243	HFP ARO BORON LETDOWN CURVES FOR S1C7	3-266
3-244	HFP ARO BORON LETDOWN CURVES FOR S1C8	3-267
3-245	HFP ARO BORON LETDOWN CURVES FOR S1C9	3-268
3-246	HFP ARO BORON LETDOWN CURVES FOR S2C2	3-269
3-247	HFP ARO BORON LETDOWN CURVES FOR S2C3	3-270
3-248	HFP ARO BORON LETDOWN CURVES FOR S2C4	3-271
3-249	HFP ARO BORON LETDOWN CURVES FOR S2C5	3-272
3-250	HFP ARO BORON LETDOWN CURVES FOR S2C6	3-273
3-251	HFP ARO BORON LETDOWN CURVES FOR S2C7	3-274
3-252	HFP ARO BORON LETDOWN CURVES FOR S2C8	3-275
3-253	HFP ARO BORON LETDOWN CURVES FOR S2C9	3-276
3-254	PREDICTED VERSUS MEASURED HZP ISOTHERMAL TEMPERATURE COEFFICIENTS	3-277

SECTION 1 - INTRODUCTION

The Virginia Electric and Power Company (Virginia Power) is updating and increasing the scope of its capability to perform nuclear utility reactor analyses for the Surry and North Anna nuclear power stations. The objective of this topical report is 1) to describe one of the computational models developed at Virginia Power for the purposes of reactor physics analyses and fuel management evaluations and 2) to demonstrate the accuracy of this model by comparing analytical results generated with the model to actual measurements from Surry and North Anna Units No. 1 and 2.

The computational model to be described is a coarse mesh (five non-uniform mesh per fuel assembly), three-dimensional (26 non-uniform axial mesh), two neutron energy group diffusion-depletion (with thermal-hydraulic feedback) calculational package and is designated as the PDQ two zone calculational model. The "two zone" designation refers to the use of two separate material zones to represent each fuel assembly in the X-Y dimension - one zone where no lumped burnable poison rods or control rods exist and one zone in which the poison rods or control rods are homogenized with the fuel materials. The PDQ two zone model uses the Virginia Power computer codes SHUFL and PDQV2, as well as input from the EPRI ARMP-02[3] CELL2[1,2] and NUPUNCHER[1] codes, the Virginia Power ETHIL code, the EPRI ESCORE[4] code, and the SCALE3[5] package from ORNL (including KENO-V.a[6]). SHUFL is an update of the SHUFFLE[7] code developed by Babcock and Wilcox and adapted by Virginia Power. PDQV2 is an update to the PDQ7V2[8] code modified for use by Virginia Power. In addition, pin power distributions and instrument thimble fluxes are reconstructed using

pointwise flux and block nuclide concentration files in conjunction with the Virginia Power computer codes PCF[9] and RECON[10]. A detailed description of the input/output, functioning, and physical models of the above computer codes can be obtained from the referenced computer code manuals. The above computer codes are maintained by Virginia Power. The EPRI computer codes are updated through contractual arrangements between Virginia Power and EPRI. The SCALE3 code package is updated periodically through notification by the ORNL Radiation Shielding Information Center.

The PDQ two zone model was designed to provide a three dimensional reactor physics analysis capability which combines the three dimensional benefits of the Virginia Power FLAME[11] 3-D nodal model with isotope depletion capability, cross section modeling complexity, more optimized mesh structure, and more reliable reflector modeling available with PDQ. In addition, the cross section representation has been improved through use of CELL2 with the ENDF/B-V option, through the use of KENO-V.a benchmarking calculations, and through the addition of multiple G-factor capability in the Virginia Power version of PDQ.

The 3-D two zone model requires more computer usage than the Virginia Power FLAME model or PDQ discrete (2-D pin by pin) model[12]. However, use of the two zone model provides the following:

1. Local power distributions for vessel fluence calculations at any axial core elevation.

2. Benchmarking of the CELL2/PDQ system without axial buckling assumptions.

3. A modeling benchmark for the faster but less detailed 3-D nodal code (FLAME).

4. A modeling benchmark for 2-D axial buckling verification.

5. A single base model from which inputs for the Virginia Power NOMAD[13] 1-D axial model can be obtained.

In addition, a 2-D collapsed version[13] of the 3-D two zone model has been developed to replace the Virginia Power PDQ one zone model[14]. Benefits of the replacement will be an improved mesh structure, more detailed cross section representation through the use of multiple G-factors, improved cross section data through use of CELL2 with KENO-V.a benchmarking, verified axial buckling inputs by direct comparison with 3-D model results, and pin power reconstruction capability. Computer requirements should be comparable to those of the one zone model.

The types of calculations that can be performed by the two zone model include:

1. Reactor Physics Analysis

   a. Three-dimensional assembly average radial power distributions, relative radial peaking factors ($F_{XY}(Z)$), enthalpy rise hot channel factors ($F_{\Delta H}(X,Y)$), assembly average axial power distribution, core average axial power distribution ($P(Z)$), and heat flux hot channel factor ($F_Q(X,Y,Z)$)

   b. Critical soluble boron concentrations

   c. Nuclide concentrations

   d. Integral and differential control rod bank worths

   e. Abnormally positioned control rod bank worths

   f. Moderator and Doppler coefficients and defects

2. Fuel Management Analysis

   a. Batch power and burnup sharing

   b. Fuel isotopics as a function of burnup

   c. Scoping studies for the evaluation of alternative future cycle designs and fuel loadings

These calculations are currently performed with other core models. However, the benchmarking data presented in this report show that the 3-D PDQ two zone model is a capable alternative. Of the above types of

calculations, the ones that are of primary interest are those which require the greatest degree of 3-D modeling detail where computer use is not limiting. For example, vessel fluence calculations require a consistent model so that predictions which have been benchmarked to capsule measurements for early cycles can be reliably extrapolated through future cycles. Calculation of the critical rod position for startups following a trip or extended outage requires that both the reactivity impact of isotope decay, the axial flux redistribution, and the partially inserted control rod worth be accurately predicted. Use of part length flux suppression rods to reduce vessel fluence requires a model which can predict the reactivity, power distribution, peaking and depletion effects in three dimensions. Scoping studies involving axial zoning, axial blankets or reduced length burnable poisons can also be performed with the 3-D two zone. Comparison of two zone model predictions with FLAME predictions has provided a basis for identifying modeling improvements for the nodal model. Similar improvements in the 1-D NOMAD model may be an additional benefit. All of these examples represent possible reasons for choosing to use the 3-D PDQ two zone model.

The Surry Nuclear Power Station and the North Anna Nuclear Power Station, each consisting of two operating units, have been selected as the operating system to be modeled for verification of the PDQ two zone model. The Surry Units Nos. 1 and 2 are identical Westinghouse designed three coolant loop pressurized water reactors with thermal ratings of 2441 Mwt. Initial criticality was achieved for Surry Unit No. 1 on July 1, 1972 and for Surry Unit No. 2 on March 7, 1973. Cycle operating summaries for the Surry units are listed in Table 1-1.

The North Anna Units Nos. 1 and 2 are identical Westinghouse designed three coolant loop pressurized water reactors with thermal ratings of 2893 Mwt (initially rated 2775 Mwt). Initial criticality was achieved for North Anna Unit No. 1 on April 5, 1978 and for North Anna Unit No. 2 on June 6, 1980. Cycle operating summaries for the North Anna units are listed in Table 1-2.

The remainder of this report describes the Surry and North Anna versions of the PDQ two zone model, the purpose and interrelationships of the various computer codes which comprise the PDQ two zone model, and the comparison of calculated results with selected reactor measurements from all completed and operating North Anna and Surry cycles.

TABLE 1-1

SURRY NUCLEAR POWER STATION OPERATING HISTORY

UNIT/CYCLE	ON LINE DATE	OFF LINE DATE	CYCLE BURNUP (MWD/MTU)	CORE RATING (MWT)
S1C1	09/12/1972	10/24/1974	13547	2441
S1C2	02/03/1975	09/26/1975	6915	2441
S1C3	12/08/1975	10/17/1976	8944	2441
S1C4	01/24/1977	04/22/1978	13107	2441
S1C5	07/09/1978	09/14/1980	14390	2441
S1C6	07/06/1981	02/07/1983	16491	2441
S1C7	05/30/1983	09/26/1984	11984	2441
S1C8	12/26/1984	05/10/1986	14040	2441
S1C9	07/12/1986	04/09/1988	16073	2441
S1C10	07/14/1988			2441
S2C1	03/19/1973	04/26/1975	14870	2441
S2C2	06/19/1975	04/22/1976	9054	2441
S2C3	06/10/1976	09/10/1977	9422	2441
S2C4	10/12/1977	02/04/1979	13678	2441
S2C5	08/19/1980	11/07/1981	13971	2441
S2C6	12/31/1981	06/30/1983	16006	2441
S2C7	09/25/1983	03/20/1985	14802	2441
S2C8	06/27/1985	10/04/1986	13359	2441
S2C9	11/30/1986	9/10/1988	15710	2441
S2C10	07/16/1989			2441

TABLE 1-2

NORTH ANNA NUCLEAR POWER STATION OPERATING HISTORY

UNIT/CYCLE	ON LINE DATE	OFF LINE DATE	CYCLE BURNUP (MWD/MTU)	CORE RATING (MWT)
N1C1	04/23/1978	09/25/1979	15590	2775
N1C2	01/24/1980	12/28/1980	10711	2775
N1C3	04/10/1981	05/17/1982	13335	2775
N1C4	11/18/1982	05/12/1984	13478	2775
N1C5	09/25/1984	11/04/1985	13398	2775
N1C6	12/23/1985	04/19/1987	15705	2775/2893
N1C7	06/29/1987	02/25/1989	16891	2893
N1C8	07/15/1989			2893
N2C1	10/23/1980	03/07/1982	14494	2775
N2C2	06/02/1982	04/02/1983	8436	2775
N2C3	05/29/1983	08/02/1984	14717	2775
N2C4	11/02/1984	02/20/1986	15534	2775
N2C5	04/01/1986	08/24/1987	17467	2775/2893
N2C6	11/03/1987	02/20/1989	17044	2893
N2C7	05/07/1989			2893

SECTION 2 - MODEL DESCRIPTION

2.1 INTRODUCTION

The PDQ two zone model incorporates a few-group, diffusion-depletion theory model, with thermal-hydraulic feedback, to perform spatial neutron flux and nuclide concentration calculations in three dimensions throughout the reactor core. This calculation is performed at each mesh point represented in the geometry of the reactor core. Furthermore, each fuel assembly is represented by a specified array of mesh blocks formed by the intersection of the mesh lines in the x and y directions (i.e., mesh points). Each mesh block is used to represent a material composition whereas the neutron flux is calculated at each mesh point.

With the exception of burnable poison rods (BP) or control rods, the material compositions of each assembly are initially homogenized so that each mesh block within an assembly represents an equal concentration of fuel rods, guide tubes, etc. Therefore, the concentrations of the various nuclides (non-BP or control rod) are initially the same in all mesh blocks within a fresh fuel assembly. For reasons detailed in section 2.2, the control rod and BP related concentrations are segregated into only that part of the assembly over which they exert the most influence. There are therefore two possible initial concentration zones for each assembly. As the assembly undergoes depletion with power operation, however, the material compositions change in each mesh block according to the neutron flux associated with that mesh block.

The two zone model performs calculations in several steps. First, a fine-group neutron flux spectrum and the appropriate cross sections as a function of neutron energy are calculated for each material composition with the cross section generating code CELL2. The fine-group flux spectrum is then used to spectrum weight and collapse the fine-group cross sections into two neutron energy groups (denoted as the fast and thermal groups). The spectrum weighted two-group cross sections associated with each material composition including the baffle and reflector are then used to perform an iterative diffusion theory calculation of the neutron flux as a function of spatial position. Solution of the diffusion theory equations consists of estimating an initial source distribution and eigenvalue, computing the flux in each group at each mesh point, and then recomputing the source and eigenvalue. This process is repeated until the change in flux and/or eigenvalue between successive iterations meets a predetermined convergence criterion. From the converged neutron flux and cross sections, the core power distribution is determined, and subsequently the fuel and moderator temperature distributions are calculated. Thermal feedback effects are included in the diffusion theory calculation by recalculating the neutron cross sections, flux and power distribution, and fuel and moderator temperature distribution iteratively until both the required nuclear and thermal convergence criteria are met.

The neutron flux in the core is not only a function of energy and position but is also a function of changes in the nuclide concentrations and cross sections which vary with burnup. The initial nuclide depletion calculation is performed with the initial two-group fluxes and

microscopic absorption and fission cross sections for the nuclides in each mesh block that vary with burnup. The neutron flux is then recalculated based upon these new values of nuclide concentrations and cross sections. This process is repeated over an interval of depletion steps until the desired burnup is achieved. Because in a 3-D model this process can lead to axial xenon concentration oscillations, an equilibrium xenon option is often used for depletion cases. The equilibrium xenon concentration is calculated in an iterative manner similar to the thermal feedback. Thermal and xenon feedback convergence parameters are chosen to assure stability and convergence of the final solution. Following execution of the PDQ code, pin powers are reconstructed in 3-D to determine peaking factors.

Several interrelated computer codes are used to perform the calculations outlined above. The computer codes comprising the PDQ two zone model and their interrelationships are presented in the flow chart of Figure 2-1. The PDQ computer code itself is the principal reactor analysis calculational tool in the PDQ two zone model and is used to perform the two-group, two-dimensional diffusion theory calculations. The other codes provide either input data, data manipulation, or use the PDQ code output. As indicated in Figure 2-1, the CELL2 computer code is used to calculate the required two-group spectrum-weighted cross sections. The ETHIL computer code formats these cross sections for use in the PDQ code (as HARMONY tablesets). NUPUNCHER reads CELL2 output files to provide cross sections for the lumped fission product representation. The KENO-V.a Monte-Carlo code is used to provide benchmark eigenvalues as a basis for adjusting the HARMONY tableset input

so that closer agreement between KENO and PDQ is obtained. KENO-V.a also provides the cross sections and worths for preparing and verifying the PDQ control rod cross section tables. The EPRI ESCORE code and XSDRNPM from the SCALE3 package are used to provide the average fuel temperature as a function of burnup and power. The SHUFL computer code is a data manipulation code that takes appropriate end-of-cycle nuclide concentrations from the PDQ computer code and shuffles this data in the reactor core according to a specified scheme which duplicates calculationally the actual replacement and movement of fuel assemblies in the reactor core as the result of a refueling. Figure 2-2 shows the calculations involved in pin power reconstruction. A database of reconstruction data is developed using PDQ single assembly models to represent each unique fuel type in the core. The data is calculated and stored by the PCF code. The RECON code is used to reconstruct in 3-D each pin power in the core to determine peaking factors and to produce data to be used with the PDQDK[15] and INCORE[16] codes. INCORE is used to determine the measured core power distribution.

Section 2-3 describes in greater detail the functioning of each of the computer codes used in the PDQ two zone model.

FIGURE 2-1

PDQ TWO ZONE MODEL FLOWCHART

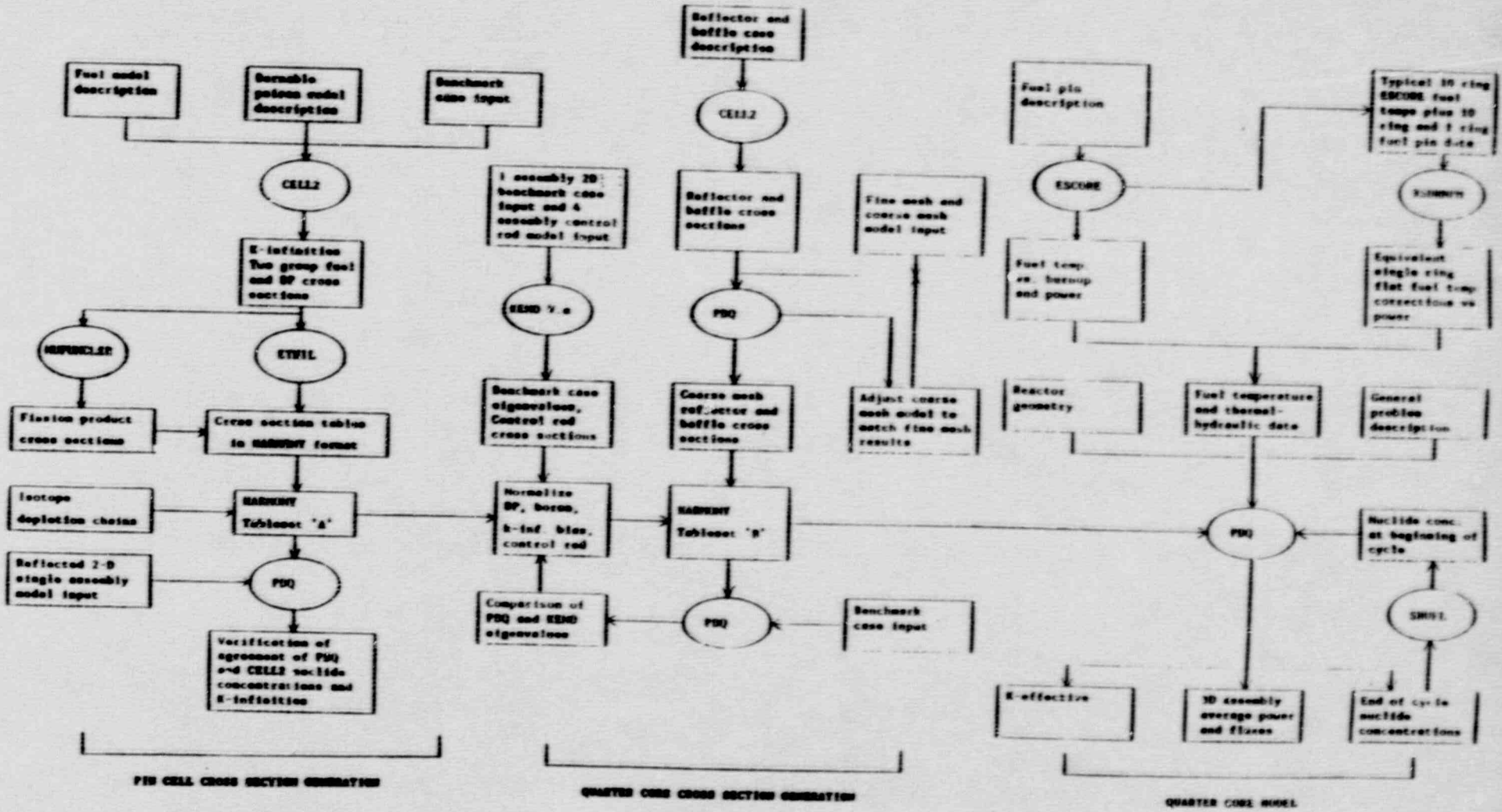

FIGURE 2-2
PIN POWER RECONSTRUCTION FLOWCHART

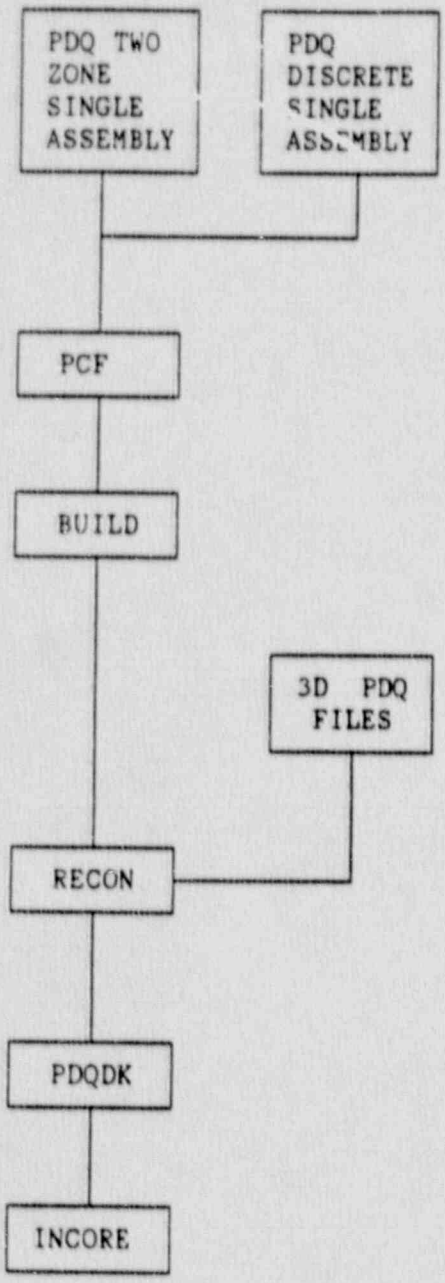

	PURPOSE
PDQ TWO ZONE SINGLE ASSEMBLY PDQ DISCRETE SINGLE ASSEMBLY	Deplete assembly models for each type of fuel/history combination. Major effects are control rods, BP, depleted BP, burnup, BP history.
PCF	Calculate and store pcf's, thimble flux multipliers for each fuel type.
BUILD	Write stored PCF data to a direct access file for RECON.
3D PDQ FILES	Write flux and concentration files.
RECON	Read direct access file, 3D PDQ flux and concentration files, user input to calculate quarter core 3D peaking factors and data for PDQDK/INCORE.
PDQDK	Read average power file and PDQDK input data written by RECON. Write INCORE input data decks.
INCORE	Read PDQDK and measured flux map data. Calculate measured power and peaking factors.

2.2 MODEL GEOMETRY

The assembly geometry for the PDQ two zone model was selected based on the conflicting needs of minimum computer usage and maximum power distribution accuracy. The primary difficulty of a coarse mesh diffusion theory model occurs at locations of rapidly changing neutron flux. This problem can be overcome to a great degree at the core boundaries by adjusting the coarse mesh reflector constants to better match a fine mesh diffusion theory solution or transport theory solution. The problem is not as severe for assemblies away from the core boundaries except when burnable poisons or control rods are involved. The presence of a discretely positioned strong neutron absorber depresses the flux in the vicinity of the absorber and creates a flux profile which rises away from the absorber. The current at the interface of a fuel assembly containing burnable poison (BP) rods and a non-BP neighbor of similar fuel characteristics will be directed inward at the poisoned assembly. The impact is an in-leakage of flux (and therefore power) from the non-BP assembly into the assembly with BP. If this current is not adequately calculated the relative power distribution among neighboring assemblies will not be accurate.

In conventional diffusion theory (with no discontinuity factors) there are two requirements for maximizing the accuracy of power distribution calculations: First, the mesh structure should be finest near important boundaries, and second, the lumped poison rods or control rods must not be homogenized over the entire assembly. The first consideration was the primary factor in the selection of the 26 mesh axial

structure shown in Figure 2-3. Both considerations were important in the selection of the X-Y mesh structure. The pin by pin orientation for Surry (15x15) fuel is given in Figure 2-4. Figure 2-5 shows the two zone X-Y geometry model chosen to represent the 15x15 assembly. The corresponding North Anna (17x17) pin by pin orientation is given in Figure 2-6 and the two zone representation is shown in Figure 2-7. The 5x5 mesh is coarse enough to reduce computer requirements by a factor of 10 versus a discrete pin by pin representation. The variable mesh size improves the ability to calculate the flux gradient with respect to either a core boundary or a neighboring assembly versus a fixed mesh model. The two zone feature, which segregates the control rods or poison closer to their region of influence within the assembly, also provides a mesh block beyond the poison region over which the flux can rise. This better represents the flux gradient in a poisoned assembly versus a model in which the poison is homogenized over the entire assembly (such as the Virginia Power PDQ one zone model). Because the PDQ option of point depletion is used, all 25 mesh blocks are used in the representation of assembly burnup gradients.

A standardized problem designed to test the effectiveness of model geometry is the 2-D IAEA benchmark[17]. This quarter core problem has a fixed set of neutron macroscopic cross sections for each fuel assembly and for the reflector region and a well defined solution for the assembly average power distribution. Figure 2-8 presents a power distribution map comparing the PDQ and benchmark solutions for a uniform 6x6 PDQ mesh structure similar to that used in the Virginia Power PDQ one zone model. Figure 2-9 shows the same comparison based on a 5x5 non-uniform mesh

structure similar to that used in the two zone model. Even though there are only 25 mesh blocks per assembly versus 36 per assembly in the 6x6 model, the non-uniform 5x5 power distribution errors are only half as large. A factor of two increase in power distribution accuracy is obtained while reducing computing time by 25%. Note that the power distribution differences in Figure 2-9 are largest at the core boundary and exhibit an in-out tilt in both sign and magnitude. Adjustments to the baffle and reflector representation can be made to remove much of the tilt. The adjustment process will be discussed further in Section 2.3.6.

The axial mesh structure was selected using the same argument that a finer mesh near the core boundary will maximize power distribution accuracy and minimize computer run time. Although no benchmark results are presented here, the process normalizing the axial reflector representation to a very fine mesh diffusion model is described in Section 2.3.6. Axial power distribution plots comparing PDQ two zone and measured data, as well as differential control rod worth comparison plots, will be presented in Section 3 to verify the accuracy of the axial structure.

FIGURE 2-3

PDQ TWO ZONE AXIAL MESH STRUCTURE

- 22 Mesh in Fuel
- 2 Mesh in Each Reflector

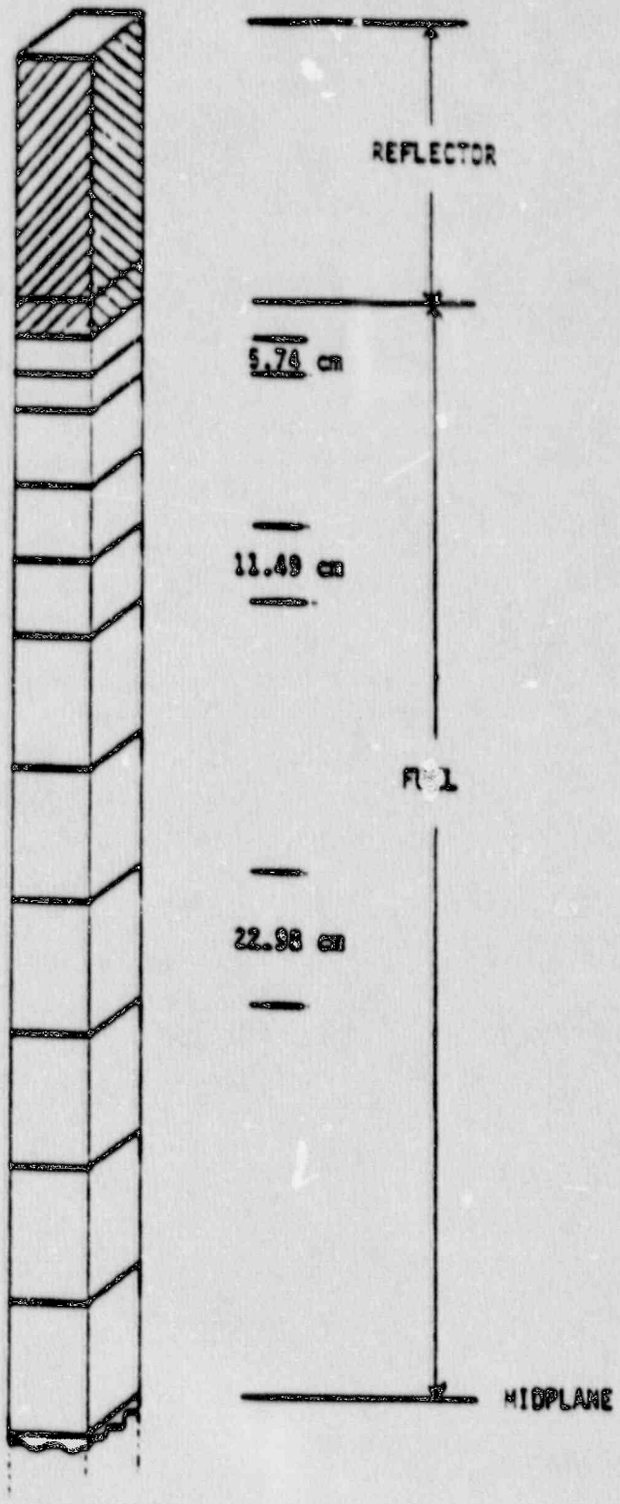

FIGURE 2-4

SURRY FUEL 15 X 15 X-Y PIN ORIENTATION

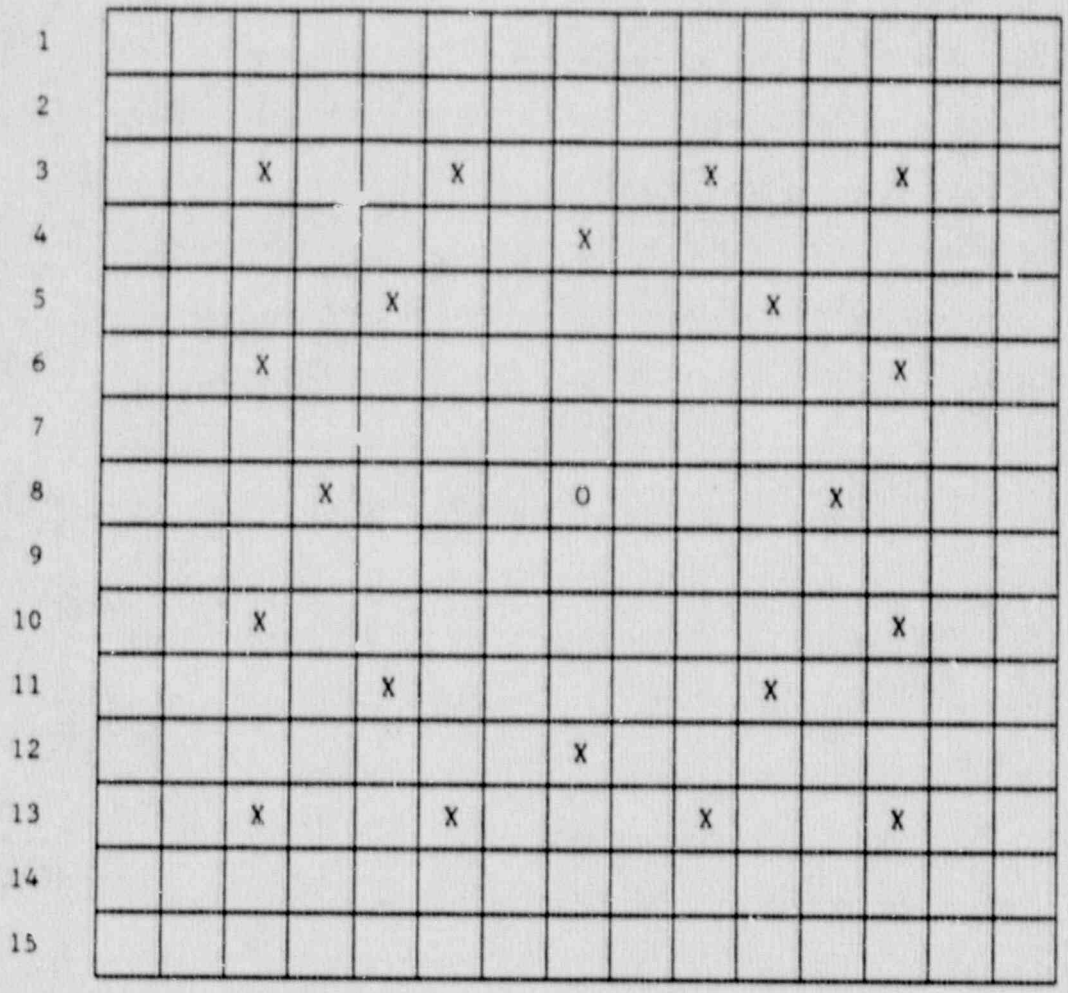

FUEL PIN CELL

X POSSIBLE BP ROD OR CONTROL ROD LOCATION

O INSTRUMENT THIMBLE

FIGURE 2-5

SURRY FUEL TWO ZONE X-Y MESH STRUCTURE

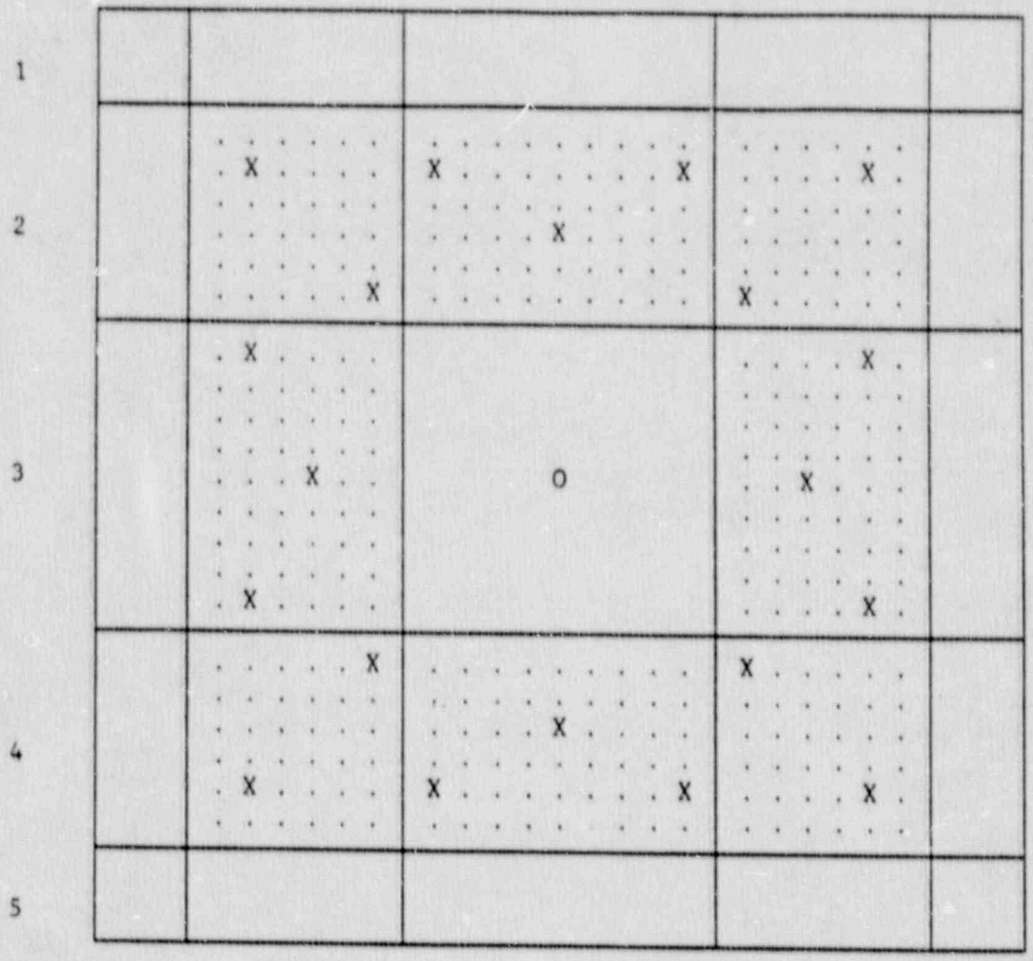

ZONE 1 - HOMOGENIZED FUEL

ZONE 2 - HOMOGENIZED MIXTURE OF FUEL AND BP OR CONTROL ROD

NOTE : BP and instrument thimble locations are shown for reference only.

FIGURE 2-6

NORTH ANNA FUEL 17 X 17 X-Y PIN ORIENTATION

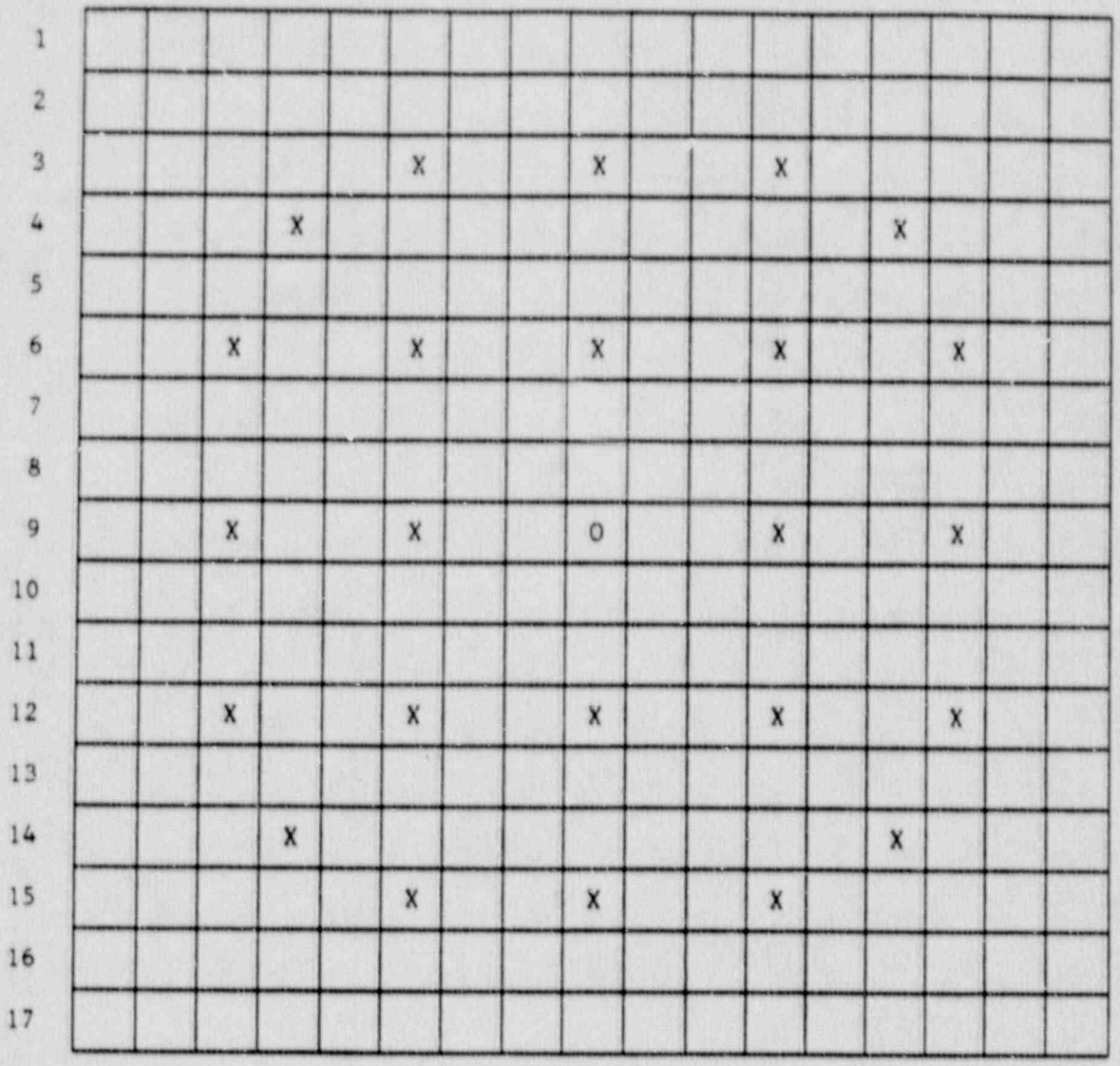

FUEL PIN CELL

X POSSIBLE BP ROD OR CONTROL ROD LOCATION

O INSTRUMENT THIMBLE

FIGURE 2-7

NORTH ANNA FUEL TWO ZONE X-Y MESH STRUCTURE

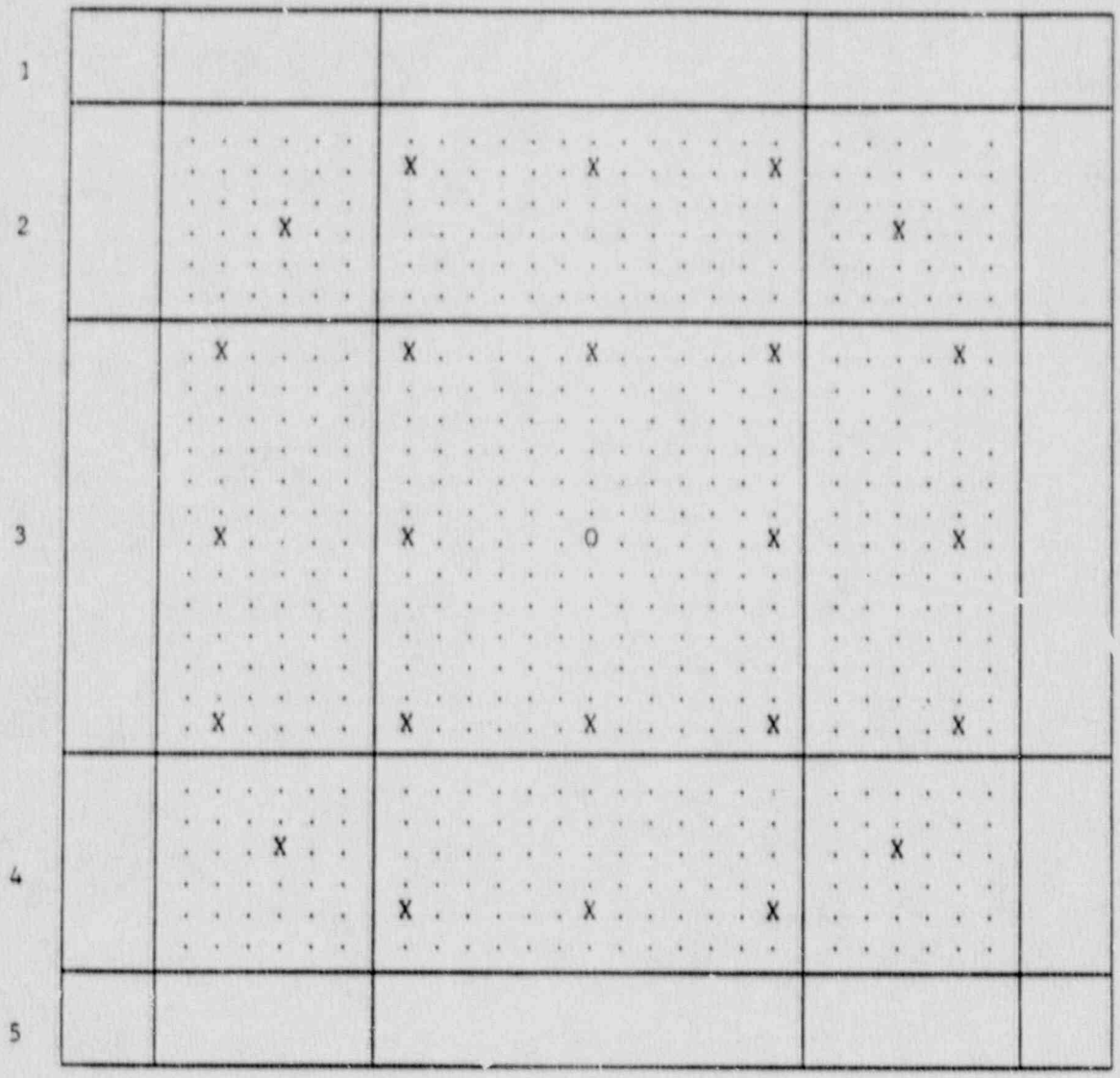

ZONE 1 - HOMOGENIZED FUEL

ZONE 2 - HOMOGENIZED MIXTURE OF FUEL AND BP OR CONTROL ROD

NOTE : BP and instrument thimble locations are shown for reference only.

FIGURE 2-8

IAEA 2-D BENCHMARK PROBLEM
PDQ 6 X 6 UNIFORM MESH RESULTS

0.746 0.728 -2.413	1.310 1.243 -5.115	1.454 1.394 -4.127	1.211 1.160 -4.211	0.610 0.610 0.000	0.935 0.927 -0.856	0.934 0.951 1.820	0.750 0.800 6.667
1.310 1.243 -5.115	1.435 1.372 -4.390	1.480 1.422 -3.919	1.315 1.270 -3.422	1.070 1.041 -2.710	1.036 1.034 -0.193	0.950 0.970 2.105	0.736 0.782 6.250
1.454 1.394 -4.127	1.480 1.422 -3.919	1.469 1.419 -3.404	1.345 1.308 -2.751	1.179 1.160 -1.612	1.071 1.075 0.373	0.975 1.003 2.872	0.692 0.758 9.538
1.211 1.160 -4.211	1.315 1.270 -3.422	1.345 1.308 -2.751	1.193 1.165 -2.347	0.967 0.952 -1.551	0.906 0.918 1.325	0.846 0.900 6.383	
0.610 0.610 0.000	1.070 1.041 -2.710	1.179 1.160 -1.612	0.967 0.952 -1.551	0.471 0.484 2.760	0.686 0.701 2.187	0.597 0.656 9.883	
0.935 0.927 -0.856	1.036 1.034 -0.193	1.071 1.075 0.373	0.906 0.918 1.325	0.686 0.701 2.187	0.585 0.642 9.744		
0.934 0.951 1.820	0.950 0.970 2.105	0.975 1.003 2.872	0.846 0.900 6.383	0.597 0.656 9.883			
0.750 0.800 6.667	0.736 0.782 6.250	0.692 0.758 9.538					

AAA BBB CCC

A - REFERENCE
B - PDQ 6 X 6
C - % DIFFERENCE

MAX DIFFERENCE = 9.883
MAX DIFF (RPD>0.9) = -5.115
RMS DIFFERENCE = 4.558

FIGURE 2-9

IAEA 2-D BENCHMARK PROBLEM
PDQ TWO ZONE 5 X 5 NON-UNIFORM MESH RESULTS

0.746 0.736 -1.344	1.310 1.274 -2.745	1.454 1.424 -2.085	1.211 1.183 -2.276	0.610 0.611 0.204	0.935 0.930 -0.529	0.934 0.944 1.038	0.750 0.772 2.981
1.310 1.274 -2.745	1.435 1.403 -2.227	1.480 1.453 -1.817	1.315 1.293 -1.686	1.070 1.056 -1.327	1.036 1.036 0.017	0.950 0.963 1.336	0.736 0.754 2.506
1.454 1.424 -2.083	1.480 1.453 -1.815	1.469 1.448 -1.423	1.345 1.329 -1.181	1.179 1.172 -0.625	1.071 1.076 0.485	0.975 0.991 1.631	0.692 0.722 4.334
1.211 1.183 -2.272	1.315 1.293 -1.681	1.345 1.329 -1.178	1.193 1.180 -1.105	0.967 0.959 -0.796	0.906 0.913 0.753	0.846 0.873 3.213	
0.610 0.611 0.213	1.070 1.056 -1.318	1.179 1.172 -0.618	0.967 0.959 -0.791	0.471 0.479 1.652	0.686 0.691 0.693	0.597 0.622 4.269	
0.935 0.930 -0.515	1.036 1.036 0.030	1.071 1.076 0.497	0.906 0.913 0.763	0.686 0.691 0.699	0.585 0.609 4.117		
0.934 0.944 1.056	0.950 0.963 1.353	0.975 0.991 1.647	0.846 0.873 3.226	0.597 0.623 4.279			
0.750 0.773 3.001	0.736 0.755 2.526	0.692 0.722 4.353					

AAA
BBB
CCC

A - REFERENCE
B - PDQ 5 X 5
C - % DIFFERENCE

MAX DIFFERENCE = 4.353
MAX DIFF (RPD>0.9) = -2.745
RMS DIFFERENCE = 2.102

2.3 CROSS SECTION GENERATION

2.3.1 FUEL CROSS SECTION GENERATION

The primary source of the basic nuclear cross section data is the ENDF/B-V library used in the EPRI CELL2 code. The library contains cross sections for 68 fast energy groups ranging from 0.414 eV to 10 MeV and 35 thermal energy groups ranging from 0.000253 eV to 1.855 eV. Additional details of the library are available in Reference 2.

The CELL2 code is used to calculate composition-dependent energy spectra and then collapse the fine-energy group cross sections to produce two-group cross sections for each unit cell. CELL2 calculates two-group spectrum weighted cross sections for each type of unit cell used to represent the reactor core. A unit cell can be either a fuel rod, a control rod guide tube, or a burnable poison rod, the moderator associated with each type of rod, and an extra region around the cell to account for the impact of other assembly materials. A supercell is defined as the combined flux weighted homogenization of all the regions comprising a unit cell. For the two zone model, the fuel unit cell consists of a fuel rod, the cladding, moderator, and an extra region to account for guide tubes (with or without BP rods) and moderator gaps between assemblies. The supercell option is used to represent the fuel assembly in the two zone model because only a homogenized assembly can be represenced due to the coarse mesh structure used. The homogenization is performed in a manner that results in all the mesh blocks within each zone initially having the same material composition. All fuel cross sections (not burnable poison

or control rods) used in the two zone model are based on the CELL2 supercell data. A more detailed description of the theory and use of the CELL2 code is available in References 1, 2, and 18.

The neutron energy spectrum calculated by CELL2 depends on the material concentrations in the unit cell. The material concentrations change during the operation of the reactor as a result of:

1) Depletion of the fuel nuclides
2) Changes in the soluble boron
3) Changes in moderator temperature
4) Removal or addition of BP rods

The neutron spectrum is also dependent on the temperature of the fuel due to Doppler broadening of the resonance absorption peaks. CELL2 is used to calculate the effect of changes in both the material concentrations and the fuel and moderator temperatures on the neutron spectrum and spectrum-weighted two-group cross sections.

To provide a base of fuel cross section data comprehensive enough for development of a thorough HARMONY tableset, CELL2 fuel cell cases are run over a wide variety of conditions. Conditions modeled include:

1) Depletion at nominal power, temperature, and soluble boron.
2) Moderator temperatures ranging from 620°F to 100°F.
3) Fuel temperatures from HFP nominal to 100°F.
4) Xenon concentrations ranging from HFP nominal equilibrium to no xenon.
5) Soluble boron ranging up to 2000 ppm.

6) Samarium concentrations ranging from 0 to two times equilibrium.

7) U^{235}, Pu^{239}, Pu^{240}, and Pu^{241} concentrations at nominal and 10% above nominal for each burnup.

8) With and without the water displacement effect of burnable poison rods.

9) With and without the neutron absorption of the BP rod B^{10}.

10) Appropriate combinations of some of the above.

After identification of significant cross section sensitivities the Virginia Power ETHIL code is used to format the cross sections into HARMONY tableset format.

2.3.2 BP CROSS SECTION GENERATION

Because CELL2 cannot represent both BP rods and fuel rods in their actual geometry simultaneously, a two stage approach is used. The unit cell for the BP model consists of the BP absorber, clad, moderator, and two extra regions consisting of fuel and moderator homogenized. The fuel and moderator homogenization is performed in such a way that the flux spectrum in the fuel region nearest the BP pin is reasonably representative of the fuel pin cell spectrum. The neutron absorption rate of the BP pin is calculated and properly volume averaged for use as input to the CELL2 fuel pin cell model for determining the sensitivity of fuel cross sections to BP neutron absorption. The BP cell model is also used to provide BP microscopic absorption cross sections and flux depression factors which are input to the HARMONY tableset as a function of fuel isotopics, boron, moderator temperature or specific volume, and BP B10 number density.

2.3.3 CROSS SECTION REPRESENTATION

Sets of HARMONY cross section tables based on these CELL2 calculations are prepared by the ETHIL code. These tables represent:

1) Microscopic fast and thermal energy group absorption, fission and transport cross sections for each material or isotope.

2) Fast and thermal Nu and Kappa for each fissioning isotope.

3) The macroscopic removal cross section.

4) Multiple G-factor tables applied to (1) and (3) above to model any important cross section dependences not accounted for in the cross section tables. The G-factor tables also model number density dependences (such as soluble boron as a function of moderator density) and flux depression factors (for BP or control rods).

The cross section representation strategy is to account for all significant cross section dependences on a microscopic cross section level. Ideally, this removes the need to identify and consciously account for 'history' effects which lead to different burnup dependent fuel isotopics. For example, one such history effect is soluble boron history. Depletion at higher boron concentrations leads to a higher production of plutonium isotopes at any given burnup relative to depletion at lower boron concentrations. Unless the impact of soluble boron on the cross sections of each affected isotope is included in the HARMONY tableset, the isotopic differences will not be accurately reproduced. For this reason, there are no lumped macroscopic cross sections or macroscopic cross section sensitivities in the two zone HARMONY tablesets except for the removal cross section and control rod cross sections. In addition, use is made of the CELL2 detailed fission product edit to model explicitly

several fission product production chains not typically modeled. The nuclide chains of interest are those leading to isotopes which have significant reactivity impact due to changing concentrations during periods of zero or low power or during full power operation following zero or low power operation. Xenon and samarium are two such nuclides which are commonly modeled. Those not typically modeled have been removed from the lumped fission product representation produced by CELL2 so as not to doubly account for any fission products.

Once all cross section dependences have been represented, the tables are assembled in a HARMONY tableset along with depletion chain and other data required for PDQ to correctly interpret the tables. A series of PDQ runs are made duplicating the initial CELL2 calculations using a 2-D fuel assembly model with reflective flux boundary conditions. The number density predictions and K-infinity values are compared to those produced by the CELL2 supercell fuel model to verify that all important cross section dependences have been accurately modeled. Additional CELL2 runs are made to check the validity of the data under other conditions, such as during long periods at zero power followed by full power operation and during depletion at non-nominal moderator temperatures. The goal is for the PDQ/HARMONY system to reasonably reproduce the CELL2 predictions for any condition within the expected range of actual core operation or analysis.

2.3.4 NORMALIZATION TO KENO-V.a BENCHMARK CASES

Prior experience with reactor core modeling has indicated that adjusting the predictions of PDQ (and by extension the cross section generation code) to higher order Monte Carlo predictions often improves the agreement between prediction and measurement. The Monte Carlo program used by Virginia Power for this purpose is the KENO-V.a code run using the SCALE3 driver package with the 218 group ENDF/B-IV cross section set. The two zone HARMONY tablesets contain adjustment factors to normalize BP worth, soluble boron worth, and overall reactivity predictions to target predictions. The target predictions are based on adjusted eigenvalues from KENO for a fresh fuel assembly (using reflective boundary conditions) at a variety of conditions. In the KENO model each fuel pin, guide tube and BP rod is explicitly modeled including clad and voids. A bias is assigned to the KENO eigenvalues on the basis of the results from several modeled critical experiments. The adjustment factors are determined in an iterative process aligning the PDQ eigenvalue for each case to the biased KENO eigenvalue. Appropriate consideration is given to the statistical uncertainty of the KENO predictions. The normalization process is applied separately to each fuel enrichment in the HARMONY tableset.

2.3.5 KENO-V.a CONTROL ROD CROSS SECTIONS

A KENO-V.a model is also used to generate control rod cross sections for the two zone PDQ model. The geometry used is a checkerboard assembly arrangement in which every other assembly can contain a control rod. The

27 group ENDF/B-IV cross section library is used because it contains fission products needed to simulate burned fuel. An edit code is used to convert K-infinity, 27 group absorption rates, fission rates, and fluxes into 2 group macroscopic absorption, fission, and removal cross sections. Rodded and unrodded cases at a variety of burnups, boron concentrations, and moderator temperatures are run to produce a set of macroscopic cross section differences due to the addition of the control rod. The cross section tables are appropriately volume weighted and added to the HARMONY tableset as microscopic cross sections and G-factors associated with the fictitious "crod" isotope. A checkerboard two zone PDQ model is used in an iterative process to determine the correct flux depression factor to be applied to the control rod cross sections in each energy group so that the overall reactivity effect produced agrees well with the KENO predictions. Comparisons of measured and predicted integral and differential control rod worths presented in Section 3 indicate excellent overall agreement using this model.

2.3.6 REFLECTOR AND BAFFLE CROSS SECTIONS

Determination of coarse mesh baffle and reflector constants for the two zone geometry is done by appropriately volume weighting and then adjusting the coarse mesh constants to better match the power distribution and flux ratios predicted by a very fine mesh PDQ model. For the X-Y plane, a quarter core geometry is used. The fine mesh geometry consists of a uniform 44X44 blocks per assembly plus additional mesh for the baffle, reflector, and core barrel. Cross section data for the stainless steel region is obtained by editing the clad region of a CELL2 stainless

steel clad fuel cell. Water and boron mixture cross sections are generated using the CELL2 non-fuel option. The coarse mesh cross sections are then calculated such that the optical thickness through each region is preserved as nearly as possible. So that two mesh blocks may be used in the baffle region to better account for flux gradients, the baffle cross section optical thickness weighting is performed over the first two mesh beyond the fuel boundary. PDQ quarter core fine and coarse mesh runs are made so that the relative power distributions and the flux ratios near the baffle can be compared. Small adjustments to the baffle constants are made until the agreement between the models for a variety of conditions is judged acceptable. The maximum RPD error obtained for all assemblies in the quarter core model is less than 1.5%. The final set of macroscopic cross sections are tabulated in the HARMONY tablesets for use in the PDQ quarter core two zone model.

A similar procedure is used to determine the axial reflector representation. CELL2 non-fuel runs are used to determine cross sections for each of several regions represented above and below the active fuel length in the very fine mesh axial PDQ fuel model. The best mesh size (using two mesh above and two mesh below the fuel) and cross sections for use in the coarse mesh PDQ two zone model are then iteratively determined on the basis of power distribution and fuel end mesh flux ratio comparisons to the fine mesh model. The chosen cross sections are tabulated in the HARMONY tableset as a function of moderator temperature or specific volume and soluble boron concentration. The reflector mesh sizes are added to the standard 3-D quarter core PDQ geometry description.

2.3.7 FUEL TEMPERATURE DATA

Fuel temperature data is obtained using the EPRI ESCORE code. Fuel pin construction, power level, and burnup data are input to the code for determination of the best estimate volume averaged fuel pin temperature as a function of burnup and power level. The temperature data is produced separately for 15x15 and 17x17 fuel.

One set of adjustments is applied to the ESCORE fuel temperatures. ESCORE is typically run using ten concentric ring temperature zones in the fuel pin. The 10 ring temperatures are volume weighted to produce a single average temperature. However, from a neutronic standpoint, a more desirable temperature is the effective single temperature which results in the same resonance absorption as the more detailed 10 ring temperature distribution. To determine a set of correction factors, an XSDRNPM[19] 10 ring fuel pin cell model is set up with a typical temperature distribution across the fuel. NITAWL[20] resonance weighting is performed for each of the 10 fuel temperatures. A ten ring model is also run using a uniform temperature distribution across the pin. The uniform temperature which produces the same pin cell K-effective is determined by interpolation of several different uniform temperature runs. The difference between the volume weighted average temperature and the equivalent uniform temperature is the correction factor. Factors are determined as a function of power level for fresh fuel and applied to the ESCORE best estimate average temperatures to provide the effective temperature tables for the PDQ two zone thermal hydraulic input data.

2.4 PDQ QUARTER CORE CYCLE CALCULATIONS

2.4.1 INTRODUCTION

The PDQ computer code, as used in the PDQ two zone calculational model, is a two-dimensional, two-group, diffusion-depletion program which is used to calculate the neutron flux, power, and nuclide concentrations as a function of position and burnup. The PDQ computer code uses the appropriate and properly formatted cross sections along with the initial description of the reactor core (i.e., geometry and material composition description) to calculate the neutron flux distribution at spatial mesh points for two energy groups at the desired core power. The spatially dependent neutron flux is then combined with the appropriate nuclide concentrations and cross sections to obtain the spatially dependent power distribution. Once the initial spatially dependent flux and power distributions are obtained, the depletion of the nuclide concentrations is calculated.

The boundary conditions used in the quarter core solution of the two dimensiona. diffusion theory equation are:

1) Zero current for the boundaries located along the core axis

2) Zero neutron flux for the boundaries located at the reactor vessel wall and at the end of the axial reflectors.

2.4.2 DEPLETION CALCULATIONS

Each mesh block in PDQ contains a single homogenous composition. The volume-weighted nuclide concentrations for each mesh block in the core are input to PDQ for beginning of life core conditions. In addition, nuclide depletion chains which describe the production and loss

mechanisms for burnup dependent nuclides are incorporated into the HARMONY tableset. The appropriate nuclide depletion equations are assigned in PDQ to each mesh block. These equations are used by PDQ to deplete the nuclide concentrations in each mesh block based on:

1) The average fast and thermal energy group neutron fluxes calculated by PDQ for the mesh block

2) The spectrum-weighted fast and thermal group cross sections determined by PDQ from the cross section tableset assigned to the mesh block

Nuclides described by these depletion equations in the two zone model are listed in Table 2-1. Detailed chains used as the source for the PDQ chains are described in Reference 21.

TABLE 2-1

NUCLIDES INCLUDED IN THE PDQ TWO ZONE DEPLETION CHAINS

FUEL NUCLIDES:

U^{234}, U^{235}, U^{236}, U^{238},

Np^{239}

Pu^{239}, Pu^{240}, Pu^{241}, Pu^{242}

Am^{241}

FISSION PRODUCTS:

Ru^{103}

Rh^{103}, Rh^{105}

I^{135}

Xe^{135}, Xe^{135m}

Nd^{147}, Nd^{148}

Pm^{147}, Pm^{148}, Pm^{148m}, Pm^{149}

Sm^{149}

Eu^{154}, Eu^{155}

F (stable lumped fission product)

2.4.3 THERMAL-HYDRAULIC FEEDBACK PARAMETERS:

Thermal-hydraulic feedback effects are represented in the PDQ two zone model in order to more accurately calculate the power and burnup distribution. The input to PDQ required for thermal-hydraulic feedback consists of:

1) Coolant inlet enthalpy and flow rate per unit area
2) Number of fuel rods per unit area
3) System pressure
4) Difference between average fuel temperature and moderator temperature as a function of relative power density and burnup

The strategy used in the feedback calculation consists of first making an initial estimate of the fuel and moderator temperature for each coolant channel. Based on this initial estimate and the cross section tables for each fuel cell, the PDQ code calculates the two-group cross sections for each mesh block. These cross sections are used in a diffusion theory calculation of power density in each mesh block. This power density is then used in a calculation of the fuel and moderator temperature for each block. In turn, the new fuel and moderator temperatures are used to calculate new two-group cross sections for another diffusion theory power distribution calculation. This process is continued until the power density for each fuel mesh in the Nth iteration differs from the power density in the (N-1)th iteration by less than the convergence criterion.

If an equilibrium xenon calculation is desired, the xenon and iodine concentrations are determined in a similar fashion to the THF iterations.

Pairs of THF and xenon iterations (each associated with a new cross section and power distribution calculation) are performed until the convergence criteria for both have been satisfied. Because the temperature distribution resulting from the latest THF iteration changes he power distribution it also changes the next xenon distribution calculation. The same is true for the effect of the xenon iteration on the next THF calculation. Due to this interdependence, relaxation parameters have been determined which ensure proper convergence with a reasonable number of iterations.

2.5 PIN POWER RECONSTRUCTION

2.5.1 USE OF SINGLE ASSEMBLY MODELS FOR PIN-TO-BLOCK POWER RATIOS

The RECON pin power reconstruction scheme is based on the following premises:

1. The 3D PDQ two zone model accurately predicts assembly power distributions and overall power gradients across assemblies.

2. Pin power behavior can be accurately calculated for the quarter core model by applying results from single assembly calculations to the 3D mesh block powers.

Support for the first premise is found later in this report through comparison to measured power distributions and based on the results of the 2D IAEA reference problem when run with the 5x5 unequal mesh geometry.

The second premise involves judging the accuracy of a number of simplifying assumptions made for practical reasons. The method used to determine pin power behavior is to use two 2D single assembly PDQ models (one a discrete pin and the second a two zone 5x5) and calculate for each pin the pin power divided by the nearest two zone block power. The PCF code is used to process the single assembly results in this way. This in effect corrects not only for pin to pin variations unknown to the two zone model but also for intra-assembly power distribution inaccuracies in the two zone caused by homogenizing the BP over blocks rather than representing them in discrete pin locations. Inherent in this approach is the need to produce a finite database of pin information. Therefore, single assembly cases are modeled with reflective boundary conditions (an

infinite lattice of the same fuel type with no cross assembly gradient), depleted at nominal power and THF conditions (not with the actual assembly power history), and history effects which are approximated (such as BP history). However, the 3D PDQ model can calculate flux gradients, power gradients, THF effects on block power, and history effects on block power. Because the pin powers are determined relative to block powers, errors are only incurred if the pin to block relationship is in error. One way to judge the magnitude of the errors is to compare the pin power distributions of the 2D discrete quarter core PDQ model to the reconstructed pin powers from the 3D.

However, differences in predicted assembly power distributions between the discrete and two zone models, and the fact that the 3D pin powers are collapsed over the axial planes with actual 3D power distributions make the comparison difficult. In the 3D pin power axial collapse, each plane has its own burnup, pin to block, and relative power sharing characteristics. This should lead to differences between a 2D approach (volume weighted burnup and peaking characteristics) and a 3D approach (power and volume weighted burnup and peaking characteristics). Comparison of the 3D and 2D pin powers therefore must allow for these physical effects. A direct comparison of peak pin to assembly average power ratios between the models shows differences of about 1% for interior assemblies and up to about 3% for peripheral assemblies. By comparing the 2-D results to a single 3-D model plane of approximately average assembly burnup and adjusting for power gradients across each assembly caused by differences in predicted power, the differences are reduced to only a few tenths of a percent in calculated peak pin powers.

Similarly, two group instrument thimble fluxes are reconstructed by multiplying ratios derived from single assembly PDQ calculations by the PDQ 3-D model fluxes in the blocks containing the instrument thimble. The validity of this approach can be demonstrated directly by comparing measured detector reaction rates to those predicted with the reconstructed thimble fluxes. Comparison data is provided in section 3.4.

2.5.2 CORRECTING FOR FLUX GRADIENTS ACROSS A BLOCK

For the purpose of determining the effect of a flux gradient on pin powers, there are two factors to consider:

1. The impact of a fast flux gradient on power is not the same as the impact of a thermal flux gradient.

2. The spatial flux-to-power relationship changes significantly if a large burnup gradient is present across the assembly.

The first problem is addressed in RECON by multiplying the fast flux by an input flux multiplier and adding the result to the thermal flux. The resulting synthesized flux is called the relative flux. The input value of the multiplier used for RECON validation calculations was based on the typical ratio of fast to thermal fission cross sections (approximately 0.05). The second concern is taken care of by calculating the block power to relative flux ratio across the assembly. This ratio will give the impact on power of a given relative flux distribution. The pin power tilt produced across each block is consistent with the power gradient from block to block within the assembly. The validity of this

approach can be seen in the smooth variation of reconstructed pin powers across block boundaries.

SECTION 3 - RESULTS

3.1 INTRODUCTION

The purpose of this section is to present a comparison of analytical predictions from the PDQ two zone model with measured data obtained from the Surry and North Anna units. These comparisons encompass both initial and reload cycles of operation in order to demonstrate both the accuracy and flexibility of the two zone model. Virginia Power intends to optionally use the two zone model for all core calculations currently performed with one zone or discrete PDQ models. To justify this, a large number of comparisons to a variety of measured data will be presented.

3.2 ANALYTICAL CALCULATIONS

The types of calculations described in this section fall into two general groups: power distribution calculations and reactivity calculations.

Power distribution calculations include:

1. Fuel assembly average relative radial power distribution as a function of cycle depletion (RPD(X,Y)).
2. Fuel assembly average relative radial power distribution with control rods inserted at beginning of cycle.
3. Core average axial power distribution as a function of cycle depletion (P(Z)).
4. Peaking factors $F_{\Delta H}(X,Y)$ and $F_Q(X,Y,Z)$ as a function of cycle depletion.

Power distribution calculations as a function of burnup are performed to assure that the assemblywise relative powers, maximum pin powers and local heat fluxes are within acceptable limits for the entire cycle depletion. Other important uses of the 3-D model for power distributions include vessel fluence predictions, benchmarking for the 2-D two zone version, benchmarking for the 3-D FLAME model, providing a good single source model for input to the 1-D NOMAD model, evaluating the merits of shortened BP rods or axial blankets, and quantifying the 3-D effects by comparing to an otherwise identical 2-D model.

Reactivity calculations include:

1. Integral control rod bank worths
2. Differential control rod bank worths
3. Critical boron concentrations and differential boron worths
4. Isothermal temperature coefficients
5. Estimated critical control rod positions (ECP) for startup

Integral control rod bank worths are calculated by holding all reactor parameters constant except for the rod bank(s) whose worth is to be determined. For early cycles, control rod worths were measured individually using the boron dilution method. More recent cycles have used the dilution method to measure the highest worth bank (the reference bank) and then use the rod swap method of inserting a test bank and withdrawing the reference bank at a constant boron. The worth of the test bank is determined by the worth of the withdrawn portion of the reference bank. For comparison to the measured data, PDQ calculations are run in the same manner as the test is conducted. For dilution cases, an all rods

out case and a reference bank in case at the same soluble boron concentration provide the reactivity worth of the reference bank. For rod swap comparisons, one case is run with the reference and test bank in their final critical configuration, and another case is run with only the reference bank at its partially inserted final configuration. This provides the test bank worth in the presence of the partially inserted reference bank. Differential control rod worths are calculated by inserting the control rod one axial node at a time. The reactivity change for each node insertion is divided by the number of rod steps associated with each node.

Core criticality is maintained by adjusting the boron concentration as a function of burnup, power level, etc. The boron concentration at which the reactor is just critical is called the critical boron concentration. This value is calculated by first using an estimated input boron concentration to determine the core K-effective and then correcting this boron concentration to a value which corresponds to the critical condition. Sufficient detail in geometry and cross section data exists in the two zone model such that the predicted critical boron falls within an acceptable uncertainty band about the measured critical boron and it is not necessary to establish a "target" K-effective based on measured data. In most of the comparison cases, the input boron concentration corresponds to the measured critical boron concentration.

The isothermal temperature coefficient is defined as the change in core reactivity per degree change in the moderator, clad, and fuel temperature (i.e., the sum of the moderator and Doppler temperature

coefficients). The calculation of the isothermal temperature coefficient values at the hot zero power (HZP) condition is important because they can be compared to plant measurements taken during startup physics testing and therefore, can provide a basis for evaluating the accuracy of isothermal temperature coefficient, moderator temperature coefficient, and Doppler coefficient design predictions. The isothermal temperature coefficient is derived by dividing the change in core reactivity caused by a uniform temperature change by the change in temperature.

Estimated critical rod positions are required prior to restarting the unit after a period of time at zero power (such as after a trip or maintenance outage). All reactivity elements of the model are tested in this prediction because boron worth, power defect, partially inserted control rod worth, axial flux redistribution effects, transient fuel isotope and fission product worth (such as Xe135, Pm149, Np239 decay to Pu239, and others) are all involved. The xenon concentration may be higher or lower than the HFP equilibrium value depending on the power history and down time. ECP calculations were run for several cycles based on the actual history and critical startup conditions.

3.3 MEASUREMENT DATA

Measurement data is obtained from the routine physics testing conducted during the startup of each cycle of operation as well as from routine core performance monitoring conducted during the depletion of each cycle. The methods used for measuring core power distribution, burnups, control rod bank worths and critical boron concentrations are

described in Reference 12. Figure 3-1 shows the core locations of all movable detector thimbles.

Several types of comparisons can be made to determine the accuracy of the power distribution and peaking factor calculations of the PDQ 3-D two zone / RECON system. First, the predicted power in monitored assemblies is compared to the inferred measured power, which was determined using the INCORE code with 2-D PDQ discrete model input as described in Reference 12. Measured peaking factors were also obtained from PDQ discrete / INCORE results for monitored assemblies. For $F_{\Delta H}$ comparisons, the peak pin power for each monitored assembly from INCORE is compared to the $F_{\Delta H}$ from RECON. For $F_Q(X,Y,Z)$, the peak local pin power at each axial plane for monitored assemblies is read from INCORE results and is output for axial planes between spacer grids. Because the grids depress power locally, power production peaks between the grids. The two zone model does not explicitly represent the grids and tends to underpredict power most versus measurement between grids. The RECON code provides $F_Q(X,Y,Z)$ interpolated using a three point Lagrangian scheme to the same axial location as the INCORE data for each monitored assembly, resulting in five points of comparison for each 15x15 assembly and six for each 17x17 assembly. Table 3-1 gives the axial location of the 15x15 and 17x17 INCORE points used for $F_Q(X,Y,Z)$ comparisons along with the three nearest PDQ two zone planes for each. For safety analysis, only powers greater than the core average are of interest. Therefore, only those observations which had measured and predicted values greater than 1.0 are used.

Note that the comparisons described above (assembly average power and peaking factors) use results from the PDQ discrete 2-D model based INCORE measurements. Because RECON can generate INCORE input, statistics can also be determined relative to INCORE measurements based on the PDQ two zone 3-D / RECON system. By calculating the measured versus predicted statistics in both ways, both the PDQ 3-D / RECON peaking factors and INCORE input generation capability can be verified. The INCORE input capability can also be verified using the average (average of the absolute percent differences) percent difference between predicted and measured thimble reaction rates. This quantity is edited by INCORE and is the most direct comparison of measurement and prediction.

Control rod bank worth determination with the rod swap method is described in Reference 22. Figure 3-2 shows the core location of all control rod banks. Isothermal temperature coefficients are measured during the startup of each cycle by monitoring with the reactivity computer the reactivity changes associated with a uniform heatup or cooldown rate. The test is performed at a very low power to assure that fuel and moderator temperatures are consistent. Reactivity is determined using the reactivity computer and is plotted against RCS temperature on an x-y recorder. The temperature coefficient is then determined from the slope of the plotted line.

TABLE 3-1
AXIAL GEOMETRY FOR POWER DISTRIBUTION COMPARISONS

NORTH ANNA UNITS:		SURRY UNITS:	
% Core Height	Description	% Core Height	Description
103.5	Grid 1	104.0	Grid 1
89.2	Grid 2	90.8	Grid 2
89.1	PDQ Plane 20	89.1	PDQ Plane 20
84.4	PDQ Plane 19	84.4	PDQ Plane 19
81.7	INCORE Node 12	83.3	INCORE Node 11
78.1	PDQ Plane 18	78.1	PDQ Plane 18
74.9	Grid 3	72.6	Grid 3
71.9	PDQ Plane 17	71.9	PDQ Plane 17
68.3	INCORE Node 20	65.6	PDQ Plane 16
65.6	PDQ Plane 16	63.3	INCORE Node 23
59.4	PDQ Plane 15	59.4	PDQ Plane 15
60.6	Grid 4	54.4	Grid 4
59.4	PDQ Plane 15	53.1	PDQ Plane 14
53.3	INCORE Node 29	46.9	PDQ Plane 13
53.1	PDQ Plane 14	45.0	INCORE Node 34
46.9	PDQ Plane 13	40.6	PDQ Plane 12
46.4	Grid 5	36.2	Grid 5
46.9	PDQ Plane 13	34.4	PDQ Plane 11
40.6	PDQ Plane 12	28.1	PDQ Plane 10
38.3	INCORE Node 38	26.7	INCORE Node 45
34.4	PDQ Plane 11	21.9	PDQ Plane 9
32.1	Grid 6	18.0	Grid 6
34.4	PDQ Plane 11	15.6	PDQ Plane 8
28.1	PDQ Plane 10	13.3	INCORE Node 53
25.0	INCORE Node 46	10.9	PDQ Plane 7
21.9	PDQ Plane 9	7.8	PDQ Plane 6
17.8	Grid 7	1.3	Grid 7
21.9	PDQ Plane 9		
15.6	PDQ Plane 8		
15.0	INCORE Node 52		
10.9	PDQ Plane 7		
0.8	Grid 8		

FIGURE 3-1
FULL CORE MONITORED ASSEMBLY LOCATIONS

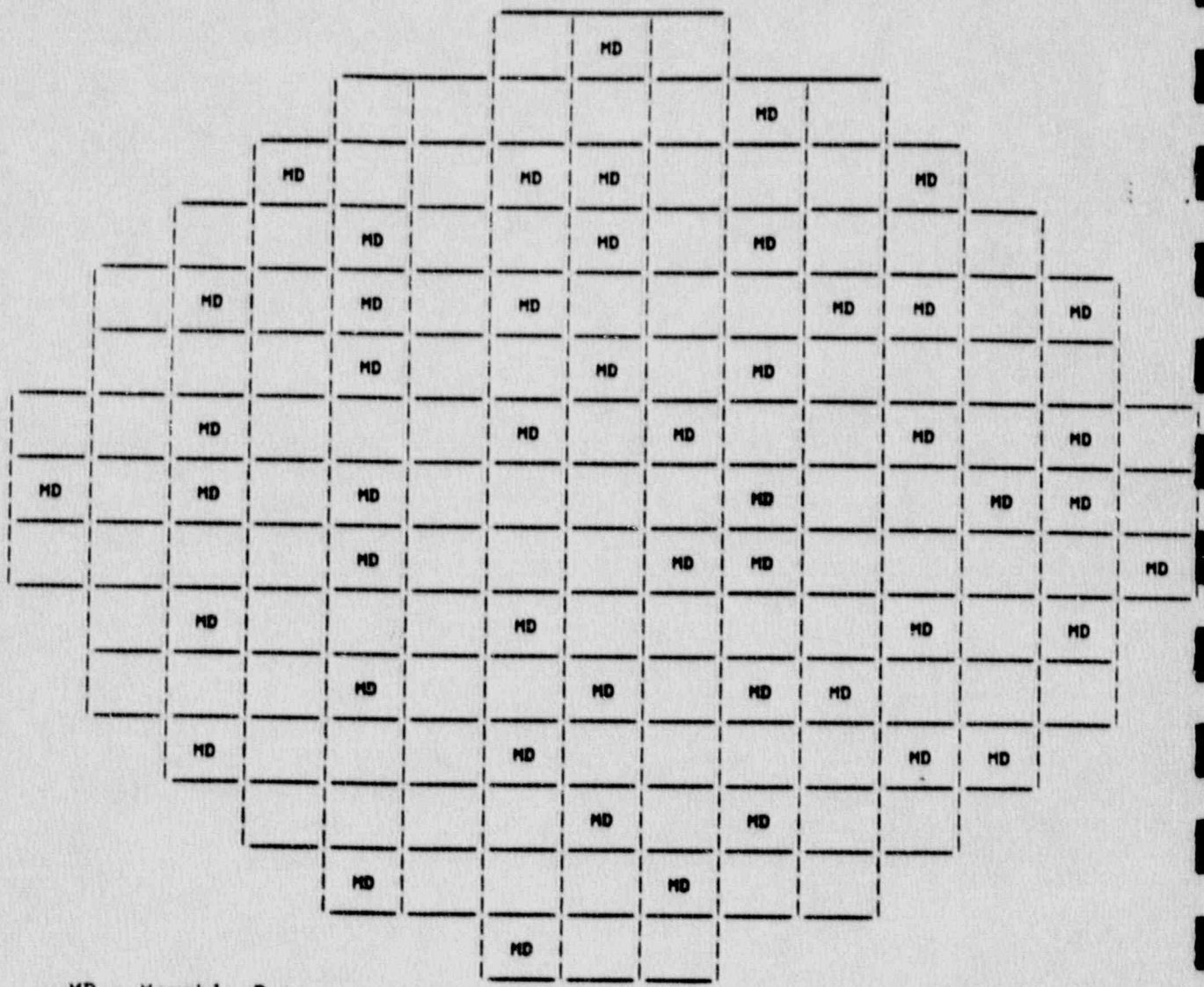

MD - Movable Detector

FIGURE 3-2
FULL CORE CONTROL ROD BANK POSITIONS

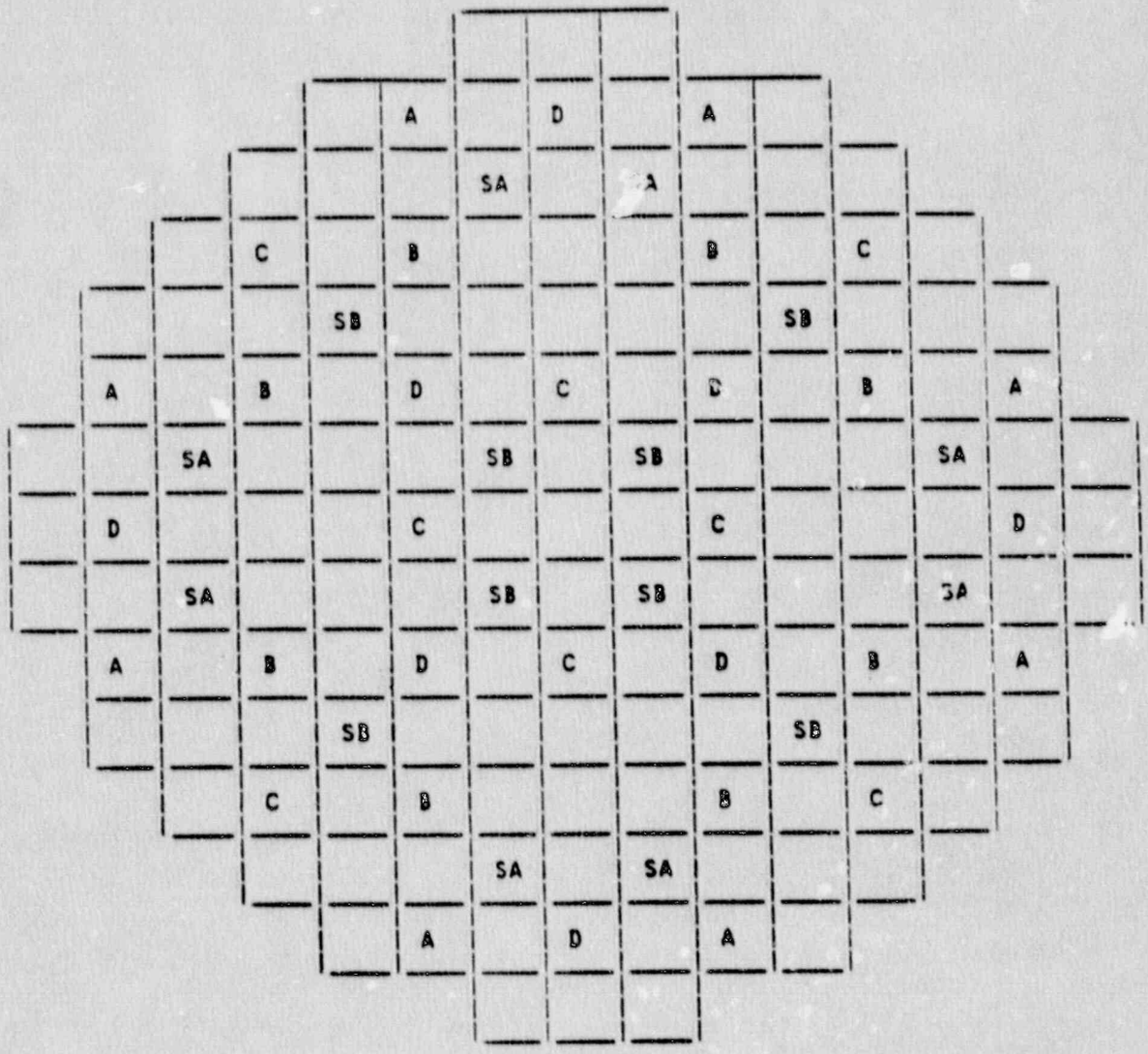

Function	Number of Clusters
Control Bank D	8
Control Bank C	8
Control Bank B	8
Control Bank A	8
Shutdown Bank SB	8
Shutdown Bank SA	8

3.4 RESULTS

Table 3-2 lists currently approved nuclear reliability factors (NRF) by which the indicated two zone model results can be judged. More information about the basis for the existing factors may be found in Reference 23. Statistical results of the two zone model power distribution predictions compared to the measurements obtained from the Surry and North Anna Power Stations are presented in Table 3-3. Statistics for reactivity parameter comparisons are given in Tables 3-5 and 3-6. The basis for the Table 3-2 two zone model nuclear uncertainty factors (NUF) is discussed below.

3.4.1 POWER DISTRIBUTIONS

Figures 3-3 through 3-104 show the predicted versus measured core average relative axial power as a function of core height (P(Z)). Data for both HZP and HFP at various core burnups is presented for each cycle. Measured values were taken from INCORE runs with inputs generated with the PDQ discrete model. Data for all cycles has been included to demonstrate the ability of the two zone model to predict both the changing HFP axial power shapes of fresh and reload cores as well as the strongly top peaked reload core HZP distributions.

Figures 3-105 through 3-192 are comparisons of measured and predicted radial power distributions. Only relative powers in monitored core locations (as listed in INCORE runs) are included in the measured data. Predictions for each full core location are symmetrically unfolded

from the quarter core PDQ model. The comparisons include HFP (> 90% power) and HZP (< 6% power) maps as well as five rodded HZP maps for further verification of the geometry and control rod model performance. For the four rodded maps for which a corresponding unrodded map exists (N1C3, S2C4, S1C5, and S2C5), RMS differences in power in the ARO and rodded maps are very similar. The very low assembly powers in the rodded assemblies are also well predicted.

The root mean square of the power distribution differences for rodded HZP maps (Figures 3-191, 3-193, 3-194, and 3-195) compares favorably to the root mean square of the differences in the corresponding unrodded maps (Figures 3-108, 3-144, 3-171, and 3-174, respectively). In the rodded assemblies, differences between measured and predicted powers are typical of all assemblies in the map, indicating no loss of accuracy in power distribution due to control rod insertion. Differences are generally smaller for the HFP maps. This is due in part to core power tilts which are larger at low power and possibly to gamma flux contributing to the measured neutron flux in some very low power cases.

Table 3-3 presents RPD, $F_{\Delta H}$ and F_Q statistics determined by comparison to PDQ discrete based INCORE measurements and to PDQ 3-D / RECON based INCORE measurements. Only monitored locations with measured and predicted values greater than the core average relative power of 1.0 were retained. Included in the table are the 95%/95% one sided upper tolerance limits (uncertainty factors) based on the mix of HZP, part power and HFP maps indicated.

The PDQ 3-D / RECON based flux map database used is listed in Table 3-4. For a common subset of 2-D discrete and RECON based INCORE maps consisting of 7 unrodded HZP and 41 unrodded HFP flux maps, the RECON based maps show the smallest average of the instrument thimble reaction rates. This indicates that the PDQ 3-D / RECON system provides somewhat better power distribution and/or thimble flux predictions than the 2-D discrete model. Use of the 3-D PDQ / RECON system for INCORE mapping data also appears to be conservative in that it results in a slightly (about 0.5%) more negative mean of the measured peaking factor differences. Because the predictions for these two cases are the same, this means that the measured peaking factors are slightly larger than those measured with the PDQ 2-D discrete based INCORE. For this reason, the reliability factors listed in Table 3-2 have been chosen from the RECON based INCORE data consisting of the full set of maps indicated in Table 3-4. The assembly $F_{\Delta H}$ 95%/95% one sided uncertainty factor of 1.034 for North Anna cycles and 1.031 for Surry cycles compares well with the existing nuclear reliability factor of 1.05. Only monitored assemblies with measured and predicted $F_{\Delta H} > 1.0$ were used. Assembly $F_Q(Z)$ comparisons from the same maps at selected axial locations between spacer grids for F_Q values > 1.0 yield uncertainty factors of 1.067 for North Anna and 1.072 for Surry. These factors compare well with the existing nuclear reliability factor of 1.075. Because of the margin to the existing reliability factors and because of the apparent conservatism in the peaking factors measured using the PDQ 3-D / RECON based predictions, no additional conservatism is considered necessary to account for possible uncertainty caused by the pin power reconstruction technique.

3.4.2 REACTIVITY PARAMETERS

Figure 3-193 is a plot of the difference between the predicted zero power critical boron concentration and the measured critical boron concentration for startups. Data includes both BOC startups and restarts in mid-cycle following a trip or maintenance outage. There is a tendency to overpredict the critical boron at hot zero power by an average of about 7 ppm. The standard deviation is 20 ppm and all but one of the predictions is within 40 ppm of the measured critical boron concentration. The administrative startup acceptance criterion is 50 ppm.

Figure 3-194 shows the difference between measured and predicted control rod bank worths plotted versus the predicted rod worth. The data includes all BOC measurements (boron dilution and rod swap method). All differences are well w thin the indicated startup criteria (± 15% or 100 pcm for banks worth 667 pcm or less). All but 5 of the 157 predicted points fall within 10% of the measured values. Of the 5 predicted points which show errors greater than 10%, three are very low worth banks averaging less than one-third of the average bank worth. The remaining two have differences of 10.3% and 10.8%. The statistical uncertainty factor for the 157 rod worths of 1.10 matches the current nuclear reliability factor. Interestingly, rod worths measured by boron dilution exhibited no significant bias, but worths measured by rod swap indicated a 1.8% average overprediction by the two zone model. Figures 3-195 through 3-224 present a representative set of differential and integral rod worth comparisons as a function of control rod bank insertion. As shown in the plots, the two zone axial mesh structure is fine enough to

obtain good worth versus insertion shapes compared to those measured. Localized dips in the measured differential rod worth are caused by the presence of fuel rod spacer grids. Grids were not explicitly modeled in the two zone due to the coarseness of the axial mesh.

Figure 3-225 shows the predicted differential boron worth at BOC plotted versus the corresponding measured value. All points fall well within the ± 10% startup acceptance criterion. There is no significant bias. The existing nuclear reliability factor cannot be met by the data as measured. However, comparison of dilution method control rod worth errors and differential boron worth errors reveals a strong linkage between these two independent parameters. The common link between measured rod worths and boron worths is the reactivity computer. Because the boron worth is calculated based on the change in boron needed to offset the reactivity inserted by one or more control rod banks, if the reactivity computer introduces a bias on the measured control rod worth, the same bias will be evident in the boron worth. This theory has been tested successfully by finding the coefficients of the best fit line described by the following equation:

$$\text{DBW ERROR (\%)} = A + B * \text{ROD WORTH ERROR (\%)}$$

The 95%/95% confidence interval for the slope (B) includes the range 0.42 to 0.80, indicating a statistically valid correlation (if the slope range includes 0, no correlation is proven). To quantify the degree of error introduced to the rod worth and boron worth statistics by the reactivity computer, the following assumptions are made:

1. Predicted control rod worth and boron worth differences from true core values are independent of each other.

2. The reactivity computer introduces a bias on the standard deviation of each set of differences by introducing a random bias (cycle to cycle) to the measured values.

If the two sets of observed percent differences (one set for rod worths and one set for boron worths) are truly independent, the standard deviation of the set of data obtained by adding the rod worth and boron worth differences together will be the same as that for the set of data obtained by subtracting the differences. Because the boron worth differences and rod worth differences are not independent, subtracting tends to cancel out the reactivity computer bias and adding tends to double it. Table 3-5 gives the statistics obtained for the dilution method rod worths differences, the associated boron worth differences, the added difference data, and the subtracted difference data. For cycles where more than one rod bank was used to determine the boron worth, the boron worth difference has been associated with each individual bank worth difference. The standard deviation of the subtracted data is the smallest (4.0%) and represents the combined root mean square of the individual true rod worth and boron worth standard deviations. The added difference data shows a standard deviation of 8.6% which suggests that the standard deviation bias introduced through use of the reactivity computer is on the order of 2%. This is verified by calculating the root mean square of the rod worth real standard deviation (observed minus 2%) and the boron worth real standard deviation. The calculated value of 3.8% is close to that calculated for the subtracted difference data. Adding two times the reactivity computer bias to this gives 7.8% which is reasonably close to the added difference data standard deviation of 8.6%. The presence of a

reactivity computer bias also explains why the rod swap control rod data exhibits a lower standard deviation (4.2%) than the dilution method control rod data (4.8%) even though the dilution method rod banks are the highest worth banks (with lower inherent test uncertainty). A portion of the reactivity computer bias is present in the rod swap data as well because it is used to obtain the reference bank worth against which the other banks are measured.

Based on this analysis, both the integral rod worth and the differential boron worth predictive uncertainties are overstated. If there were an error of 5% in the total boron worth at beginning of cycle (when the average boron concentration is about 1400 ppm), a critical boron error of 70 ppm would be expected unless offset or added to by some other factor. In 30 cycles, the largest BOC HZP critical boron difference is 58 ppm (4.4%). Using a 2% estimate for the bias in the Table 3-5 rod worth and boron worth statistics, the integral control rod worth uncertainty can be reduced to 1.057 and an uncertainty factor of 1.05 for boron worth error is reasonable based on the estimated standard deviation of 2.4%. The boron worth sample is small (31 points) and is non-normal so the statistical uncertainty factor is not easily calculated if the reactivity computer bias is to be accounted for. However, the magnitude of the standard deviation, the observed maximum critical boron difference, and the 20 ppm (1.4%) standard deviation of the BOC HZP critical boron differences all support the 1.05 estimated uncertainty factor.

Figures 3-227 through 3-254 show the predicted versus measured boron letdown curves based on HFP all rods out (ARO) operation. Both measured

and predicted data have been modified to remove the effects of off-nominal operation (operation at reduced power, reduced temperature, or with control rods partially inserted). Data for all cycles has been included to demonstrate the flexibility of the model to handle high and low leakage loadings, large or small numbers of fresh or depleted burnable poison rods, and a wide range of fuel enrichments without re-normalization of the model to measured data. Significant scatter in the measured data makes quantification of differences difficult. Letdown curve slope, shape, and overall agreement indicate that the 50 ppm reliability factor is appropriate for HFP predictions as well. Differences are typically limited to about 30 ppm which is consistent with the HZP startup data.

Figure 3-255 presents a comparison of predicted versus measured isothermal temperature coefficients for both rodded and unrodded configurations at BOC. All points are within the ± 3 pcm/°F startup criteria. A bias of approximately - 0.8 pcm/°F in the predicted data can be seen in the plot.

TABLE 3-2

SUMMARY OF NUCLEAR RELIABILITY FACTORS

PARAMETER	VEP-FRD-45A NRF	PDQ TWO ZONE NUF*
Individual Integral Bank Worth	x 1.10	x 1.06
Cumulative Integral Bank Worth	x 1.10	x 1.06
Differential Bank Worth Worth	2 pcm/step	< 2 pcm/step
Critical Boron Concentration	50 ppm	50 ppm
Differential Boron Worth	x 1.05	x 1.05
Moderator Temperature Coefficient	3 pcm/°F	3 pcm/°F
$F_{\Delta H}$	x 1.05	x 1.034 North Anna x 1.031 Surry
F_Q	x 1.075	x 1.067 North Anna x 1.072 Surry

* Nuclear uncertainty factor -- defined as the 95%/95% one sided upper tolerance limit.

TABLE 3-3

POWER DISTRIBUTION STATISTICS

NORTH ANNA UNIT DIFFERENCE FROM MEASURED (%)

DESCRIPTION	NUMBER OF PTS.	MEAN	STANDARD DEVIATION	TOTAL UNC. FACTOR	MAX.	MIN.
(1) HZP & HFP RPD > 1.0	540	0.49%	1.9 %	1.028	8.7	-12.3
HZP & HFP $F_{\Delta H}$ > 1.0	696	0.54%	2.1 %	1.031	9.4	-12.1
HZP & HFP F_Q > 1.0	4205	-1.67%	2.8 %	1.062	9.2	-14.1
(2) HZP & HFP RPD > 1.0	550	0.11%	1.6 %	1.025	7.7	-8.8
HZP & HFP $F_{\Delta H}$ > 1.0	701	0.03%	1.8 %	1.029	7.8	-9.6
HZP & HFP F_Q > 1.0	4205	-2.24%	2.6 %	1.065	8.1	-14.1
(3) ALL RPD > 1.0	1175	0.23%	1.8 %	1.028	7.8	-8.8
ALL $F_{\Delta H}$ > 1.0	1479	0.12%	1.9 %	1.034	8.8	-9.6
ALL F_Q > 1.0	9246	-2.16%	2.8 %	1.067	11.2	-14.1

(1) Based on 4 HZP and 17 HFP flux maps (PDQ 2-D discrete based INCORE)
(2) Based on 4 HZP and 17 HFP flux maps (PDQ 3-D / RECON based INCORE)
(3) Based on 6 HZP, 2 part power, and 32 HFP flux maps (PDQ 3-D / RECON based INCORE)

TABLE 3-3 (Continued)

SURRY UNIT DIFFERENCE FROM MEASURED (%)

DESCRIPTION	NUMBER OF PTS.	MEAN	STANDARD DEVIATION	TOTAL UNC. FACTOR	MAX.	MIN.
(4) HZP & HFP RPD > 1.0	775	0.50%	1.9 %	1.030	6.7	-11.1
HZP & HFP $F_{\Delta H}$ > 1.0	1018	0.51%	2.0 %	1.031	10.9	-10.9
HZP & HFP F_Q > 1.0	5080	-2.09%	3.1 %	1.070	13.6	-13.0
(5) HZP & HFP RPD > 1.0	773	0.09%	1.7 %	1.028	5.9	-10.8
HZP & HFP $F_{\Delta H}$ > 1.0	1016	-0.02%	1.7 %	1.031	7.2	-10.7
HZP & HFP F_Q > 1.0	5044	-2.61%	2.8 %	1.070	12.6	-13.0
(6) ALL RPD > 1.0	1447	0.10%	1.7 %	1.027	5.9	-10.8
ALL $F_{\Delta H}$ > 1.0	1878	-0.02%	1.7 %	1.031	7.2	-10.7
ALL F_Q > 1.0	9372	-2.57%	3.0 %	1.072	12.6	-16.2

(4) Based on 4 HZP and 25 HFP flux maps (PDQ 2-D discrete based INCORE)
(5) Based on 4 HZP and 25 HFP flux maps (PDQ 3-D / RECON based INCORE)
(6) Based on 8 HZP, 2 part power, and 44 HFP flux maps (PDQ 3-D / RECON based INCORE)

TABLE 3-4

FLUX MAP DATABASE LISTING

Cycle	Map	Power (%)	D-Bank	Burnup (MWD/T)	Measured A.O.(%)	PDQ A.O.(%)	
N1C1	01A	HZP	228	0	+0.6	-0.2	*
N1C1	25A	96	216	300	-8.5	-9.8	
N1C1	52A	96	218	8405	-3.0	-1.5	
N1C1	68A	100	220	14070	-1.9	-1.7	
N1C2	07A	30	165	28	+0.8	-2.7	
N1C2	15A	99	228	300	+0.1	-0.8	*
N1C2	26A	100	222	3277	-1.5	-2.5	
N1C2	44A	100	210	8109	-4.1	-3.0	
N1C3	02A	HZP	220	0	+17.0	+17.6	
N1C3	14A	100	224	486	-7.9	-7.3	
N1C3	33A	100	213	6883	-5.[illegible]	-2.2	
N1C3	84A	100	216	11434	-3.9	-1.7	
N1C4	02A	29	180	13	+4.4	+6.4	
N1C4	07A	100	221	305	-1.2	-0.5	
N1C4	17A	100	216	5520	-3.1	-1.9	
N1C4	25A	100	226	10170	-4.0	-2.9	*
N1C5	01A	HZP	228	0	+26.0	+25.6	*
N1C5	15A	100	224	225	-6.2	-5.6	*
N1C5	23A	100	224	6831	-4.0	-2.1	*
N1C5	34A	100	228	12983	-3.2	-1.8	*
N1C6	09A	100	219	378	-3.0	-2.5	*
N1C6	17A	100	228	6690	-4.0	-2.6	*
N1C6	29A	100	228	14340	-3.9	-2.8	*
N2C2	02A	HZP	228	0	+57.5	+59.3	*
N2C2	20A	100	224	3225	-0.6	-2.2	*
N2C2	27A	100	218	6750	-4.0	-3.0	*
N2C3	01A	HZP	211	0	+23.0	+21.4	
N2C3	14A	100	228	1566	-4.6	-4.9	*
N2C3	25A	100	217	7647	-4.0	-2.8	
N2C3	37A	100	221	13040	-2.7	-2.3	
N2C4	01A	HZP	211	0	+31.6	+34.5	
N2C4	08A	100	228	1060	-2.4	-2.3	
N2C4	22A	100	220	6610	-3.8	-2.4	*
N2C4	28A	100	228	11267	-3.2	-2.0	*
N2C5	08A	100	228	250	-1.7	-2.3	*
N2C5	19A	100	228	6075	-4.2	-2.9	*
N2C5	29A	100	228	13671	-4.5	-2.8	*
N2C6	04A	100	228	222	-2.6	-4.0	
N2C6	13A	100	228	4930	-3.9	-2.6	
N2C6	22A	100	228	13175	-5.2	-3.2	

* SUBSET FOR DISCRETE 2-D PDQ INCORE COMPARISON

TABLE 3-4 (Continued)

Cycle	Map	Power (%)	D-Bank	Burnup (MWD/T)	Measured A.O.(%)	PDQ A.O.(%)	
S1C2	12A	98	222	1085	+1.6	-0.4	*
S1C2	17A	99	223	4065	-1.8	-2.4	*
S1C3	20C	100	225	7175	-1.8	-2.5	*
S1C4	02A	HZP	220	0	+24.0	+19.9	
S1C4	10A	100	215	930	-2.1	-4.3	
S1C4	17A	100	214	4444	-3.4	-2.0	
S1C4	23A	100	206	8400	-4.2	-2.7	
S1C5	01A	HZP	218	0	+27.4	+24.8	
S1C5	11A	100	220	1300	-1.2	-3.4	
S1C5	23A	100	224	7411	-3.2	-2.2	*
S1C5	32A	100	216	11580	-3.5	-1.9	
S1C6	01A	HZP	201	0	+21.4	+19.6	
S1C6	13A	100	217	973	-1.9	-2.2	*
S1C6	56A	100	228	7518	-2.5	-1.5	*
S1C6	70A	100	222	13207	-3.0	-1.9	*
S1C7	02A	HZP	221	0	+40.3	+40.0	*
S1C7	03A	51	180	6	-0.1	-2.8	
S1C7	08A	100	223	807	-0.2	-1.3	*
S1C7	14A	100	228	4329	-2.5	-1.7	*
S1C7	22A	100	226	7630	-2.9	-2.1	*
S1C8	08A	100	228	925	-4.0	-4.2	*
S1C8	37A	100	227	8081	-3.3	-2.3	*
S1C9	06A	100	220	240	-0.4	-0.4	*
S1C9	28A	100	222	7295	-2.5	-0.8	*
S1C9	40A	100	217	14606	-4.0	-3.0	*
S1CA	06A	100	225	238	-0.2	-1.8	
S1CA	22A	100	225	5254	-1.6	-1.8	

* SUBSET FOR DISCRETE 2-D PDQ INCORE COMPARISON

TABLE 3-4 (Continued)

Cycle	Map	Power (%)	D-Bank	Burnup (MWD/T)	Measured A.O.(%)	PDQ A.O.(%)	
S2C2	01A	HZP	199	0	+20.3	+21.8	
S2C2	07A	100	210	730	+2.5	+1.1	
S2C3	08A	100	219	137	+0.1	-0.3	
S2C3	13C	100	221	3127	-1.0	-1.6	*
S2C4	01A	HZP	228	0	+21.9	+21.6	*
S2C4	10A	100	223	1186	-2.9	-3.7	*
S2C4	23A	100	201	8250	-4.5	-6.1	
S2C4	34A	100	226	11934	-0.8	+1.5	
S2C5	01A	HZP	216	0	+35.9	+35.9	
S2C5	17A	100	217	1690	+1.0	+0.9	
S2C5	23A	100	219	5619	-0.5	-1.5	
S2C5	35A	100	220	11320	-4.1	-3.6	
S2C6	01A	HZP	223	0	+24.8	+25.0	*
S2C6	07A	100	228	1116	-2.2	-3.7	*
S2C6	18A	100	228	7390	-3.0	-1.3	*
S2C6	29A	100	227	13900	-2.7	-1.4	*
S2C7	02A	47	178	10	+0.2	-0.4	
S2C7	13A	99	226	1647	-1.2	-1.2	*
S2C7	19A	100	226	5781	-2.4	-1.4	*
S2C7	38A	100	223	13122	-2.5	-2.0	*
S2C8	01A	HZP	228	0	+29.5	+30.9	*
S2C8	13A	100	211	2423	-2.7	-1.2	
S2C8	23A	100	218	6525	-2.2	-1.1	
S2C8	34A	100	221	12391	-2.7	-1.2	
S2C9	09A	100	208	1072	+2.2	+0.6	*
S2C9	17A	100	223	6887	-1.5	-1.7	*
S2C9	27A	100	224	13553	-3.7	-2.5	

* SUBSET FOR DISCRETE 2-D PDQ INCORE COMPARISON

TABLE 3-5

REACTIVITY PARAMETER STATISTICS

CRITICAL BORON CONCENTRATIONS
DIFFERENCE FROM CRITICAL (ppm)

DESCRIPTION	NUMBER OF POINTS	MEAN	STANDARD DEVIATION	TOTAL UNC. FACTOR	MAX.	MIN.
HZP	54	6.3	20. ppm	47.4 ppm	57.9	-30.3

BORON WORTHS
DIFFERENCE FROM MEASURED (%)

DESCRIPTION	NUMBER OF POINTS	MEAN	STANDARD DEVIATION	TOTAL UNC. FACTOR	MAX.	MIN.
HZP	30	-0.3	4.4	----	7.4	-6.1
* ADJUSTED	30	-0.3	2.4	< 1.05	----	----

ISOTHERMAL TEMPERATURE COEFFICIENTS
DIFFERENCE FROM MEASURED (pcm/°F)

DESCRIPTION	NUMBER OF POINTS	MEAN	STANDARD DEVIATION	TOTAL UNC. FACTOR	MAX.	MIN.
HZP	57	-0.8	0.96	2.9 pcm/F	2.6	-2.9

CONTROL ROD BANK WORTHS
DIFFERENCE FROM MEASURED (%)

DESCRIPTION	NUMBER OF POINTS	MEAN	STANDARD DEVIATION	TOTAL UNC. FACTOR	MAX.	MIN.
BORON DILUTION	62	0.2%	4.8 %	1.099	10.7	-9.9
ROD SWAP	95	1.8%	4.2 %	1.099	11.5	-11.3
COMBINED	157	1.0%	4.5 %	1.095	11.5	-11.3
* ADJUSTED	157	1.0%	2.5 %	1.057	----	----

* See Table 3-6

TABLE 3-6

REACTIVITY COMPUTER INDUCED BIAS ERROR ESTIMATE

DATA ANALYZED	MEAN	STANDARD DEVIATION	DATA POINTS	COMMENTS
BORON WORTH % DIFFERENCE (RAW DATA)	-0.1%	4.6%	62	31 actual points repeated for cycles which used multiple bank dilutions.
CONTROL ROD % DIFFERENCE (RAW DILUTION METHOD DATA)	-0.2%	4.8%	62	Early cycles used dilution method for more than one rod bank.
BORON WORTH % DIFFERENCE PLUS CONTROL ROD % DIFFERENCE	-0.3%	8.6%	62	Represents combined std. dev. impacts of rod worth error, boron worth error and double reactivity computer bias.
BORON WORTH % DIFFERENCE MINUS CONTRCL ROD % DIFFERENCE	0.0%	4.0%	62	Represents combined std. dev. impacts of rod worth error and boron worth error. Reactivity computer bias cancelled out.

Estimated standard deviation bias due to use of the reactivity computer: 2%

Estimated standard deviation of boron worth data excluding bias: 2.4%

Estimated standard deviation of integral control rod worth data excluding bias: 2.5%

NORTH ANNA P(Z) COMPARISON

TWO ZONE PDQ3D RESULTS AND INCORE DATA
UNIT=NICI BURNUP=0

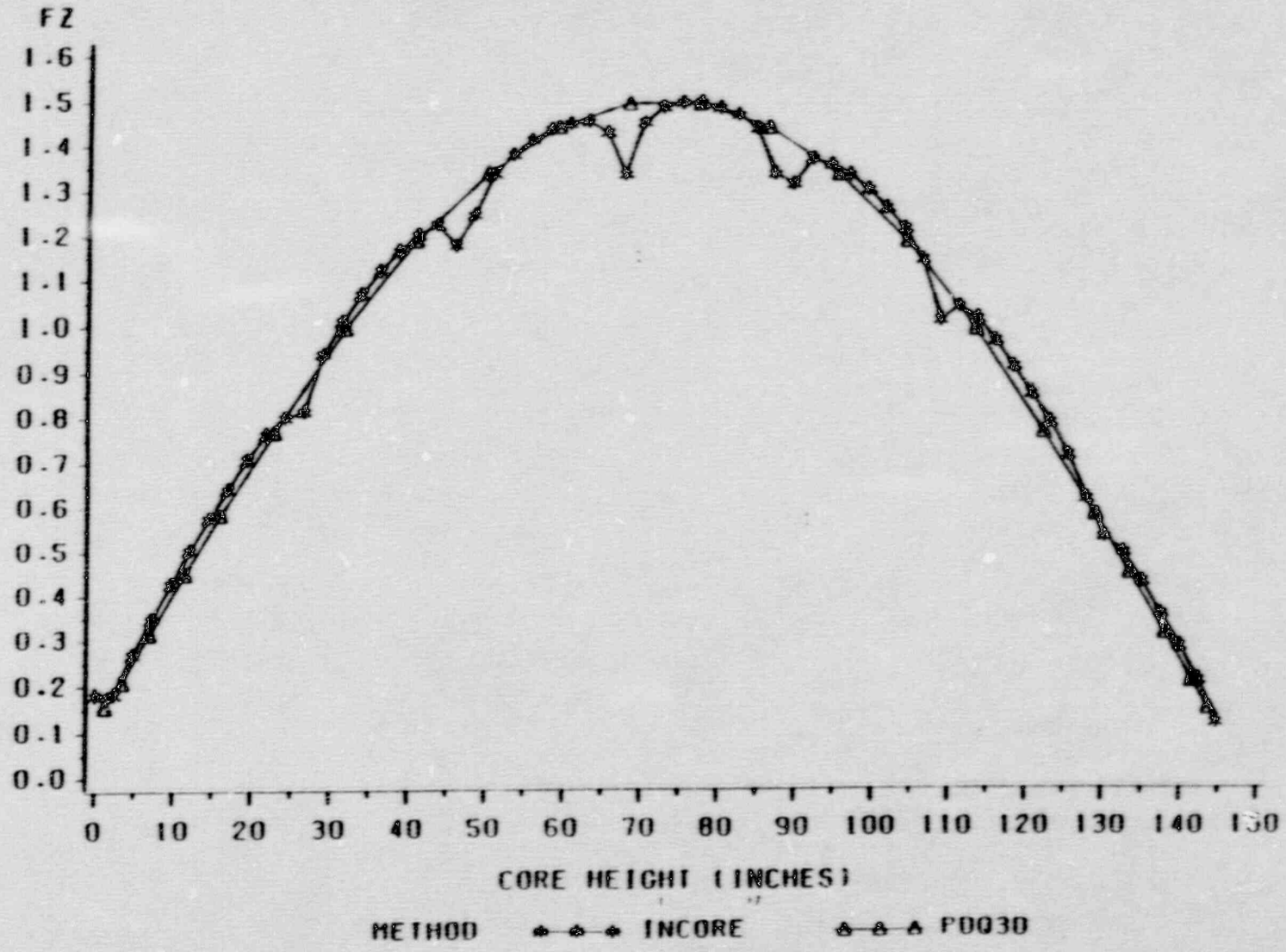

FIGURE 3-3

NORTH ANNA P(Z) COMPARISON

TWO ZONE PD03D RESULTS AND INCORE DATA
UNIT=N1C1 BURNUP=881

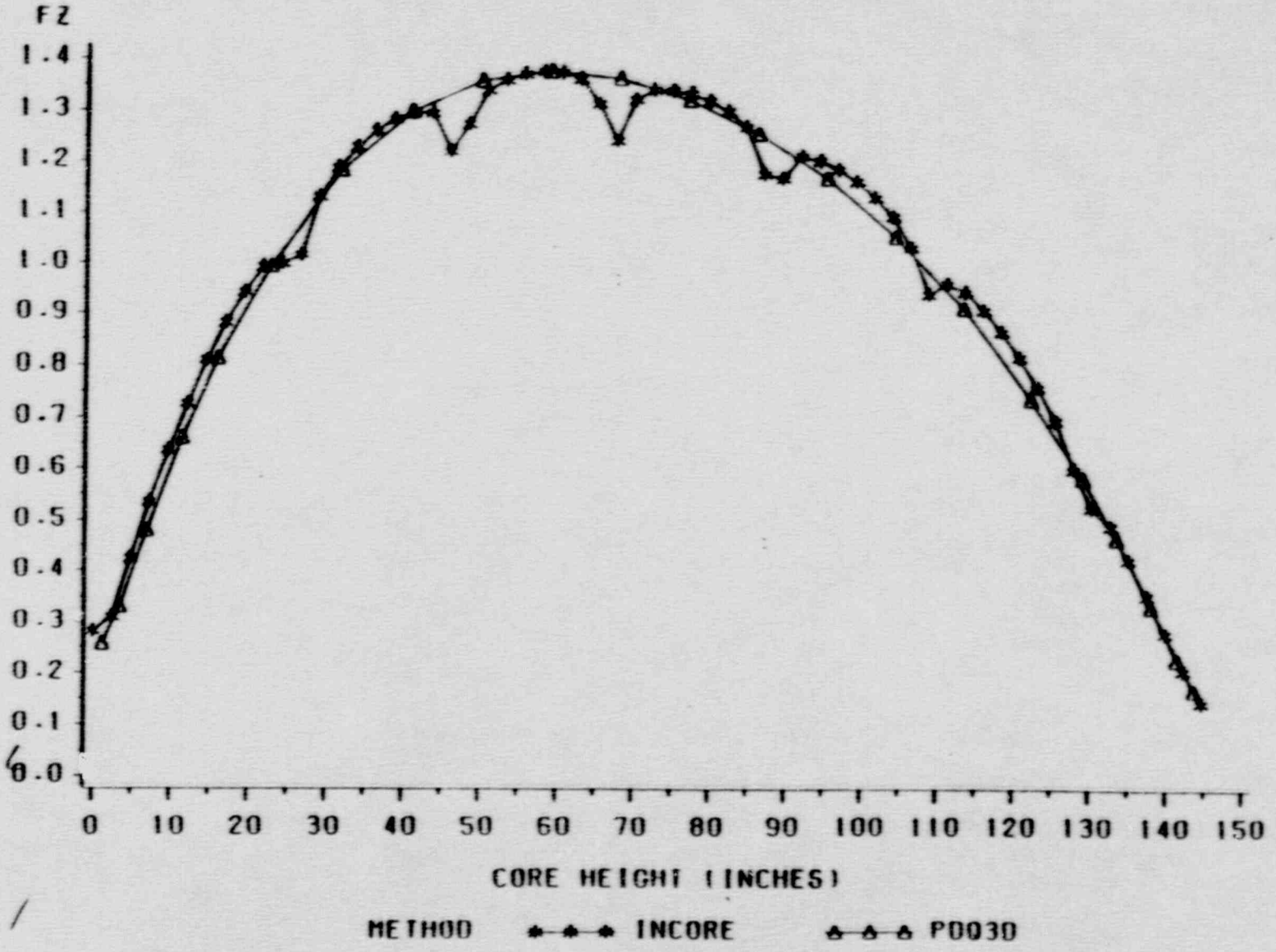

FIGURE 3-4

NORTH ANNA P(Z) COMPARISON

TWO ZONE PDQ3D RESULTS AND INCORE DATA
UNIT=NIC1 BURNUP=8405

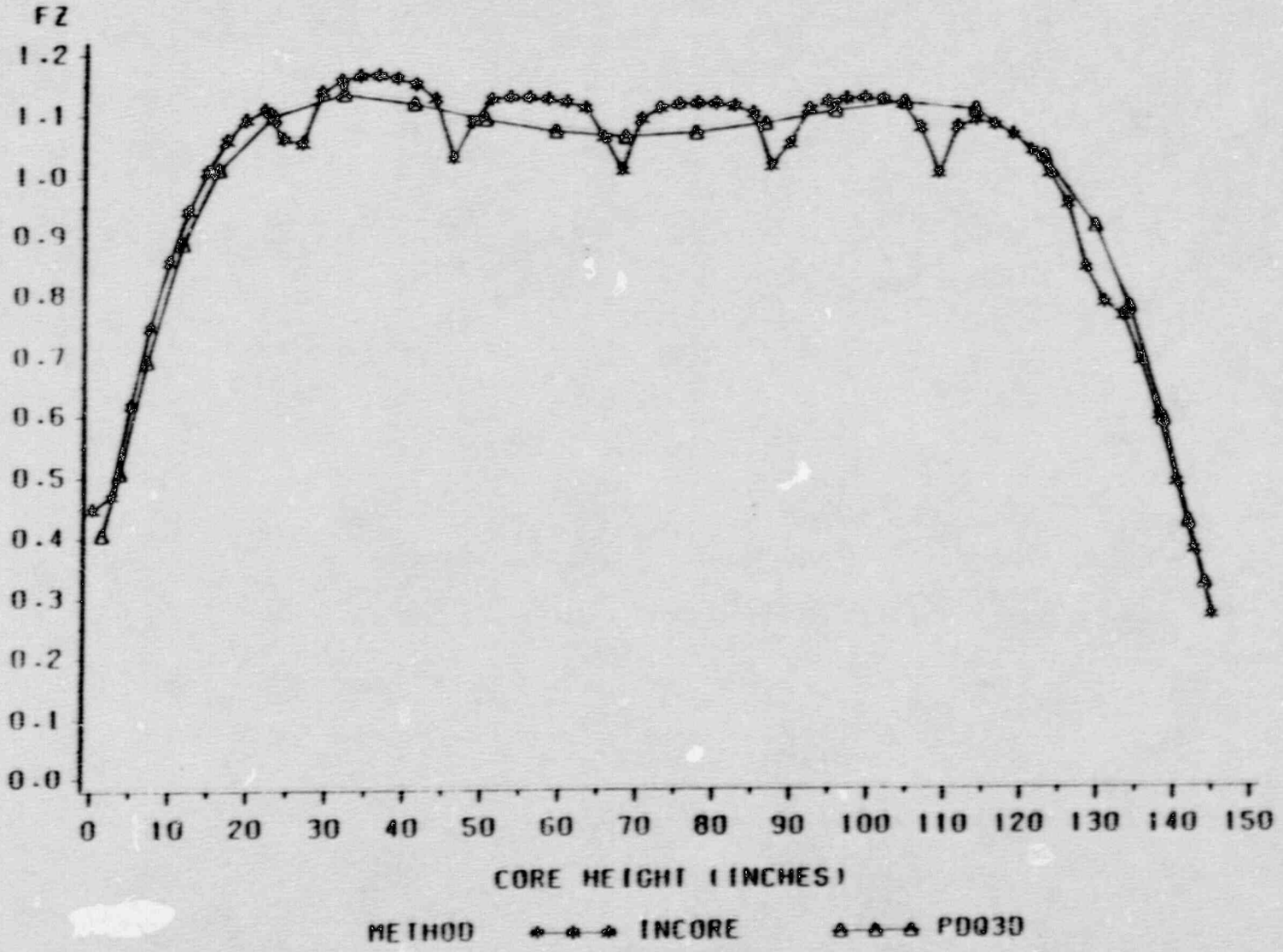

FIGURE 3-5

NORTH ANNA P(Z) COMPARISON

TWO ZONE PDQ3D RESULTS AND INCORE DATA
UNIT=NIC1 BURNUP=14070

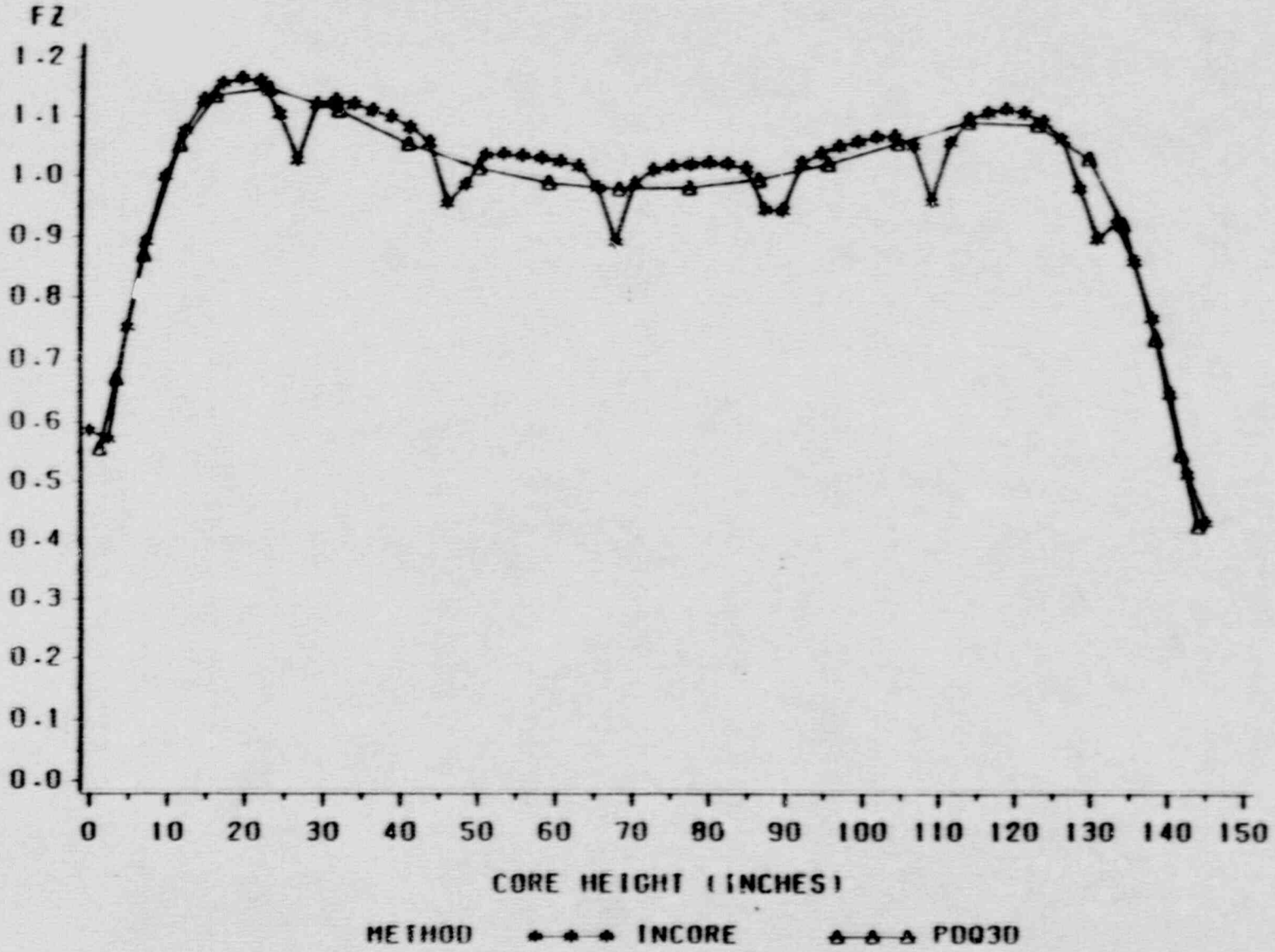

FIGURE 3-6

NORTH ANNA P(Z) COMPARISON

TWO ZONE PDQ3D RESULTS AND INCORE DATA

UNIT=NIC2 BURNUP=0

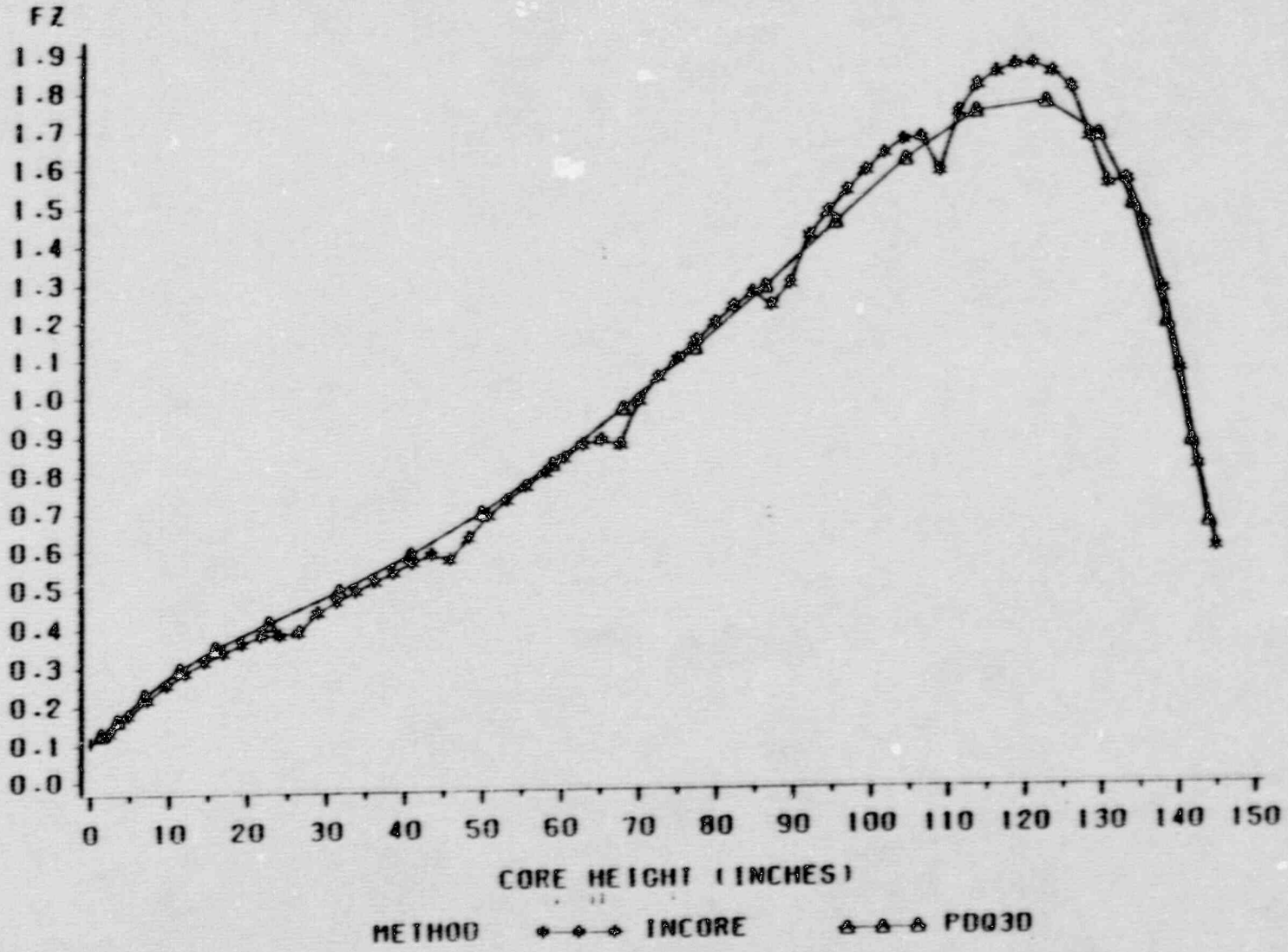

FIGURE 3-7

NORTH ANNA P(Z) COMPARISON

TWO ZONE PDQ3D RESULTS AND INCORE DATA
UNIT=NIC2 BURNUP=305

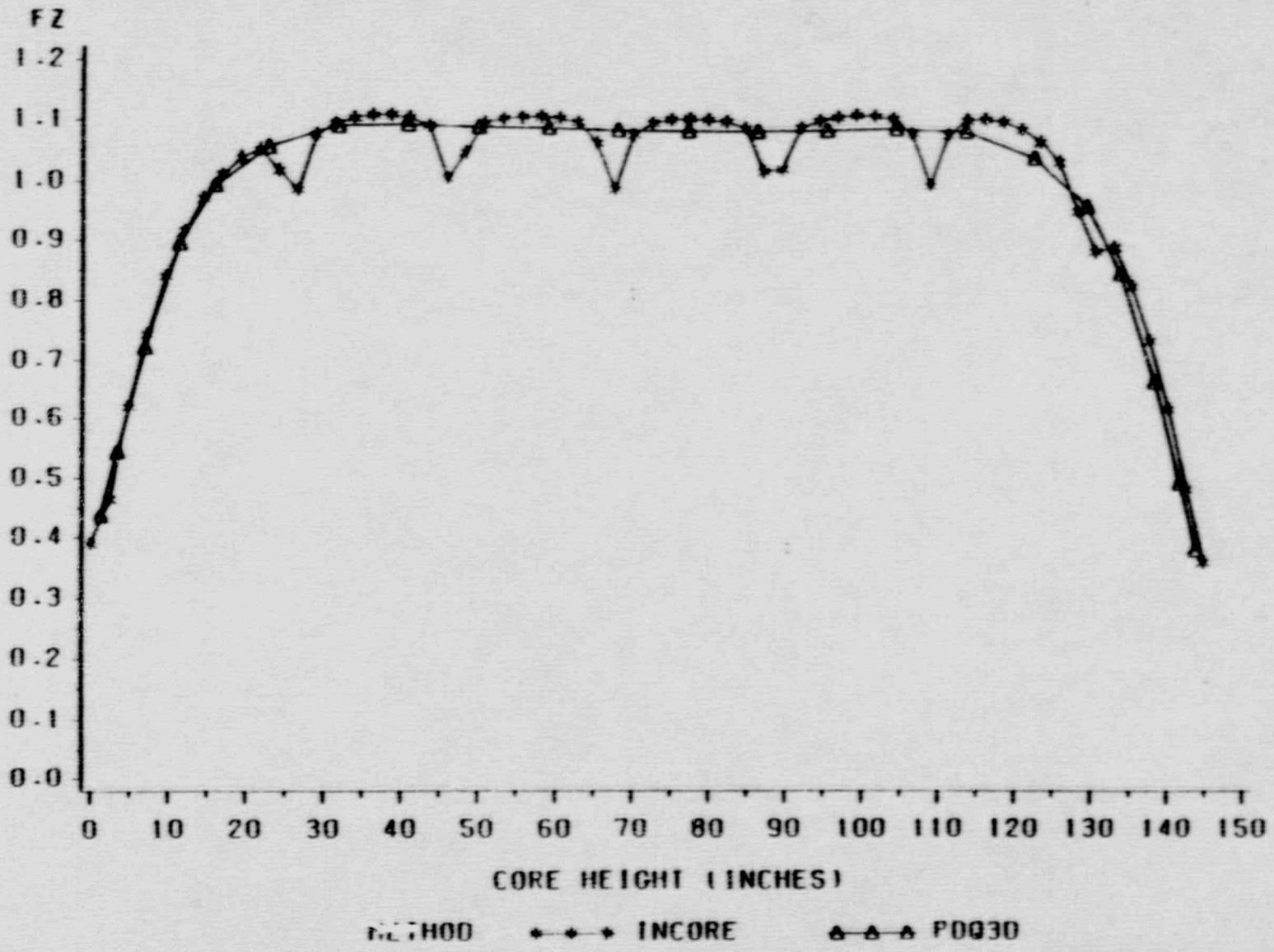

FIGURE 3-8

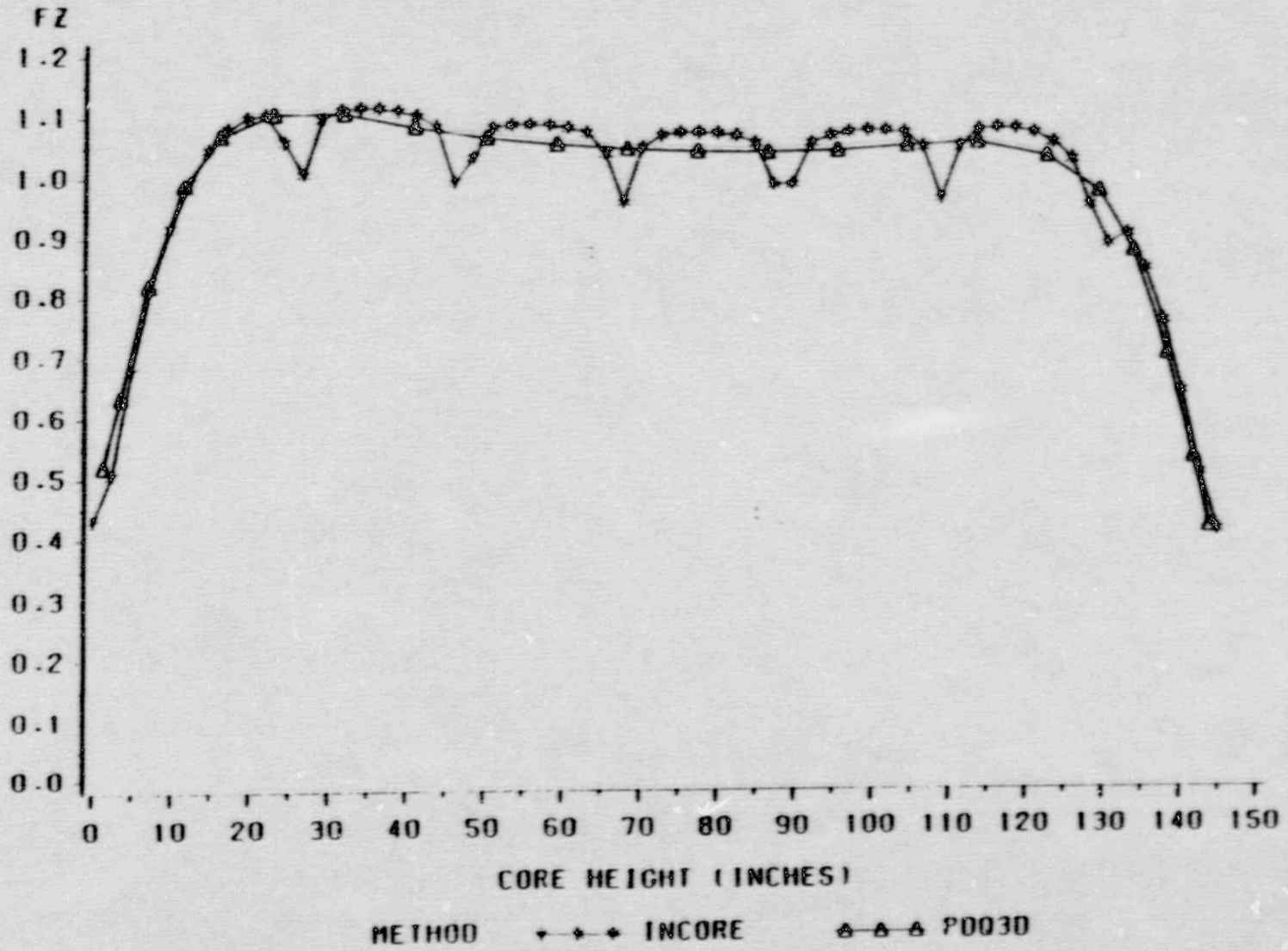
NORTH ANNA P(Z) COMPARISON
TWO ZONE PDQ3D RESULTS AND INCORE DATA
UNIT=N1C2 BURNUP=3277
FZ
1.2
1.1
1.0
0.9
0.8
0.7
0.6
0.5
0.4
0.3
0.2
0.1
0.0
0
10
20
30
40
50
60
70
80
90
100
110
120
130
140
150
CORE HEIGHT (INCHES)
METHOD
INCORE
PDQ3D

FIGURE 3-9

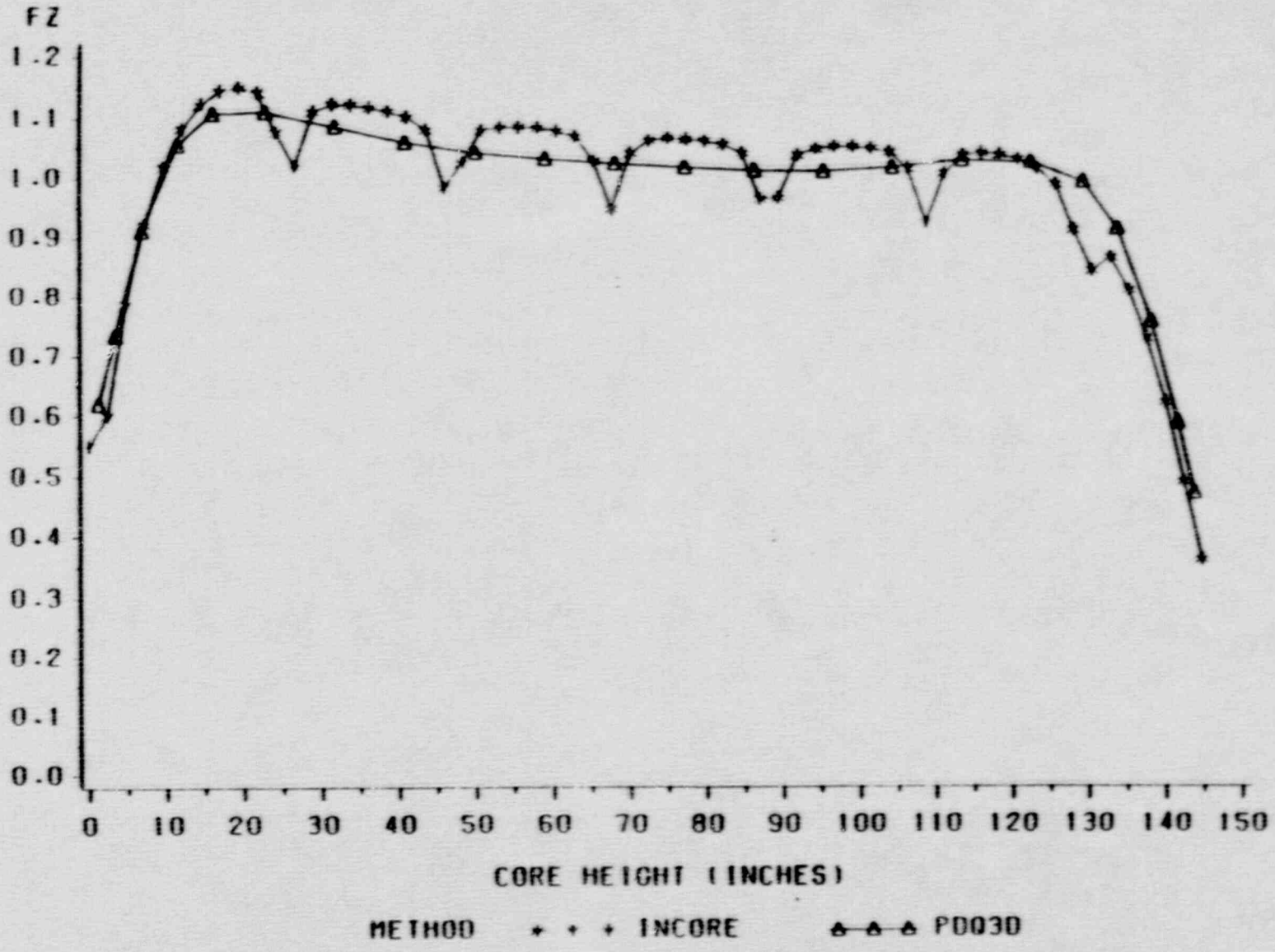
NORTH ANNA P(Z) COMPARISON
TWO ZONE PDQ3D RESULTS AND INCORE DATA
UNIT=NIC2 BURNUP=8109
FZ
1.2
1.1
1.0
0.9
0.8
0.7
0.6
0.5
0.4
0.3
0.2
0.1
0.0
0
10
20
30
40
50
60
70
80
90
100
110
120
130
140
150
CORE HEIGHT (INCHES)
METHOD
INCORE
PDQ3D

FIGURE 3-10

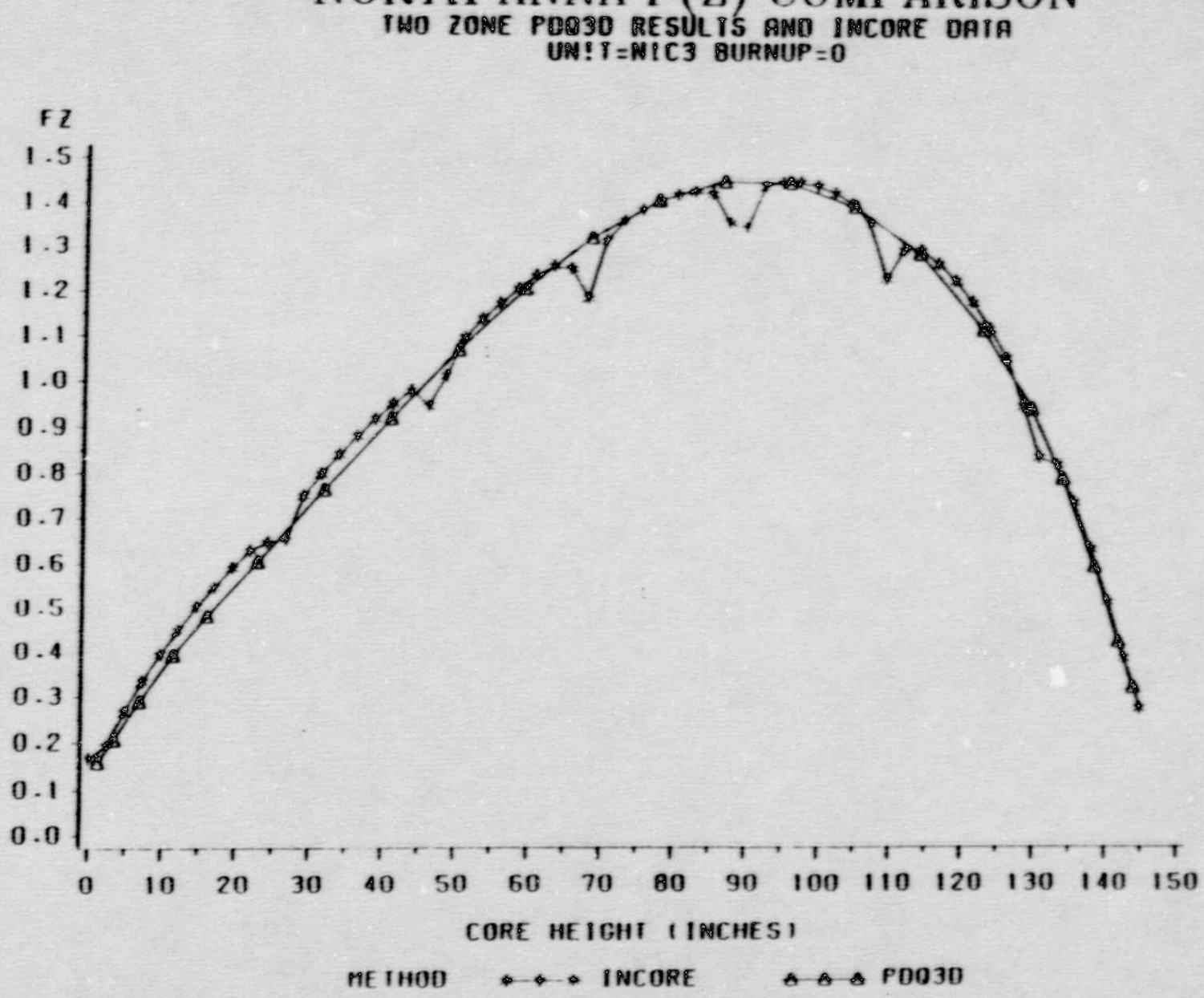
NORTH ANNA P(Z) COMPARISON
TWO ZONE PDQ3D RESULTS AND INCORE DATA
UNIT=NIC3 BURNUP=0
FZ
1.5
1.4
1.3
1.2
1.1
1.0
0.9
0.8
0.7
0.6
0.5
0.4
0.3
0.2
0.1
0.0
0
10
20
30
40
50
60
70
80
90
100
110
120
130
140
150
CORE HEIGHT (INCHES)
METHOD
INCORE
PDQ3D

FIGURE 3-11

NORTH ANNA P(Z) COMPARISON

TWO ZONE PDQ3D RESULTS AND INCORE DATA
UNIT=NIC3 BURNUP=487

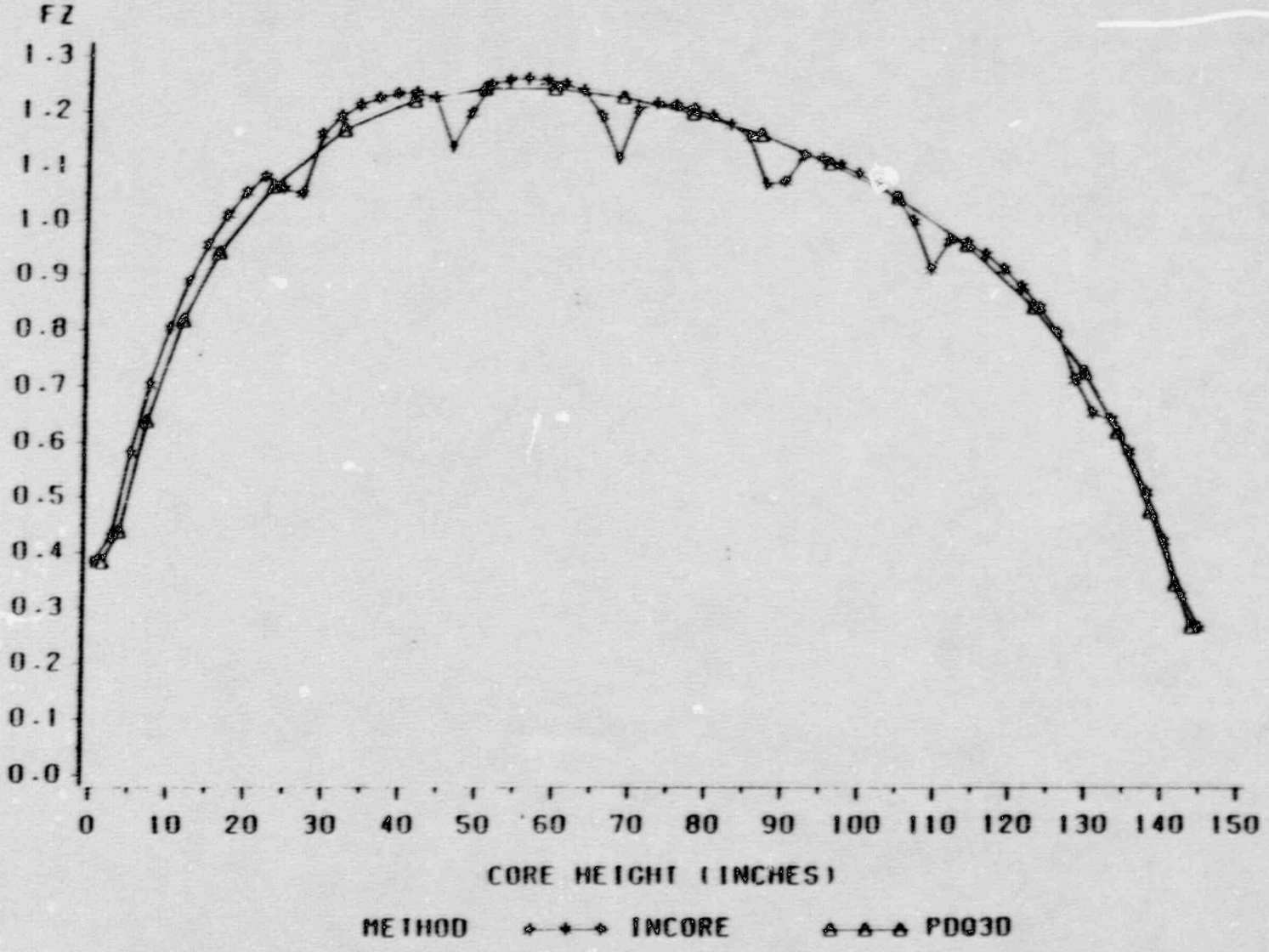

FIGURE 3-12

FIGURE 3-13

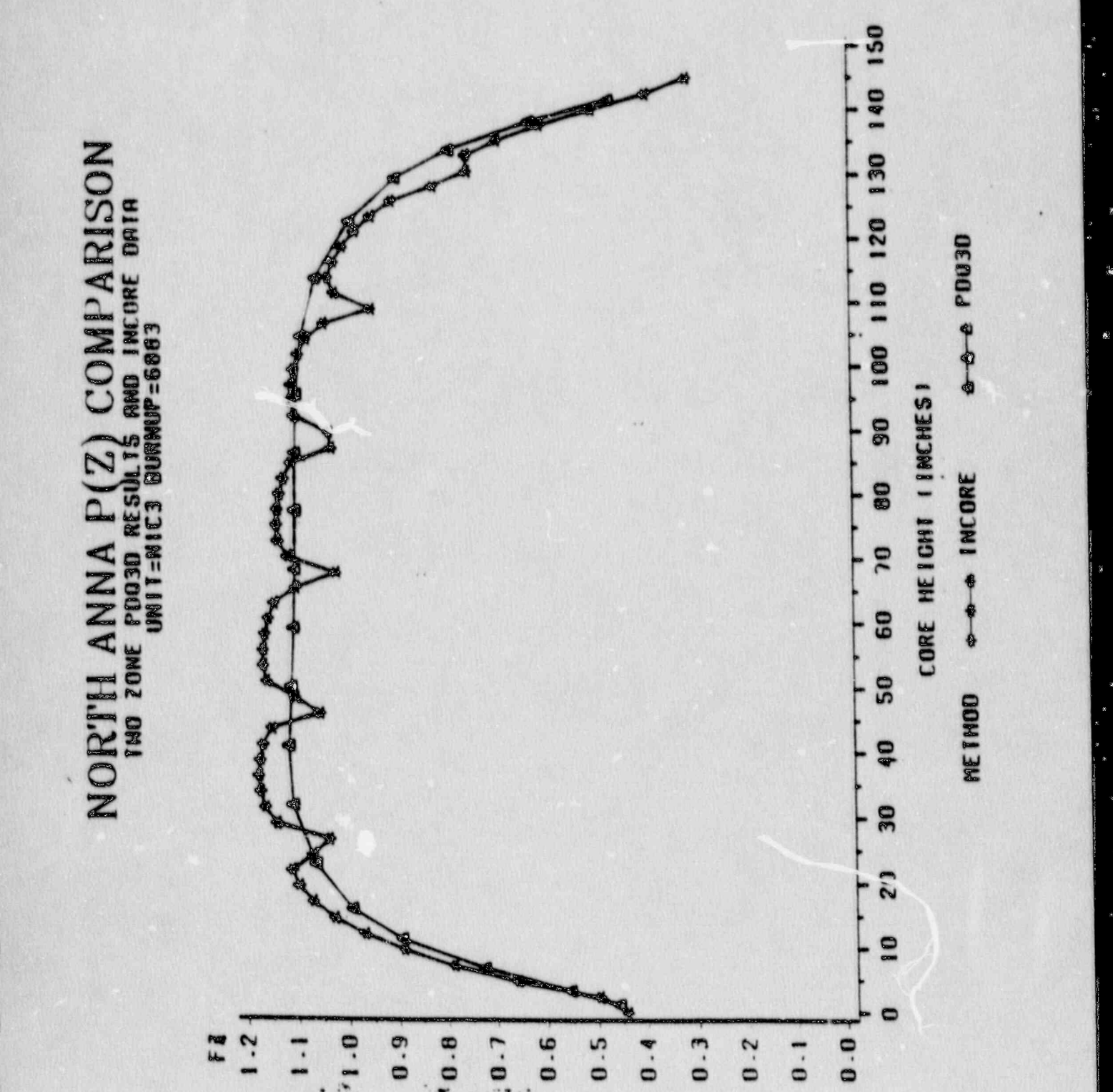
NORTH ANNA P(Z) COMPARISON
TWO ZONE PDQ3D RESULTS AND INCORE DATA
UNIT=NIC3 BURNUP=6003
FZ
1.2
1.1
1.0
0.9
0.8
0.7
0.6
0.5
0.4
0.3
0.2
0.1
0.0
0 10 20 30 40 50 60 70 80 90 100 110 120 130 140 150
CORE HEIGHT (INCHES)
METHOD INCORE PDQ3D

NORTH ANNA P(Z) COMPARISON

TWO ZONE PDQ3D RESULTS AND INCORE DATA
UNIT=NIC3 BURNUP=11434

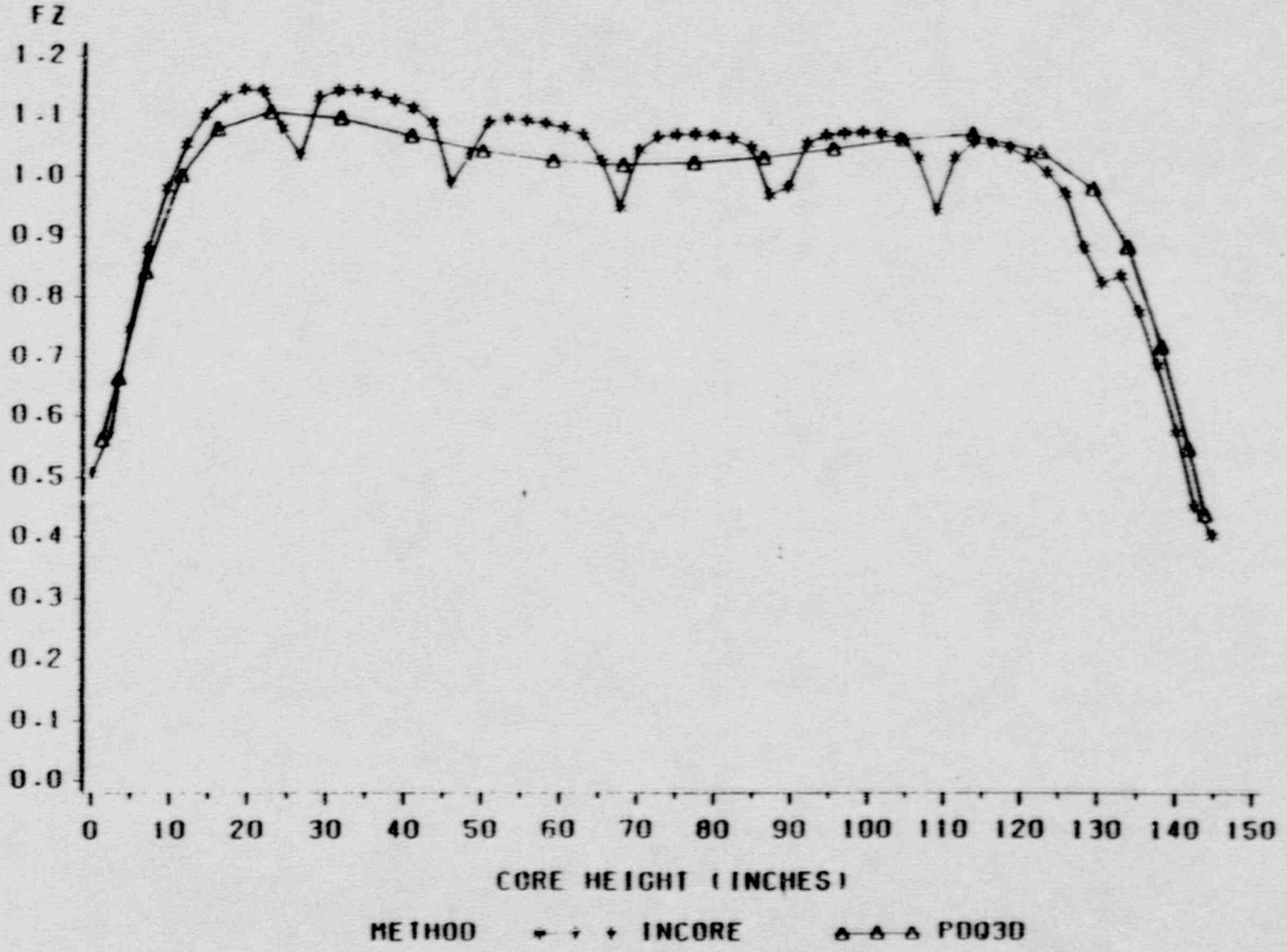

FIGURE 3-14

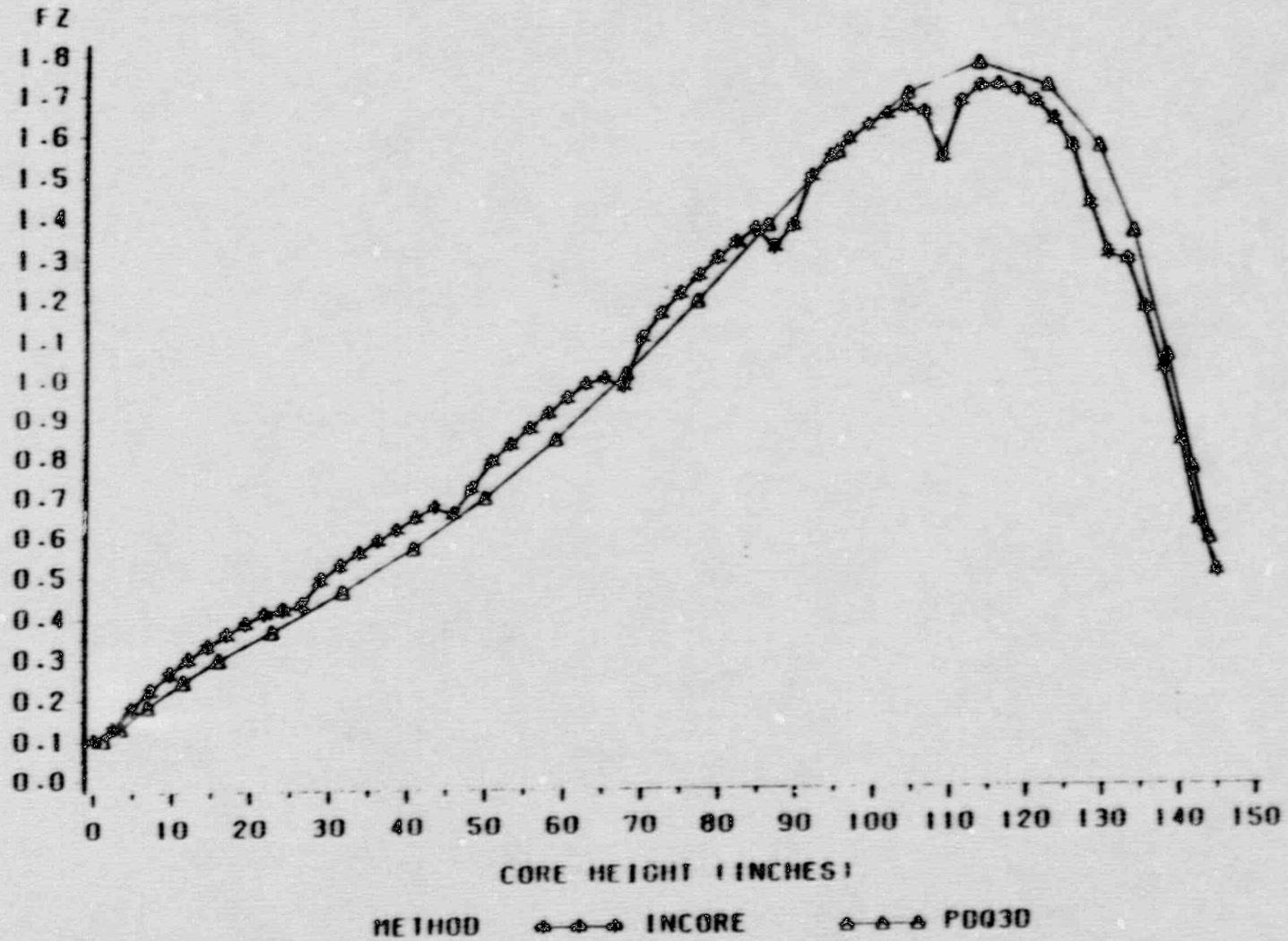
NORTH ANNA P(Z) COMPARISON
TWO ZONE PDQ3D RESULTS AND INCORE DATA
UNIT=NIC4 BURNUP=0
FZ
1.8
1.7
1.6
1.5
1.4
1.3
1.2
1.1
1.0
0.9
0.8
0.7
0.6
0.5
0.4
0.3
0.2
0.1
0.0
0
10
20
30
40
50
60
70
80
90
100
110
120
130
140
150
CORE HEIGHT (INCHES)
METHOD
INCORE
PDQ3D

FIGURE 3-15

NORTH ANNA P(Z) COMPARISON

TWO ZONE PDQ3D RESULTS AND INCORE DATA
UNIT=NIC4 BURNUP=305

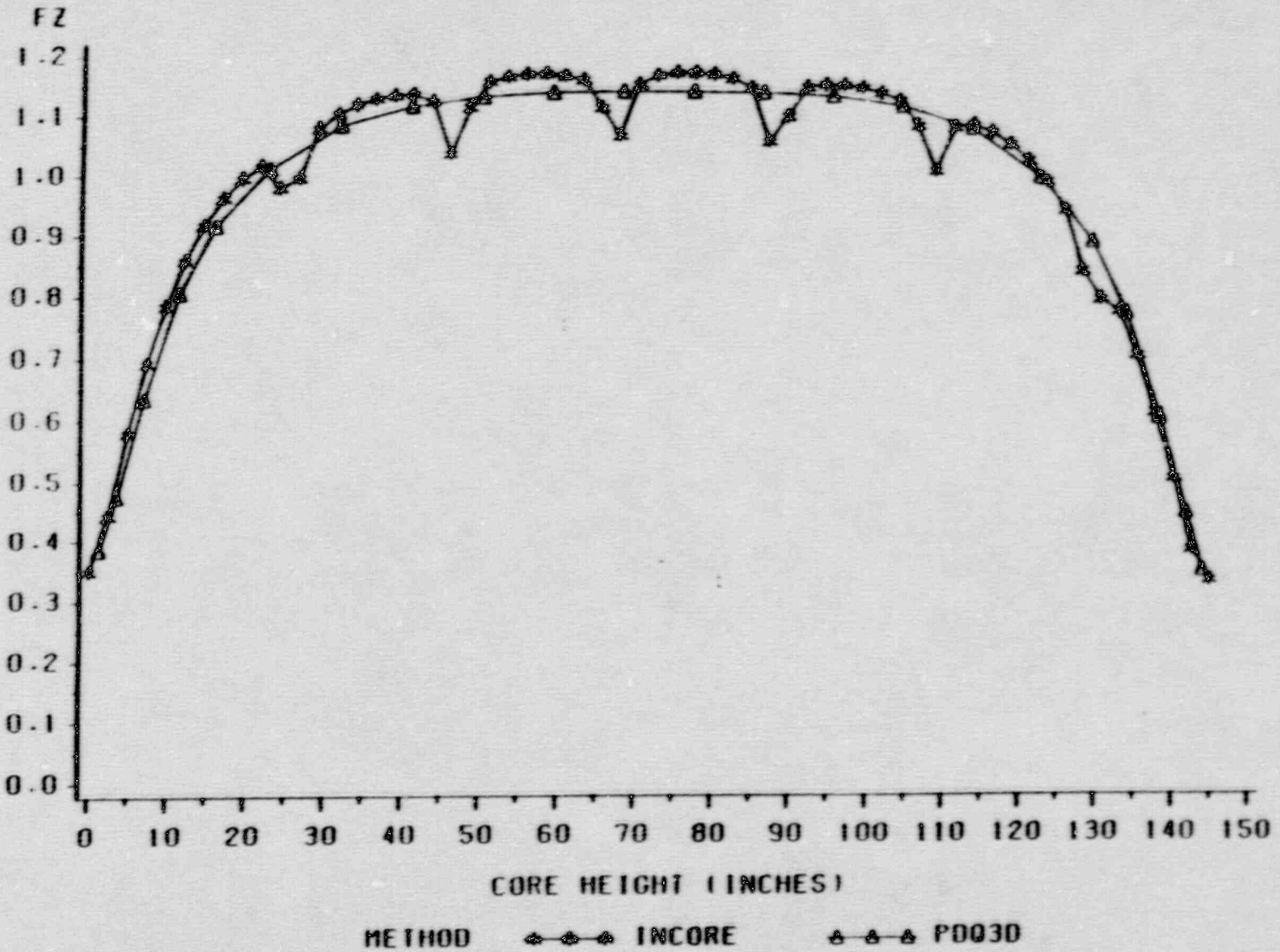

FIGURE 3-16

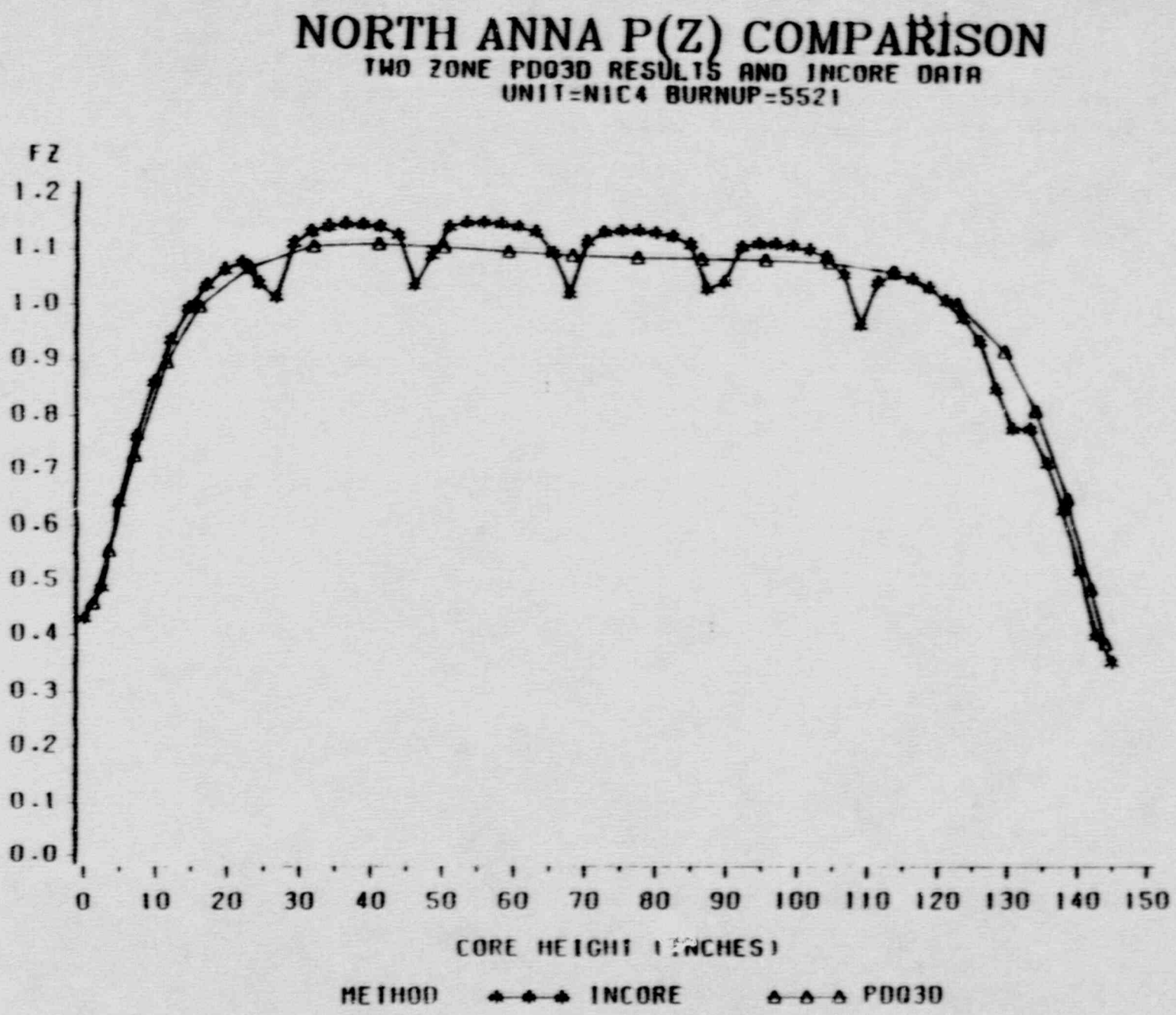
NORTH ANNA P(Z) COMPARISON
TWO ZONE PD03D RESULTS AND INCORE DATA
UNIT=N1C4 BURNUP=5521
FZ
1.2
1.1
1.0
0.9
0.8
0.7
0.6
0.5
0.4
0.3
0.2
0.1
0.0
0 10 20 30 40 50 60 70 80 90 100 110 120 130 140 150
CORE HEIGHT (INCHES)
METHOD INCORE PD03D

FIGURE 3-17

NORTH ANNA P(Z) COMPARISON

TWO ZONE PDQ3D RESULTS AND INCORE DATA
UNIT=NIC4 BURNUP=10170

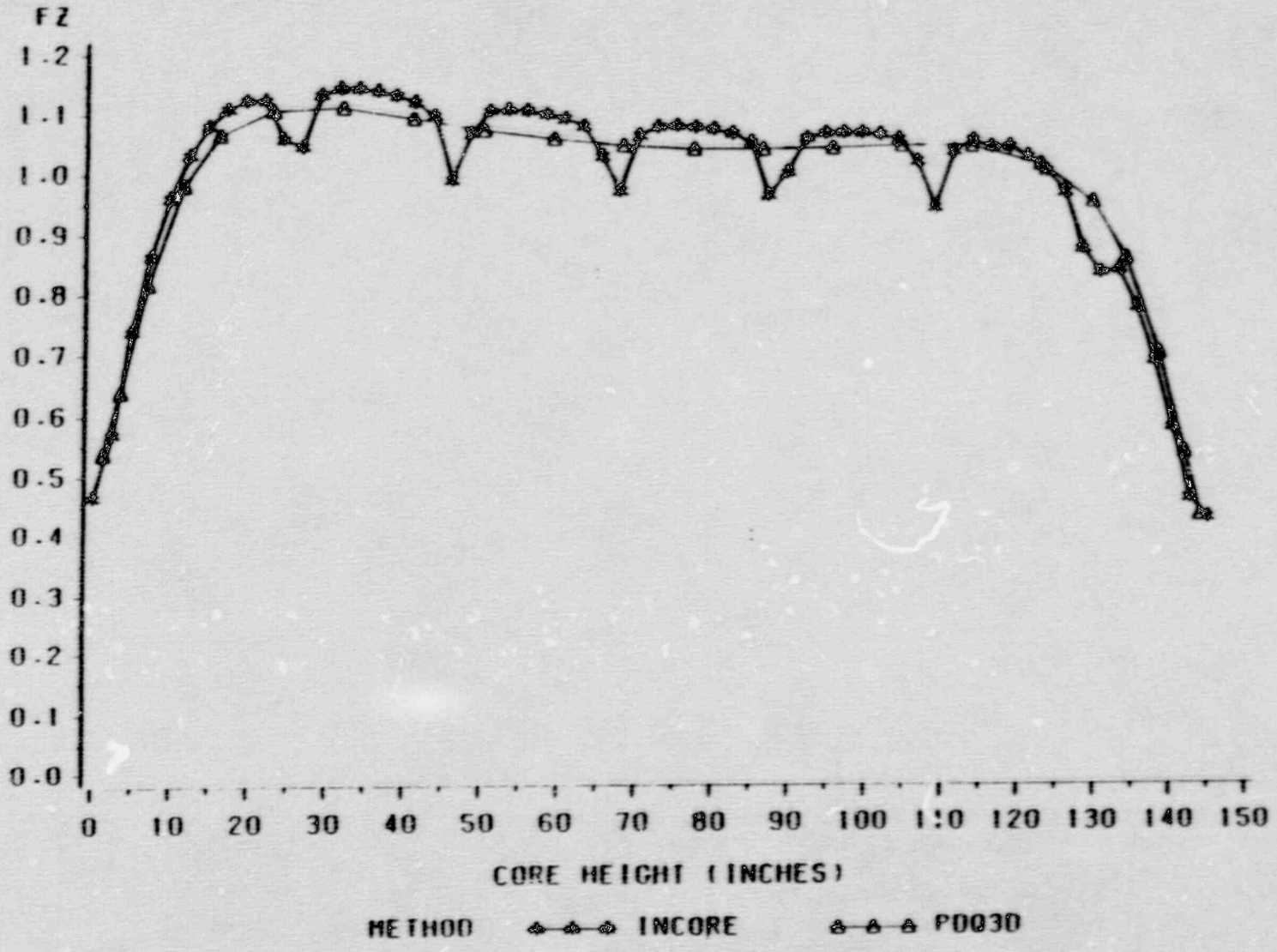

FIGURE 3-18

NORTH ANNA P(Z) COMPARISON

TWO ZONE PDQ3D RESULTS AND INCORE DATA
UNIT=NIC5 BURNUP=0

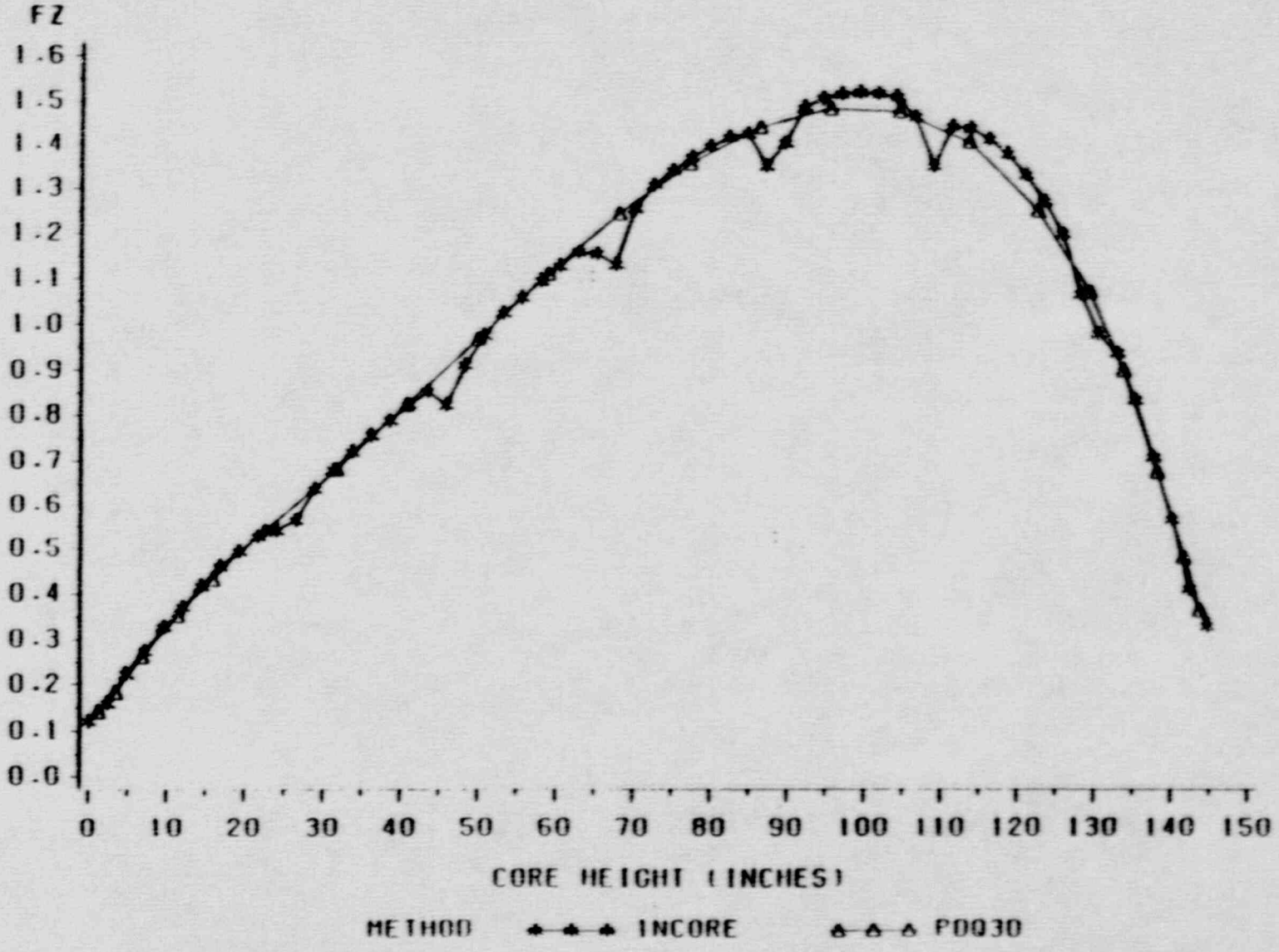

FIGURE 3-19

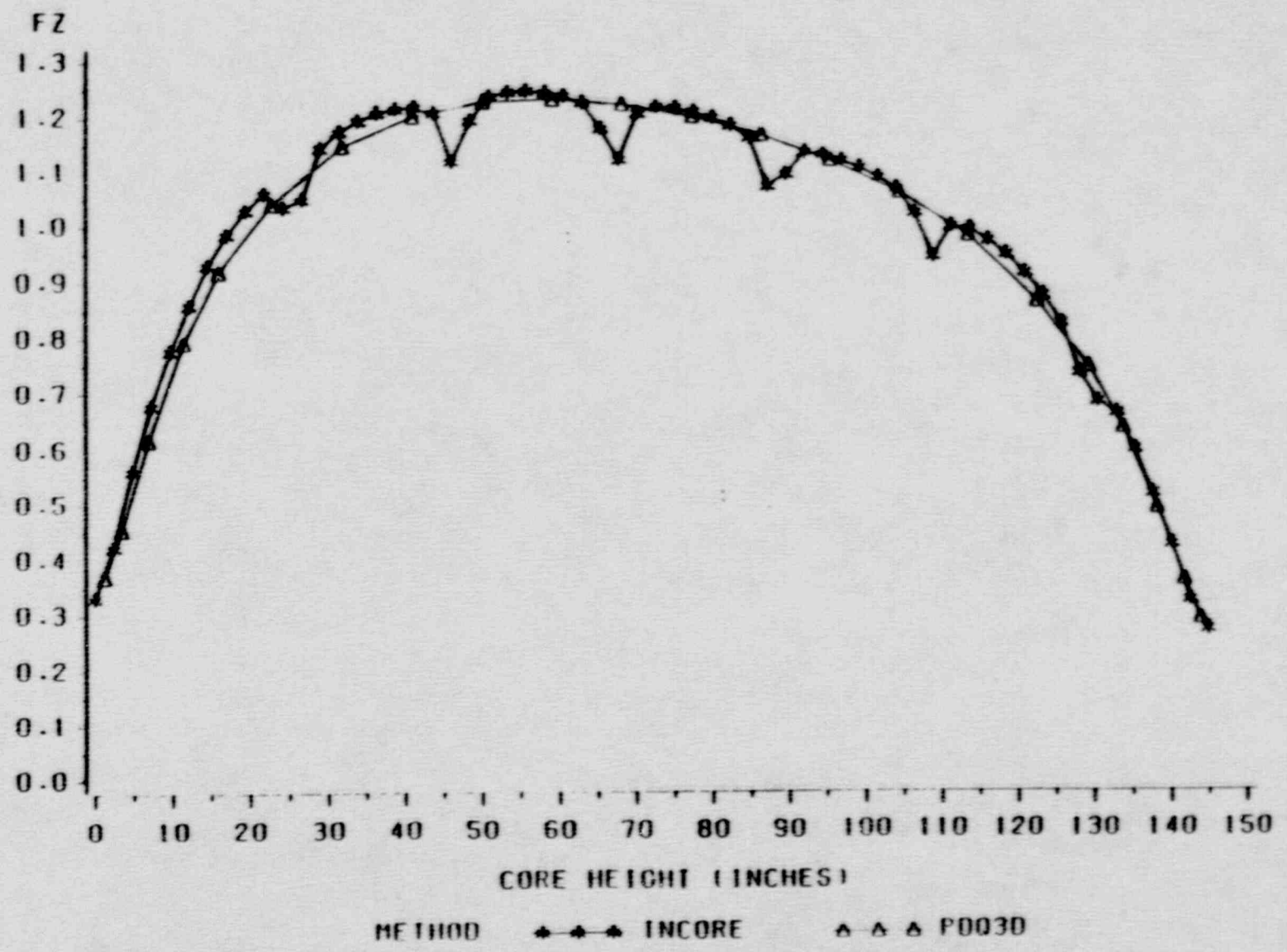
NORTH ANNA P(Z) COMPARISON
TWO ZONE PDQ3D RESULTS AND INCORE DATA
UNIT=NIC5 BURNUP=225
FZ
1.3
1.2
1.1
1.0
0.9
0.8
0.7
0.6
0.5
0.4
0.3
0.2
0.1
0.0
0
10
20
30
40
50
60
70
80
90
100
110
120
130
140
150
CORE HEIGHT (INCHES)
METHOD
INCORE
PDQ3D

FIGURE 3-20

NORTH ANNA P(Z) COMPARISON

TWO ZONE PDQ3D RESULTS AND INCORE DATA

UNIT=NICS BURNUP=6831

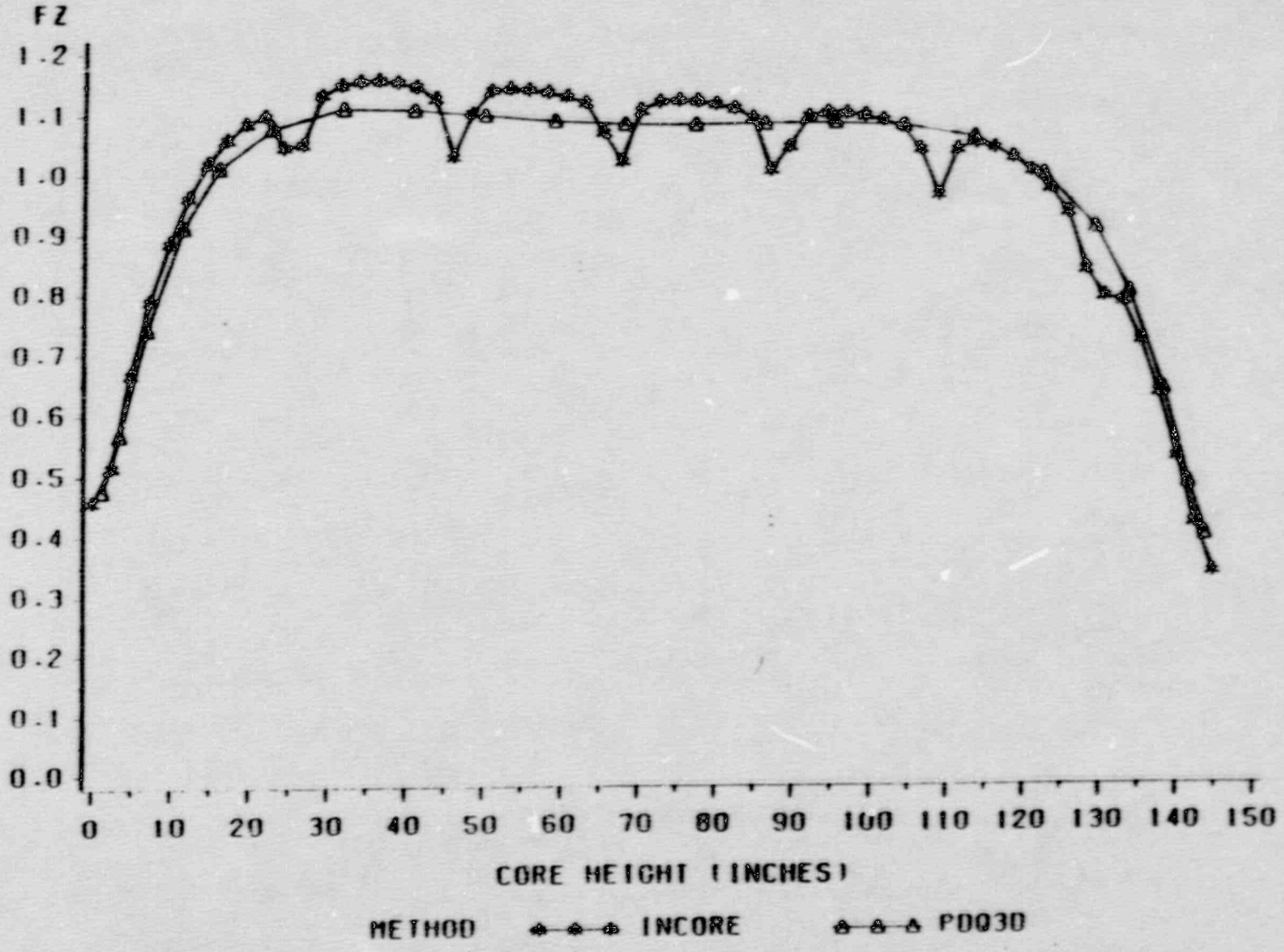

FIGURE 3-21

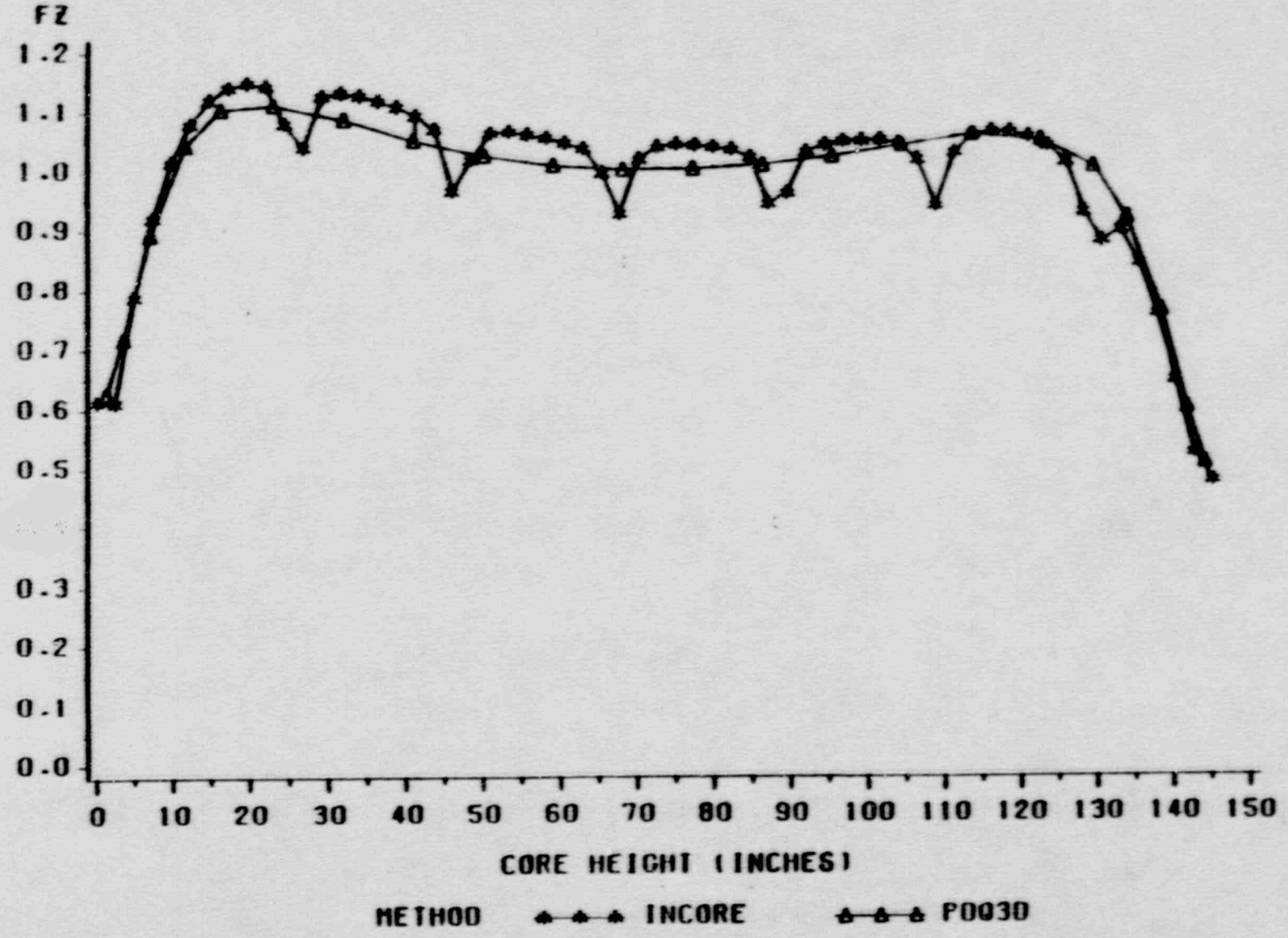
NORTH ANNA P(Z) COMPARISON
TWO ZONE PDQ3D RESULTS AND INCORE DATA
UNIT=NIC5 BURNUP=12983
FZ
1.2
1.1
1.0
0.9
0.8
0.7
0.6
0.5
0.3
0.2
0.1
0.0
0 10 20 30 40 50 60 70 80 90 100 110 120 130 140 150
CORE HEIGHT (INCHES)
METHOD INCORE PDQ3D

FIGURE 3-22

NORTH ANNA P(Z) COMPARISON

TWO ZONE PDQ3D RESULTS AND INCORE DATA
UNIT=NIC6 BURNUP=379

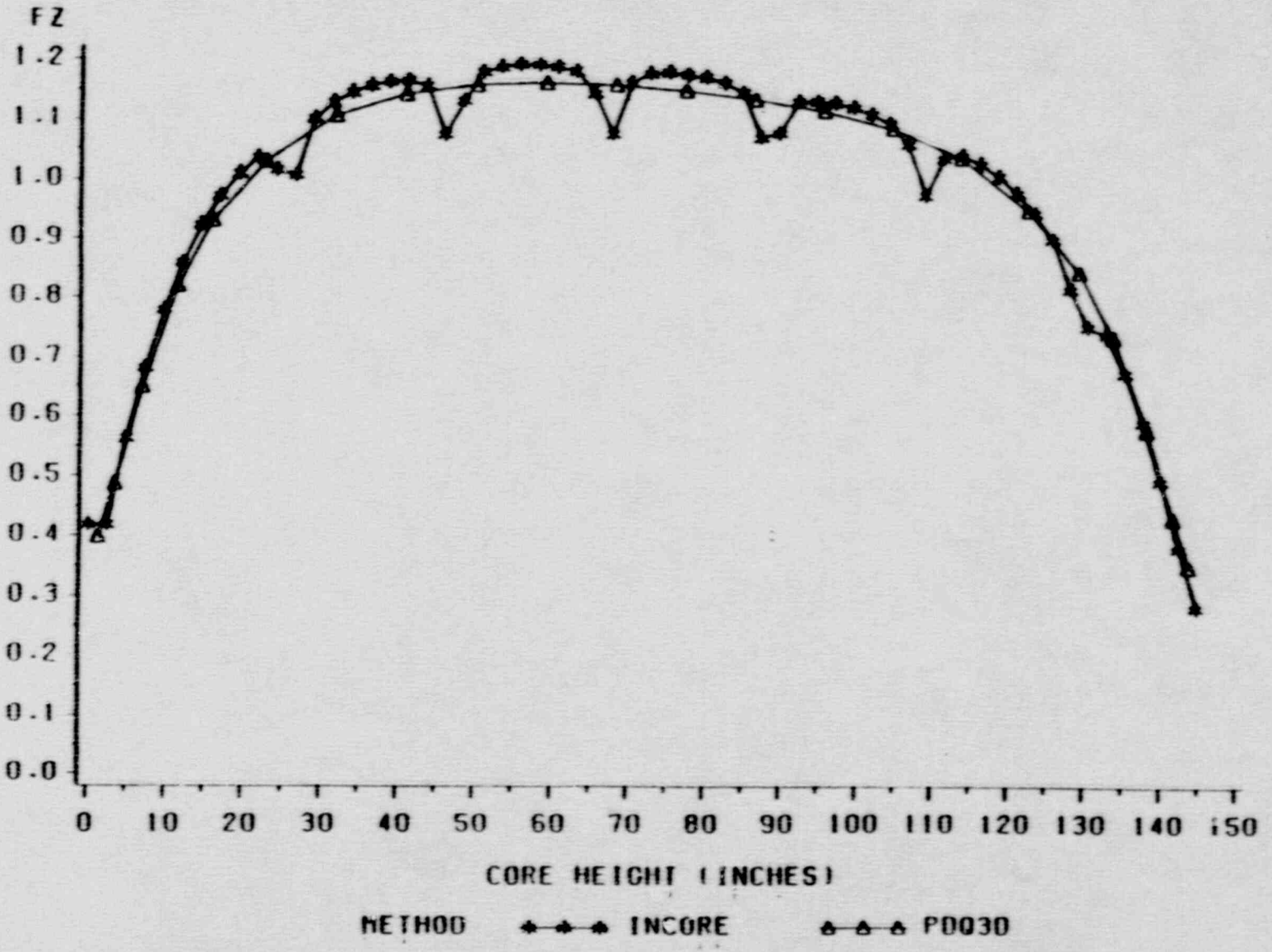

FIGURE 3-23

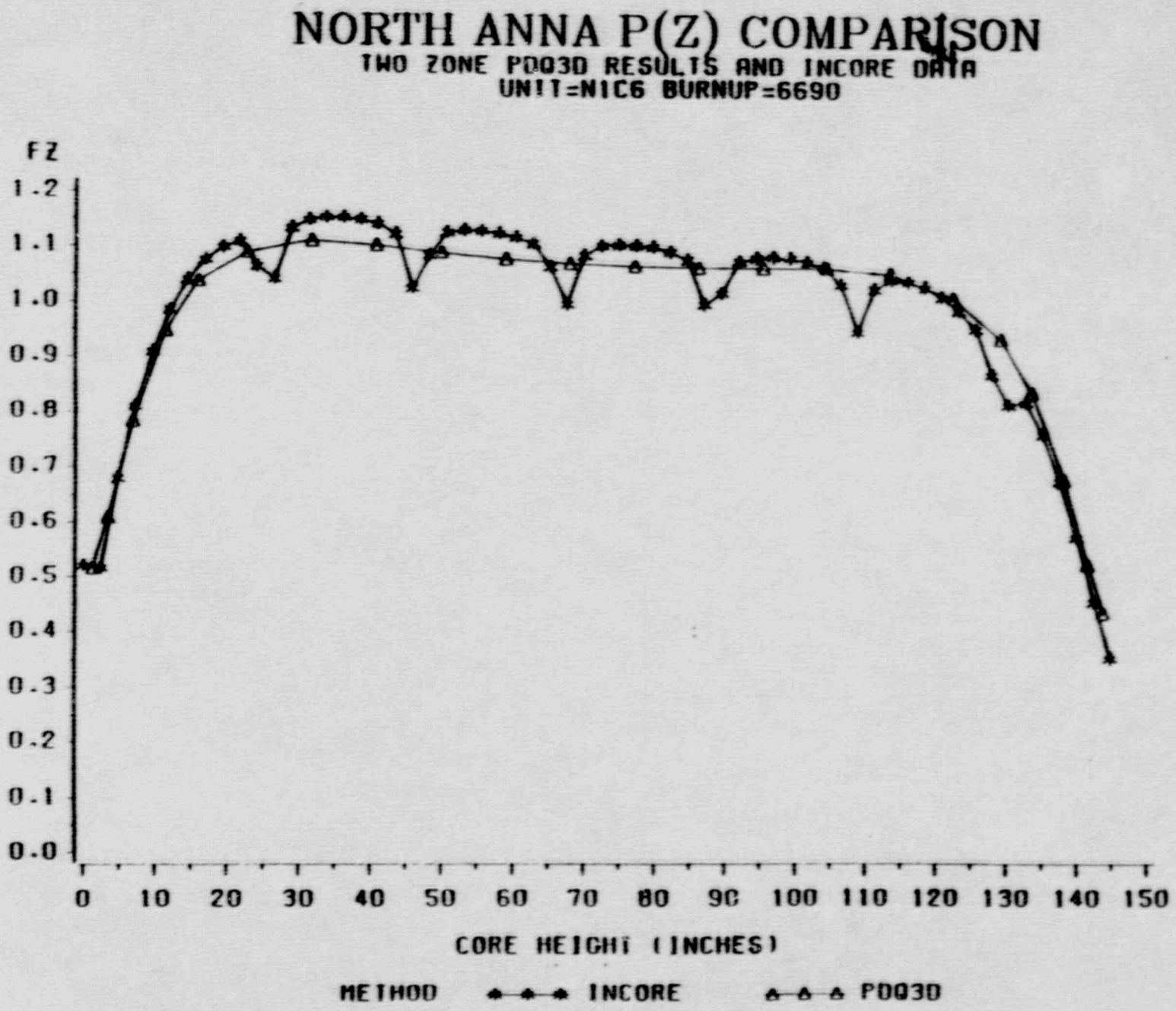
NORTH ANNA P(Z) COMPARISON
TWO ZONE PDQ3D RESULTS AND INCORE DATA
UNIT=N1C6 BURNUP=6690
FZ
1.2
1.1
1.0
0.9
0.8
0.7
0.6
0.5
0.4
0.3
0.2
0.1
0.0
0 10 20 30 40 50 60 70 80 90 100 110 120 130 140 150
CORE HEIGHT (INCHES)
METHOD INCORE PDQ3D

FIGURE 3-24

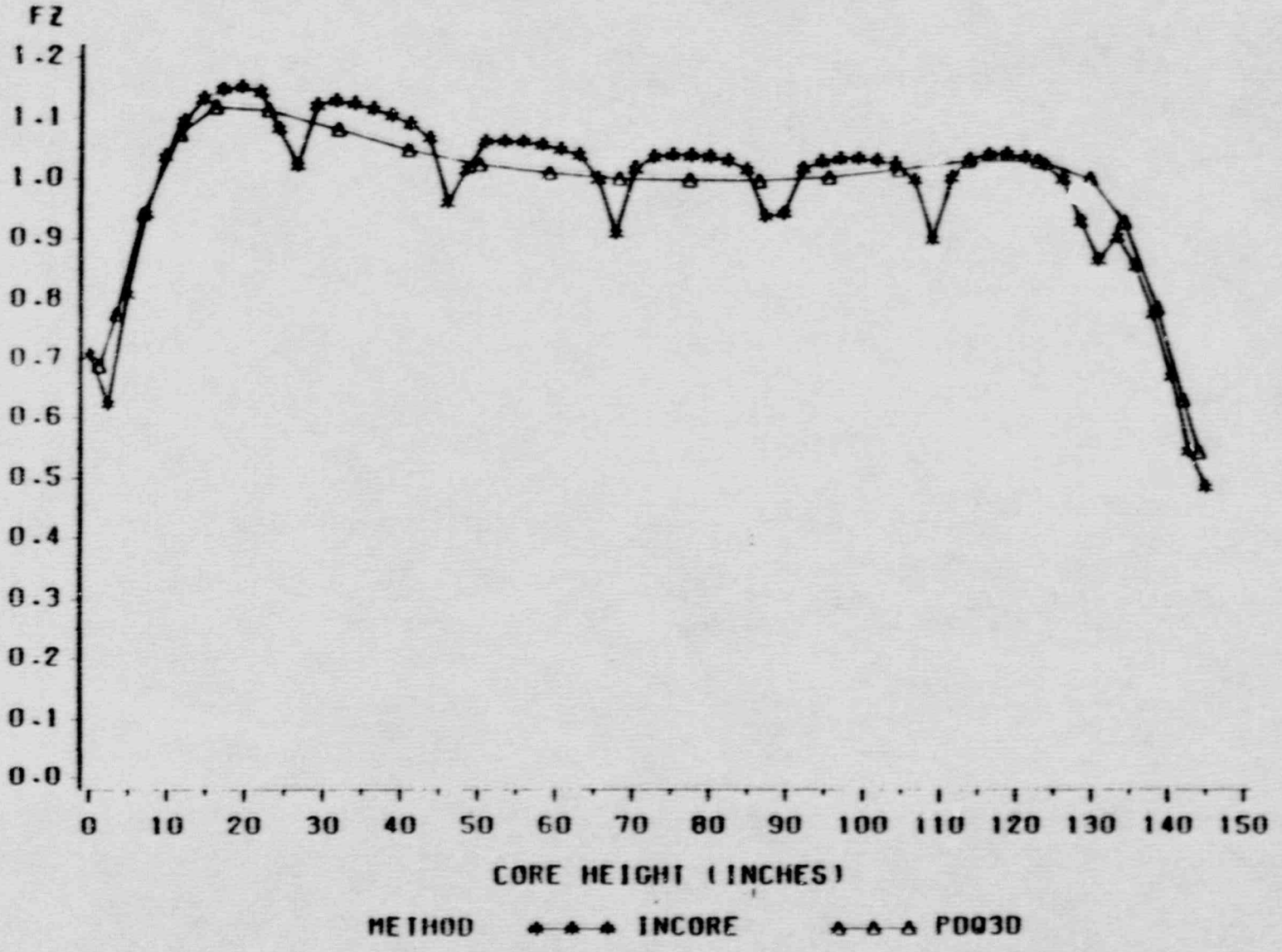
NORTH ANNA P(Z) COMPARISON
TWO ZONE PDQ3D RESULTS AND INCORE DATA
UNIT=N1C6 BURNUP=14340
FZ
1.2
1.1
1.0
0.9
0.8
0.7
0.6
0.5
0.4
0.3
0.2
0.1
0.0
0
10
20
30
40
50
60
70
80
90
100
110
120
130
140
150
CORE HEIGHT (INCHES)
METHOD
INCORE
PDQ3D

FIGURE 3-25

NORTH ANNA P(Z) COMPARISON

TWO ZONE PDQ3D RESULTS AND INCORE DATA

UNIT=N1C7 BURNUP=1062

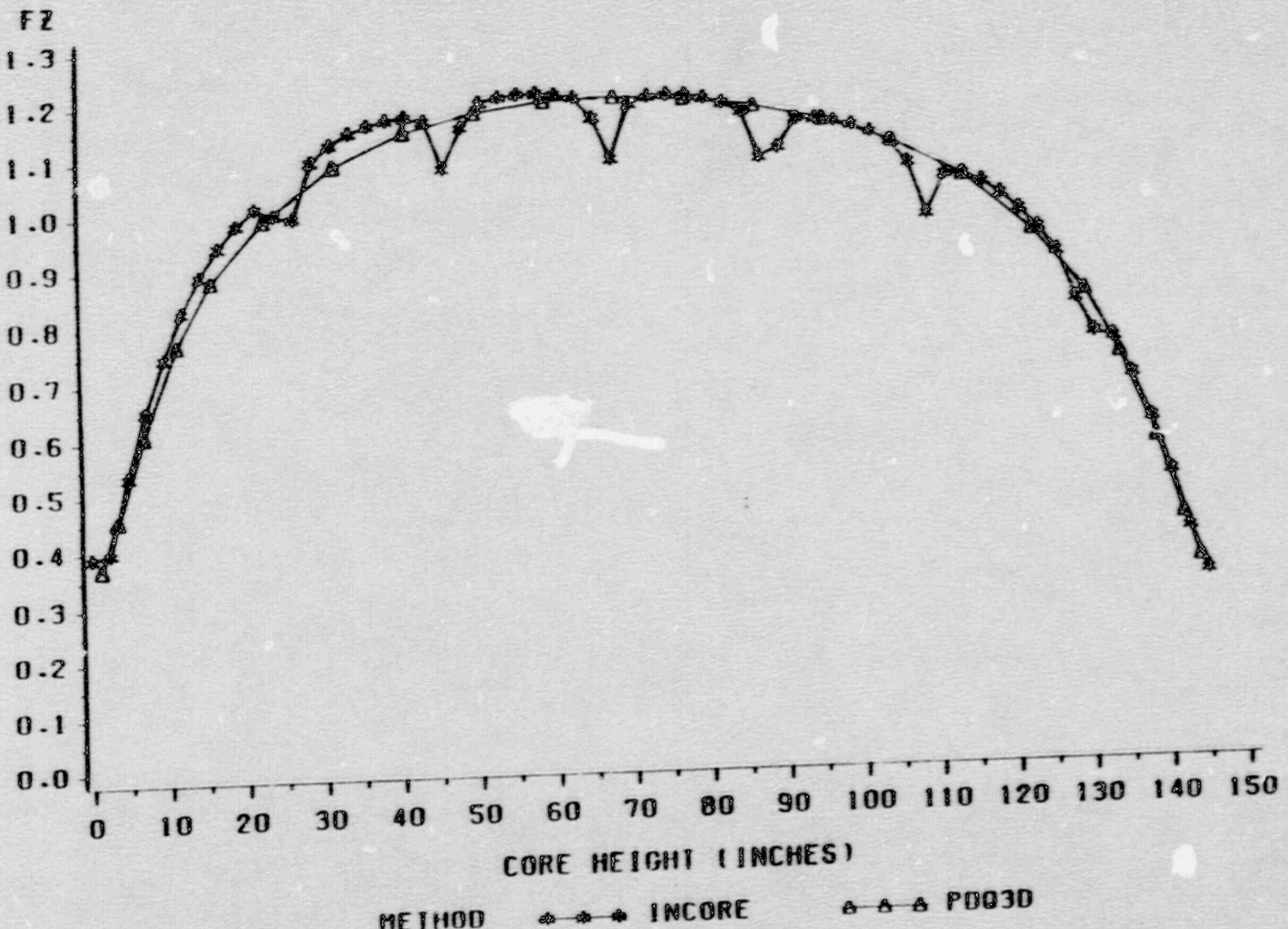

FIGURE 3-26

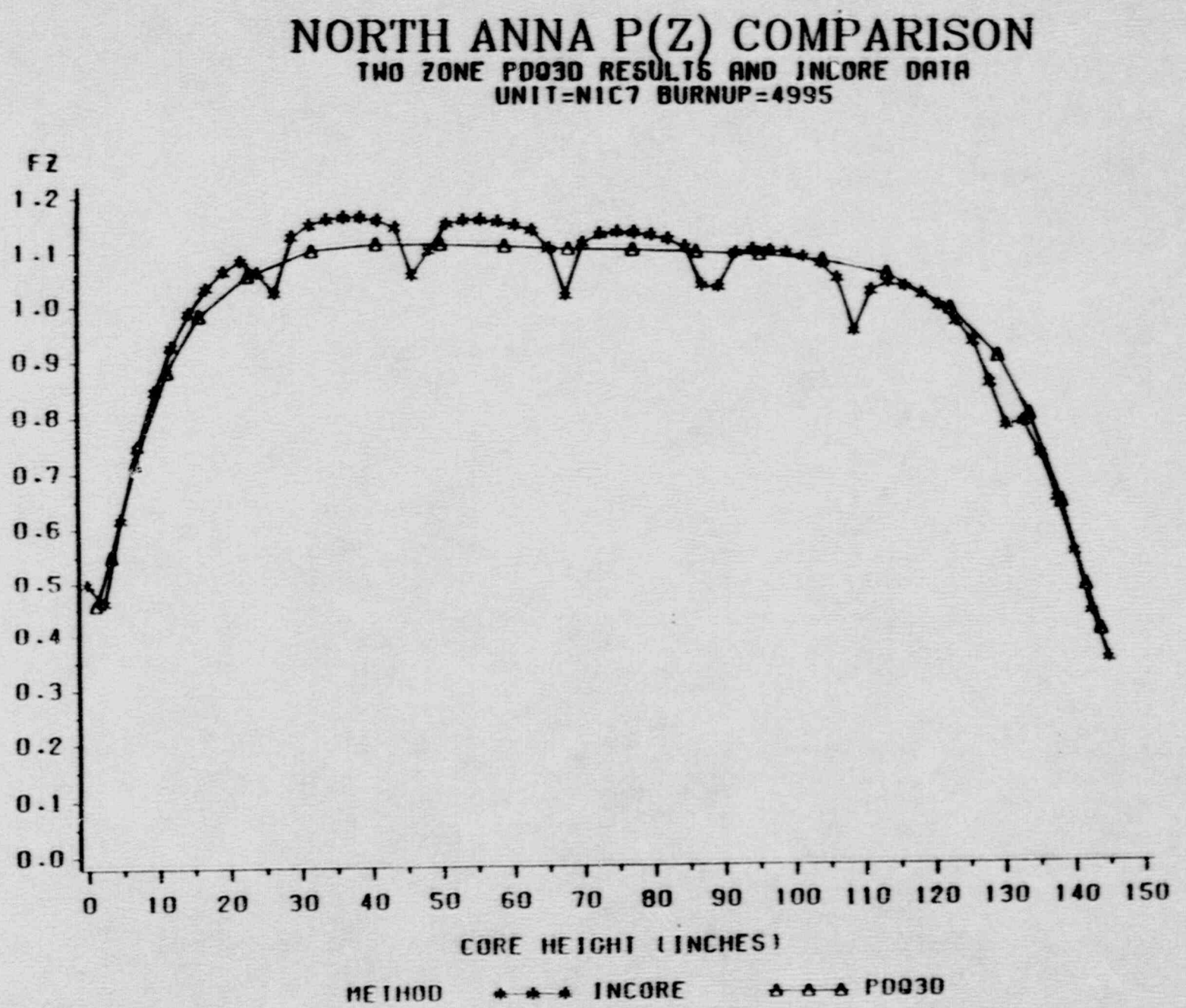
NORTH ANNA P(Z) COMPARISON
TWO ZONE PDQ3D RESULTS AND INCORE DATA
UNIT=N1C7 BURNUP=4995
FZ
1.2
1.1
1.0
0.9
0.8
0.7
0.6
0.5
0.4
0.3
0.2
0.1
0.0
0
10
20
30
40
50
60
70
80
90
100
110
120
130
140
150
CORE HEIGHT (INCHES)
METHOD
INCORE
PDQ3D

FIGURE 3-27

NORTH ANNA P(Z) COMPARISON

TWO ZONE PDQ3D RESULTS AND INCORE DATA
UNIT=N2C1 BURNUP=0

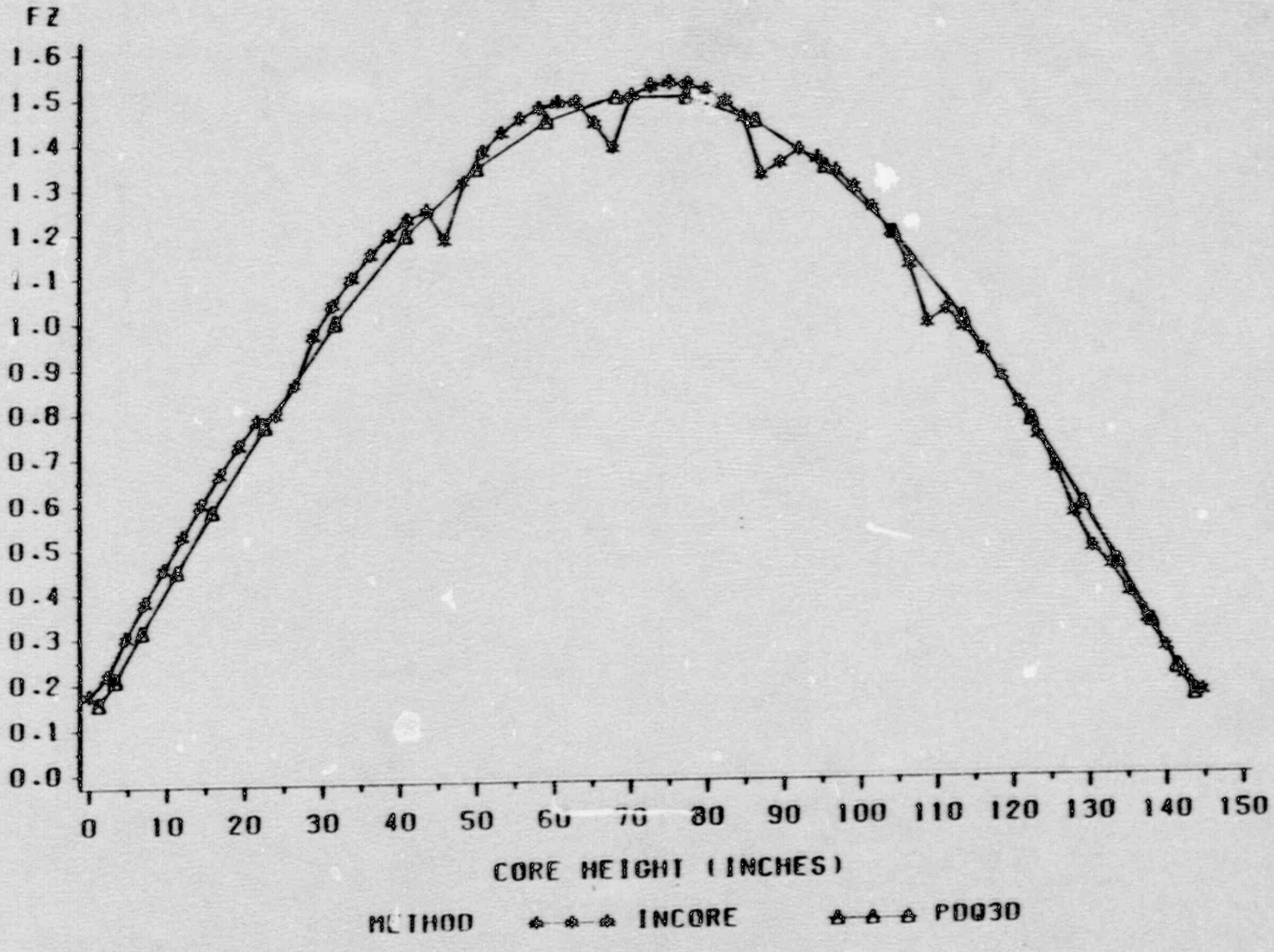

FIGURE 3-28

NORTH ANNA F(Z) COMPARISON

TWO ZONE PDQ3D RESULTS AND INCORE DATA
UNIT=N2C2 BURNUP=0

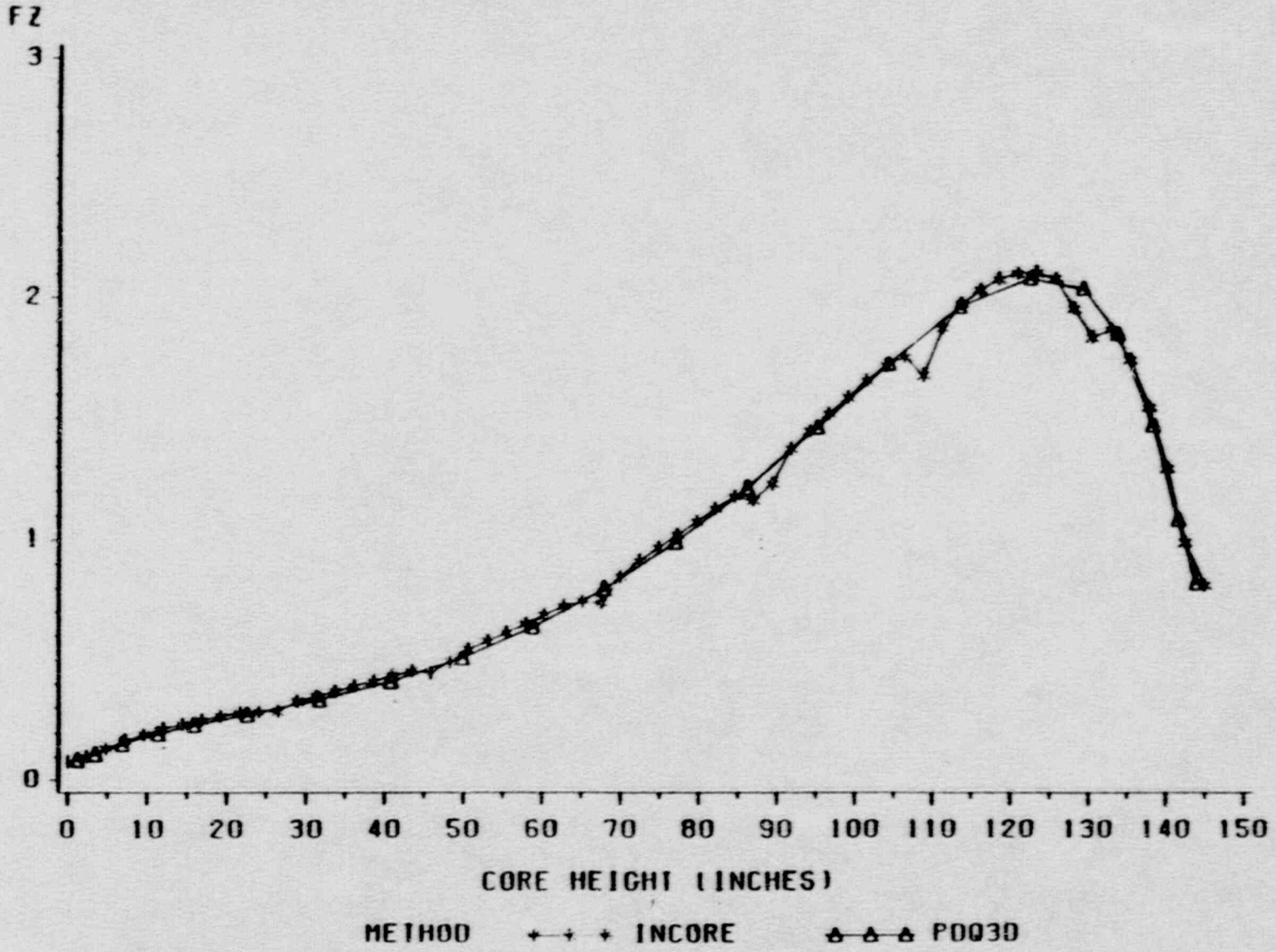

FIGURE 3-29

NORTH ANNA P(Z) COMPARISON

TWO ZONE PDQ3D RESULTS AND INCORE DATA

UNIT=N2C2 BURNUP=3225

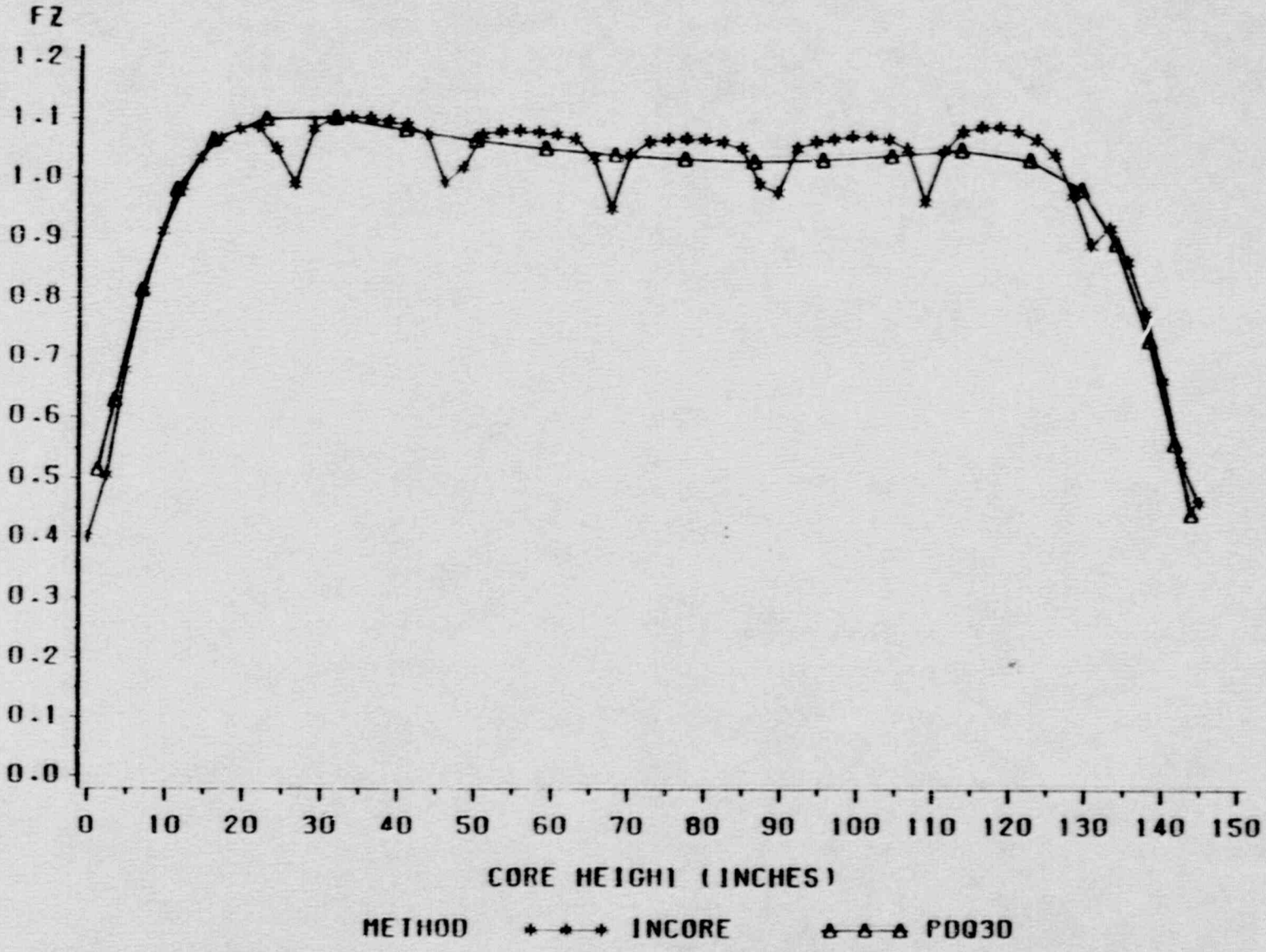

FIGURE 3-30

NORTH ANNA P(Z) COMPARISON

TWO ZONE PDQ3D RESULTS AND INCORE DATA

UNIT=N2C2 BURNUP=6751

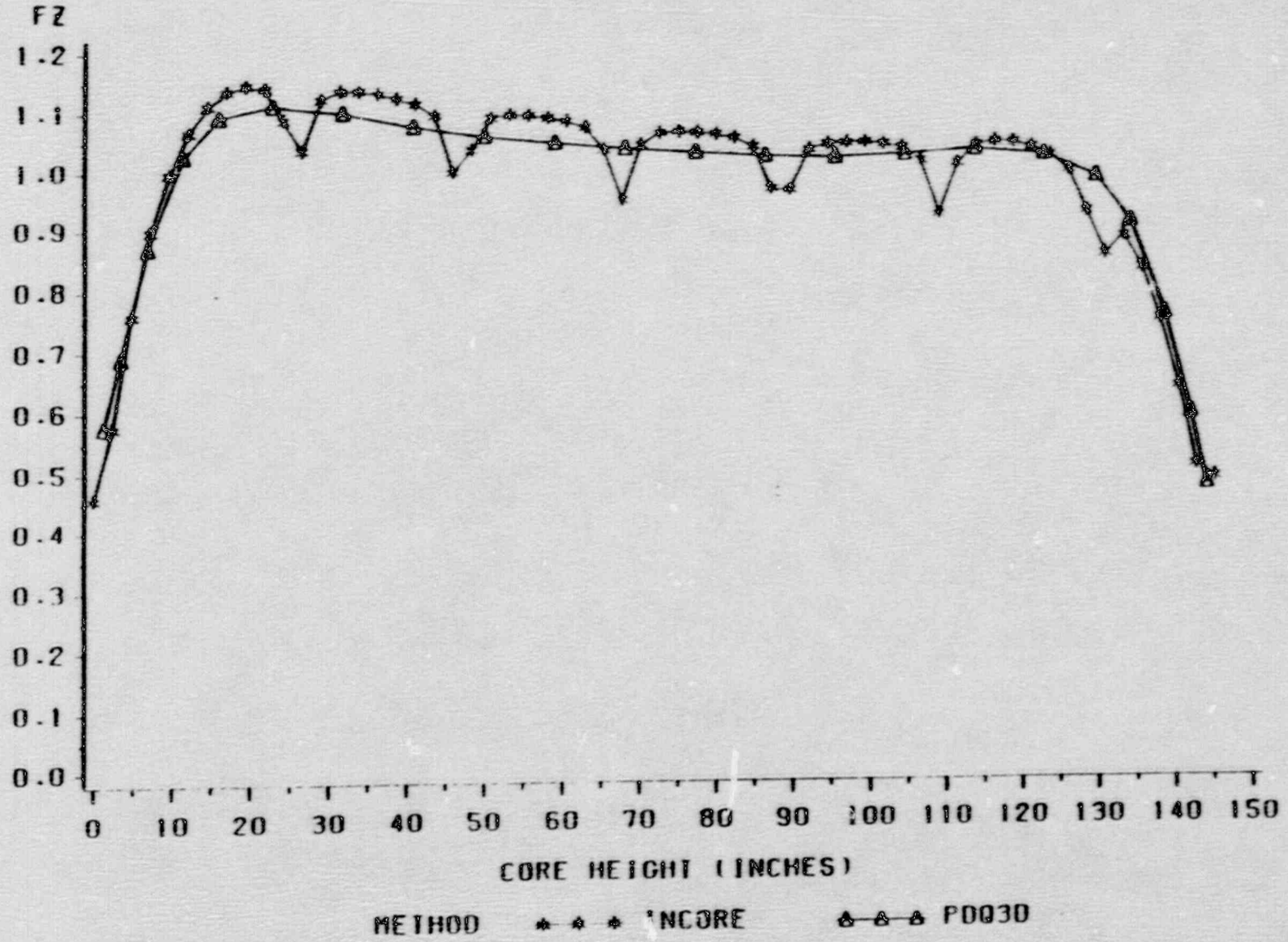

FIGURE 3-31

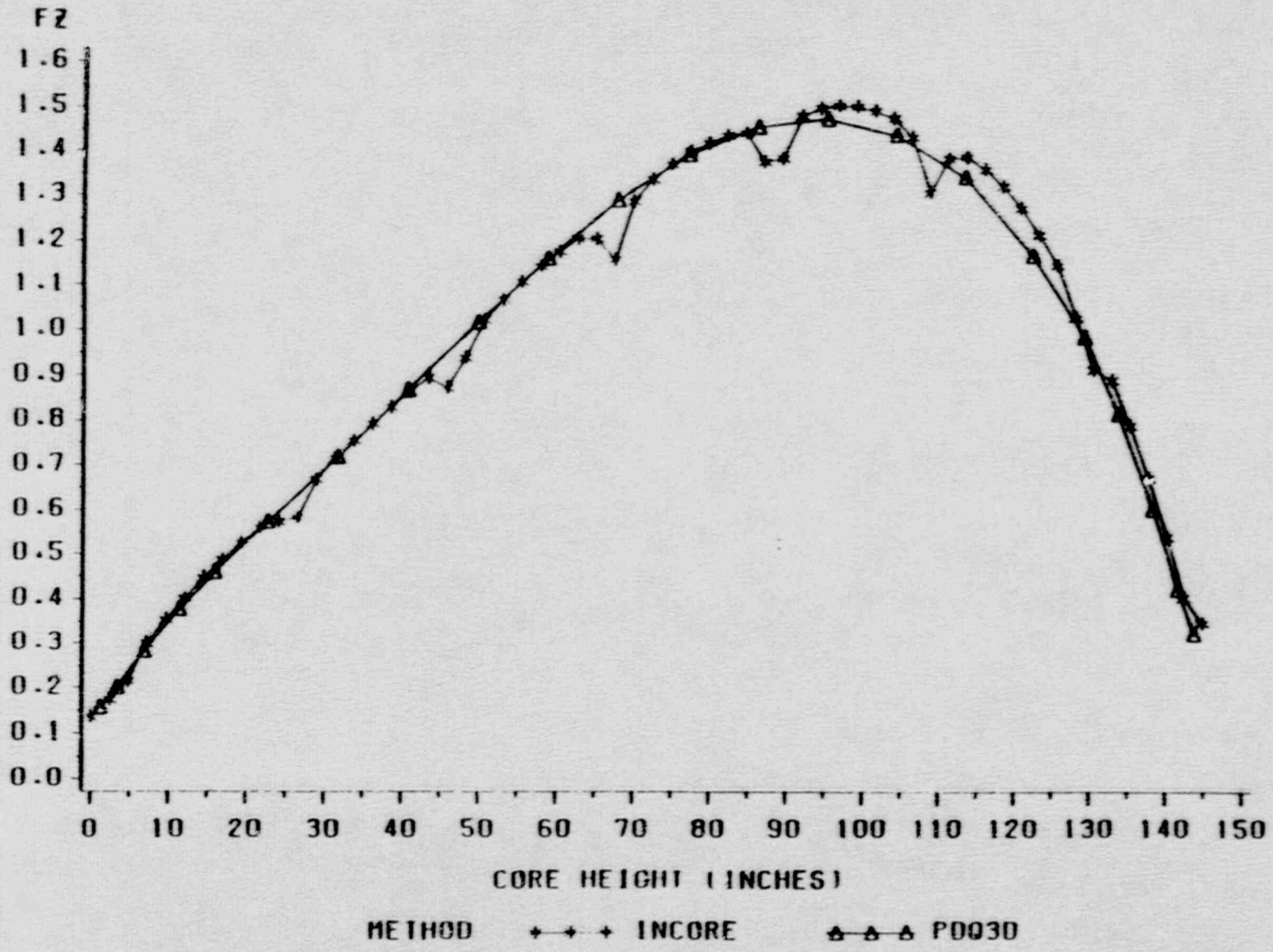
NORTH ANNA P(Z) COMPARISON
TWO ZONE PDQ3D RESULTS AND INCORE DATA
UNIT=N2C3 BURNUP=0
FZ
1.6
1.5
1.4
1.3
1.2
1.1
1.0
0.9
0.8
0.7
0.6
0.5
0.4
0.3
0.2
0.1
0.0
0
10
20
30
40
50
60
70
80
90
100
110
120
130
140
150
CORE HEIGHT (INCHES)
METHOD
INCORE
PDQ3D

FIGURE 3-32

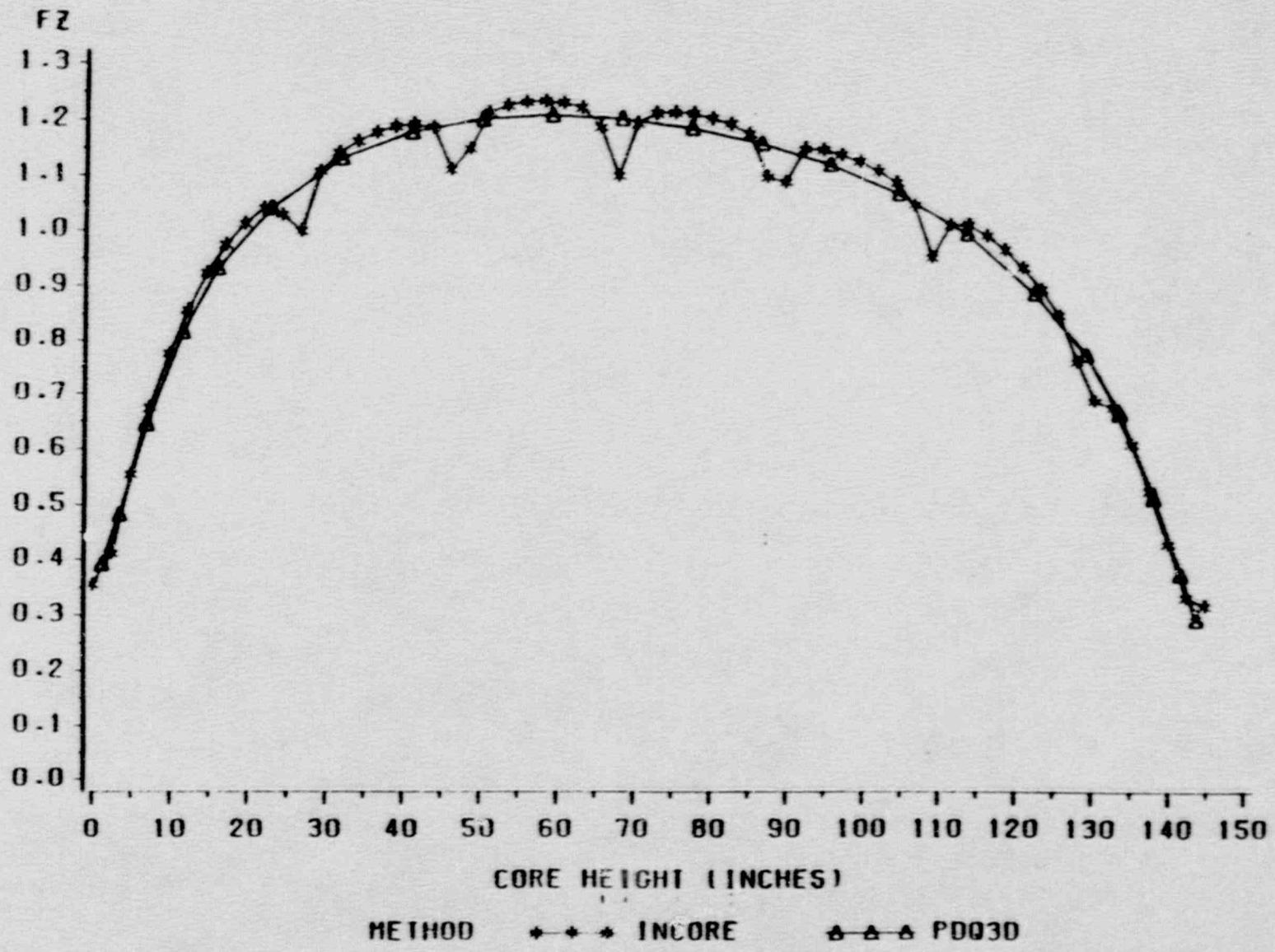
NORTH ANNA P(Z) COMPARISON
TWO ZONE PDQ3D RESULTS AND INCORE DATA
UNIT=N2C3 BURNUP=1566
FZ
1.3
1.2
1.1
1.0
0.9
0.8
0.7
0.6
0.5
0.4
0.3
0.2
0.1
0.0
0 10 20 30 40 50 60 70 80 90 100 110 120 130 140 150
CORE HEIGHT (INCHES)
METHOD * * * INCORE Δ Δ Δ PDQ3D

FIGURE 3-33

NORTH ANNA P(Z) COMPARISON

TWO ZONE PDQ3D RESULTS AND INCORE DATA
UNIT=N2C3 BURNUP=7647

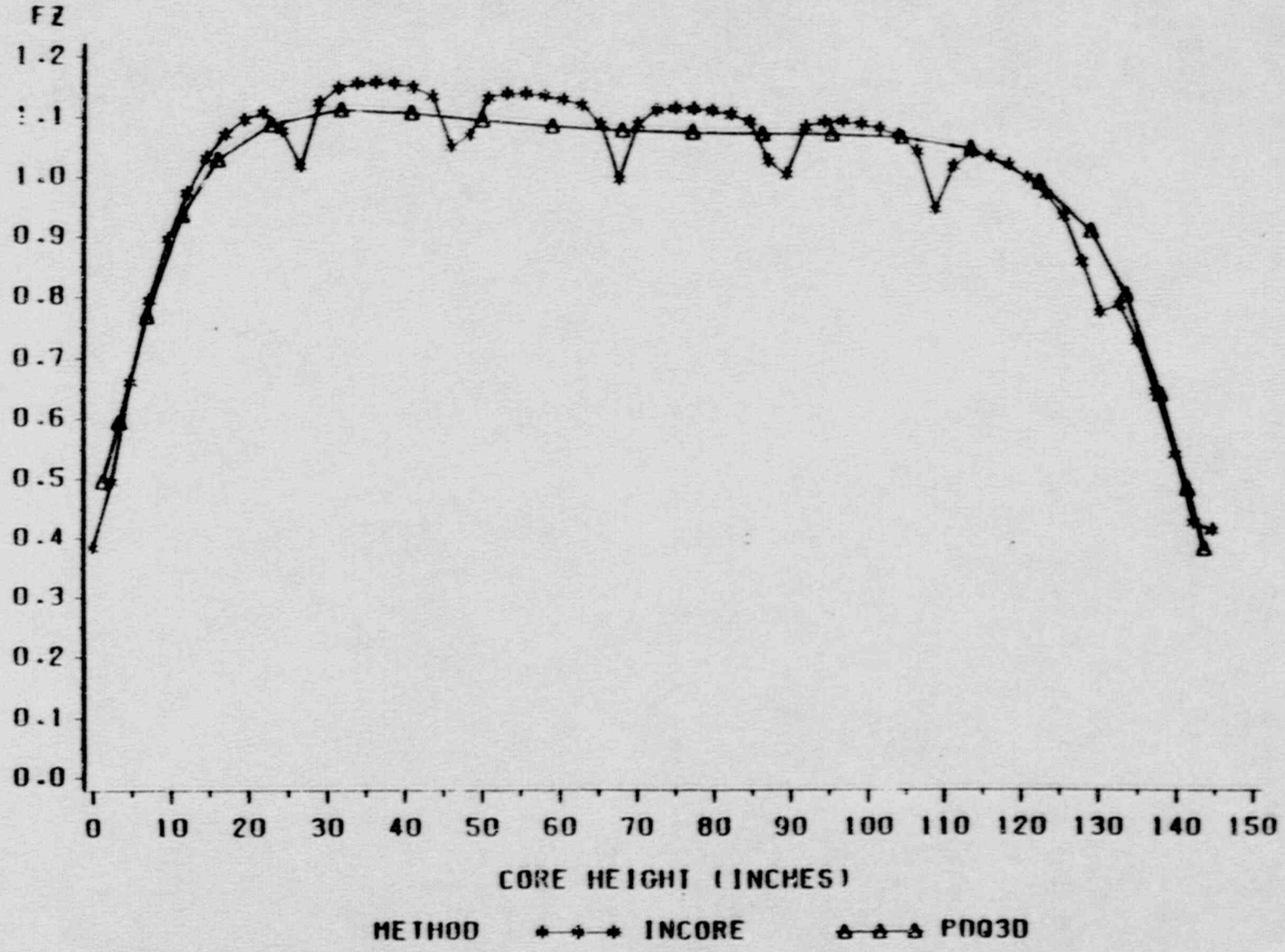

FIGURE 3-34

NORTH ANNA P(Z) COMPARISON

TWO ZONE PDQ3D RESULTS AND INCORE DATA
UNIT=N2C3 BURNUP=13040

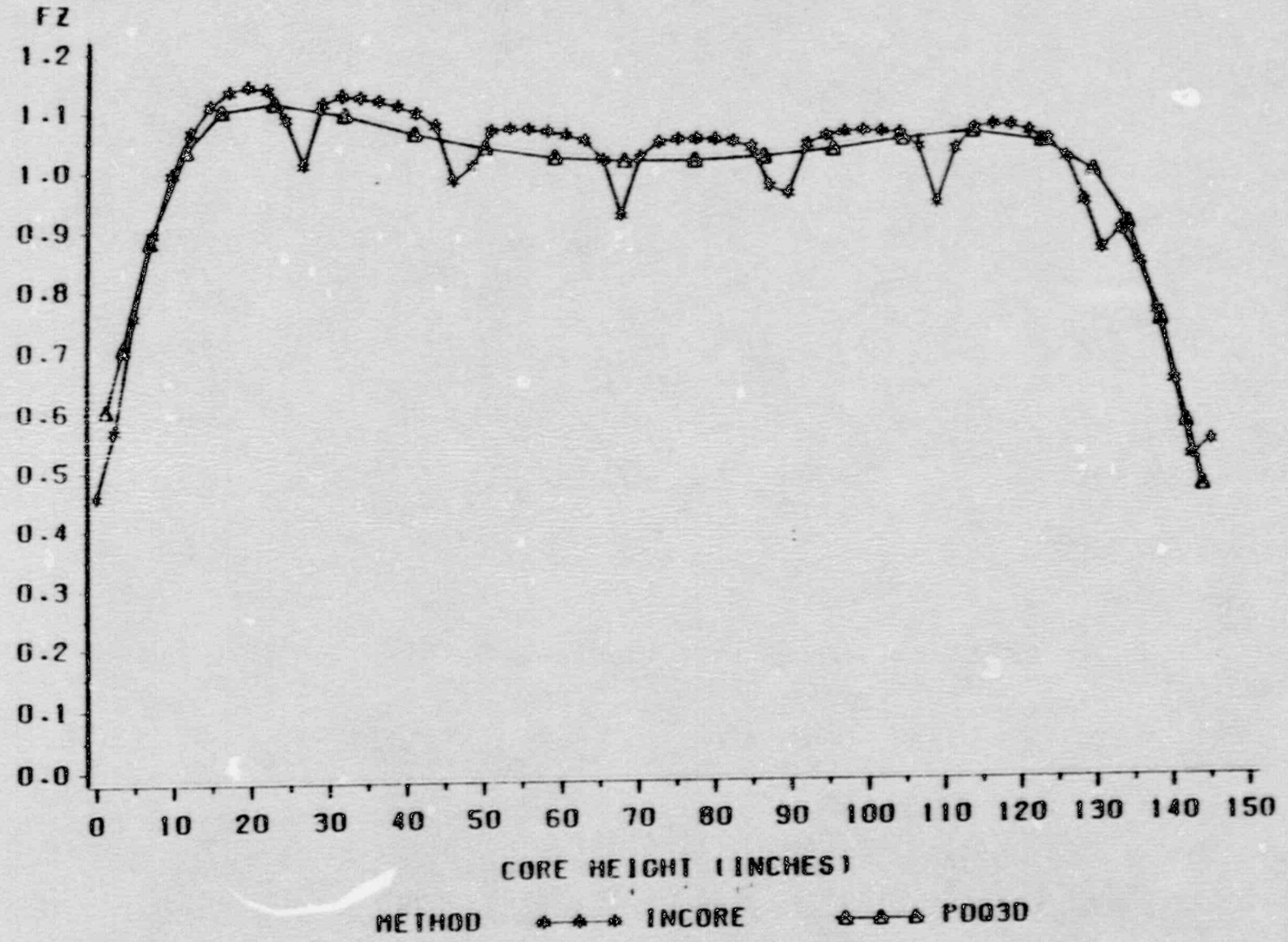

FIGURE 3-35

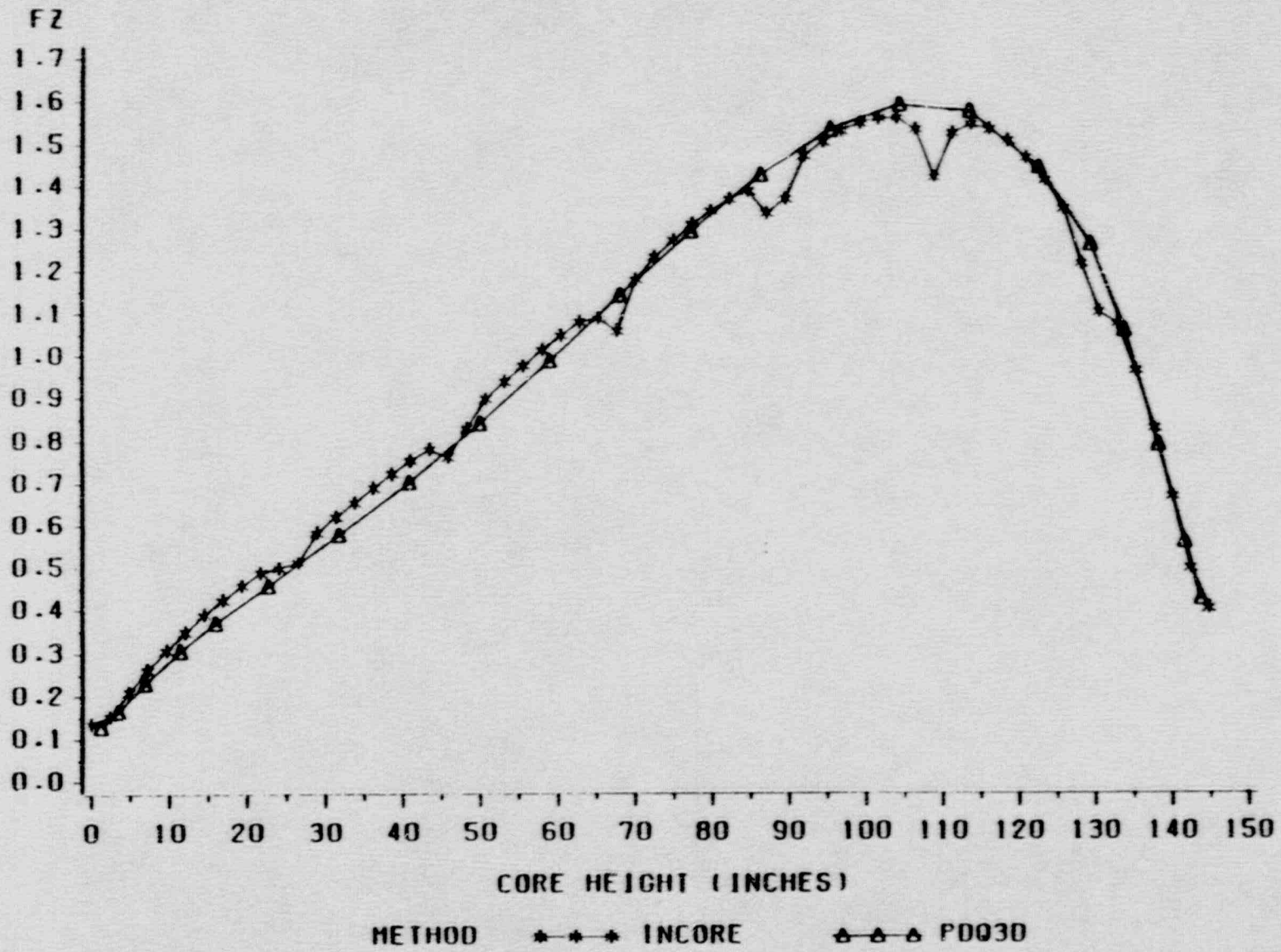
NORTH ANNA P(Z) COMPARISON
TWO ZONE PDQ3D RESULTS AND INCORE DATA
UNIT=N2C4 BURNUP=0
FZ
1.7
1.6
1.5
1.4
1.3
1.2
1.1
1.0
0.9
0.8
0.7
0.6
0.5
0.4
0.3
0.2
0.1
0.0
0
10
20
30
40
50
60
70
80
90
100
110
120
130
140
150
CORE HEIGHT (INCHES)
METHOD
INCORE
PDQ3D

FIGURE 3-36

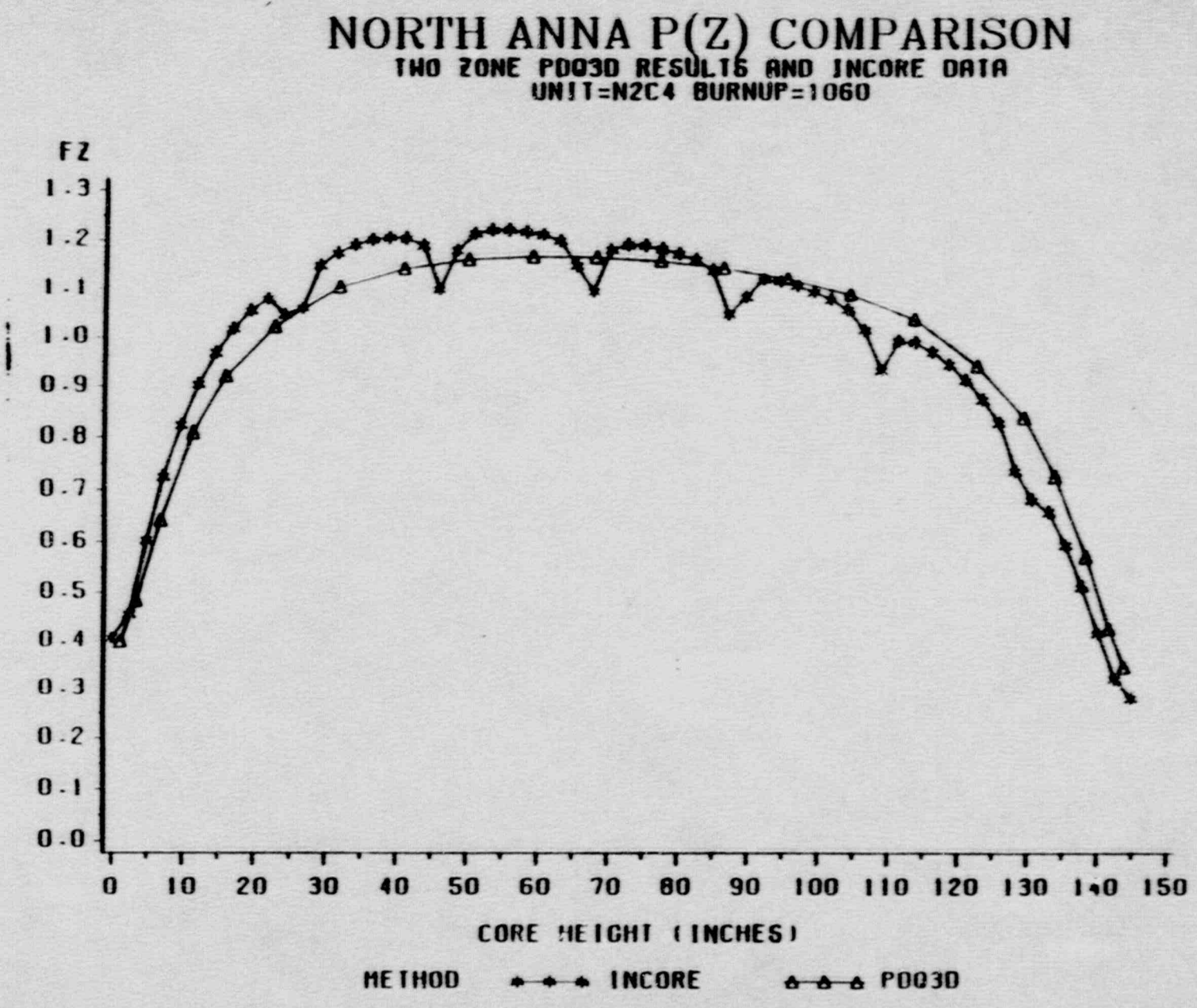
NORTH ANNA P(Z) COMPARISON
TWO ZONE PDQ3D RESULTS AND INCORE DATA
UNIT=N2C4 BURNUP=1060
FZ
1.3
1.2
1.1
1.0
0.9
0.8
0.7
0.6
0.5
0.4
0.3
0.2
0.1
0.0
0 10 20 30 40 50 60 70 80 90 100 110 120 130 140 150
CORE HEIGHT (INCHES)
METHOD INCORE PDQ3D

FIGURE 3-37

NORTH ANNA P(Z) COMPARISON

TWO ZONE PDQ3D RESULTS AND INCORE DATA
UNIT=N2C4 BURNUP=6610

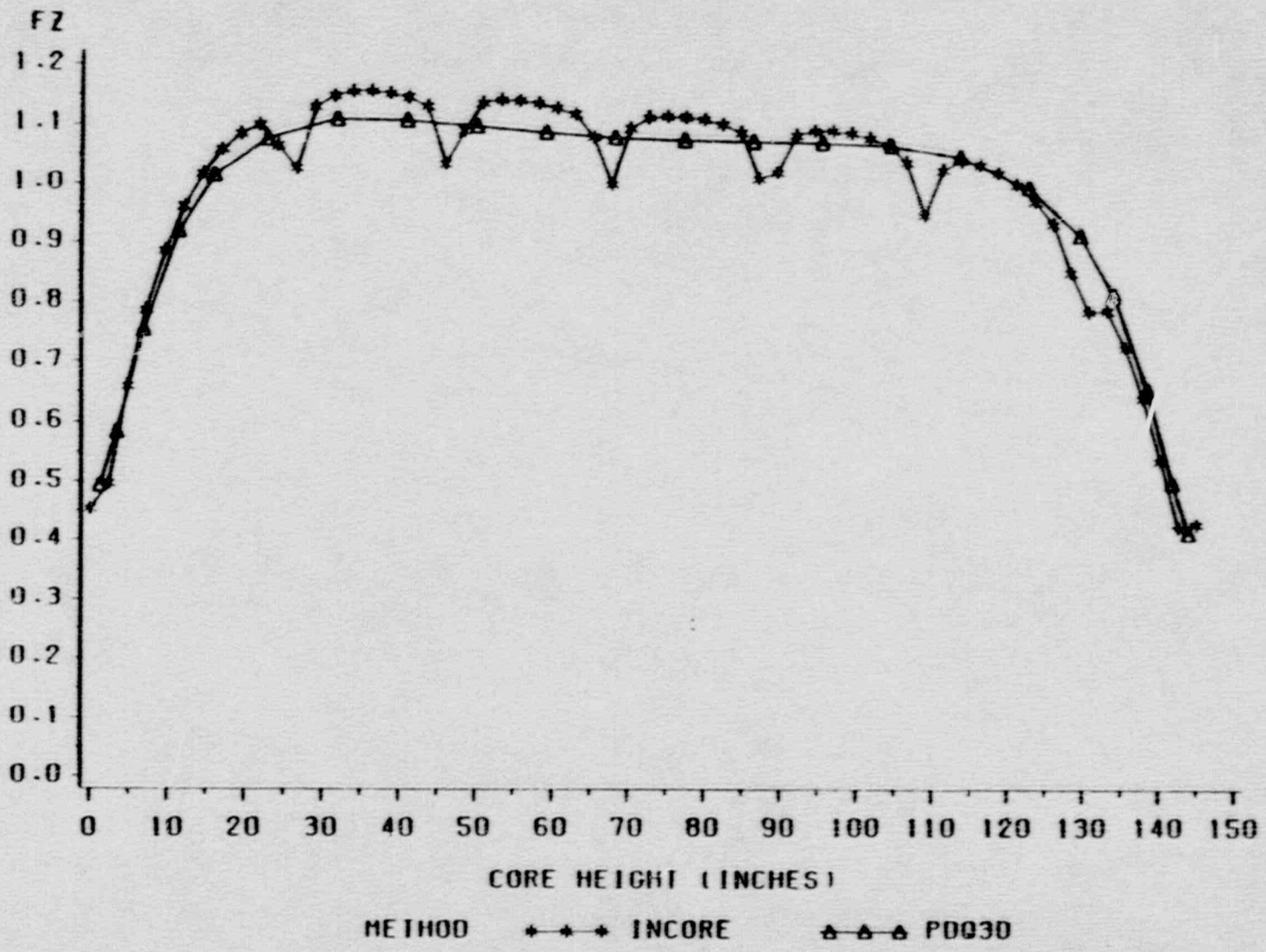

FIGURE 3-38

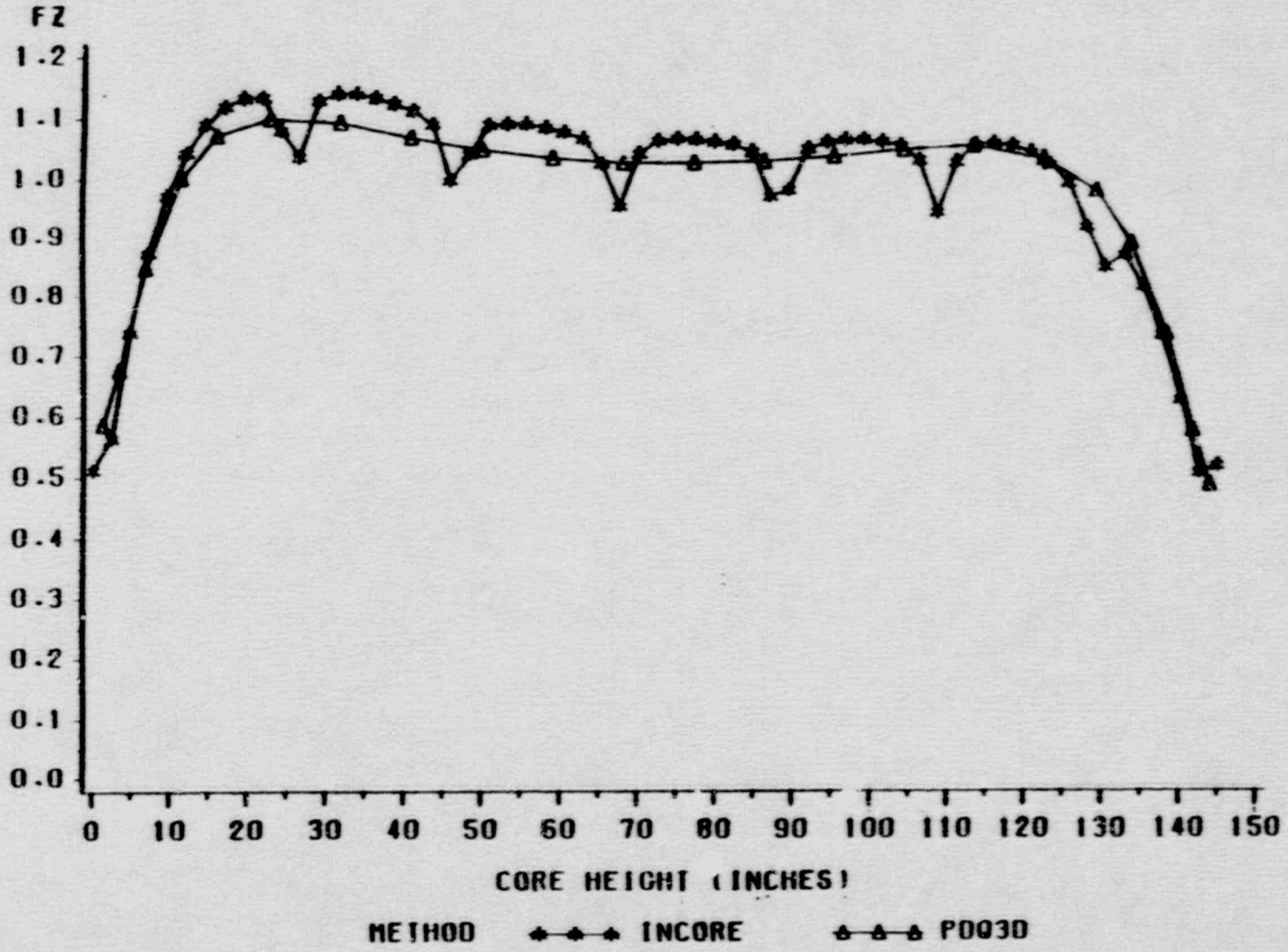
NORTH ANNA P(Z) COMPARISON
TWO ZONE PDQ3D RESULTS AND INCORE DATA
UNIT=N2C4 BURNUP=11267
FZ
1.2
1.1
1.0
0.9
0.8
0.7
0.6
0.5
0.4
0.3
0.2
0.1
0.0
0
10
20
30
40
50
60
70
80
90
100
110
120
130
140
150
CORE HEIGHT (INCHES)
METHOD
INCORE
PDQ3D

FIGURE 3-39

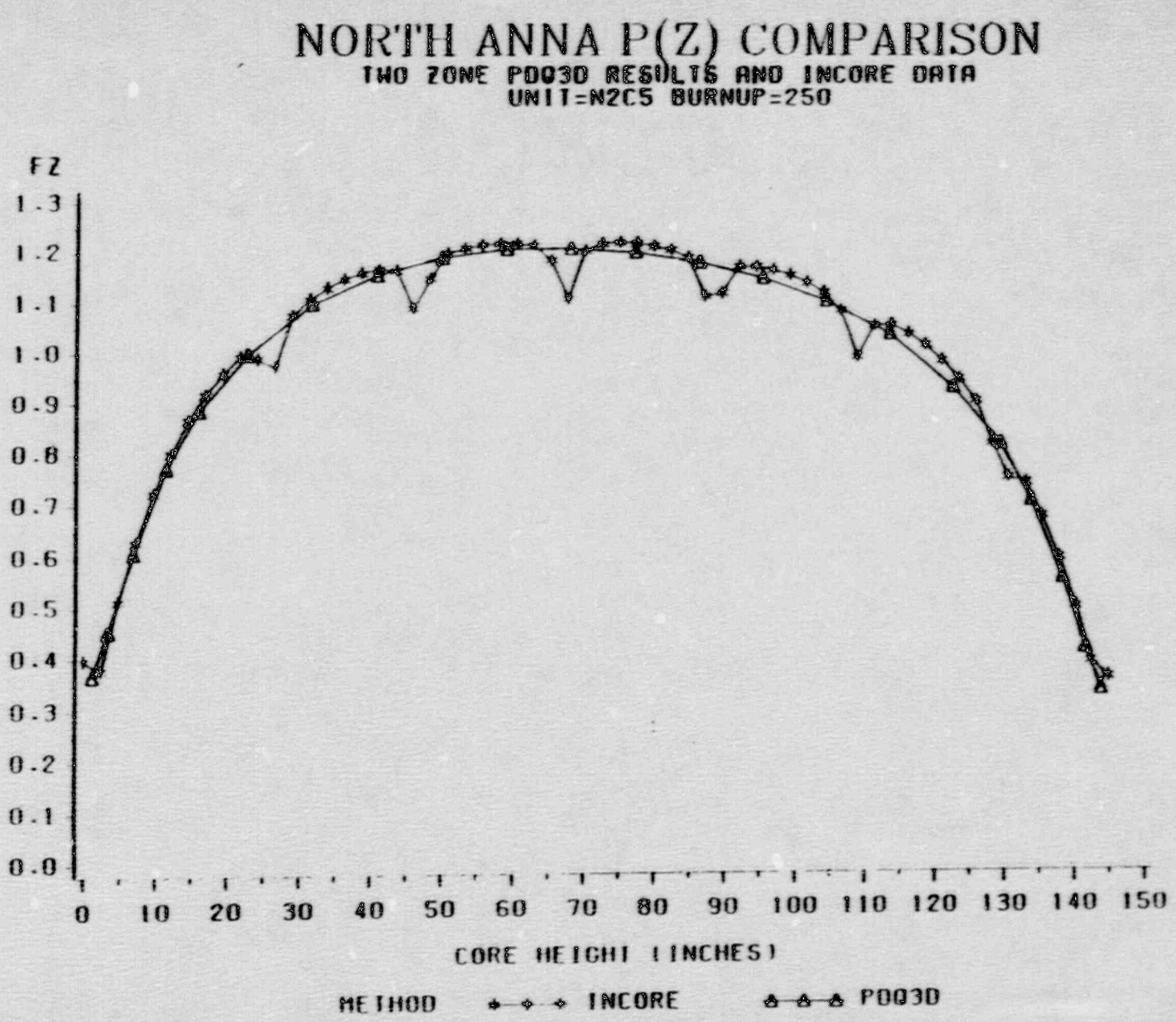
NORTH ANNA P(Z) COMPARISON
TWO ZONE P003D RESULTS AND INCORE DATA
UNIT=N2C5 BURNUP=250
FZ
1.3
1.2
1.1
1.0
0.9
0.8
0.7
0.6
0.5
0.4
0.3
0.2
0.1
0.0
0 10 20 30 40 50 60 70 80 90 100 110 120 130 140 150
CORE HEIGHT (INCHES)
METHOD INCORE P003D

FIGURE 3-40

NORTH ANNA P(Z) COMPARISON

TWO ZONE PDQ3D RESULTS AND INCORE DATA
UNIT=N2C5 BURNUP=6075

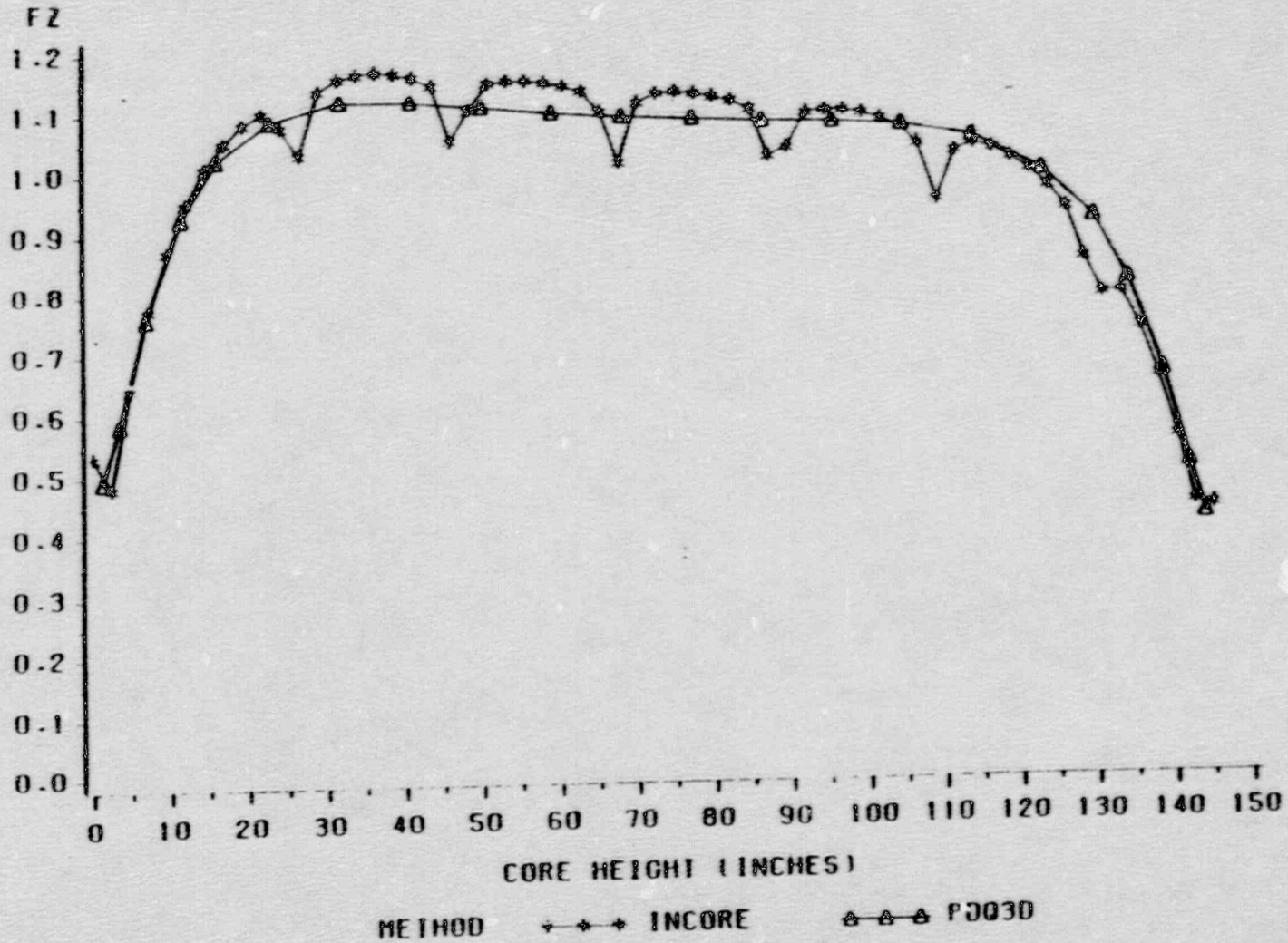

FIGURE 3-41

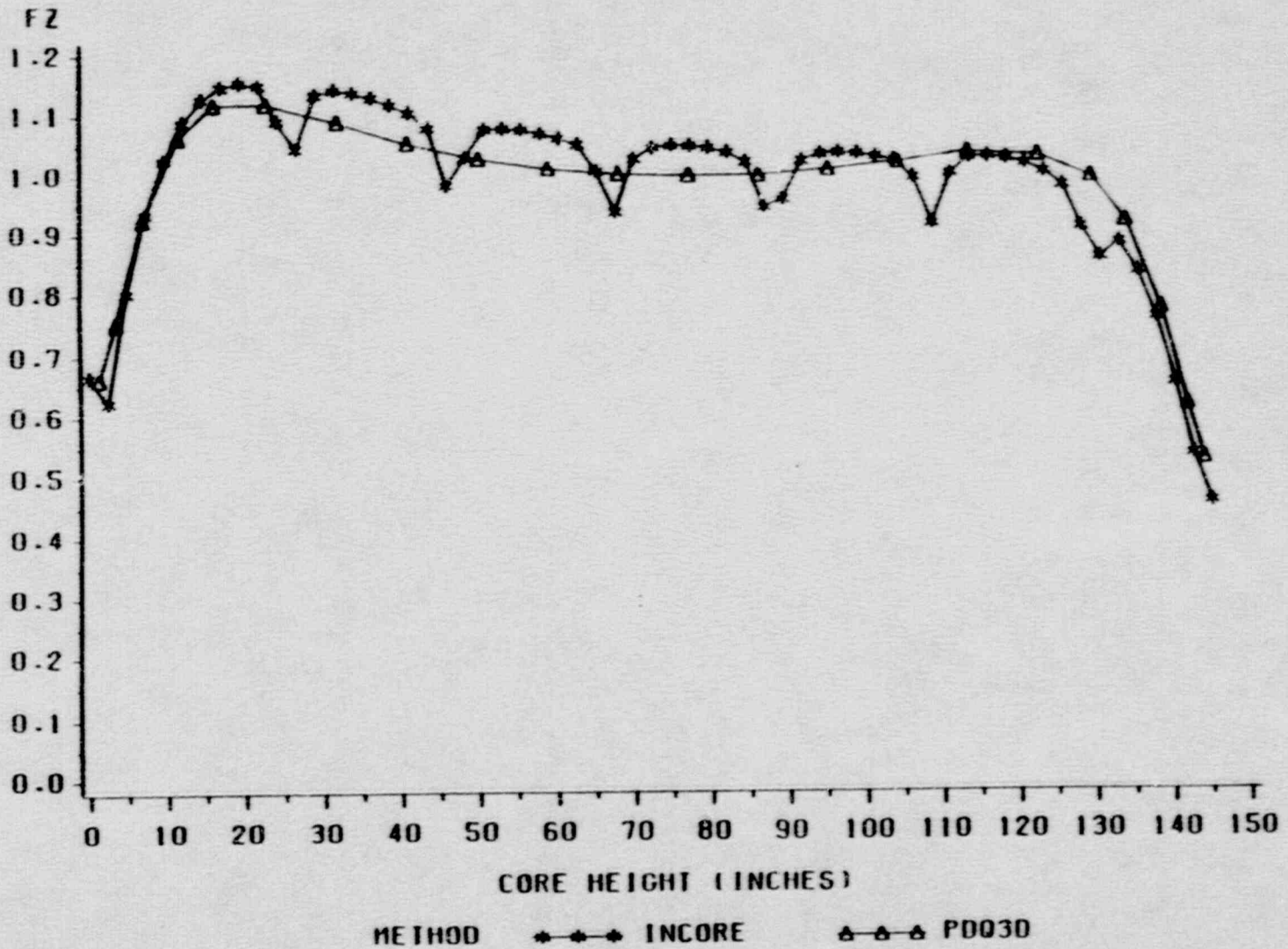
NORTH ANNA P(Z) COMPARISON
TWO ZONE PDQ3D RESULTS AND INCORE DATA
UNIT=N2C5 BURNUP=13671
FZ
1.2
1.1
1.0
0.9
0.8
0.7
0.6
0.5
0.4
0.3
0.2
0.1
0.0
0
10
20
30
40
50
60
70
80
90
100
110
120
130
140
150
CORE HEIGHT (INCHES)
METHOD
INCORE
PDQ3D

FIGURE 3-42

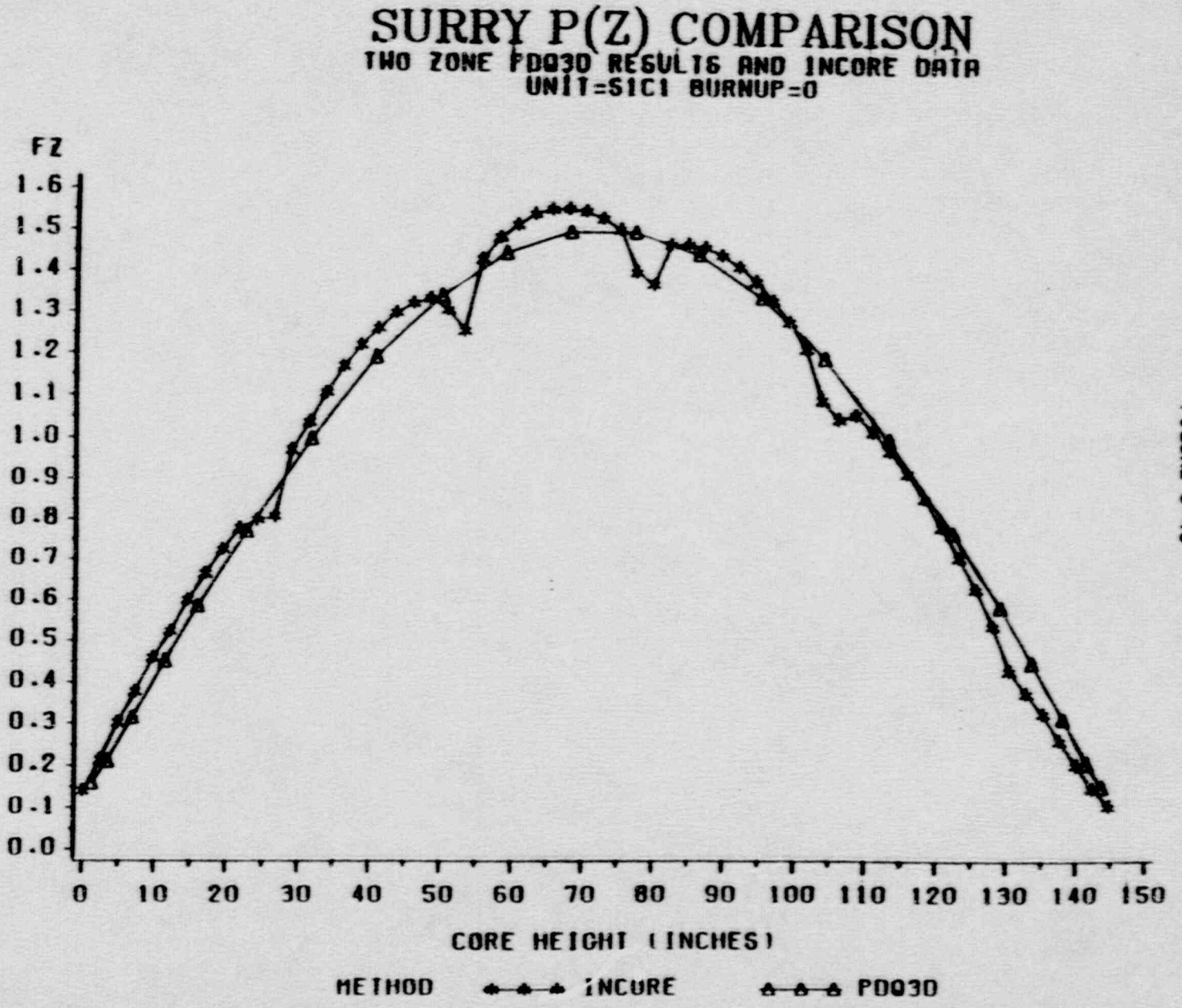
SURRY P(Z) COMPARISON
TWO ZONE PDQ3D RESULTS AND INCORE DATA
UNIT=SIC1 BURNUP=0
FZ
1.6
1.5
1.4
1.3
1.2
1.1
1.0
0.9
0.8
0.7
0.6
0.5
0.4
0.3
0.2
0.1
0.0
0
10
20
30
40
50
60
70
80
90
100
110
120
130
140
150
CORE HEIGHT (INCHES)
METHOD
INCORE
PDQ3D

FIGURE 3-43

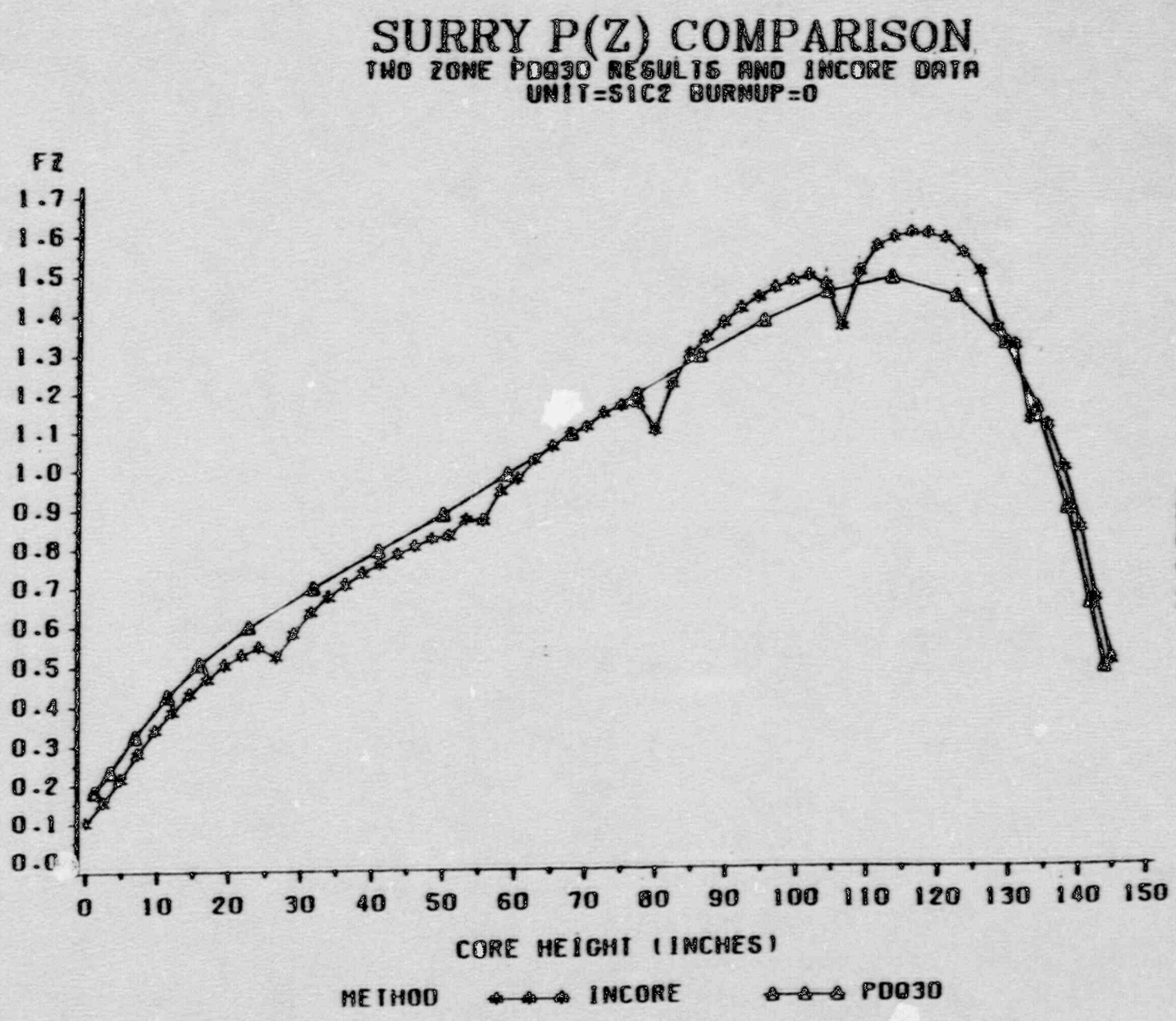
SURRY P(Z) COMPARISON
TWO ZONE PDQ3D RESULTS AND INCORE DATA
UNIT=S1C2 BURNUP=0
FZ
1.7
1.6
1.5
1.4
1.3
1.2
1.1
1.0
0.9
0.8
0.7
0.6
0.5
0.4
0.3
0.2
0.1
0.0
0 10 20 30 40 50 60 70 80 90 100 110 120 130 140 150
CORE HEIGHT (INCHES)
METHOD INCORE PDQ3D

FIGURE 3-44

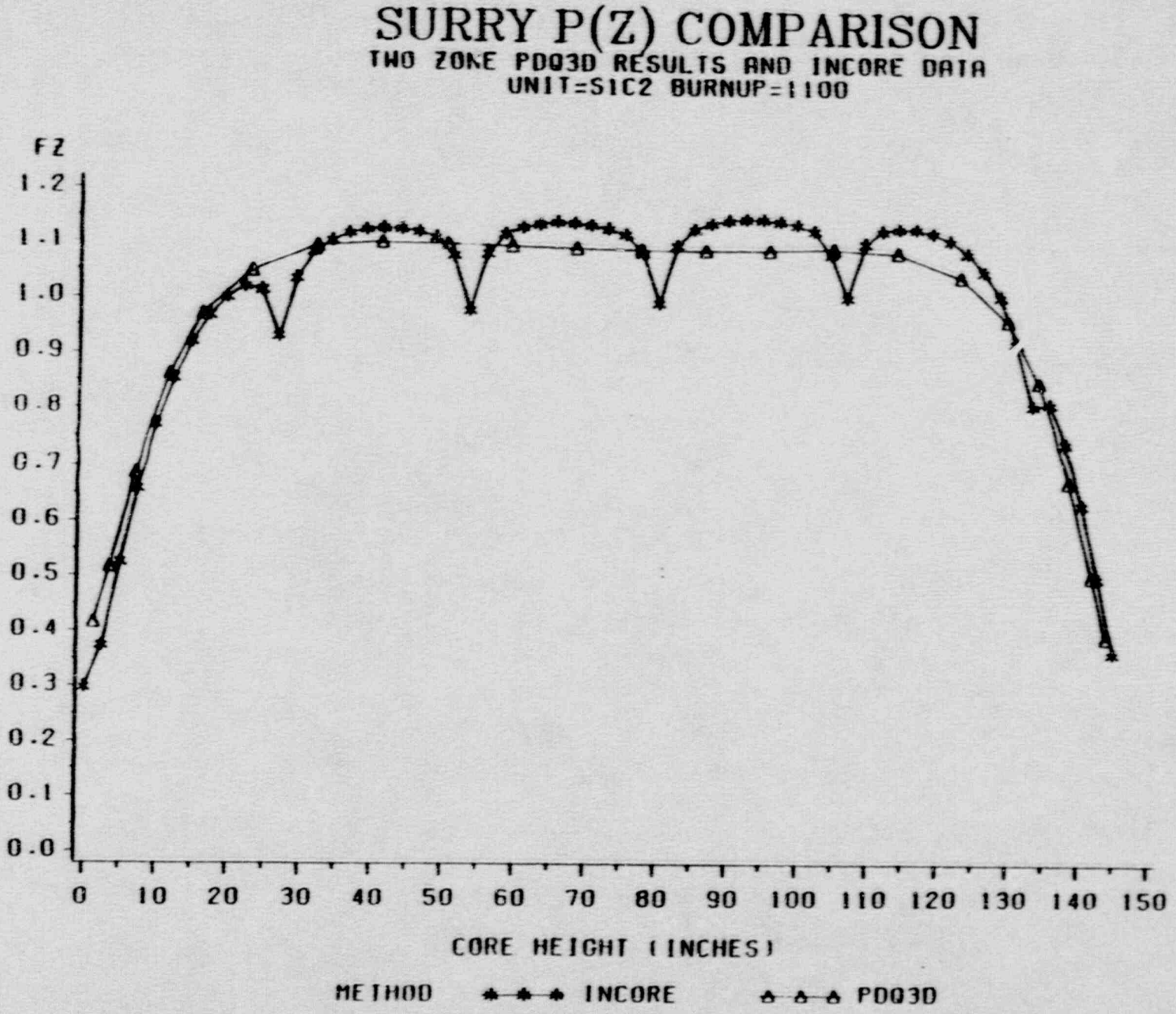
SURRY P(Z) COMPARISON
TWO ZONE PDQ3D RESULTS AND INCORE DATA
UNIT=S1C2 BURNUP=1100
FZ
1.2
1.1
1.0
0.9
0.8
0.7
0.6
0.5
0.4
0.3
0.2
0.1
0.0
0
10
20
30
40
50
60
70
80
90
100
110
120
130
140
150
CORE HEIGHT (INCHES)
METHOD
INCORE
PDQ3D

FIGURE 3-45

SURRY P(Z) COMPARISON

TWO ZONE PDQ3D RESULTS AND INCORE DATA
UNIT=S1C2 BURNUP=4050

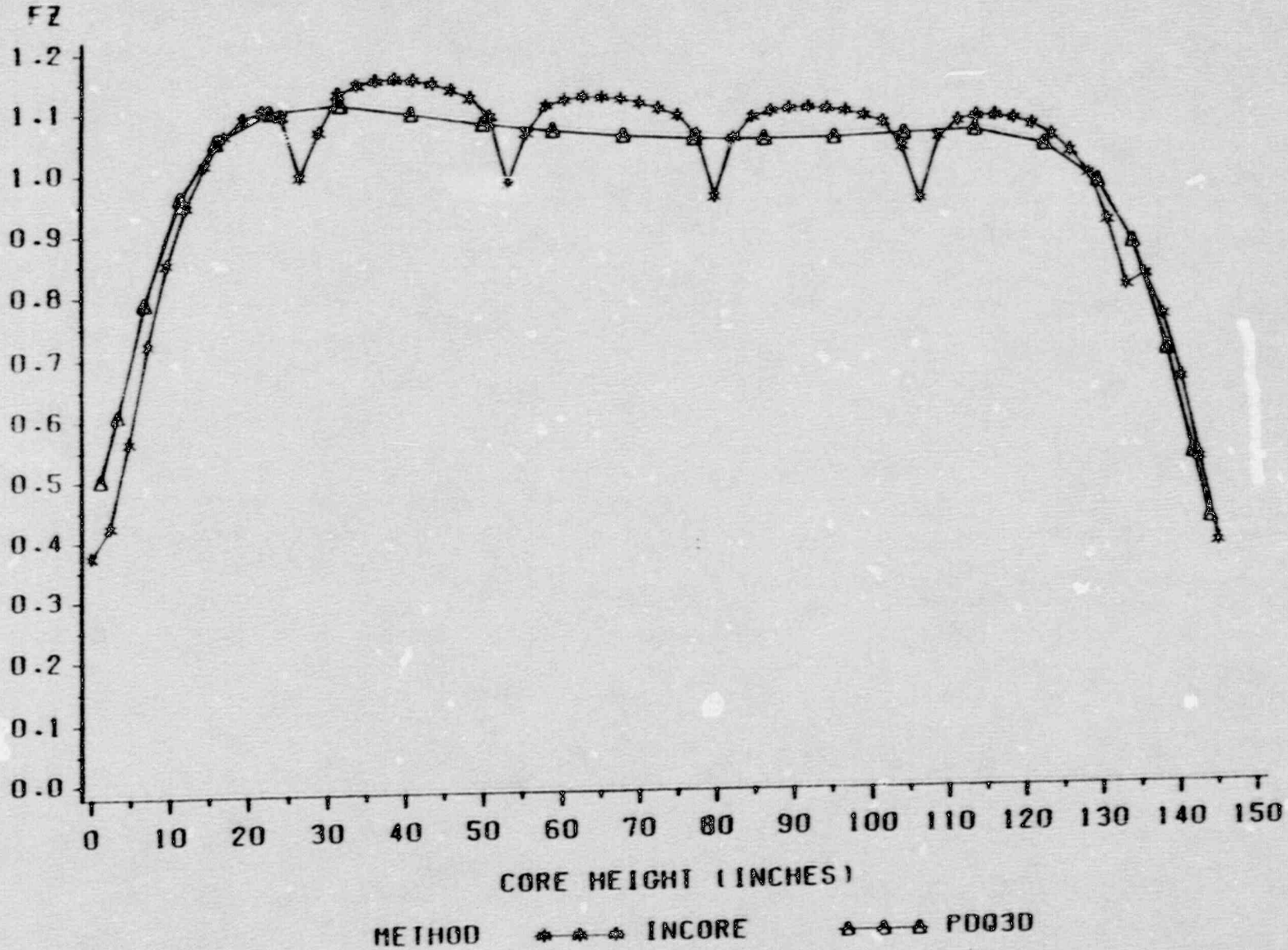

FIGURE 3-46

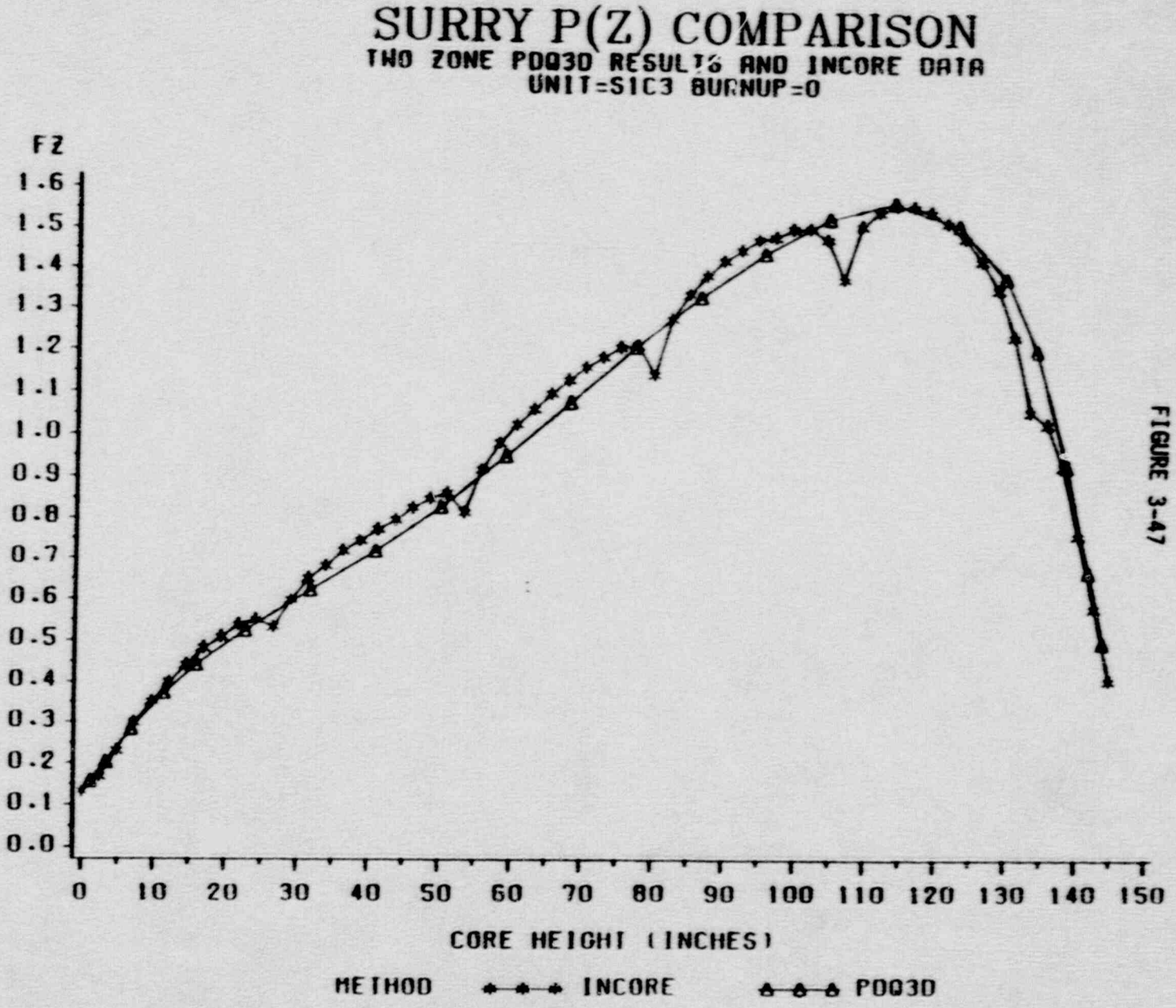
SURRY P(Z) COMPARISON
TWO ZONE PDQ3D RESULTS AND INCORE DATA
UNIT=S1C3 BURNUP=0
FZ
1.6
1.5
1.4
1.3
1.2
1.1
1.0
0.9
0.8
0.7
0.6
0.5
0.4
0.3
0.2
0.1
0.0
0
10
20
30
40
50
60
70
80
90
100
110
120
130
140
150
CORE HEIGHT (INCHES)
METHOD
INCORE
PDQ3D

FIGURE 3-47

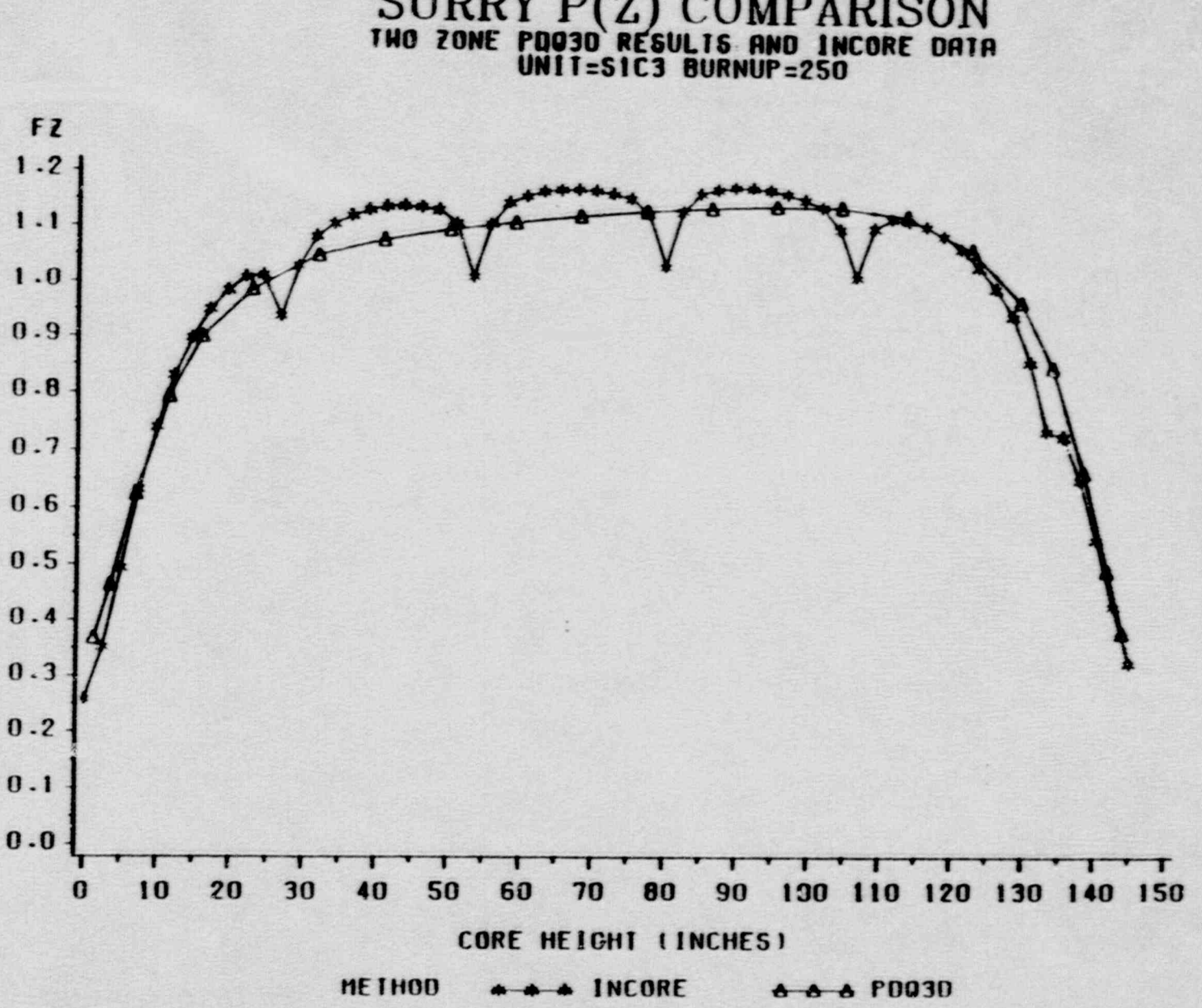
SURRY P(Z) COMPARISON
TWO ZONE PDQ3D RESULTS AND INCORE DATA
UNIT=S1C3 BURNUP=250
FZ
1.2
1.1
1.0
0.9
0.8
0.7
0.6
0.5
0.4
0.3
0.2
0.1
0.0
0 10 20 30 40 50 60 70 80 90 100 110 120 130 140 150
CORE HEIGHT (INCHES)
METHOD INCORE PDQ3D

FIGURE 3-48

SURRY P(Z) COMPARISON

TWO ZONE PDQ3D RESULTS AND INCORE DATA
UNIT=S1C3 BURNUP=7175

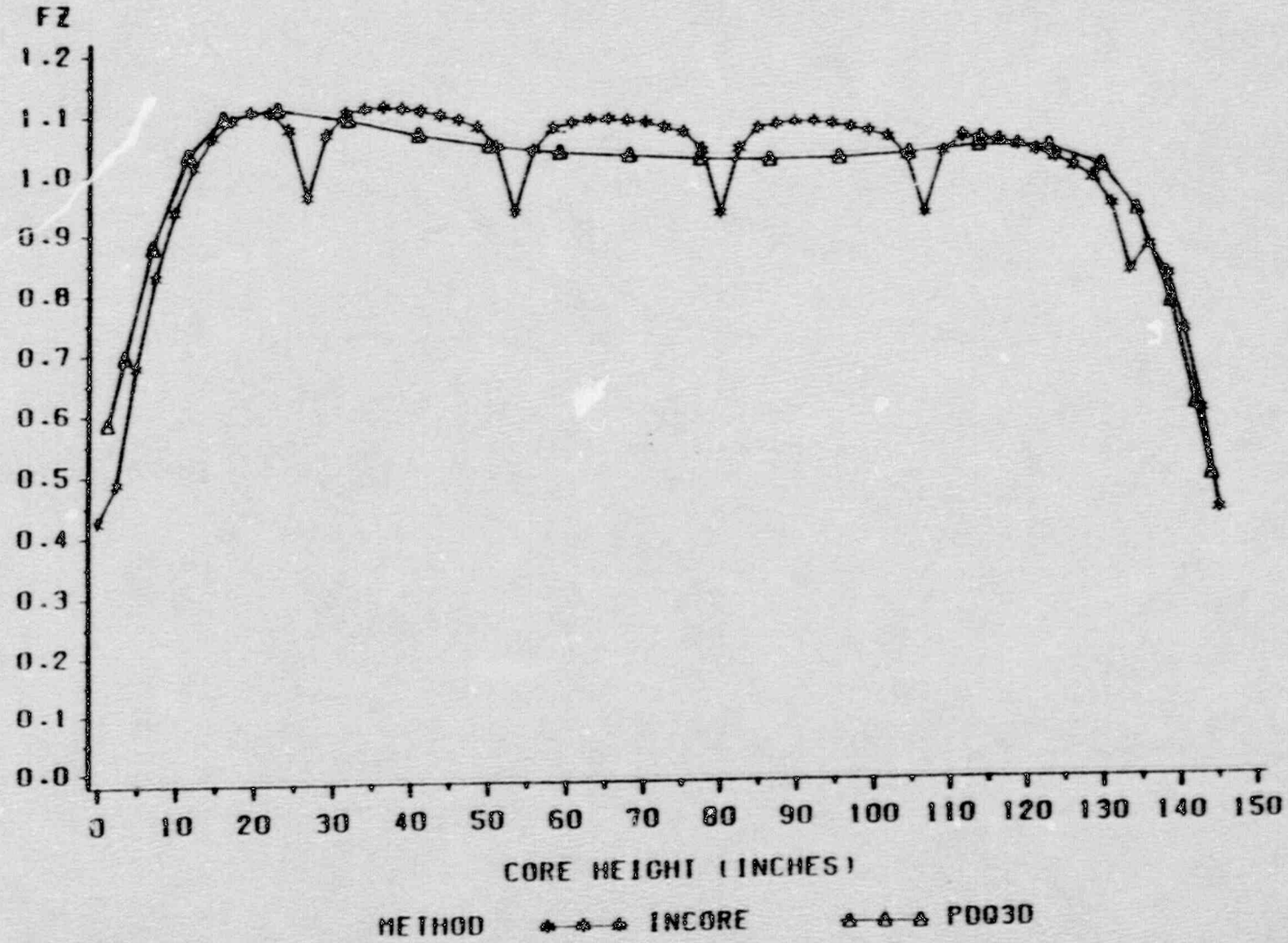

FIGURE 3-49

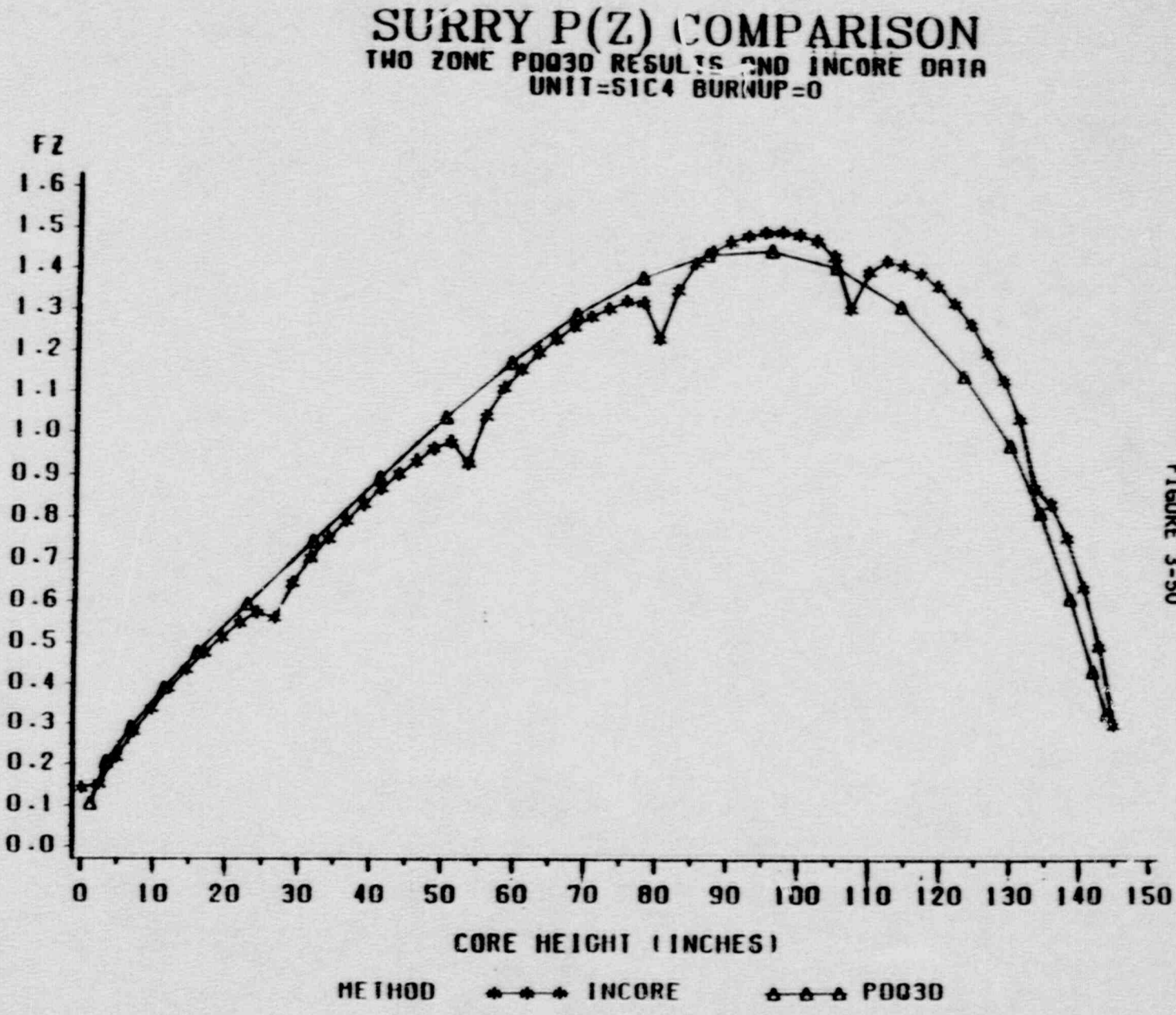
SURRY P(Z) COMPARISON
TWO ZONE PDQ3D RESULTS AND INCORE DATA
UNIT=S1C4 BURNUP=0
FZ
1.6
1.5
1.4
1.3
1.2
1.1
1.0
0.9
0.8
0.7
0.6
0.5
0.4
0.3
0.2
0.1
0.0
0 10 20 30 40 50 60 70 80 90 100 110 120 130 140 150
CORE HEIGHT (INCHES)
METHOD INCORE PDQ3D

FIGURE 3-50

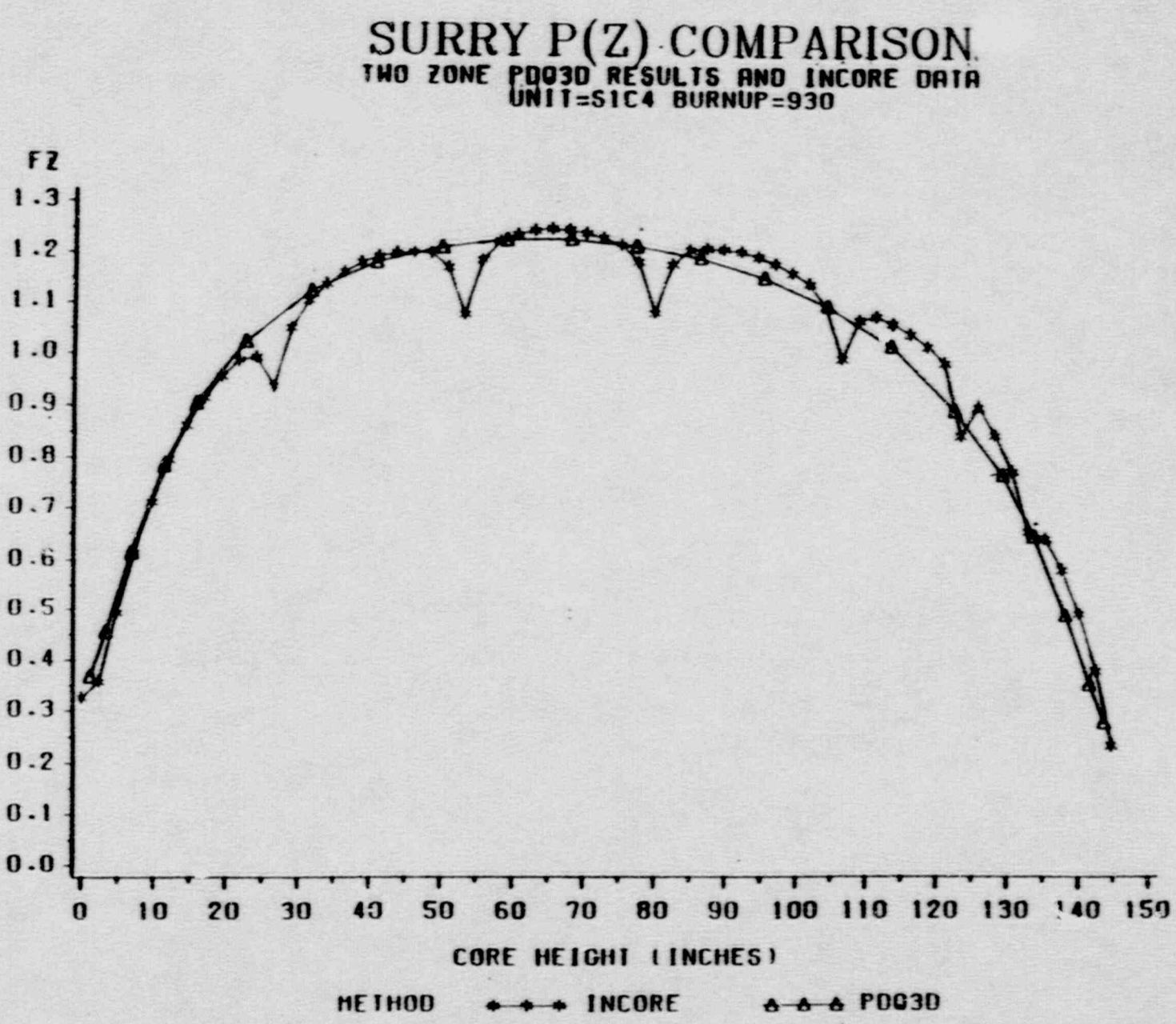
SURRY P(Z) COMPARISON
TWO ZONE PDQ3D RESULTS AND INCORE DATA
UNIT=S1C4 BURNUP=930
FZ
1.3
1.2
1.1
1.0
0.9
0.8
0.7
0.6
0.5
0.4
0.3
0.2
0.1
0.0
0 10 20 30 40 50 60 70 80 90 100 110 120 130 140 150
CORE HEIGHT (INCHES)
METHOD INCORE PDQ3D

FIGURE 3-51

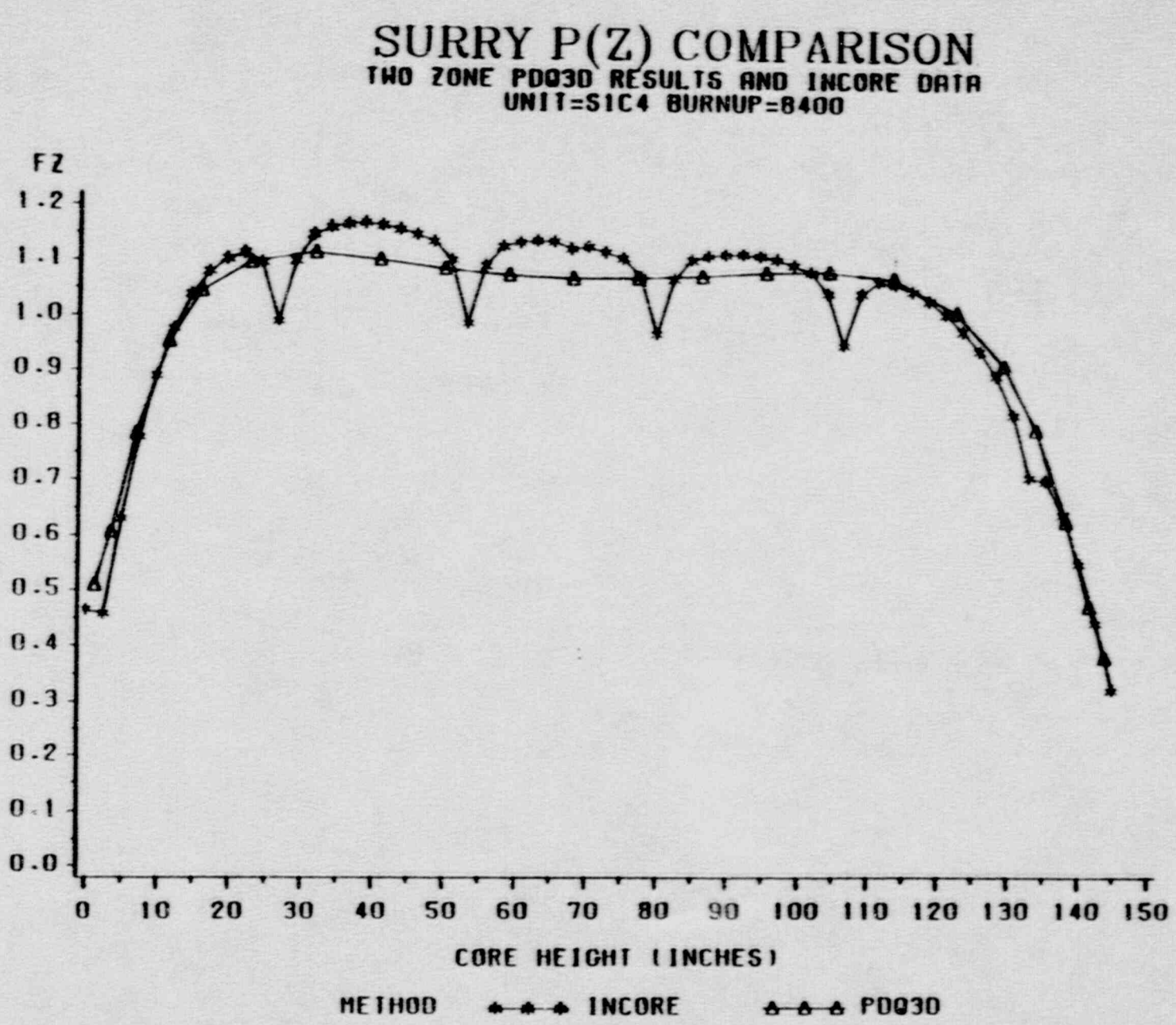
SURRY P(Z) COMPARISON
TWO ZONE PDQ3D RESULTS AND INCORE DATA
UNIT=S1C4 BURNUP=8400
FZ
1.2
1.1
1.0
0.9
0.8
0.7
0.6
0.5
0.4
0.3
0.2
0.1
0.0
0
10
20
30
40
50
60
70
80
90
100
110
120
130
140
150
CORE HEIGHT (INCHES)
METHOD
INCORE
PDQ3D

FIGURE 3-52

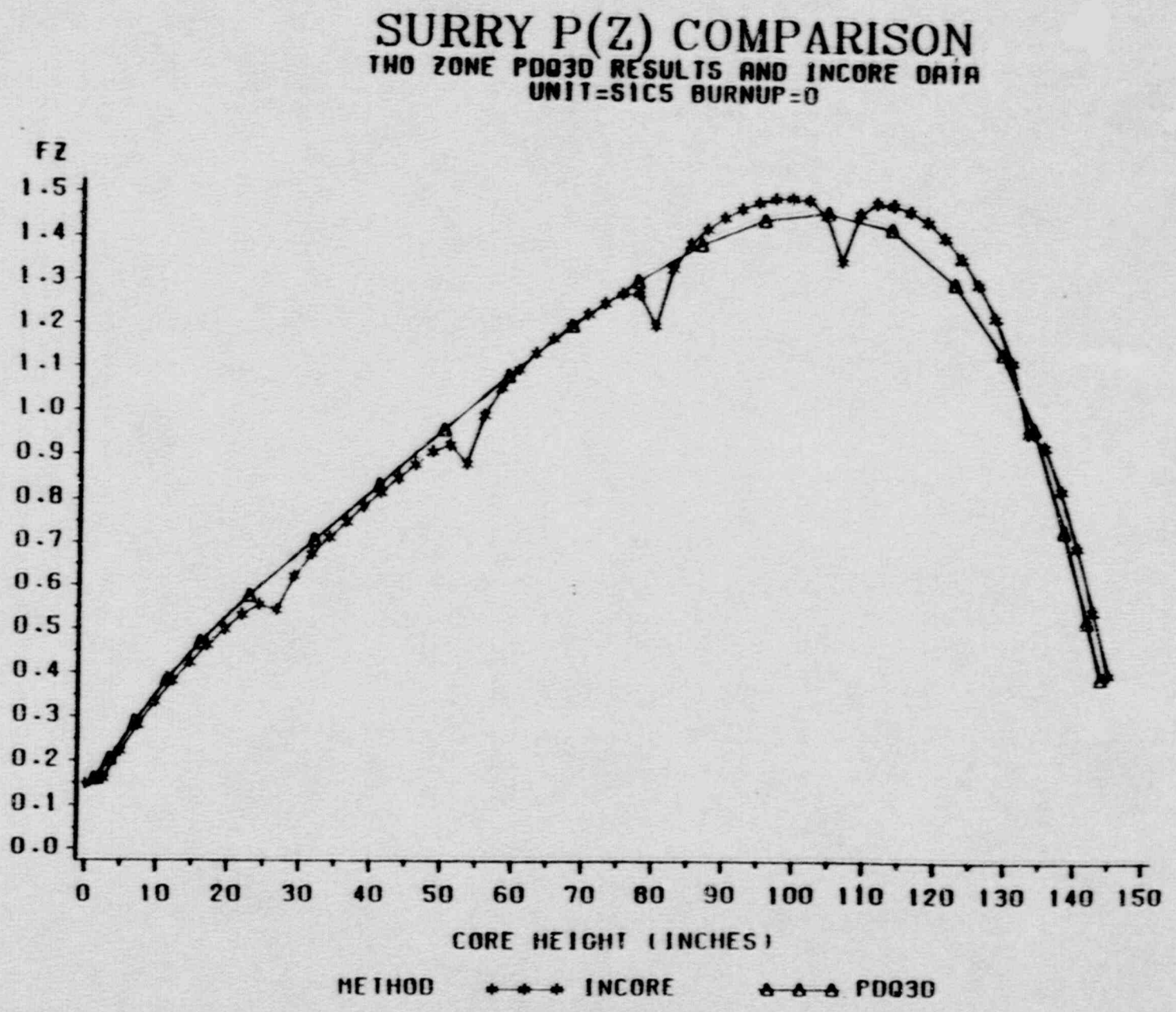
SURRY P(Z) COMPARISON
TWO ZONE PDQ3D RESULTS AND INCORE DATA
UNIT=SIC5 BURNUP=0
FZ
1.5
1.4
1.3
1.2
1.1
1.0
0.9
0.8
0.7
0.6
0.5
0.4
0.3
0.2
0.1
0.0
0
10
20
30
40
50
60
70
80
90
100
110
120
130
140
150
CORE HEIGHT (INCHES)
METHOD
INCORE
PDQ3D

FIGURE 3-53

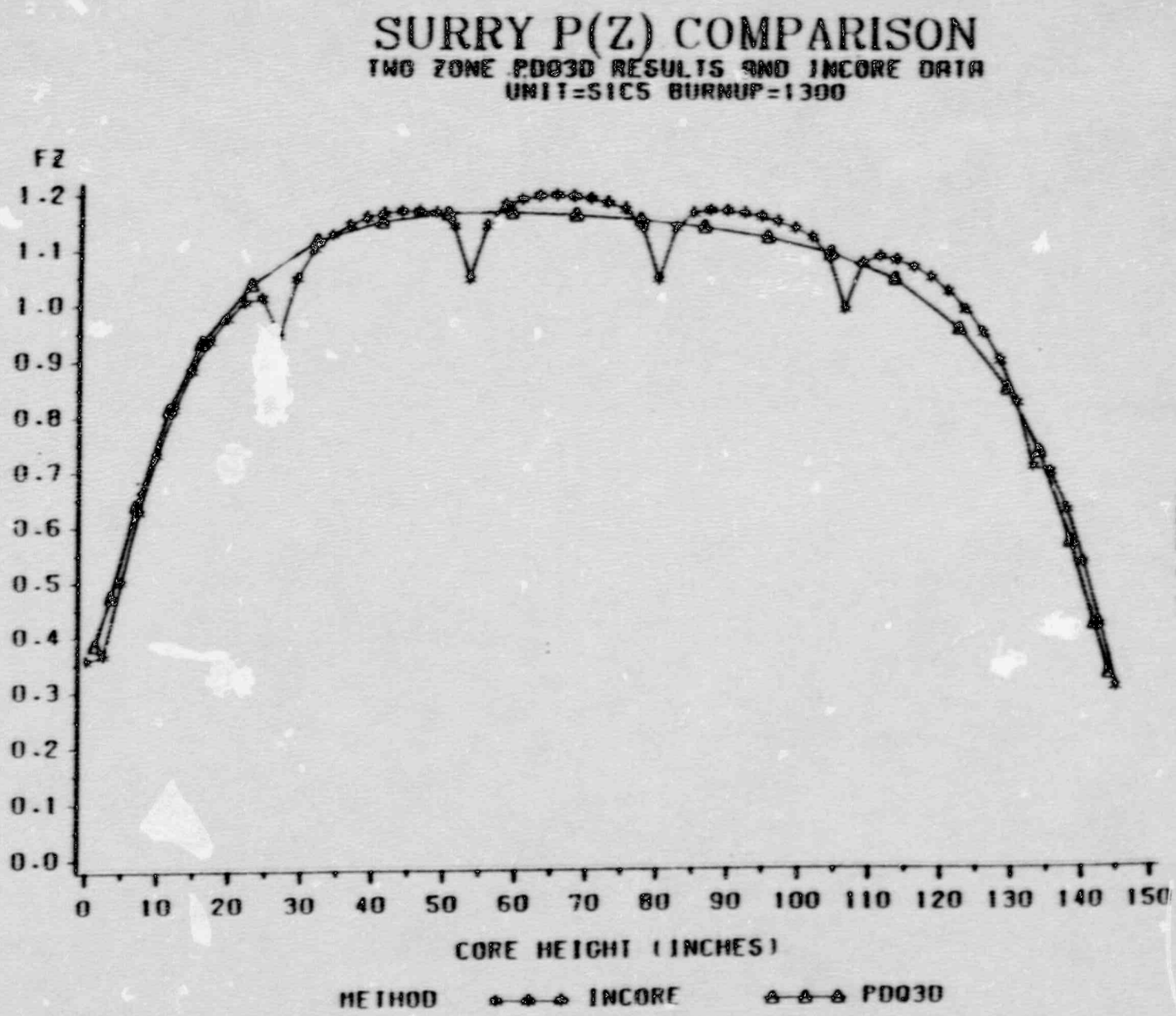
SURRY P(Z) COMPARISON
TWO ZONE PDQ3D RESULTS AND INCORE DATA
UNIT=SIC5 BURNUP=1300
FZ
1.2
1.1
1.0
0.9
0.8
0.7
0.6
0.5
0.4
0.3
0.2
0.1
0.0
0
10
20
30
40
50
60
70
80
90
100
110
120
130
140
150
CORE HEIGHT (INCHES)
METHOD
INCORE
PDQ3D

FIGURE 3-54

SURRY P(Z) COMPARISON

TWO ZONE PDQ3D RESULTS AND INCORE DATA
UNIT=SICS BURNUP=7411

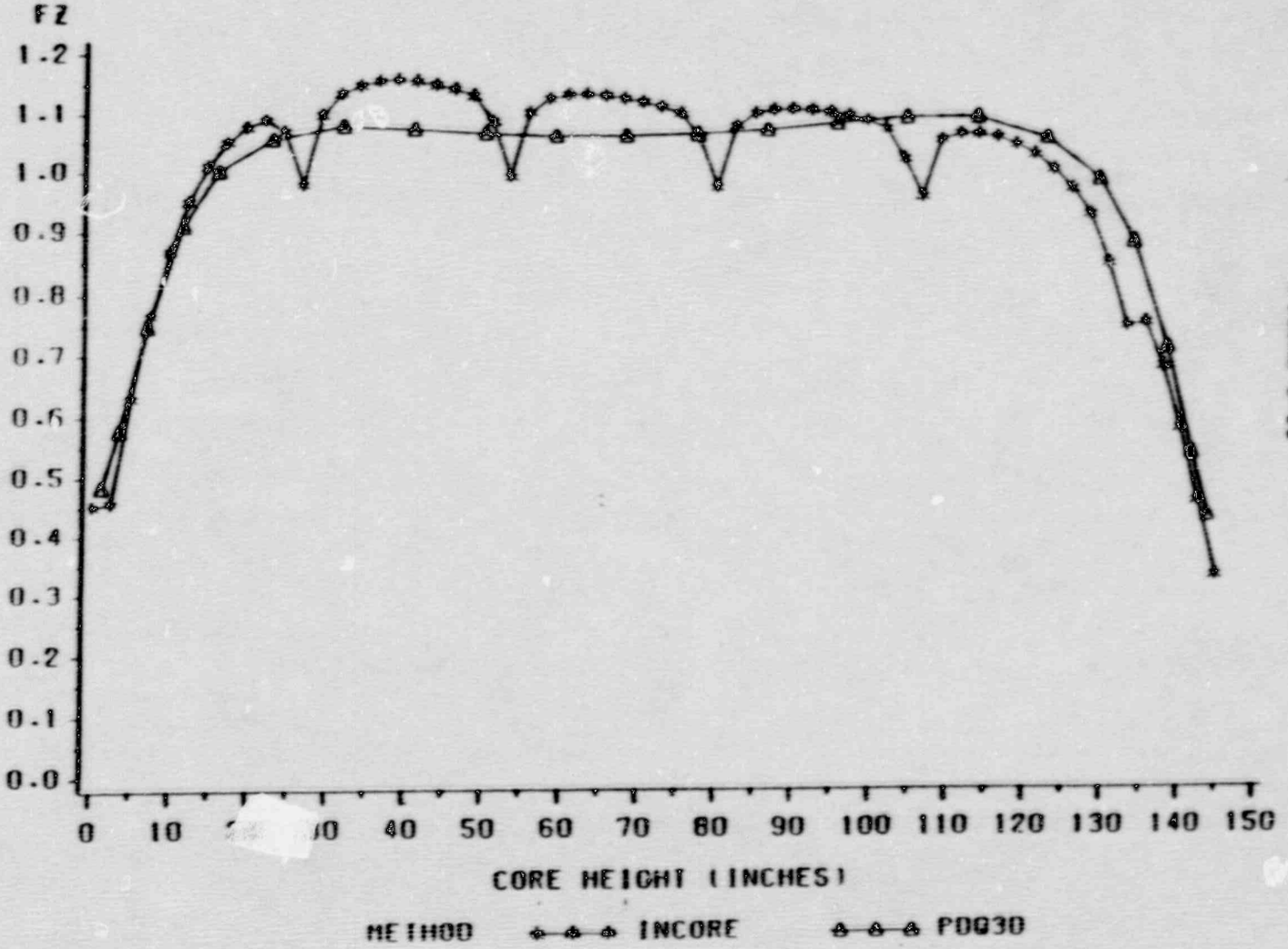

FIGURE 3-55

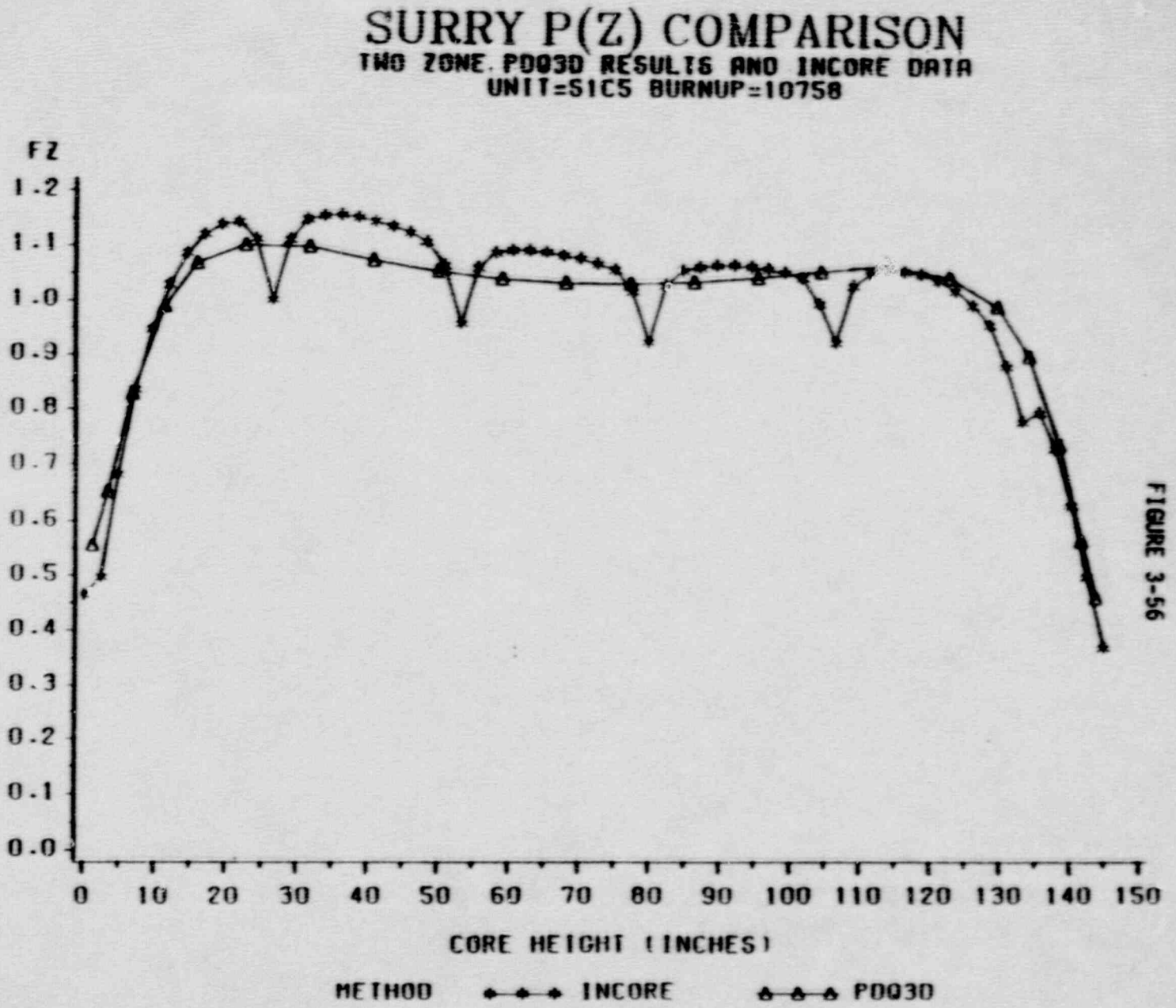
SURRY P(Z) COMPARISON
TWO ZONE PDQ3D RESULTS AND INCORE DATA
UNIT=S1C5 BURNUP=10758
FZ
1.2
1.1
1.0
0.9
0.8
0.7
0.6
0.5
0.4
0.3
0.2
0.1
0.0
0 10 20 30 40 50 60 70 80 90 100 110 120 130 140 150
CORE HEIGHT (INCHES)
METHOD INCORE PDQ3D

FIGURE 3-56

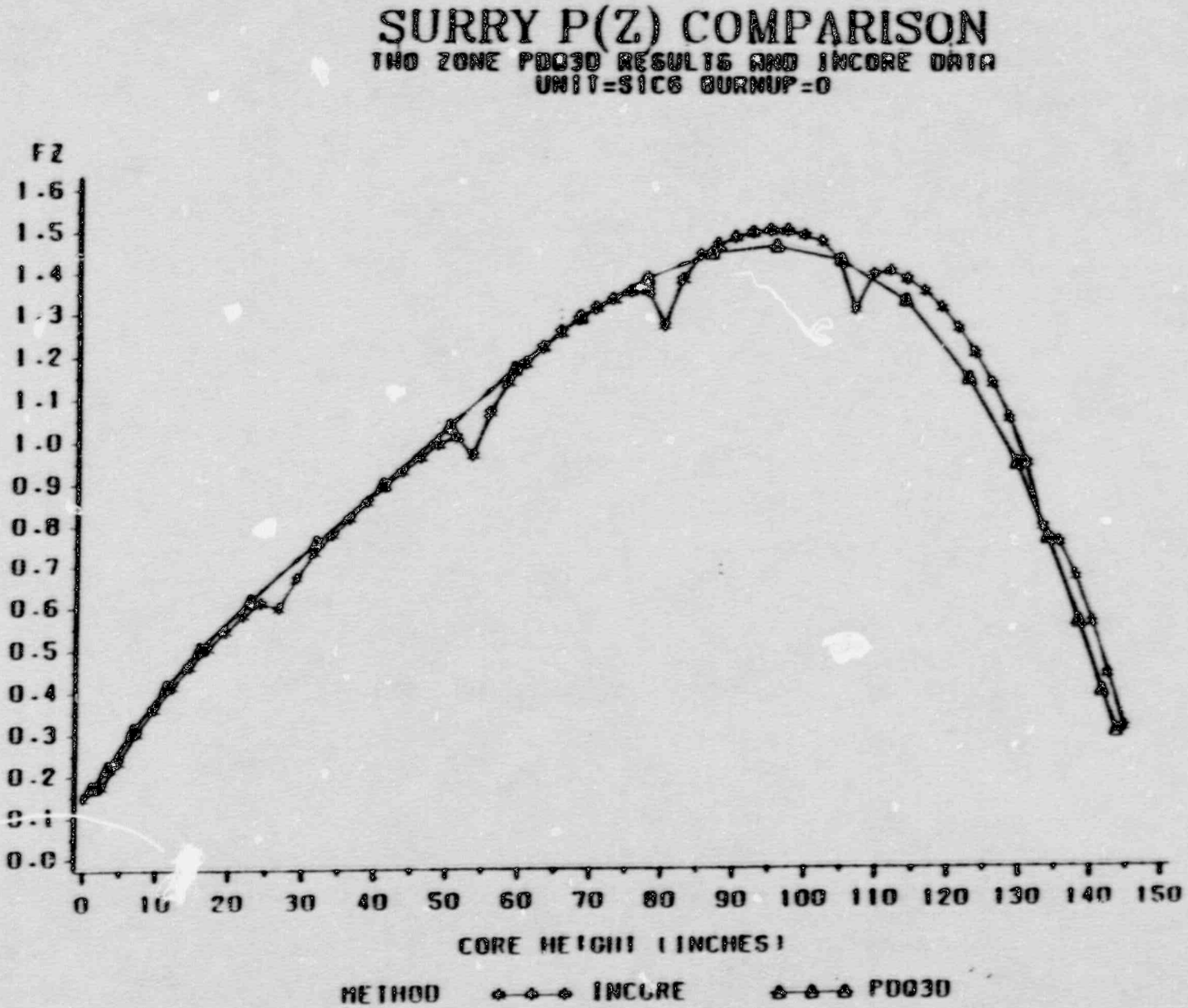
SURRY P(Z) COMPARISON
TWO ZONE PDQ3D RESULTS AND INCORE DATA
UNIT=SIC6 BURNUP=0
FZ
1.6
1.5
1.4
1.3
1.2
1.1
1.0
0.9
0.8
0.7
0.6
0.5
0.4
0.3
0.2
0.1
0.0
0 10 20 30 40 50 60 70 80 90 100 110 120 130 140 150
CORE HEIGHT (INCHES)
METHOD INCORE PDQ3D

FIGURE 3-57

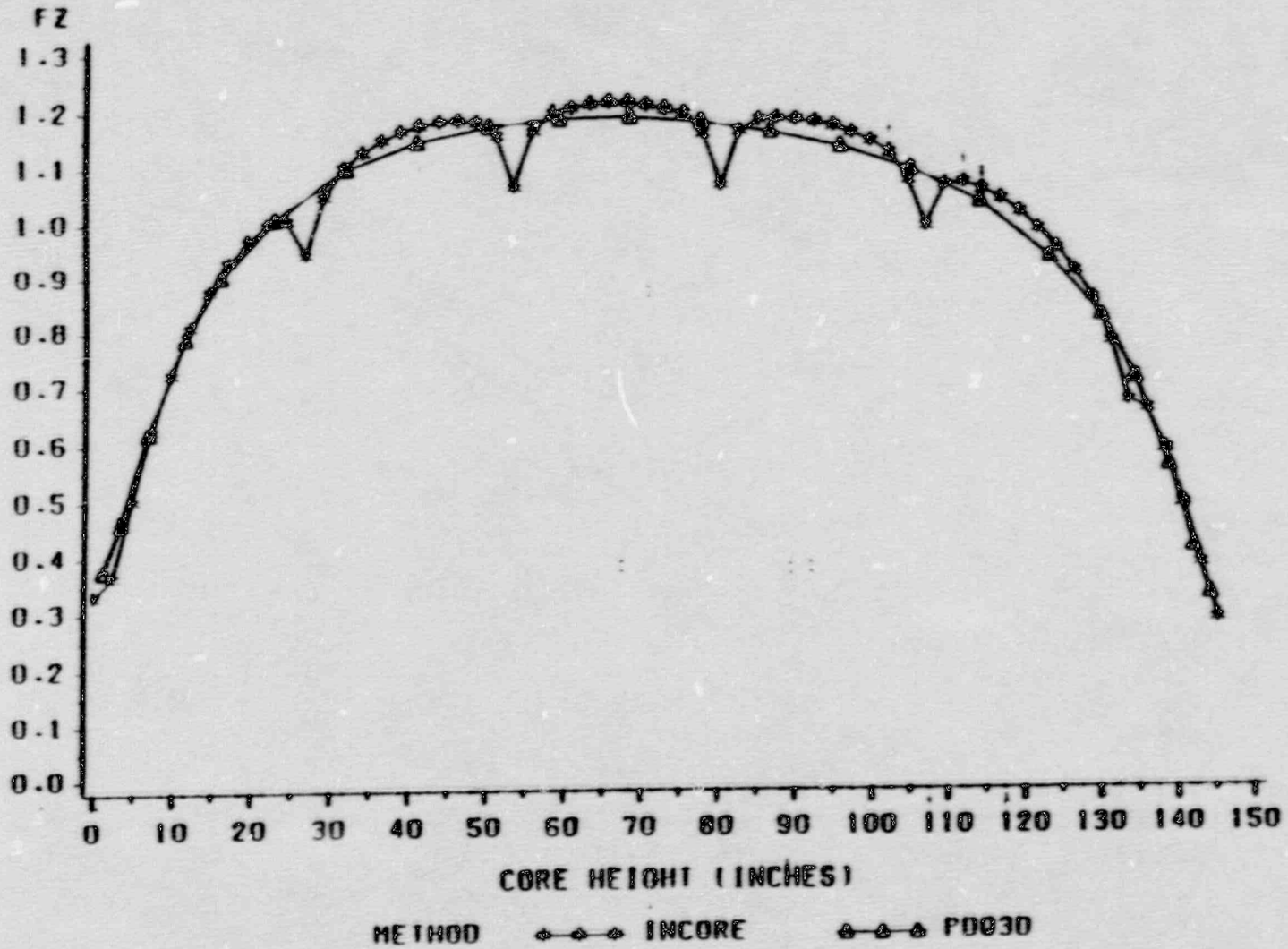
SURRY P(Z) COMPARISON
TWO ZONE PD03D RESULTS AND INCORE DATA
UNIT=61C6 BURNUP=973
FZ
1.3
1.2
1.1
1.0
0.9
0.8
0.7
0.6
0.5
0.4
0.3
0.2
0.1
0.0
0 10 20 30 40 50 60 70 80 90 100 110 120 130 140 150
CORE HEIGHT (INCHES)
METHOD INCORE PD03D

FIGURE 3-58

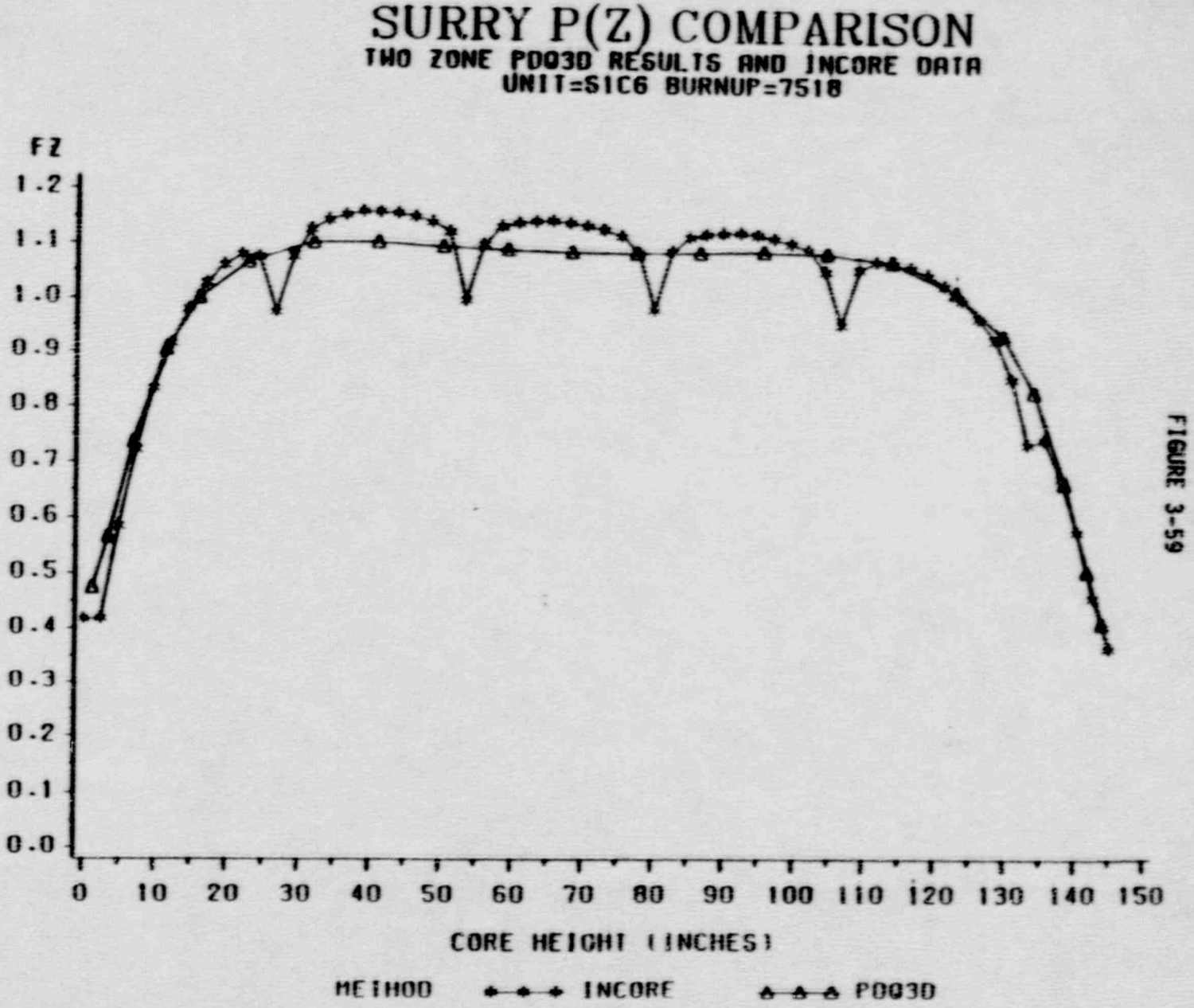
SURRY P(Z) COMPARISON
TWO ZONE PDQ3D RESULTS AND INCORE DATA
UNIT=SIC6 BURNUP=7518
FZ
1.2
1.1
1.0
0.9
0.8
0.7
0.6
0.5
0.4
0.3
0.2
0.1
0.0
0 10 20 30 40 50 60 70 80 90 100 110 120 130 140 150
CORE HEIGHT (INCHES)
METHOD INCORE PDQ3D

FIGURE 3-59

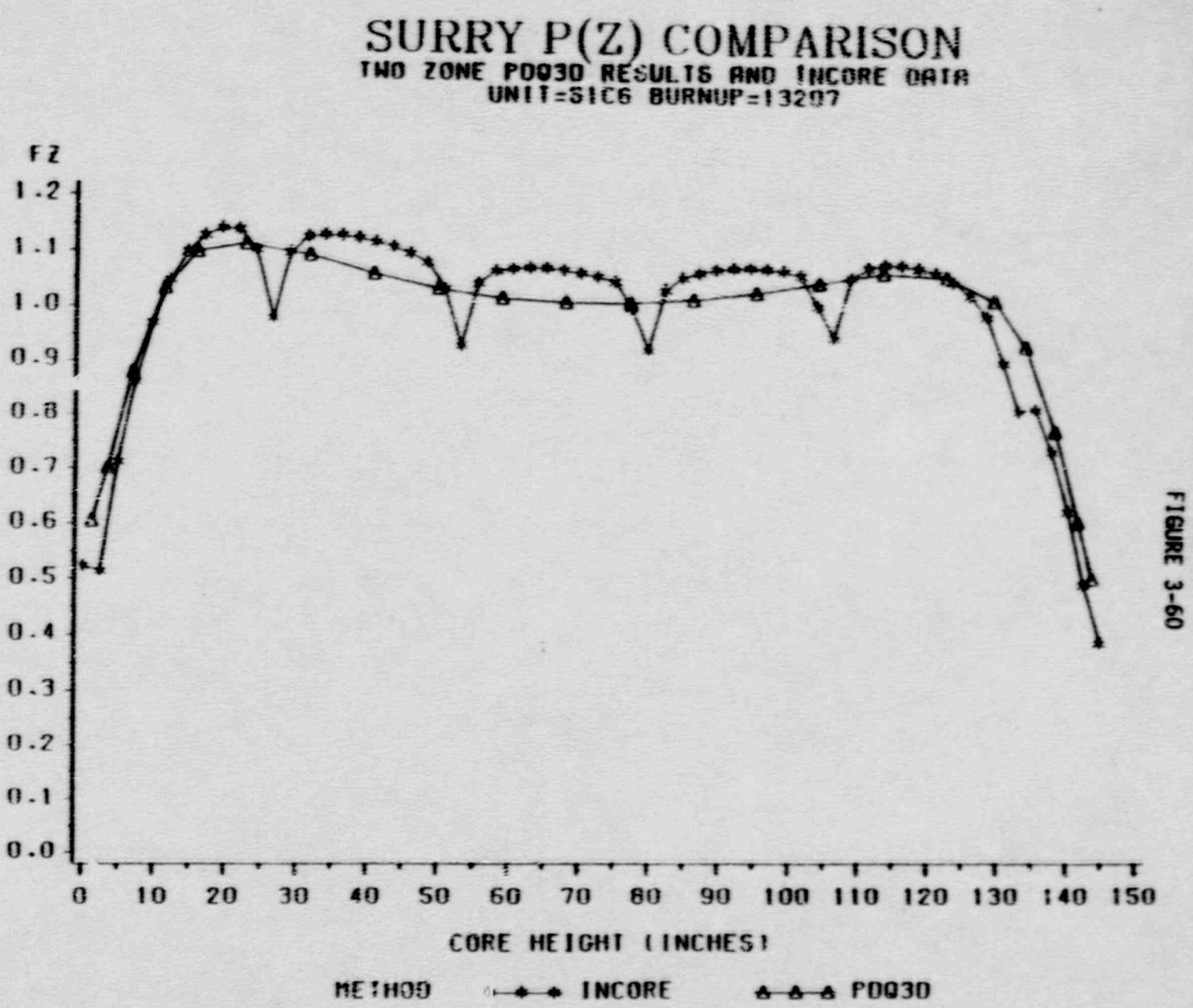
SURRY P(Z) COMPARISON
TWO ZONE PDQ3D RESULTS AND INCORE DATA
UNIT=SIC6 BURNUP=13207
FZ
1.2
1.1
1.0
0.9
0.8
0.7
0.6
0.5
0.4
0.3
0.2
0.1
0.0
0
10
20
30
40
50
60
70
80
90
100
110
120
130
140
150
CORE HEIGHT (INCHES)
METHOD
INCORE
PDQ3D

FIGURE 3-60

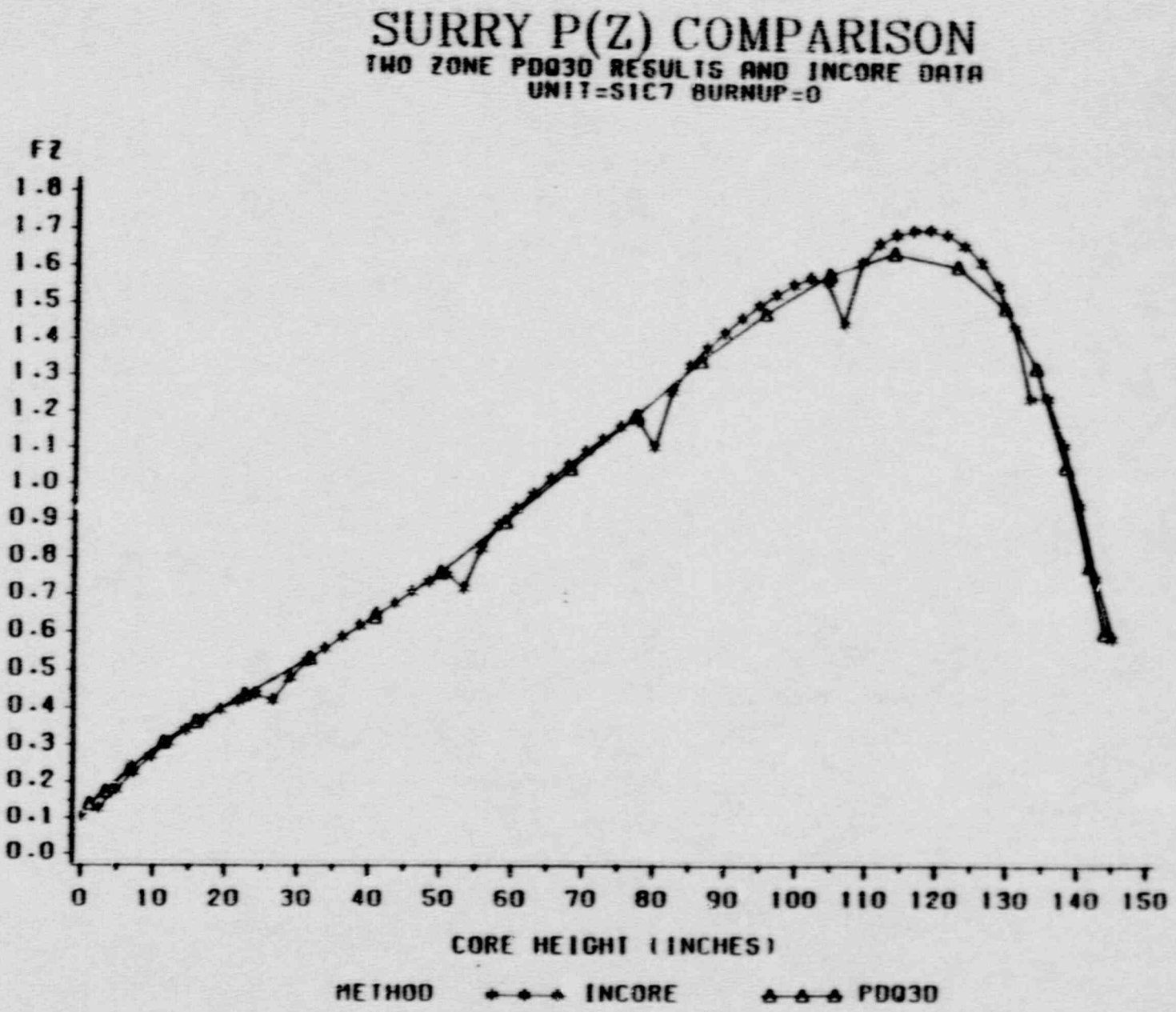
SURRY P(Z) COMPARISON
TWO ZONE PDQ3D RESULTS AND INCORE DATA
UNIT=SIC7 BURNUP=0
FZ
1.8
1.7
1.6
1.5
1.4
1.3
1.2
1.1
1.0
0.9
0.8
0.7
0.6
0.5
0.4
0.3
0.2
0.1
0.0
0
10
20
30
40
50
60
70
80
90
100
110
120
130
140
150
CORE HEIGHT (INCHES)
METHOD
INCORE
PDQ3D

FIGURE 3-61

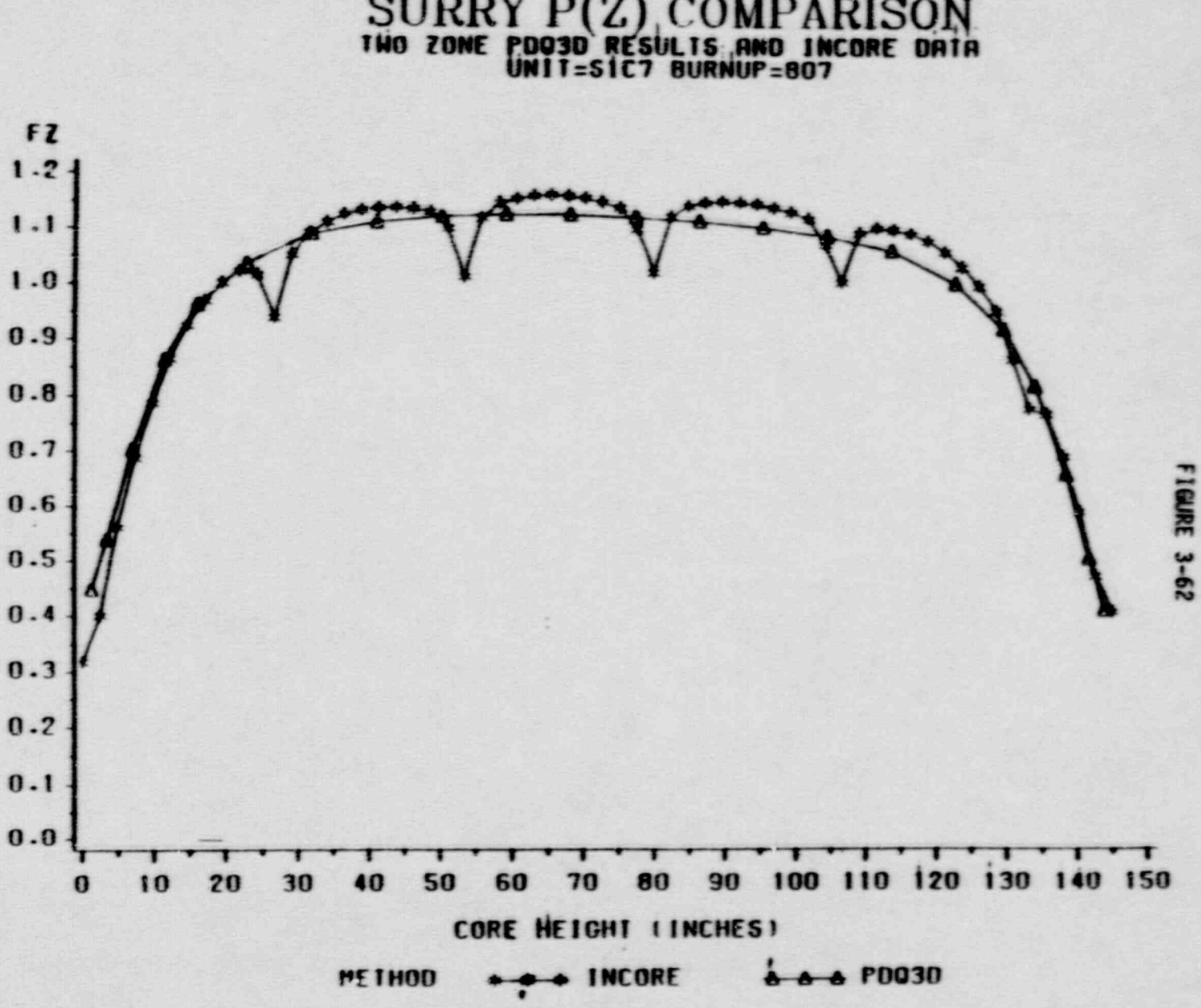
SURRY P(Z) COMPARISON
TWO ZONE PDQ3D RESULTS AND INCORE DATA
UNIT=SIC7 BURNUP=807
FZ
1.2
1.1
1.0
0.9
0.8
0.7
0.6
0.5
0.4
0.3
0.2
0.1
0.0
0 10 20 30 40 50 60 70 80 90 100 110 120 130 140 150
CORE HEIGHT (INCHES)
METHOD
INCORE
PDQ3D

FIGURE 3-62

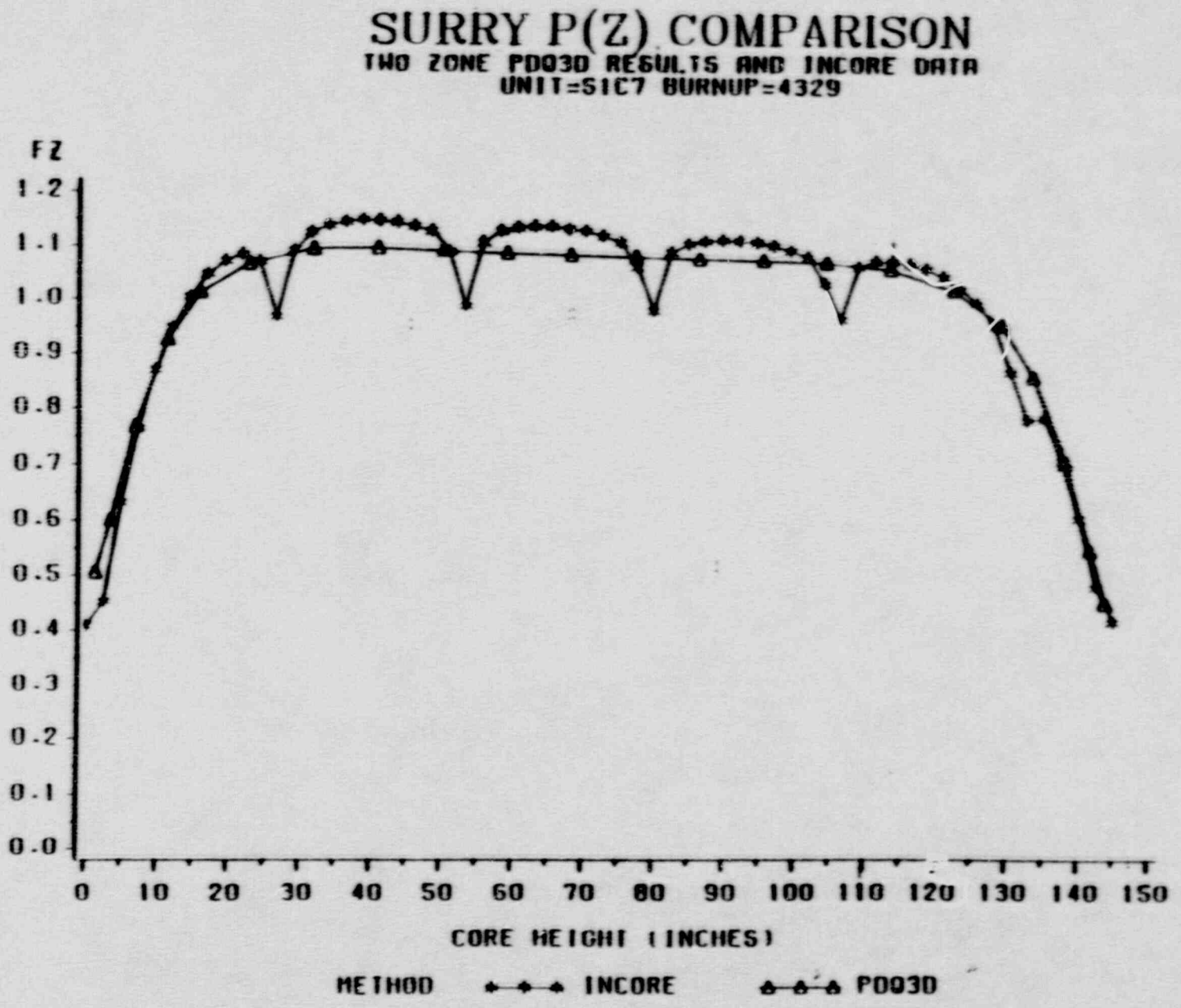
SURRY P(Z) COMPARISON
TWO ZONE PDQ3D RESULTS AND INCORE DATA
UNIT=S1C7 BURNUP=4329
FZ
1.2
1.1
1.0
0.9
0.8
0.7
0.6
0.5
0.4
0.3
0.2
0.1
0.0
0 10 20 30 40 50 60 70 80 90 100 110 120 130 140 150
CORE HEIGHT (INCHES)
METHOD INCORE PDQ3D

FIGURE 3-63

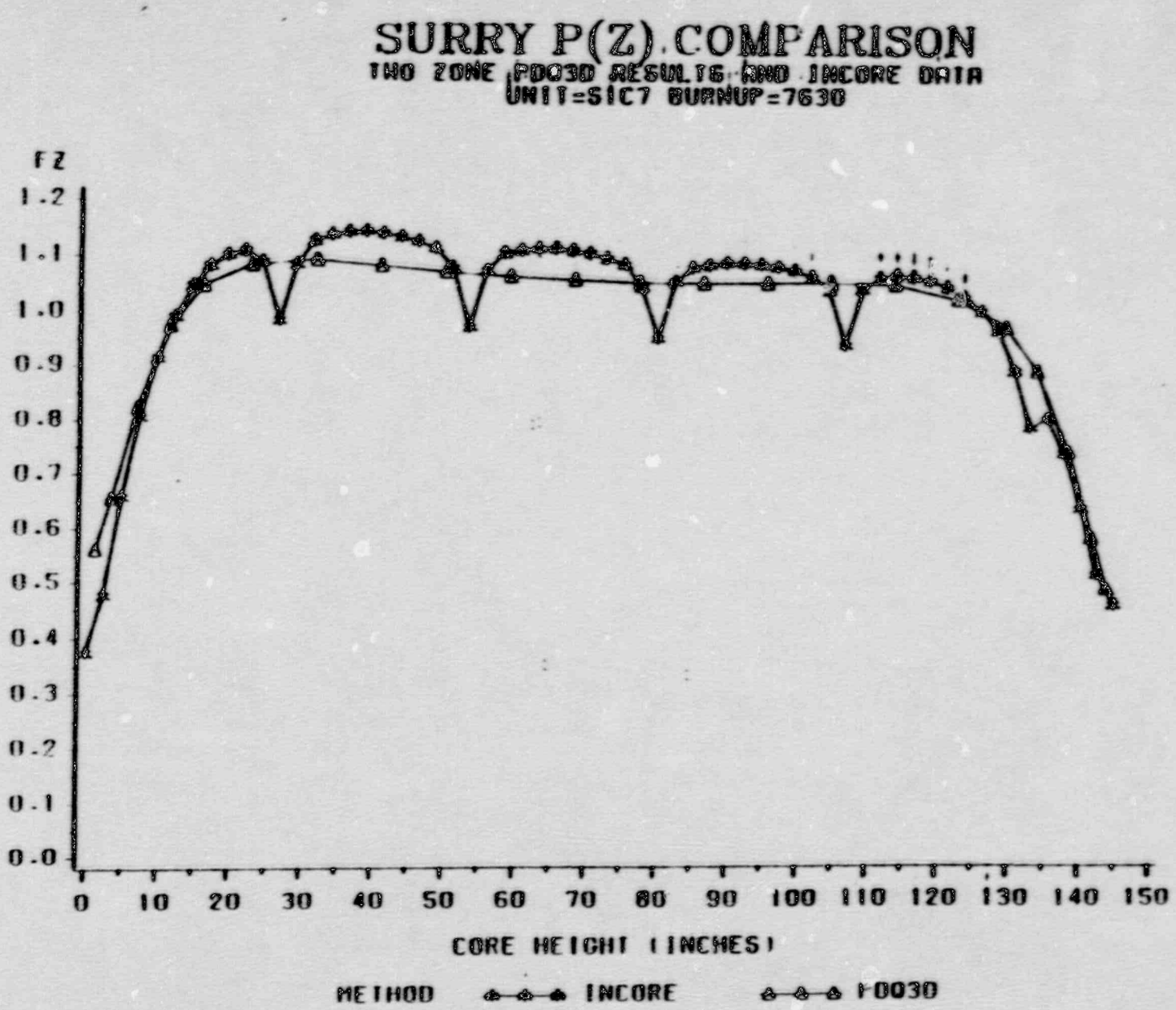
SURRY P(Z) COMPARISON
TWO ZONE PDQ3D RESULTS AND INCORE DATA
UNIT=SIC7 BURNUP=7630
FZ
1.2
1.1
1.0
0.9
0.8
0.7
0.6
0.5
0.4
0.3
0.2
0.1
0.0
0
10
20
30
40
50
60
70
80
90
100
110
120
130
140
150
CORE HEIGHT (INCHES)
METHOD
INCORE
PDQ3D

FIGURE 3-64

SURRY P(Z) COMPARISON

TWO ZONE PDQ3D RESULTS AND INCORE DATA
UNIT=SIC8 BURNUP=0

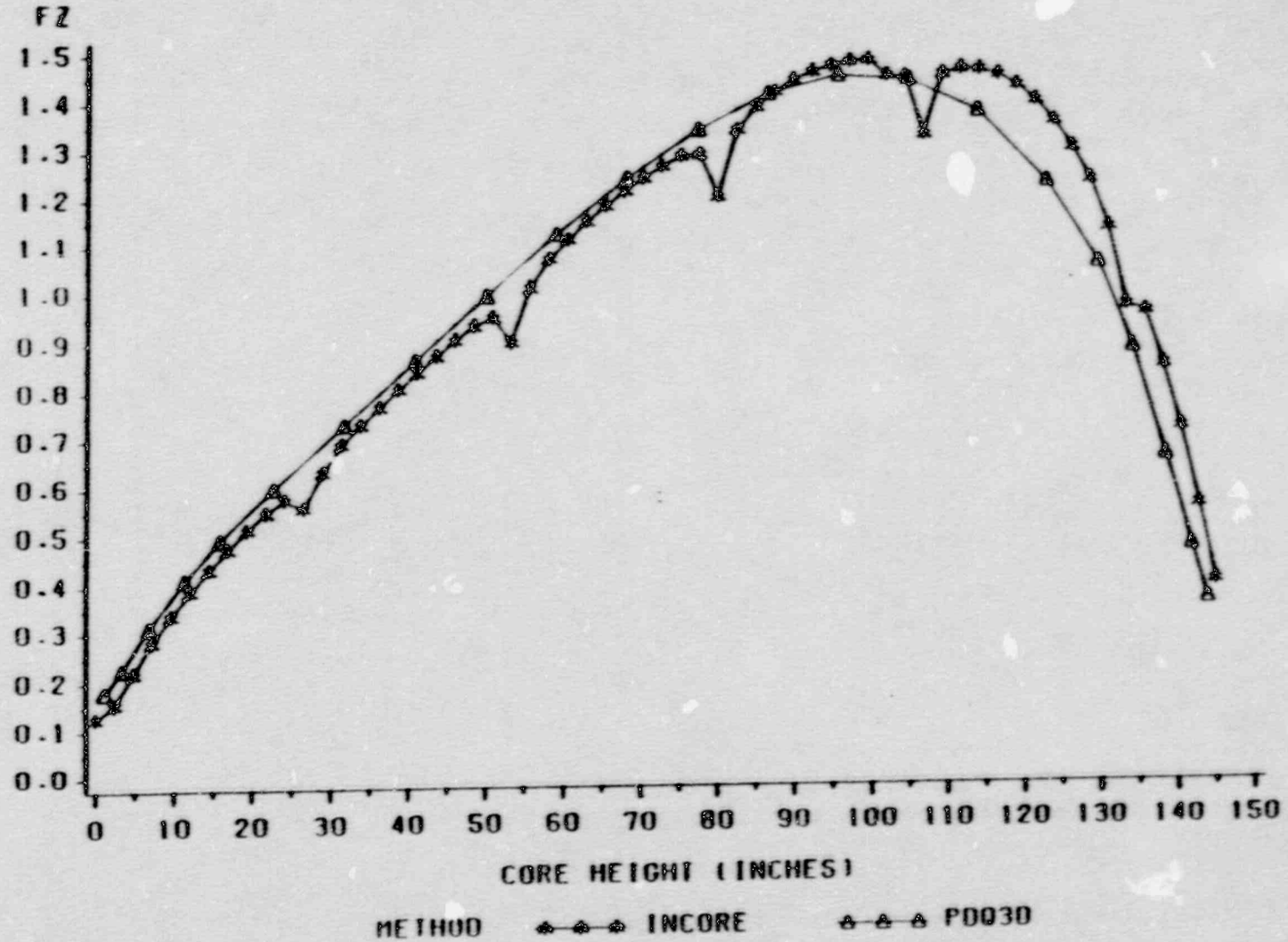

FIGURE 3-65

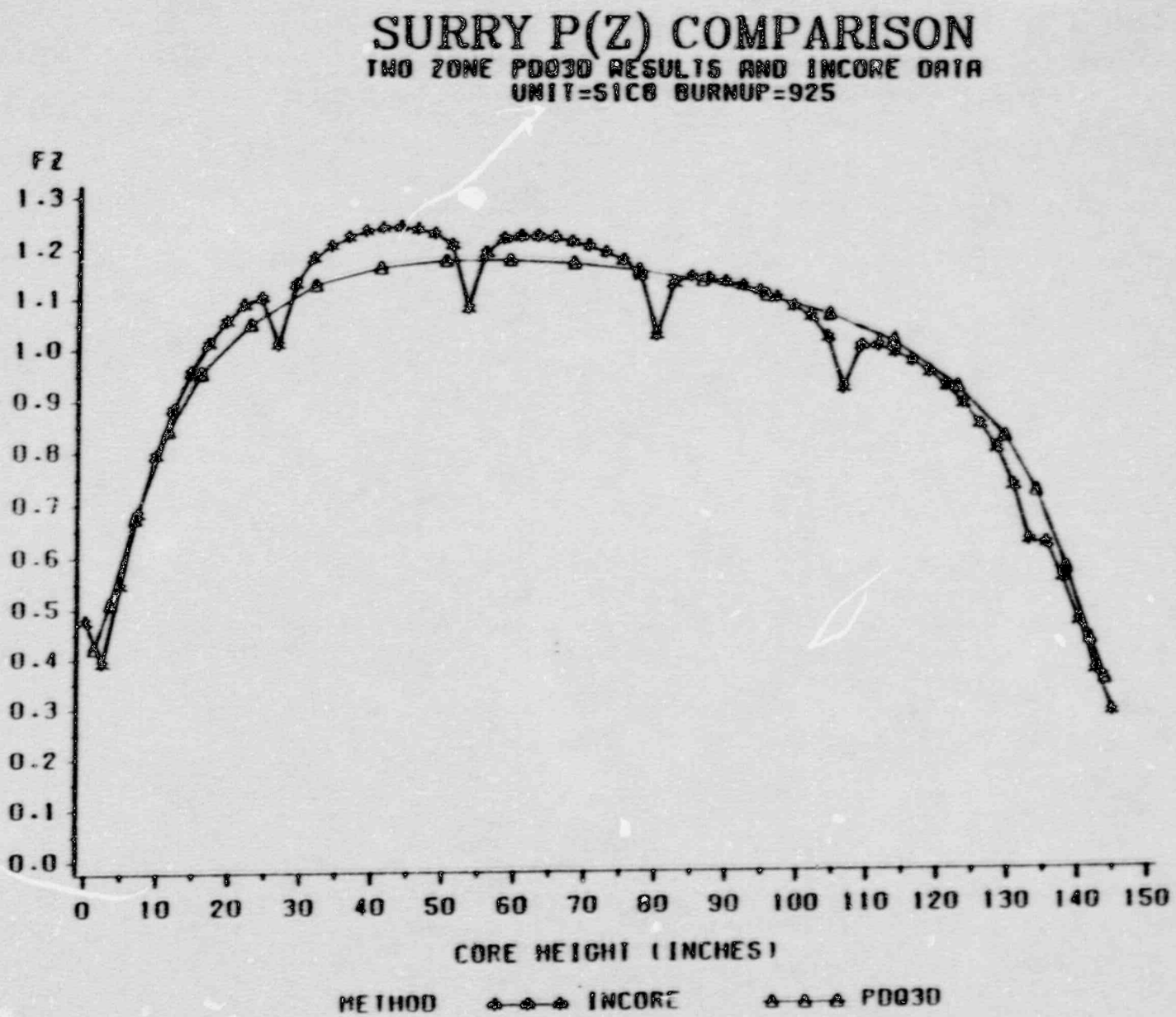
SURRY P(Z) COMPARISON
TWO ZONE PDQ3D RESULTS AND INCORE DATA
UNIT=SIC8 BURNUP=925
FZ
1.3
1.2
1.1
1.0
0.9
0.8
0.7
0.6
0.5
0.4
0.3
0.2
0.1
0.0
0 10 20 30 40 50 60 70 80 90 100 110 120 130 140 150
CORE HEIGHT (INCHES)
METHOD INCORE PDQ3D

FIGURE 3-66

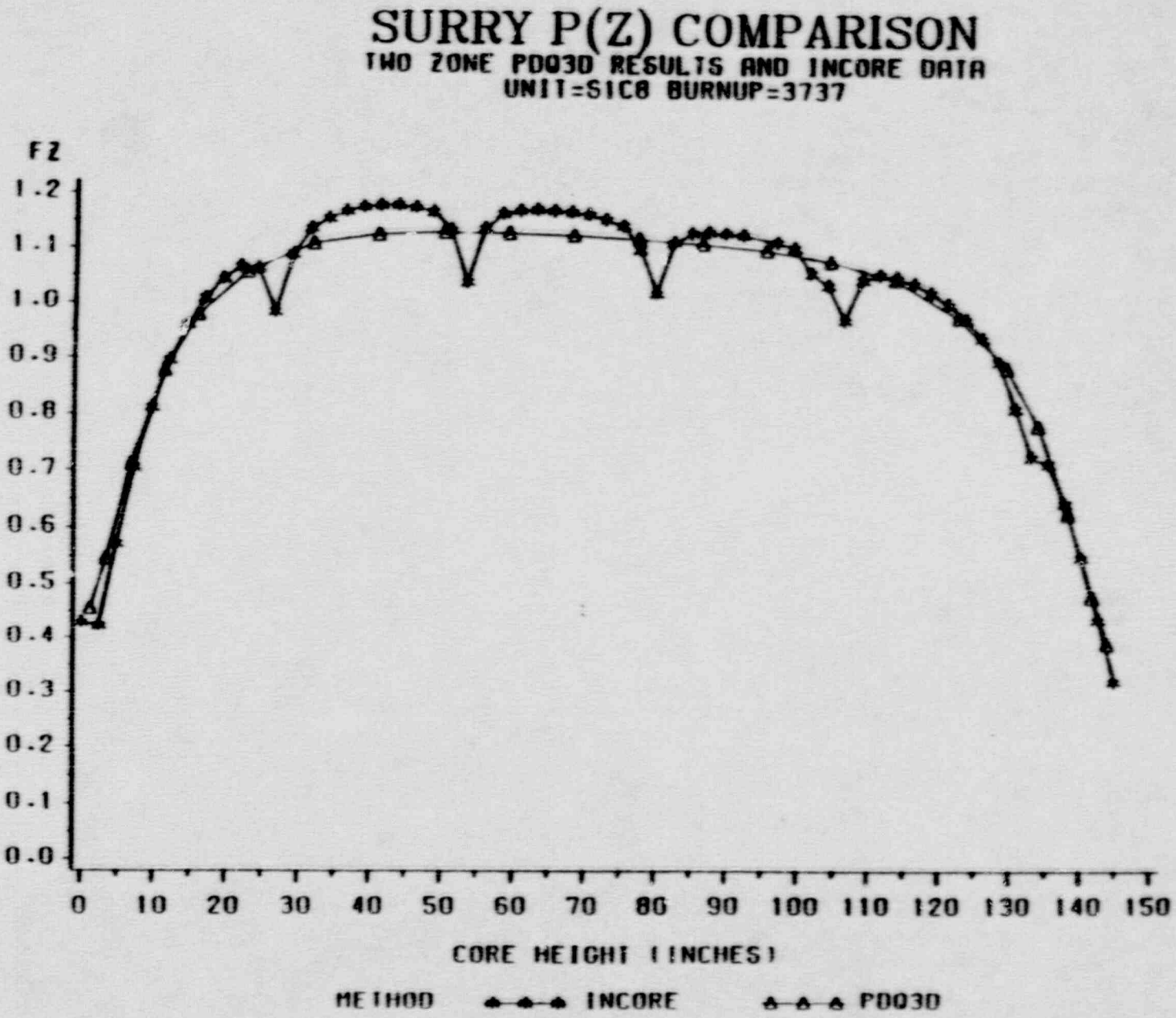
SURRY P(Z) COMPARISON
TWO ZONE PDQ3D RESULTS AND INCORE DATA
UNIT=SIC8 BURNUP=3737
FZ
1.2
1.1
1.0
0.9
0.8
0.7
0.6
0.5
0.4
0.3
0.2
0.1
0.0
0
10
20
30
40
50
60
70
80
90
100
110
120
130
140
150
CORE HEIGHT (INCHES)
METHOD
INCORE
PDQ3D

FIGURE 3-67

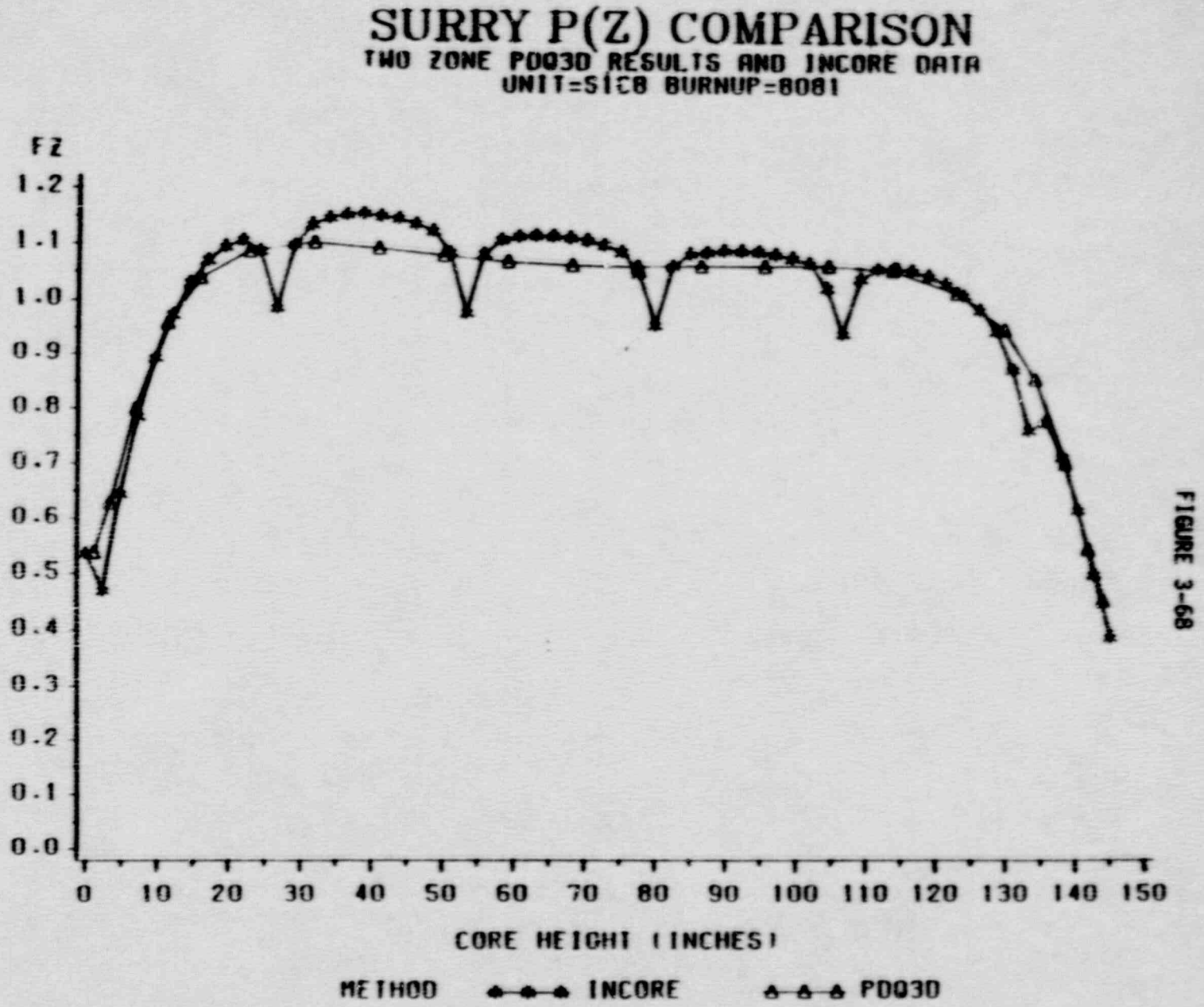
SURRY P(Z) COMPARISON
TWO ZONE PDQ3D RESULTS AND INCORE DATA
UNIT=SIC8 BURNUP=8081
FZ
1.2
1.1
1.0
0.9
0.8
0.7
0.6
0.5
0.4
0.3
0.2
0.1
0.0
0
10
20
30
40
50
60
70
80
90
100
110
120
130
140
150
CORE HEIGHT (INCHES)
METHOD
INCORE
PDQ3D

FIGURE 3-68

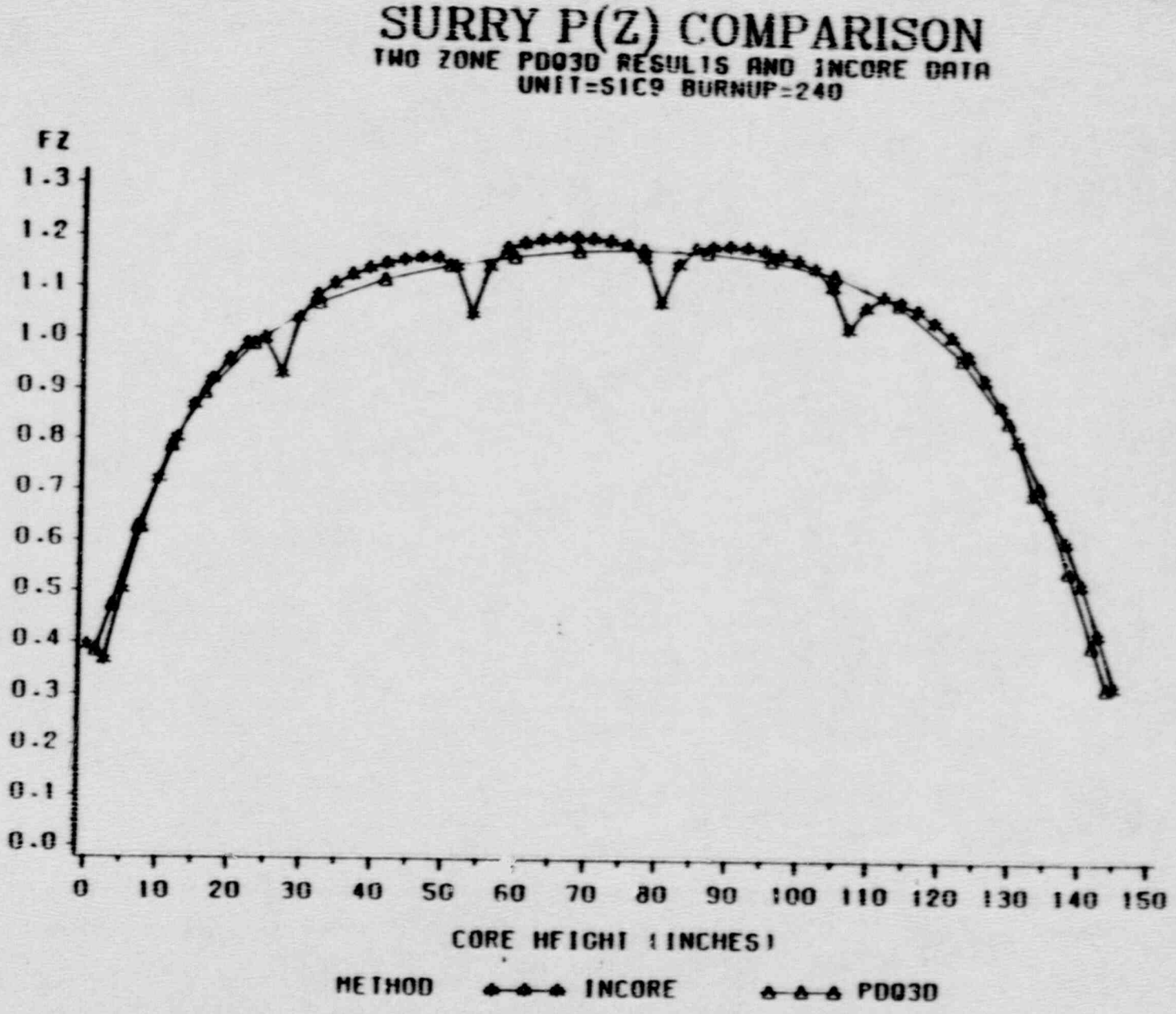
SURRY P(Z) COMPARISON
TWO ZONE PDQ3D RESULTS AND INCORE DATA
UNIT=SIC9 BURNUP=240
FZ
1.3
1.2
1.1
1.0
0.9
0.8
0.7
0.6
0.5
0.4
0.3
0.2
0.1
0.0
0
10
20
30
40
50
60
70
80
90
100
110
120
130
140
150
CORE HEIGHT (INCHES)
METHOD
INCORE
PDQ3D

FIGURE 3-69

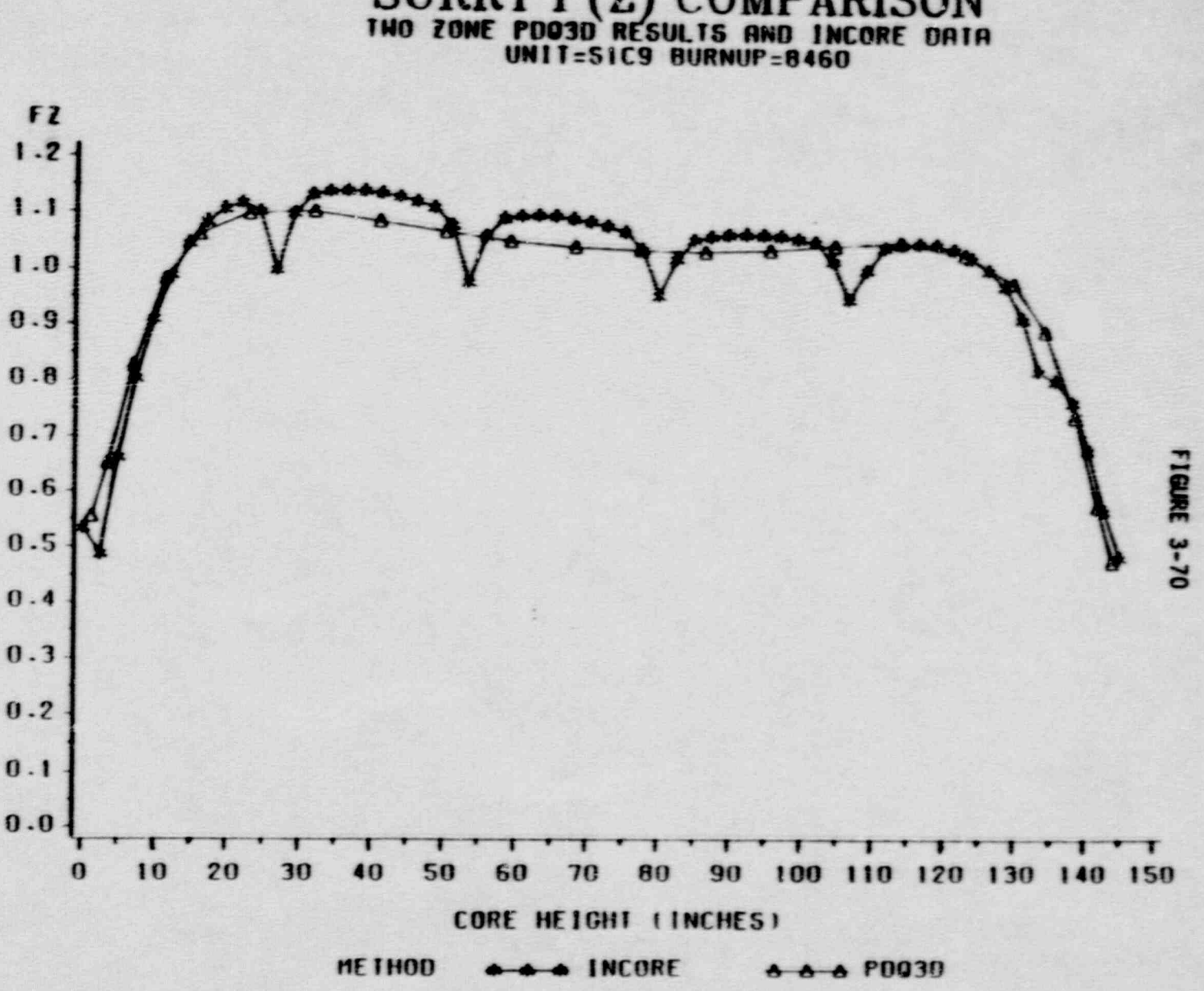
SURRY P(Z) COMPARISON
TWO ZONE PDQ3D RESULTS AND INCORE DATA
UNIT=SIC9 BURNUP=8460
FZ
1.2
1.1
1.0
0.9
0.8
0.7
0.6
0.5
0.4
0.3
0.2
0.1
0.0
0
10
20
30
40
50
60
70
80
90
100
110
120
130
140
150
CORE HEIGHT (INCHES)
METHOD
INCORE
PDQ3D

FIGURE 3-70

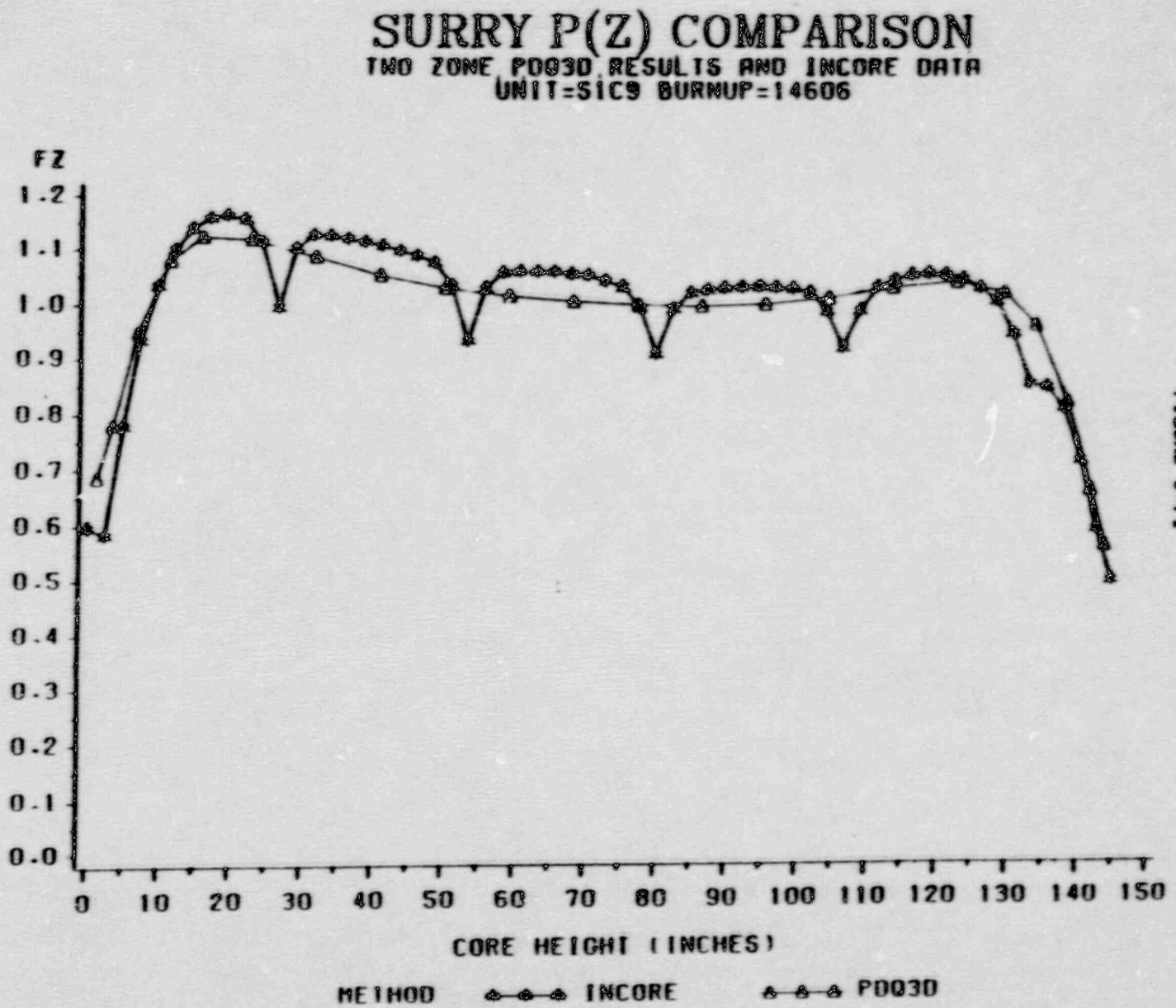
SURRY P(Z) COMPARISON
TWO ZONE PDQ3D RESULTS AND INCORE DATA
UNIT=SIC9 BURNUP=14606
FZ
1.2
1.1
1.0
0.9
0.8
0.7
0.6
0.5
0.4
0.3
0.2
0.1
0.0
0 10 20 30 40 50 60 70 80 90 100 110 120 130 140 150
CORE HEIGHT (INCHES)
METHOD INCORE PDQ3D

FIGURE 3-71

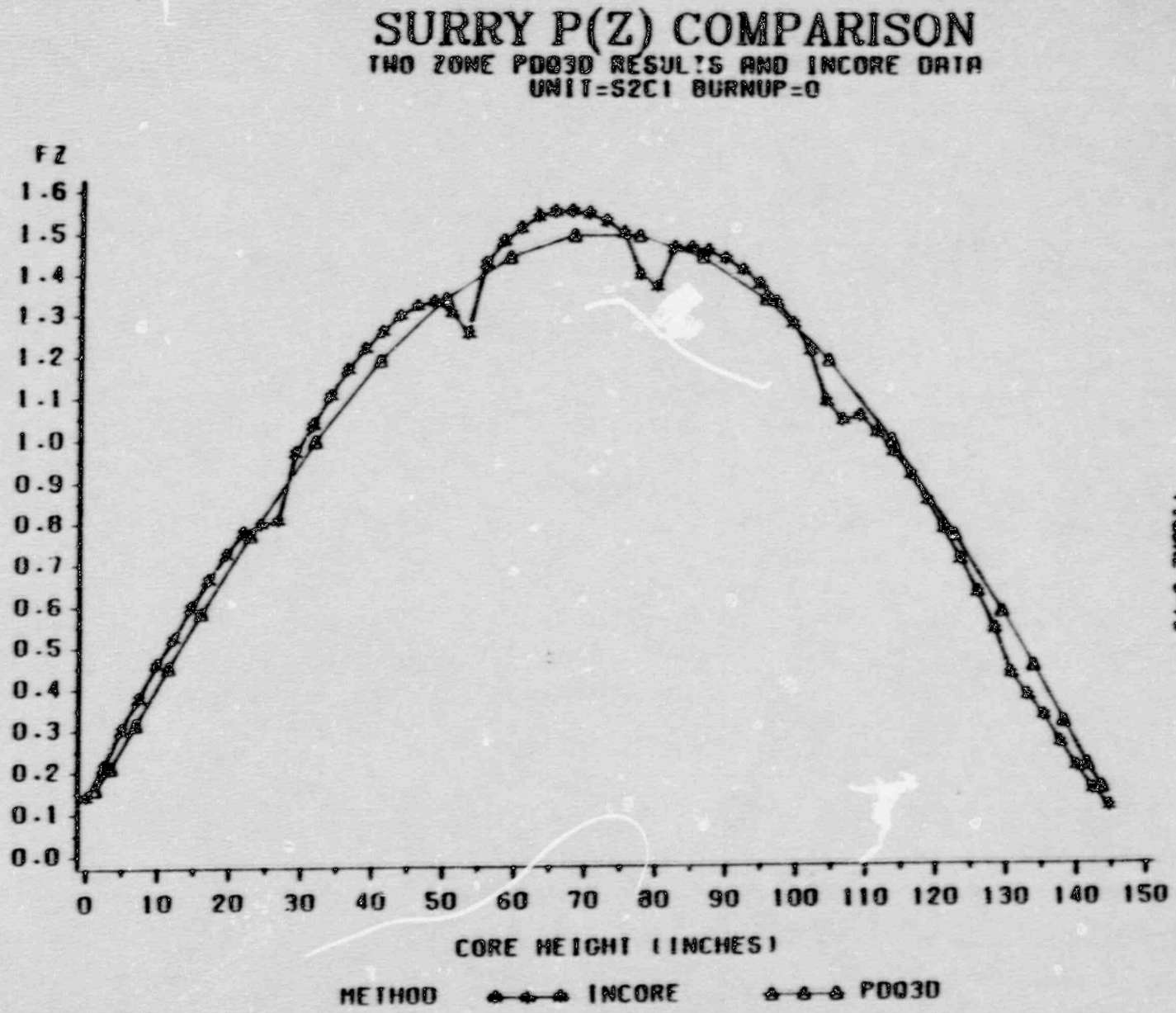
SURRY P(Z) COMPARISON
TWO ZONE PDQ3D RESULTS AND INCORE DATA
UNIT=S2C1 BURNUP=0
FZ
1.6
1.5
1.4
1.3
1.2
1.1
1.0
0.9
0.8
0.7
0.6
0.5
0.4
0.3
0.2
0.1
0.0
0 10 20 30 40 50 60 70 80 90 100 110 120 130 140 150
CORE HEIGHT (INCHES)
METHOD INCORE PDQ3D

FIGURE 3-72

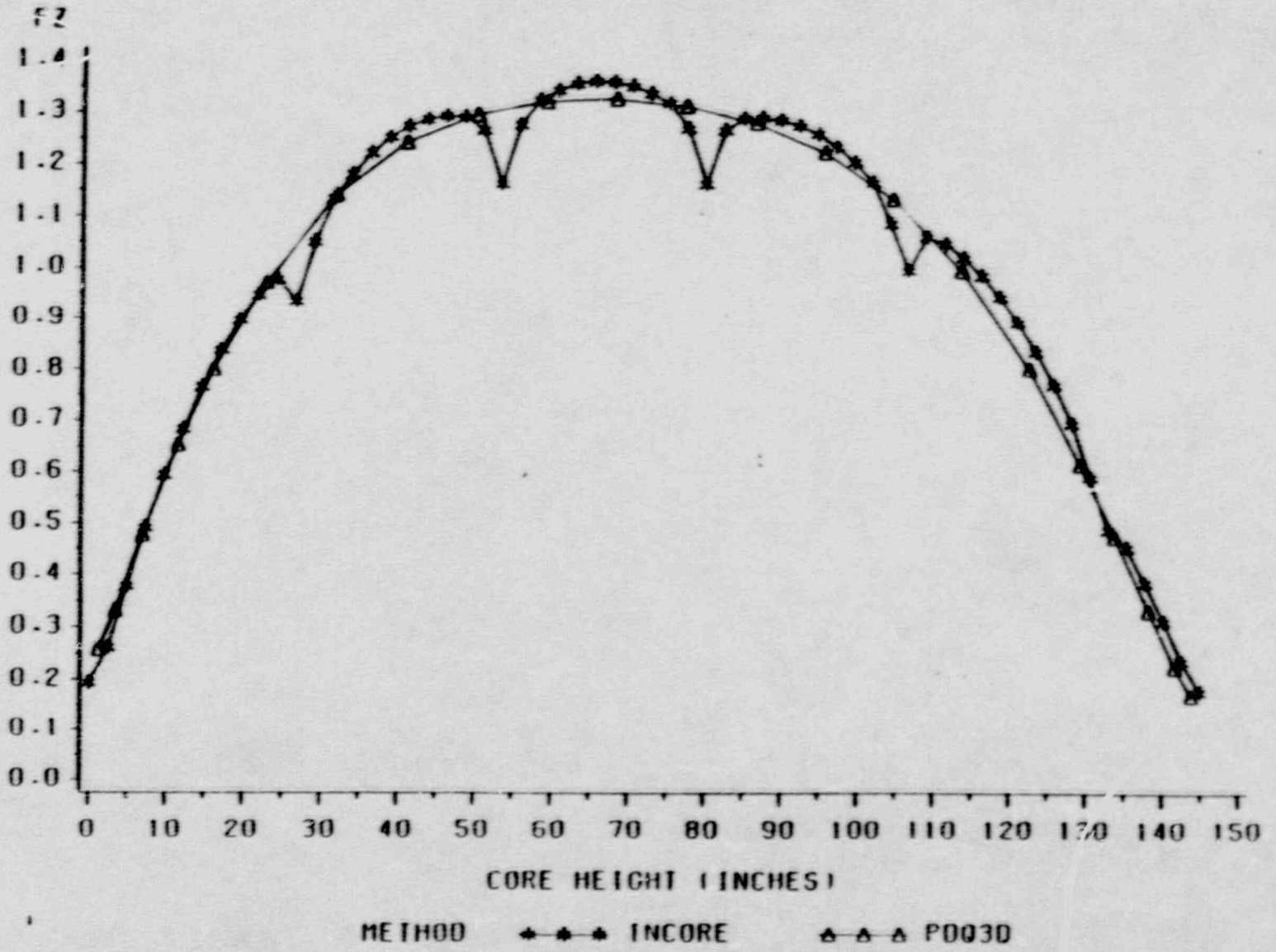
SURRY P(Z) COMPARISON
T40 ZONE PDQ3D RESULTS AND INCORE DATA
UNIT=S2C1 BURNUP=2030
FZ
1.4
1.3
1.2
1.1
1.0
0.9
0.8
0.7
0.6
0.5
0.4
0.3
0.2
0.1
0.0
0
10
20
30
40
50
60
70
80
90
100
110
120
130
140
150
CORE HEIGHT (INCHES)
METHOD
INCORE
PDQ3D

FIGURE 3-73

SURRY P(Z) COMPARISON

TWO ZONE PDQ3D RESULTS AND INCORE DATA
UNIT=S2C1 BURNUP=7310

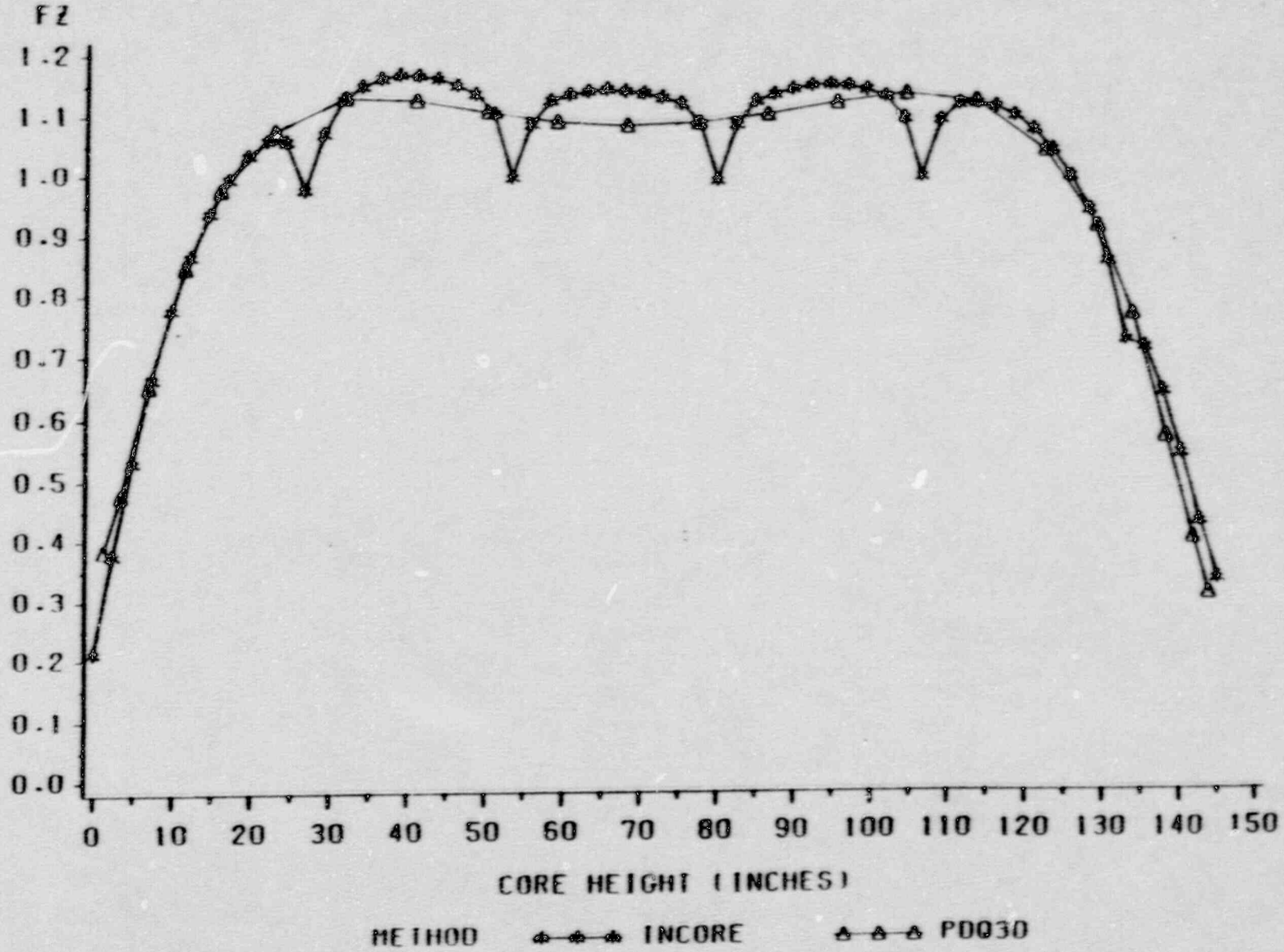

FIGURE 3-74

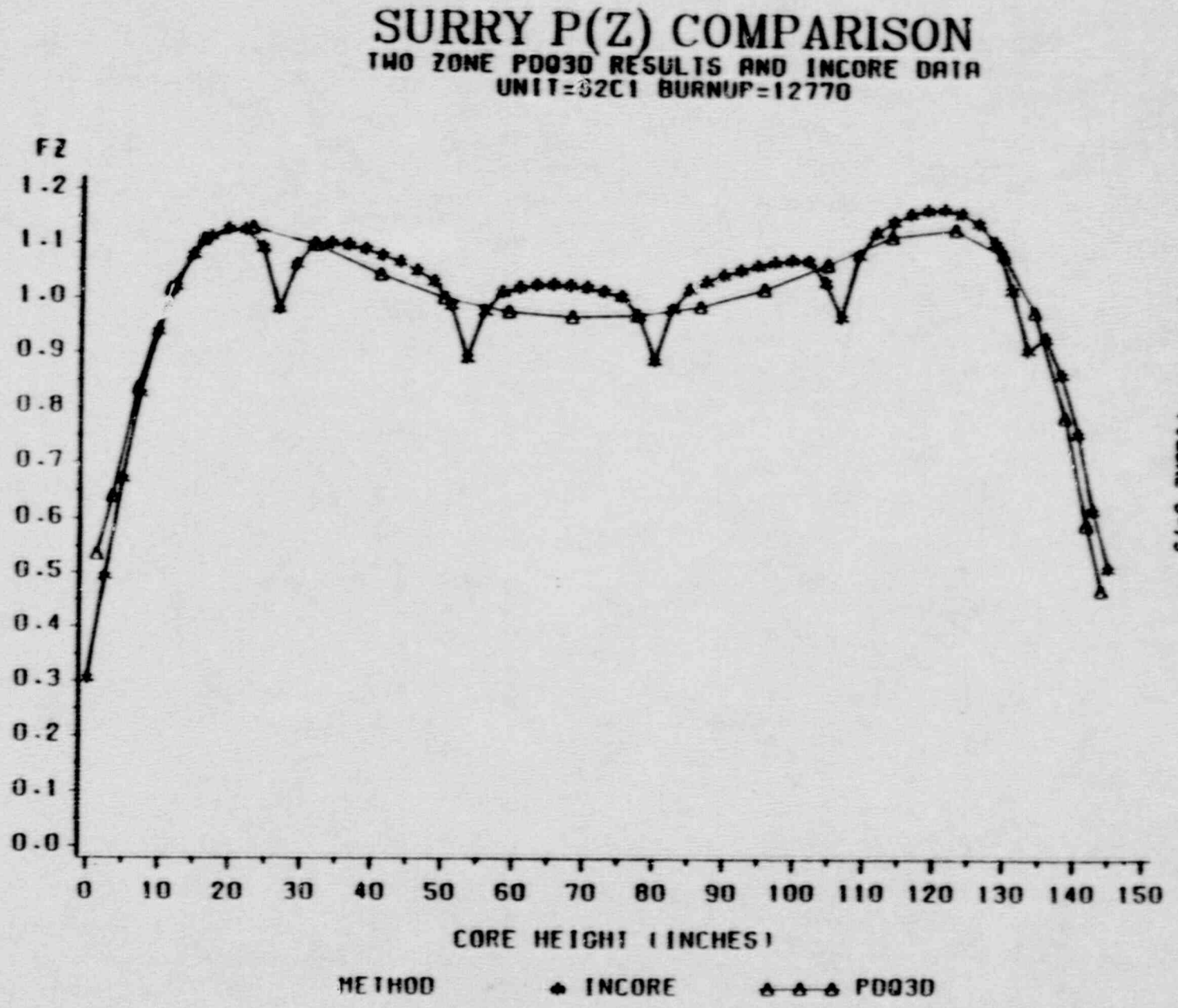
SURRY P(Z) COMPARISON
TWO ZONE PDQ3D RESULTS AND INCORE DATA
UNIT=S2C1 BURNUP=12770
FZ
1.2
1.1
1.0
0.9
0.8
0.7
0.6
0.5
0.4
0.3
0.2
0.1
0.0
0
10
20
30
40
50
60
70
80
90
100
110
120
130
140
150
CORE HEIGHT (INCHES)
METHOD
INCORE
PDQ3D

FIGURE 3-75

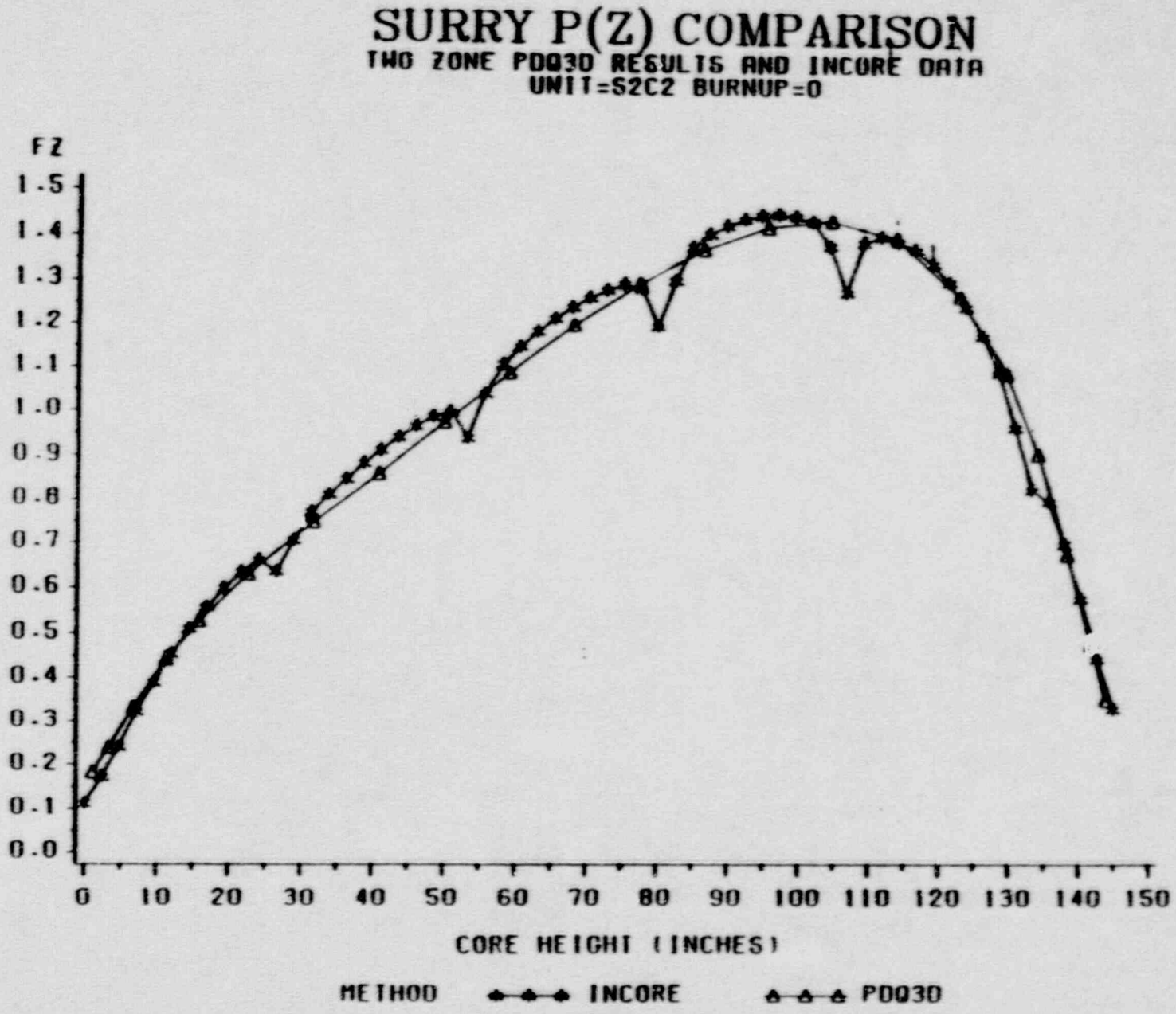
SURRY P(Z) COMPARISON
TWO ZONE PDQ3D RESULTS AND INCORE DATA
UNIT=S2C2 BURNUP=0
FZ
1.5
1.4
1.3
1.2
1.1
1.0
0.9
0.8
0.7
0.6
0.5
0.4
0.3
0.2
0.1
0.0
0
10
20
30
40
50
60
70
80
90
100
110
120
130
140
150
CORE HEIGHT (INCHES)
METHOD
INCORE
PDQ3D

FIGURE 3-76

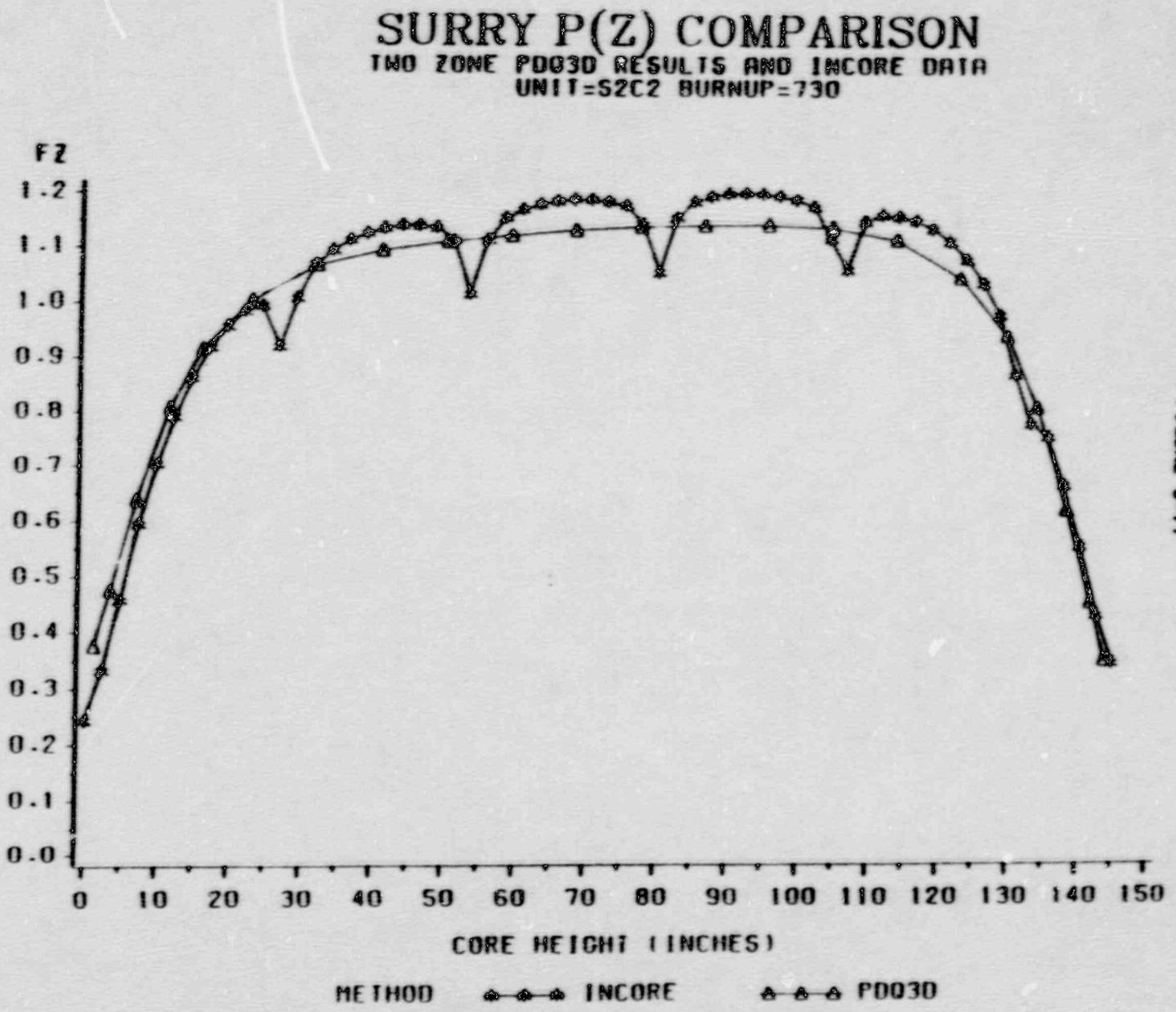
SURRY P(Z) COMPARISON
TWO ZONE PD03D RESULTS AND INCORE DATA
UNIT=S2C2 BURNUP=730
FZ
1.2
1.1
1.0
0.9
0.8
0.7
0.6
0.5
0.4
0.3
0.2
0.1
0.0
0
10
20
30
40
50
60
70
80
90
100
110
120
130
140
150
CORE HEIGHT (INCHES)
METHOD
INCORE
PD03D

FIGURE 3-77

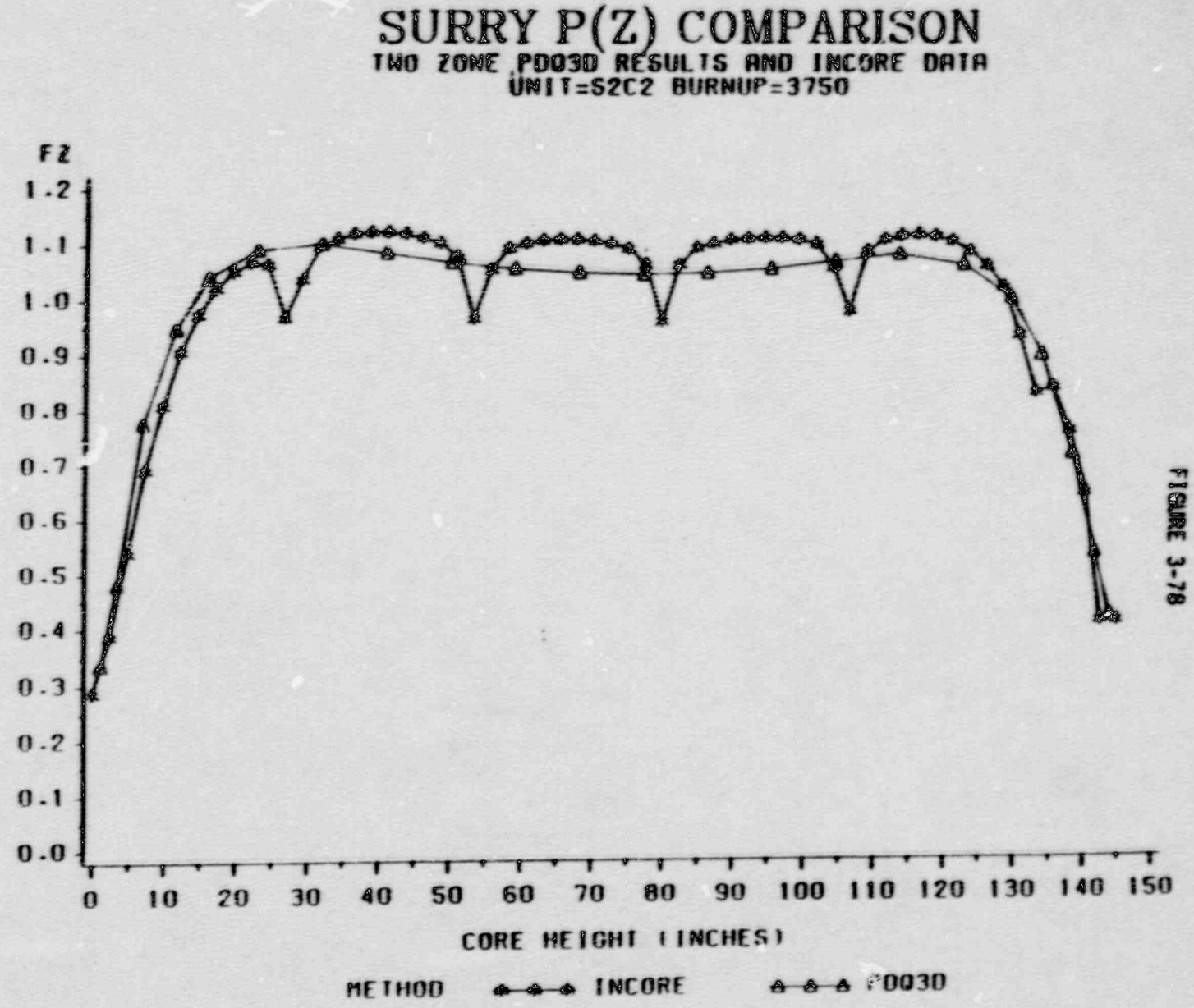
SURRY P(Z) COMPARISON
TWO ZONE PDQ3D RESULTS AND INCORE DATA
UNIT=S2C2 BURNUP=3750
FZ
1.2
1.1
1.0
0.9
0.8
0.7
0.6
0.5
0.4
0.3
0.2
0.1
0.0
0 10 20 30 40 50 60 70 80 90 100 110 120 130 140 150
CORE HEIGHT (INCHES)
METHOD INCORE PDQ3D

FIGURE 3-78

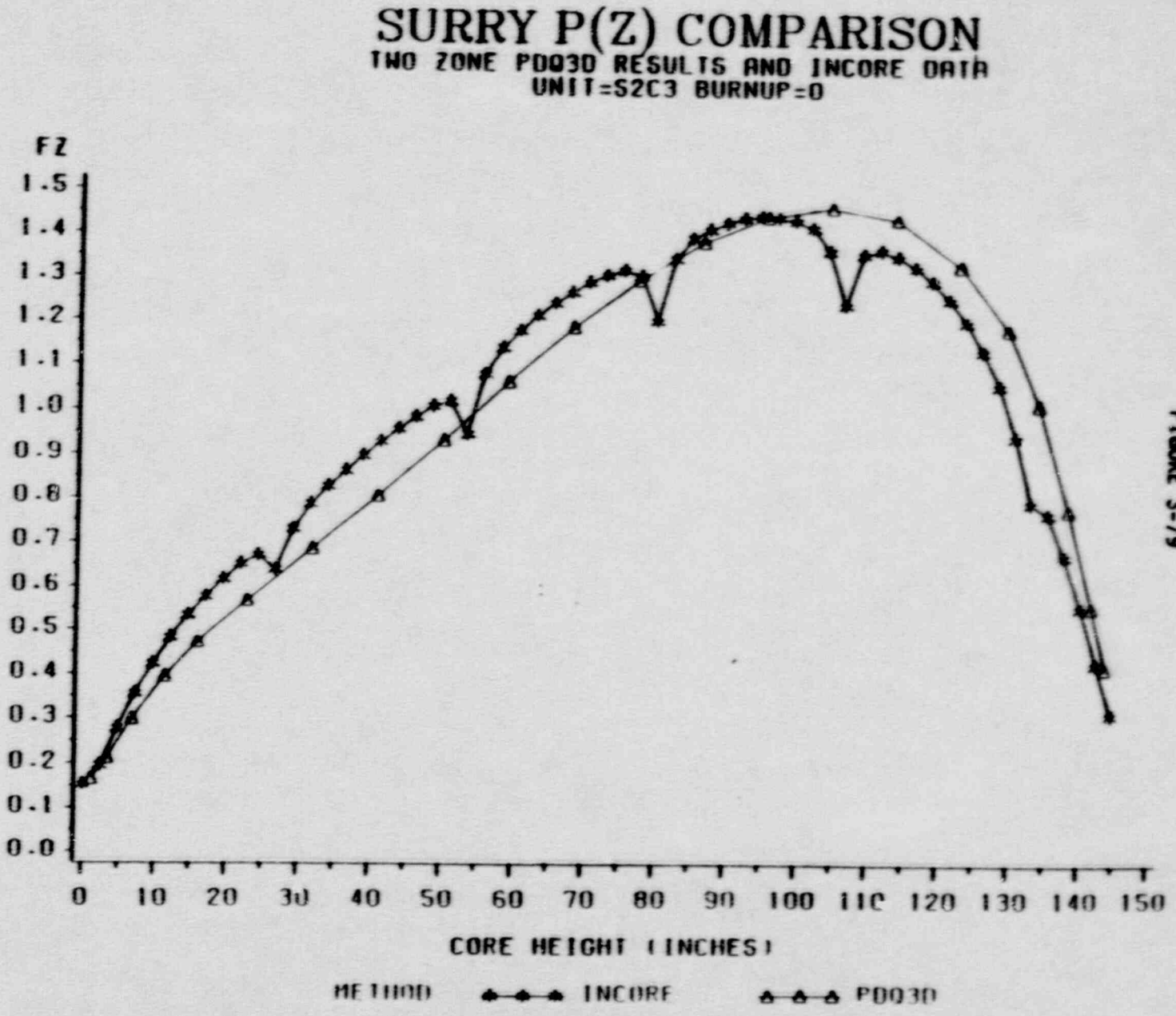
SURRY P(Z) COMPARISON
TWO ZONE PDQ3D RESULTS AND INCORE DATA
UNIT=S2C3 BURNUP=0
FZ
1.5
1.4
1.3
1.2
1.1
1.0
0.9
0.8
0.7
0.6
0.5
0.4
0.3
0.2
0.1
0.0
0
10
20
30
40
50
60
70
80
90
100
110
120
130
140
150
CORE HEIGHT (INCHES)
METHOD
INCORE
PDQ3D

FIGURE 3-79

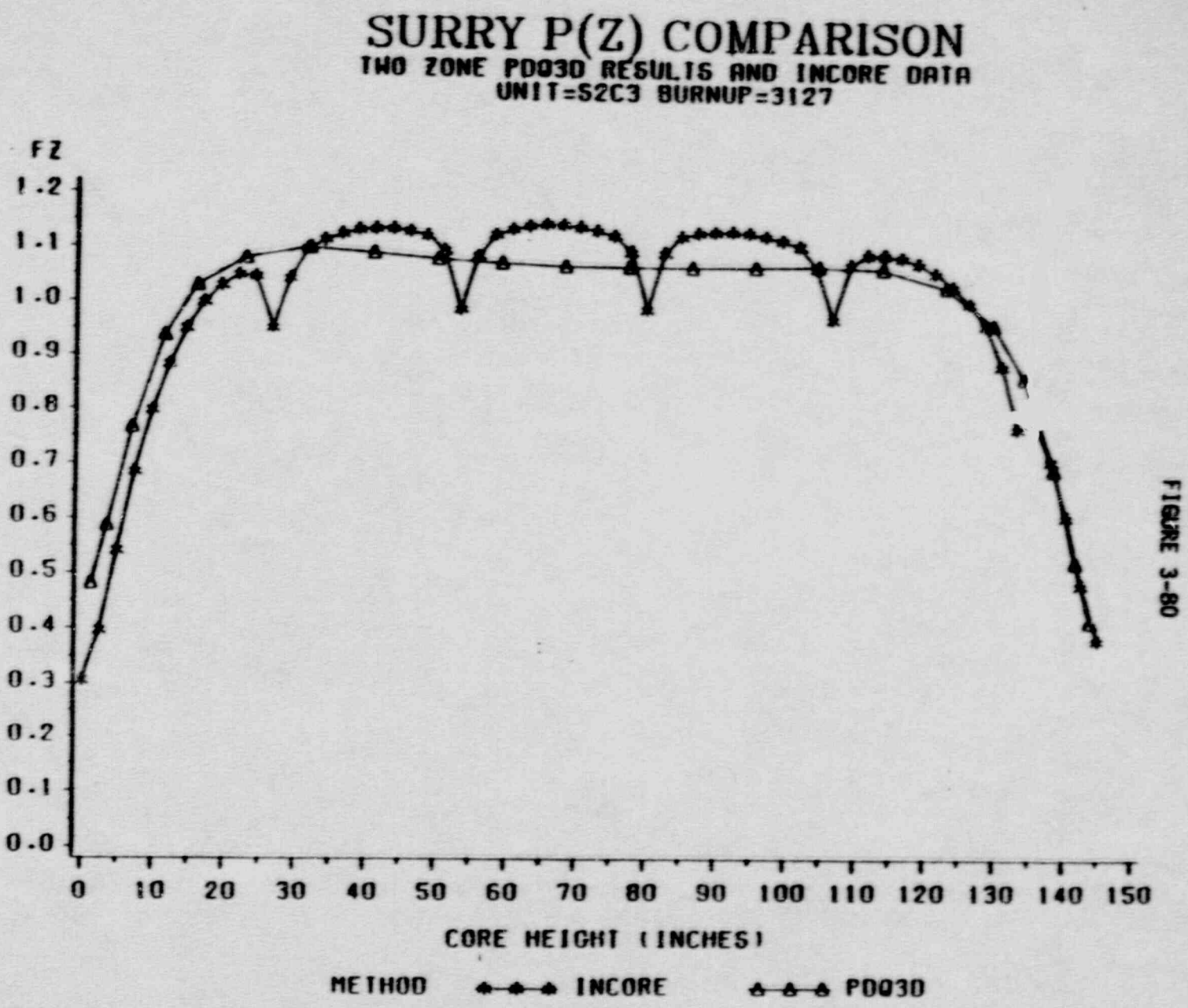
SURRY P(Z) COMPARISON
TWO ZONE PDQ3D RESULTS AND INCORE DATA
UNIT=S2C3 BURNUP=3127
FZ
1.2
1.1
1.0
0.9
0.8
0.7
0.6
0.5
0.4
0.3
0.2
0.1
0.0
0
10
20
30
40
50
60
70
80
90
100
110
120
130
140
150
CORE HEIGHT (INCHES)
METHOD
INCORE
PDQ3D

FIGURE 3-80

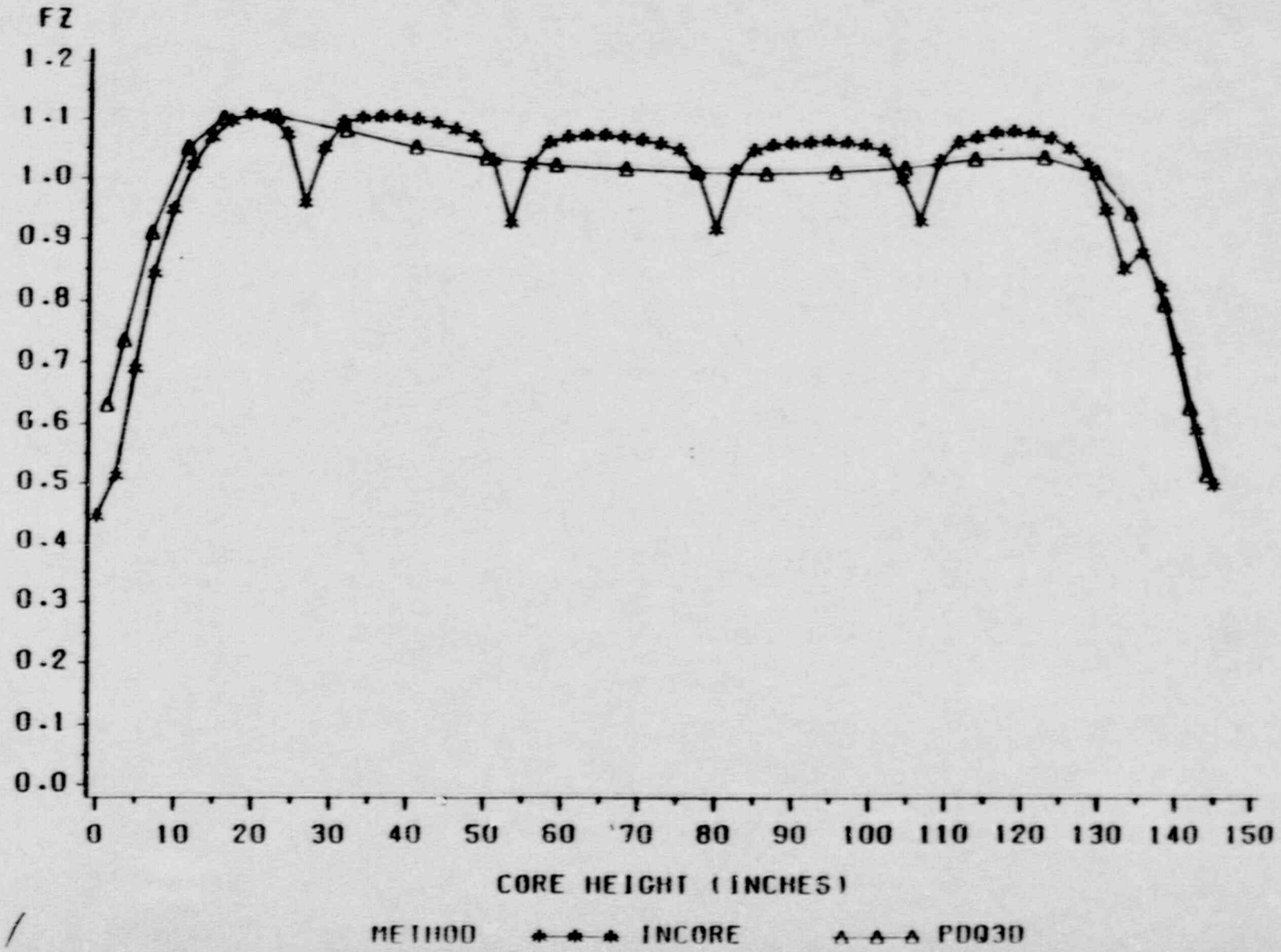
SURRY P(Z) COMPARISON
TWO ZONE PDQ3D RESULTS AND INCORE DATA
UNIT=S2C3 BURNUP=9025
FZ
1.2
1.1
1.0
0.9
0.8
0.7
0.6
0.5
0.4
0.3
0.2
0.1
0.0
0
10
20
30
40
50
60
70
80
90
100
110
120
130
140
150
CORE HEIGHT (INCHES)
METHOD
INCORE
PDQ3D

FIGURE 3-81

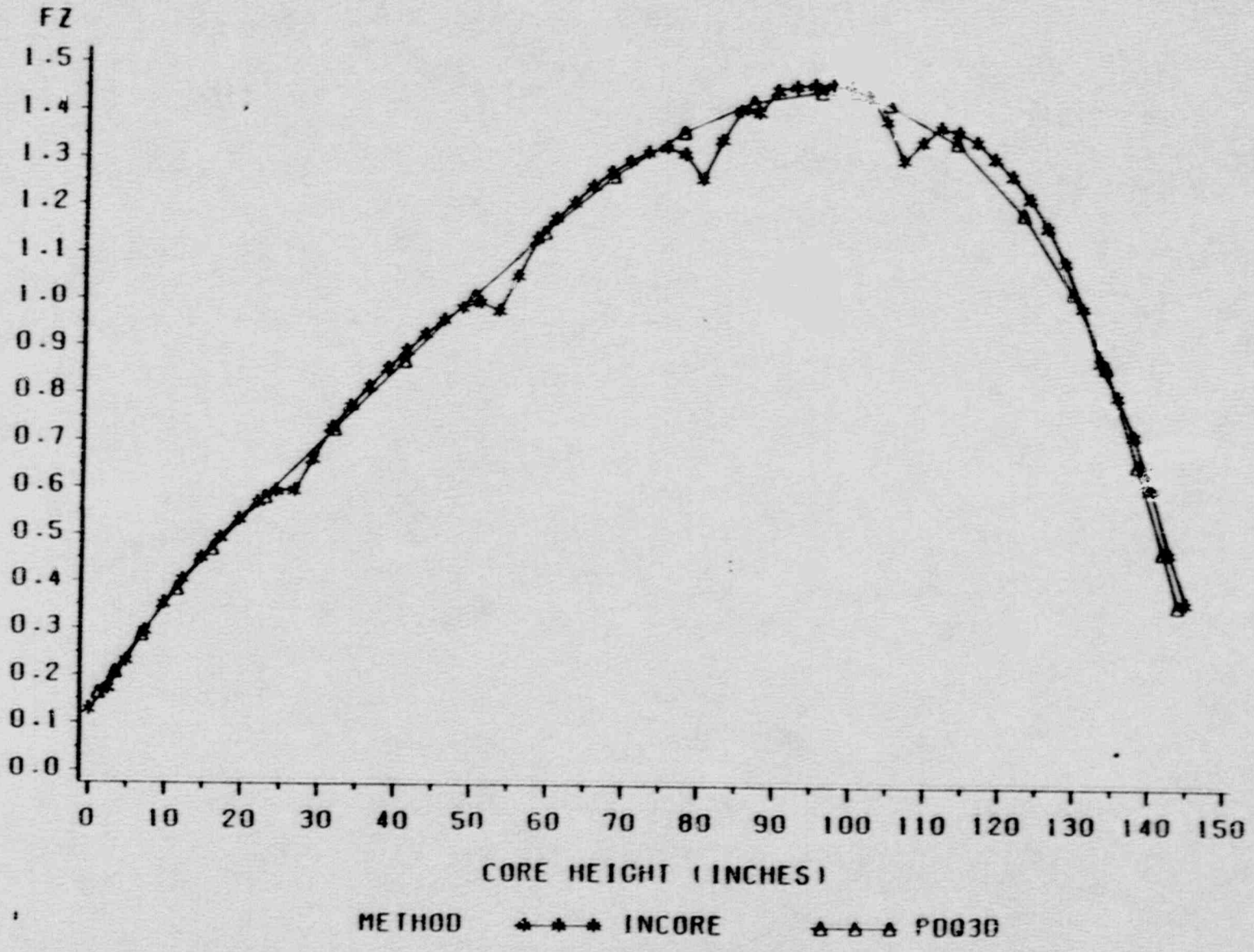
SURRY P(Z) COMPARISON
TWO ZONE PDQ3D RESULTS AND INCORE DATA
UNIT=S2C4 BURNUP=0
FZ
1.5
1.4
1.3
1.2
1.1
1.0
0.9
0.8
0.7
0.6
0.5
0.4
0.3
0.2
0.1
0.0
0
10
20
30
40
50
60
70
80
90
100
110
120
130
140
150
CORE HEIGHT (INCHES)
METHOD
INCORE
PDQ3D

FIGURE 3-82

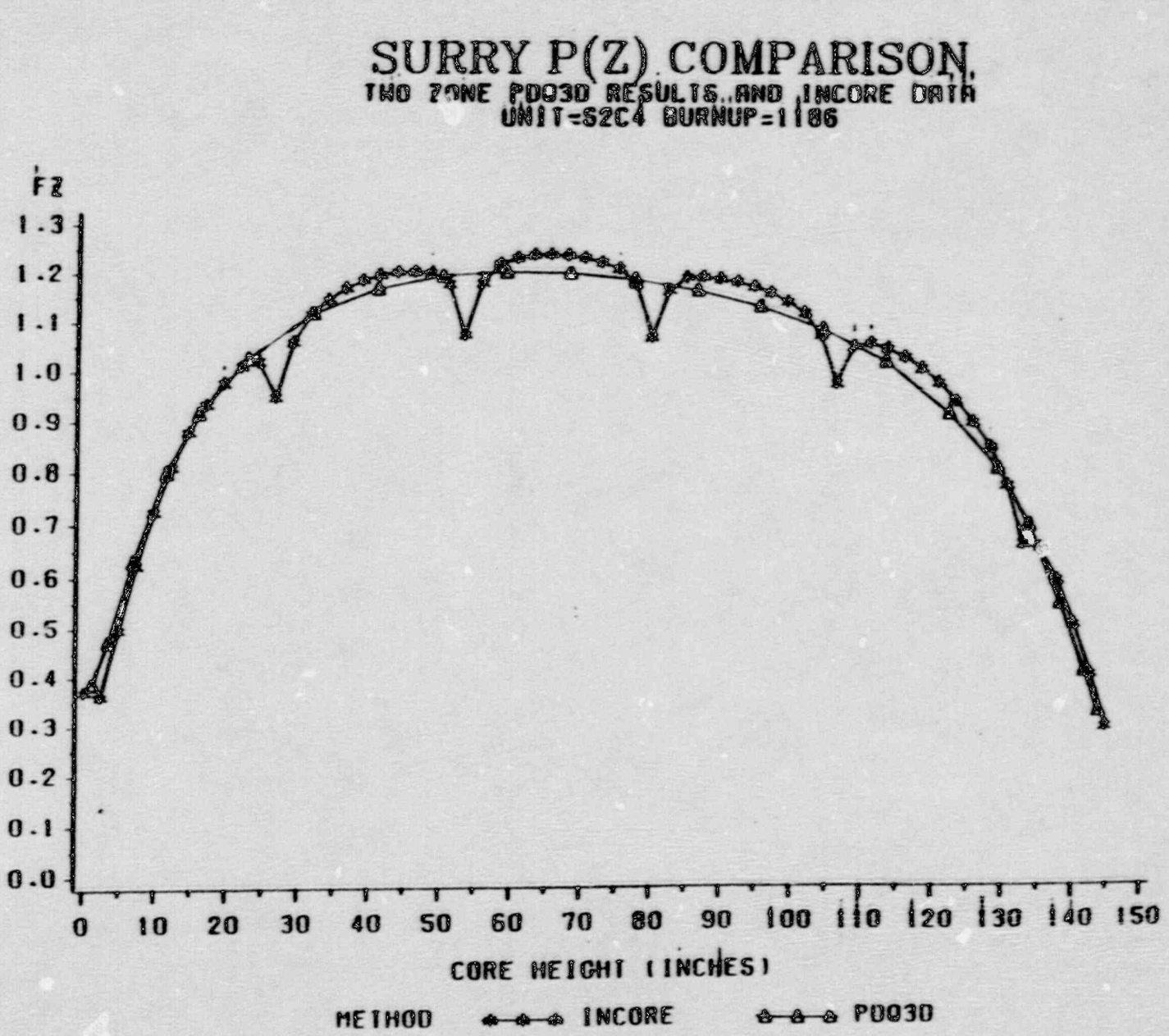
SURRY P(Z) COMPARISON
TWO ZONE PDQ3D RESULTS AND INCORE DATA
UNIT=S2C4 BURNUP=1186
FZ
1.3
1.2
1.1
1.0
0.9
0.8
0.7
0.6
0.5
0.4
0.3
0.2
0.1
0.0
0 10 20 30 40 50 60 70 80 90 100 110 120 130 140 150
CORE HEIGHT (INCHES)
METHOD INCORE PDQ3D

FIGURE 3-83

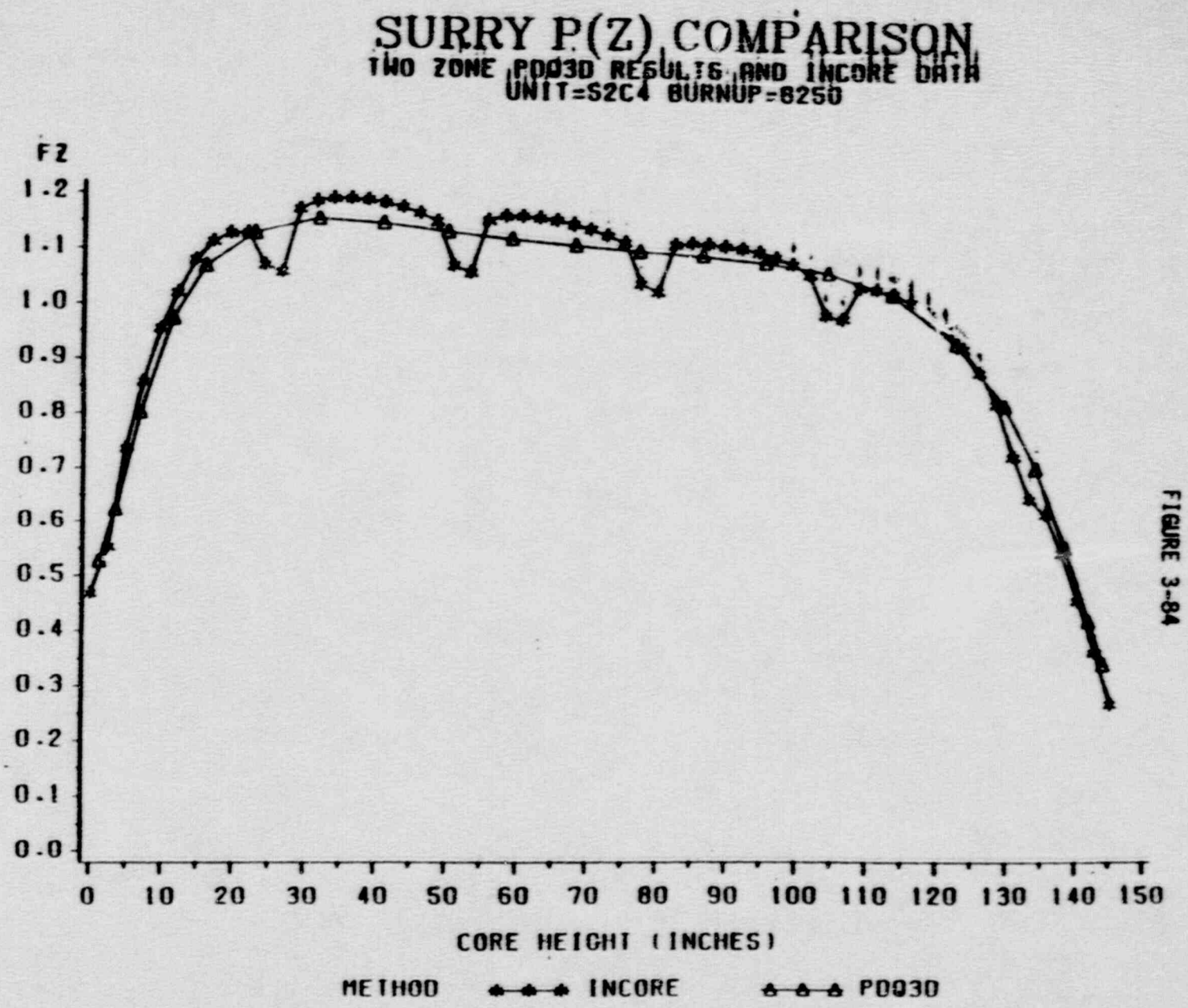
SURRY P(Z) COMPARISON
TWO ZONE PDQ3D RESULTS AND INCORE DATA
UNIT=S2C4 BURNUP=6250
FZ
1.2
1.1
1.0
0.9
0.8
0.7
0.6
0.5
0.4
0.3
0.2
0.1
0.0
0 10 20 30 40 50 60 70 80 90 100 110 120 130 140 150
CORE HEIGHT (INCHES)
METHOD INCORE PDQ3D

FIGURE 3-84

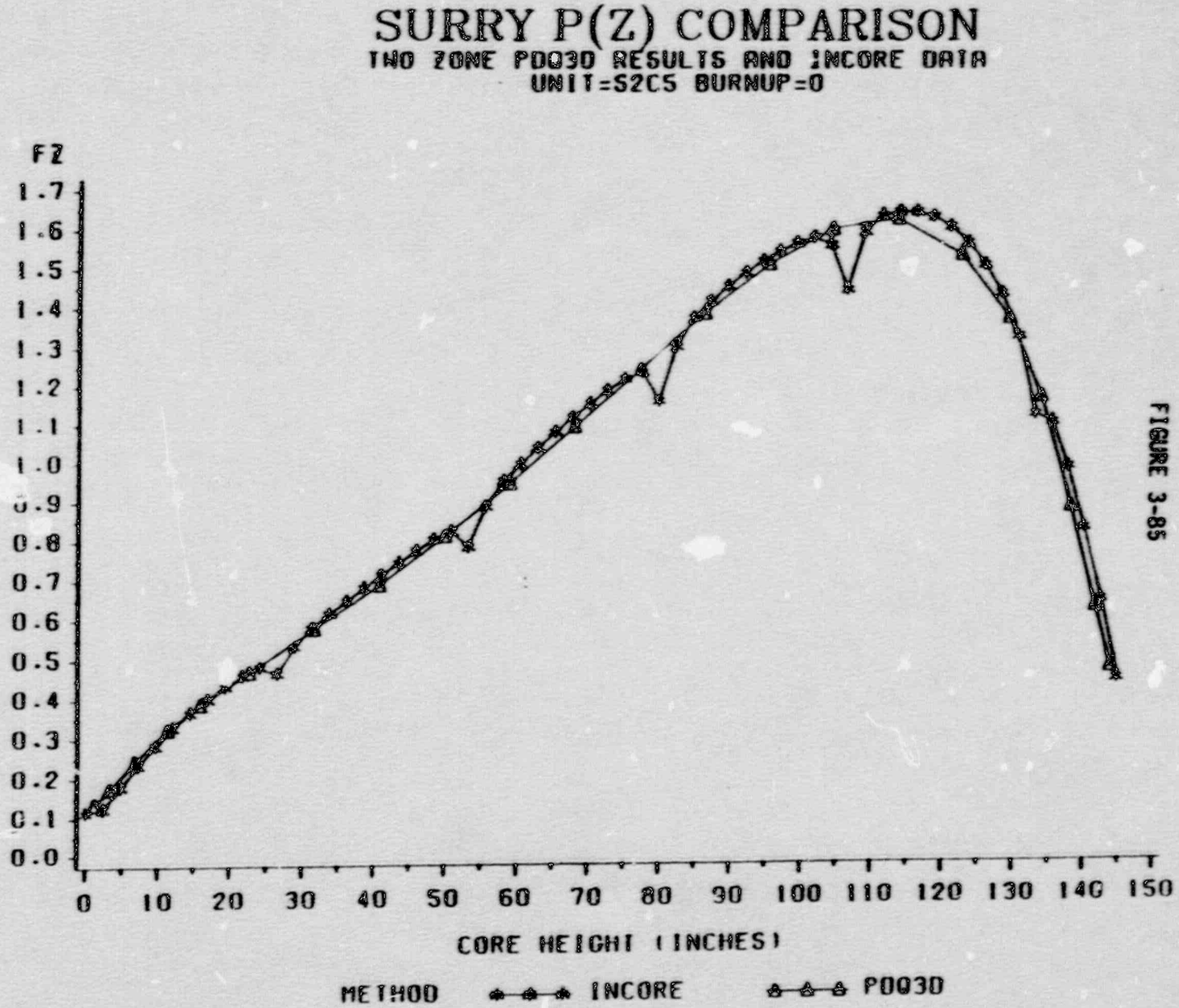
SURRY P(Z) COMPARISON
TWO ZONE P003D RESULTS AND INCORE DATA
UNIT=S2C5 BURNUP=0
FZ
1.7
1.6
1.5
1.4
1.3
1.2
1.1
1.0
0.9
0.8
0.7
0.6
0.5
0.4
0.3
0.2
0.1
0.0
0
10
20
30
40
50
60
70
80
90
100
110
120
130
140
150
CORE HEIGHT (INCHES)
METHOD
INCORE
P003D

FIGURE 3-85

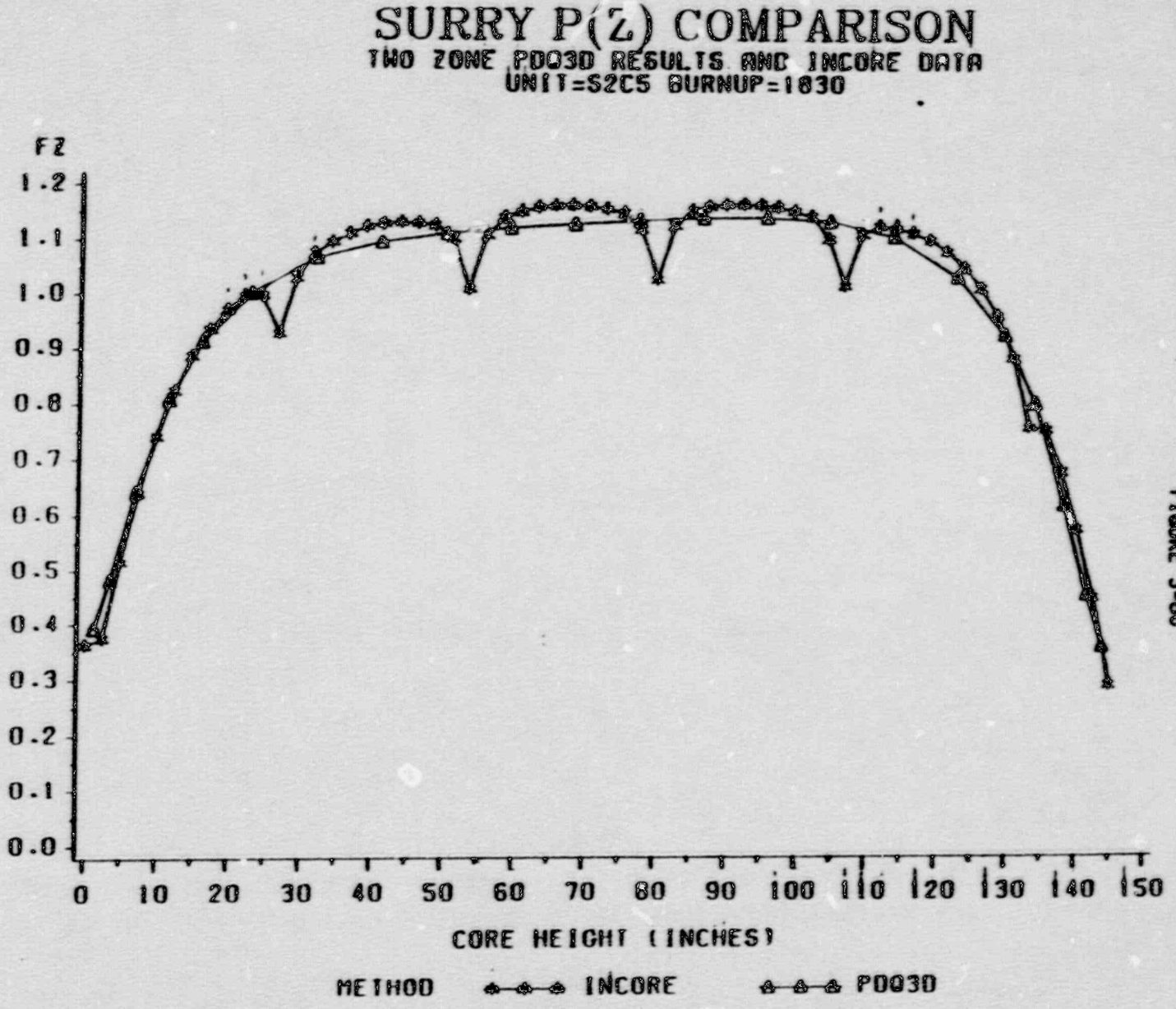
SURRY P(Z) COMPARISON
TWO ZONE PDQ3D RESULTS AND INCORE DATA
UNIT=S2C5 BURNUP=1830
FZ
1.2
1.1
1.0
0.9
0.8
0.7
0.6
0.5
0.4
0.3
0.2
0.1
0.0
0 10 20 30 40 50 60 70 80 90 100 110 120 130 140 150
CORE HEIGHT (INCHES)
METHOD INCORE PDQ3D

FIGURE 3-86

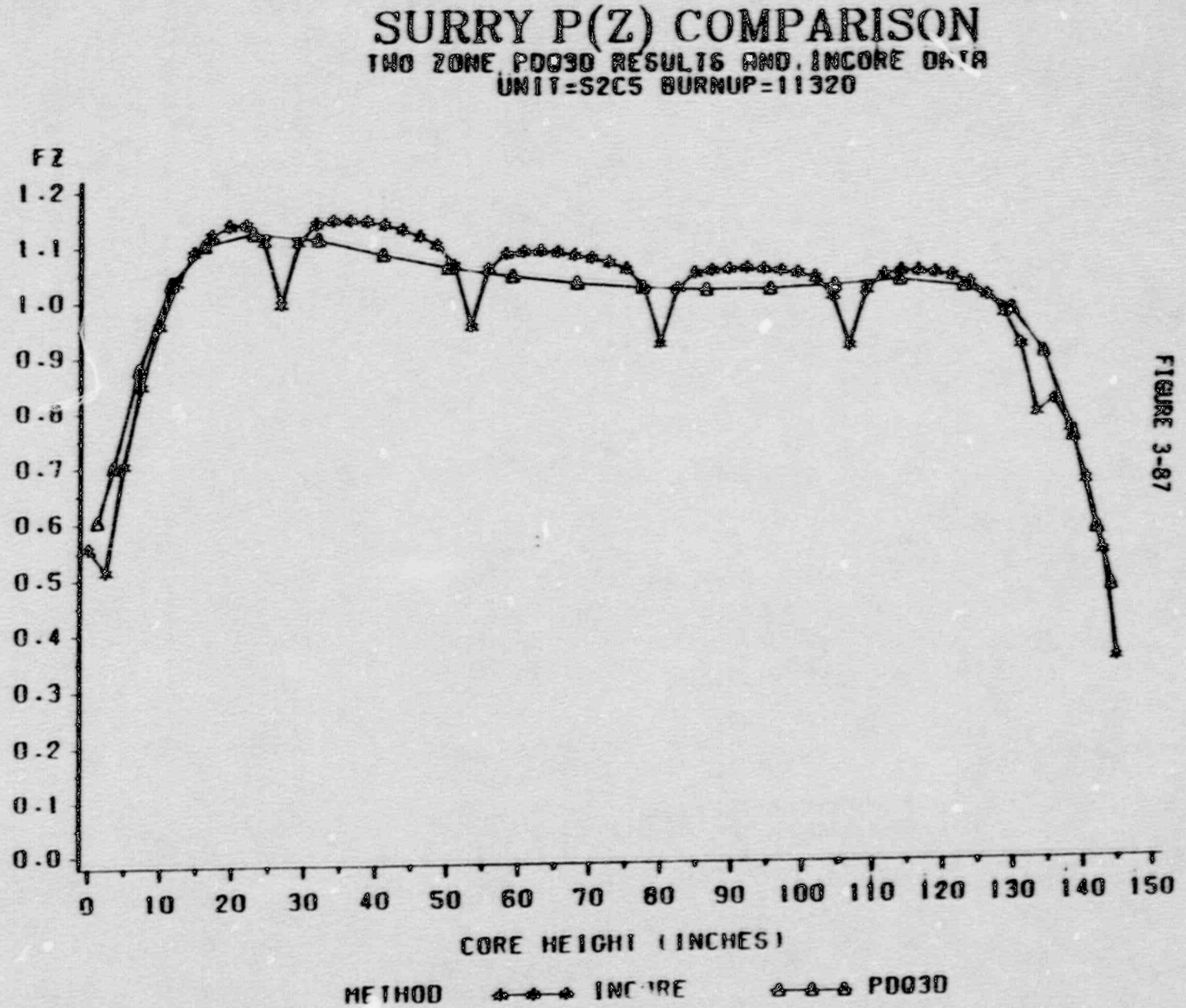
SURRY P(Z) COMPARISON
TWO ZONE PDQ3D RESULTS AND INCORE DATA
UNIT=S2C5 BURNUP=11320
FZ
1.2
1.1
1.0
0.9
0.8
0.7
0.6
0.5
0.4
0.3
0.2
0.1
0.0
0 10 20 30 40 50 60 70 80 90 100 110 120 130 140 150
CORE HEIGHT (INCHES)
METHOD INCORE PDQ3D

FIGURE 3-87

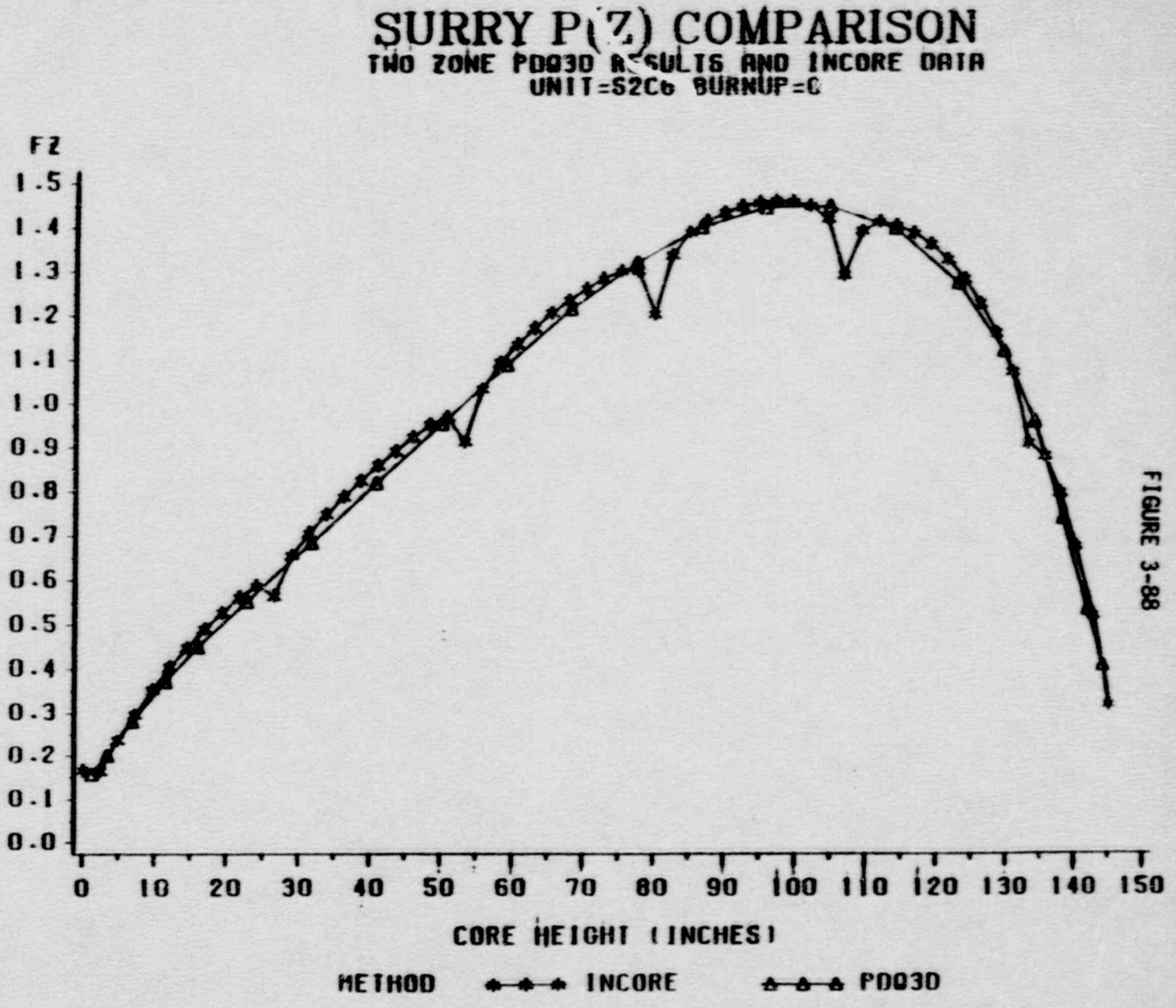
SURRY P(Z) COMPARISON
TWO ZONE PDQ3D RESULTS AND INCORE DATA
UNIT=S2C6 BURNUP=0
FZ
1.5
1.4
1.3
1.2
1.1
1.0
0.9
0.8
0.7
0.6
0.5
0.4
0.3
0.2
0.1
0.0
0 10 20 30 40 50 60 70 80 90 100 110 120 130 140 150
CORE HEIGHT (INCHES)
METHOD INCORE PDQ3D

FIGURE 3-88

SURRY P(Z) COMPARISON

TWO ZONE PDQ3D RESULTS AND INCORE DATA

UNIT=S2C6 BURNUP=1116

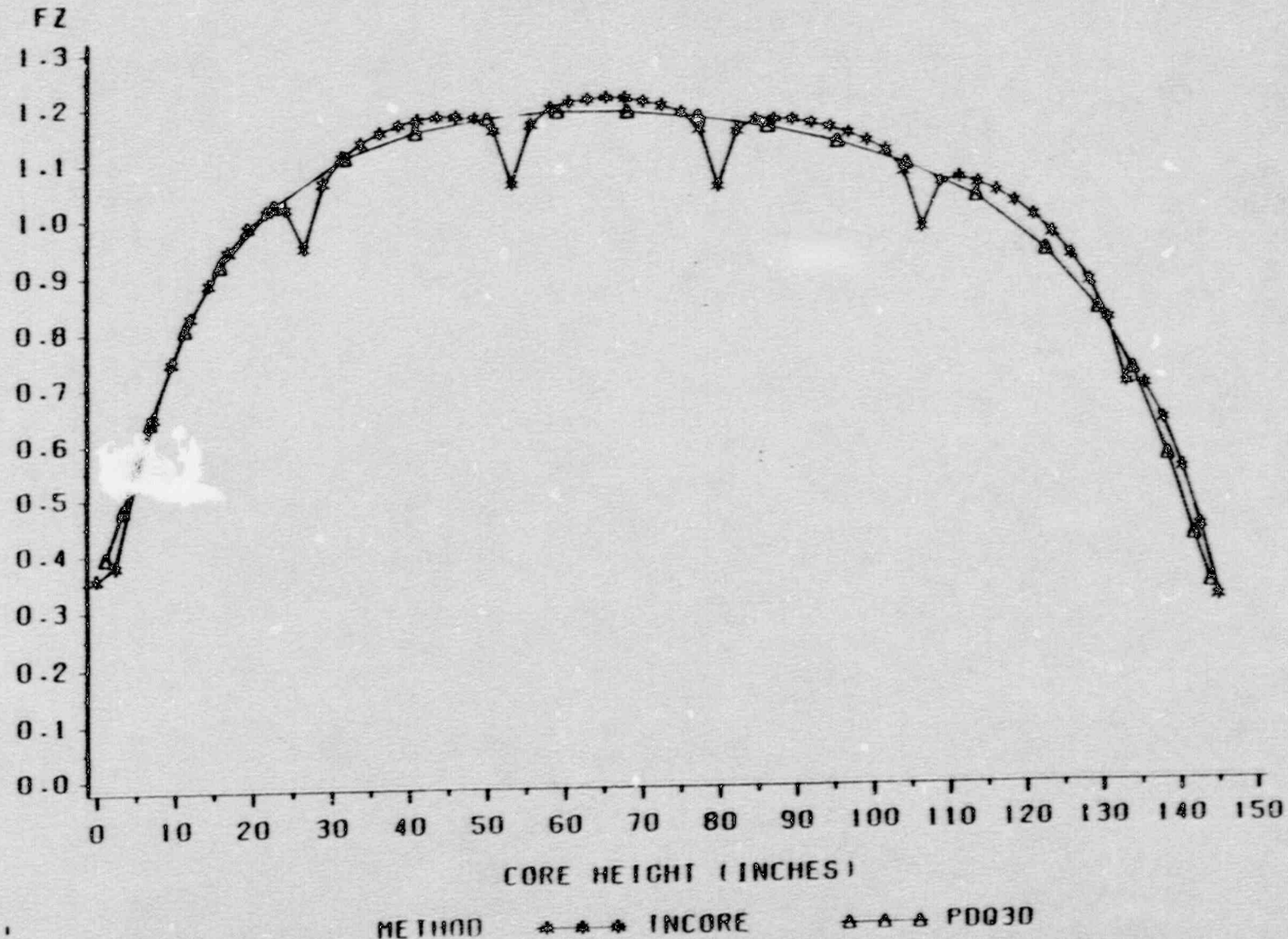

FIGURE 3-89

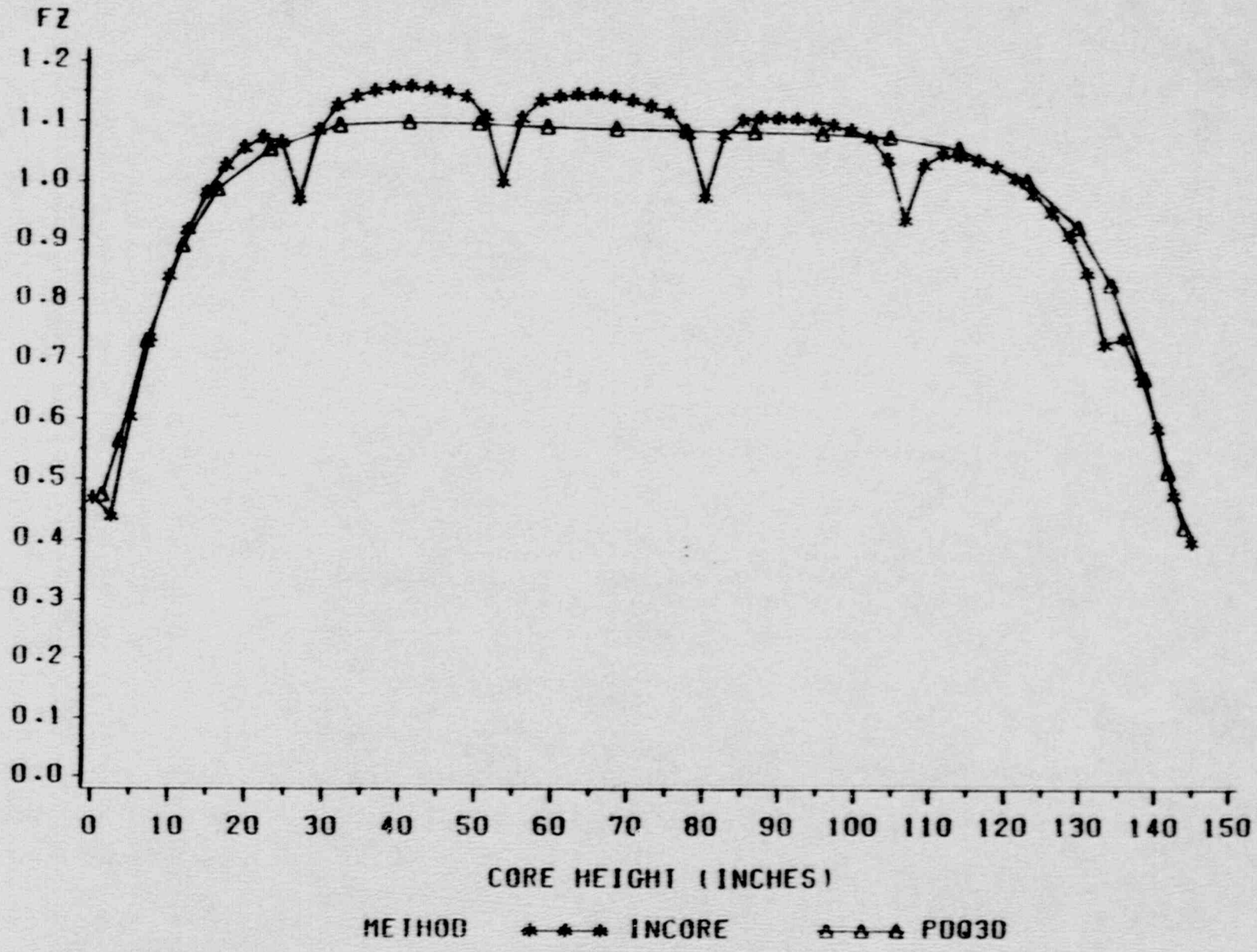
SURRY P(Z) COMPARISON
TWO ONE PDQ3D RESULTS AND INCORE DATA
UNIT=S2C6 BURNUP=7390
FZ
1.2
1.1
1.0
0.9
0.8
0.7
0.6
0.5
0.4
0.3
0.2
0.1
0.0
0 10 20 30 40 50 60 70 80 90 100 110 120 130 140 150
CORE HEIGHT (INCHES)
METHOD INCORE PDQ3D

FIGURE 3-90

SURRY P(Z) COMPARISON

TWO ZONE PDQ3D RESULTS AND INCORE DATA
UNIT=S2C6 BURNUP=13900

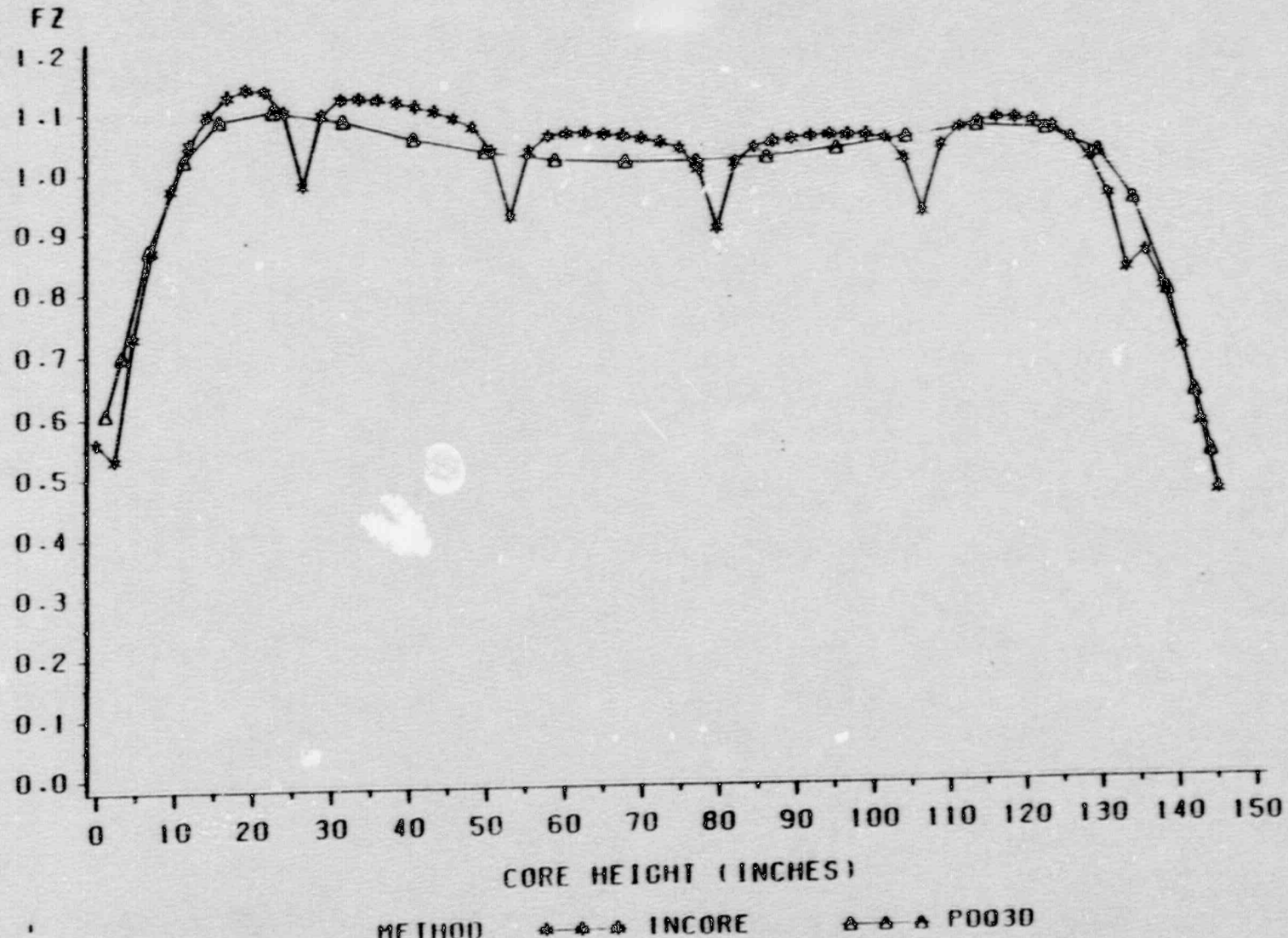

FIGURE 3-91

SURRY P(Z) COMPARISON

TWO ZONE PDQ3D RESULTS AND INCORE DATA
UNIT=S2C7 BURNUP=0

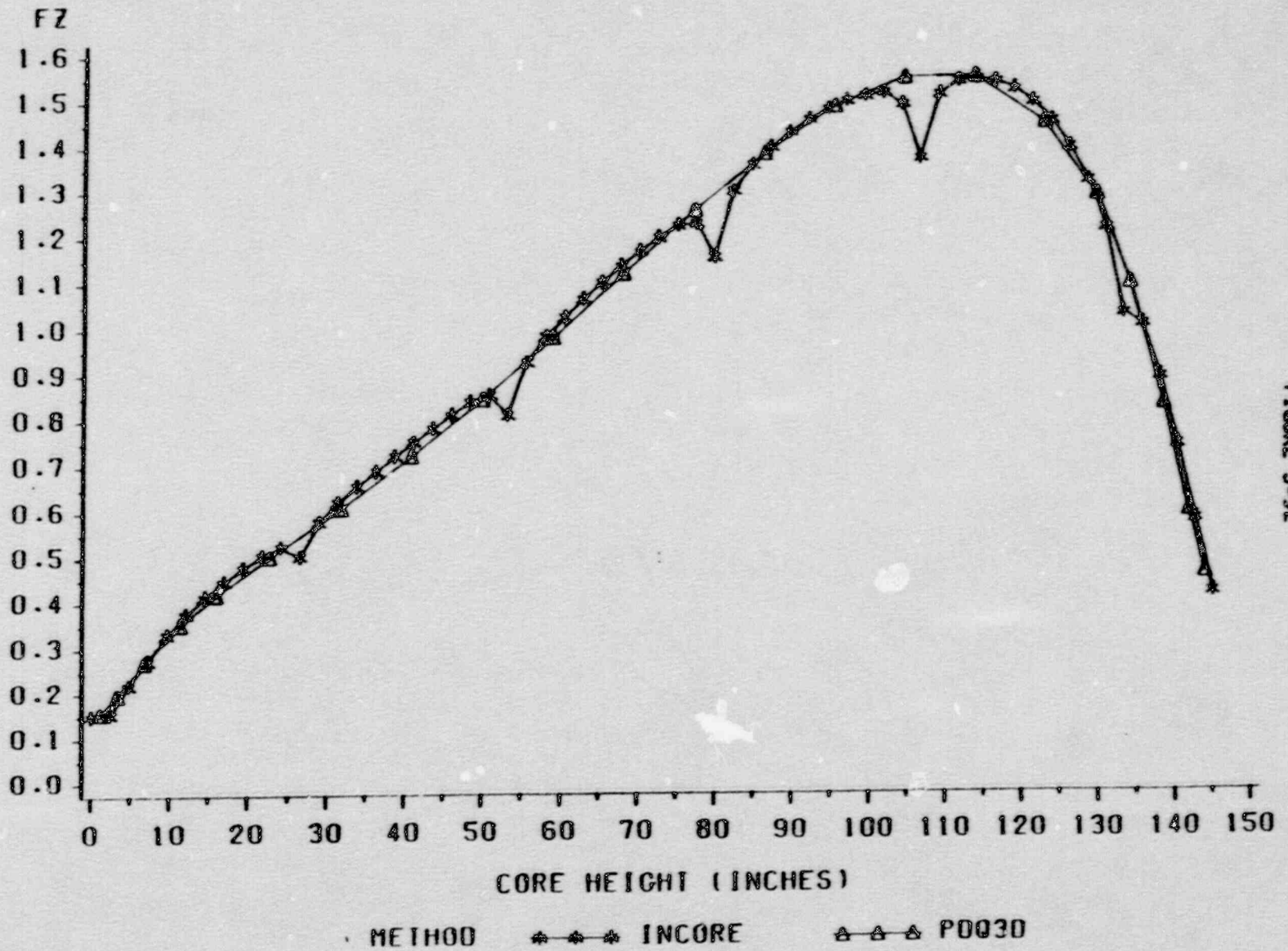

FIGURE 3-92

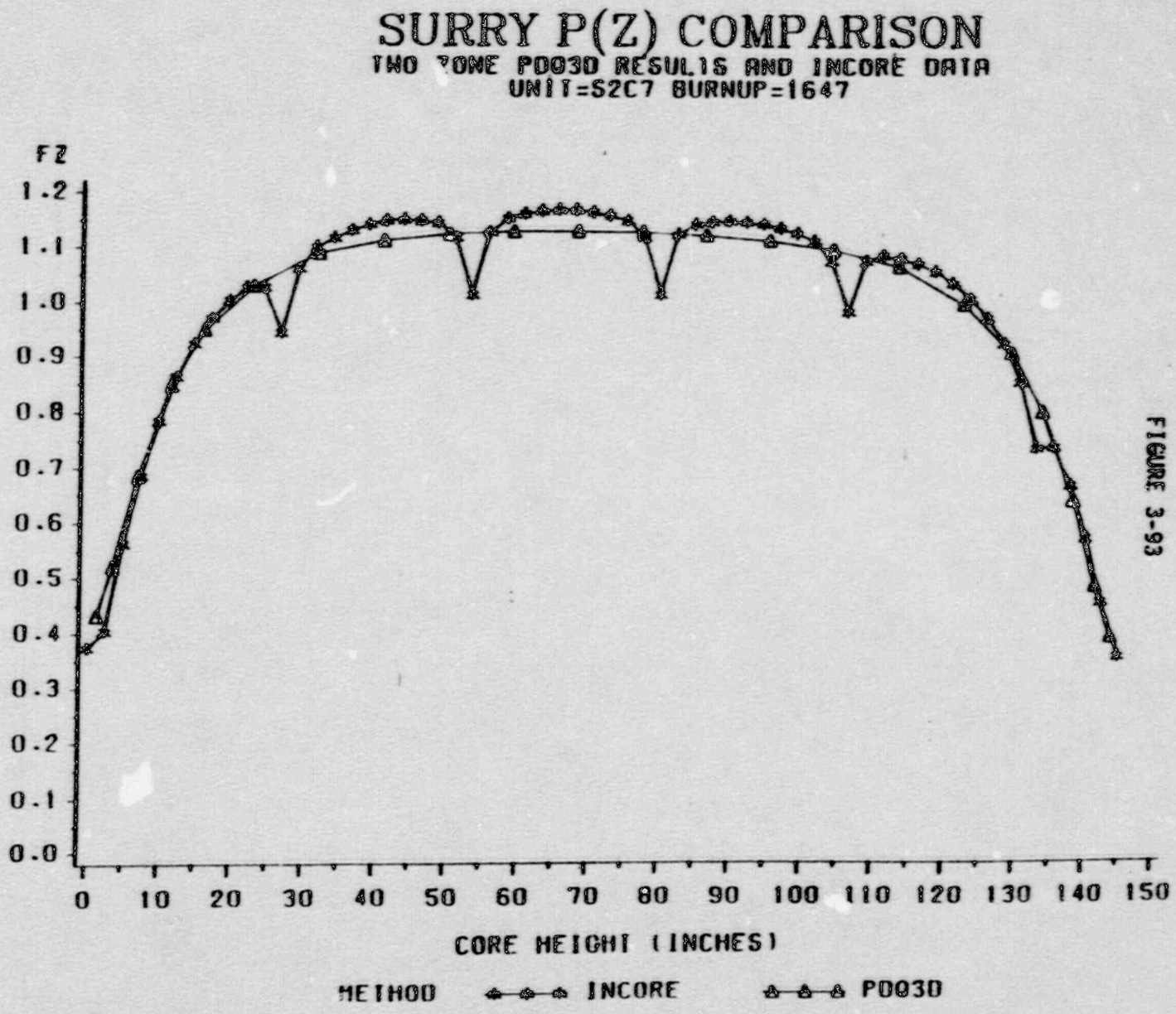
SURRY P(Z) COMPARISON
TWO ZONE PD03D RESULTS AND INCORE DATA
UNIT=S2C7 BURNUP=1647
FZ
1.2
1.1
1.0
0.9
0.8
0.7
0.6
0.5
0.4
0.3
0.2
0.1
0.0
0 10 20 30 40 50 60 70 80 90 100 110 120 130 140 150
CORE HEIGHT (INCHES)
METHOD INCORE PD03D

FIGURE 3-93

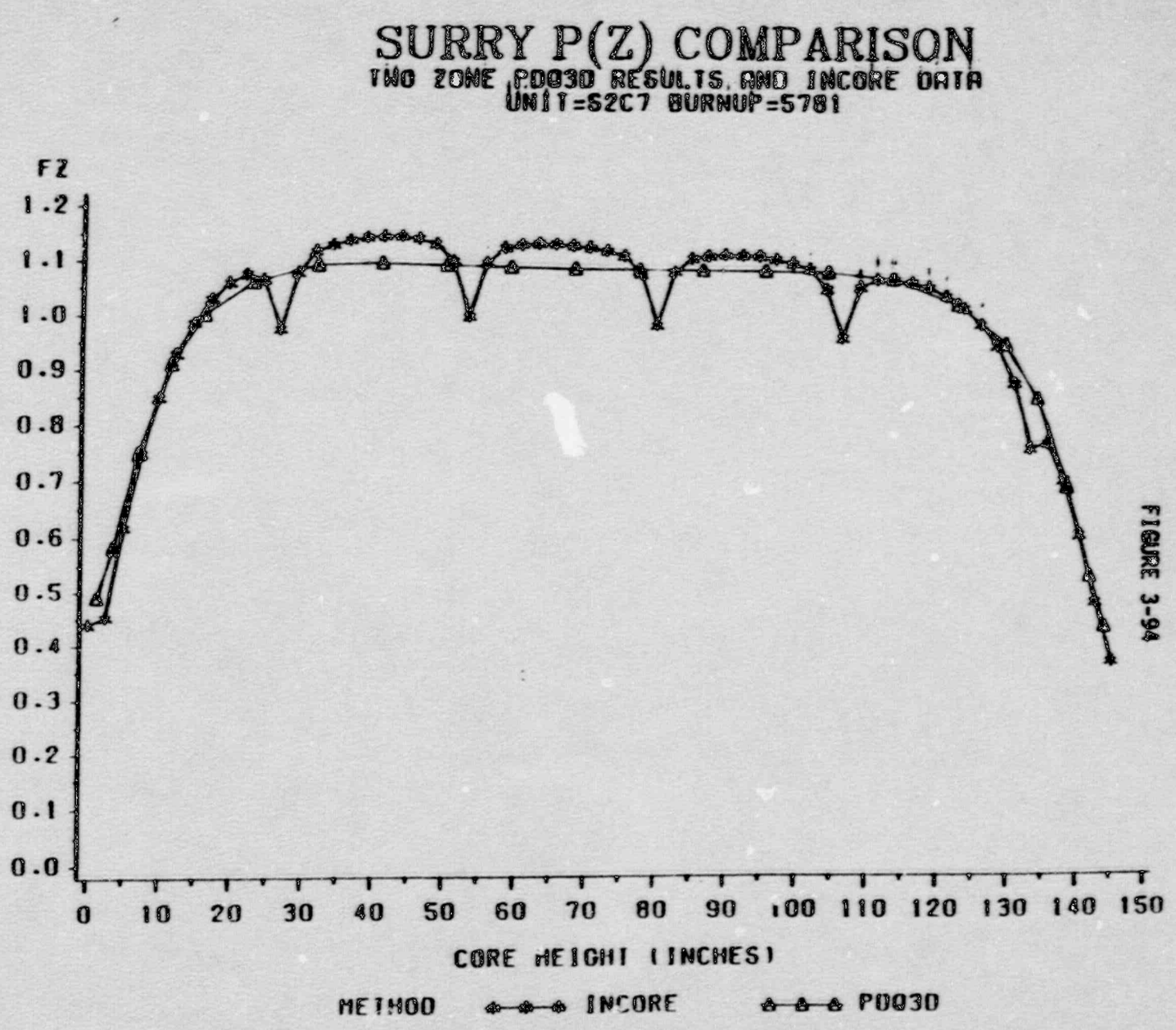
SURRY P(Z) COMPARISON
TWO ZONE PD03D RESULTS AND INCORE DATA
UNIT=S2C7 BURNUP=5781
FZ
1.2
1.1
1.0
0.9
0.8
0.7
0.6
0.5
0.4
0.3
0.2
0.1
0.0
0 10 20 30 40 50 60 70 80 90 100 110 120 130 140 150
CORE HEIGHT (INCHES)
METHOD INCORE PD03D

FIGURE 3-94

SURRY P(Z) COMPARISON

TWO ZONE PDQ3D RESULTS AND INCORE DATA
UNIT=S2C7 BURNUP=13122

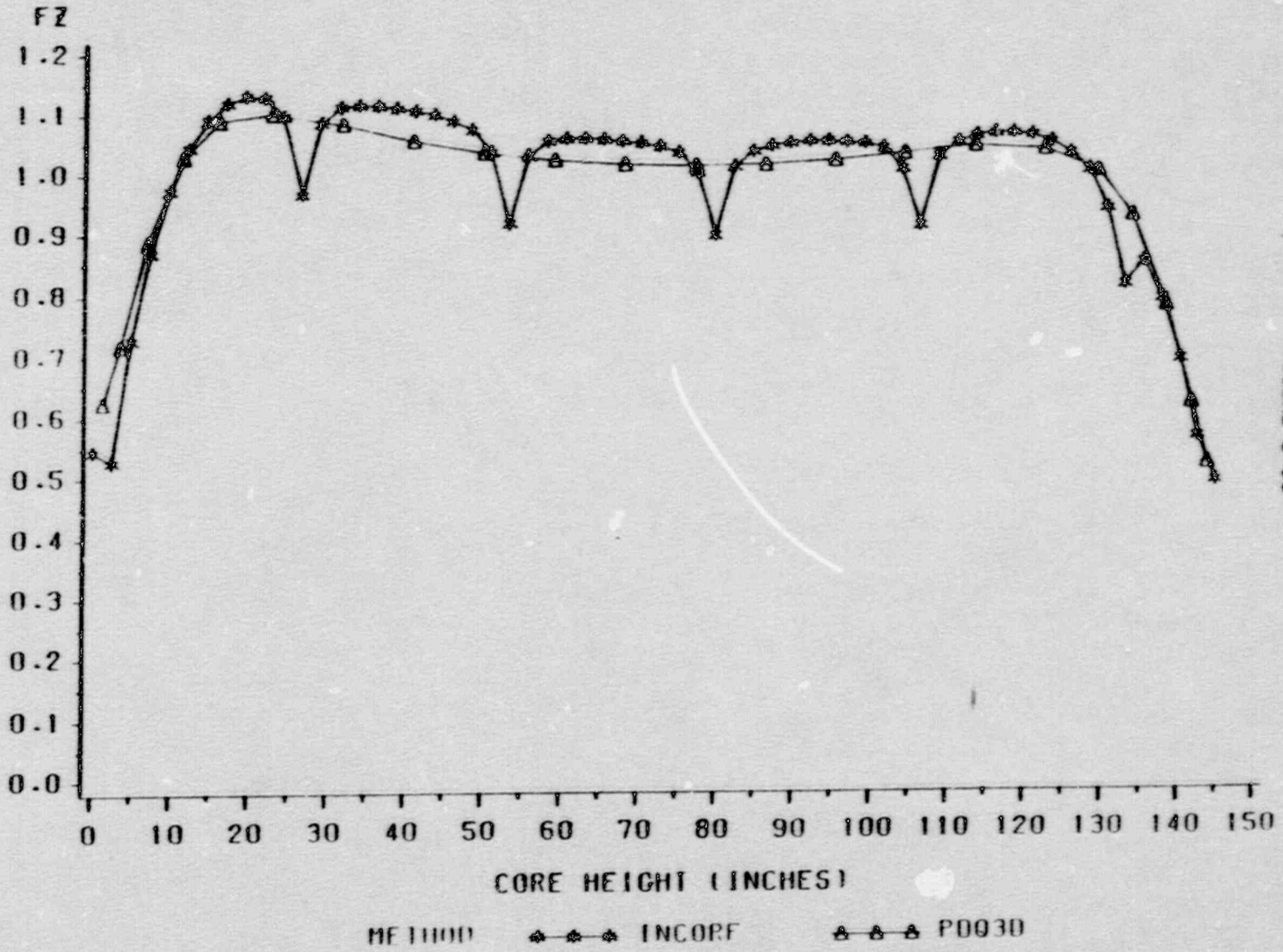

FIGURE 3-95

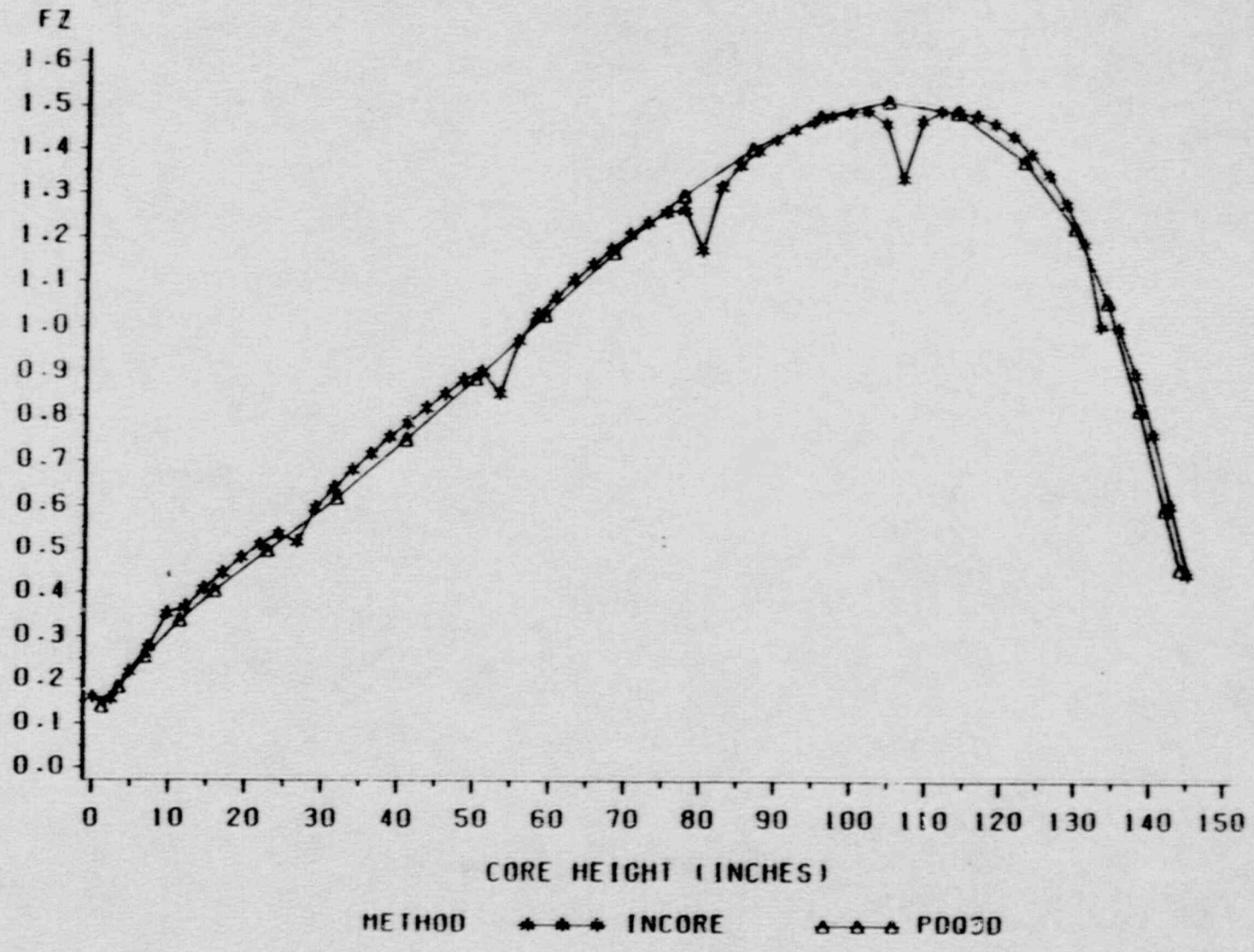
SURRY P(Z) COMPARISON
TWO ZONE PDQ3D RESULTS AND INCORE DATA
UNIT=S2C8 BURNUP=0
FZ
1.6
1.5
1.4
1.3
1.2
1.1
1.0
0.9
0.8
0.7
0.6
0.5
0.4
0.3
0.2
0.1
0.0
0 10 20 30 40 50 60 70 80 90 100 110 120 130 140 150
CORE HEIGHT (INCHES)
METHOD INCORE PDQ3D

FIGURE 3-96

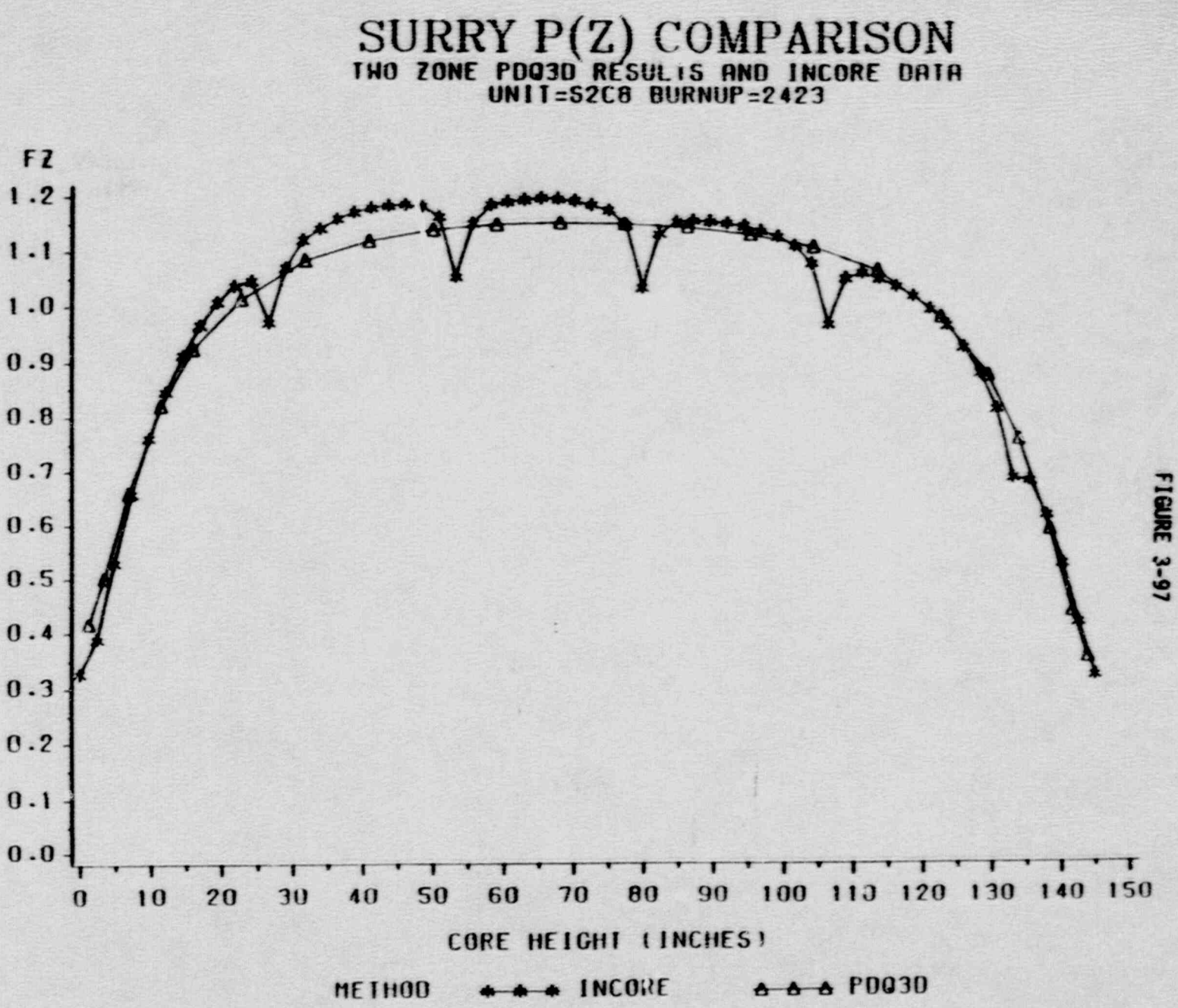
SURRY P(Z) COMPARISON
TWO ZONE PDQ3D RESULTS AND INCORE DATA
UNIT=S2C8 BURNUP=2423
FZ
1.2
1.1
1.0
0.9
0.8
0.7
0.6
0.5
0.4
0.3
0.2
0.1
0.0
0
10
20
30
40
50
60
70
80
90
100
110
120
130
140
150
CORE HEIGHT (INCHES)
METHOD
INCORE
PDQ3D

FIGURE 3-97

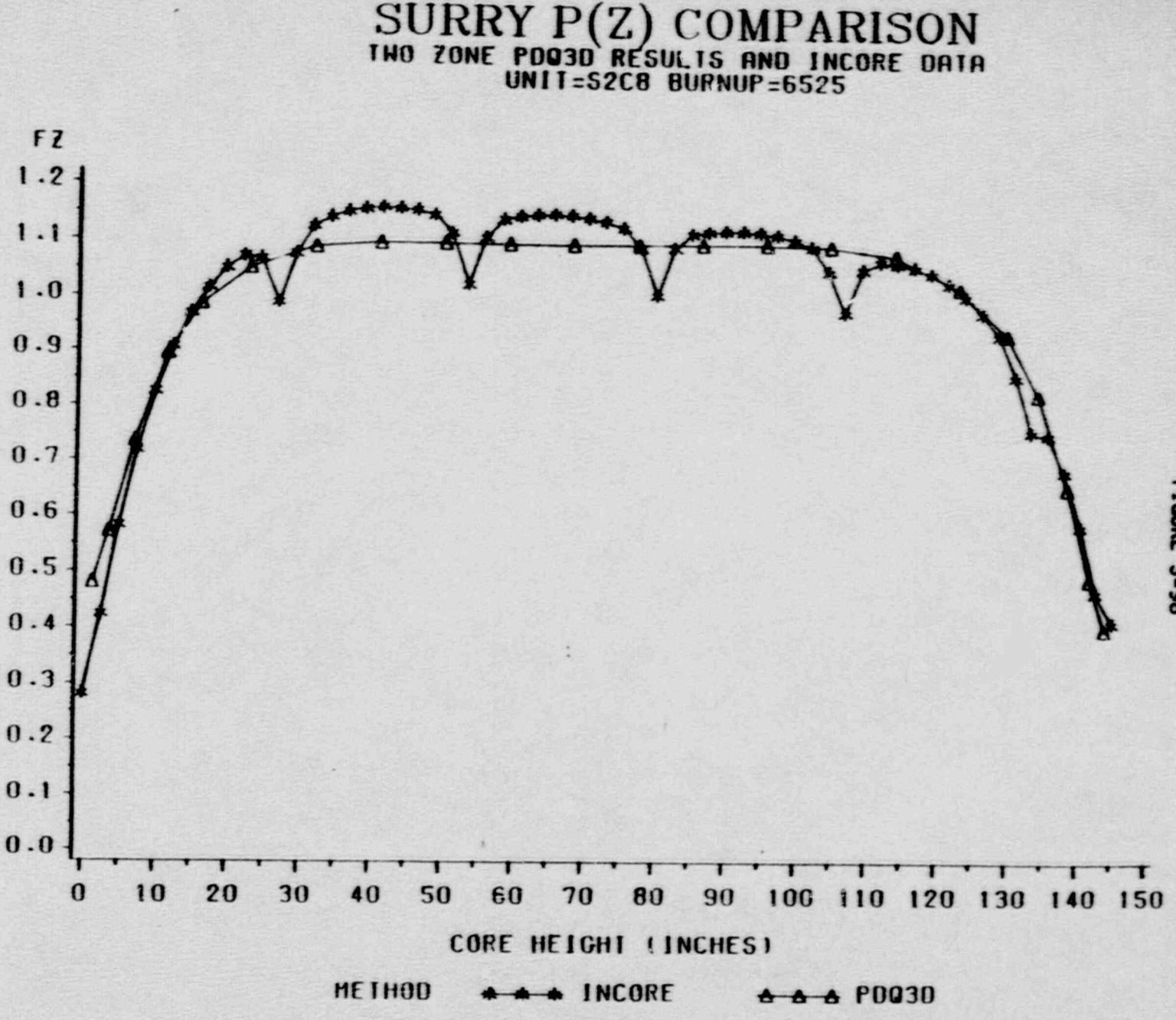
SURRY P(Z) COMPARISON
TWO ZONE PDQ3D RESULTS AND INCORE DATA
UNIT=S2C8 BURNUP=6525
FZ
1.2
1.1
1.0
0.9
0.8
0.7
0.6
0.5
0.4
0.3
0.2
0.1
0.0
0 10 20 30 40 50 60 70 80 90 100 110 120 130 140 150
CORE HEIGHT (INCHES)
METHOD INCORE PDQ3D

FIGURE 3-98

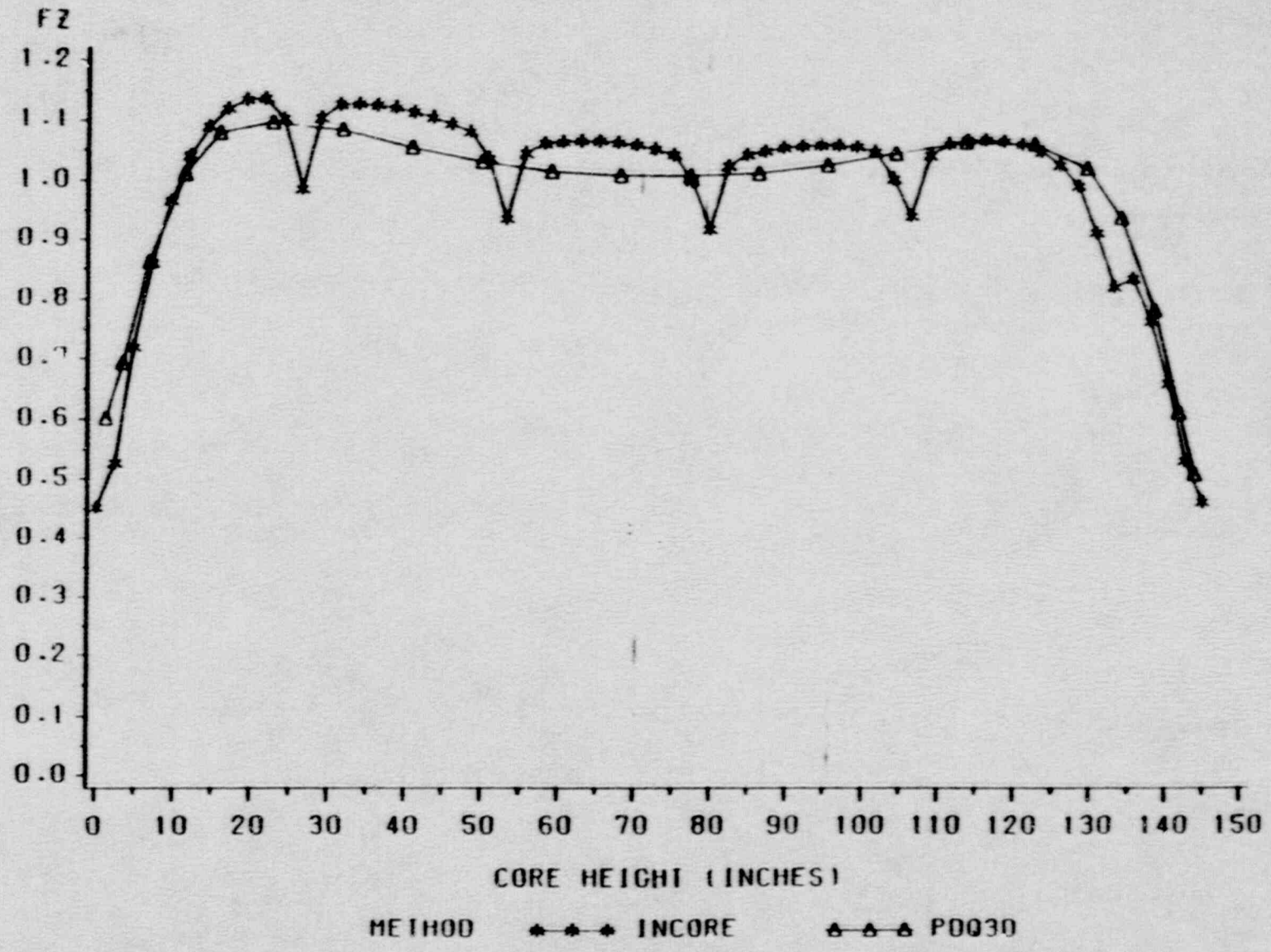
SURRY P(Z) COMPARISON
TWO ZONE PDQ3D RESULTS AND INCORE DATA
UNIT=S2C8 BURNUP=12391
FZ
1.2
1.1
1.0
0.9
0.8
0.7
0.6
0.5
0.4
0.3
0.2
0.1
0.0
0
10
20
30
40
50
60
70
80
90
100
110
120
130
140
150
CORE HEIGHT (INCHES)
METHOD
INCORE
PDQ3D

FIGURE 3-99

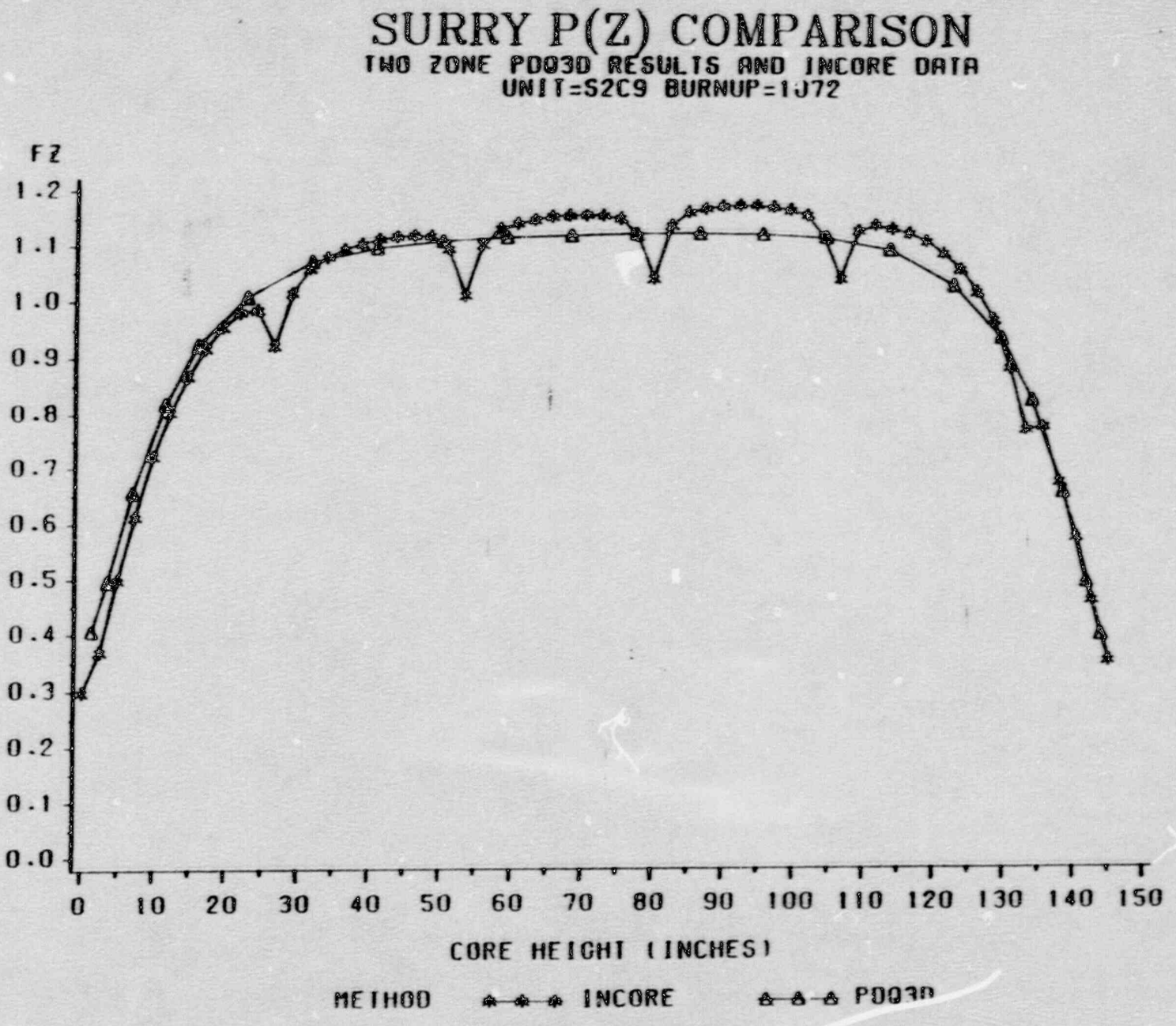
SURRY P(Z) COMPARISON
TWO ZONE PDQ3D RESULTS AND INCORE DATA
UNIT=S2C9 BURNUP=1J72
FZ
1.2
1.1
1.0
0.9
0.8
0.7
0.6
0.5
0.4
0.3
0.2
0.1
0.0
0
10
20
30
40
50
60
70
80
90
100
110
120
130
140
150
CORE HEIGHT (INCHES)
METHOD
INCORE
PDQ3D

FIGURE 3-100

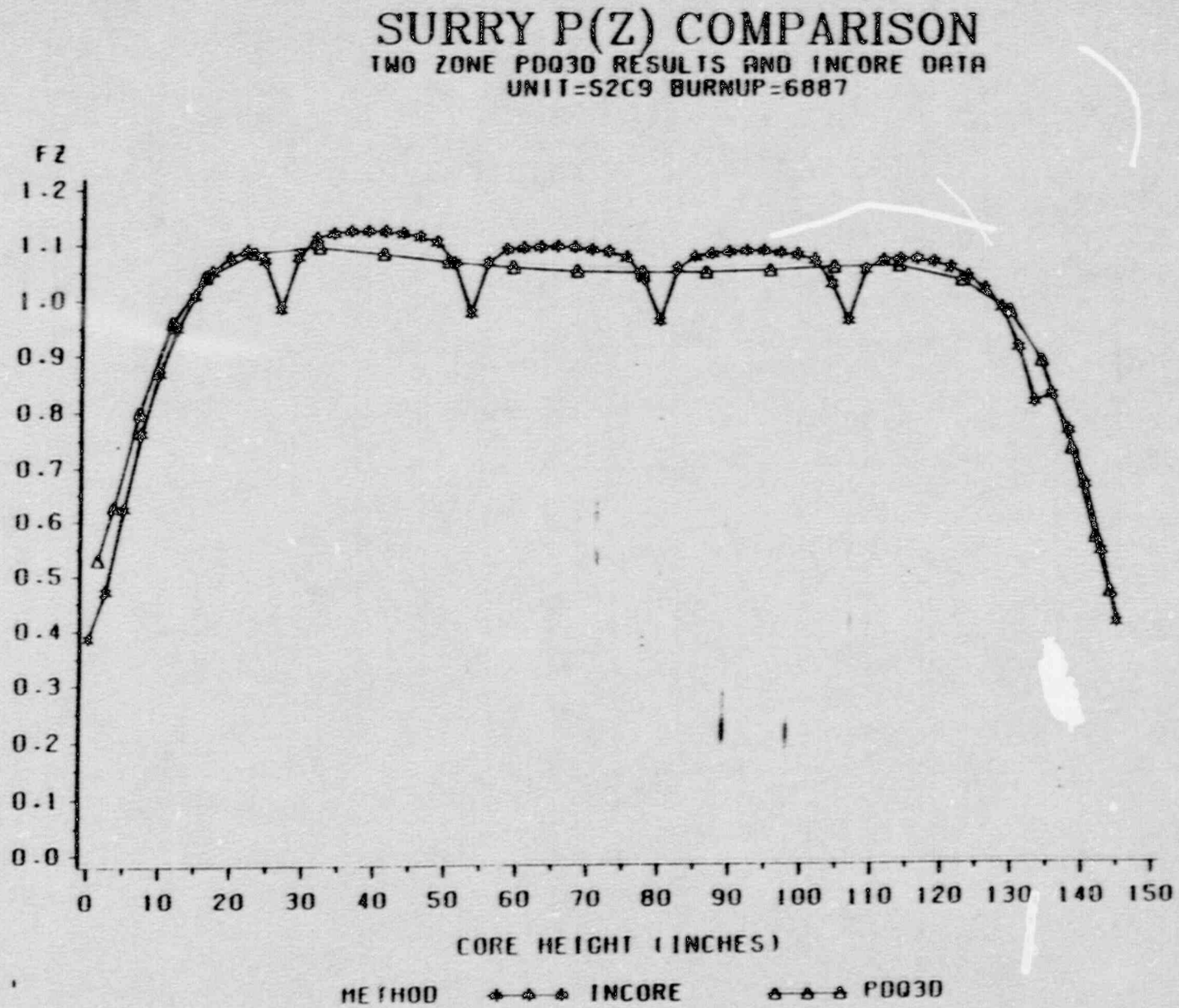
SURRY P(Z) COMPARISON
TWO ZONE PDQ3D RESULTS AND INCORE DATA
UNIT=S2C9 BURNUP=6887
FZ
1.2
1.1
1.0
0.9
0.8
0.7
0.6
0.5
0.4
0.3
0.2
0.1
0.0
0
10
20
30
40
50
60
70
80
90
100
110
120
130
140
150
CORE HEIGHT (INCHES)
METHOD
INCORE
PDQ3D

FIGURE 3-101

FIGURE 3-102

N1C1 3D PDQ VS. MEASURED RPD COMPARISON
HZP, D-228, 0 MWD/MTU N1C1-01A

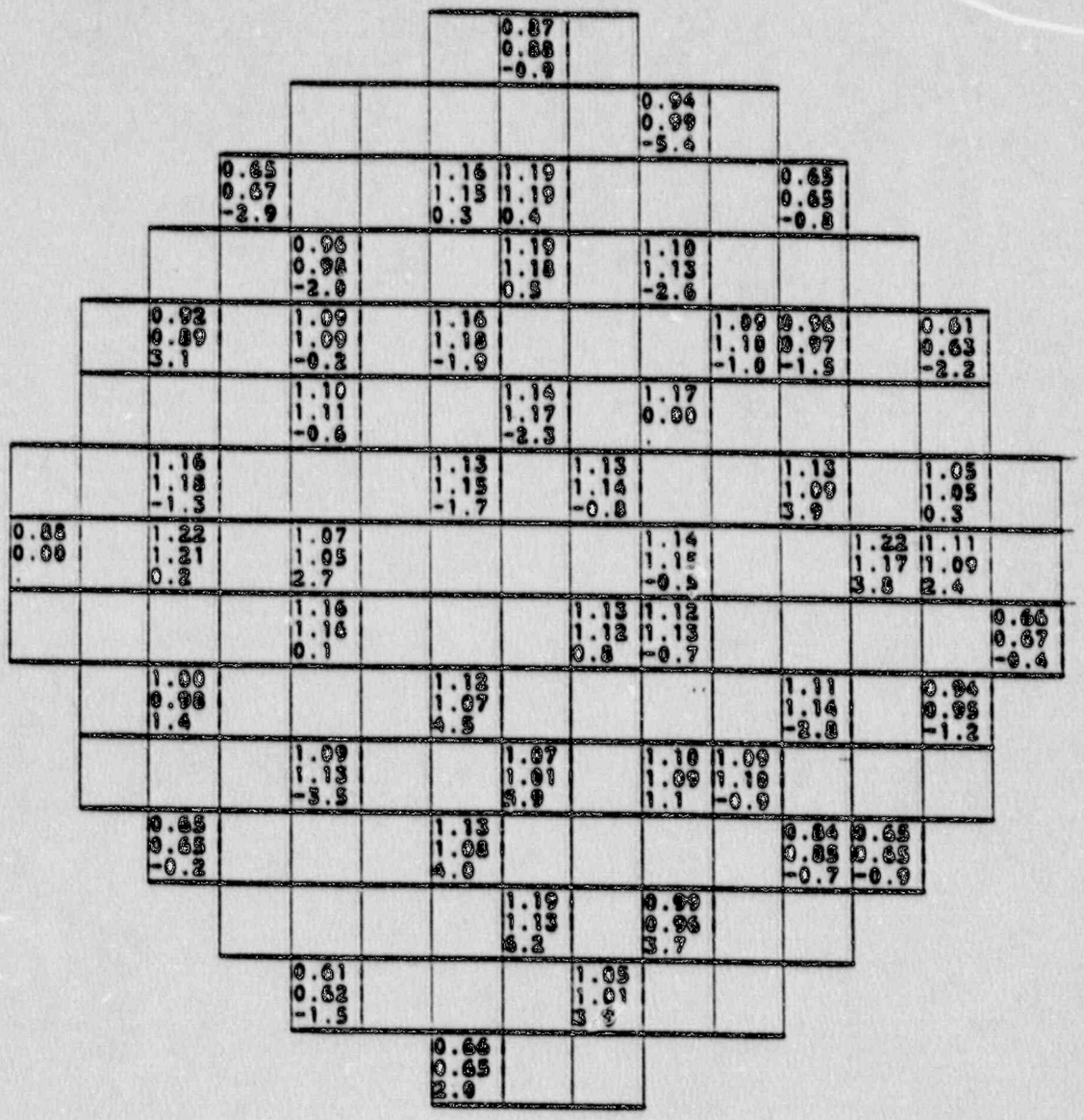

MAX DIFFERENCE = 6.22
MAX DIFF (RPD>0.9) = 4.22
RMS DIFFERENCE = 2.50

X.XX PREDICTED
X.XX MEASURED
X.X PERCENT DIFFERENCE

FIGURE 3-103

N1C1 3D PDQ VS. MEASURED RPD COMPARISON
HFP, D-220, 14070 MWD/MTU N1C1-66A

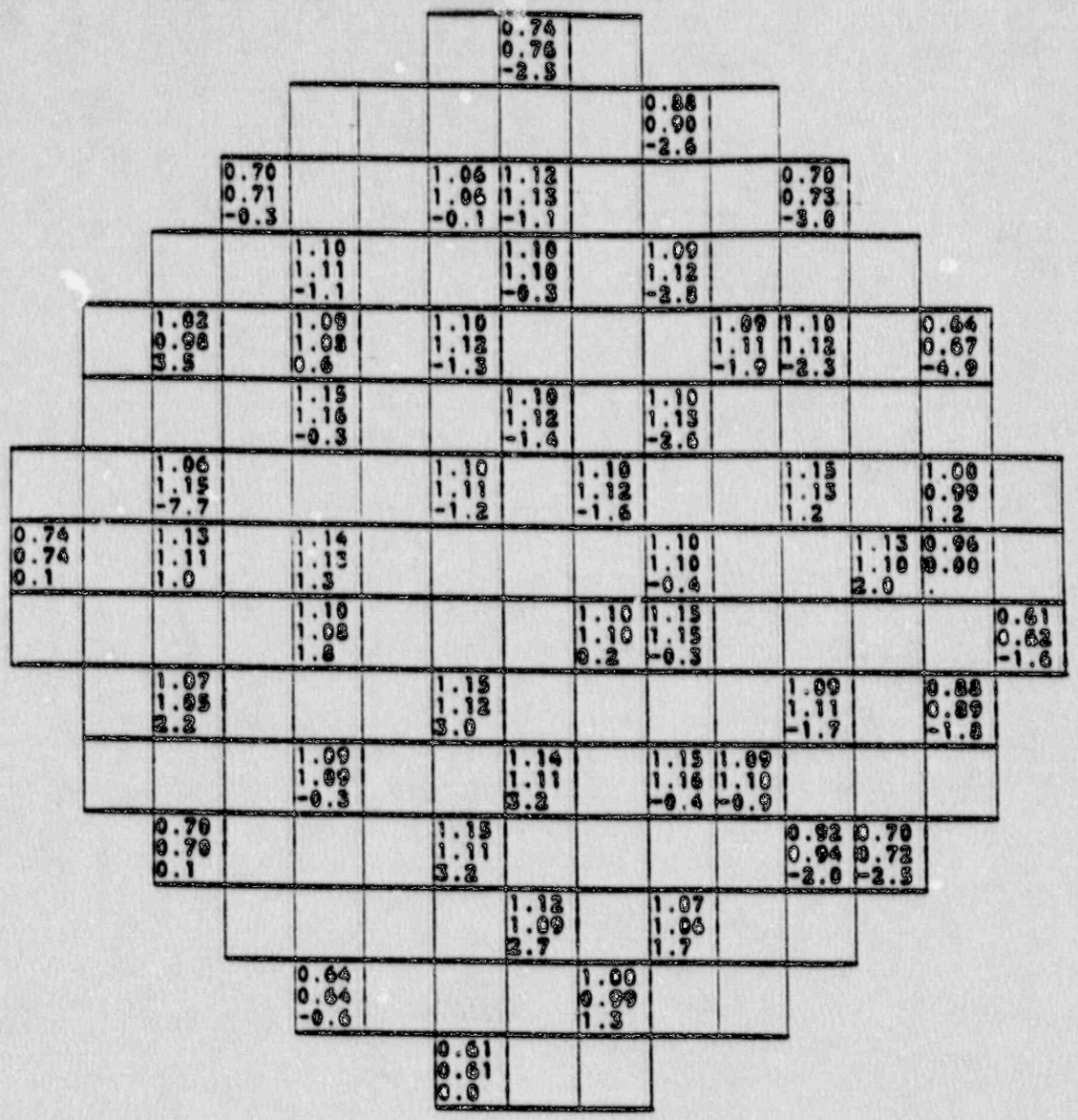

MAX DIFFERENCE = -7.7
MAX DIFF (RPD>0.9) = -7.7
RMS DIFFERENCE = 2.17

X.XX	PREDICTED
X.XX	MEASURED
X.X	PERCENT DIFFERENCE

FIGRE 3-104

N1C2 3D PDQ VS. MEASURED RPD COMPARISON
HZP, D-228, 0 MWD/MTU N1C2-03A

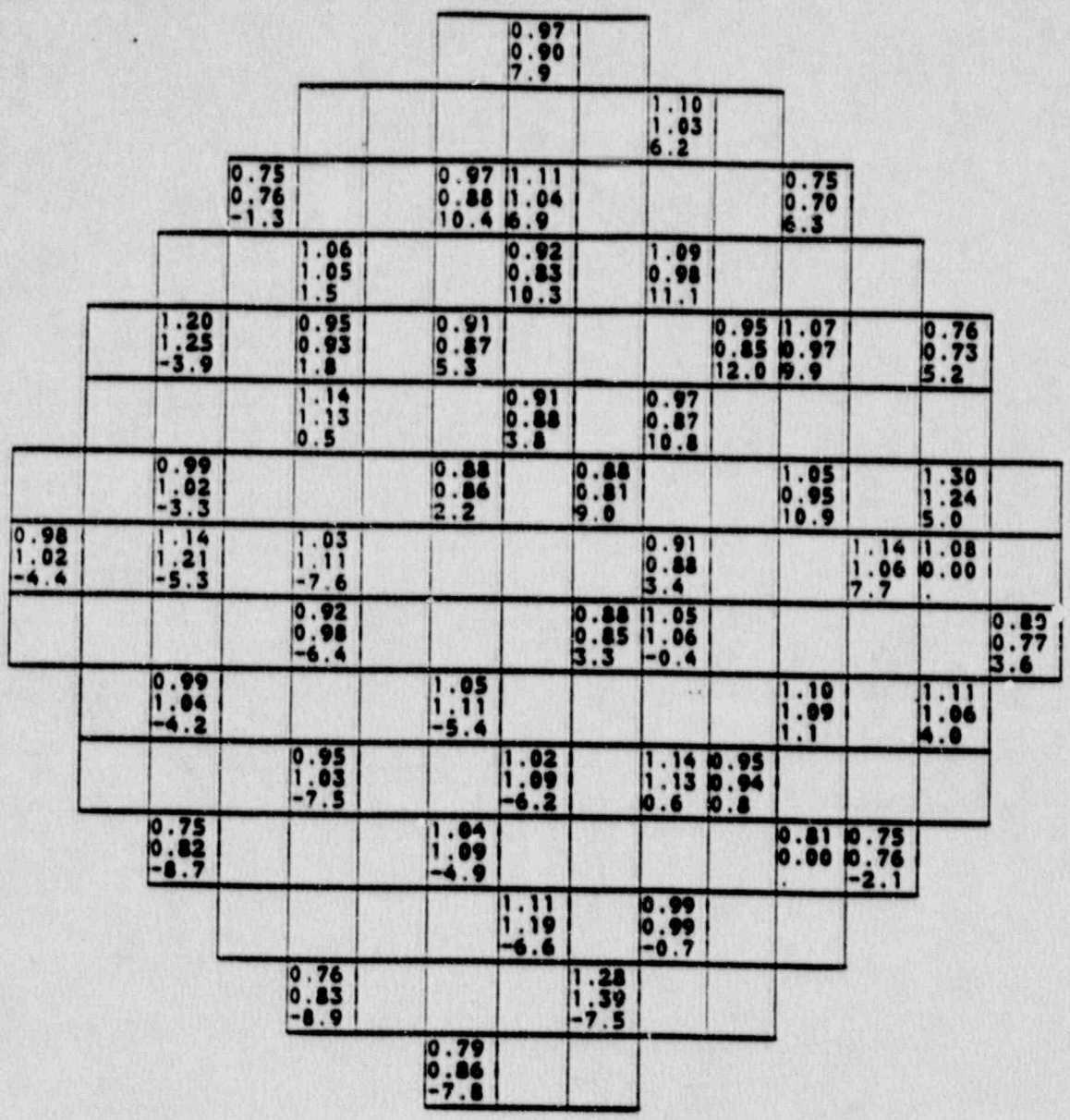

MAX DIFFERENCE = 12
MAX DIFF (RPD>0.9) = 12
RMS DIFFERENCE = 6.39

X.XX PREDICTED
X.XX MEASURED
X.X PERCENT DIFFERENCE

FIGURE 3-105

N1C2 3D PDQ VS. MEASURED RPD COMPARISON
HFP, D-220, 300 MWD/MTU N1C2-1SA

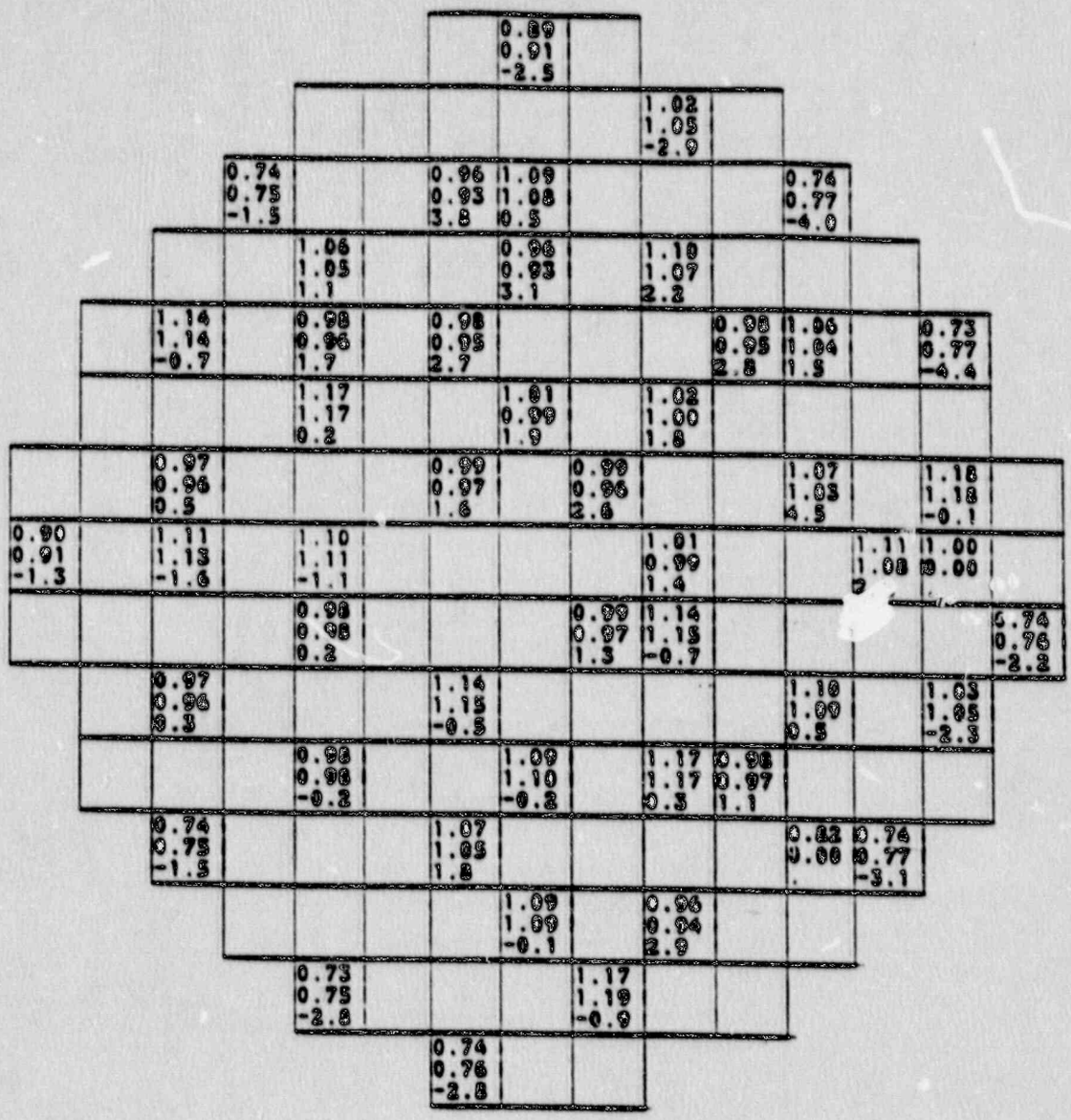

MAX DIFFERENCE = 4.47
MAX DIFF (RPD>0.9) = 4.47
RMS DIFFERENCE = 2.08

X.XX PREDICTED
X.XX MEASURED
X.X PERCENT DIFFERENCE

FIGURE 3-106

N1C2 3D PDQ VS. MEASURED RPD COMPARISON
KFP, D-222, 3277 MWD/MTU N1C2-26A

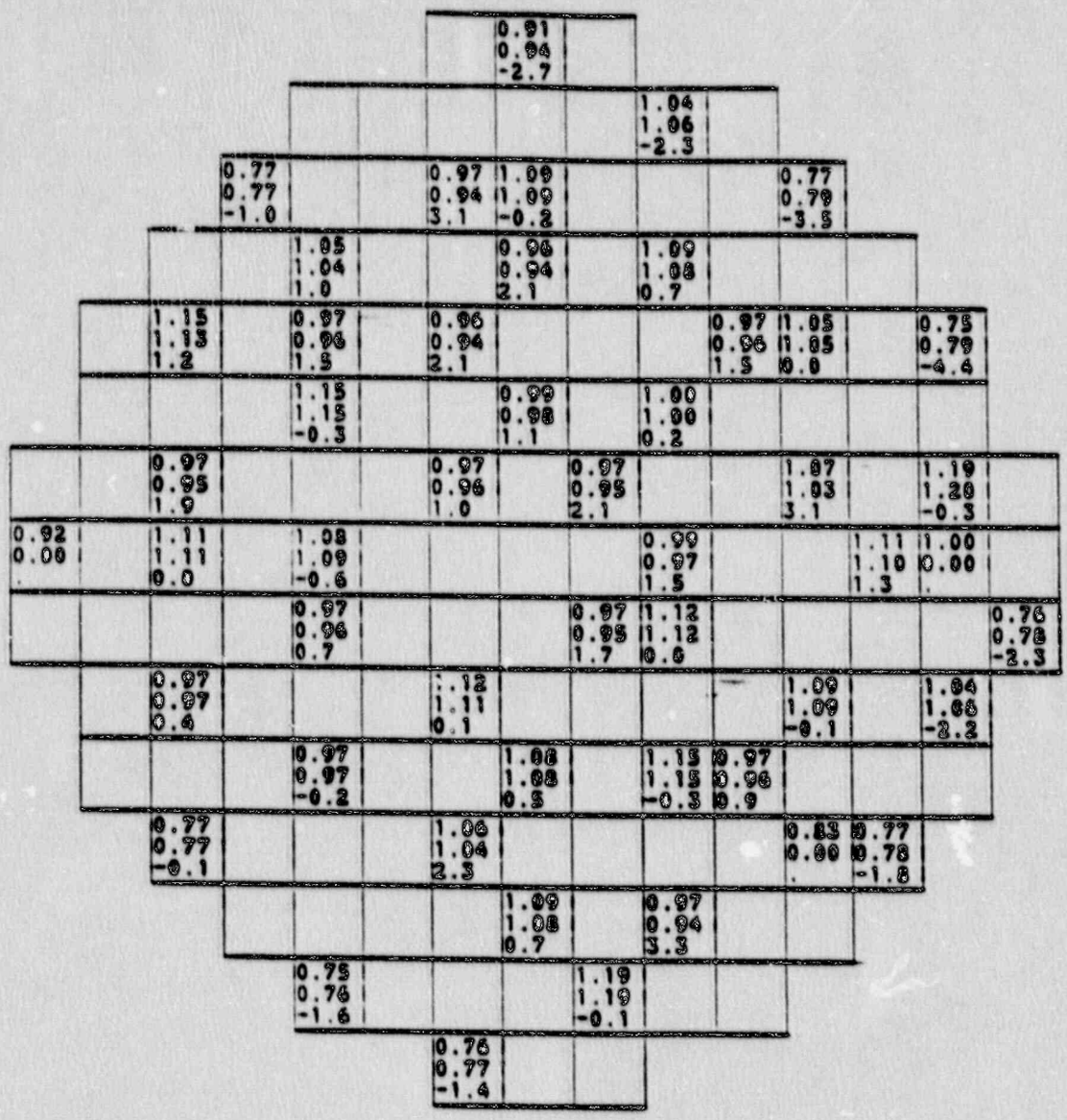

MAX DIFFERENCE = -4.4
MAX DIFF (RPD>0.9) = 3.30
RMS DIFFERENCE = 1.[illegible]

X.XX PREDICTED
X.XX MEASURED
X.X PERCENT DIFFERENCE

FIGURE 3-107

N1C2 3D PDQ VS. MEASURED RPD COMPARISON
HFP, D-210, 8109 MWD/MTU N1C2-44A

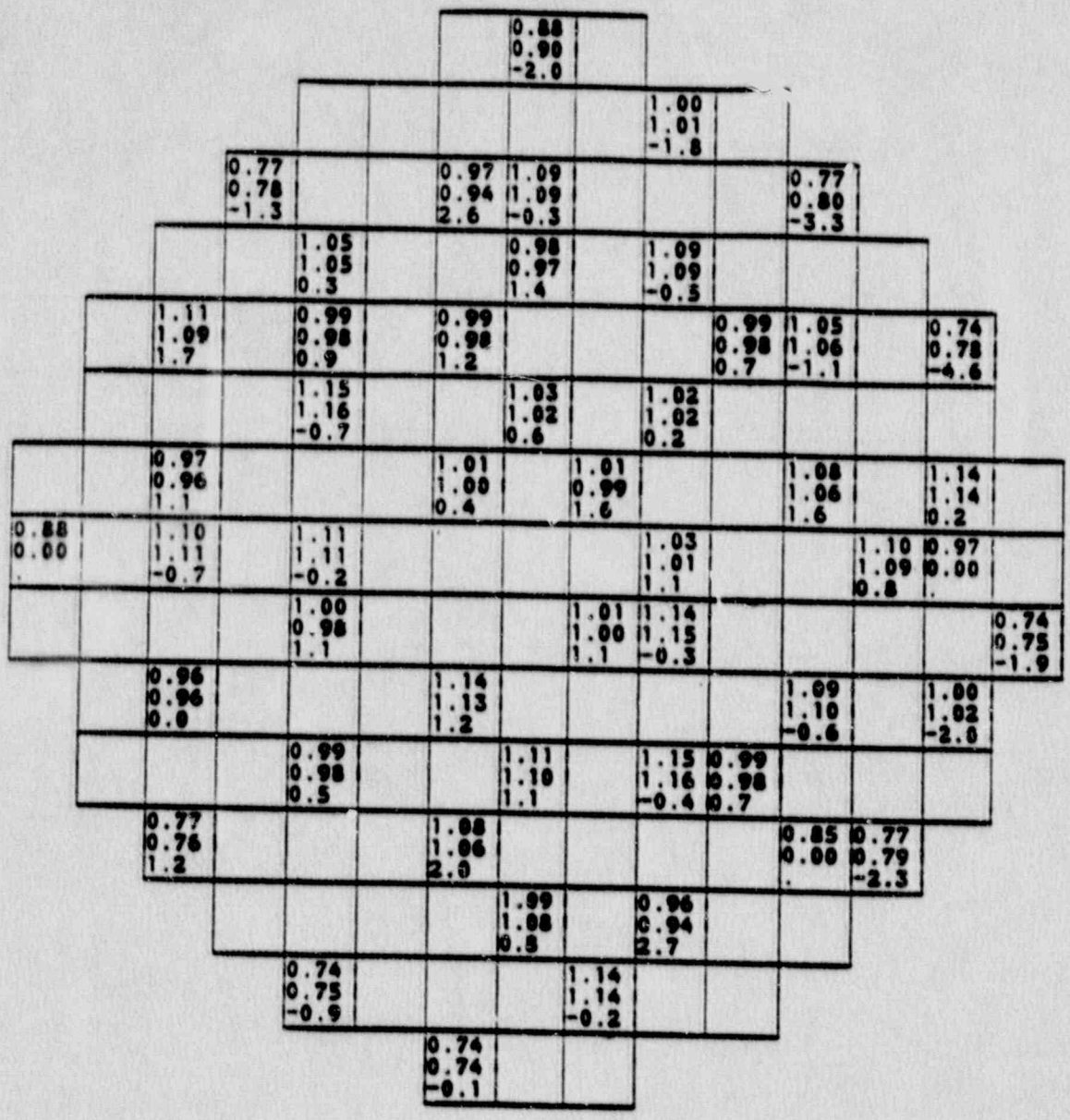

MAX DIFFERENCE = -4.6
MAX DIFF (RPD>0.9) = 2.67
RMS DIFFERENCE = 1.46

X.XX PREDICTED
X.XX MEASURED
X.X PERCENT DIFFERENCE

FIGURE 3-108

N1C3 3D PDQ VS. MEASURED RPD COMPARISON
MZP, D-22C, 0 MWD/MTU N1C3-02A

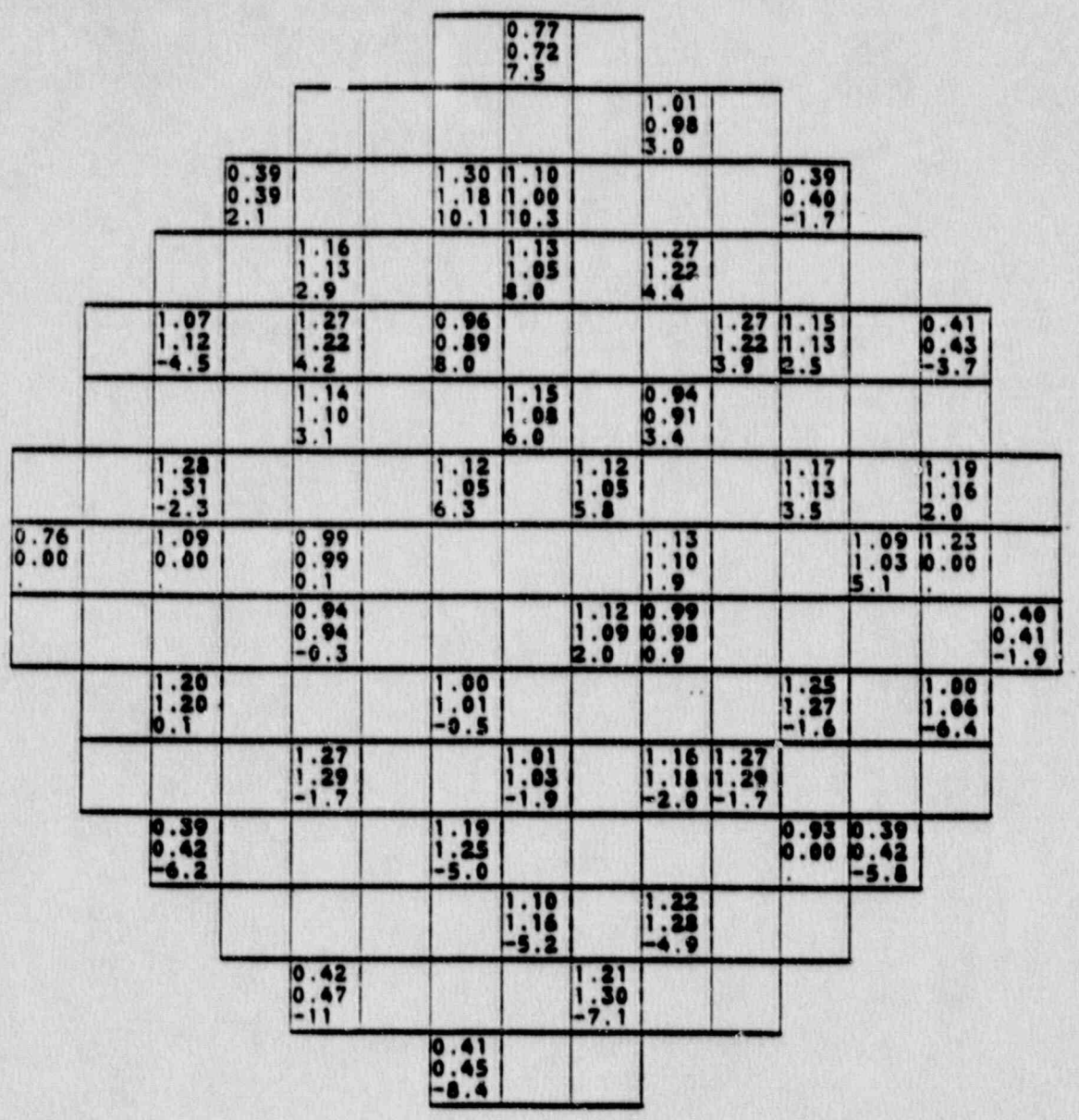

MAX DIFFERENCE = -11
MAX DIFF (RPD>0.9) = 10.3
RMS DIFFERENCE = 5.02

X.XX	PREDICTED
X.XX	MEASURED
X.X	PERCENT DIFFERENCE

FIGURE 3-109

N1C3 3D PDQ VS. MEASURED RPD COMPARISON
HFP, D-213, 6883 MWD/MTU N1C3-33A

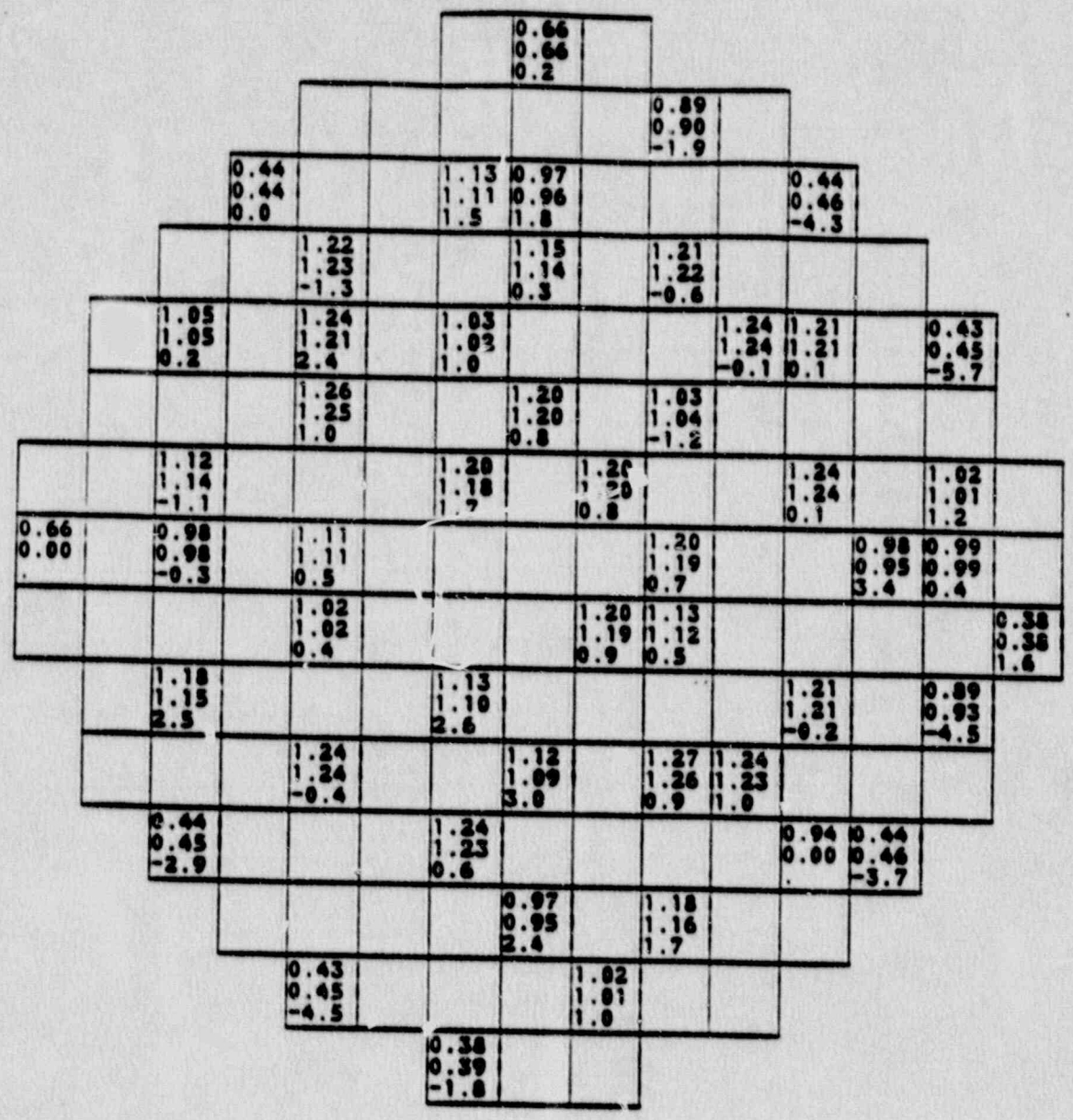

MAX DIFFERENCE = -5.7
MAX DIFF (RPD>0.9) = 3.38
RMS DIFFERENCE = 2.02

X.XX	PREDICTED
X.XX	MEASURED
X.X	PERCENT DIFFERENCE

FIGURE 3-110

NIC3 3D PDQ VS. MEASURED RPD COMPARISON
KFP, D-216, 11434 MWD/MTU NICE-84A

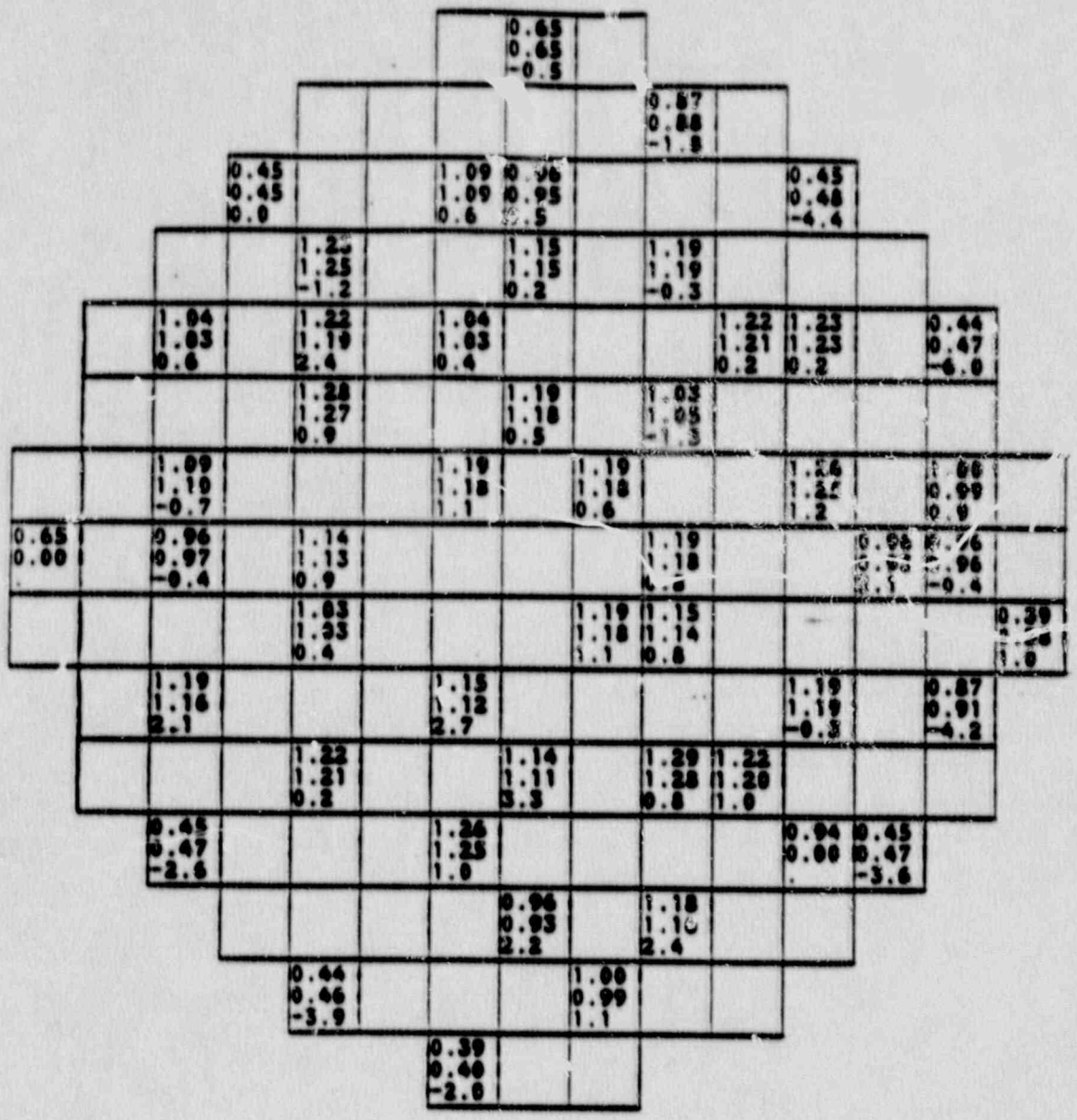

MAX DIFFERENCE = -6
MAX DIFF (RPD>0.9) = 3.25
RMS DIFFERENCE = 1.95

X.XX PREDICTED
X.XX MEASURED
X.X PERCENT DIFFERENCE

FIGURE 3-111

N1C4 3D PDQ VS. MEASURED RPD COMPARISON
HZP, D-228, 0 MWD/MTU N1C4-01A

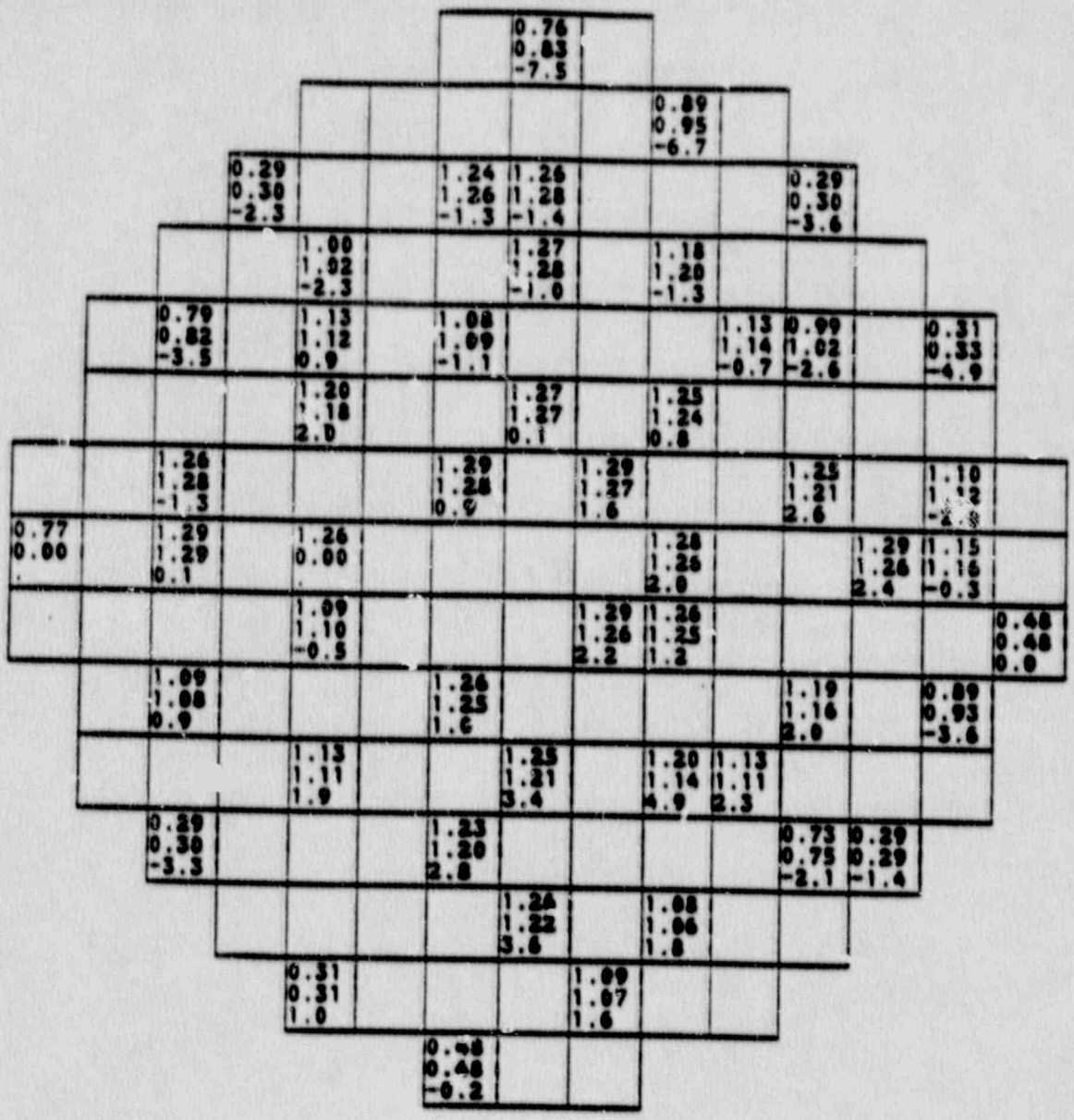

MAX DIFFERENCE = -7.5
MAX DIFF (RPD>0.9) = 4.91
RMS DIFFERENCE = 2.59

X.XX PREDICTED
X.XX MEASURED
X.X PERCENT DIFFERENCE

FIGURE 3-112

N1C4 3D PDQ VS. MEASURED RPD COMPARISON
HFP, D-221, 305 MWD/MTU N1C4-07A

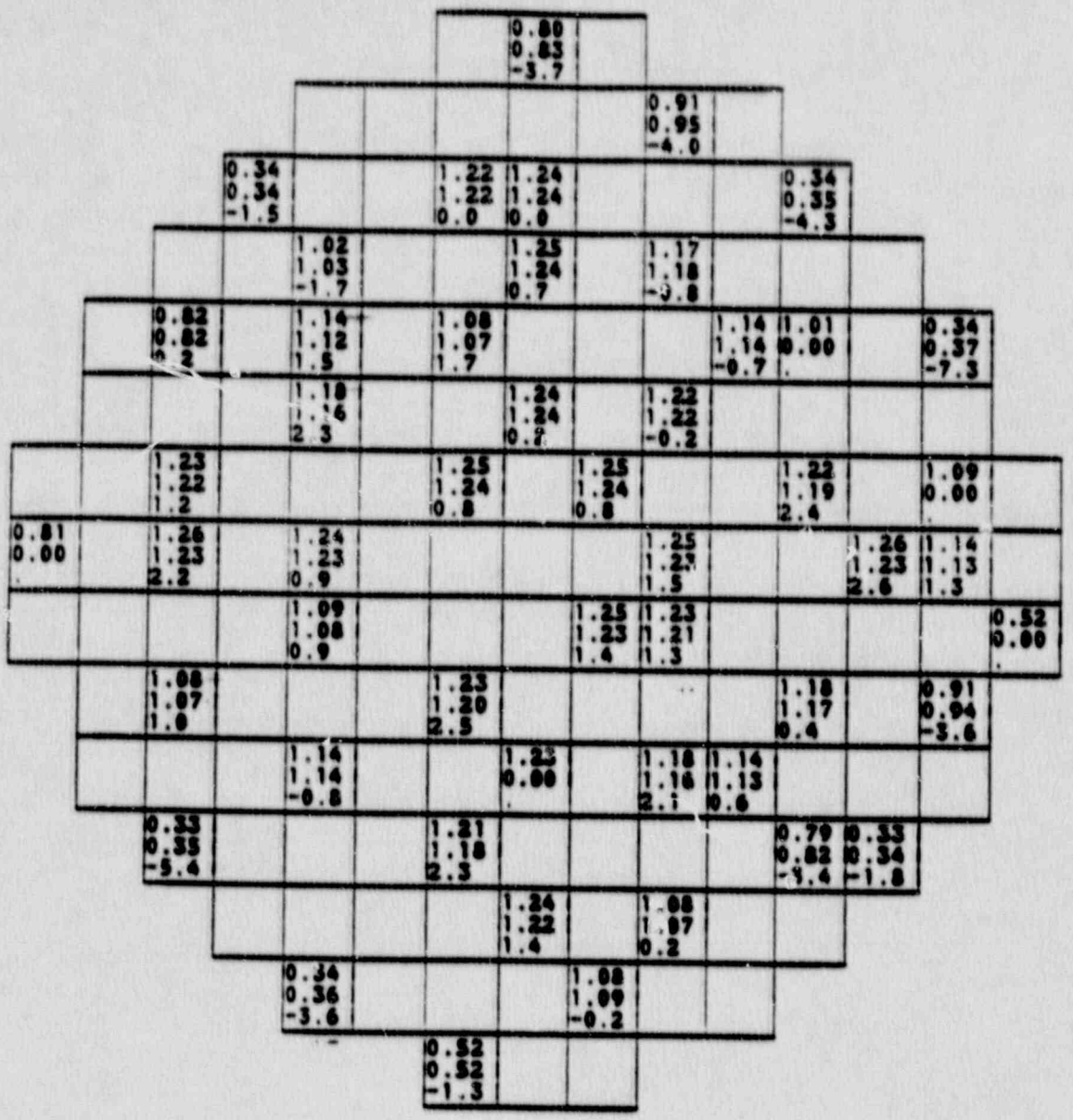

MAX DIFFERENCE = -7.3
MAX DIFF (RPD>0.9) = -4
RMS DIFFERENCE = 2.31

X.XX
X.XX
X.X

PREDICTED
MEASURED
PERCENT DIFFERENCE

FIGURE 3-113

N1C4 3D PD0 VS. MEASURED RPD COMPARISON
HFP, D-216, 5520 MWD/MTU N1C4-17A

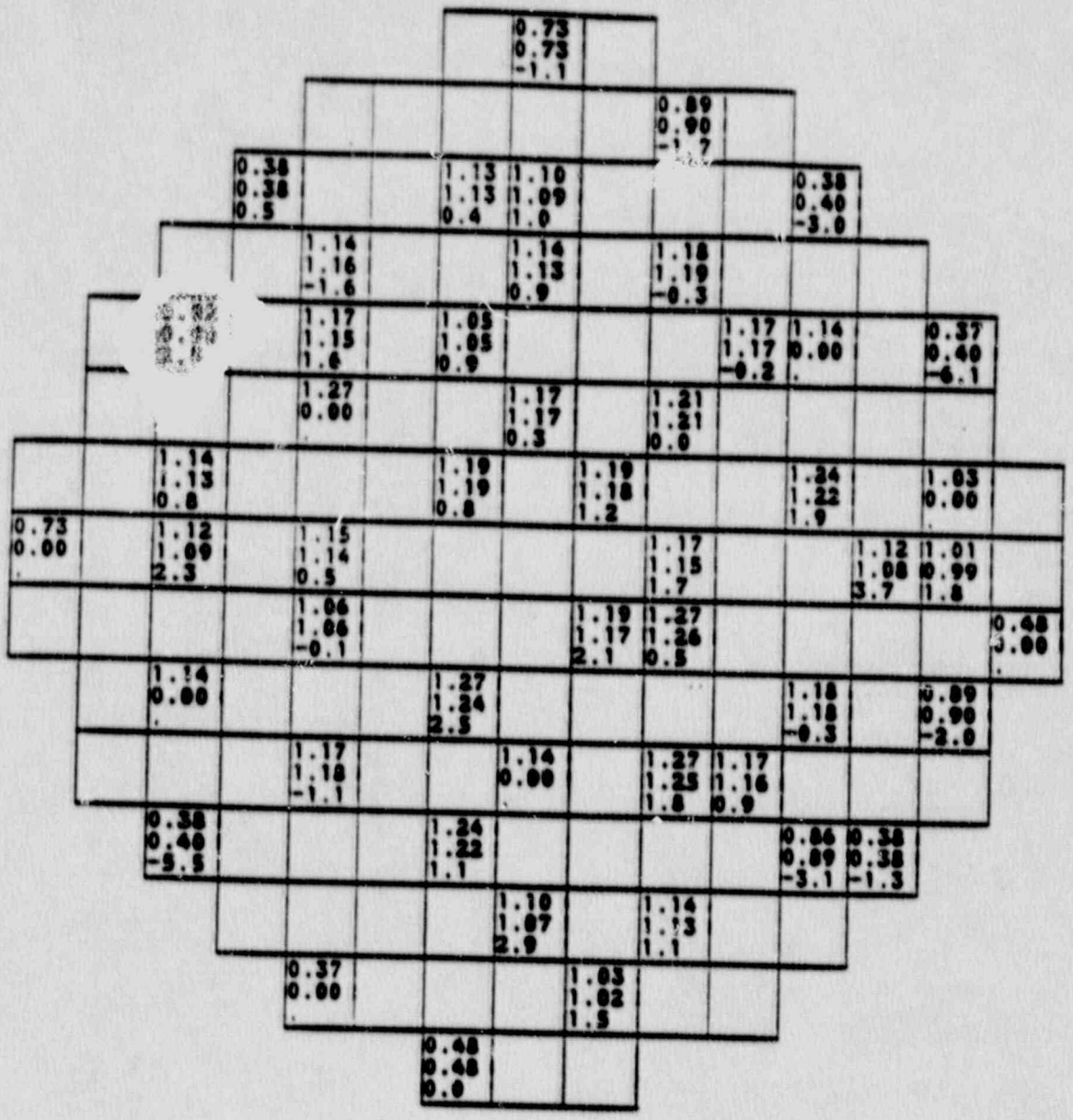

MAX DIFFERENCE = -6.1
MAX DIFF (RPD>0.9) = 3.71
RMS DIFFERENCE = 2.02

X.XX PREDICTED
X.XX MEASURED
X.X PERCENT DIFFERENCE

FIGURE 3-114

N1C4 3D PDQ VS. MEASURED RPD COMPARISON
HFP, D-226, 10170 MWD/MTU N1C4-25A

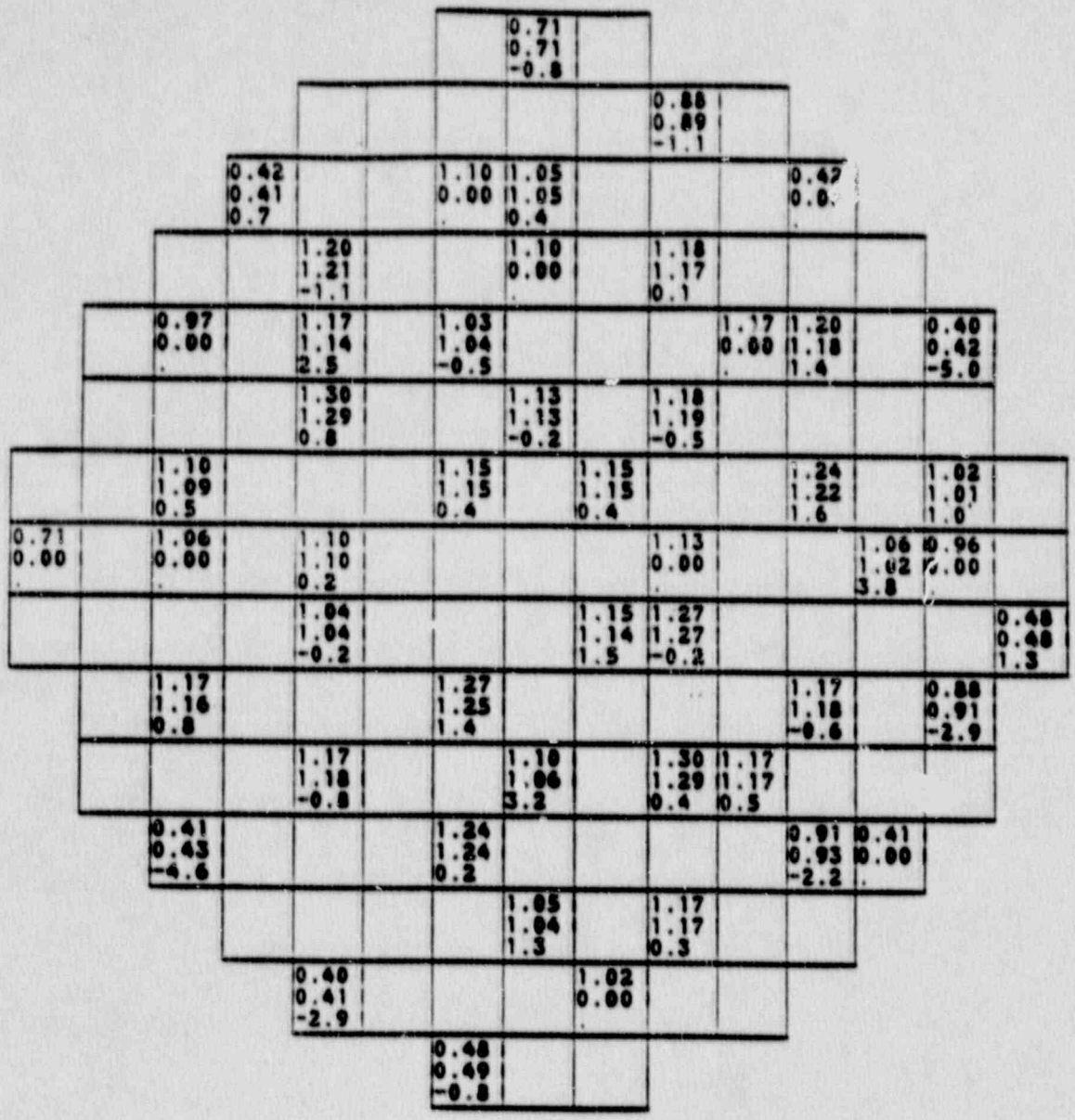

MAX DIFFERENCE = -5
MAX DIFF (RPD>0.9) = 3.82
RMS DIFFERENCE = 1.75

X.XX PREDICTED
X.XX MEASURED
X.X PERCENT DIFFERENCE

FIGURE 3-115

N1C5 3D PDQ VS. MEASURED RPD COMPARISON
MZP, D-228, 0 MWD/MTU N1C5-01

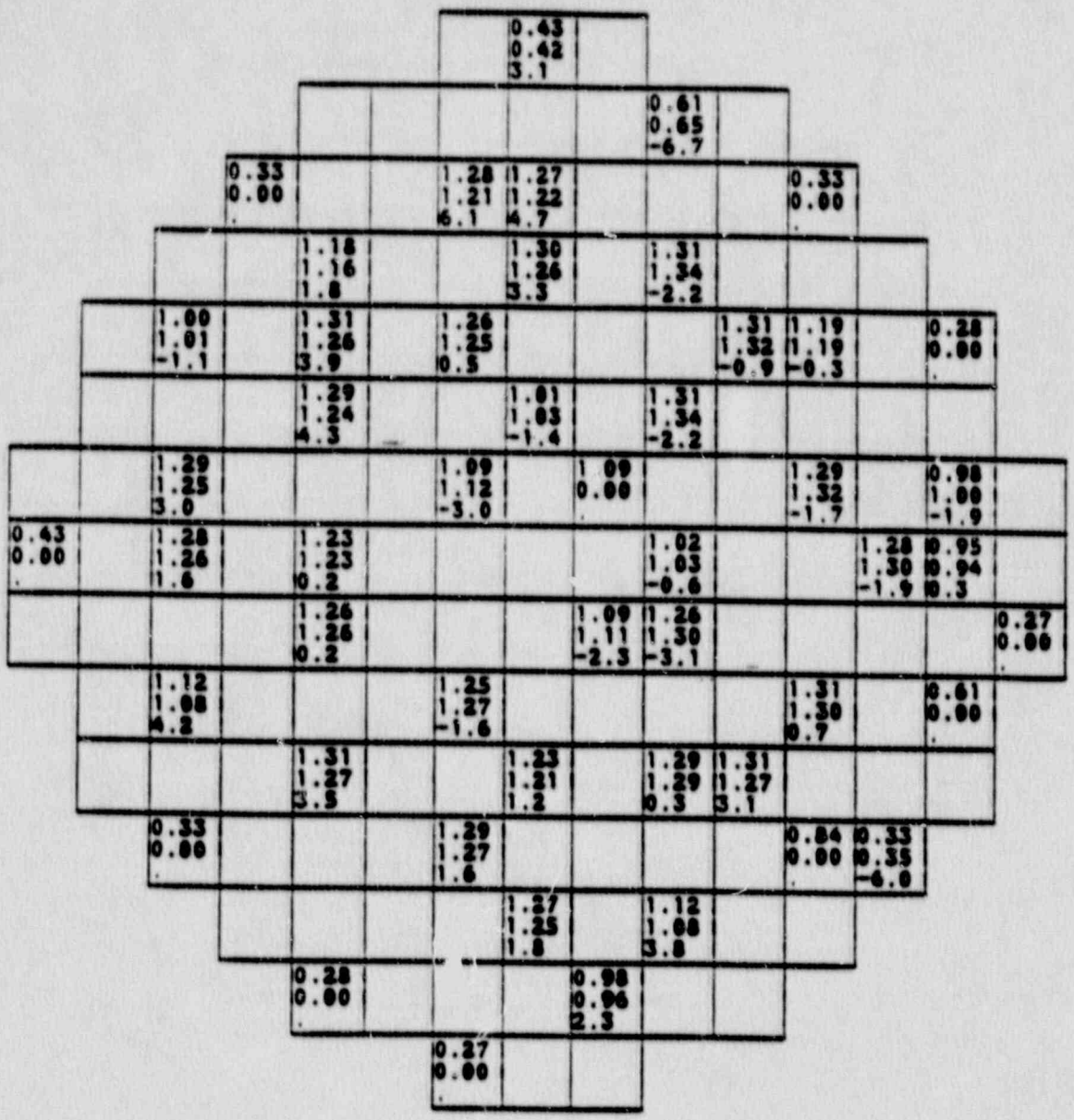

MAX DIFFERENCE = -6.7
MAX DIFF (RPD>0.9) = 6.12
RMS DIFFERENCE = 2.90

X.XX PREDICTED
X.XX MEASURED
X.X PERCENT DIFFERENCE

FIGURE 3-116

N1C5 3D PDQ VS. MEASURED RPD COMPARISON
MFP, D-224, 225 MWD/MTU N1C5-15A

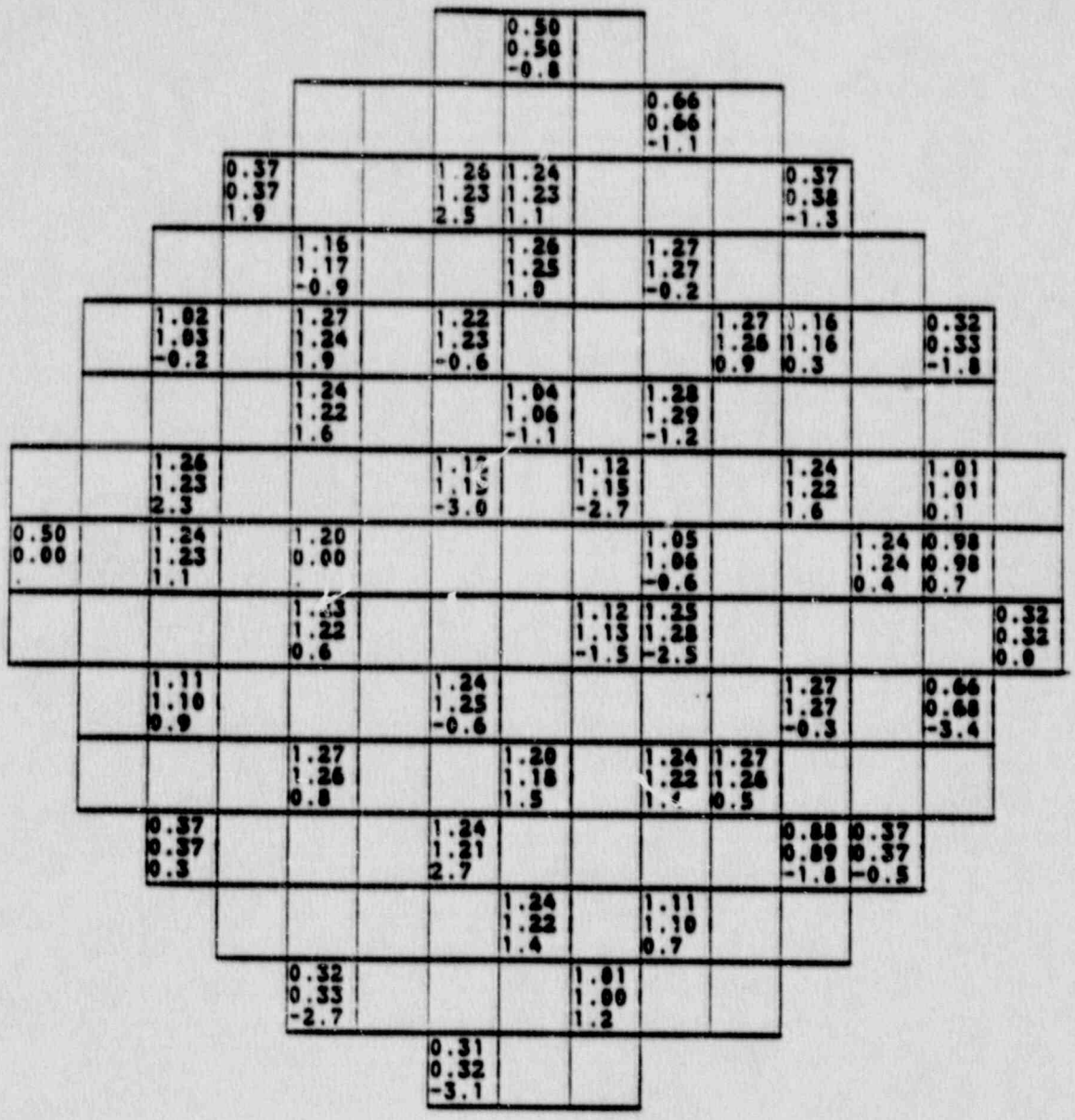

MAX DIFFERENCE = -3.4
MAX DIFF (RPD>0.9) = -3
RMS DIFFERENCE = 1.55

X.XX
X.XX
X.X

PREDICTED
MEASURED
PERCENT DIFFERENCE

FIGURE 3-117

W1C3 3D FDQ VS. MEASURED RPD COMPARISON
HFP, D-224, 6831 MWD/MTU W1C5-23A

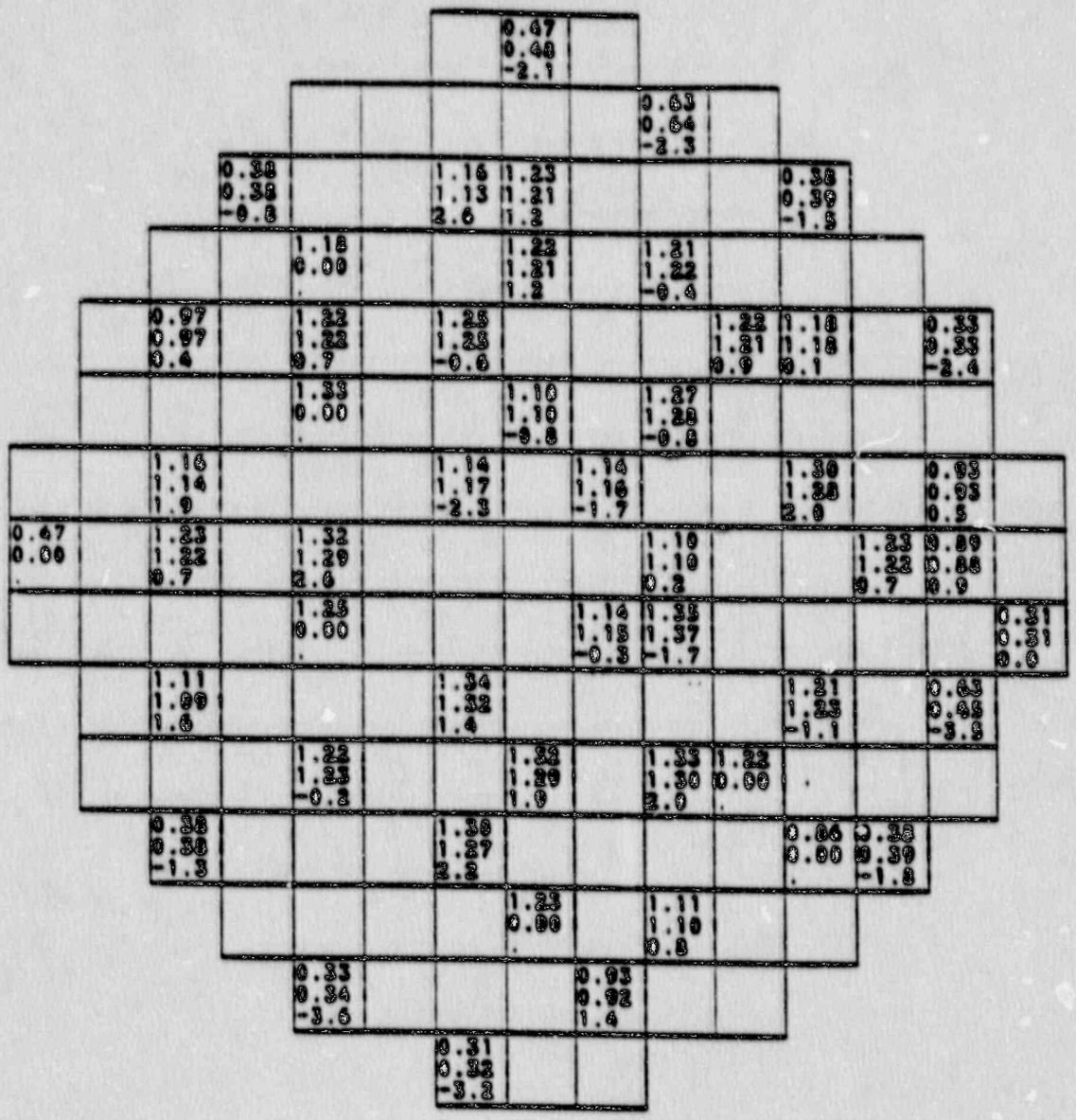

MAX DIFFERENCE : -3.6
MAX DIFF (RPD>0.9) : 2.97
RMS DIFFERENCE : 1.66

X.XX PREDICTED
X.XX MEASURED
X.X PERCENT DIFFERENCE

FIGURE 3-118

N1C5 3D PDQ VS. MEASURED RPD COMPARISON
HFP, D-228, 12983 MWD/MTU N1C5-34A

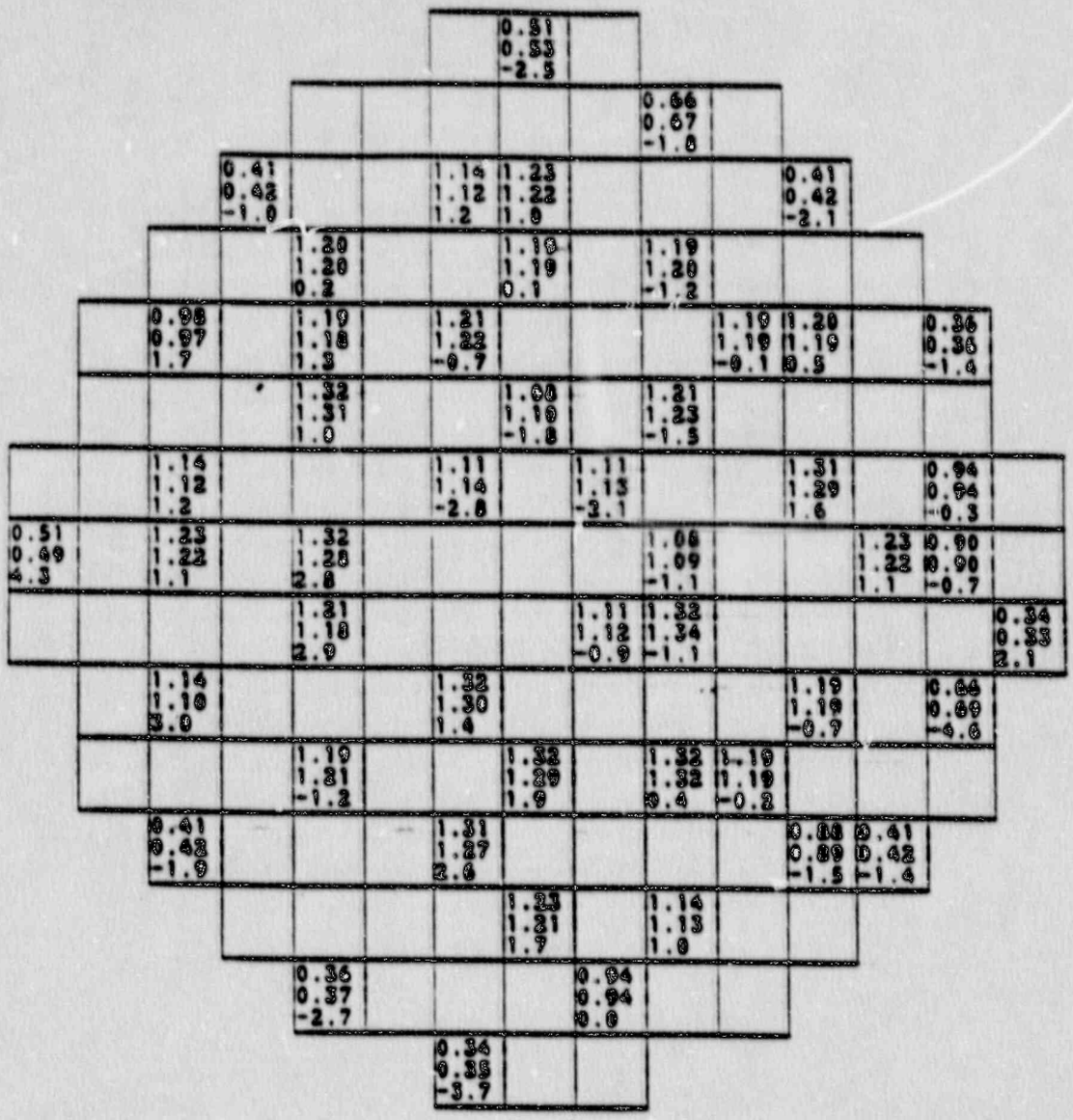

MAX DIFFERENCE = -4.6
MAX DIFF (RPD>0.9) = 2.99
RMS DIFFERENCE = 1.85

X.XX PREDICTED
X.XX MEASURED
X.X PERCENT DIFFERENCE

FIGURE 3-119

N1C6 3D PDQ VS. MEASURED RPD COMPARISON
KFP, D-219, 378 MWD/MTU N1C6-09A

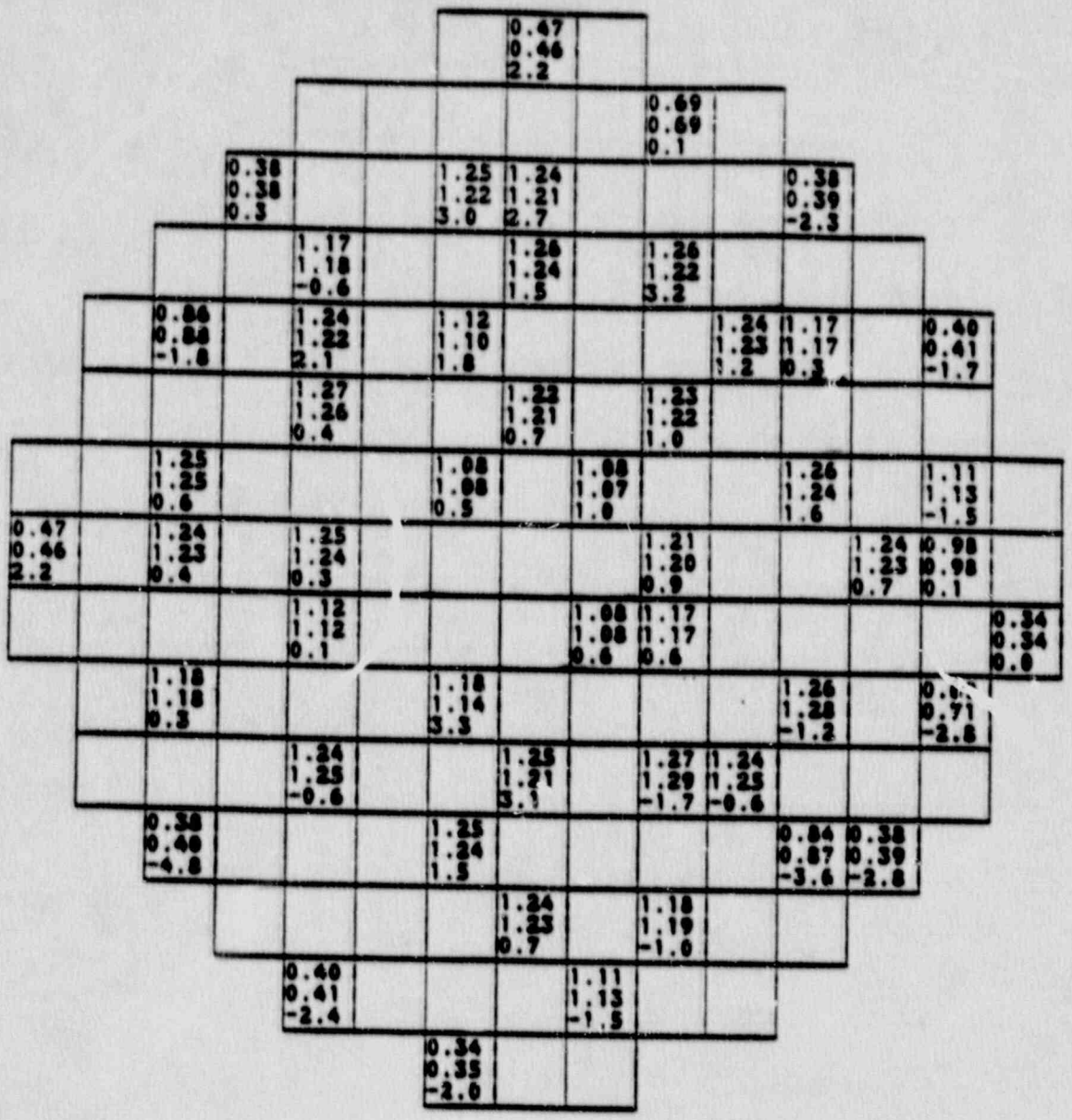

MAX DIFFERENCE = -4.8
MAX DIFF (RPD>0.9) = 3.34
RMS DIFFERENCE = 1.80

X.XX PREDICTED
X.XX MEASURED
X.X PERCENT DIFFERENCE

FIGURE 3-120

N1C6 3D PDQ VS. MEASURED LPD COMPARISON
HF[illegible], D-228, 6690 MWD/MTU N1C6-17A

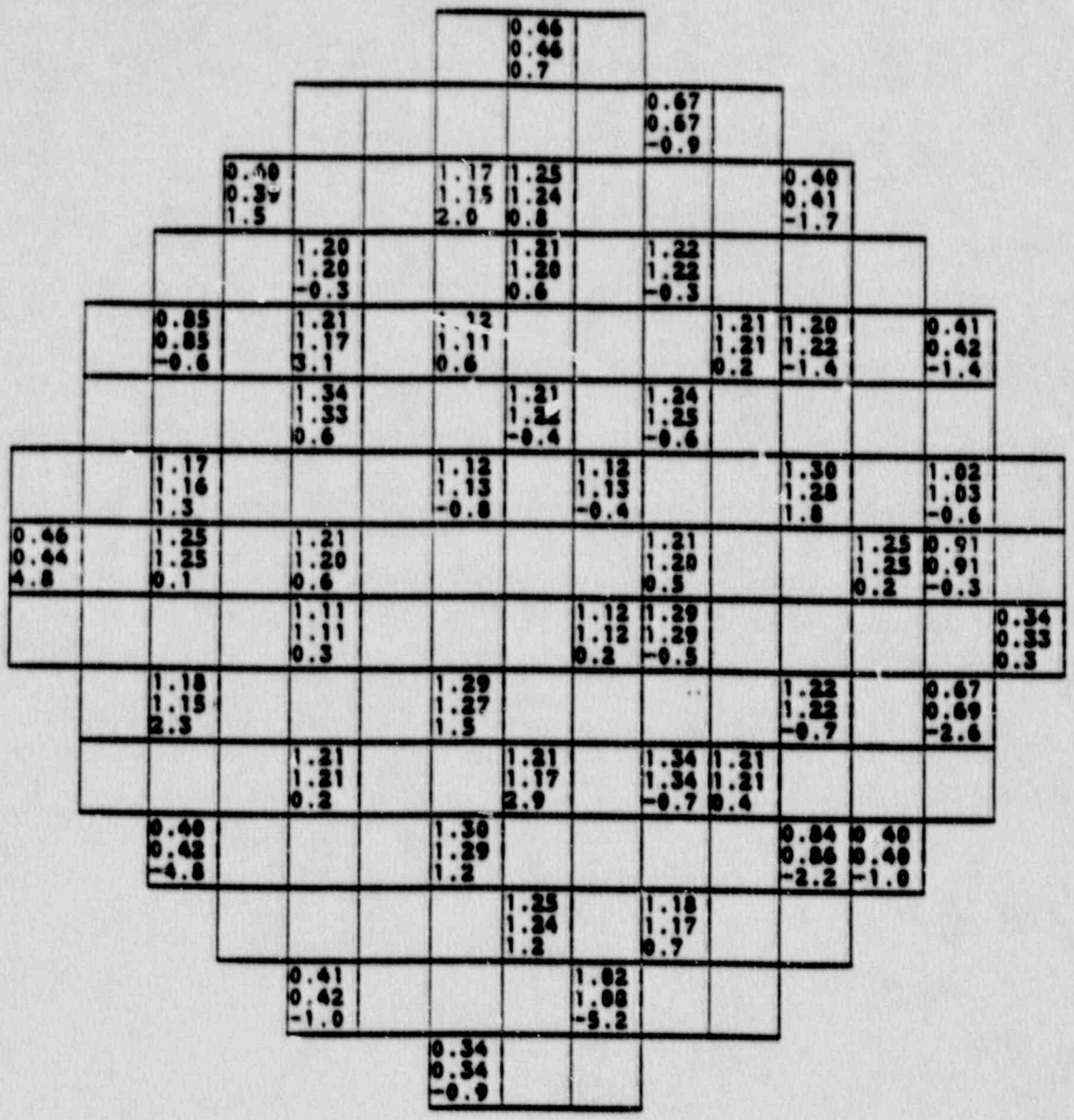

MAX DIFFERENCE = -5.2
MAX DIFF (RPD>0.9) = -5.2
RMS DIFFERENCE = 1.68

X.XX PREDICTED
X.XX MEASURED
X.X PERCENT DIFFERENCE

FIGURE 3-121

N1C6 3D FDQ VS. MEASURED RPD COMPARISON
HFP, D-228, 14340 MWD/MTU N1C6-29A

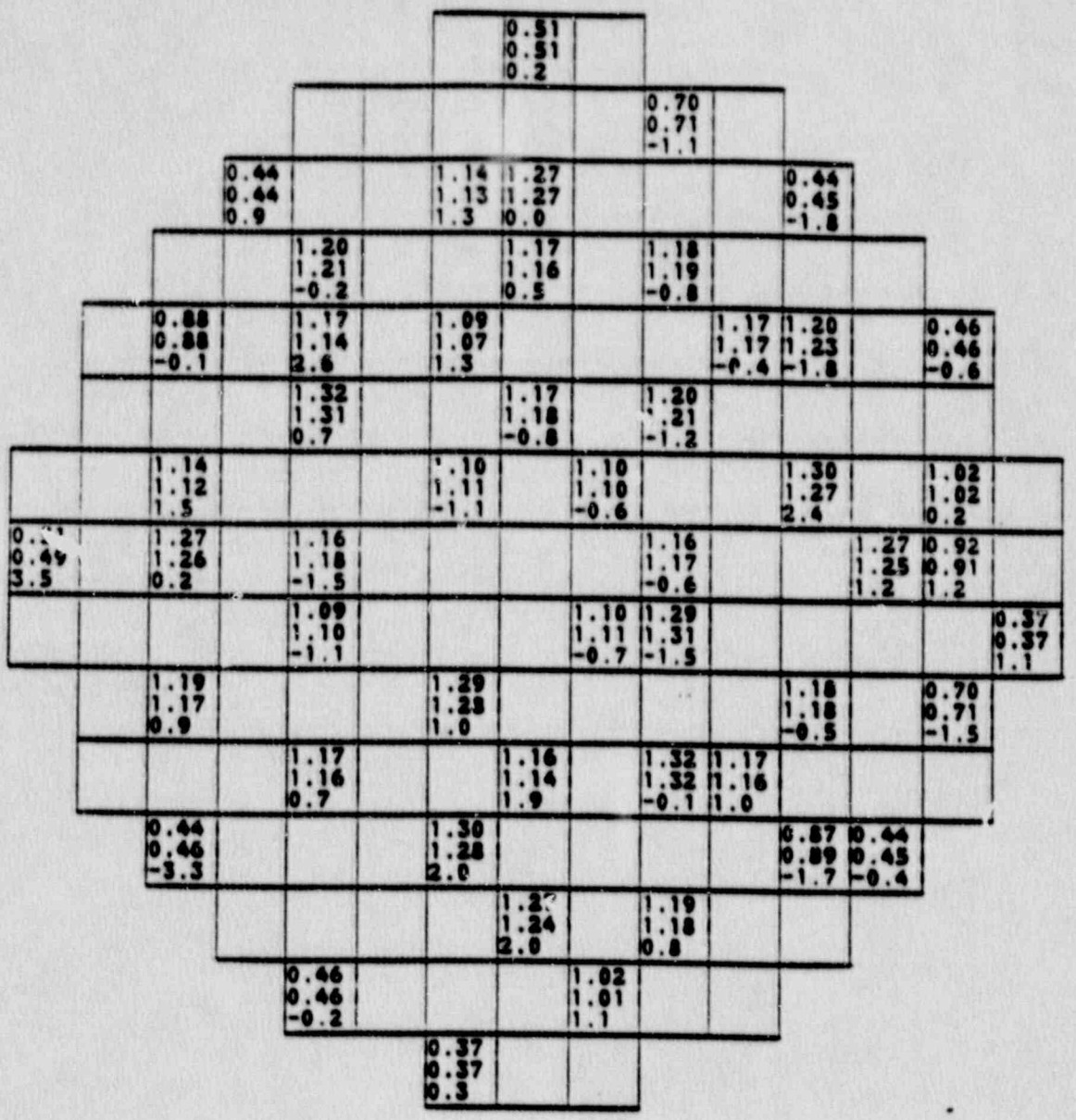

MAX DIFFERENCE = 3.46
MAX DIFF (RPD>0.9) = 2.64
RMS DIFFERENCE = 1.33

X.XX PREDICTED
X.XX MEASURED
X.X PERCENT DIFFERENCE

FIGURE 3-122

N2C2 3D PDQ VS. MEASURED RPD COMPARISON
HZP, D-228, 0 MWD/MTU N2C2-02A

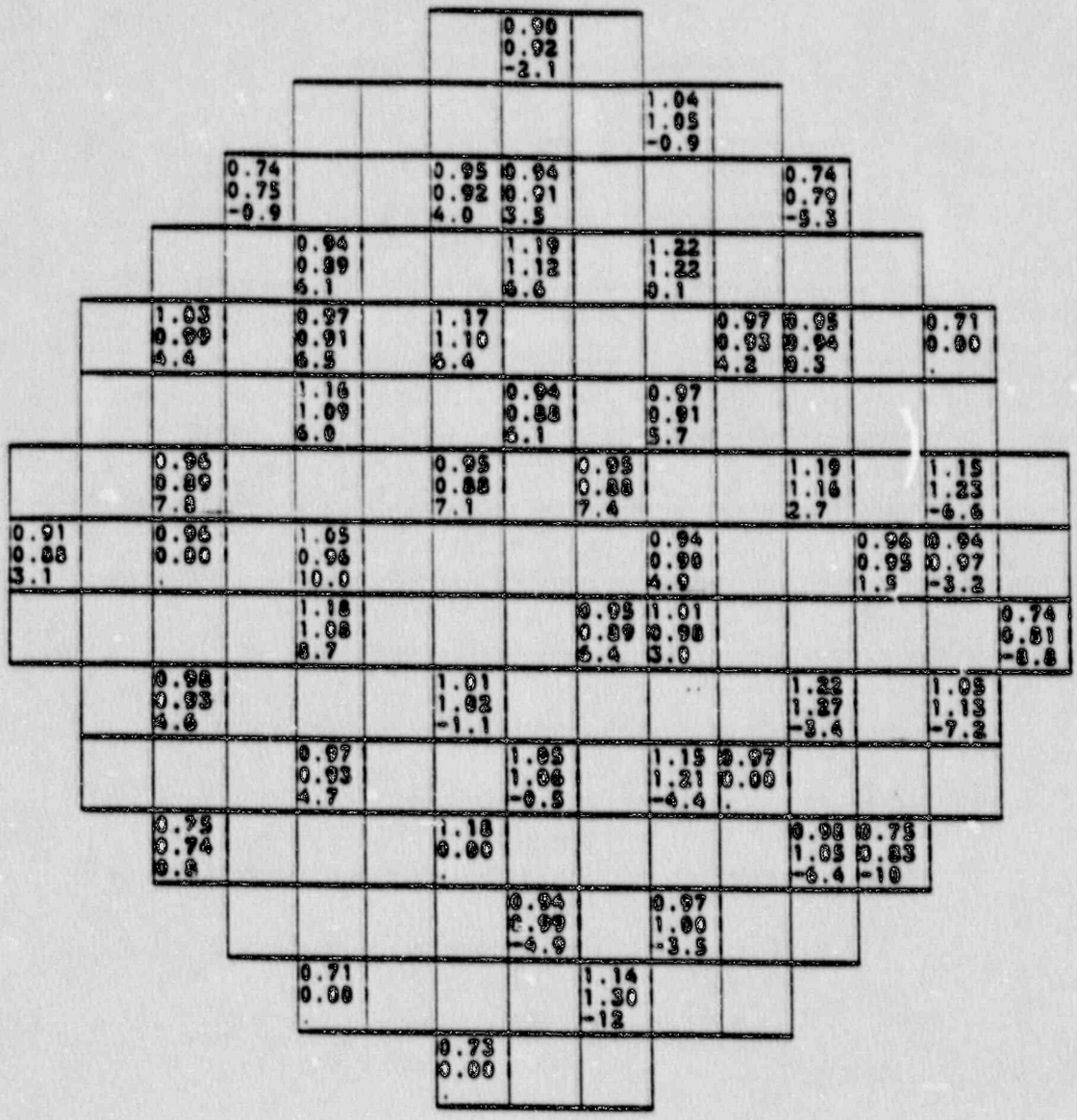

MAX DIFFERENCE = -12
MAX DIFF (RPD>0.9) = -12
RMS DIFFERENCE = 5.62

X.XX PREDICTED
X.XX MEASURED
X.X PERCENT DIFFERENCE

FIGURE 3-123

N2C2 3D PDQ VS. MEASURED RPD COMPARISON
HFP, D-224, 3225 MWD/MTU N2C2-20A

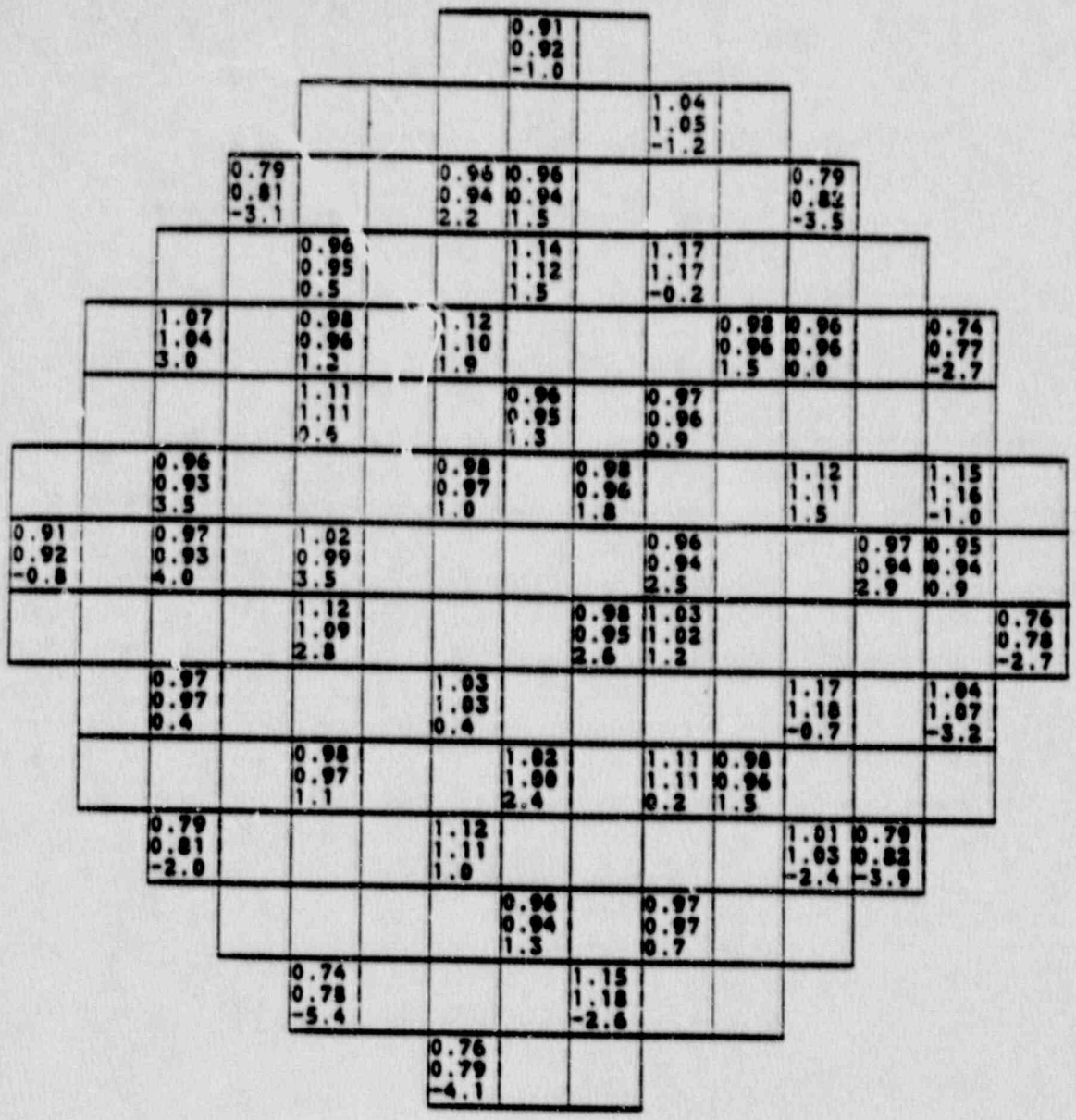

MAX DIFFERENCE = -5.4
MAX DIFF (RPD>0.9) = 3.97
RMS DIFFERENCE = 2.23

X.XX PREDICTED
X.XX MEASURED
X.X PERCENT DIFFERENCE

FIGURE 3-124

N2C2 3D PDQ VS. MEASURED RPD COMPARISON
HFP, D-218, 6751 MWD/MTU N2C2-27A

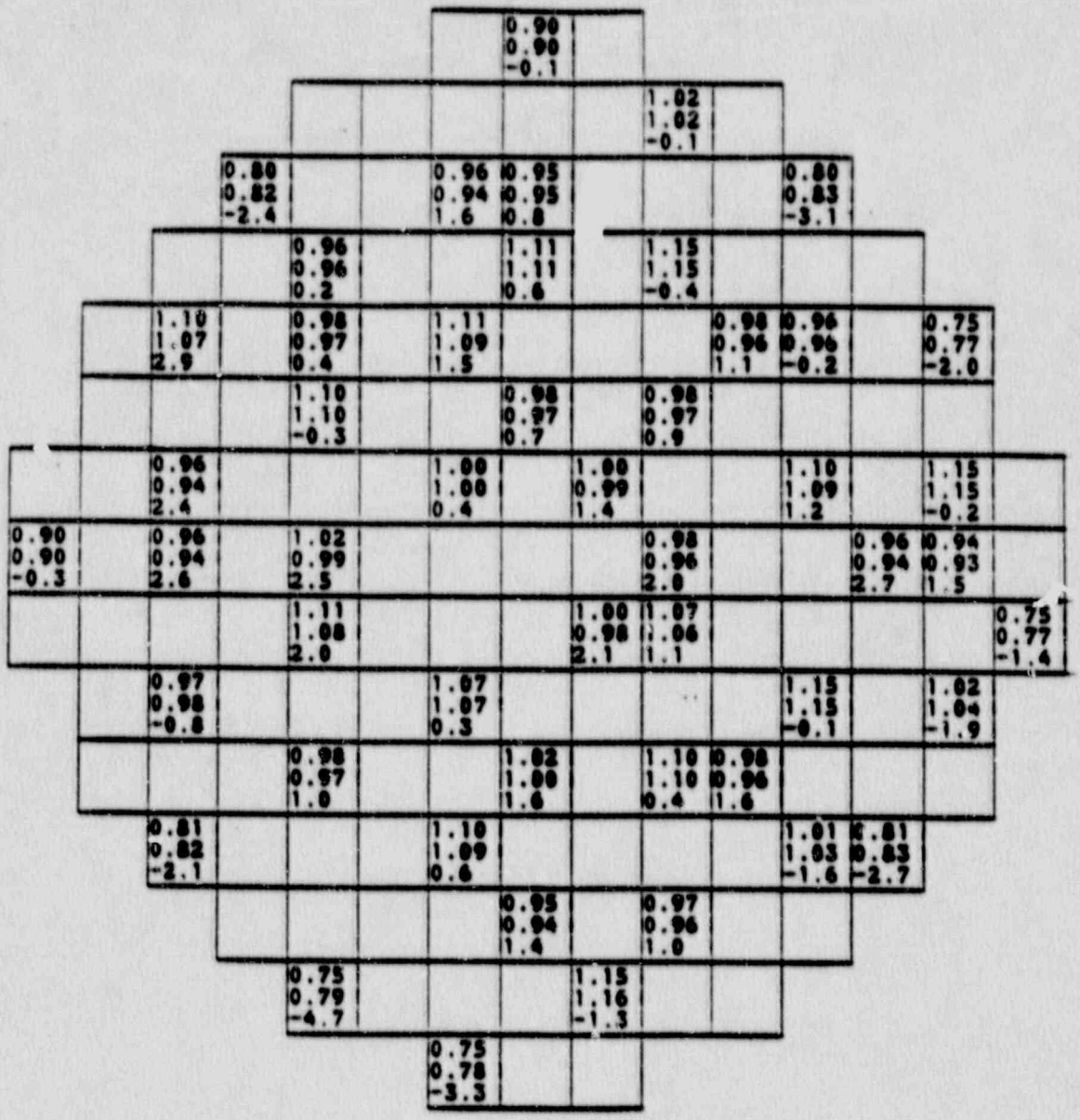

MAX DIFFERENCE = -4.7
MAX DIFF (RPD>0.9) = 2.90
RMS DIFFERENCE = 1.71

X.XX PREDICTED
X.XX MEASURED
X.X PERCENT DIFFERENCE

FIGURE 3-12

N2C3 3D PDQ VS. MEASURED P'D COMPARISON
MZP, D-211, 0 MWD/MTU N2C3-01A

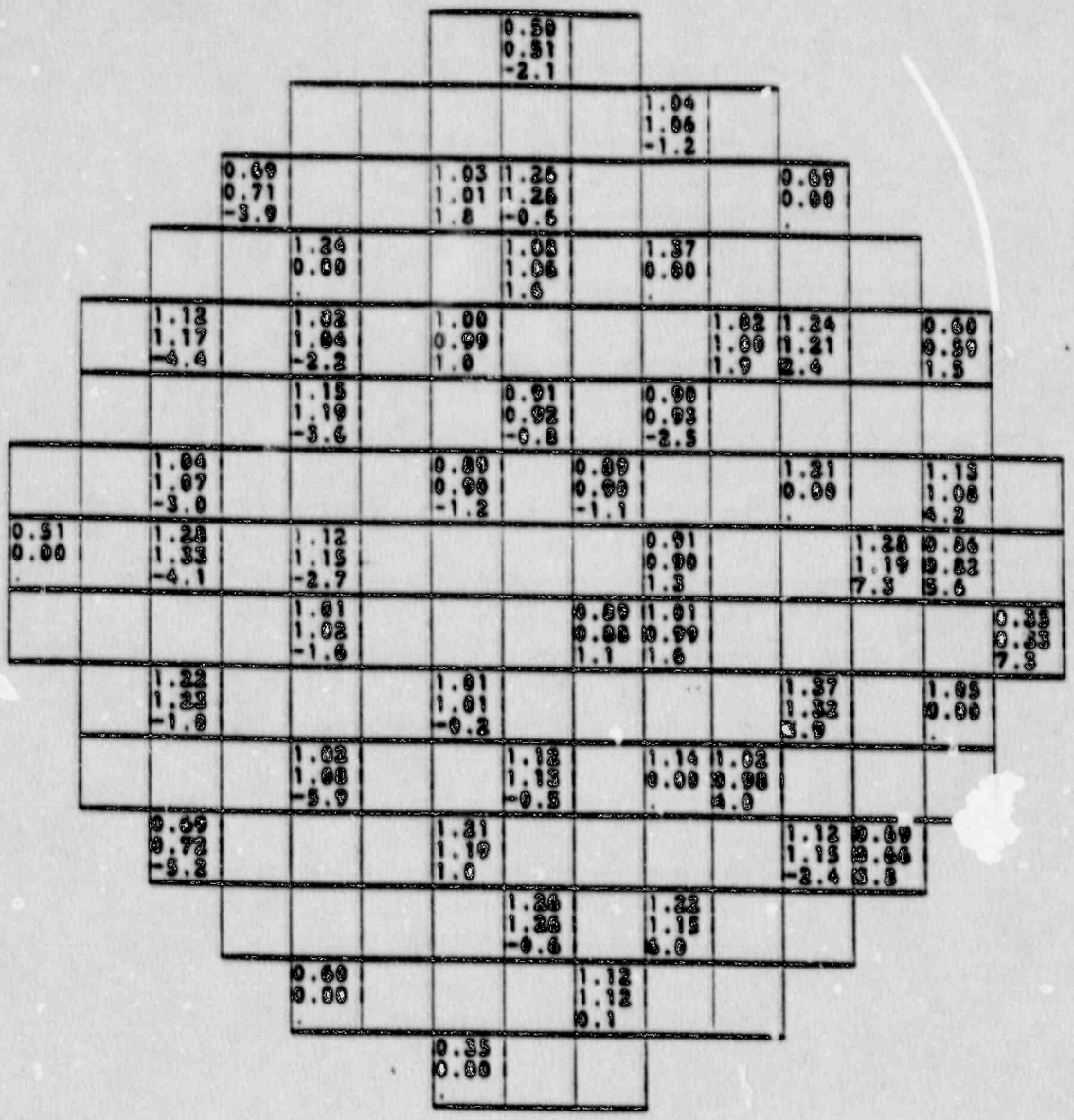

MAX DIFFERENCE = 7.32
MAX DIFF (EXP>0.6) = 7.32
RMS DIFFERENCE = 3.26

X.XX PREDICTED
X.XX MEASURED
X.X PERCENT DIFFERENCE

FIGURE 3-126

N2C3 3D PDQ VS. MEASURED RPD COMPARISON
HFP, D-212, 1566 MWD/MTU N2C3-14A

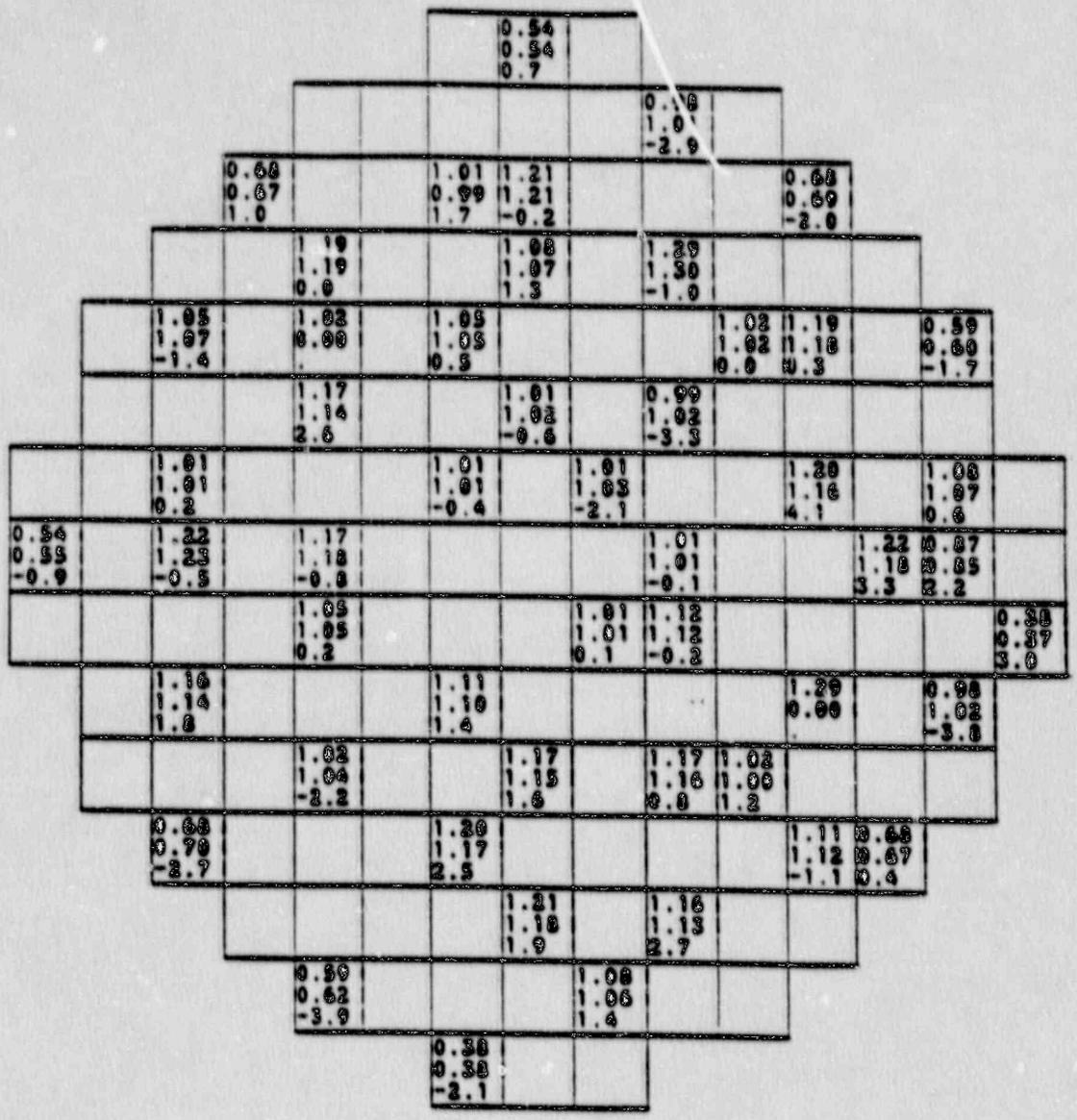

MAX DIFFERENCE = 4.07
MAX DIFF (RPD>0.9) = 4.07
RMS DIFFERENCE = 1.87

X.XX PREDICTED
X.XX MEASURED
X.X PERCENT DIFFERENCE

FIGURE 3-127

N2C3 3D PDQ VS. MEASURED RPD COMPARISON
HFP, D-217, 7647 MWD/MTU N2C3-25A

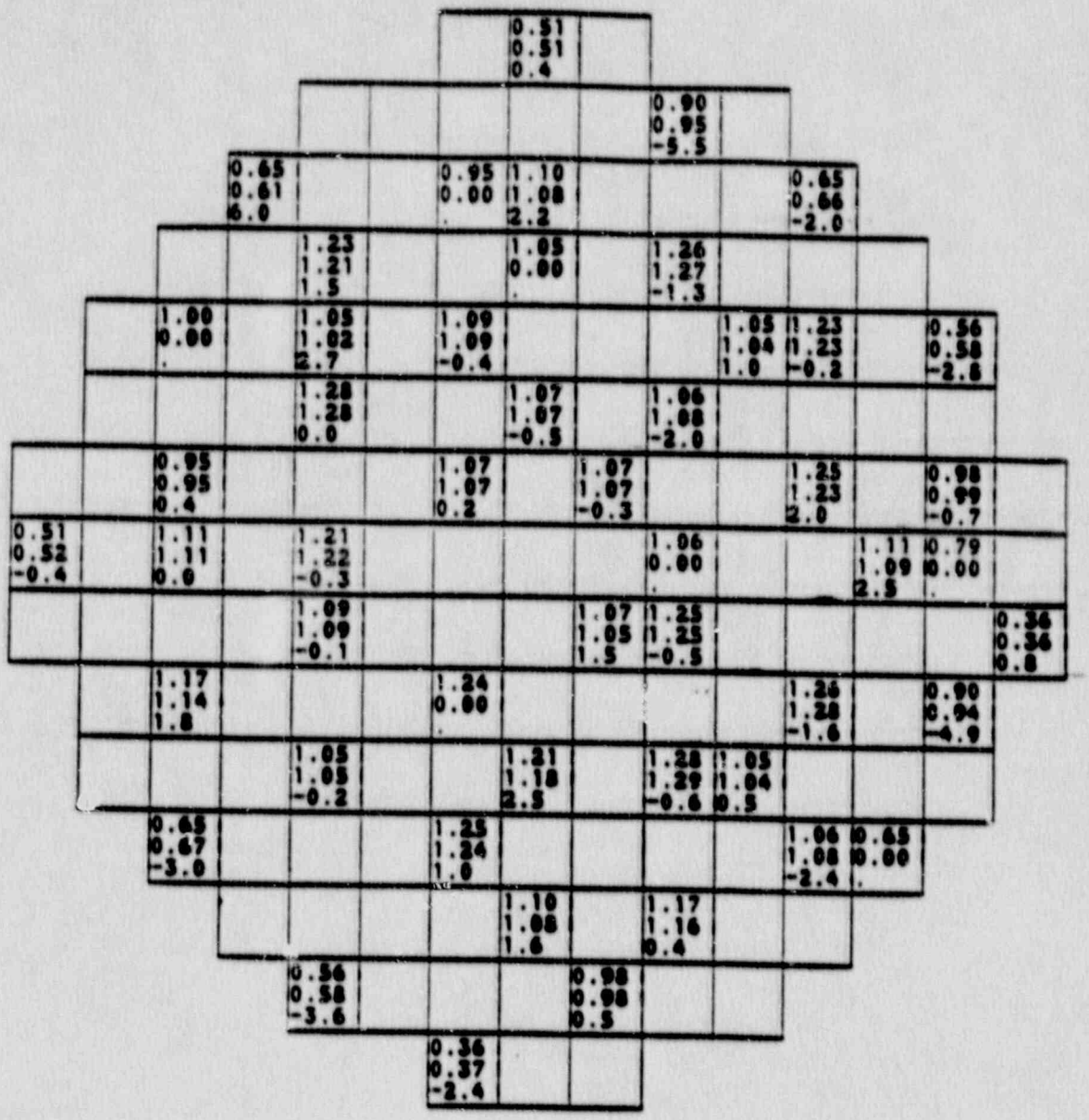

MAX DIFFERENCE = 6.04
MAX DIFF (RPD>0.9) = 2.74
RMS DIFFERENCE = 2.09

X.XX PREDICTED
X.XX MEASURED
X.X PERCENT DIFFERENCE

FIGURE 3-128

N2C3 3D PDO VS. MEASURED RPD COMPARISON
HFP, D-221, 13040 MWD/MTU N2C3-37A

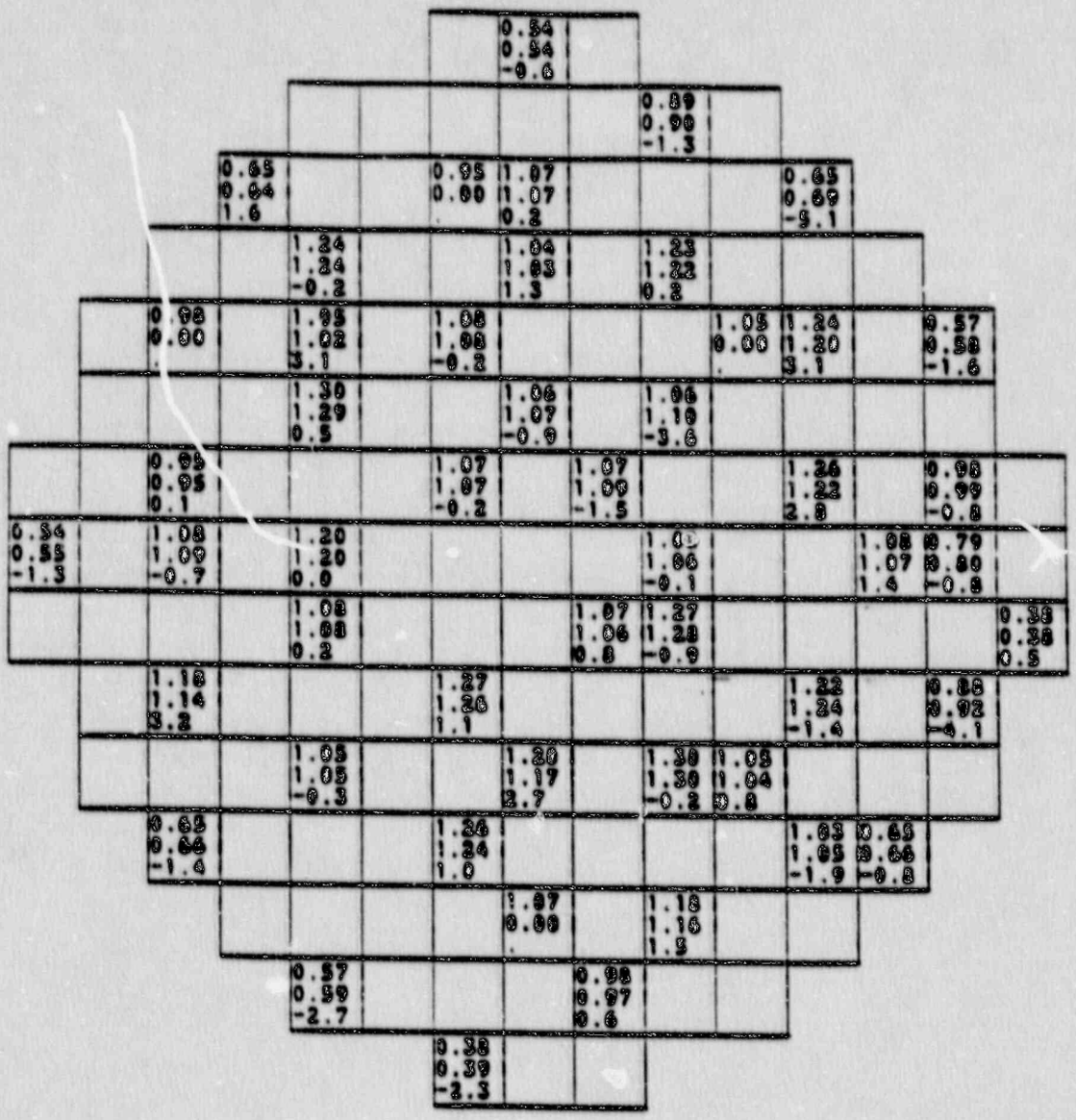

MAX DIFFERENCE = -5.1
MAX DIFF (RPD>0.9) = -3.6
RMS DIFFERENCE = 1.78

X.XX PREDICTED
X.XX MEASURED
X.X PERCENT DIFFERENCE

FIGURE 3-129

N2C4 3D PDQ VS. MEASURED RPD COMPARISON
KZP, D-211, 0 MWD/MTU N2C4-01A

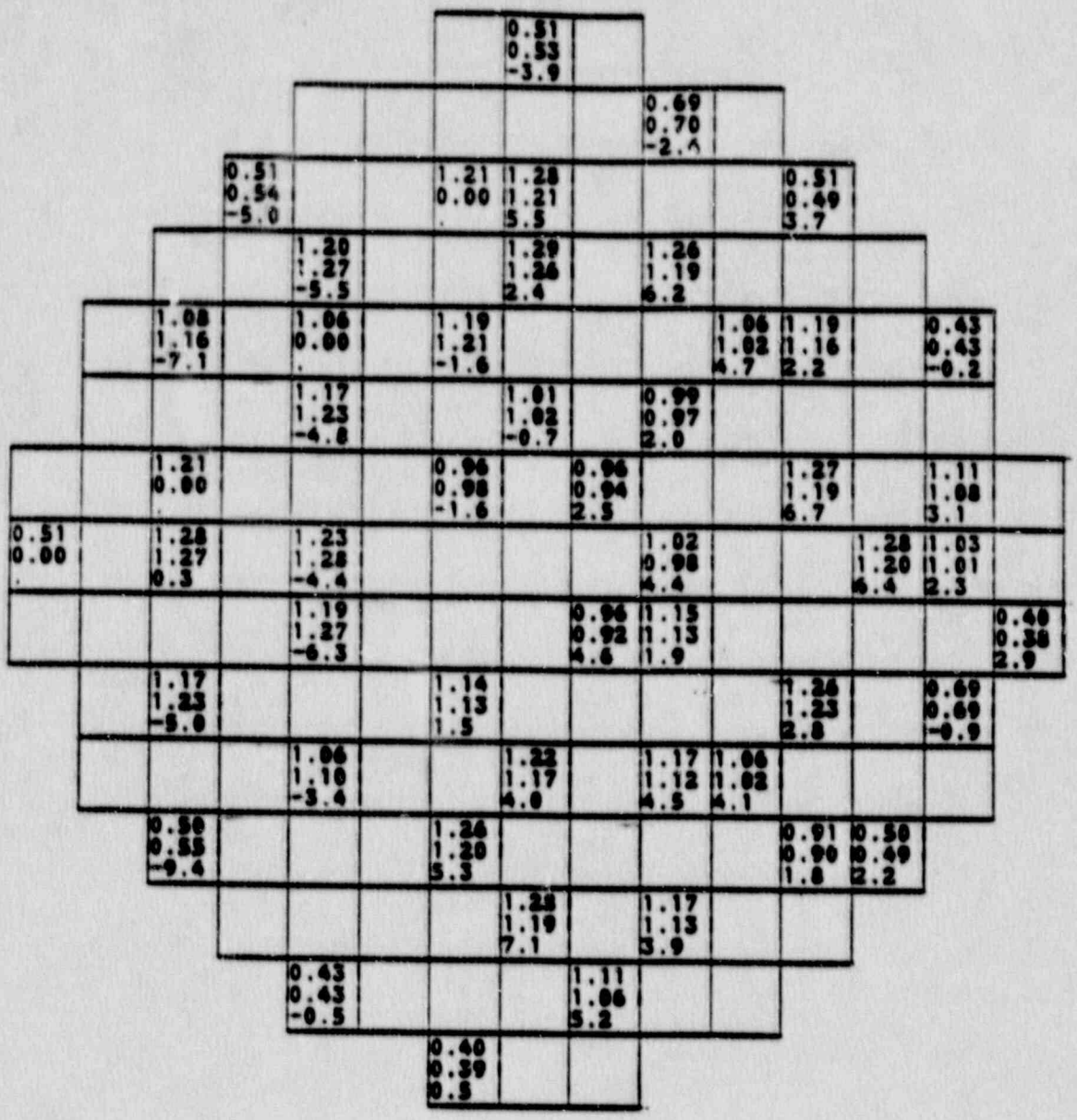

MAX DIFFERENCE = -9.4
MAX DIFF (RPD>0.9) = 7.14
RMS DIFFERENCE = 4.20

X.XX
X.XX
X.X

PREDICTED
MEASURED
PERCENT DIFFERENCE

FIGURE 3-130

N2C4 3D PDQ VS. MEASURED RPD COMPARISON
HFP, D-220, 6610 MWD/MTU N2C4-22A

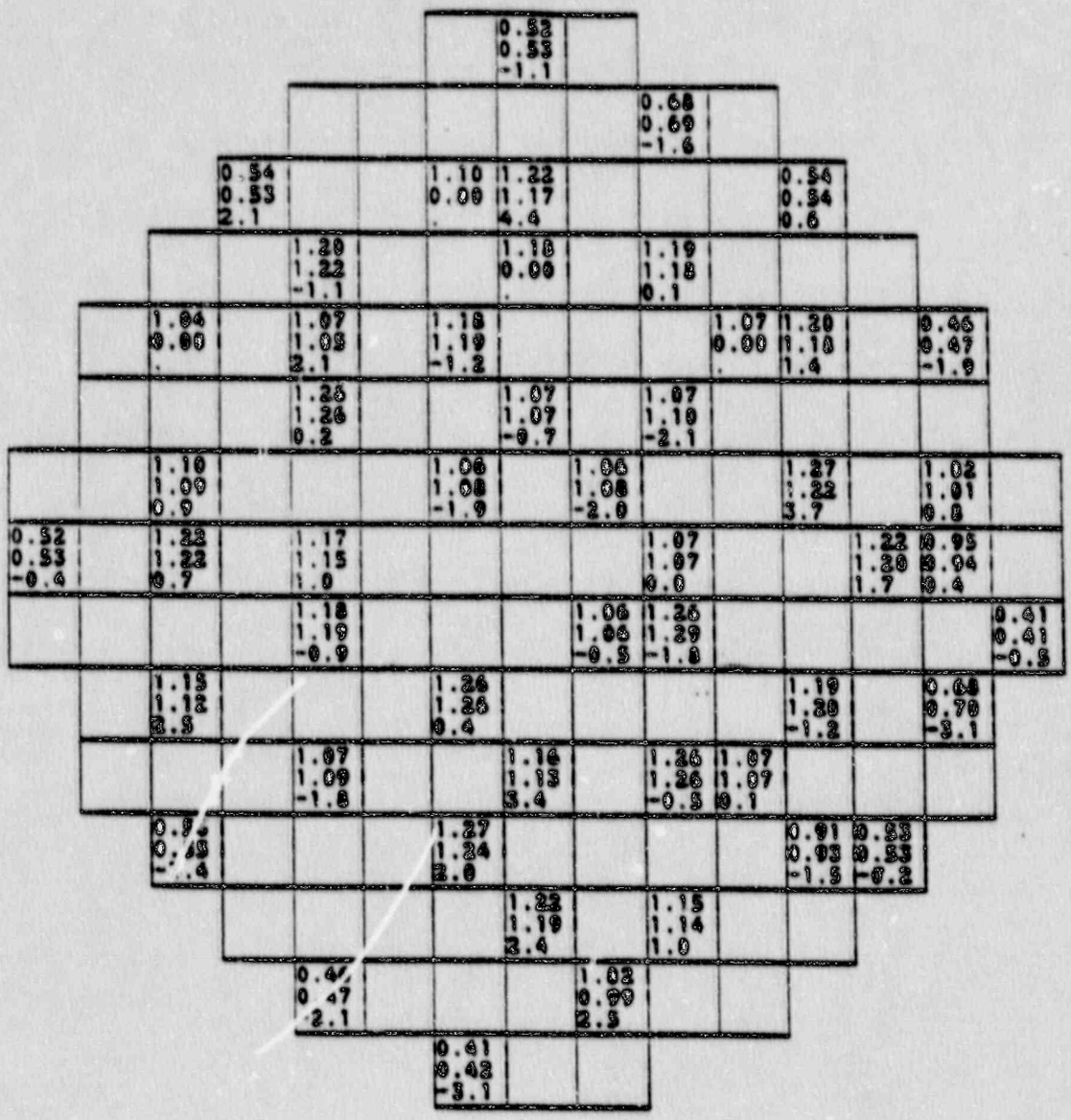

MAX DIFFERENCE = 4.64
MAX DIFF (RPD>0.9) = 4.44
RMS DIFFERENCE = 1.84

X.XX PREDICTED
X.XX MEASURED
X.X PERCENT DIFFERENCE

FIGURE 3-131

N2C4 3D PDQ VS. MEASURED RPD COMPARISON
KFP, D-228, 11267 MWD/MTU N2C4-28A

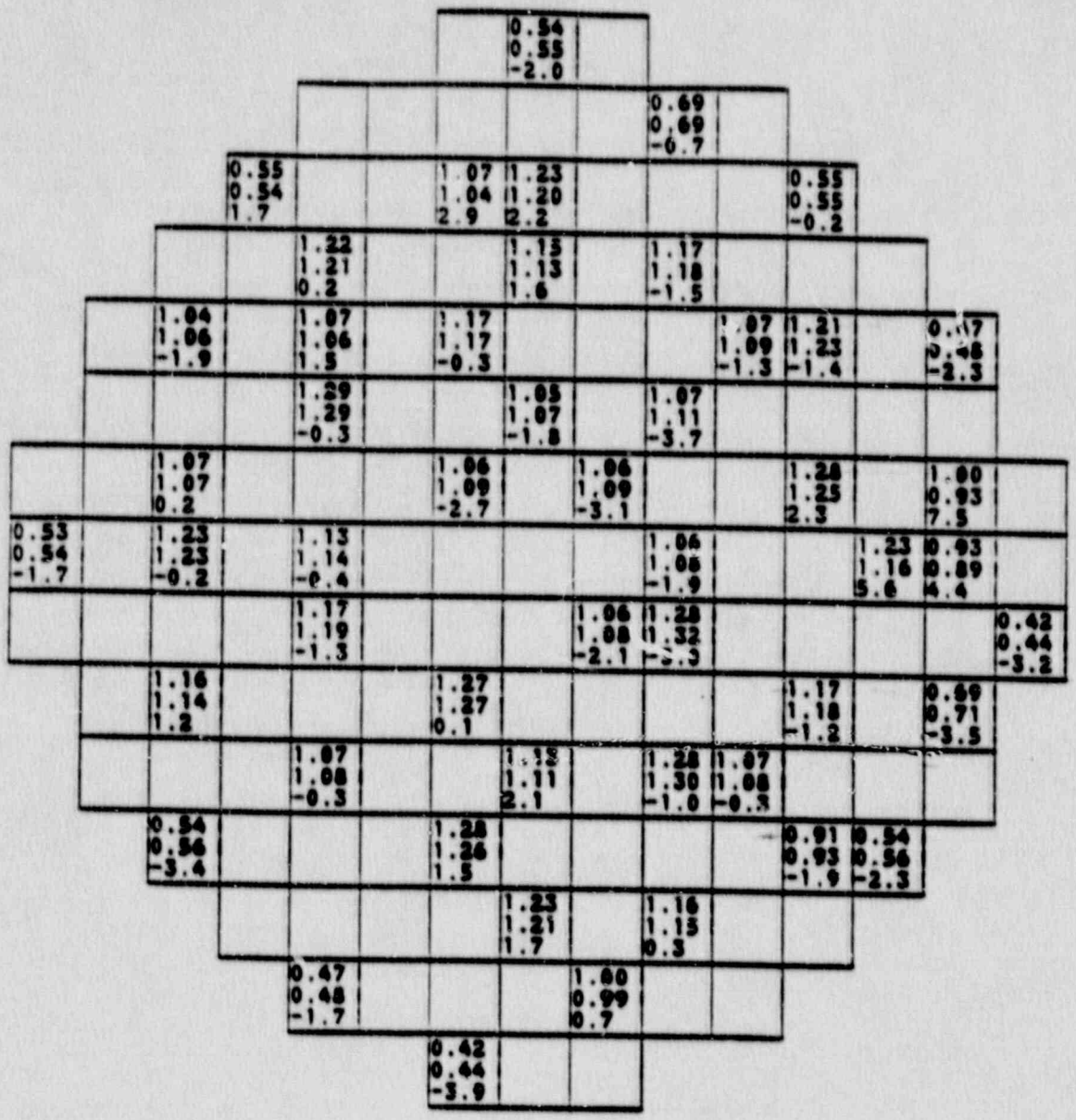

MAX DIFFERENCE = 7.51
MAX DIFF (RPD>0.9) = 7.51
RMS DIFFERENCE = 2.38

X.XX PREDICTED
X.XX MEASURED
X.X PERCENT DIFFERENCE

FIGURE 3-132

N2C5 3D PDQ VS. MEASURED RPD COMPARISON
MFP, D-228, 250 MWD/MTU N2C5-08A

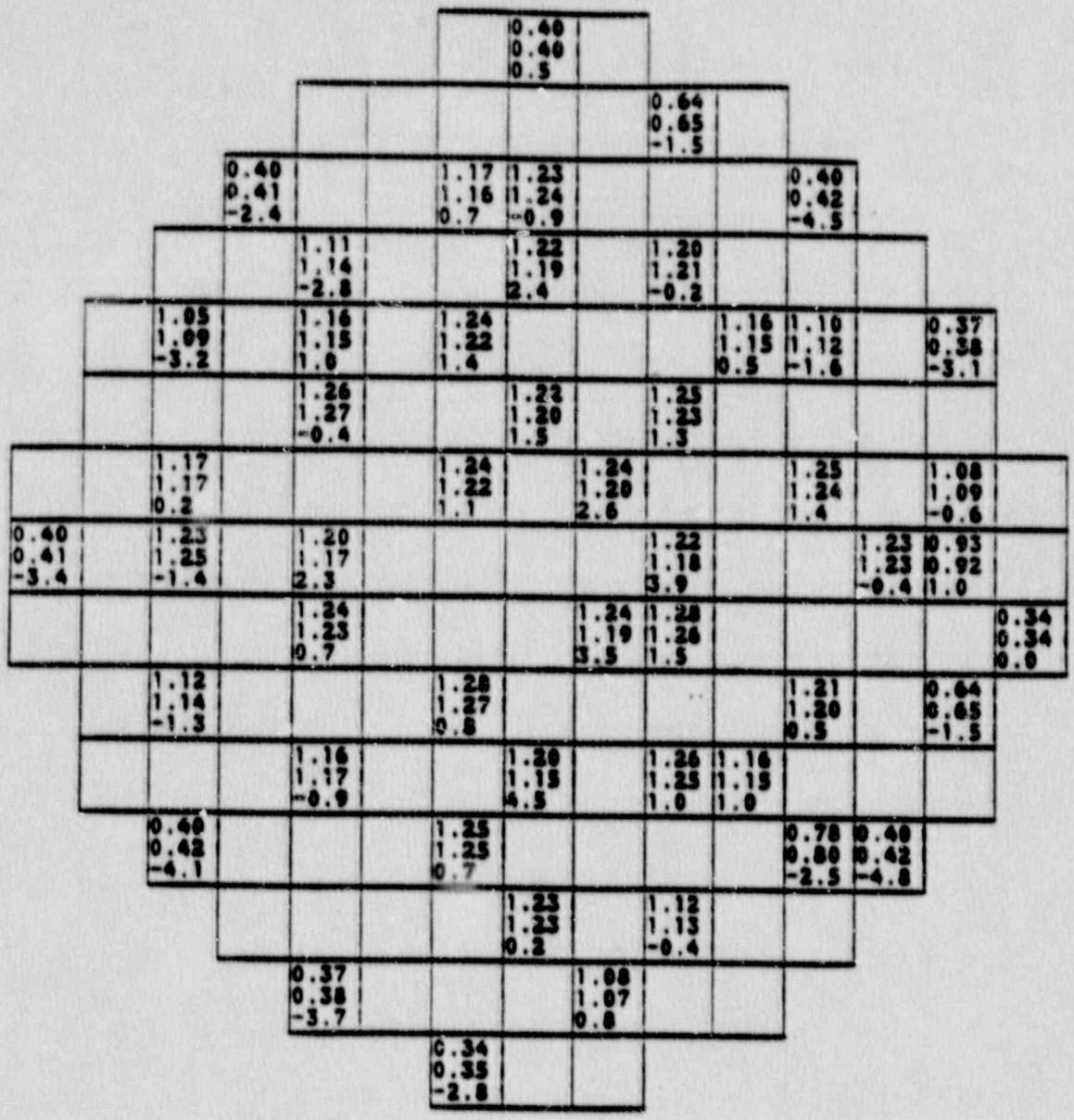

MAX DIFFERENCE = -4.8
MAX DIFF (RPD>0.9) = 4.53
RMS DIFFERENCE = 2.15

X.XX PREDICTED
X.XX MEASURED
X.X PERCENT DIFFERENCE

FIGURE 3-133

N2C5 3D PDQ VS. MEASURED RPD COMPARISON
HFP, D-228, 6075 MWD/MTU N2C5-19A

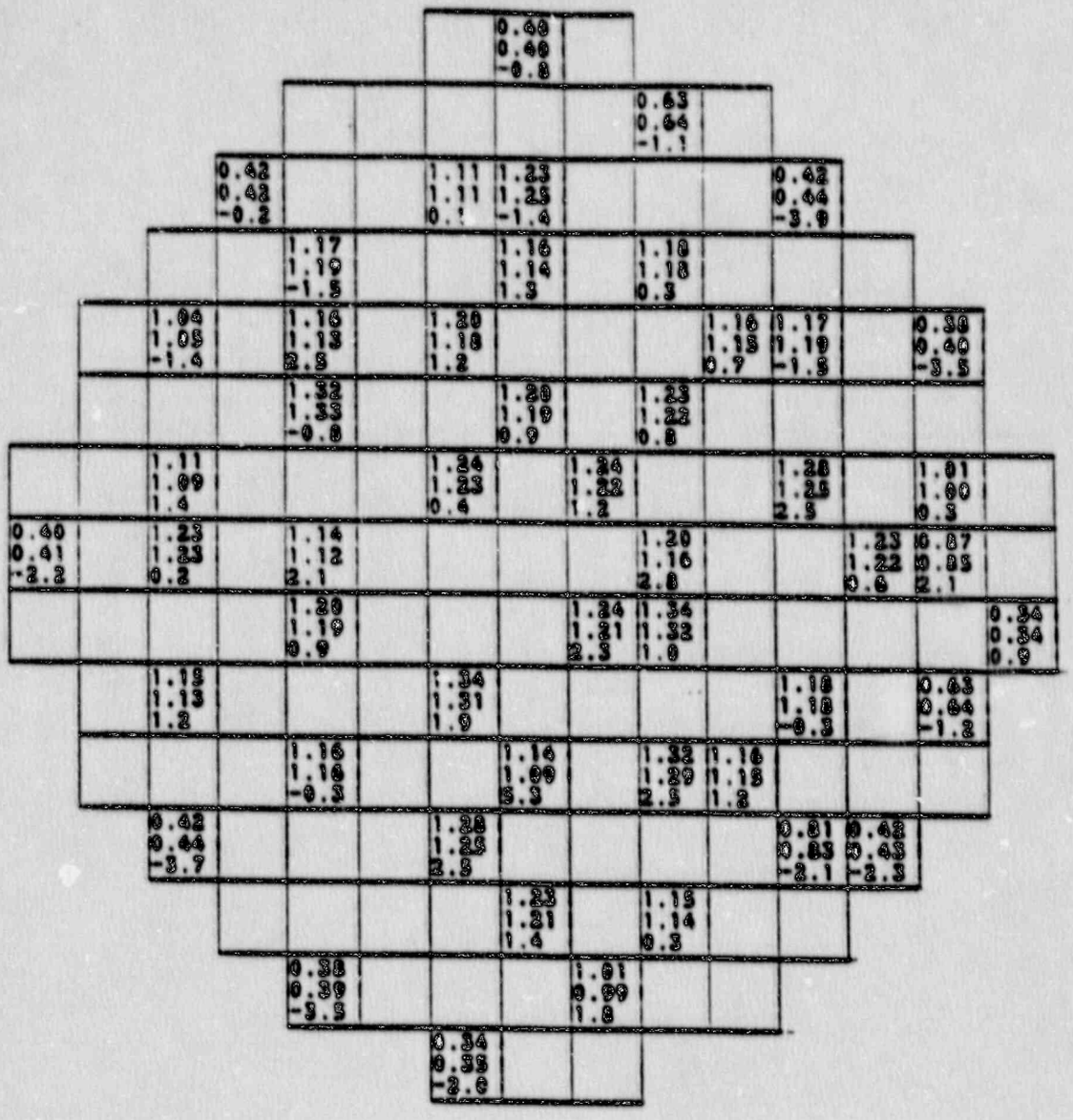

MAX DIFFERENCE = 5.34
MAX DIFF (RPD>0.9) = 5.34
RMS DIFFERENCE = 1.92

X.XX PREDICTED
X.XX MEASURED
X.X PERCENT DIFFERENCE

FIGURE 3-134

N2C5 3D PDQ VS. MEASURED RPD COMPARISON
HFP, D-228, 13871 MWD/MTU N2C5-29A

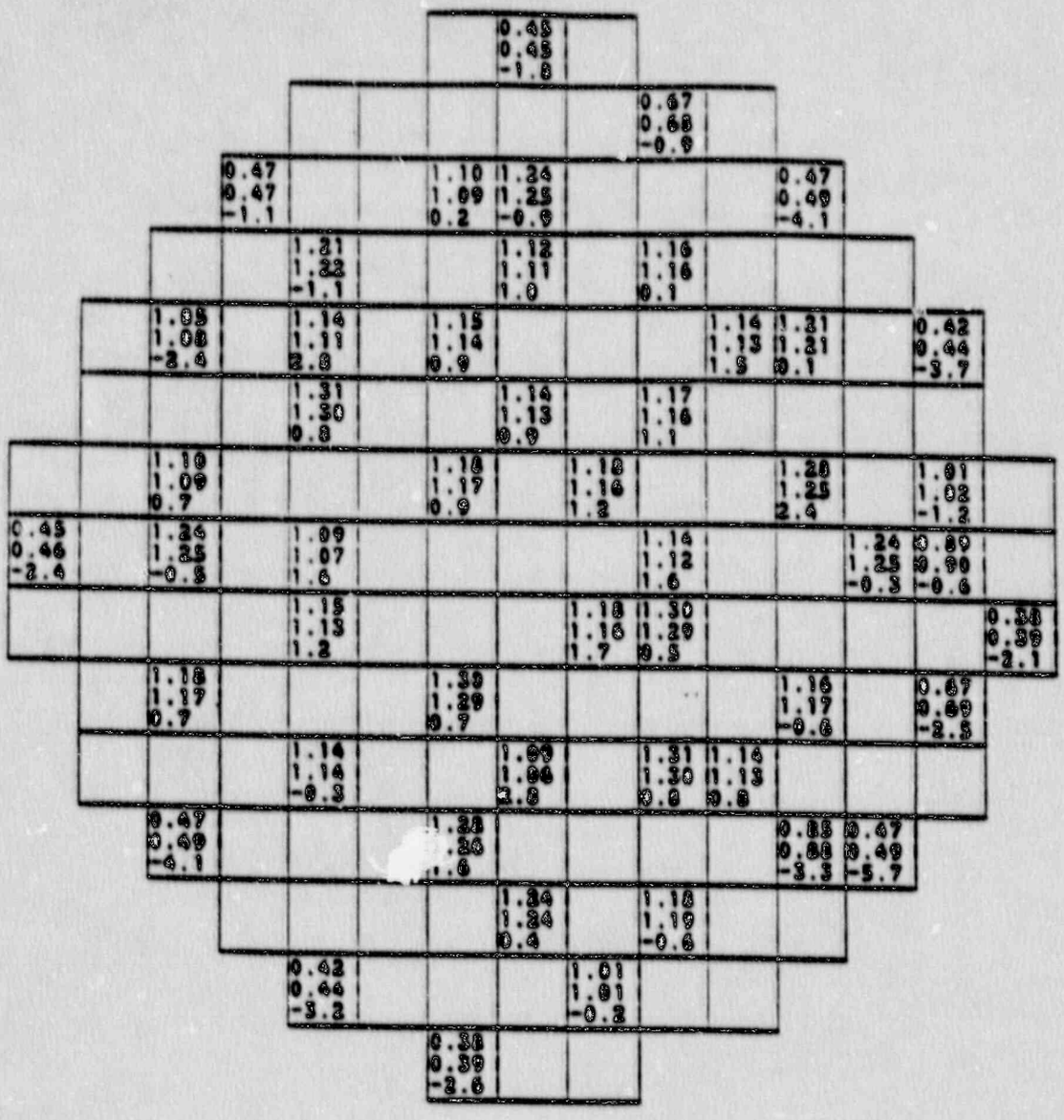

MAX DIFFERENCE = -5.7
MAX DIFF (RPD>0.0) = 2.83
RMS DIFFERENCE = 1.92

X.XX PREDICTED
X.XX MEASURED
X.X PERCENT DIFFERENCE

FIGURE 3-135

S1C2 3D PDQ VS. MEASURED RPD COMPARISON
MZP, D-314, 0 MWD/MTU S1-2-02A

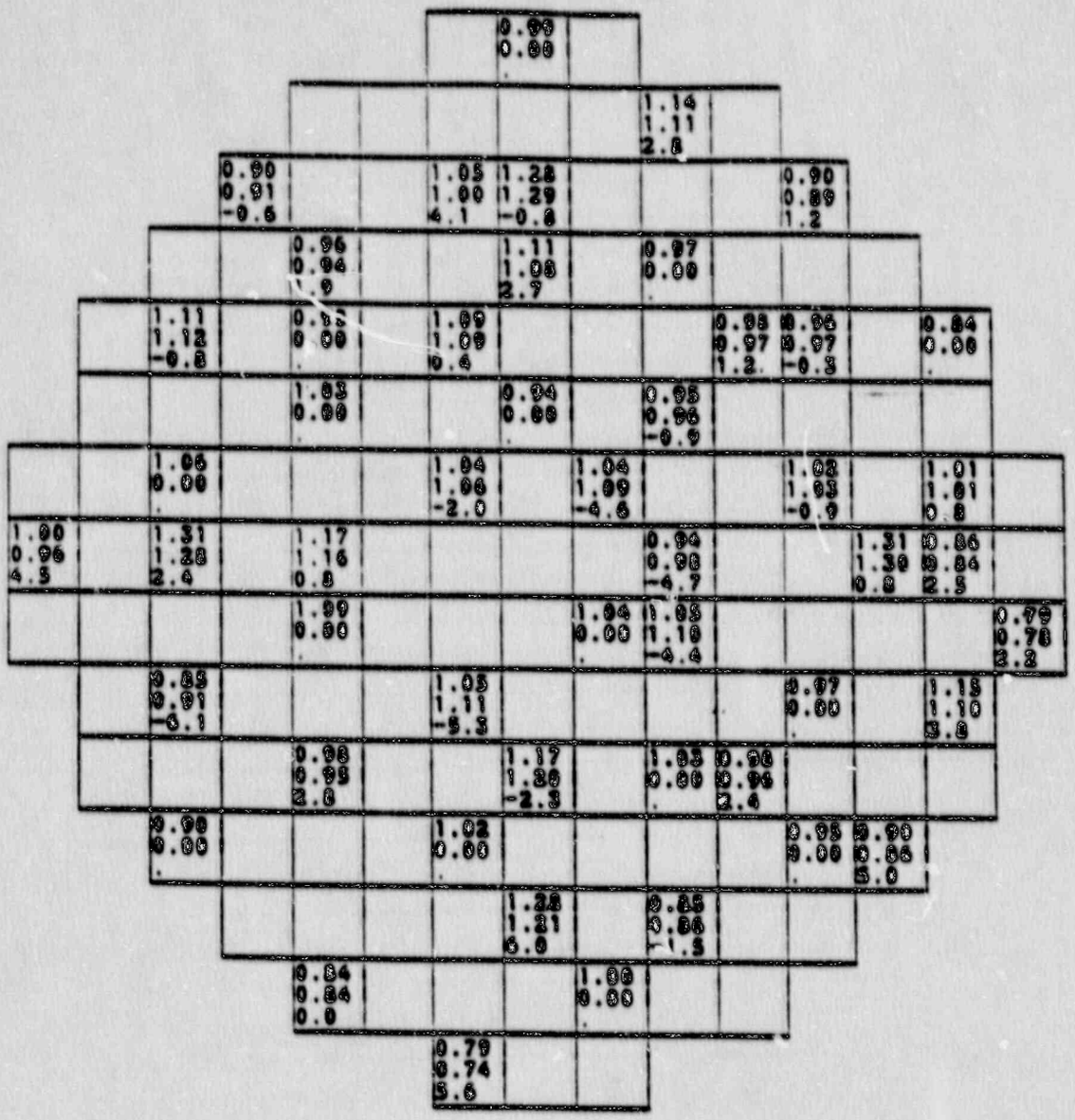

MAX DIFFERENCE = -6.1
MAX DIFF (RPD>0.9) = 5.97
RMS DIFFERENCE = 3.12

X.XX PREDICTED
X.XX MEASURED
X.X PERCENT DIFFERENCE

FIGURE 3-136

S1CR 3D PDQ VS. MEASURED RPD COMPARISON
HFP, D-222, 1100 MWD/MTU S1-2-12A

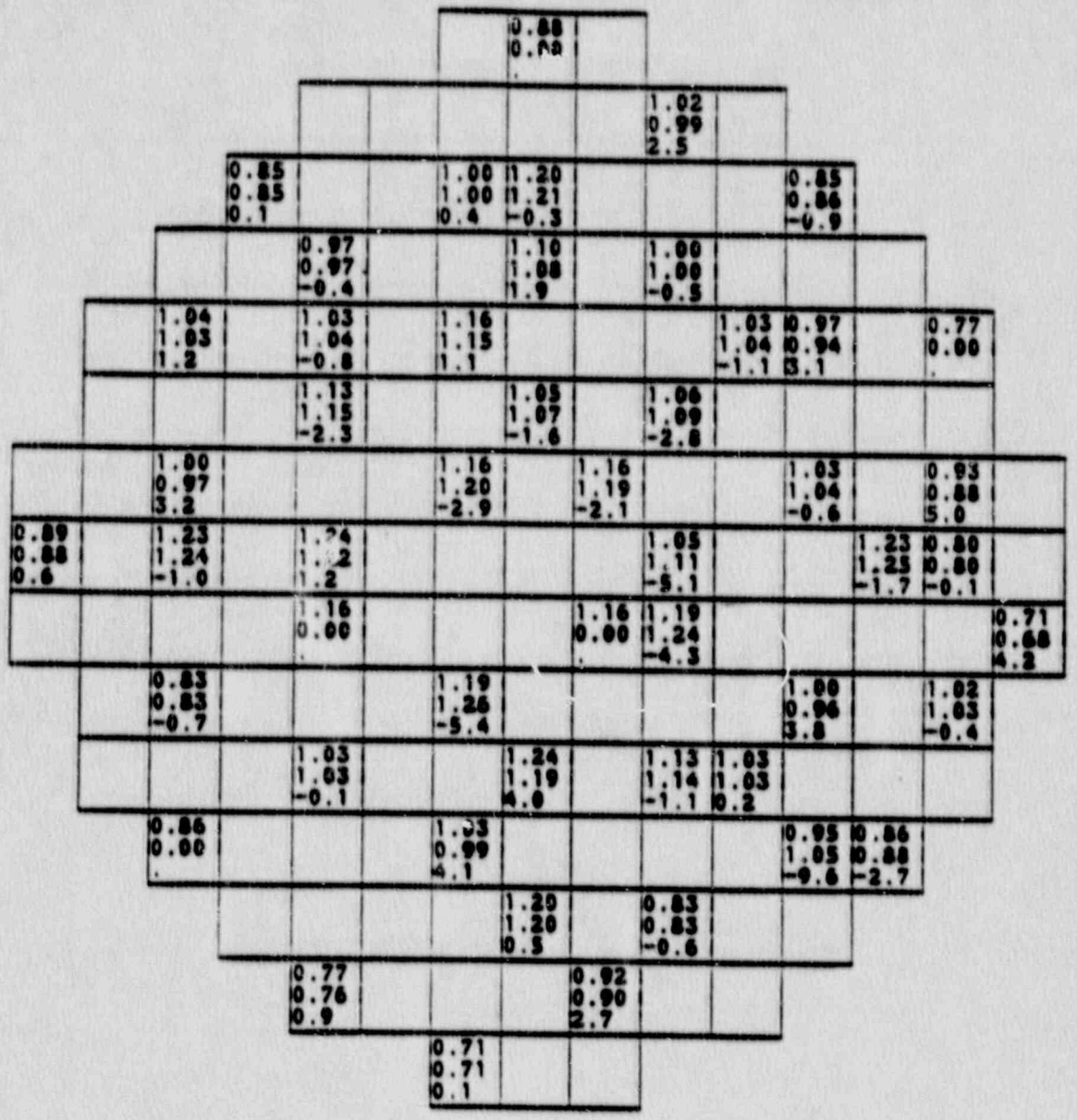

MAX DIFFERENCE = -9.6
MAX DIFF (RPD>0.9) = -9.6
RMS DIFFERENCE = 2.77

X.XX PREDICTED
X.XX MEASURED
X.X PERCENT DIFFERENCE

FIGURE 3-137

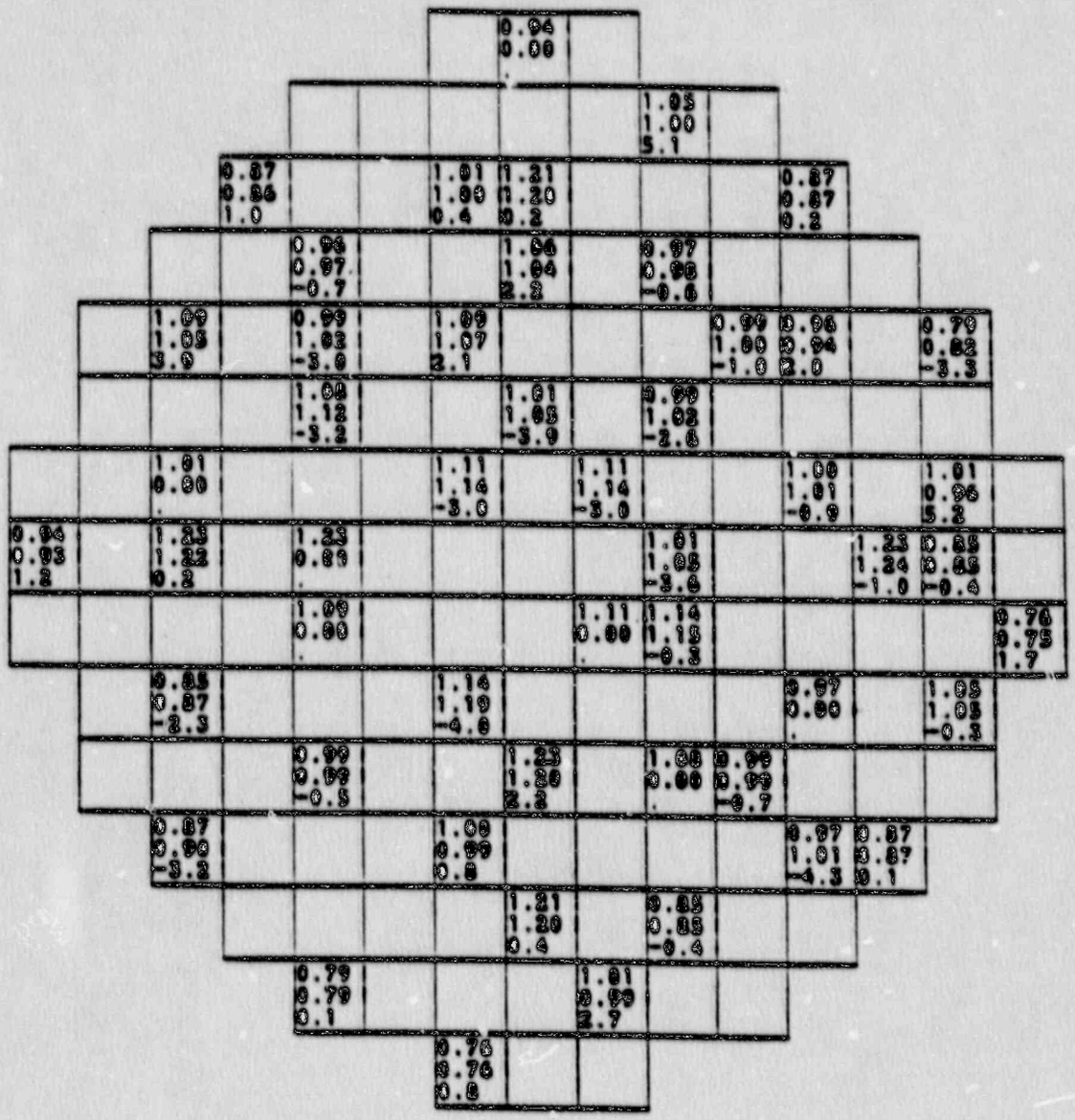

MAX DIFFERENCE = 5.18
MAX DIFF (REF>0.0) = 5.18
RMS DIFFERENCE = 2.36

X.XX PREDICTED
X.XX MEASURED
X.X PERCENT DIFFERENCE

FIGURE 3-138

S1C3 3D FDG VS. MEASURED RFD COMPARISON
HFP, D-212, 250 MWD/MTU S1-3-09B

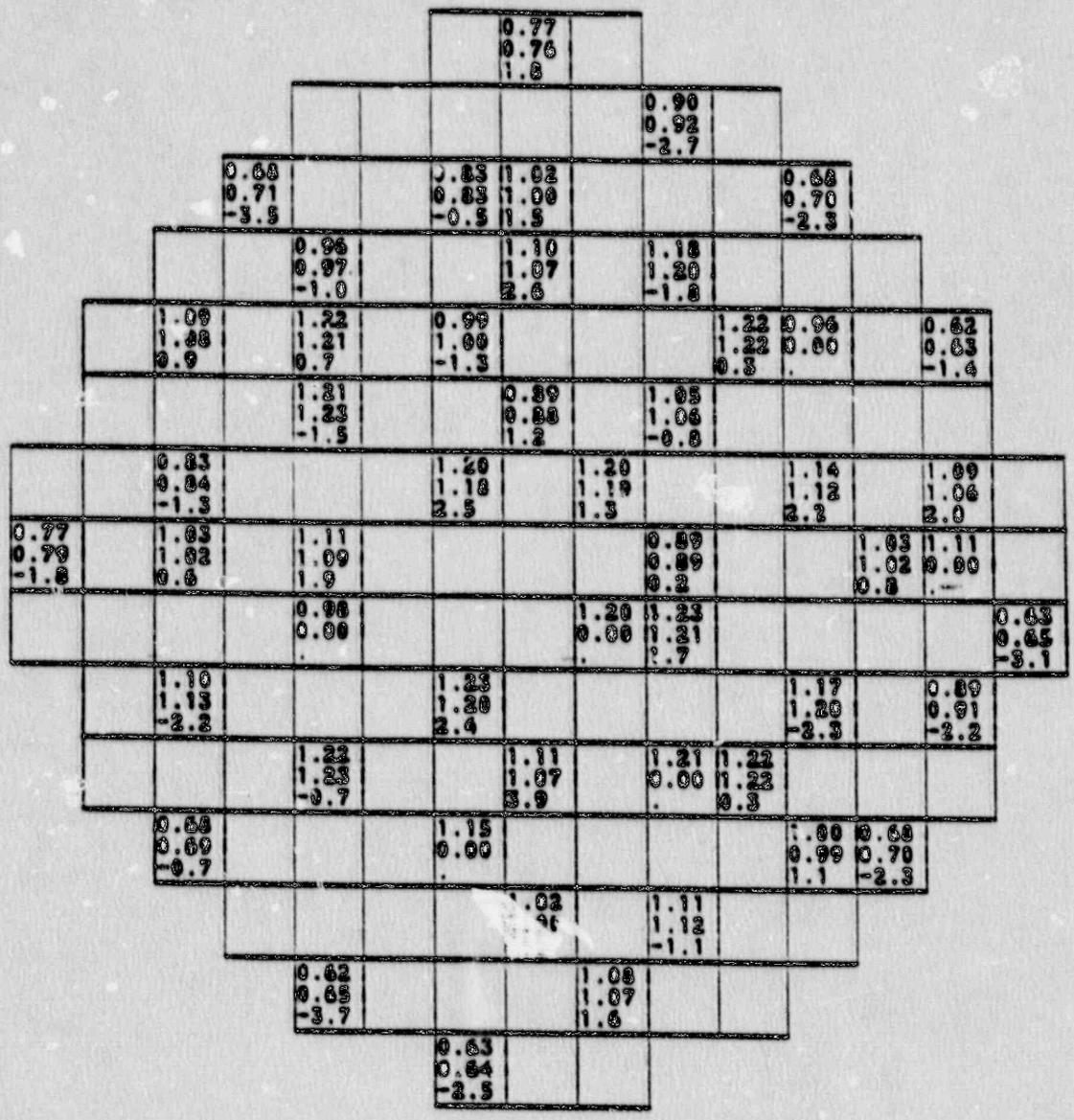

MAX DIFFERENCE = 3.91
MAX DIFF (RFD>0.9) = 3.91
RMS DIFFERENCE = 1.91

X.XX PREDICTED
X.XX MEASURED
X.X PERCENT DIFFERENCE

FIGURE 3-139

S1C3 3D PDQ VS. MEASURED RPD COMPARISON
HFP, D-225 7175 MWD/MTU S1-3-20B

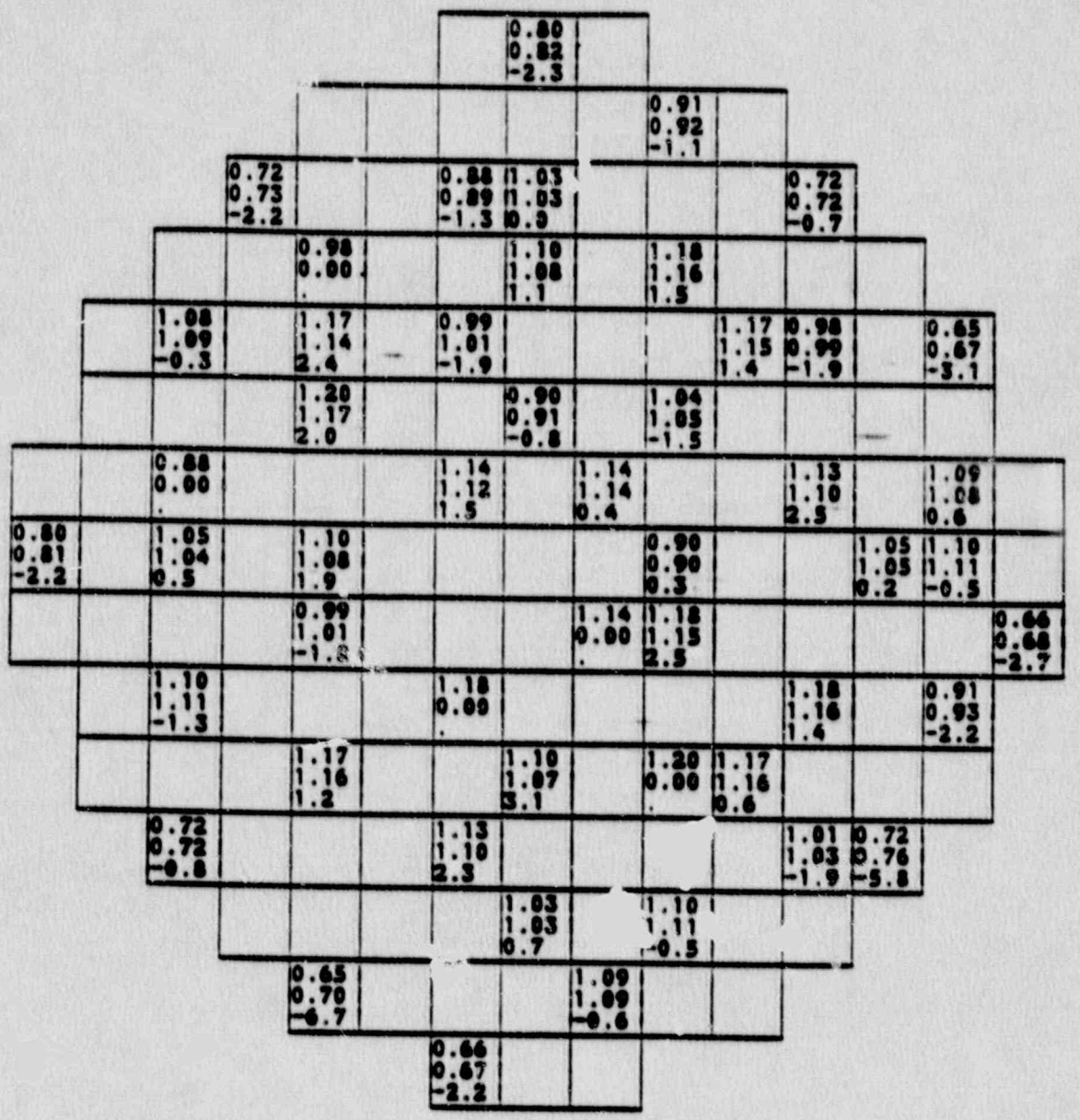

MAX DIFFERENCE = -6.7
MAX DIFF (RPD>0.9) = 3.09
RMS DIFFERENCE = 2.10

X.XX	PREDICTED
X.XX	MEASURED
X.X	PERCENT DIFFERENCE

FIGURE 3-140

S1C4 3D PDQ VS. MEASURED RPD COMPARISON
HZP, D-220, 0 MWD/MTU S1-4-02A

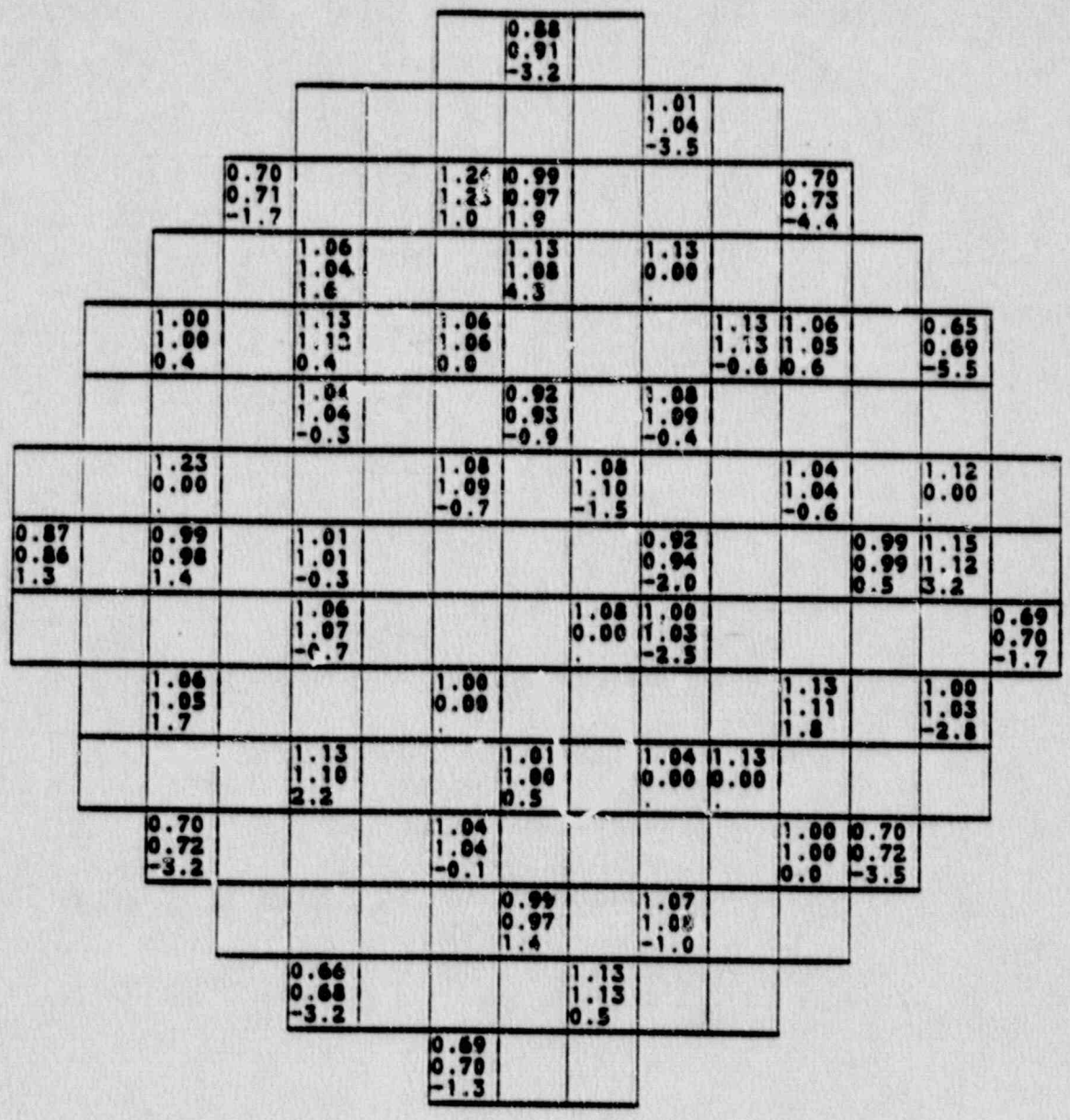

MAX DIFFERENCE = -5.5
MAX DIFF (RPD>0.9) = 4.26
RMS DIFFERENCE = 2.10

X.XX PREDICTED
X.XX MEASURED
X.X PERCENT DIFFERENCE

FIGURE 3-141

S1C4 3D FDQ VS. MEASURED RFD COMPARISON
HFP, D-215, 930 MWD/MTU S1-4-10A

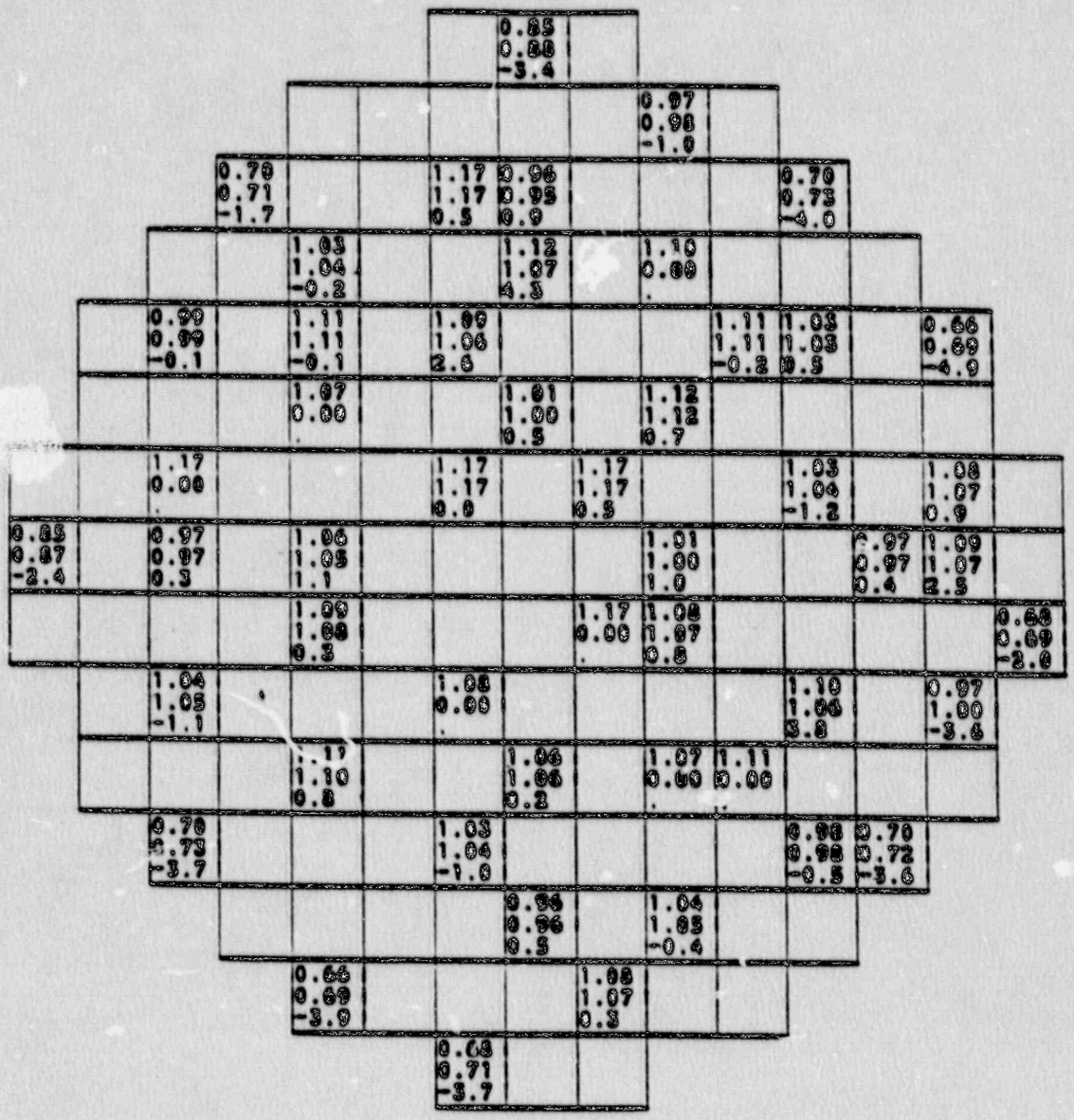

MAX DIFFERENCE = -4.9
MAX DIFF (RFD>0.9) = 4.29
RMS DIFFERENCE = 2.11

X.XX
X.XX
X.X

PREDICTED
MEASURED
PERCENT DIFFERENCE

FIGURE 3-142

S1C4 3D PDQ VS. MEASURED RPD COMPARISON
HFP, D-206, 8400 MWD/MTU S1-4-23A

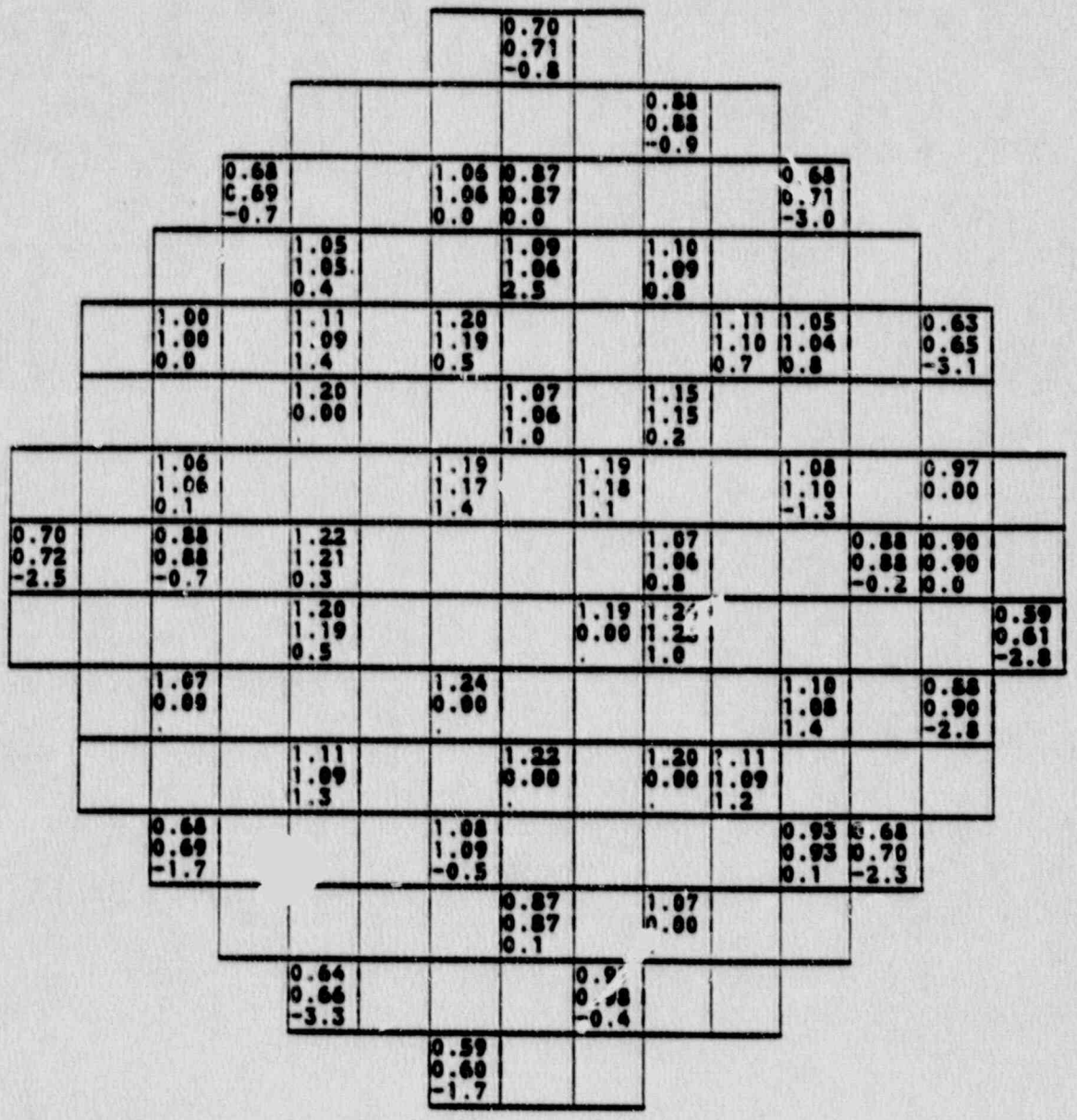

MAX DIFFERENCE = -3.3
MAX DIFF (RPD>0.9) = 2.54
RMS DIFFERENCE = 1.45

X.XX	PREDICTED
X.XX	MEASURED
X.X	PERCENT DIFFERENCE

FIGURE 3-143

S1C5 3D PDQ VS. MEASURED RPD COMPARISON
HZP, D-218, 0 MWD/MTU S1-5-01A

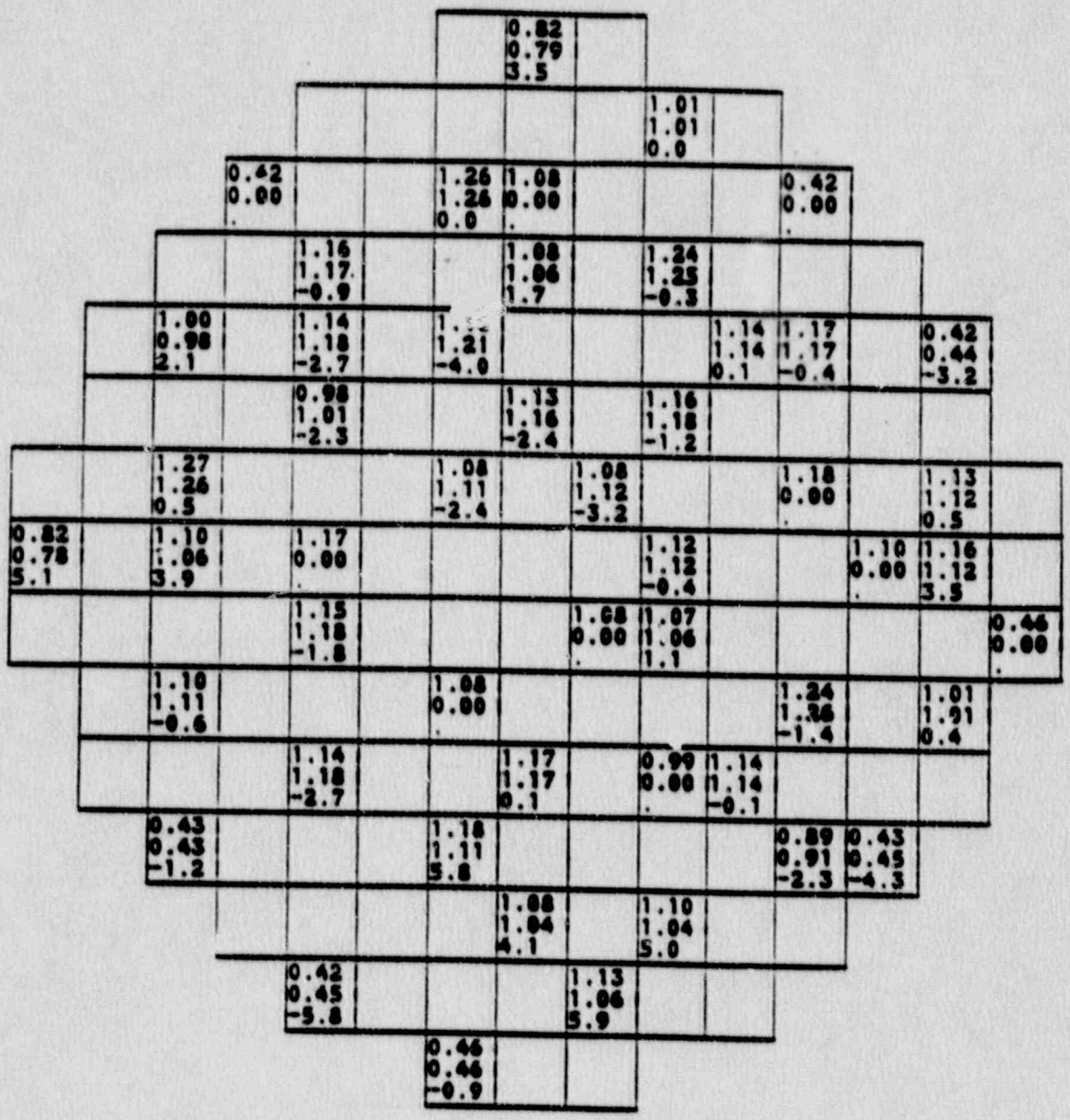

MAX DIFFERENCE = 5.93
MAX DIFF (RPD>0.9) = 5.93
RMS DIFFERENCE = 2.84

XX.XX PREDICTED
XX.XX MEASURED
X.X PERCENT DIFFERENCE

FIGURE 3-144

S1CS 3D PDQ VS. MEASURED R'D COMPARISON
HFP, D-220, 1300 MWD/MTU S1-5-11A

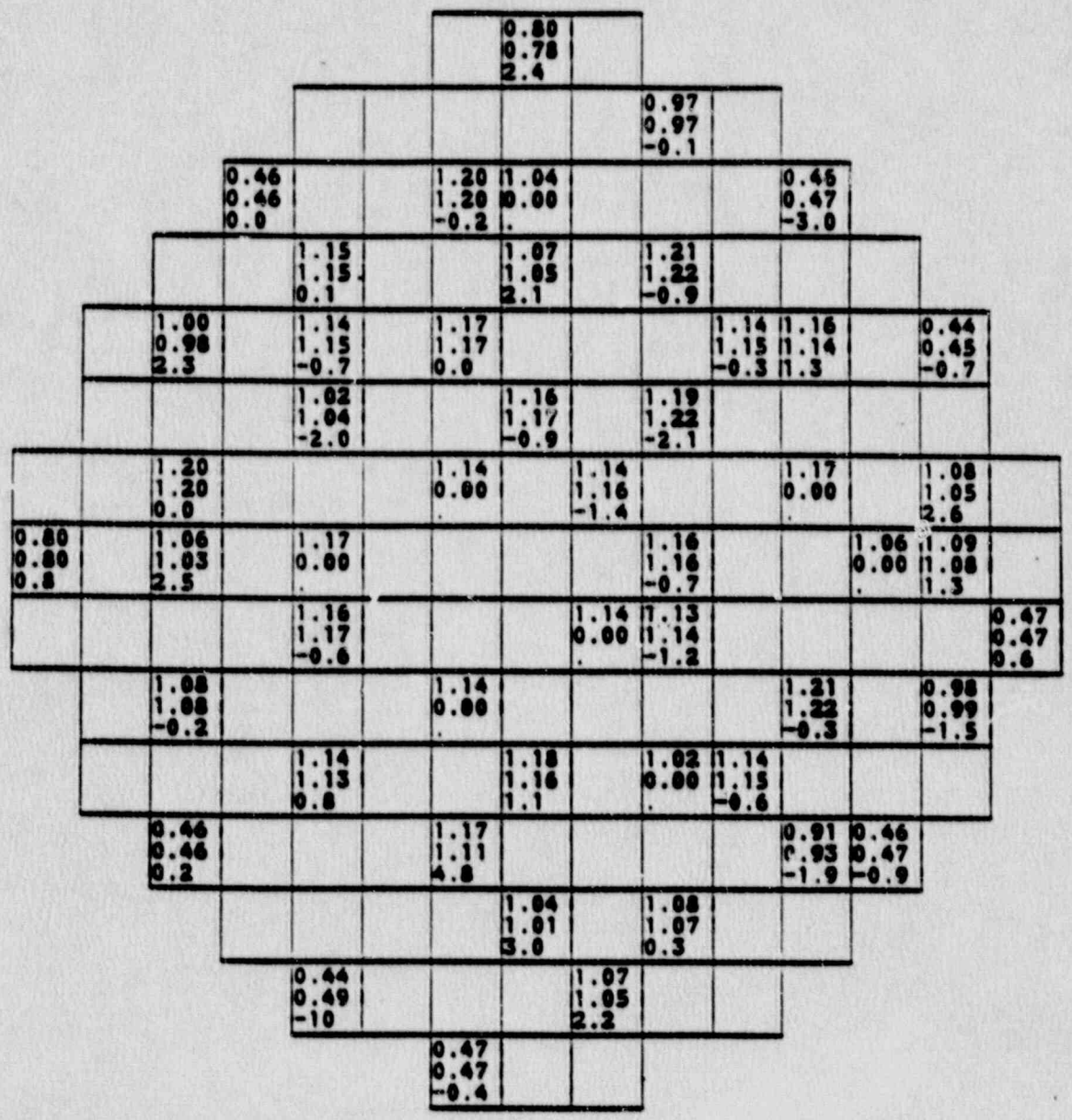

MAX DIFFERENCE = -10
MAX DIFF (RPD>0.9) = 4.85
RMS DIFFERENCE = 2.24

X.XX PREDICTED
X.XX MEASURED
X.X PERCENT DIFFERENCE

FIGURE 3-145

SICS 3D PDQ VS. MEASURED RPD COMPARISON
MFP, D-224, 7411 MWD/MTU S1-S-23A

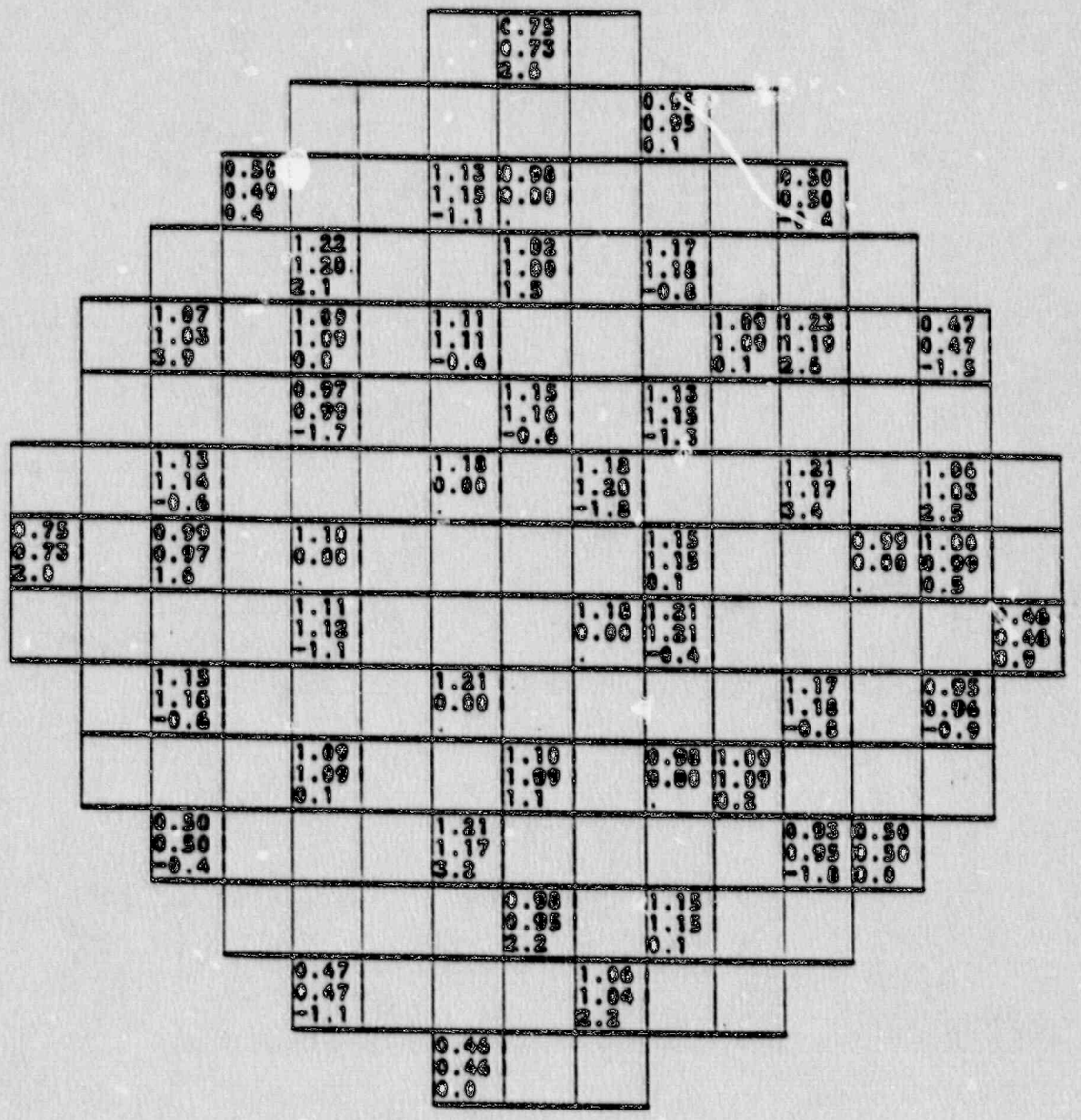

MAX DIFFERENCE = 3.90
MAX DIFF (RPD>0.9) = 3.90
RMS DIFFERENCE = 1.55

X.XX PREDICTED
X.XX MEASURED
X.X PERCENT DIFFERENCE

FIGURE 3-146

S1CS 3D PDQ VS. MEASURED RFD COMPARISON
HFP, D-226, 10758 MWD/MTU S1-5-31A

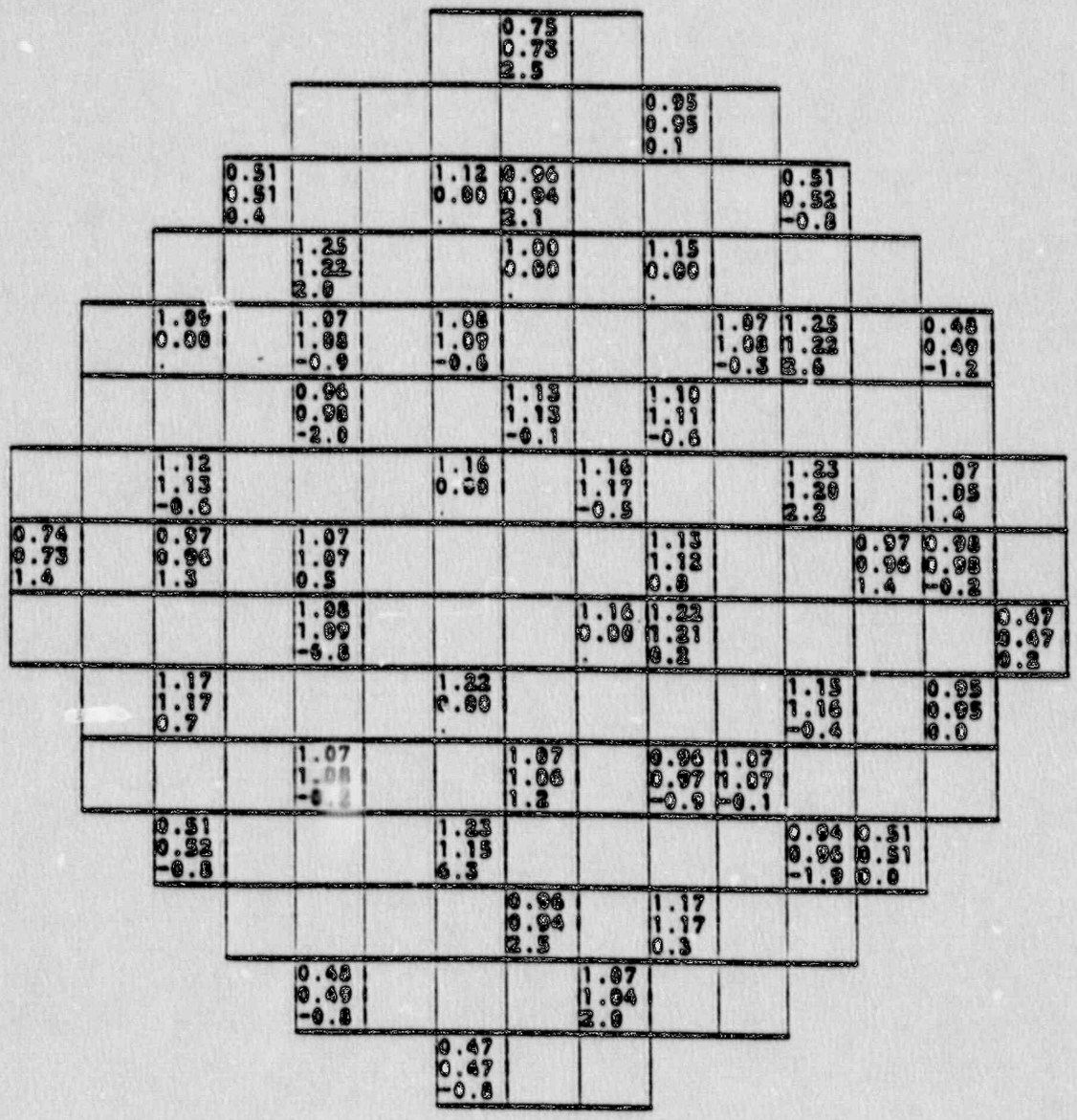

MAX DIFFERENCE = 6.32
MAX DIFF (RFD>0.9) = 6.32
RMS DIFFERENCE = 1.55

X.XX PREDICTED
X.XX MEASURED
X.X PERCENT DIFFERENCE

FIGURE 3-147

S1C6 3D PDQ VS. MEASURED RPD COMPARISON
HZP, D-201, 0 MWD/MTU S1-6-01A

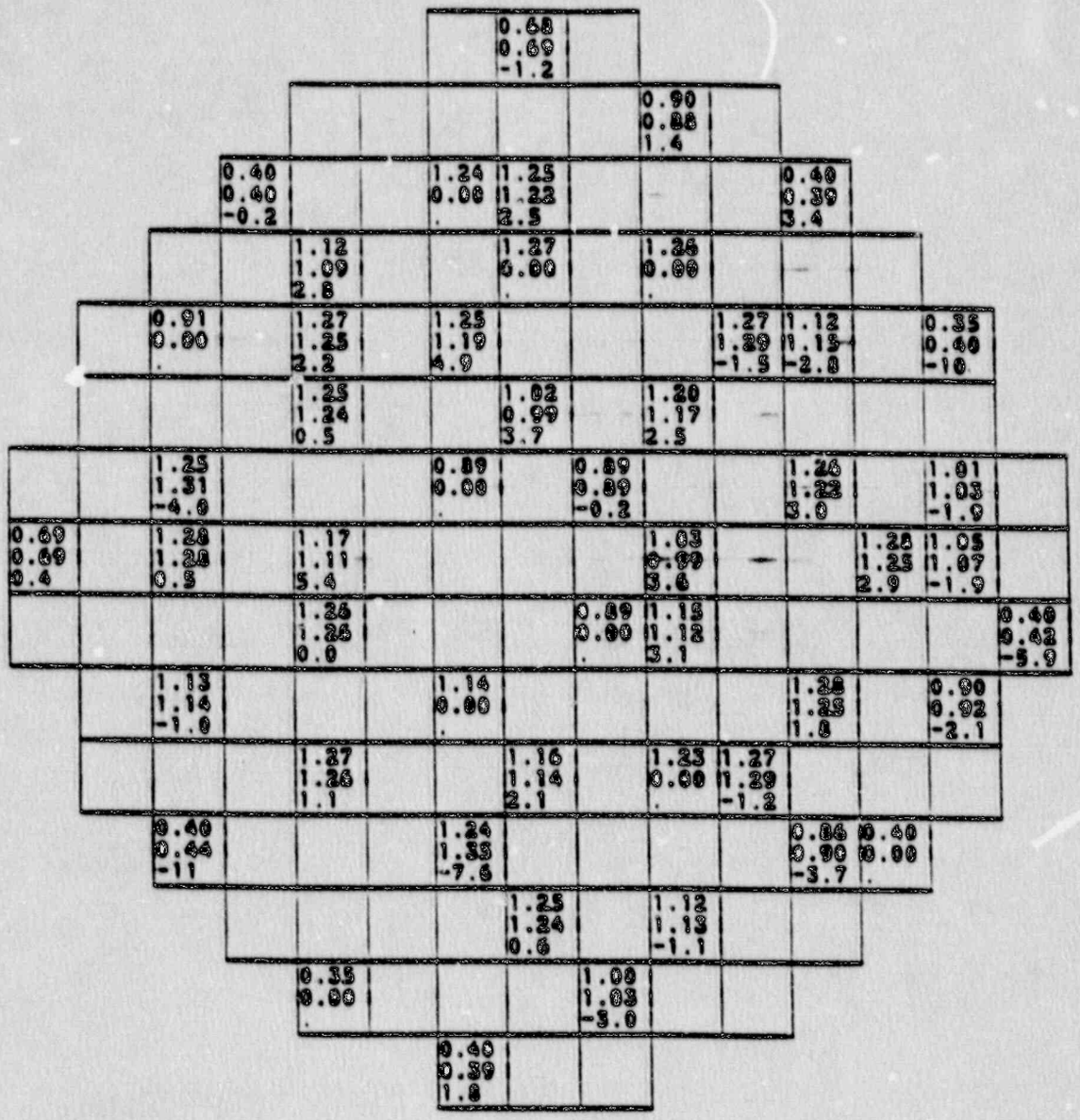

MAX DIFFERENCE = -11
MAX DIFF (RPD>0.9) = -7.6
RMS DIFFERENCE = 3.69

X.XX
X.XX
X.X

PREDICTED
MEASURED
PERCENT DIFFERENCE

FIGURE 3-148

S1C6 3D PDQ VS. MEASURED RPD COMPARISON
HFP, D-217, 973 MWD/MTU S1-6-13A

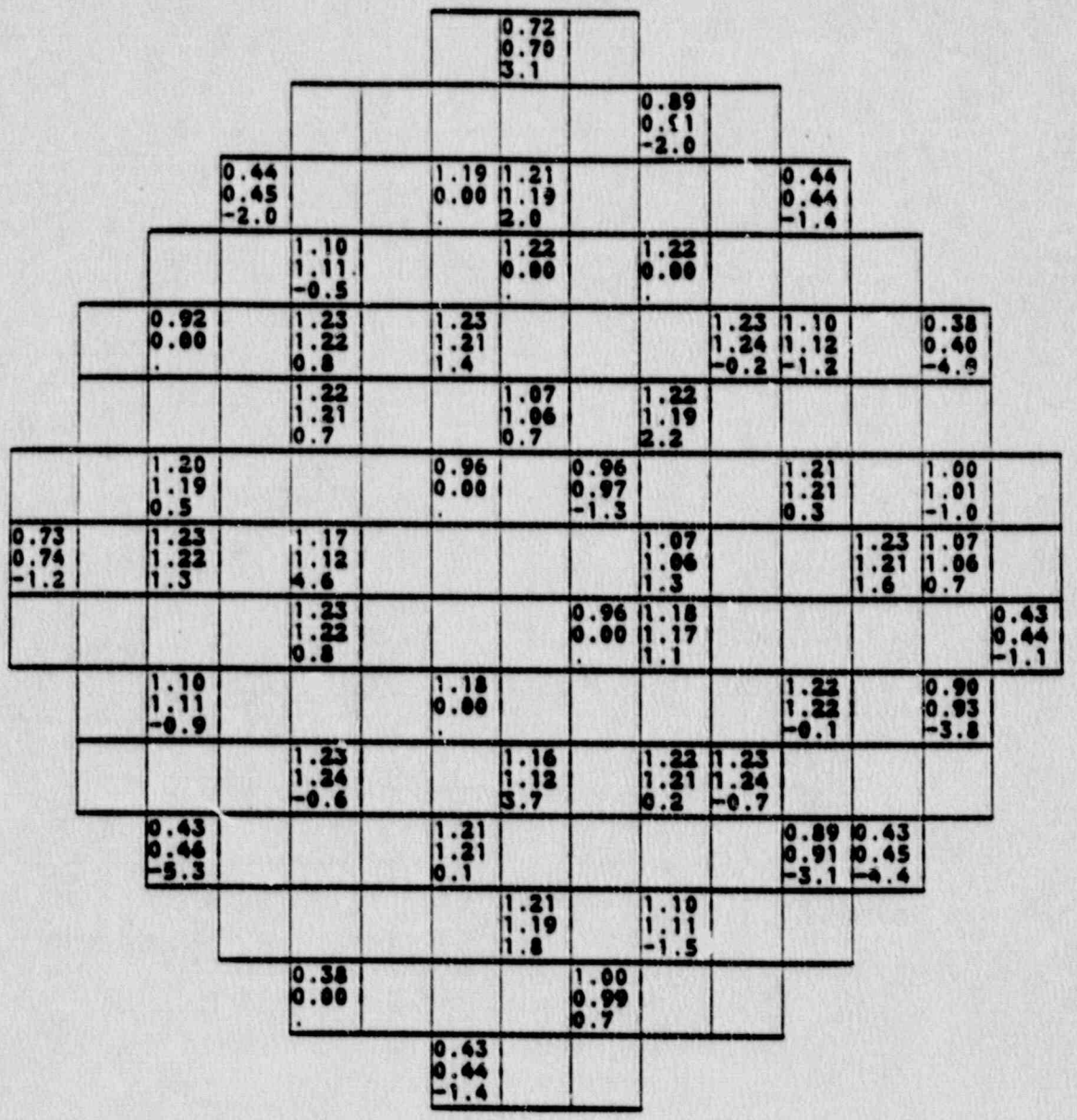

MAX DIFFERENCE = -5.3
MAX DIFF (RPD>0.9) = 4.57
RMS DIFFERENCE = 2.11

X.XX PREDICTED
X.XX MEASURED
X.X PERCENT DIFFERENCE

FIGURE 3-149

S1C6 3D PDQ VS. MEASURED RPD COMPARISON
HFP, D-228, 7518 MWD/MTU S1-6-56A

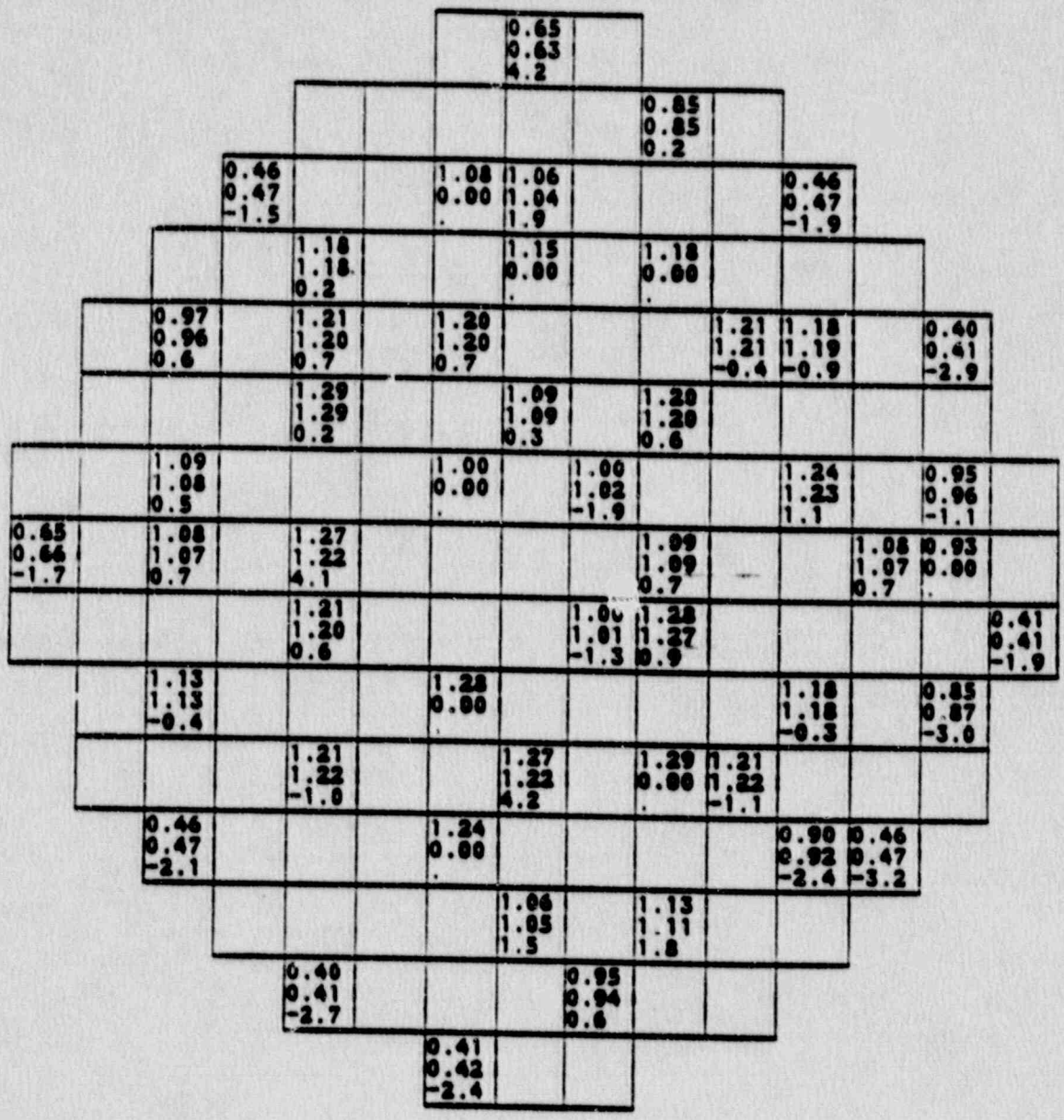

MAX DIFFERENCE = 4.18
MAX DIFF (RPD>0.9) = 4.18
RMS DIFFERENCE = 1.83

X.XX PREDICTED
X.XX MEASURED
(X.X) PERCENT DIFFERENCE

FIGURE 3-150

S1C6 3D PDQ VS. MEASURED RPD COMPARISON
KFP, D-222, 13207 MWD/MTU S1-6-70A

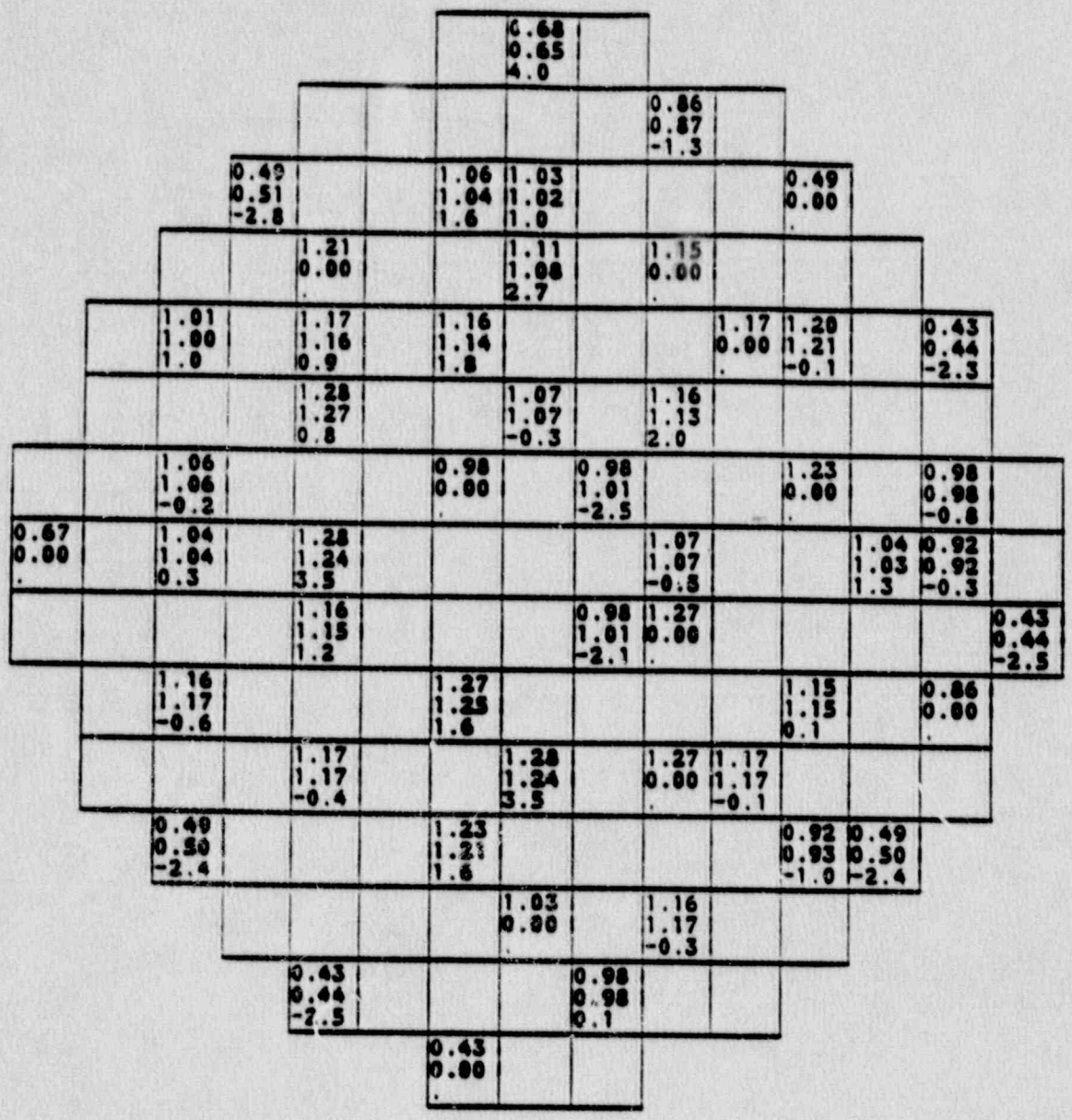

MAX DIFFERENCE = 4.00
MAX DIFF (RPD>0.9) = 3.47
RMS DIFFERENCE = 1.78

X.XX PREDICTED
X.XX MEASURED
X.X PERCENT DIFFERENCE

FIGURE 3-151

S1C7 3D PDQ VS. MEASURED RPD COMPARISON
HZP, D-221, 0 MWD/MTU S1-7-02A

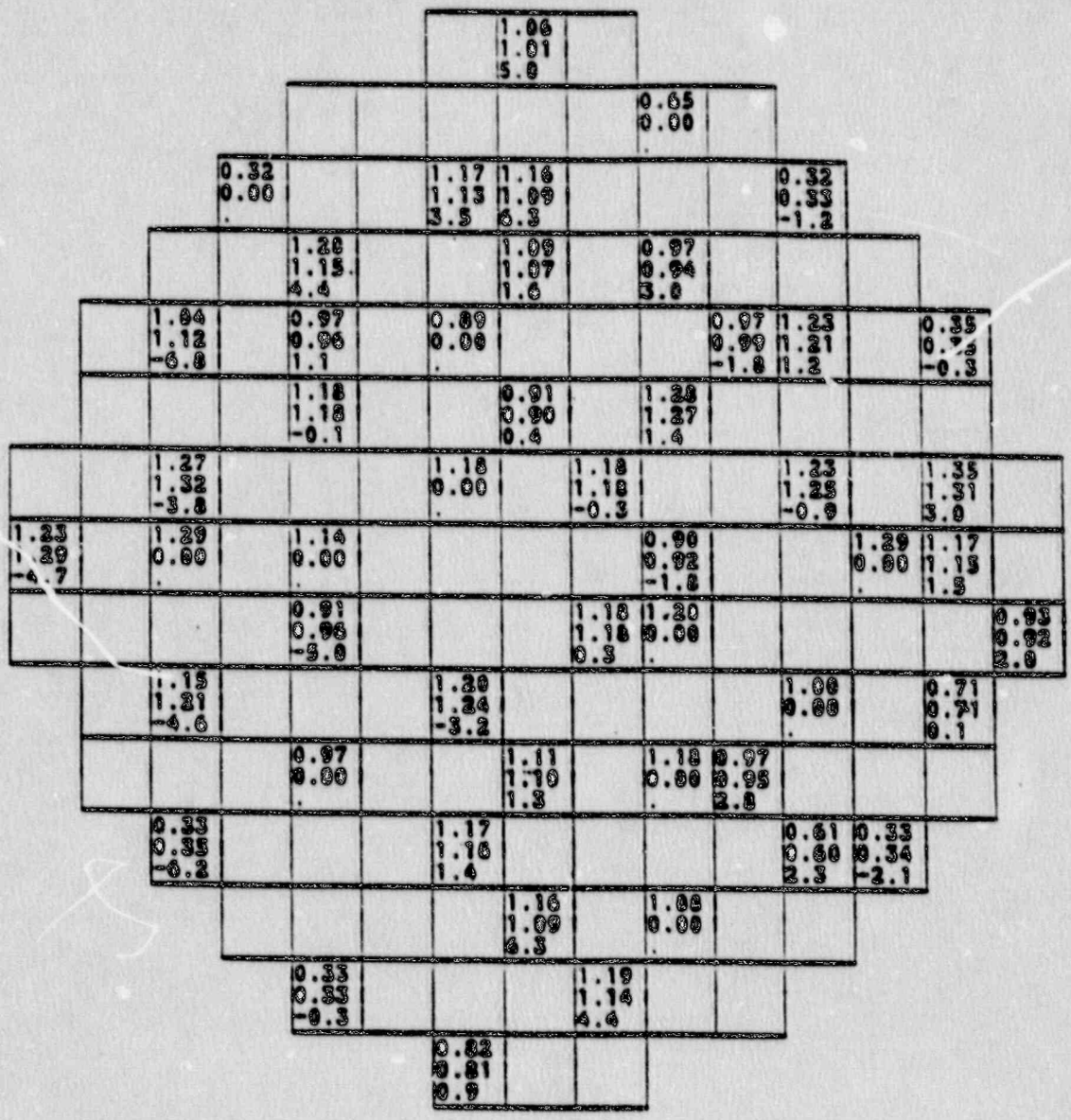

MAX DIFFERENCE = -6.8
MAX DIFF (RPD>0.9) = -6.8
RMS DIFFERENCE = 3.23

X.XX	PREDICTED
X.XX	MEASURED
X.X	PERCENT DIFFERENCE

FIGURE 3-152

S1C7 3D PDQ VS. MEASURED RPD COMPARISON
HFP, D-228, 807 MWD, WTU S1-7-08A

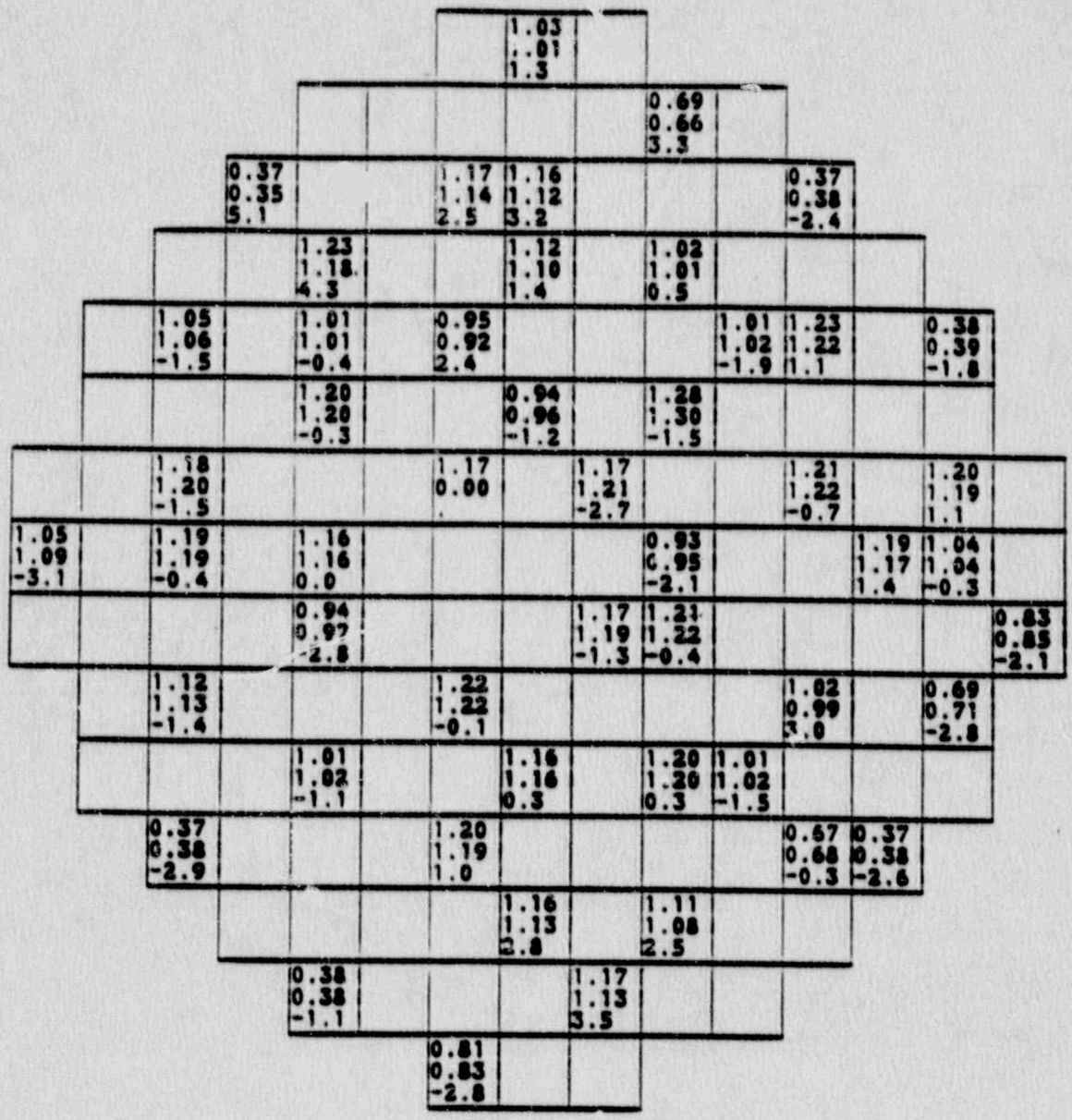

MAX DIFFERENCE = 5.11
MAX DIFF (RPD>0.9) = 4.31
RMS DIFFERENCE = 2.10

X.XX	PREDICTED
X.XX	MEASURED
X.X	PERCENT DIFFERENCE

FIGURE 3-153

S1C7 3D PDQ VS. MEASURED RPD COMPARISON
HFP, D-228, 4329 MWD/MTU 81-7-14A

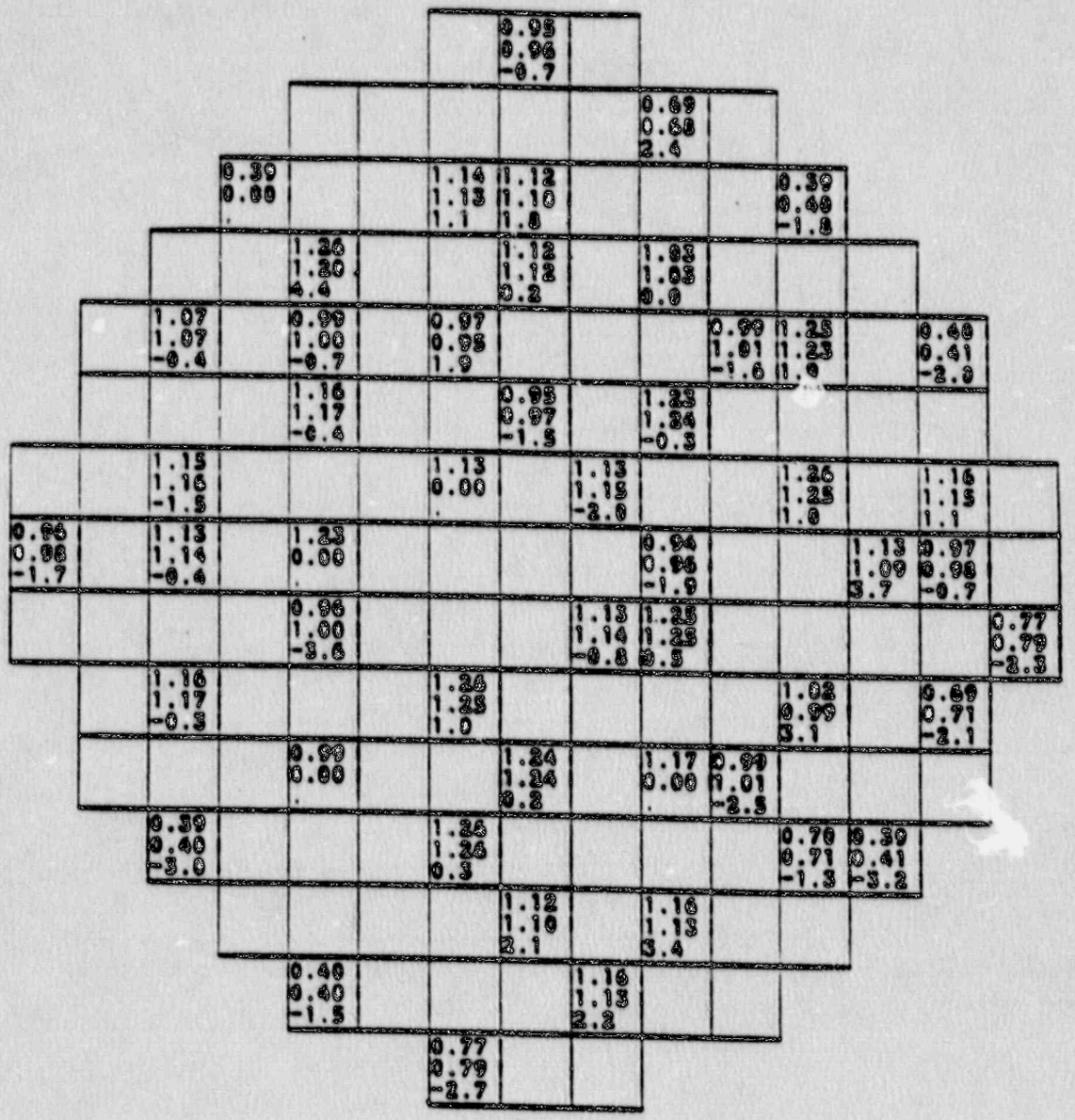

MAX DIFFERENCE = 4.40
MAX DIFF (RPD>0.9) = 4.40
RMS DIFFERENCE = 1.98

X.XX PREDICTED
X.XX MEASURED
X.X PERCENT DIFFERENCE

FIGURE 3-154

S1C7 3D PDQ VS. MEASURED RPD COMPARISON
HFP, D-228, 7630 MWD/MTU S1-7-22A

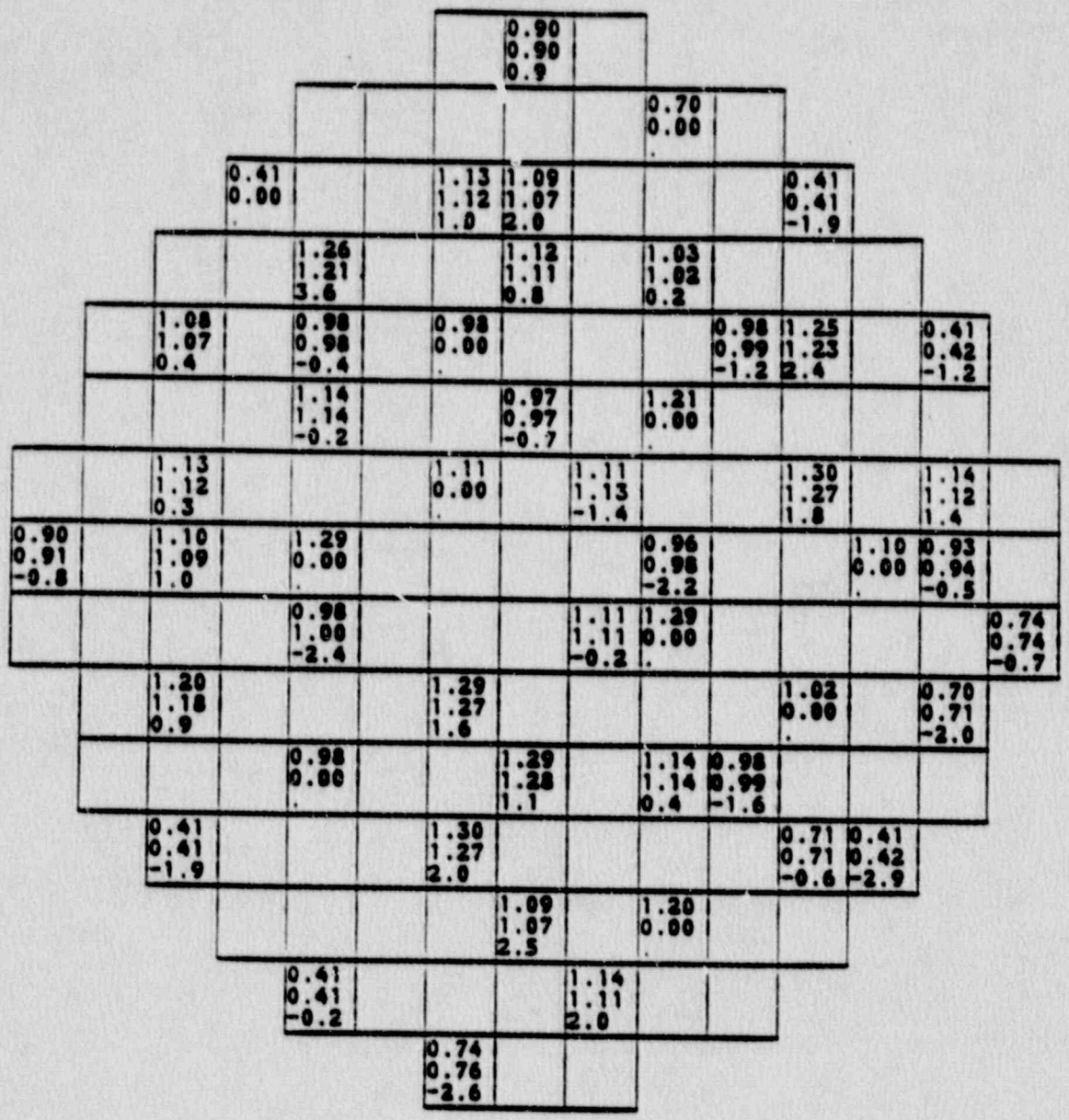

MAX DIFFERENCE = 3.63
MAX DIFF (RPD>0.9) = 3.63
RMS DIFFERENCE = 1.58

X.XX	PREDICTED
X.XX	MEASURED
X.X	PERCENT DIFFERENCE

FIGURE 3-155

S1C8 3D PDQ VS. MEASURED RPD COMPARISON
HZP, D-212, 0 MWD/MTU S1-8-03A

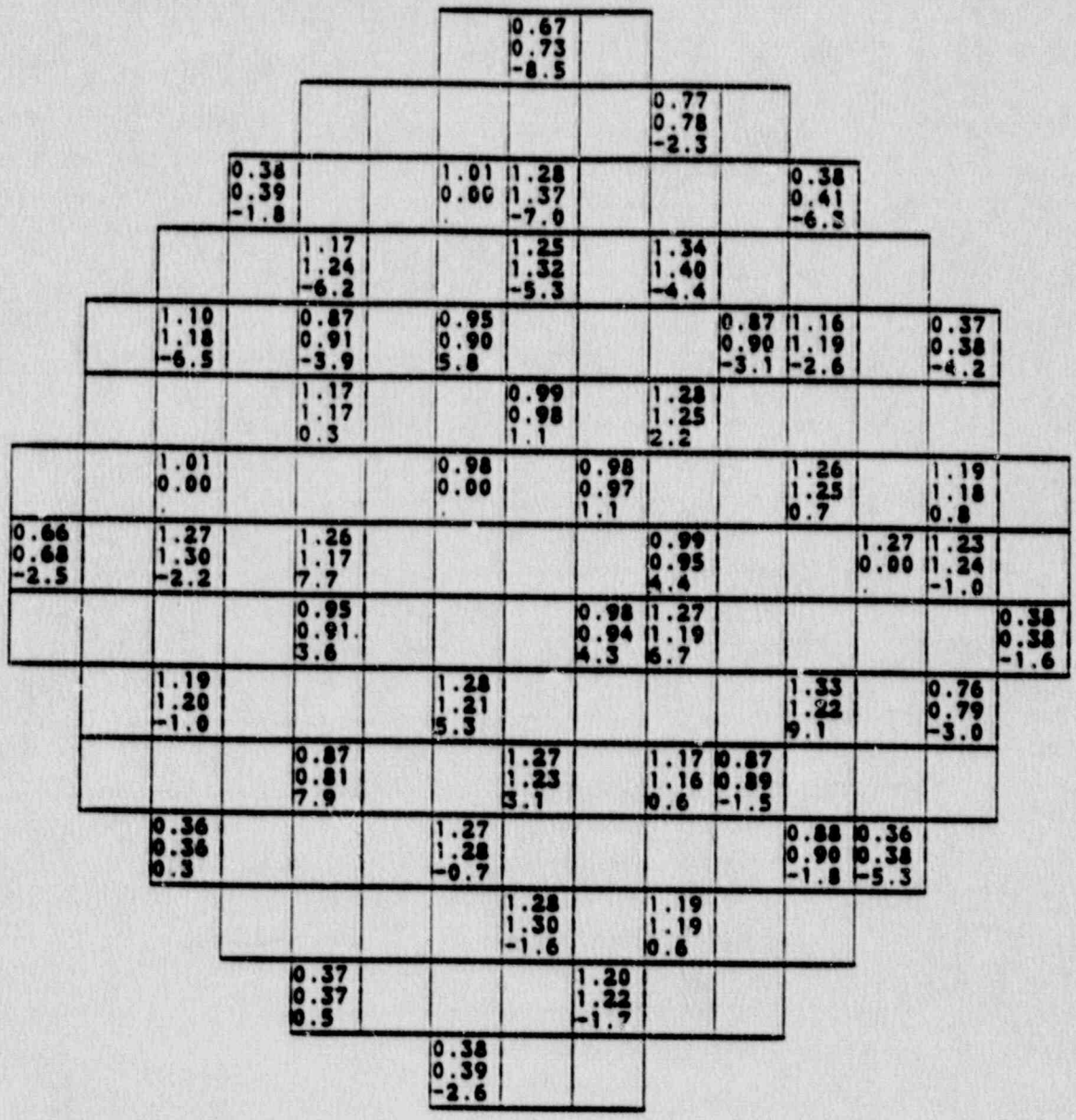

MAX DIFFERENCE = 9.10
MAX DIFF (RPD>0.9) = 9.10
RMS DIFFERENCE = 4.17

X.XX	PREDICTED
X.XX	MEASURED
X.X	PERCENT DIFFERENCE

FIGURE 3-156

S1C8 3D PDQ VS. MEASURED RPD COMPARISON
MFP, D-238, 900 MWD/MTU S1-8-08A

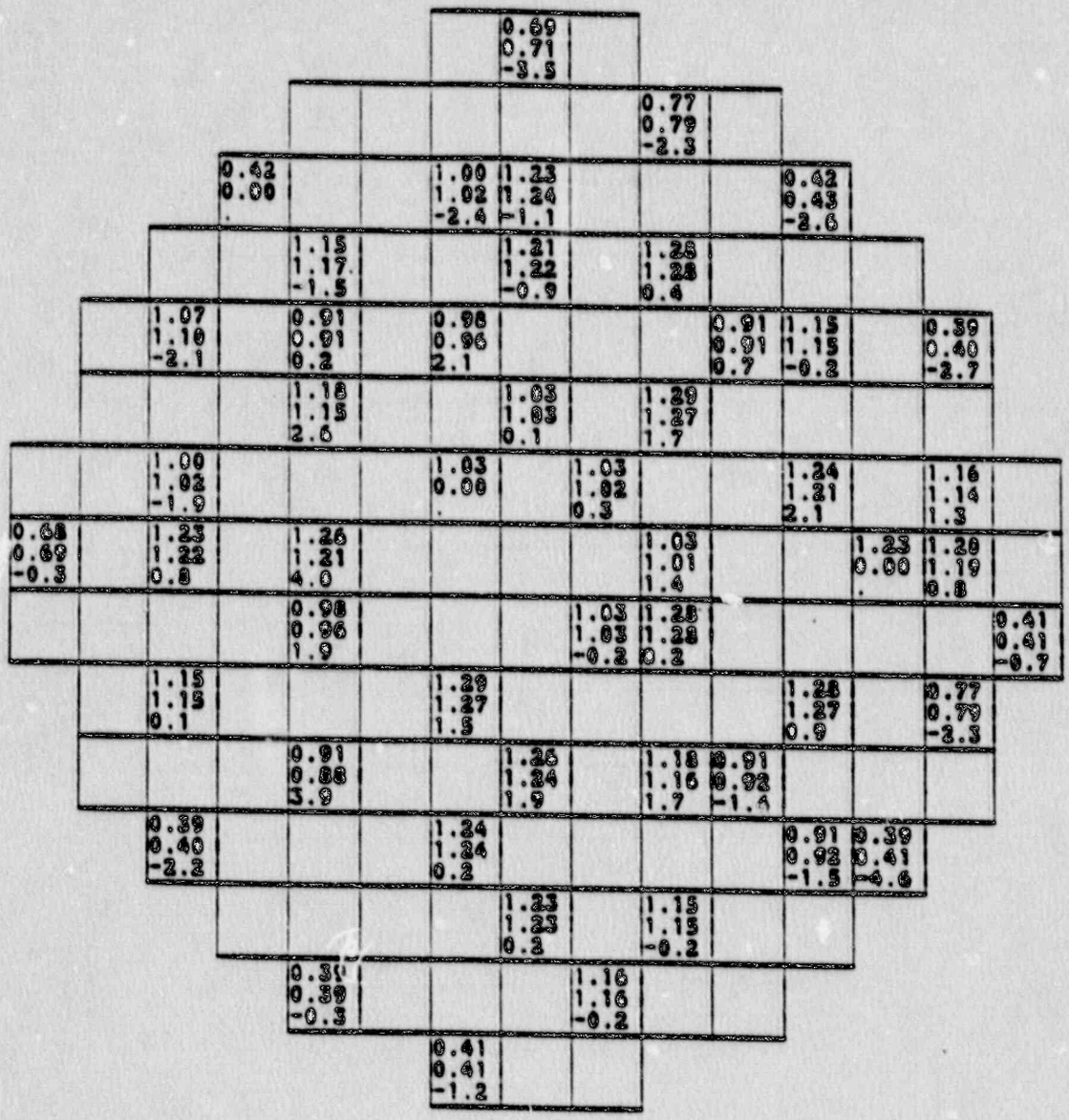

MAX DIFFERENCE = -4.6
MAX DIFF (REF>0.9) = 3.95
RMS DIFFERENCE = 1.82

X.XX PREDICTED
X.XX MEASURED
X.X PERCENT DIFFERENCE

FIGURE 3-157

S1C8 3D PDQ VS. MEASURED RPD COMPARISON
HFP, D-227, 8081 MWD/MTU S1-8-37A

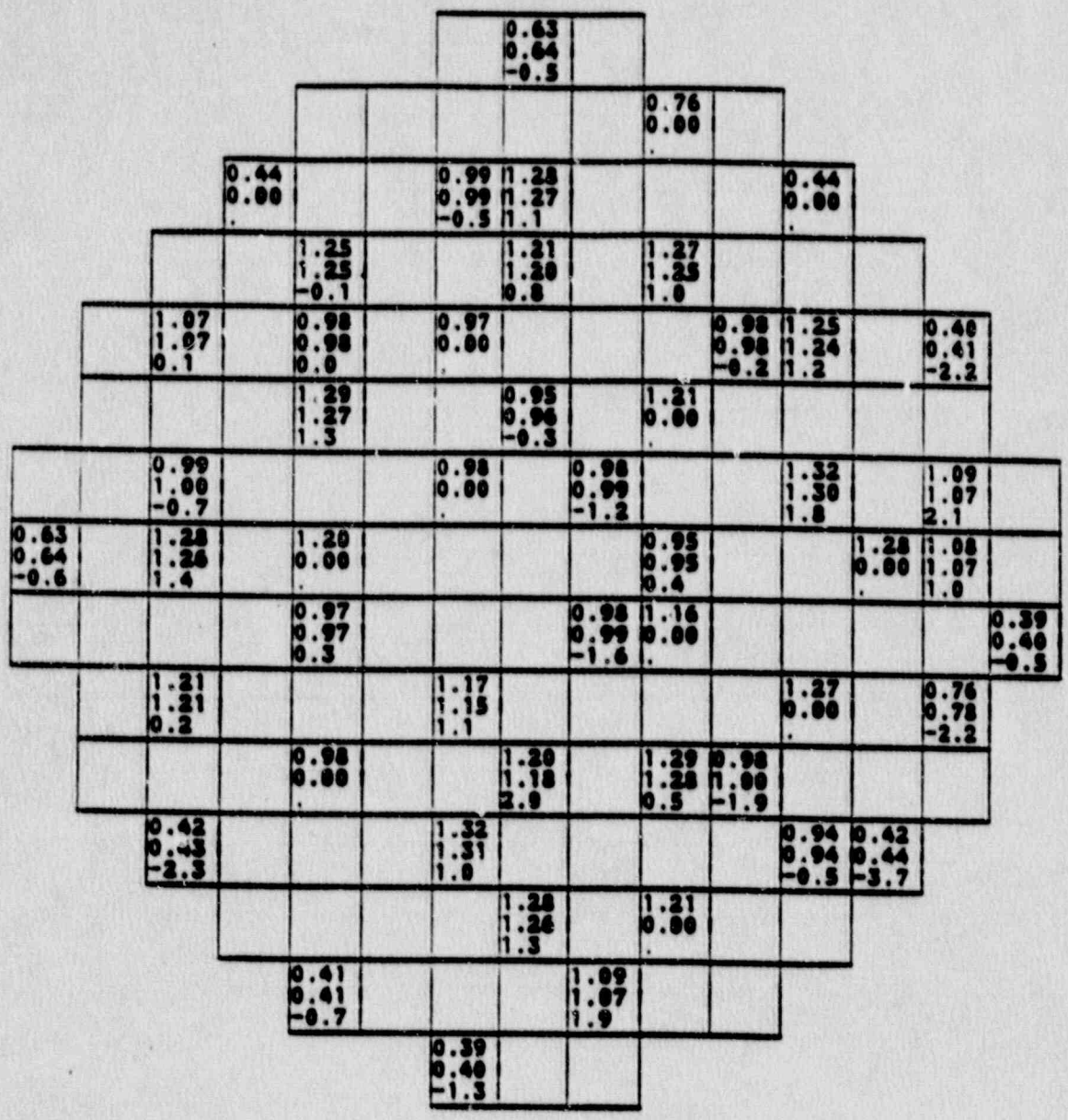

MAX DIFFERENCE = -3.7
MAX DIFF (RPD>0.9) = 2.15
RMS DIFFERENCE = 1.35

X.XX	PREDICTED
X.XX	MEASURED
X.X	PERCENT DIFFERENCE

FIGURE 3-158

S1C8 3D PDQ VS. MEASURED RPD COMPARISON
HFP, D-212, 13212 MWD/MTU S1-8-M50

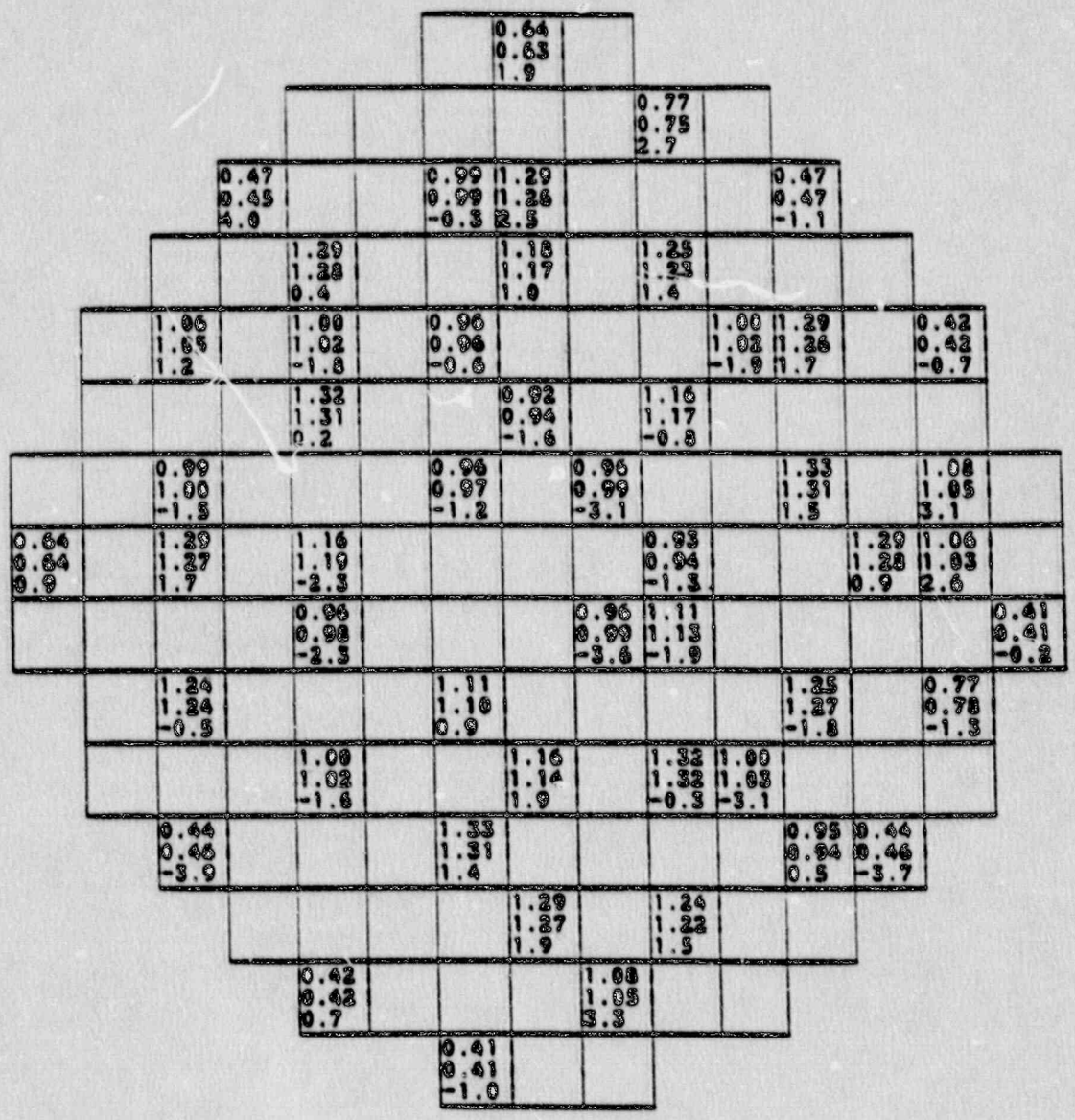

MAX DIFFERENCE = 4.01
MAX DIFF (RPD>0.9) = -3.6
RMS DIFFERENCE = 1.95

X.XX PREDICTED
X.XX MEASURED
X.X PERCENT DIFFERENCE

FIGURE 3-159

S1C9 3D PDQ VS. MEASURED RPD COMPARISON
HFP, D-220, 240 MWD/MTU S1-9-06A

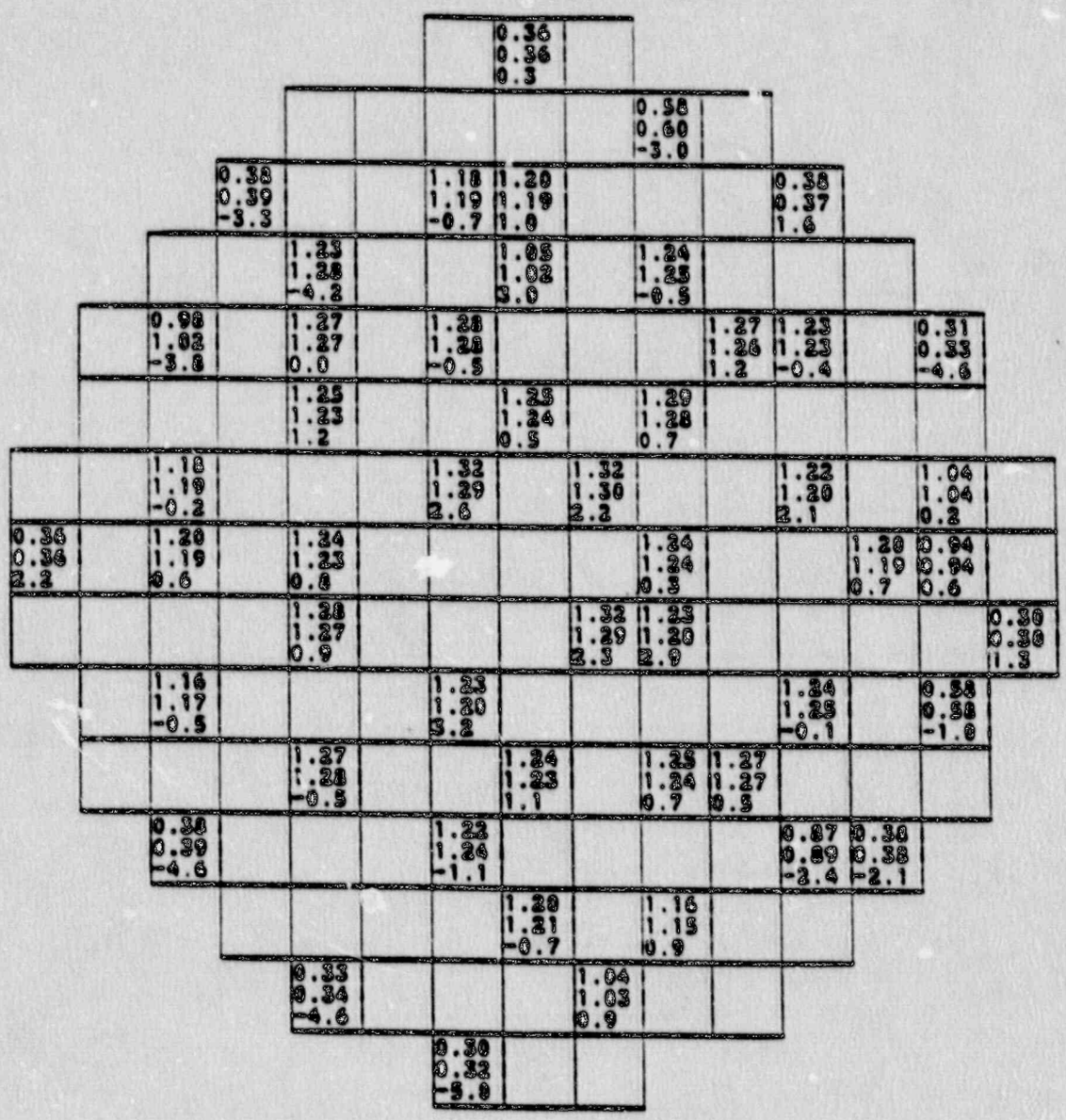

MAX DIFFERENCE = -5
MAX DIFF (RPD>0.9) = -4.2
RMS DIFFERENCE = 2.12

X.XX	PREDICTED
X.XX	MEASURED
X.X	PERCENT DIFFERENCE

FIGURE 3-160

S1C9 3D PDQ VS. MEASURED RPD COMPARISON
HFP, D-222, 7295 MWD/MTU S1-9-28A

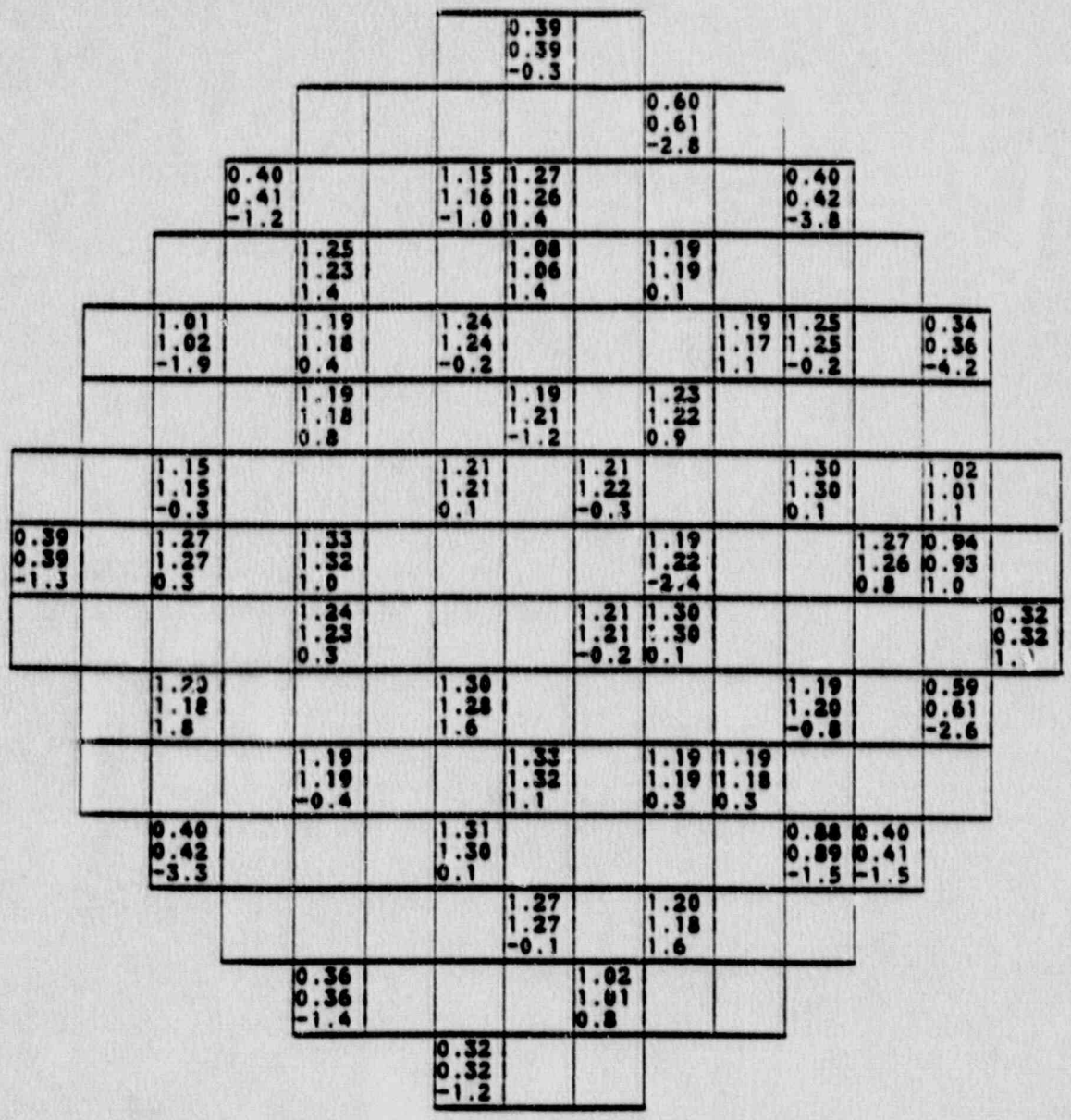

MAX DIFFERENCE = -4.2
MAX DIFF (RPD>0.9) = -2.4
RMS DIFFERENCE = 1.47

X.XX	PREDICTED
X.XX	MEASURED
X.X	PERCENT DIFFERENCE

FIGURE 3-161

S1C9 3D FDQ VS. MEASURED RPD COMPARISON
MFP, D-217, 14606 MWD/MTU S1-9-M40A

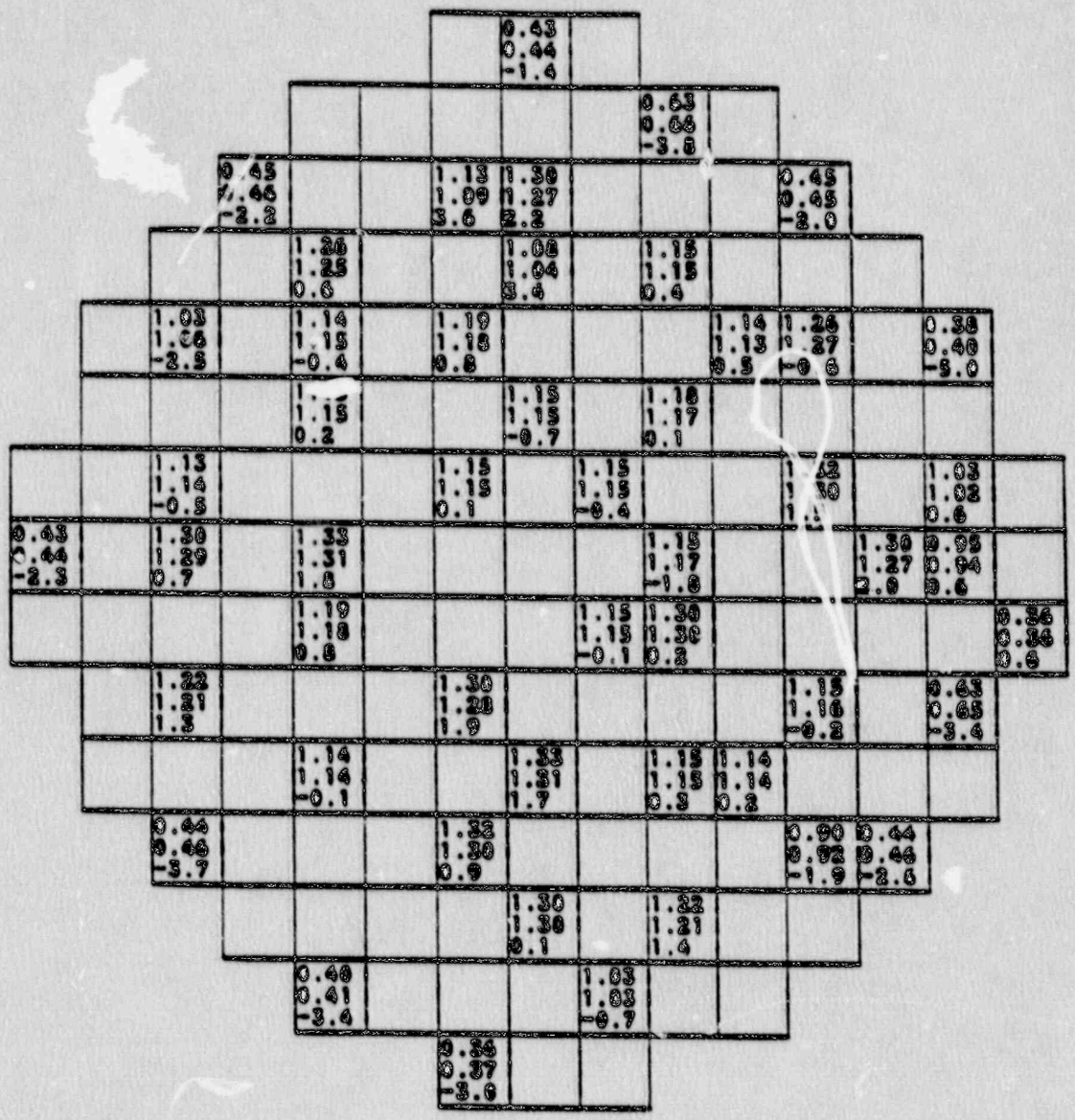

MAX DIFFERENCE = -5
MAX DIFF (REF>0.9) = 3.57
RMS DIFFERENCE = 1.87

X.XX PREDICTED
X.XX MEASURED
X.X PERCENT DIFFERENCE

FIGURE 3-162

S2C1 3D PDQ VS. MEASURED RPD COMPARISON
HZP, D- 300, 0 MWD/MTU S2-1-01A

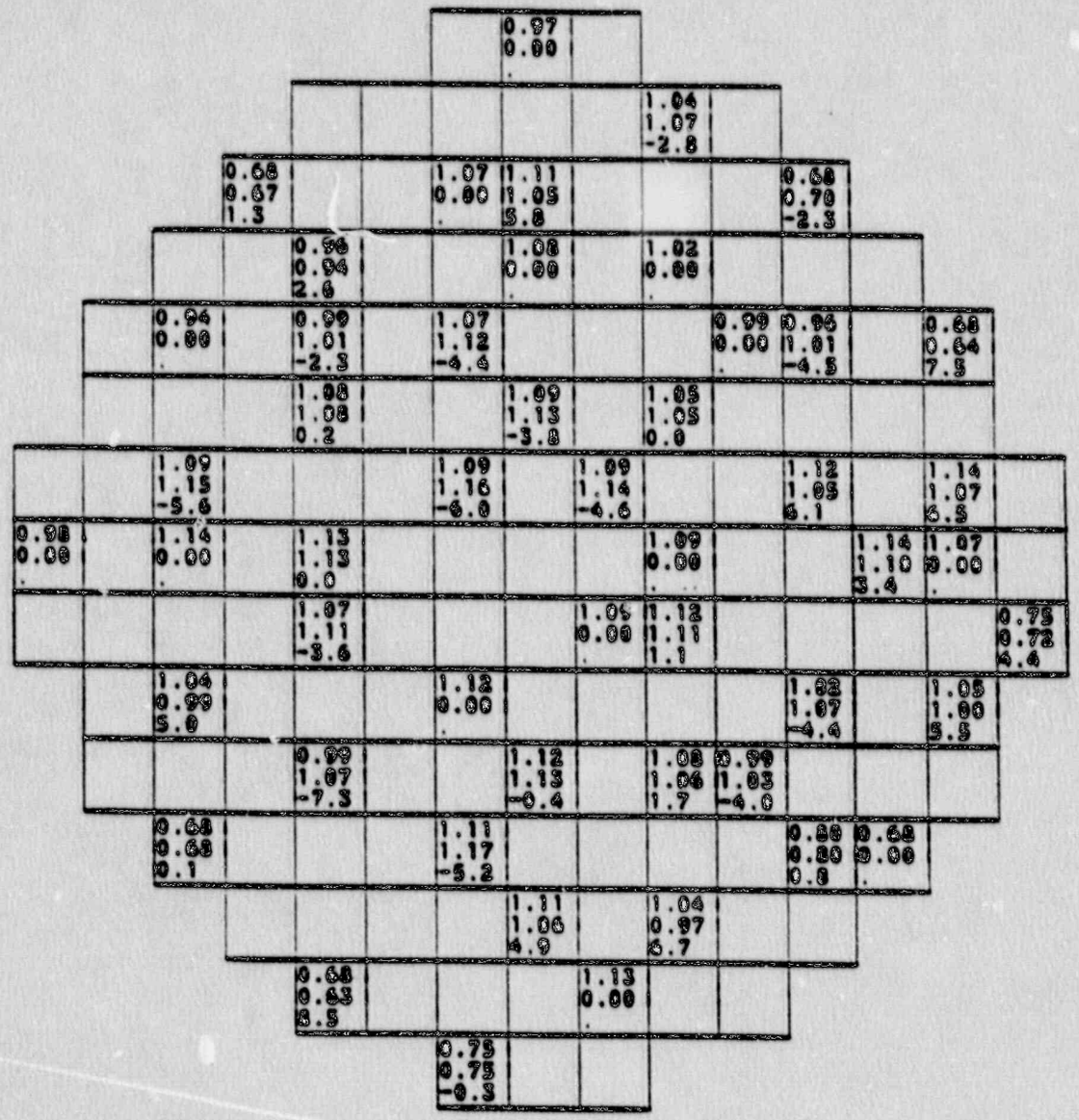

MAX DIFFERENCE = 8.45
MAX DIFF (RPD>0.9) = -7.3
RMS DIFFERENCE = 4.41

X.XX PREDICTED
X.XX MEASURED
X.X PERCENT DIFFERENCE

FIGURE 3-163

S2C1 3D PDQ VS. MEASURED RFO COMPARISON
MFP, D-203, 2030 MWD/MTU S2-1-34

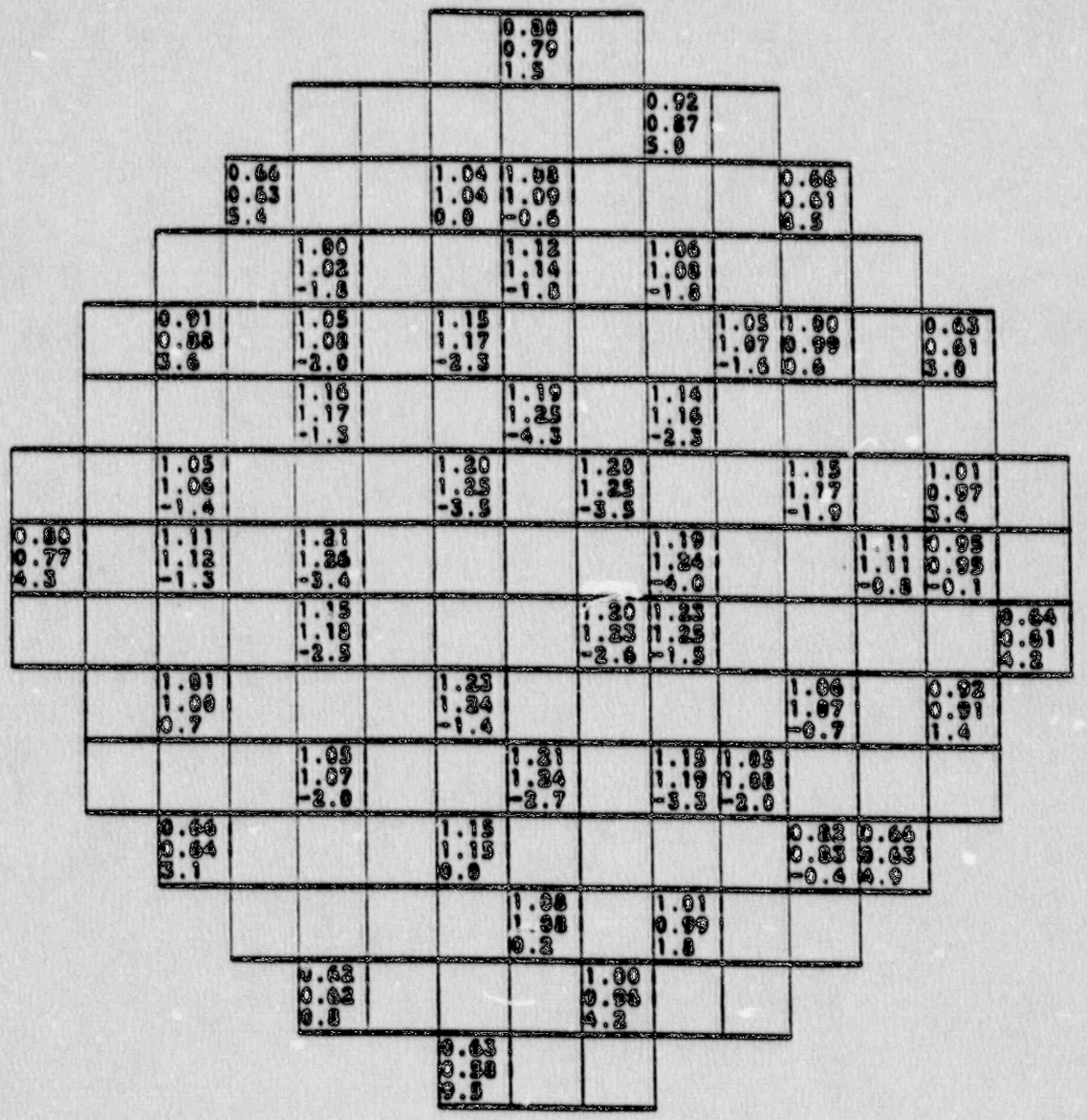

MAX DIFFERENCE : 9.48
MAX DIFF (RFO>0.9) : 5.05
RMS DIFFERENCE : 3.16

X.XX PREDICTED
X.XX MEASURED
X.X PERCENT DIFFERENCE

FIGURE 3-164

S2C1 3D PDQ VS. MEASURED RPD COMPARISON
HFP, D-215, 7310 MWD/MTU S2-1-49

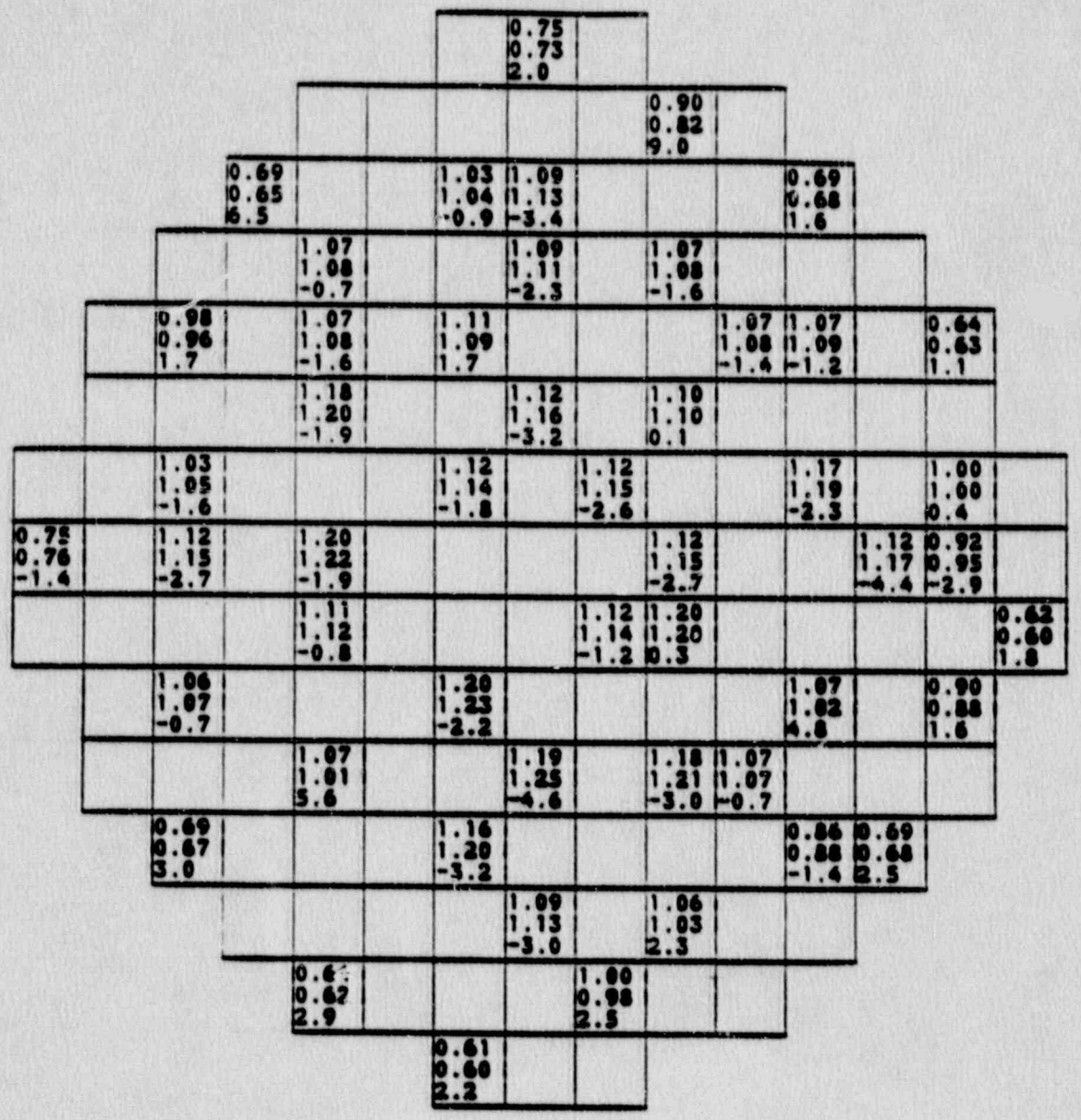

MAX DIFFERENCE = 8.99
MAX DIFF (RPD>0.9) = 5.65
RMS DIFFERENCE = 2.84

X.XX PREDICTED
X.XX MEASURED
X.X PERCENT DIFFERENCE

FIGURE 3-165

S2C2 3D PDQ VS. MEASURED RPD COMPARISON
HZP, D-199, 0 MWD/MTU S2-2-01A

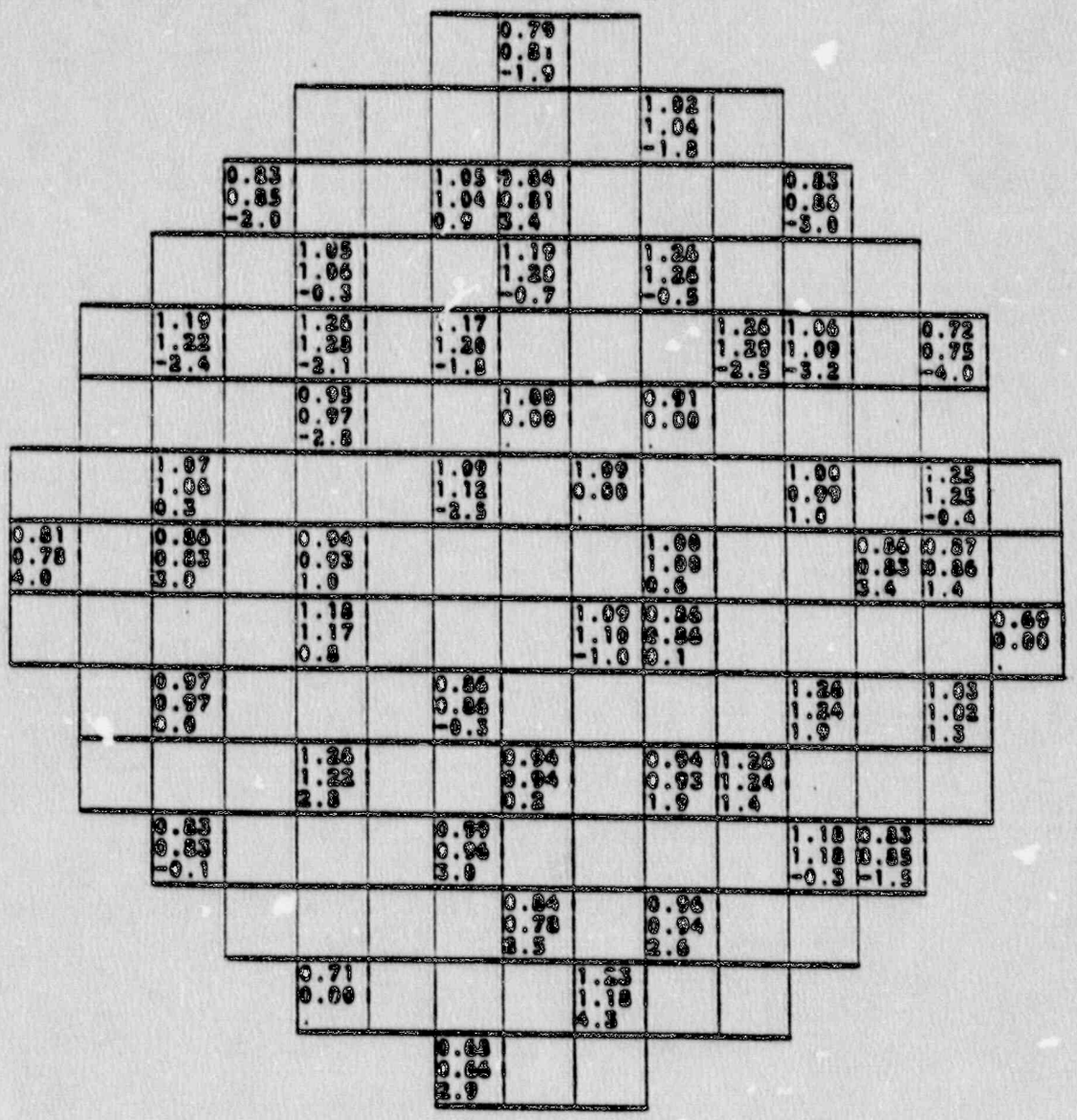

MAX DIFFERENCE = 0.49
MAX DIFF (RPD>0.9) = 4.33
RMS DIFFERENCE = 2.44

X.XX WEIGHTED
X.XX MEASURED
X.X PERCENT DIFFERENCE

FIGURE 3-166

S2C2 3D PD0 VS. MEASURED RPD COMPARISON
HFP, D-210, 730 MWD/MTU S2-2-07A

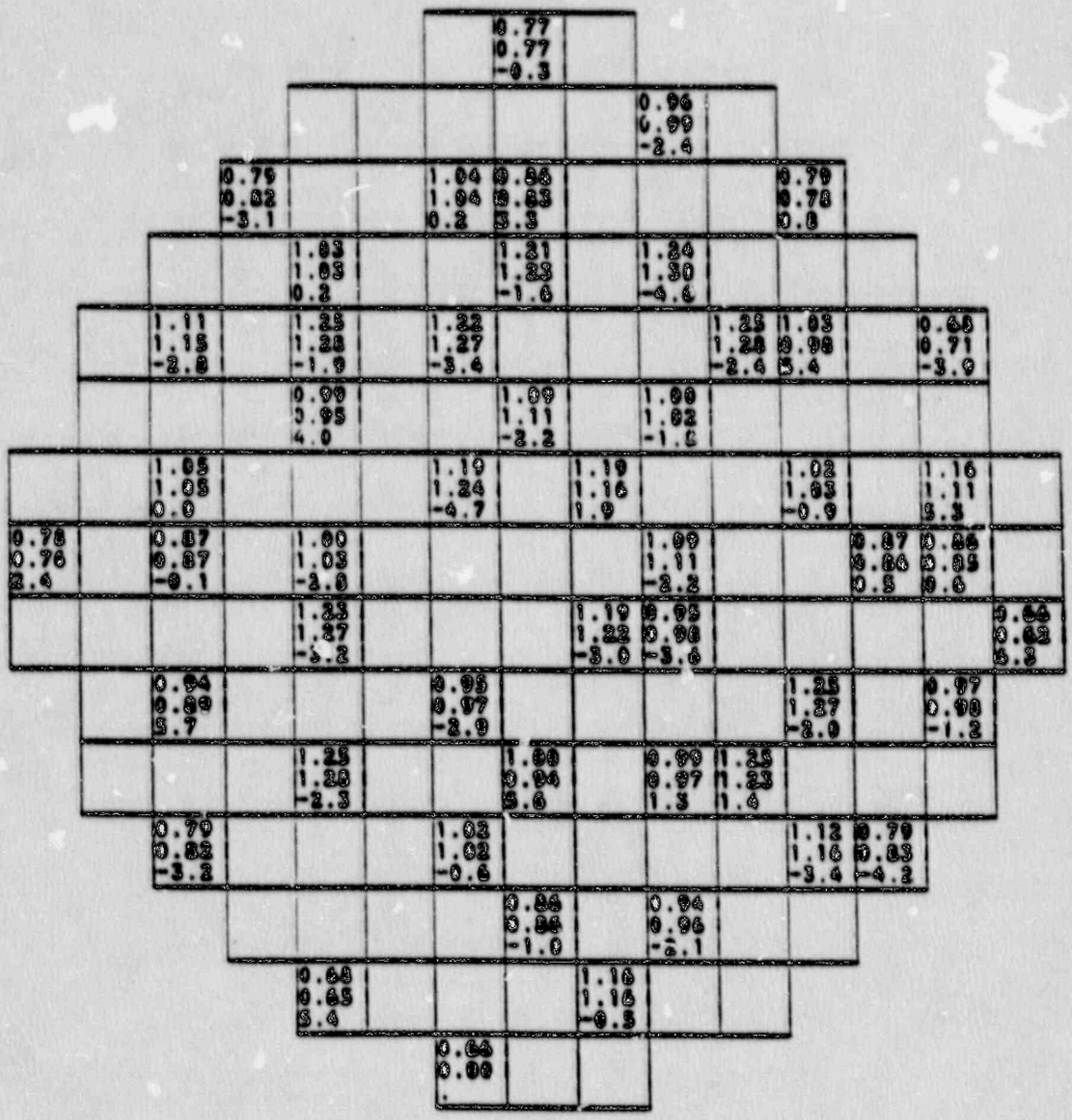

MAX DIFFERENCE = 6.26
MAX DIFF (EXP>0.9) = 5.70
RMS DIFFERENCE = 3.05

X.XX PREDICTED
X.XX MEASURED
X.X PERCENT DIFFERENCE

FIGURE 3-167

S2C2 3D PDQ VS. MEASURED RPD COMPARISON
KFP, D-216, 3750 MWD/MTU S2-2-15A

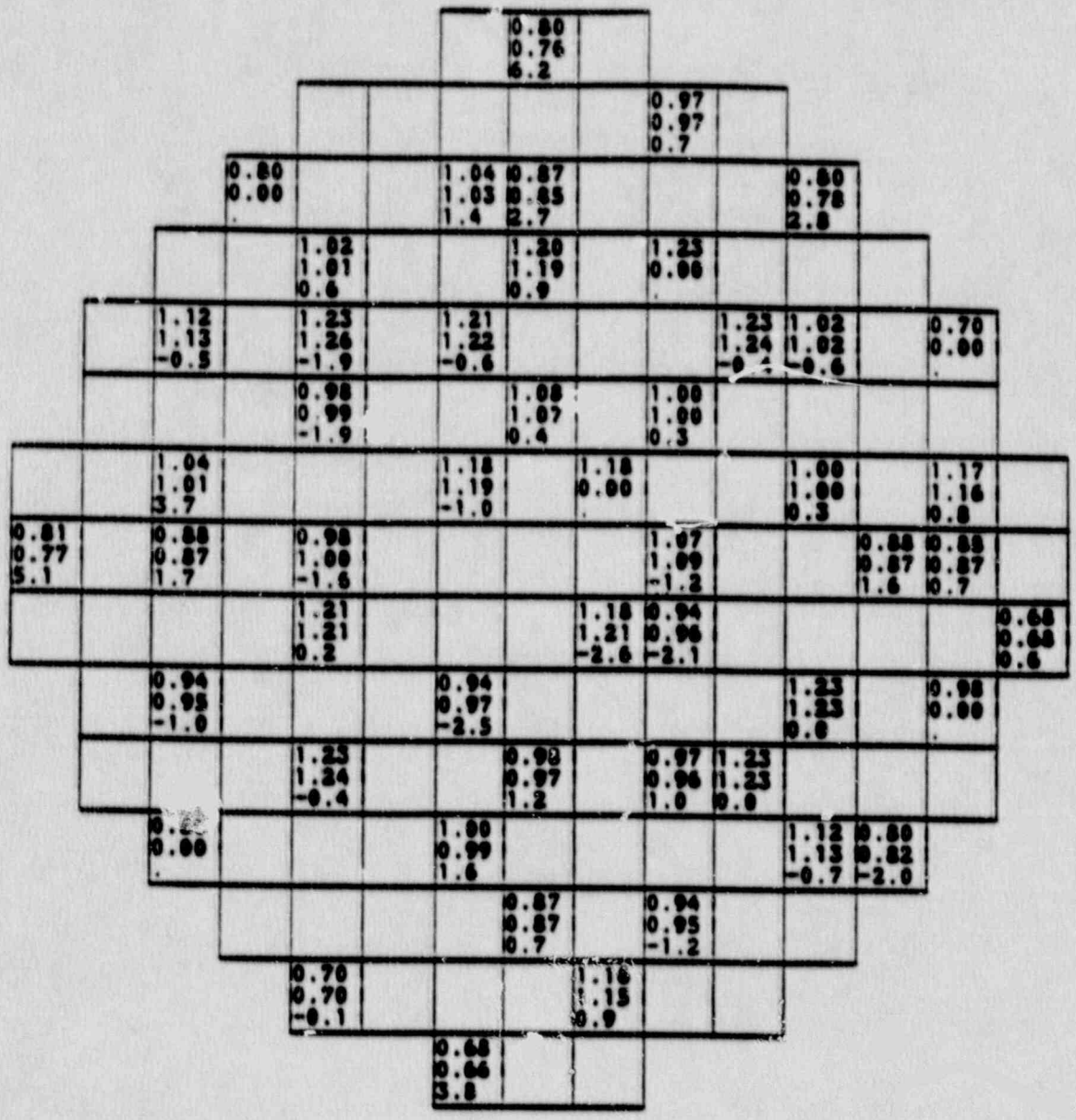

MAX DIFFERENCE = 6.20
MAX DIFF (RFP>0.9) = 3.68
RMS DIFFERENCE = 1.92

X.XX PREDICTED
X.XX MEASURED
X.X PERCENT DIFFERENCE

FIGURE 3-168

S2C3 3D PDQ VS. MEASURED RPD COMPARISON
HFP, D-221, 3127 MWD/MTU S2-3-13B

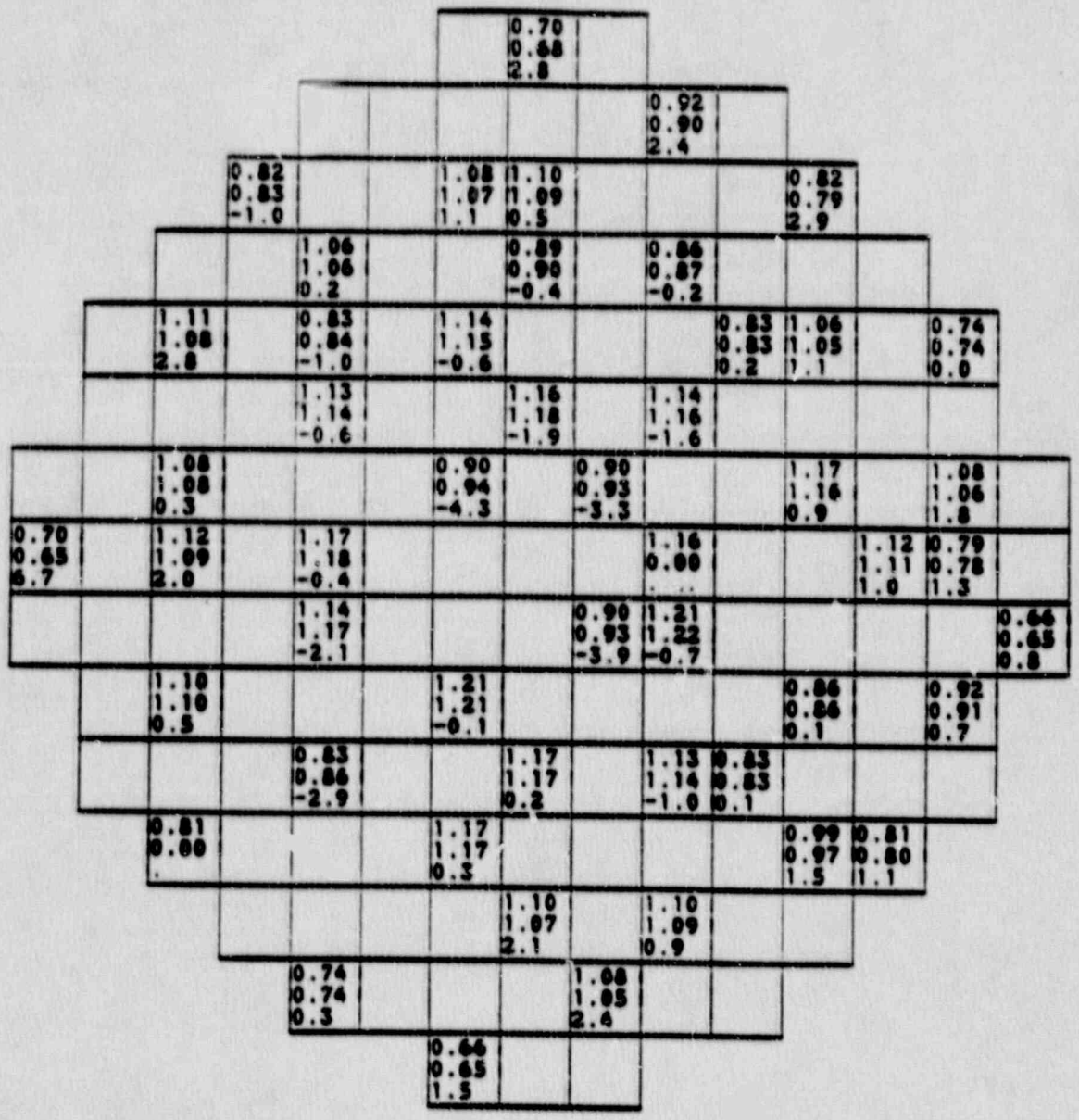

MAX DIFFERENCE = 6.73
MAX DIFF (RPD>0.9) = 2.77
RMS DIFFERENCE = 1.91

X.XX	PREDICTED
X.XX	MEASURED
X.X	PERCENT DIFFERENCE

FIGURE 3-169

S2C3 3D FDQ VS. MEASURED RFD COMPARISON
MFP, D-224, 8688 MWD/MTU S2-3-268

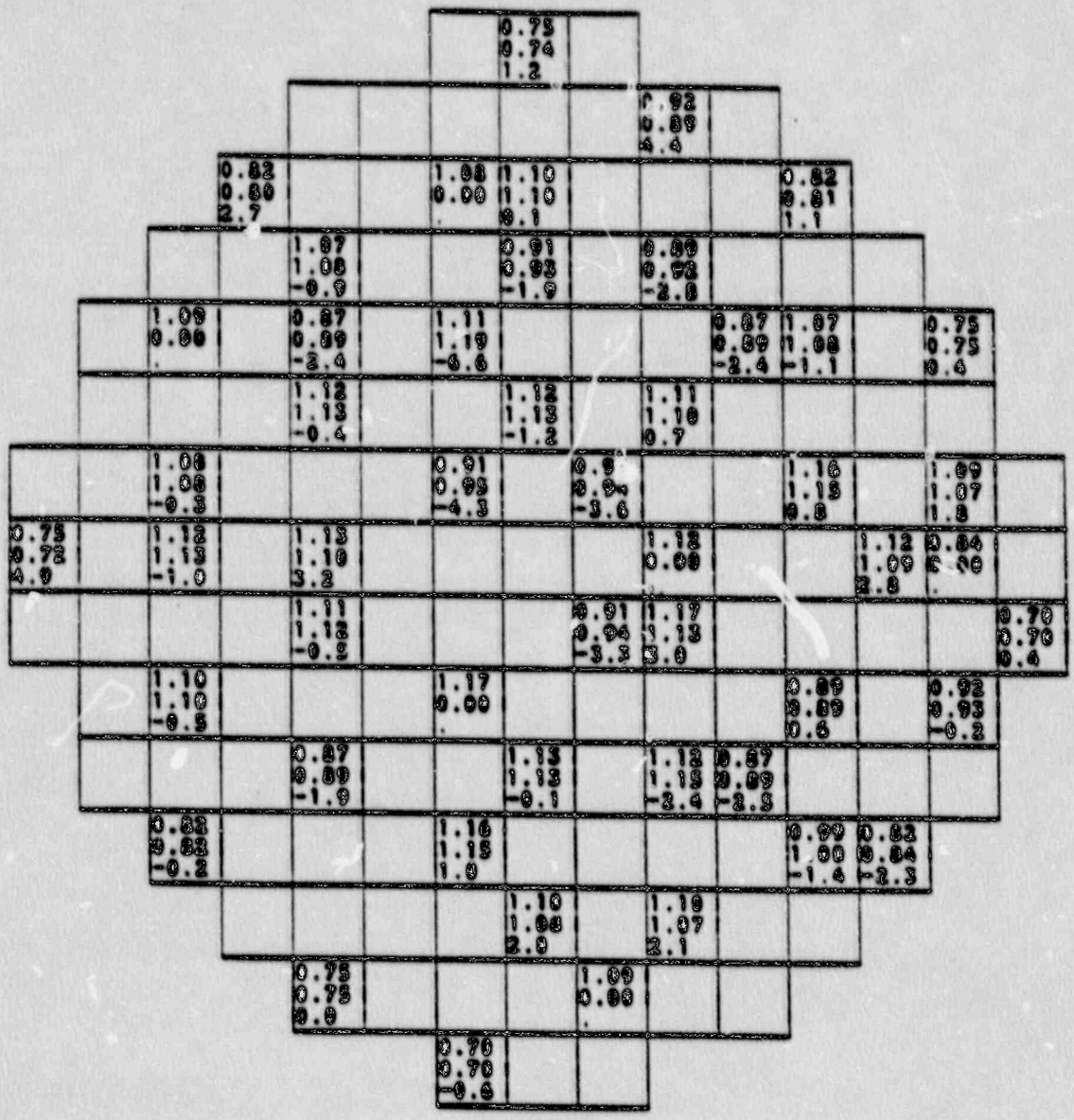

MAX DIFFERENCE = -6.6
MAX DIFF (RFD>0.9) = -6.6
RMS DIFFERENCE = 2.29

X.XX PREDICTED
X.XX MEASURED
X.X PERCENT DIFFERENCE

FIGURE 3-170

S2C4 3D PDQ VS. MEASURED RPD COMPARISON
HZP, D-228, 0 MWD/MTU S2-4-01A

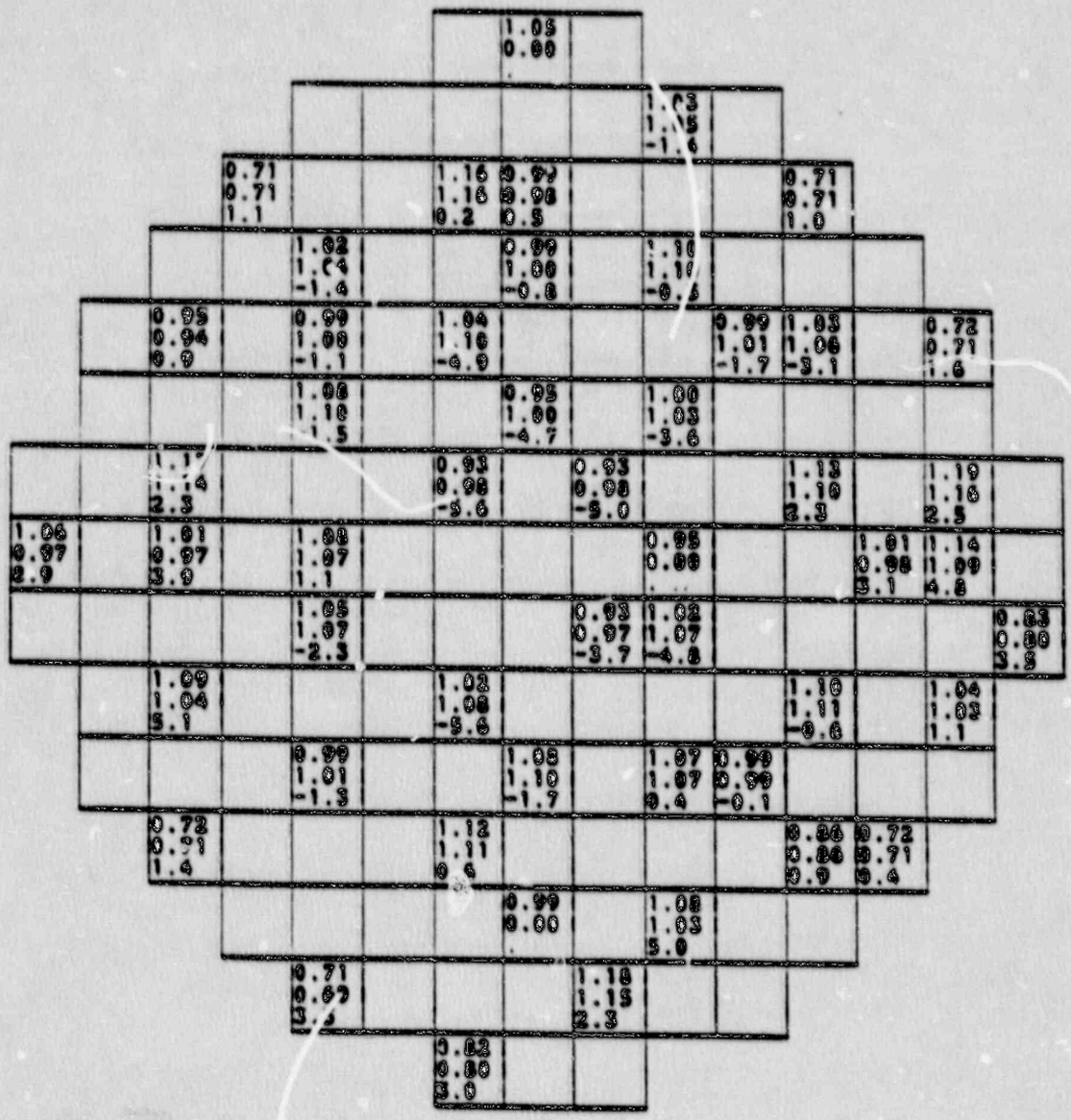

MAX DIFFERENCE = 8.93
MAX DIFF (RPD>0.9) = 8.93
MAX DIFFERENCE = 3.13

X.XX PREDICTED
X.XX MEASURED
X.X PERCENT DIFFERENCE

FIGURE 3-171

S2C4 3D PDQ VS. MEASURED RPD COMPARISON
KFP, D-223, 1186 MWD/MTU S2-4-10A

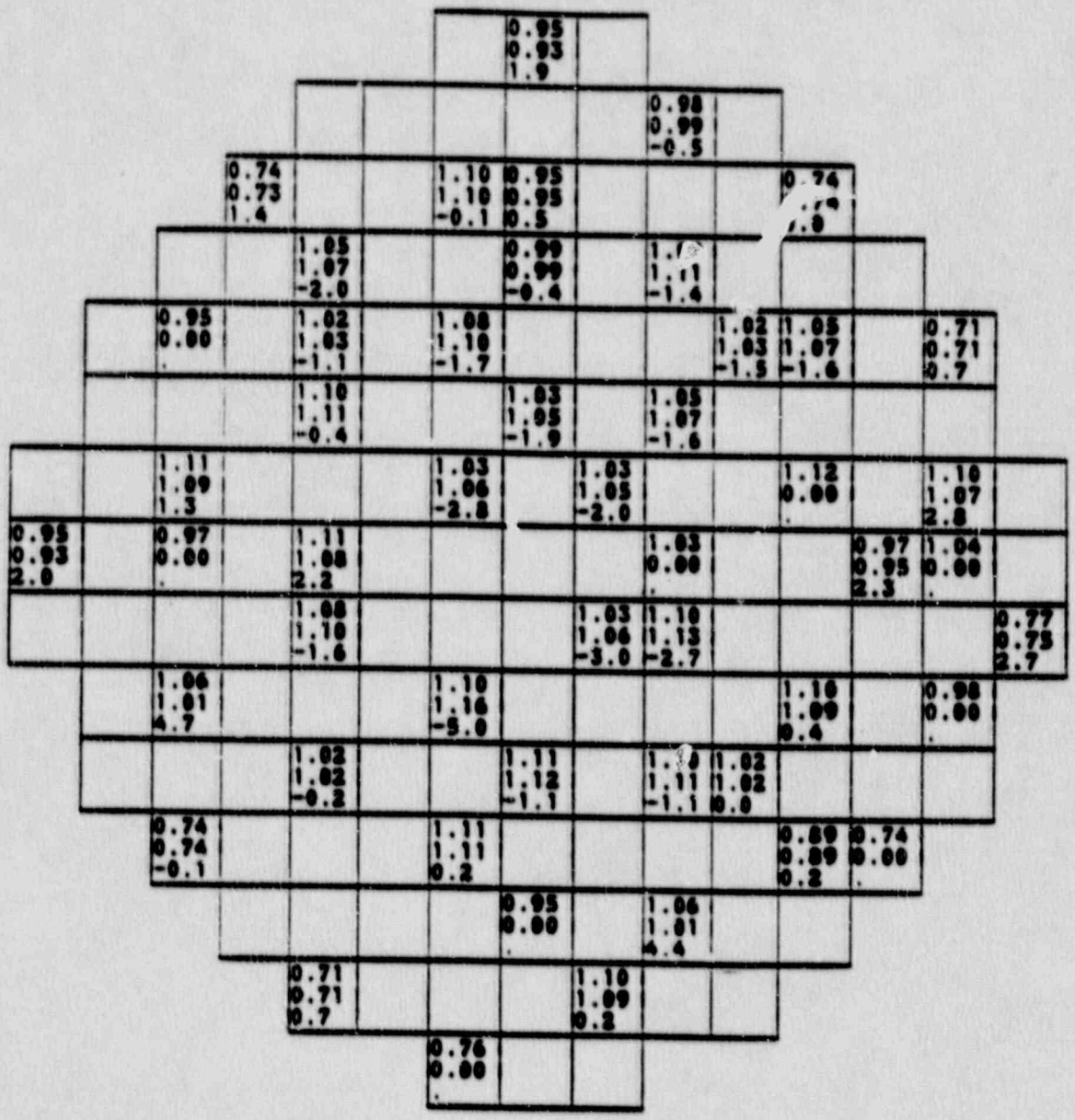

MAX DIFFERENCE = -5
MAX DIFF (REF>0.9) = -5
RMS DIFFERENCE = 1.97

X.XX PREDICTED
X.XX MEASURED
X.X PERCENT DIFFERENCE

FIGURE 3-172

S2C4 3D PDG VS. MEASURED RPD COMPARISON
HFP, D-201, 8250 MWD/MTU S2-4-23A

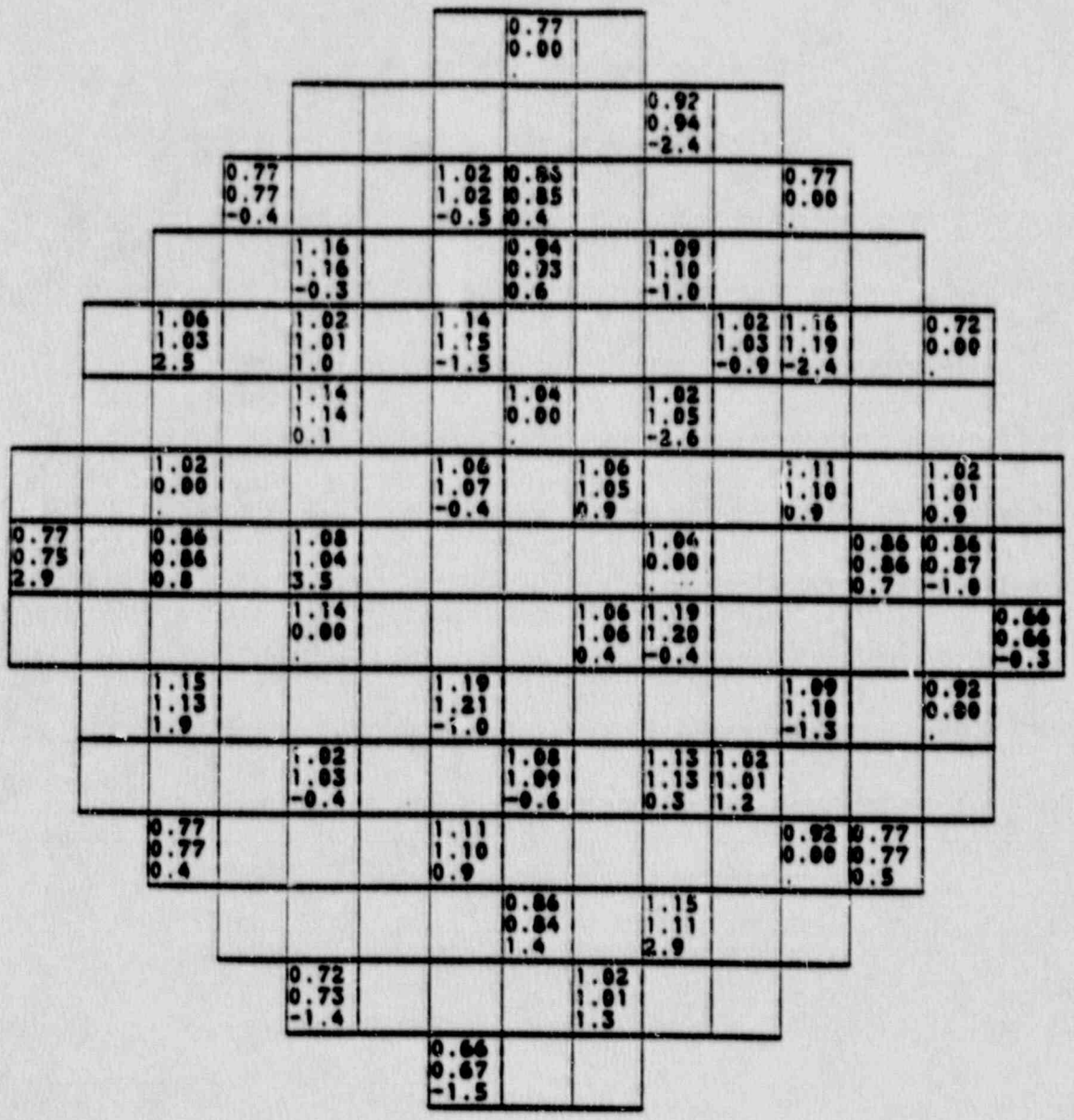

MAX DIFFERENCE = 3.55
MAX DIFF (RPD>0.9) = 3.55
RMS DIFFERENCE = 1.41

X.XX PREDICTED
X.XX MEASURED
X.X PERCENT DIFFERENCE

FIGURE 3-173

S2C5 3D PDQ VS. MEASURED RPD COMPARISON
HZP, D-216, 0 MWD/MTU S2-5-01A

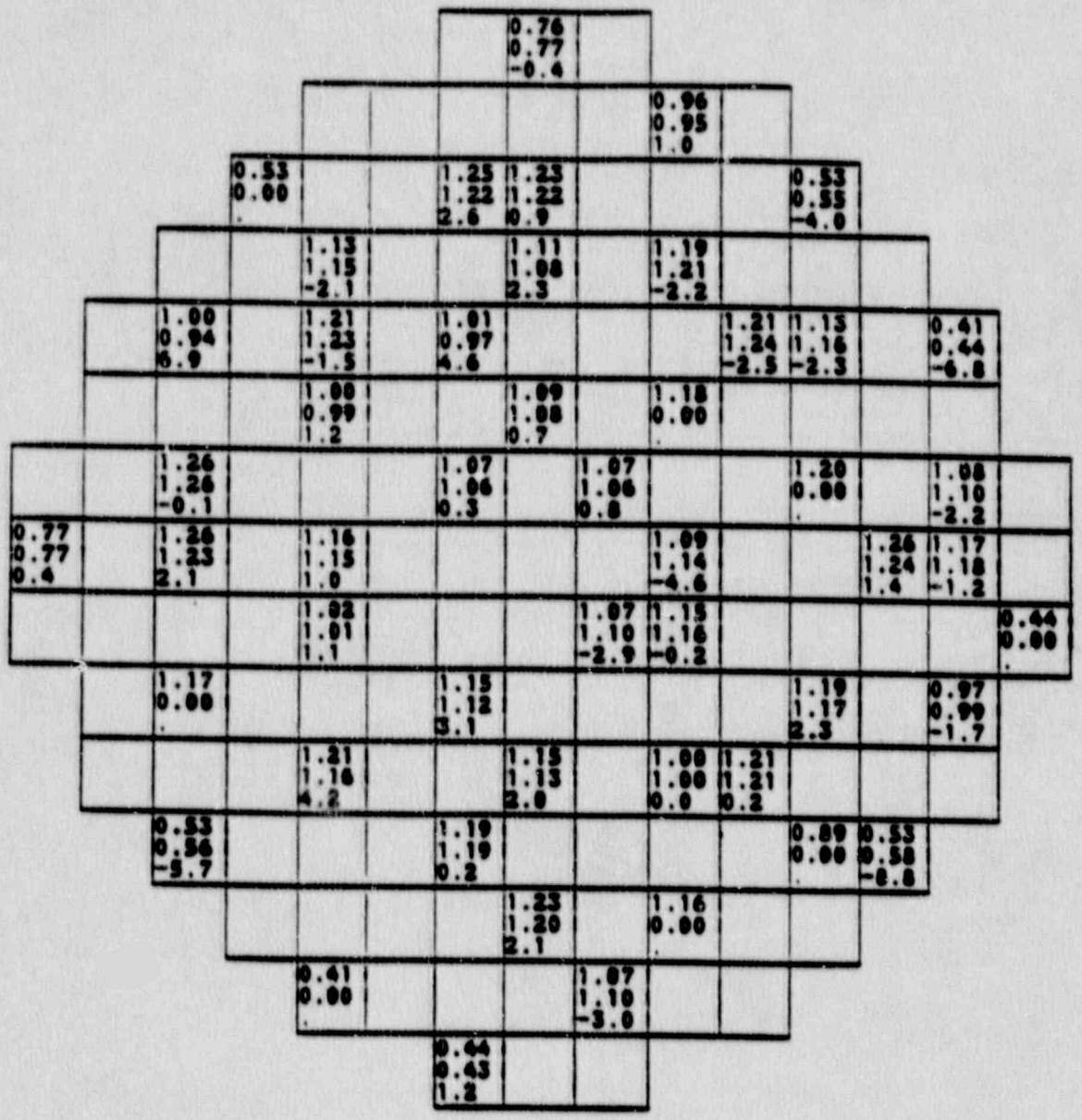

MAX DIFFERENCE : -8.8
MAX DIFF (RPD>0.9) : 6.94
RMS DIFFERENCE : 3.01

X.XX
X.XX
X.X

PREDICTED
MEASURED
PERCENT DIFFERENCE

FIGURE 3-174

S2C5 3D PDQ VS. MEASURED RPD COMPARISON
HFP, D-217, 1690 MWD/MTU S2-5-17A

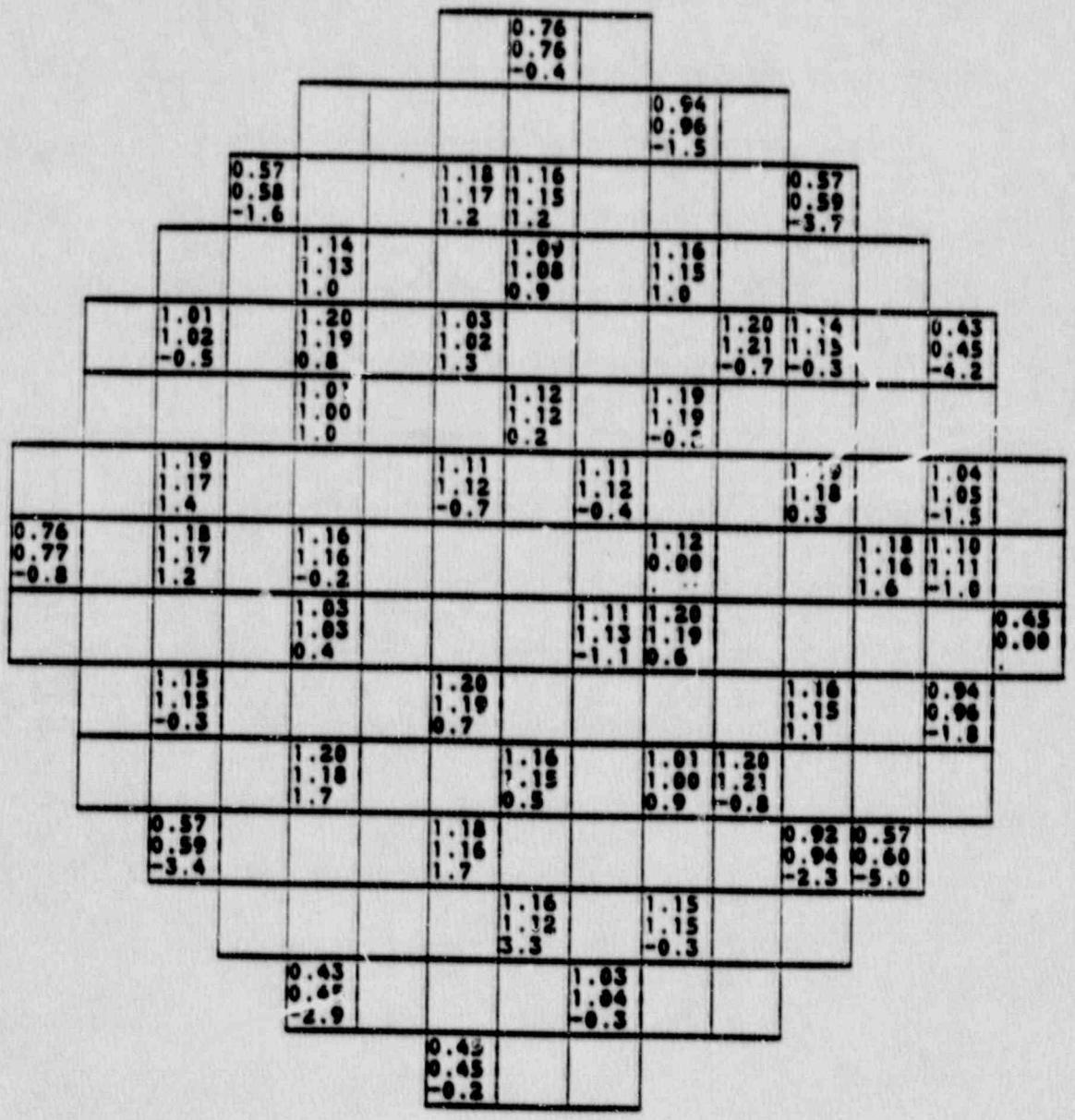

MAX DIFFERENCE = -5
MAX DIFF (RPD>0.9) = 3.29
RMS DIFFERENCE = 1.66

X.XX PREDICTED
X.XX MEASURED
X.X PERCENT DIFFERENCE

FIGURE 3-175

S2L5 3D PDQ VS. MEASURED RPD COMPARISON
H.P. D-220, 11320 MWD/MTU S2-5-35A

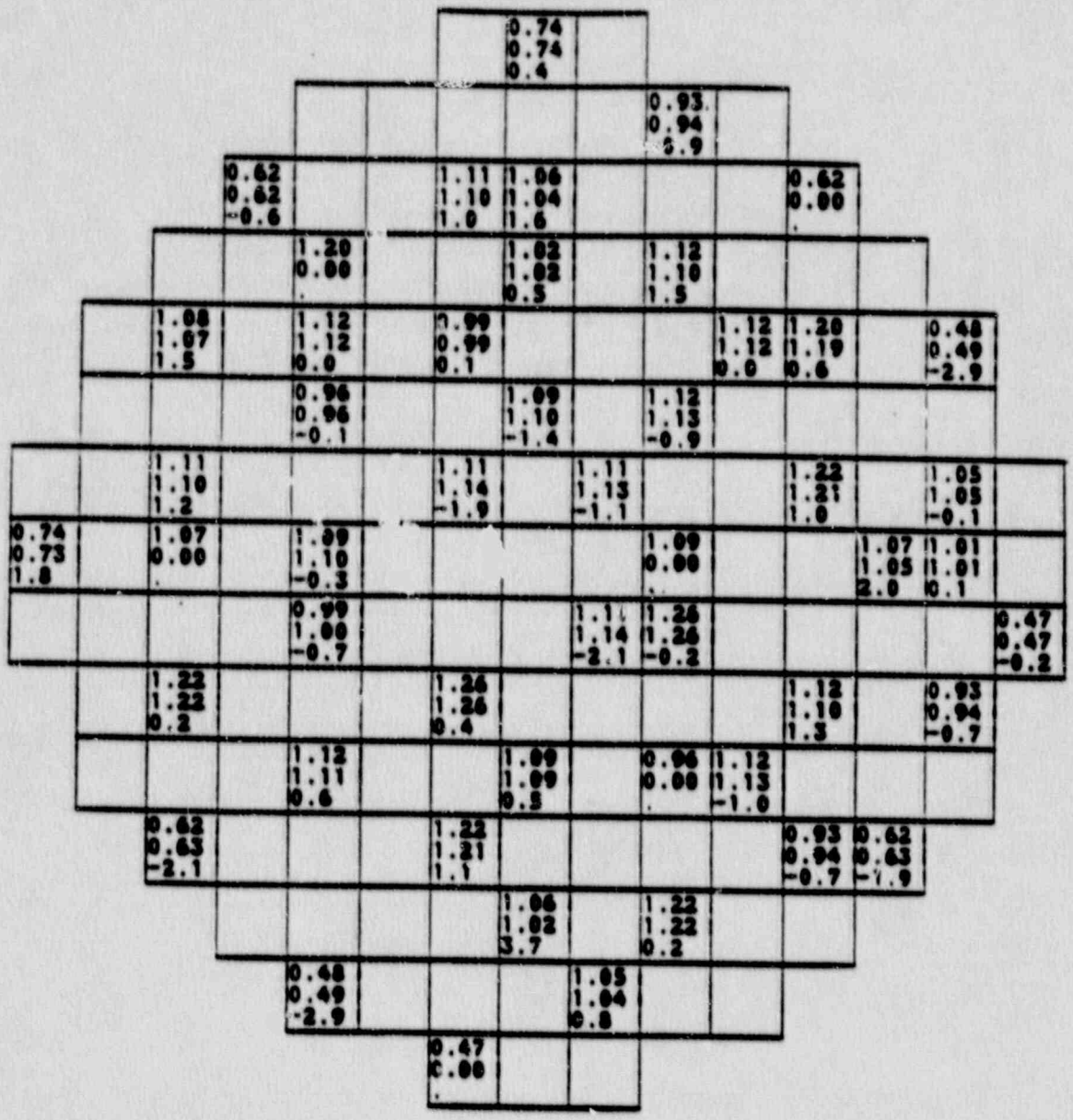

MAX DIFFERENCE = 3.73
MAX DIFF (RPD>0.9) = 3.73
RMS DIFFERENCE = 1.32

X.XX PREDICTED
X.XX MEASURED
X.X PERCENT DIFFERENCE

FIGURE 3-176

S2C6 3D PDQ VS. MEASURED RPD COMPARISON
HZP, D-223, 0 MWD/MTU S2-6-01A

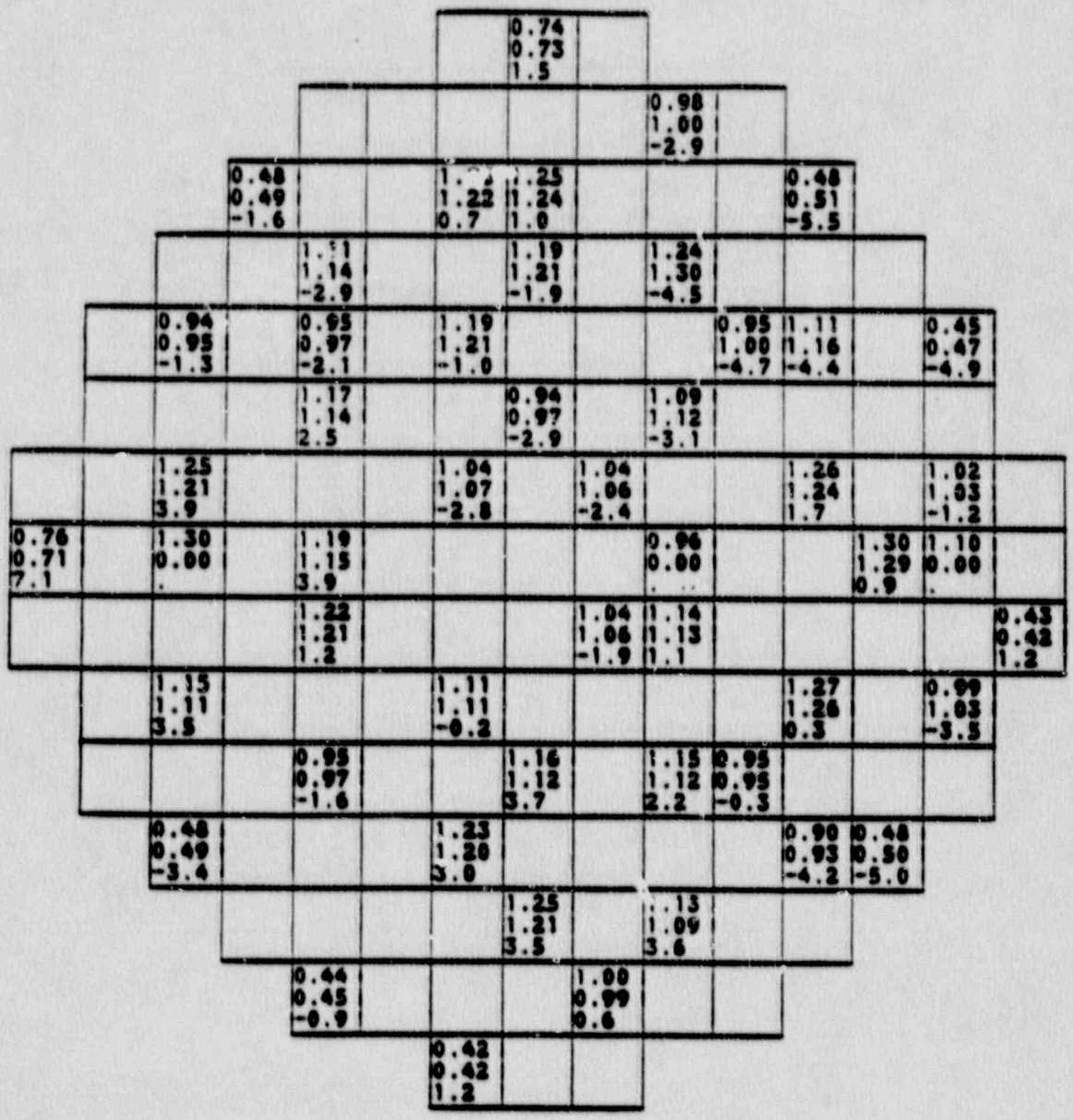

MAX DIFFERENCE = 7.08
MAX DIFF (RPD>0.9) = -4.7
RMS DIFFERENCE = 2.98

X.XX PREDICTED
X.XX MEASURED
X.X PERCENT DIFFERENCE

FIGURE 3-177

S2C6 3D PDQ VS. MEASURED RPD COMPARISON
HFP, D-228, 1116 MWD/MTU S2-6-07A

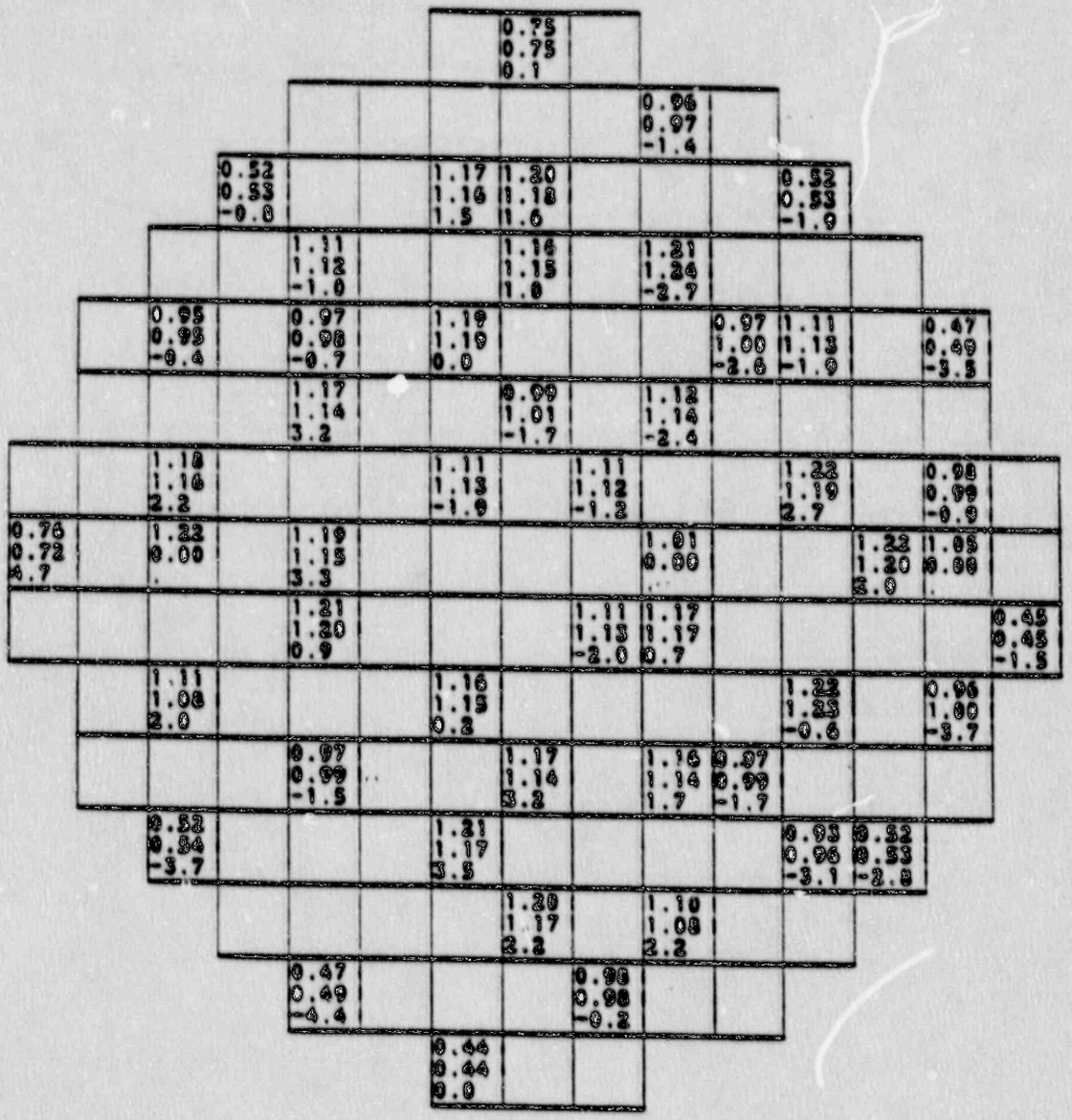

MAX DIFFERENCE = 4.71
MAX DIFF (RPD>0.9) = -3.7
RMS DIFFERENCE = 2.24

X.XX PREDICTED
X.XX MEASURED
X.X PERCENT DIFFERENCE

FIGURE 3-178

S2C6 3D PDQ VS. MEASURED RPD COMPARISON
HFP, D-228, 7390 MWD/MTU S2-6-18A

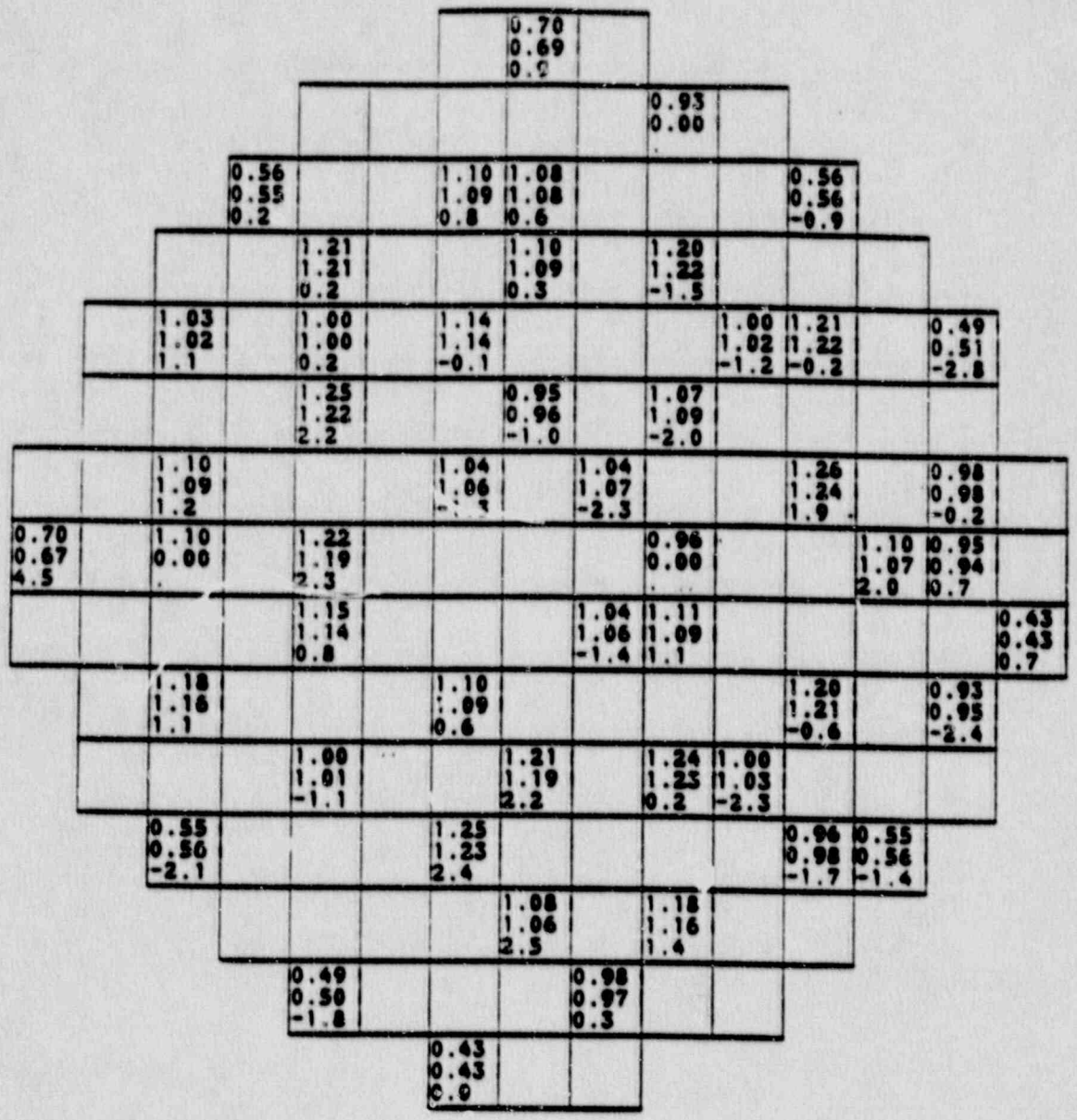

MAX DIFFERENCE = 4.48
MAX DIFF (RPD>0.9) = 2.46
RMS DIFFERENCE = 1.58

X.XX	PREDICTED
X.XX	MEASURED
X.X	PERCENT DIFFERENCE

FIGURE 3-179

S2C6 3D FDQ VS. MEASURED RPD COMPARISON
HFP, D-237, 13900 MWD/MTU S2-6-29A

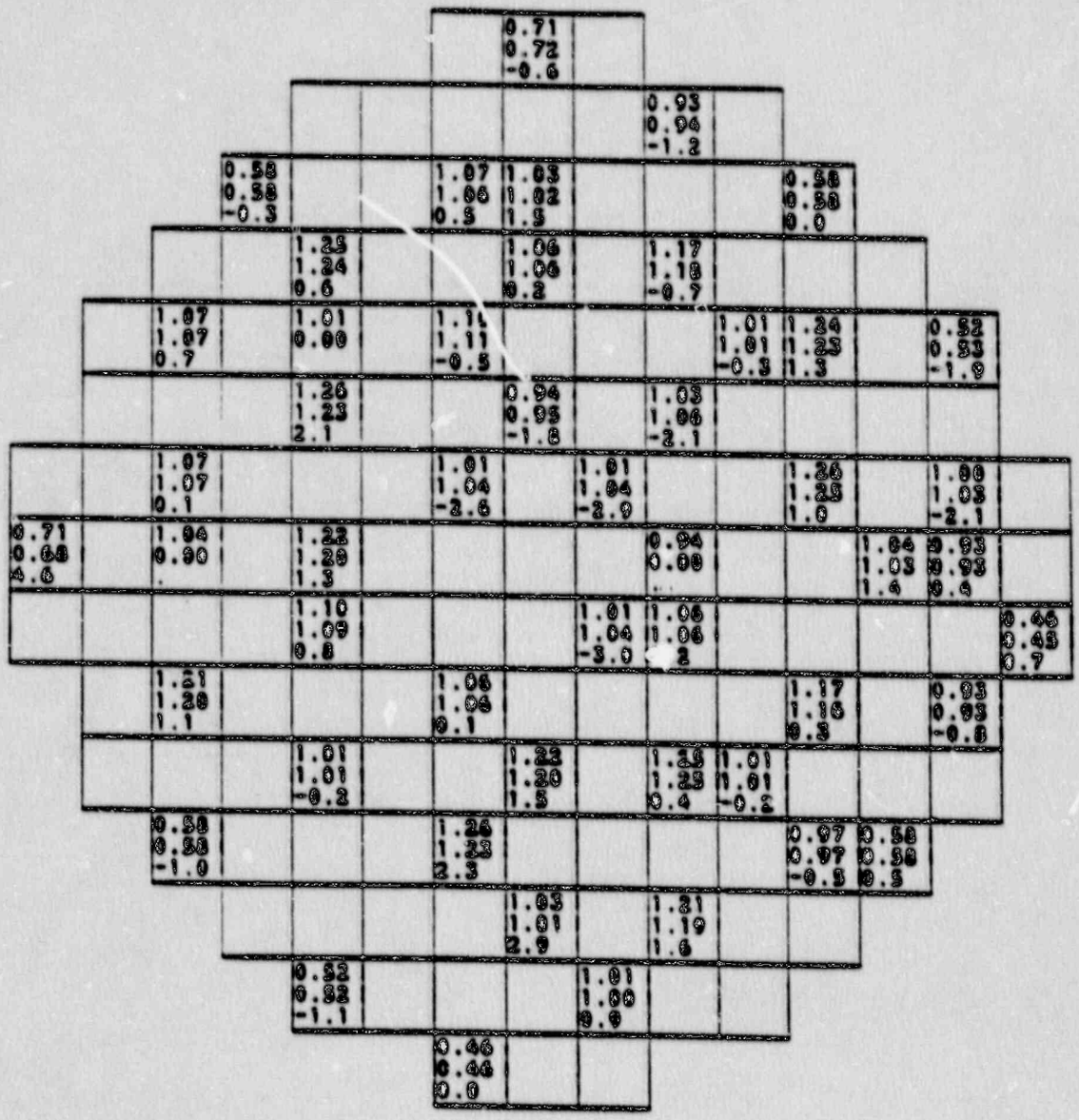

MAX DIFFERENCE = 4.56
MAX DIFF (P/F)>0.9) = -3
RMS DIFFERENCE = 1.48

X.XX PREDICTED
X.XX MEASURED
X.X PERCENT DIFFERENCE

FIGURE 3-180

S2C7 3D PDQ VS. MEASURED RPD COMPARISON
HZP, D-211, 0 MWD/MTU S2-7-01A

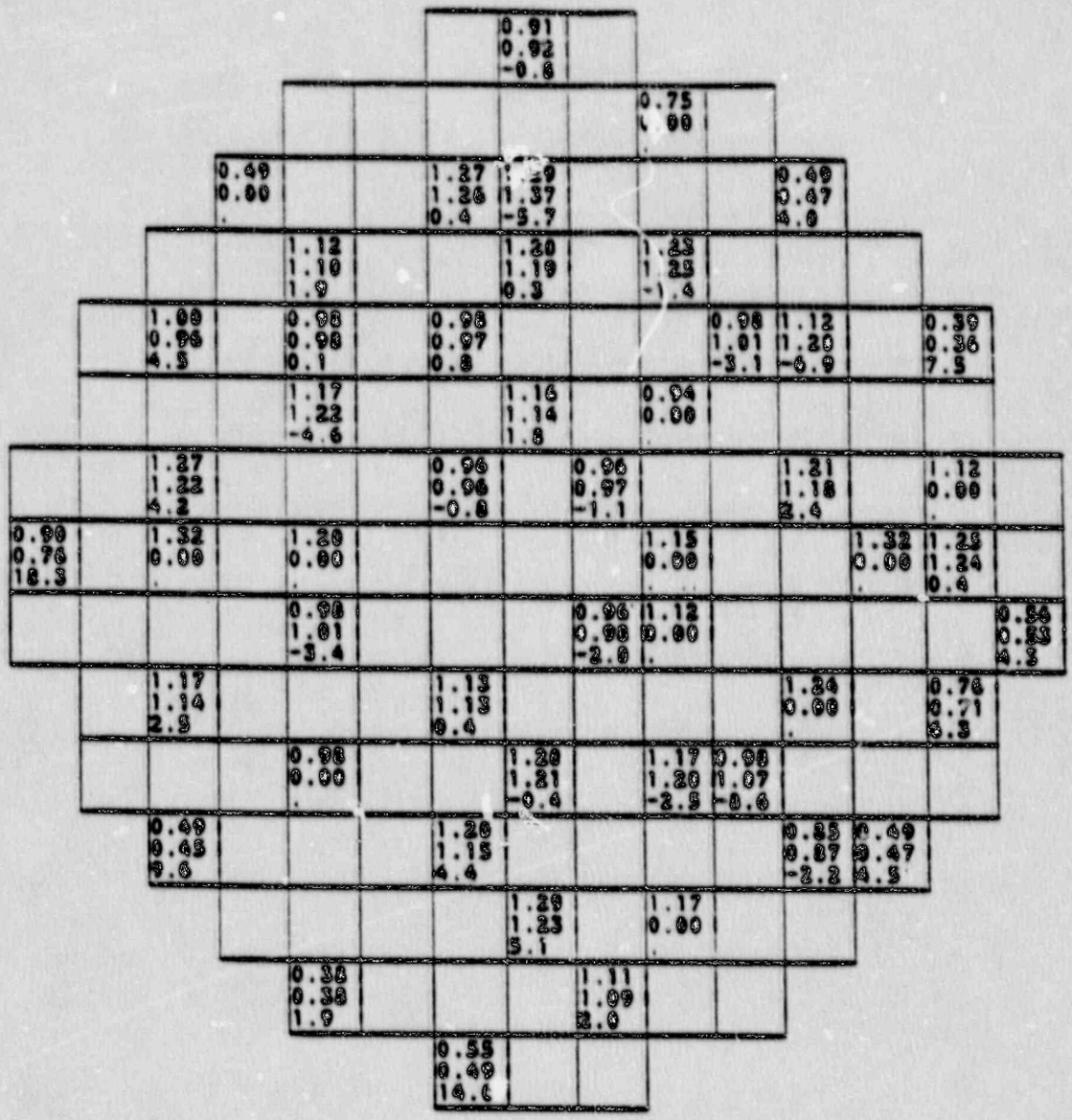

MAX DIFFERENCE = 18.3
MAX DIFF (EXCEPT 0.0) = 18.3
RMS DIFFERENCE = 5.38

X.XX PREDICTED
X.XX MEASURED
X.X PERCENT DIFFERENCE

FIGURE 3-181

S2C7 3D PDQ VS. MEASURED RPD COMPARISON
HFP, D-226, 1647 MWD/MTU S2-7-13A

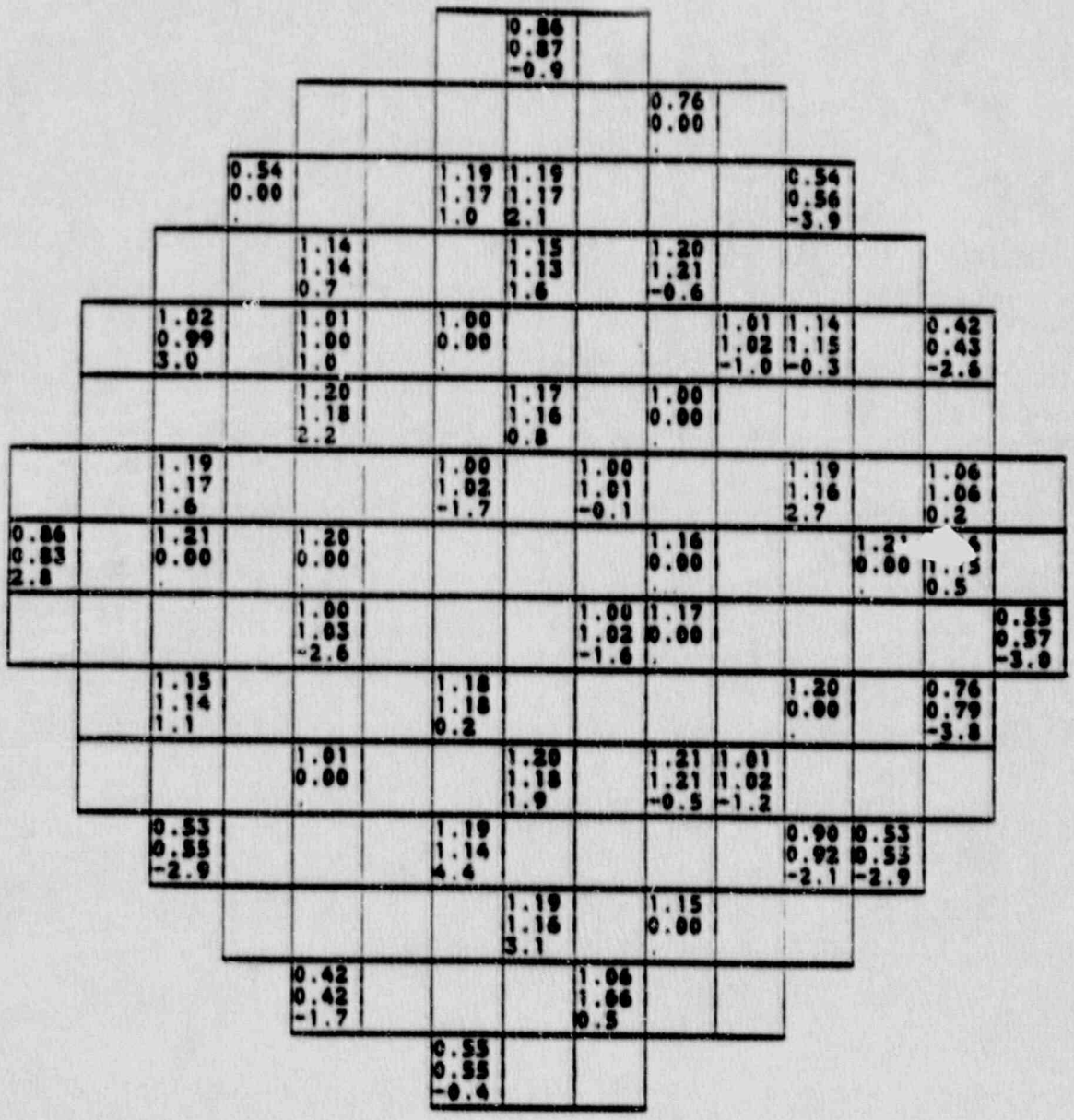

MAX DIFFERENCE = 4.40
MAX DIFF (RPD>0.9) = 4.40
RMS DIFFERENCE = 2.06

X.XX PREDICTED
X.XX MEASURED
X.X PERCENT DIFFERENCE

FIGURE 3-182

S2C7 3D PDQ VS. MEASURED RPD COMPARISON
KFP, D-226, 5781 MWD/MTU S2-7-19A

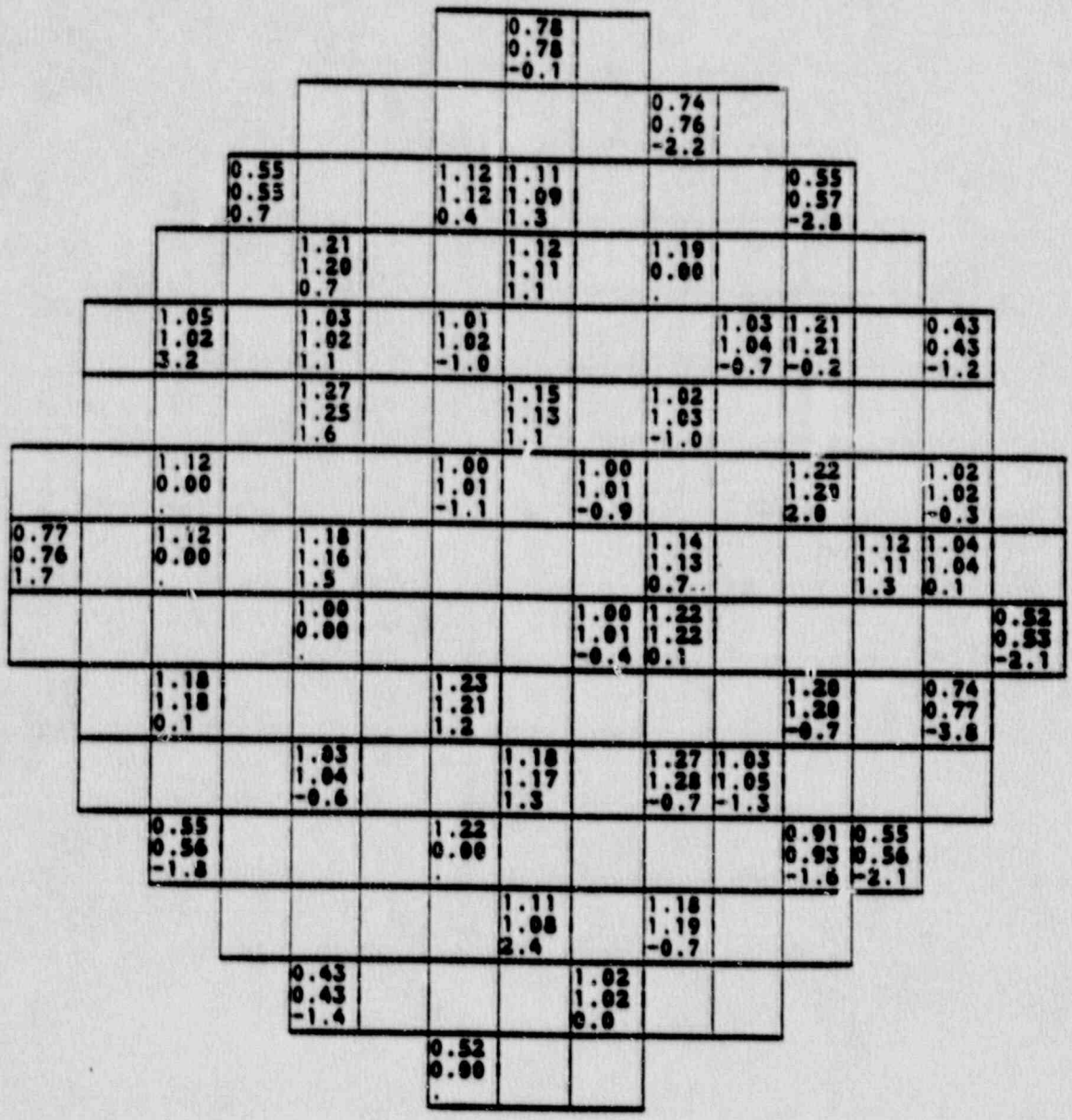

MAX DIFFERENCE = -7.8
MAX DIFF (RPD>0.9) = 7.24
RMS DIFFERENCE = 1.45

X.XX PREDICTED
X.XX MEASURED
X.X PERCENT DIFFERENCE

FIGURE 3-183

S2C7 3D PDQ VS. MEASURED RPD COMPARISON
MFP, D-223, 15122 MWD/MTU S2-7-38A

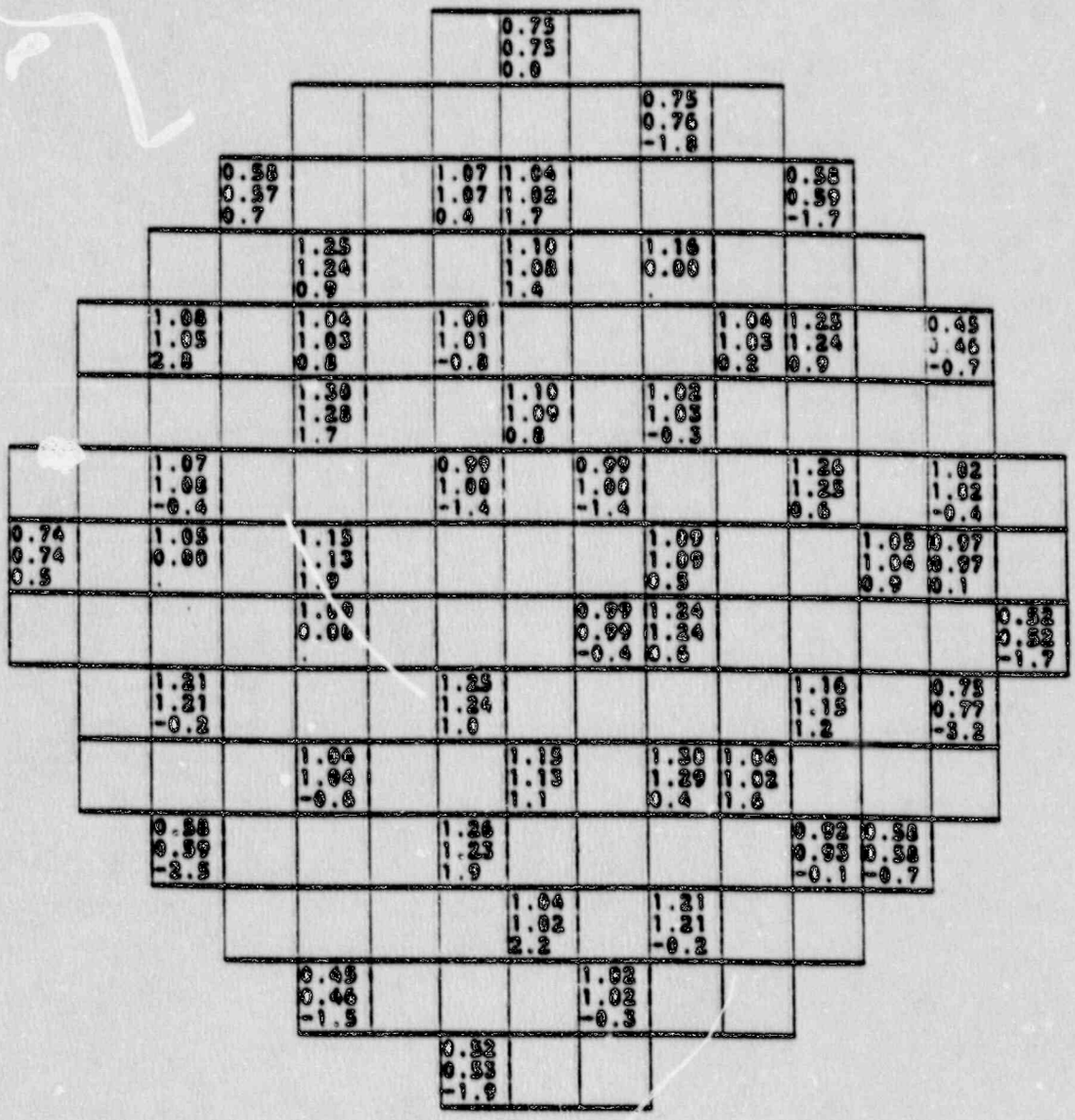

MAX DIFFERENCE = -3.2
MAX DIFF (RPD>0.9) = 2.76
RMS DIFFERENCE = 1.28

X.XX PREDICTED
X.XX MEASURED
X.X PERCENT DIFFERENCE

FIGURE 3-184

S2C8 3D PDQ VS. MEASURED RPD COMPARISON
HZP, D-220, 0 MWD/MTU S2-0-01A

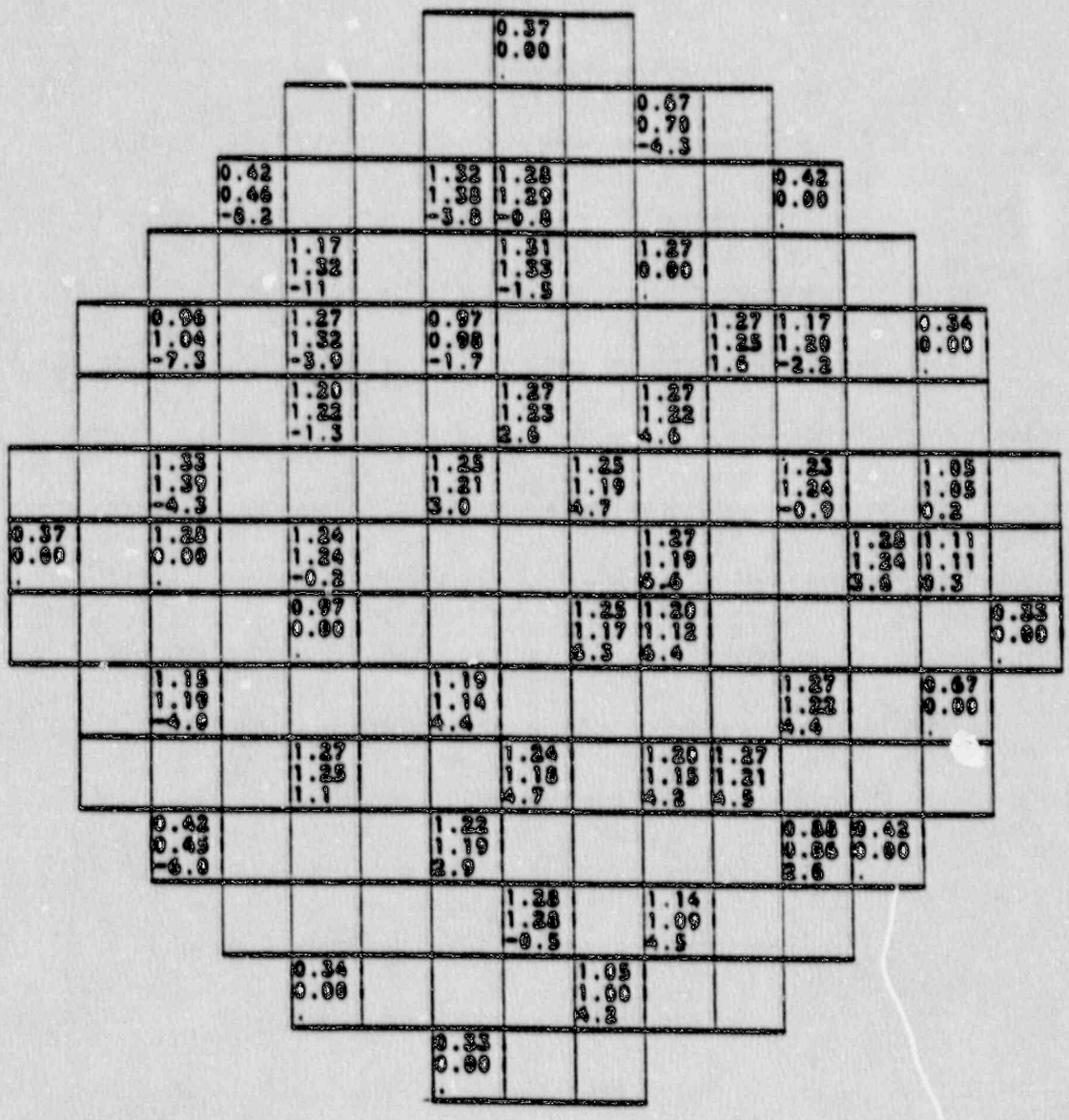

MAX DIFFERENCE = -11
MAX DIFF (REF>0.9) = -11
RMS DIFFERENCE = 4.37

X.XX PREDICTED
X.XX MEASURED
X.X PERCENT DIFFERENCE

FIGURE 3-105

S2C8 3D PDQ VS. MEASURED RPD COMPARISON
RFP. D-228 .8423 MWD/MTU S2-8-13A

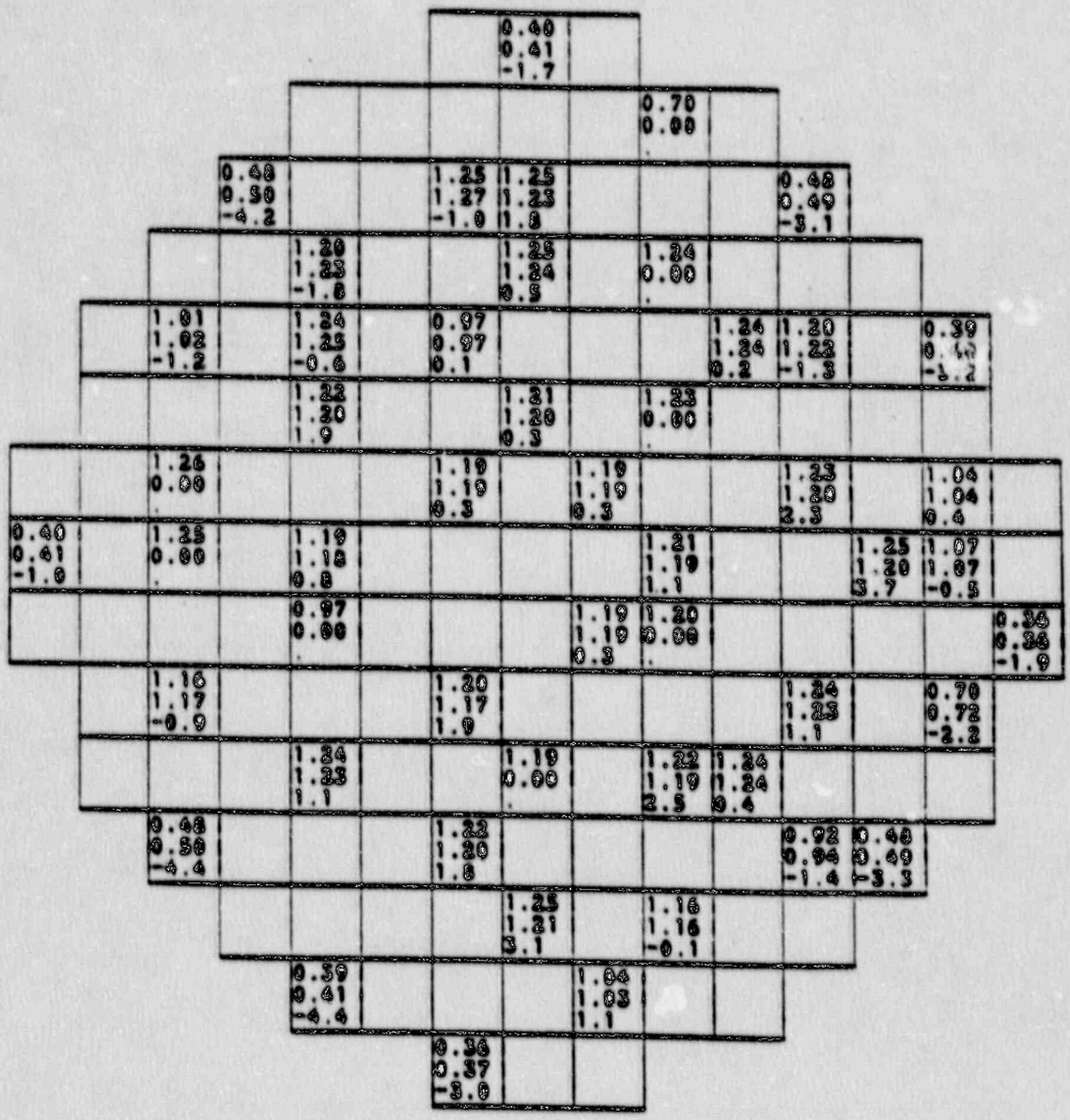

MAX DIFFERENCE : -4.4
MAX DIFF (REF>0.9) : 3.65
RMS DIFFERENCE : 2.03

X.XX PREDICTED
X.XX MEASURED
X.X PERCENT DIFFERENCE

FIGURE 3-186

S2C8 3D PDQ VS. MEASURED RPD COMPARISON
HFP, D-218, 6525 MWD/MTU S2C8-M23A

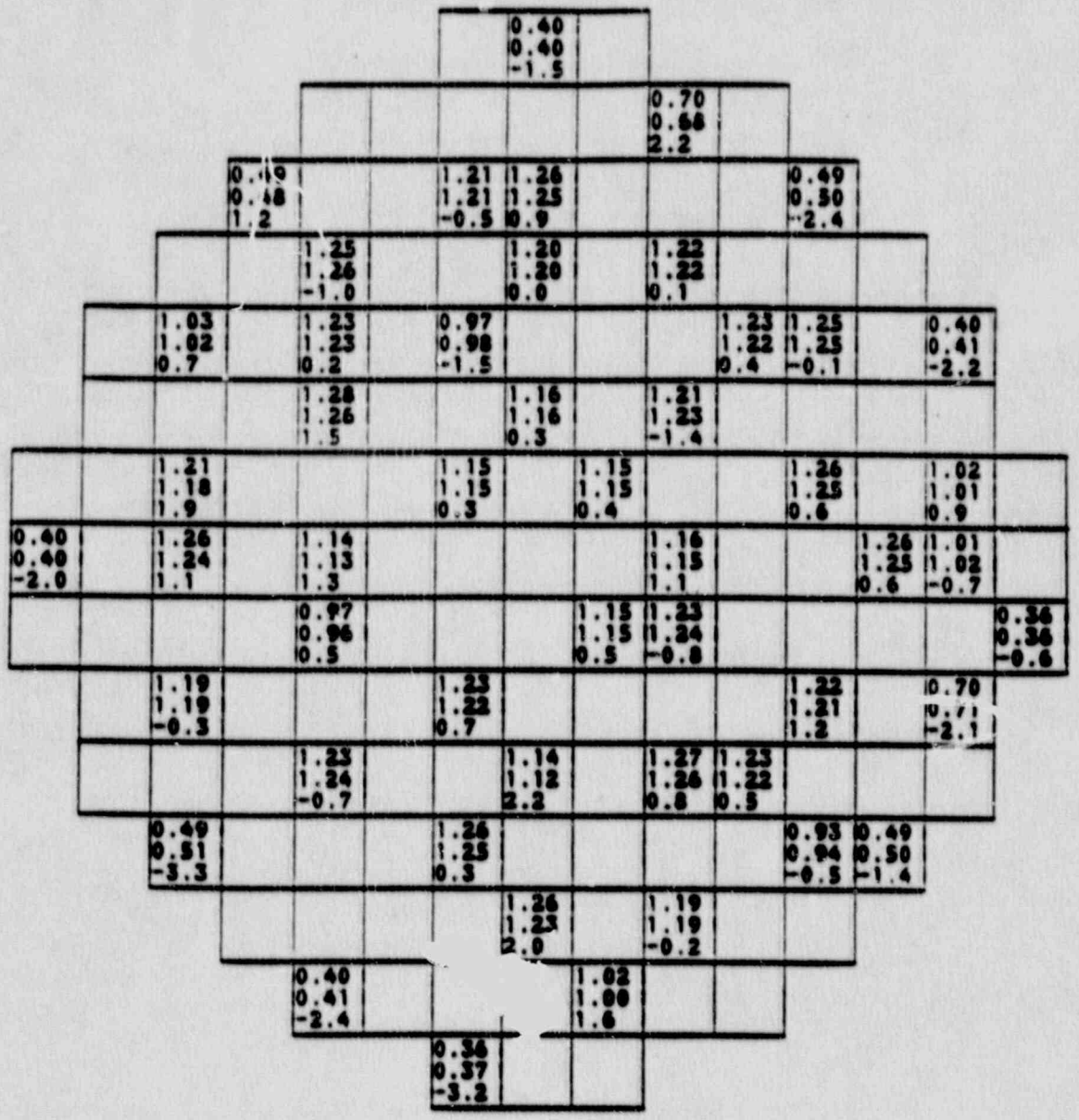

MAX DIFFERENCE = -3.3
MAX DIFF (RPD>0.9) = 2.24
RMS DIFFERENCE = 1.37

X.XX PREDICTED
X.XX MEASURED
X.X PERCENT DIFFERENCE

FIGURE 3-187

S2C8 3D PDQ VS. MEASURED RPD COMPARISON
KFP, D-221, 12391 MWD/MTU S2-8-N34A

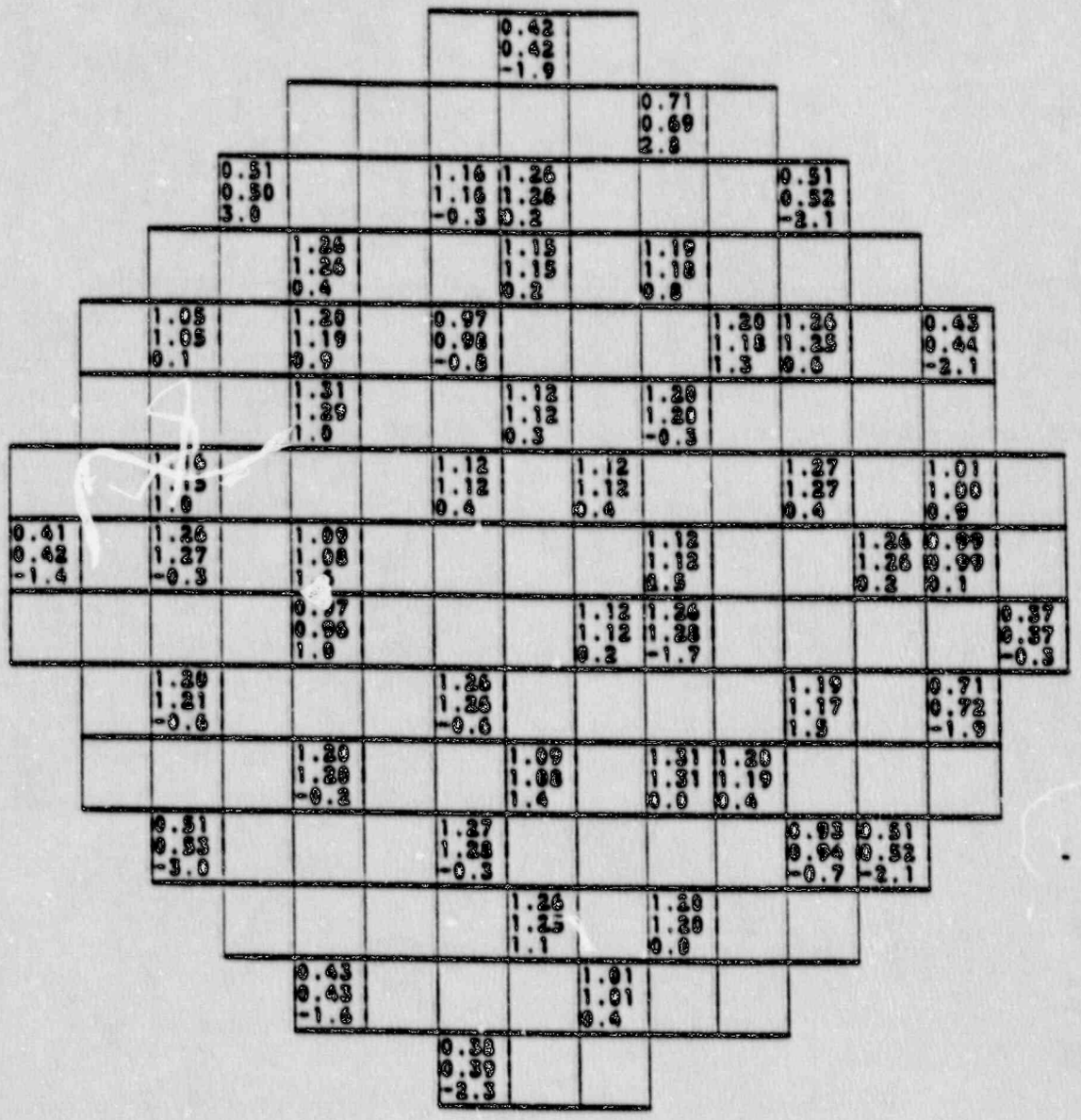

MAX DIFFERENCE = -3
MAX DIFF (RPD>0.9) = -1.7
RMS DIFFERENCE = 1.25

X.XX PREDICTED
X.XX MEASURED
X.X PERCENT DIFFERENCE

FIGURE 3-188

S2C9 3[illegible] FDH VS. MEASURED RPD COMPARISON
HFP, D-208, 1072 MWD/MTU S2-9-M09A

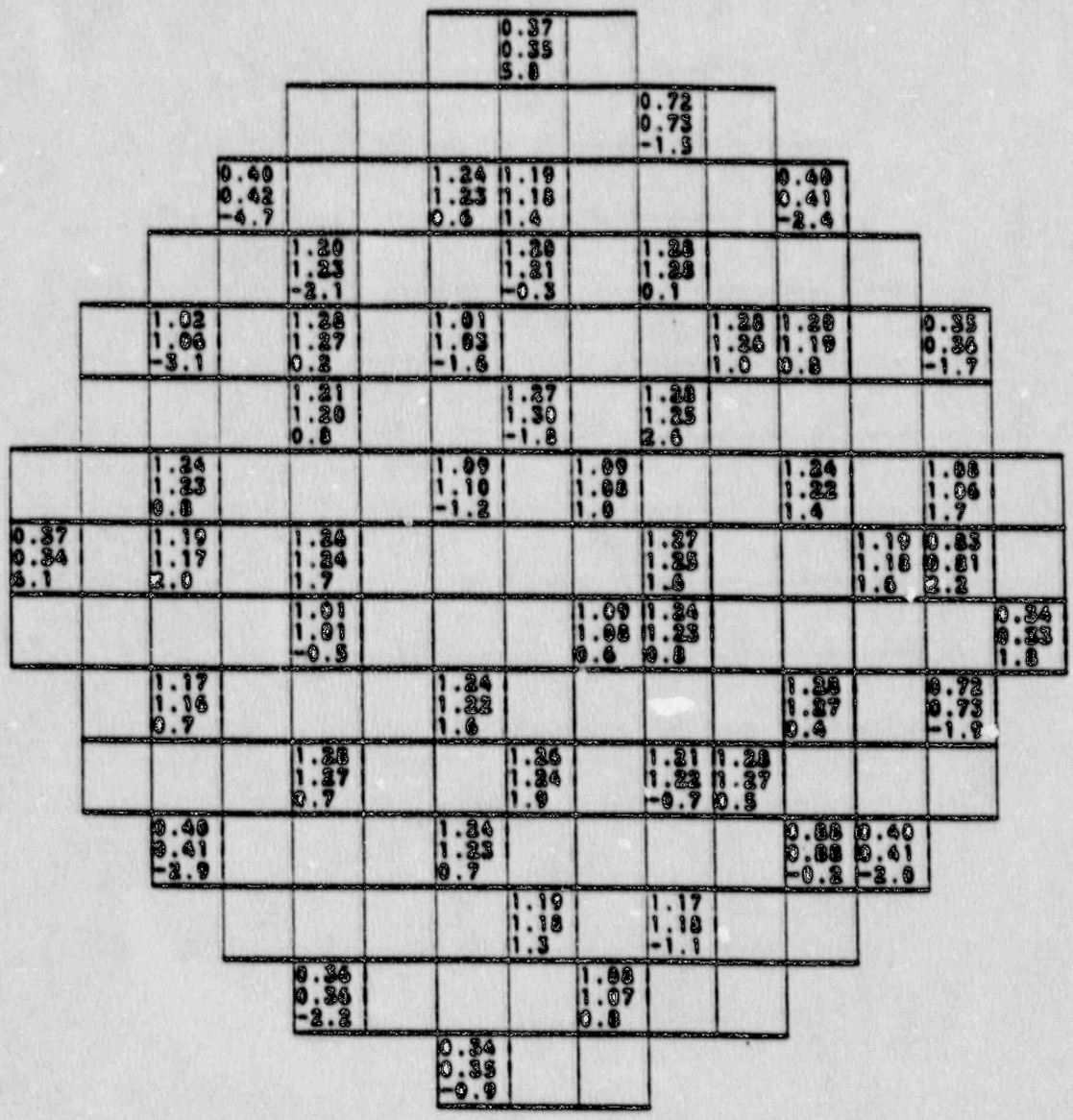

MAX DIFFERENCE = 8.09
MAX DIFF (RPD>0.9) = -3.1
RMS DIFFERENCE = 1.99

X.XX PREDICTED
X.XX MEASURED
X.X PERCENT DIFFERENCE

FIGURE 3-189

S2C9 3D PDQ VS. MEASURED RPD COMPARISON
HFP, D-223, 6887 MWD/MTU S2-9-H17A

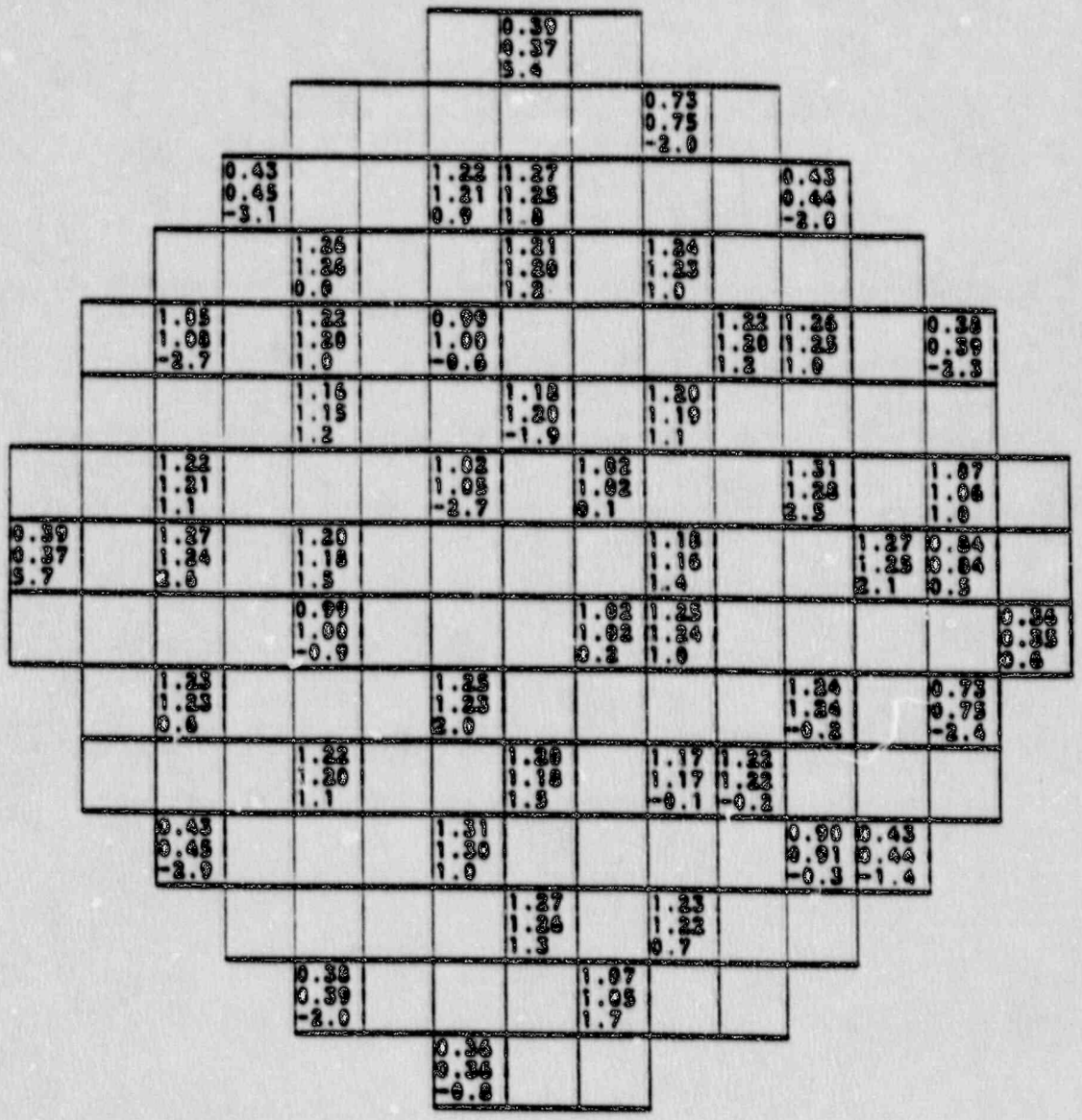

MAX DIFFERENCE = 5.71
MAX DIFF (RPD>0.9) = -2.7
RMS DIFFERENCE = 1.88

X.XX PREDICTED
X.XX MEASURED
X.X PERCENT DIFFERENCE

FIGURE 3-190

N1C3 3D PDQ VS. MEASURED RPD COMPARISON
HZP, D-2, C/130 0 MWD/MTU N1C3-03A

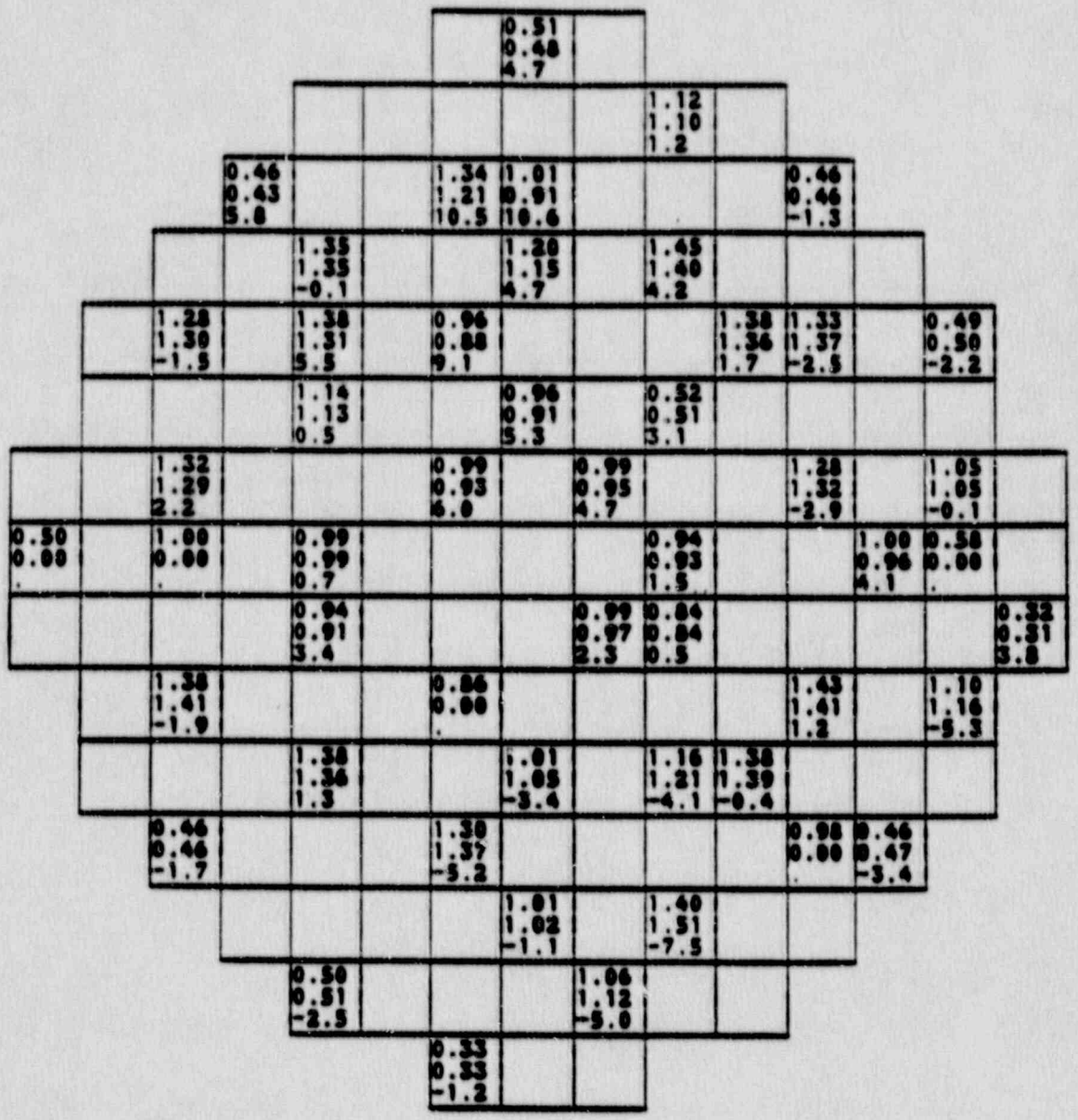

MAX DIFFERENCE = 10.6
MAX DIFF (RPD>0.9) = 10.6
RMS DIFFERENCE = 4.23

X.XX PREDICTED
X.XX MEASURED
X.X PERCENT DIFFERENCE

FIGURE 3-191

N1C6 3D FDQ VS. MEASURED RPD COMPARISON
HZP, D-2S, 0 MWD/MTU N1C6-01A

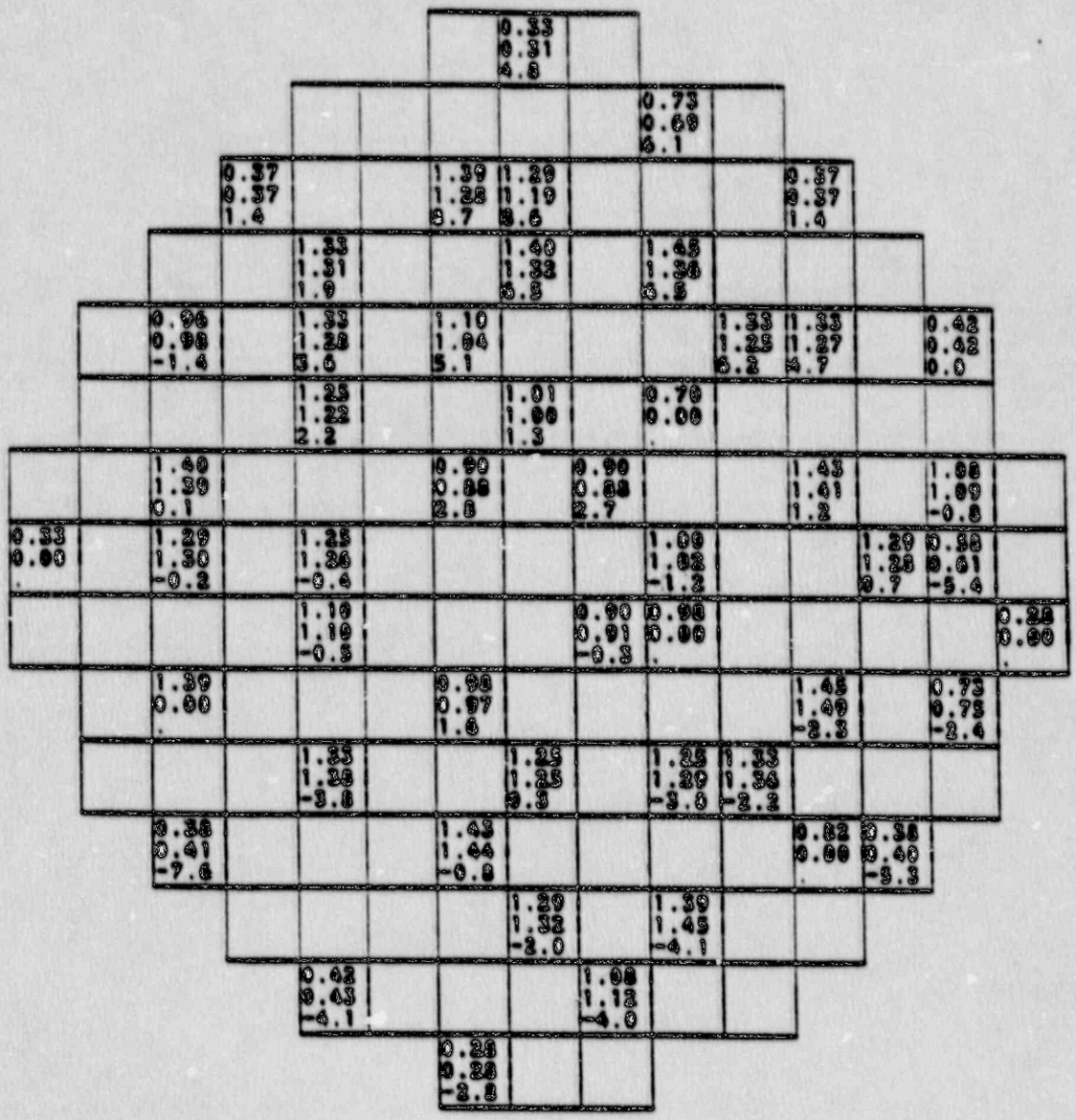

MAX DIFFERENCE = 8.74
MAX DIFF (RPD>0.9) = 8.74
RMS DIFFERENCE = 3.84

X.XX PREDICTED
X.XX MEASURED
X.X PERCENT DIFFERENCE

FIGURE 3-192

SICS 3D FDG VS. MEASURED RPD COMPARISON
MZP, D-0, C219, 0 MWD/MTU S1-S-03

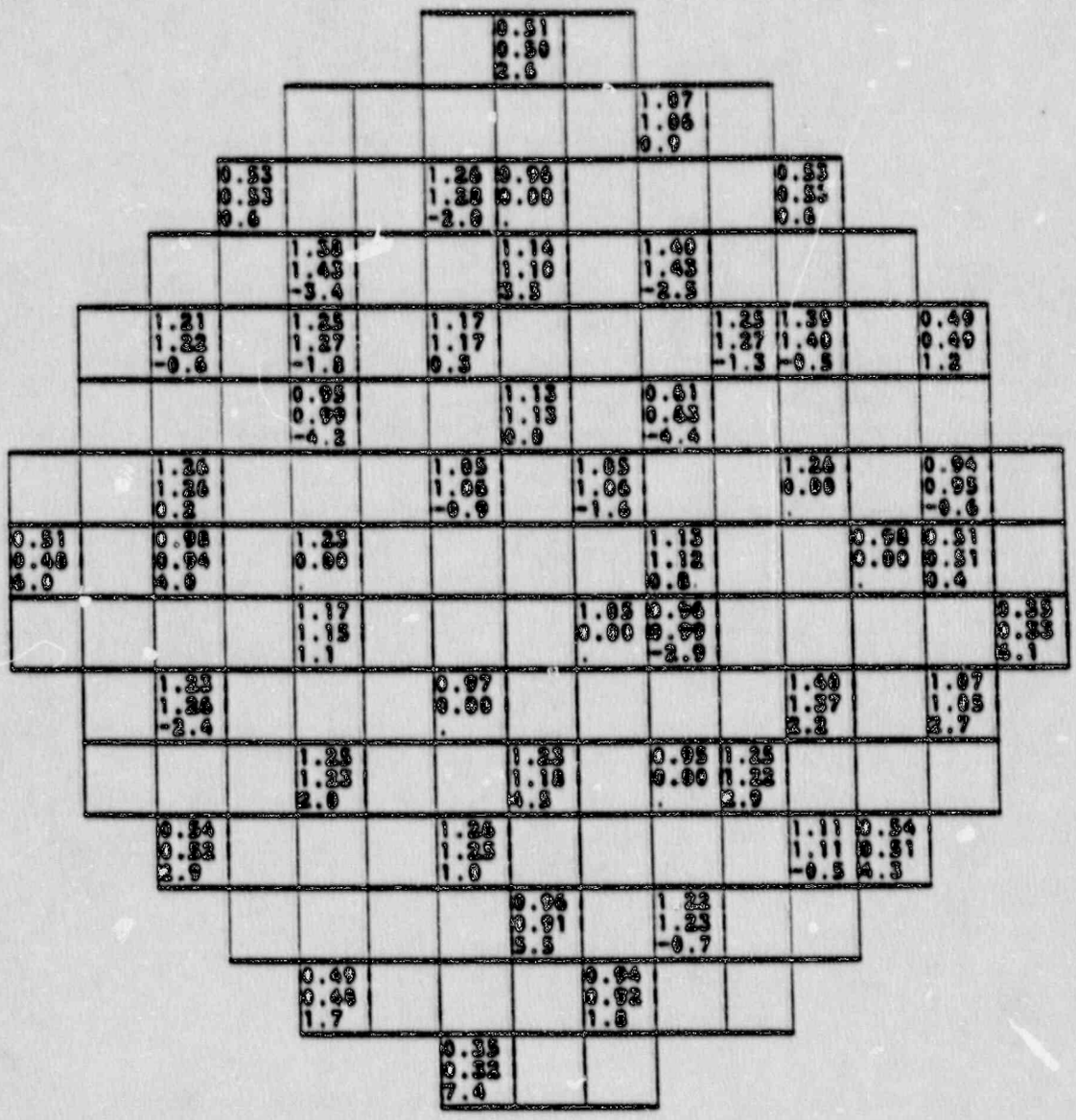

MAX DIFFERENCE = 7.41
MAX DIFF (REF>0.6 = 5.49
RMS DIFFERENCE = 2.89

X.XX PREDICTED
X.XX MEASURED
X.X PERCENT DIFFERENCE

FIGURE 3-193

S2C4 3D PDQ VS. MEASURED RPD COMPARISON
HZP, D-0, 0 MWD/MTU S2-4-02A

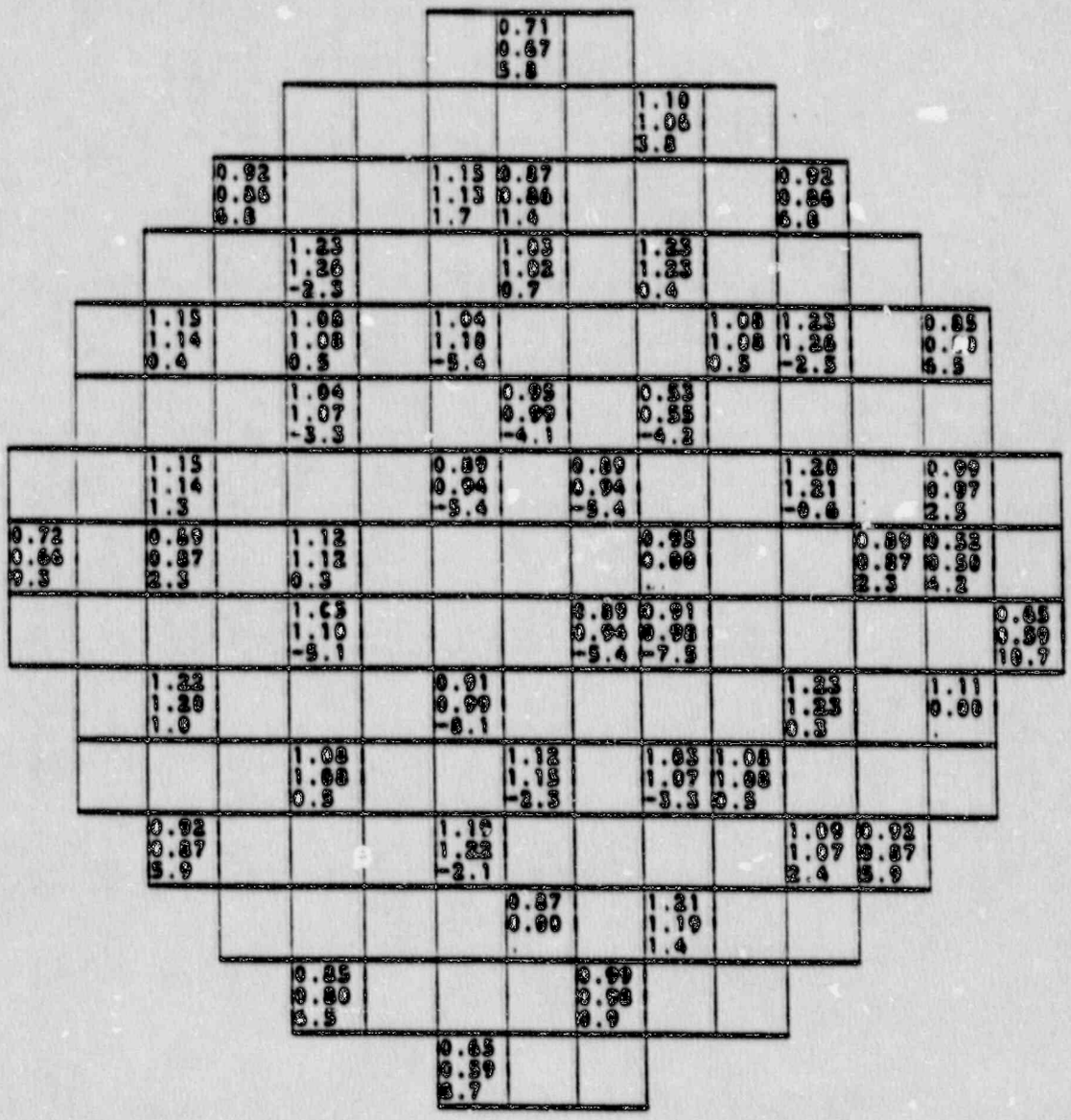

MAX DIFFERENCE = 10.7
MAX DIFF (REF>0.9) = -8.1
RMS DIFFERENCE = 4.93

X.XX PREDICTED
X.XX MEASURED
X.X PERCENT DIFFERENCE

FIGURE 3-104

S2C5 3D PDQ VS. MEASURED RPD COMPARISON
HZP, D-228, B/33-34, 0 MWD/MTU S2-5-02A

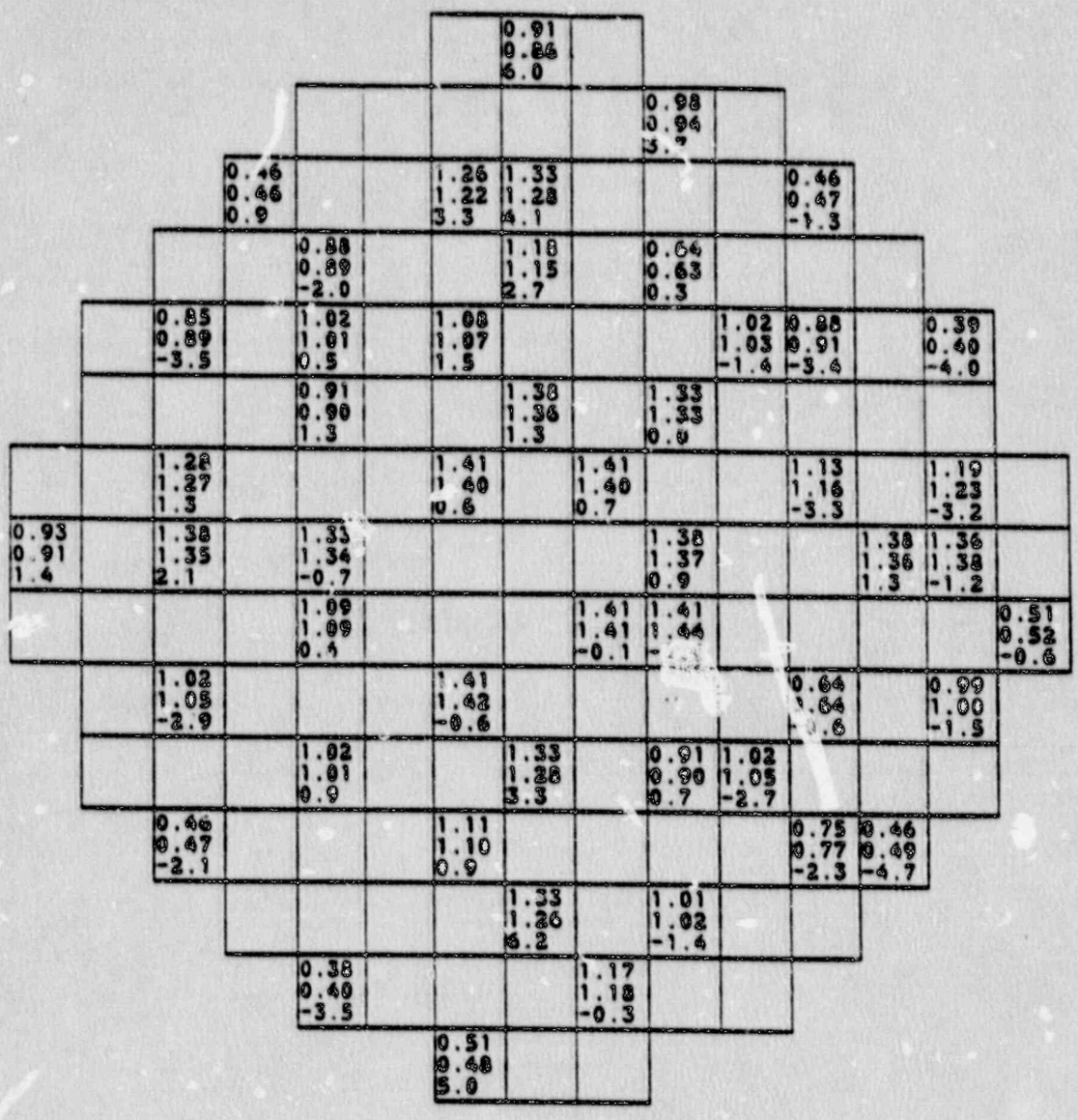

MAX DIFFERENCE = 6.21
MAX DIFF (RPD>0.9) = 6.21
RMS DIFFERENCE = 2.52

X.XX PREDICTED
X.XX MEASURED
X.X PERCENT DIFFERENCE

HZP CRITICAL BORON CONCENTRATION DIFFERENCES
+/- 50 PPM STARTUP CRITERIA

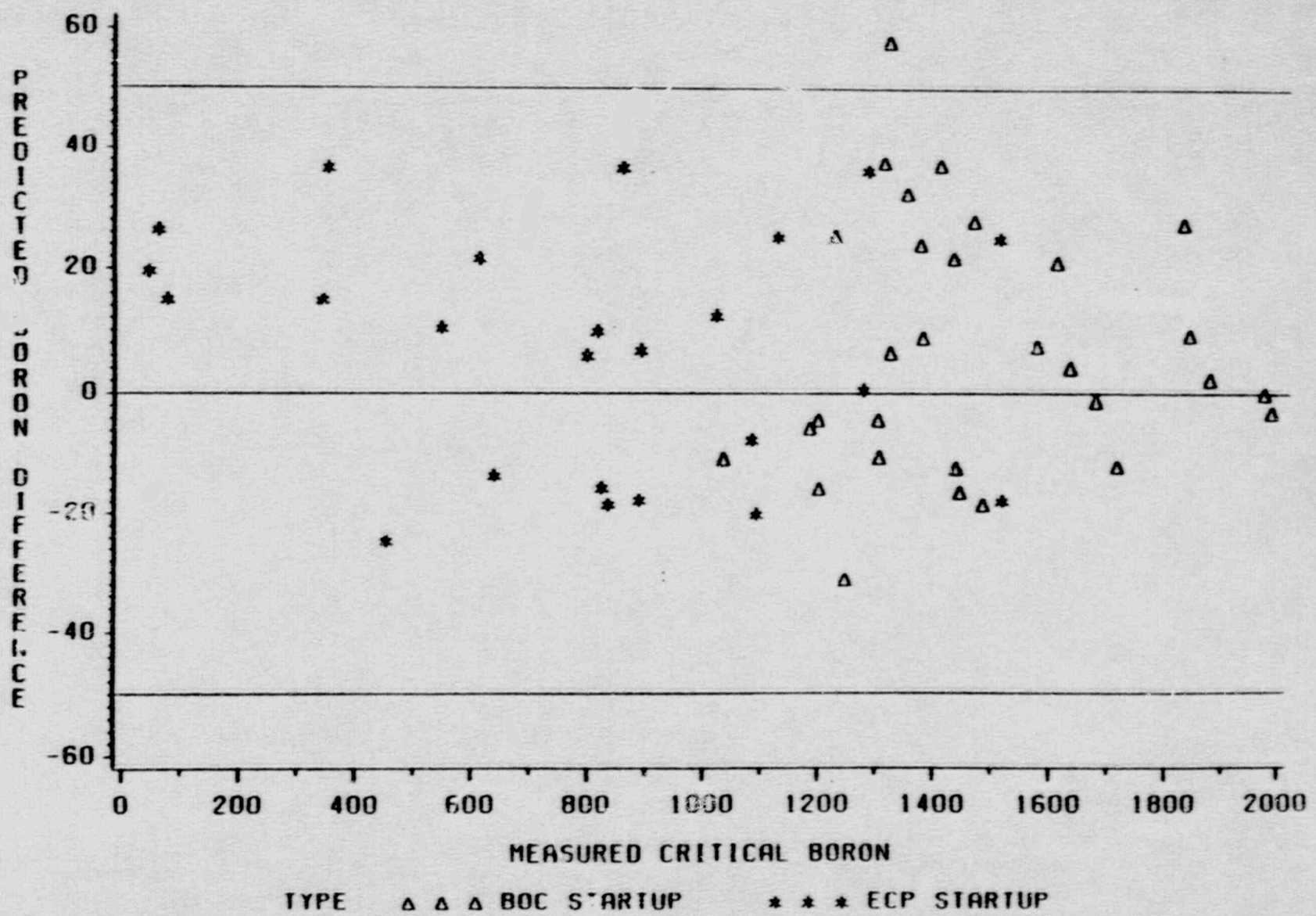

FIGURE 3-195

INTEGRAL CONTROL ROD WORTH DIFFERENCES

TWO ZONE PDQ3D MODEL

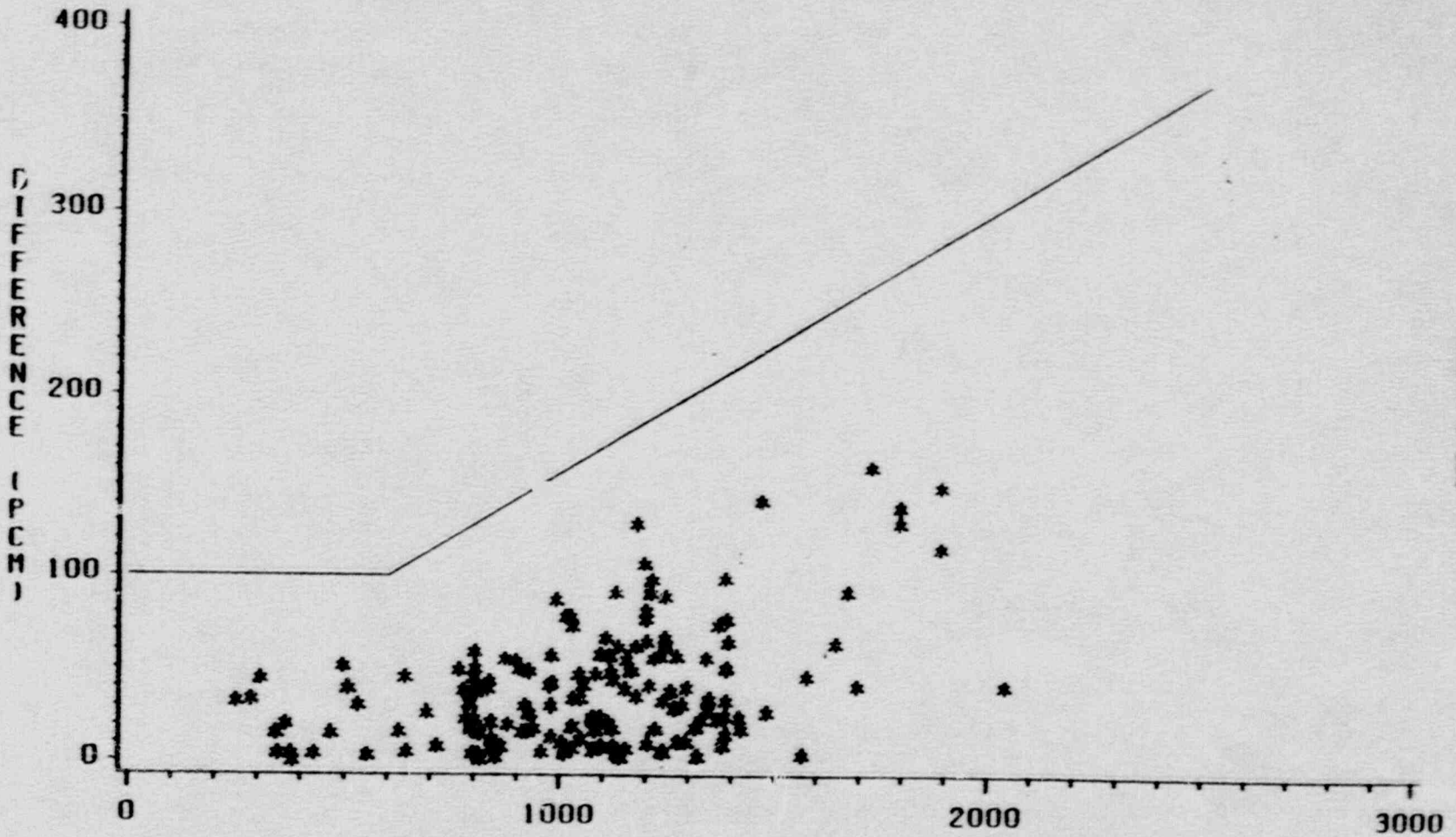

15% ACCEPTANCE CRITERIA. MINIMUM OF 100 PCM
% DIFFERENCE CALCULATED AS ABS(MEAS-PDQ3D)/PDQ3D

FIGURE 3-196

B BANK INTEGRAL WORTH FOR NORTH ANNA 1, CYCLE 5

PDQ 5X5 AND MEASURED DATA

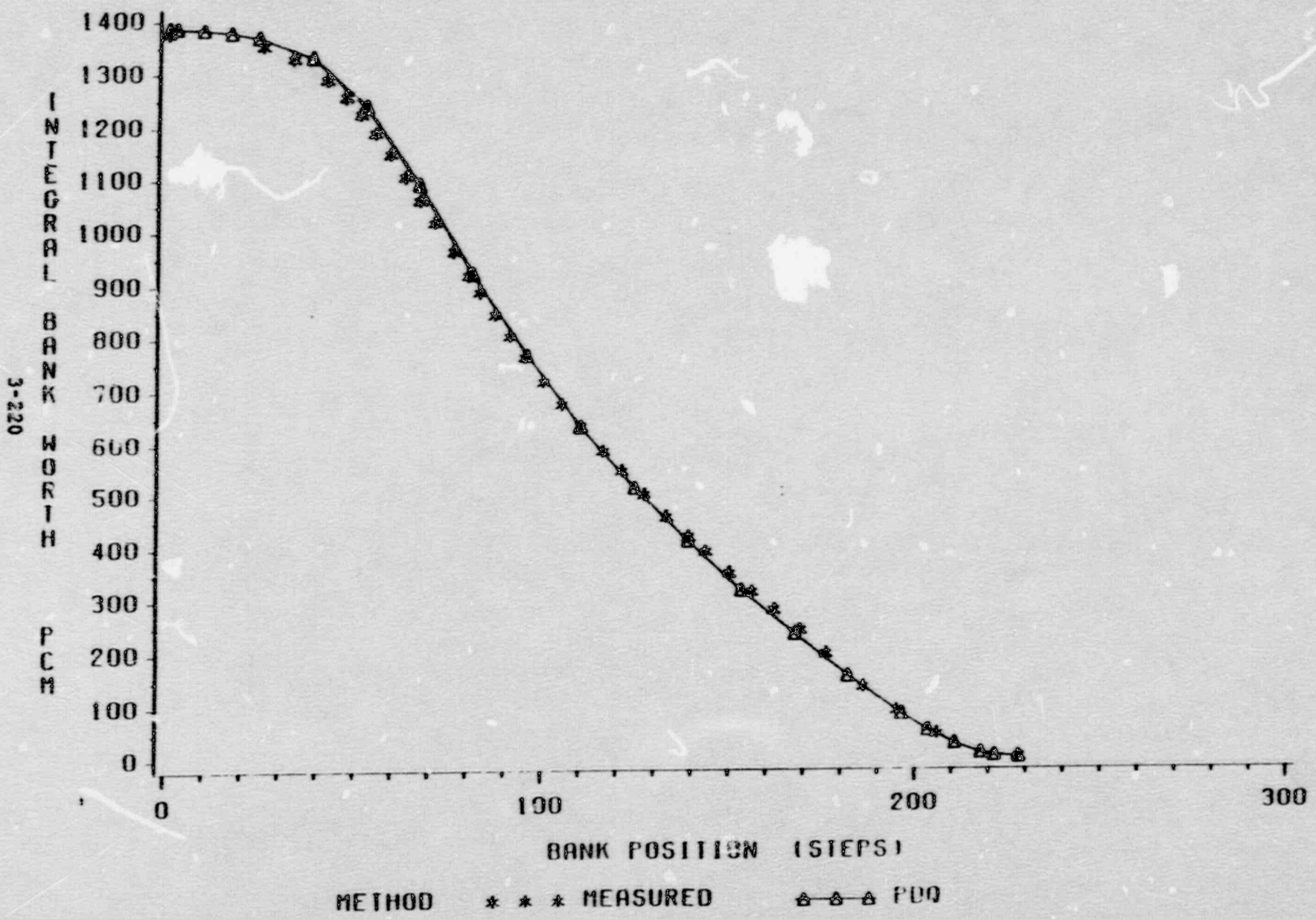

FIGURE 3-197

B BANK DIFFERENTIAL WORTH FOR NORTH ANNA 1, CYCLE 5

PDQ 5X5 AND MEASURED DATA

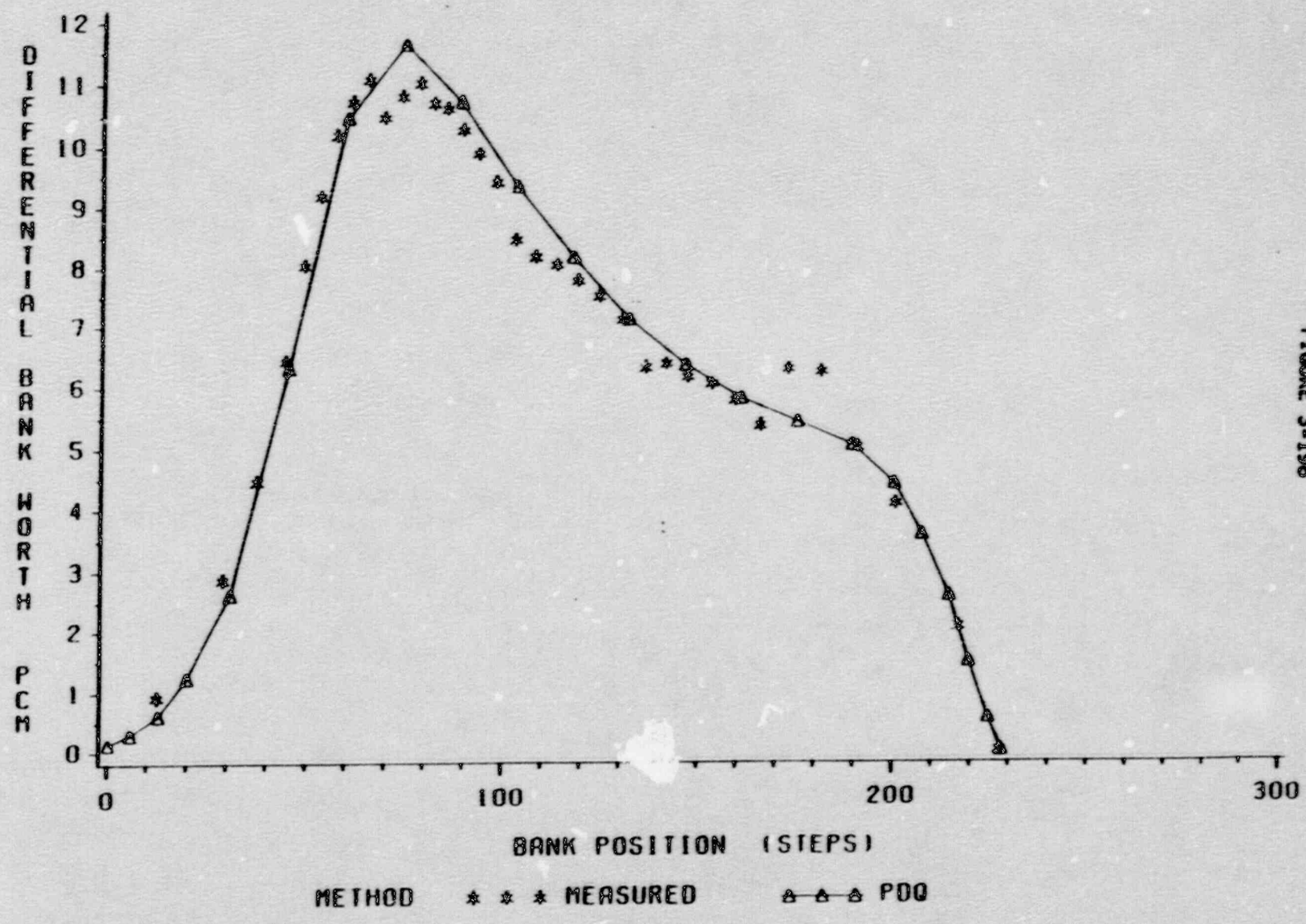

FIGURE 3-198

B BANK INTEGRAL WORTH FOR NORTH ANNA 1, CYCLE 6

POD 5X5 AND MEASURED DATA

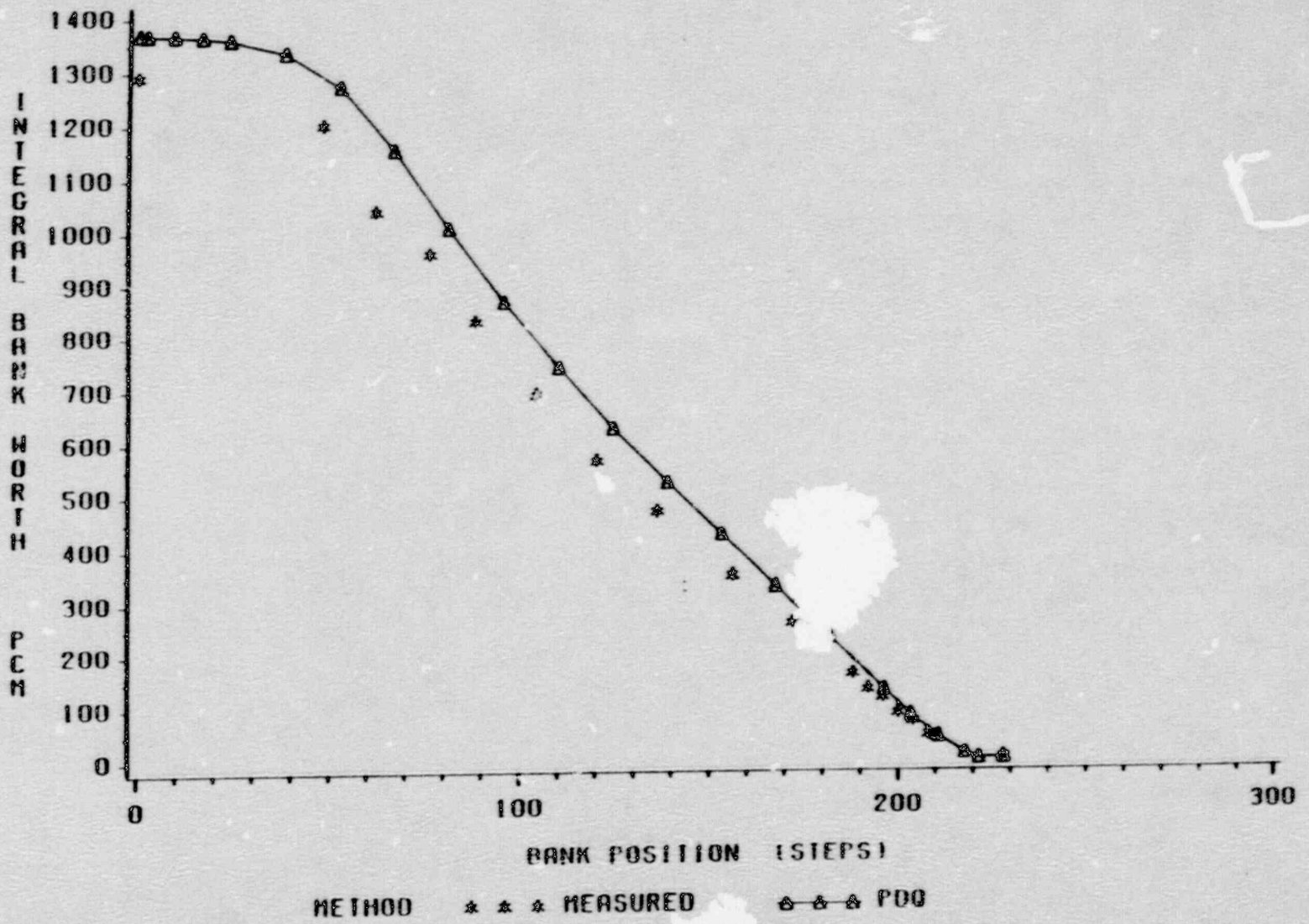

FIGURE 3-199

B BANK DIFFERENTIAL WORTH FOR NORTH ANNA 1, CYCLE 6

PDQ 5X5 AND MEASURED DATA

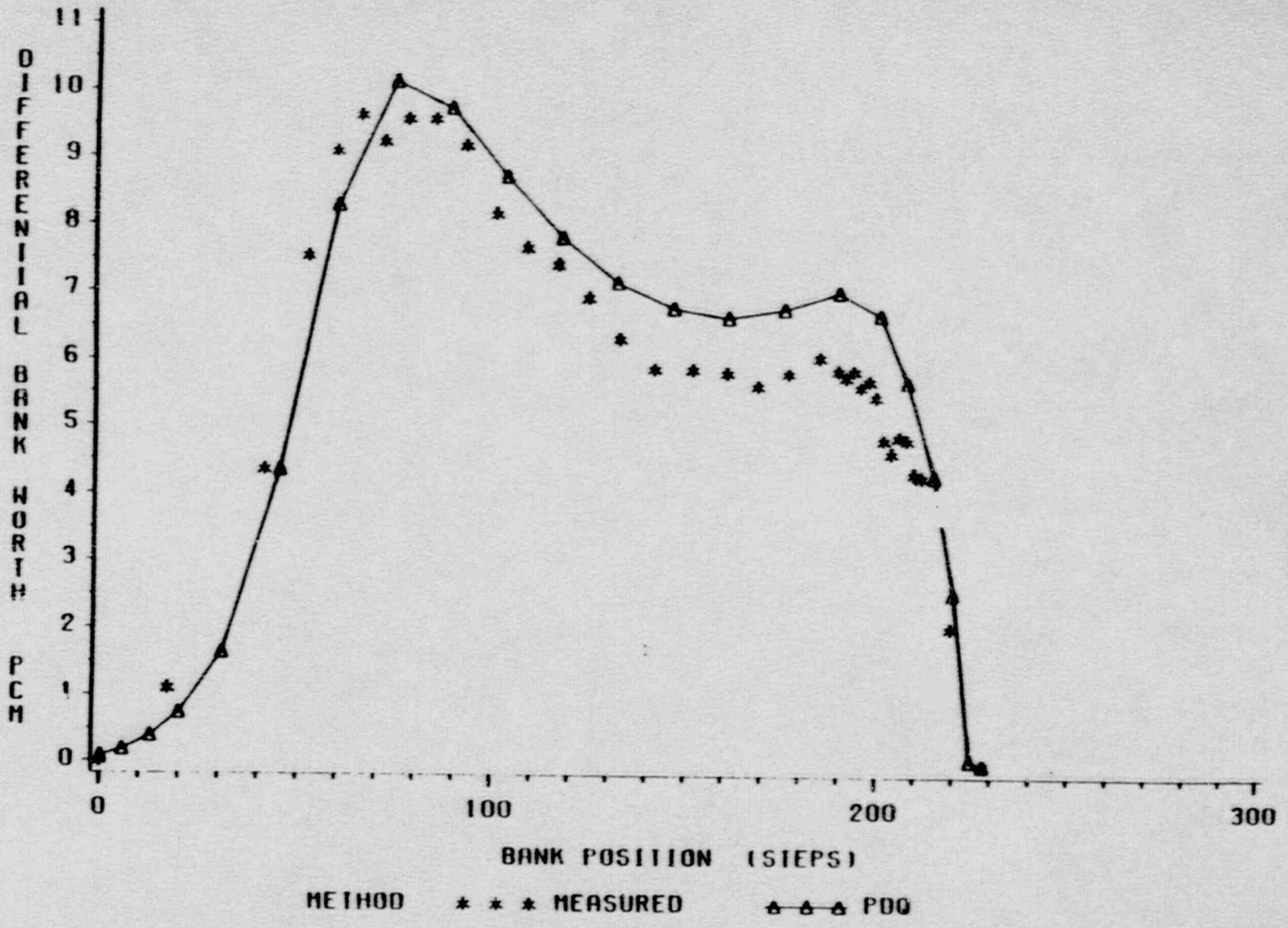

FIGURE 3-200

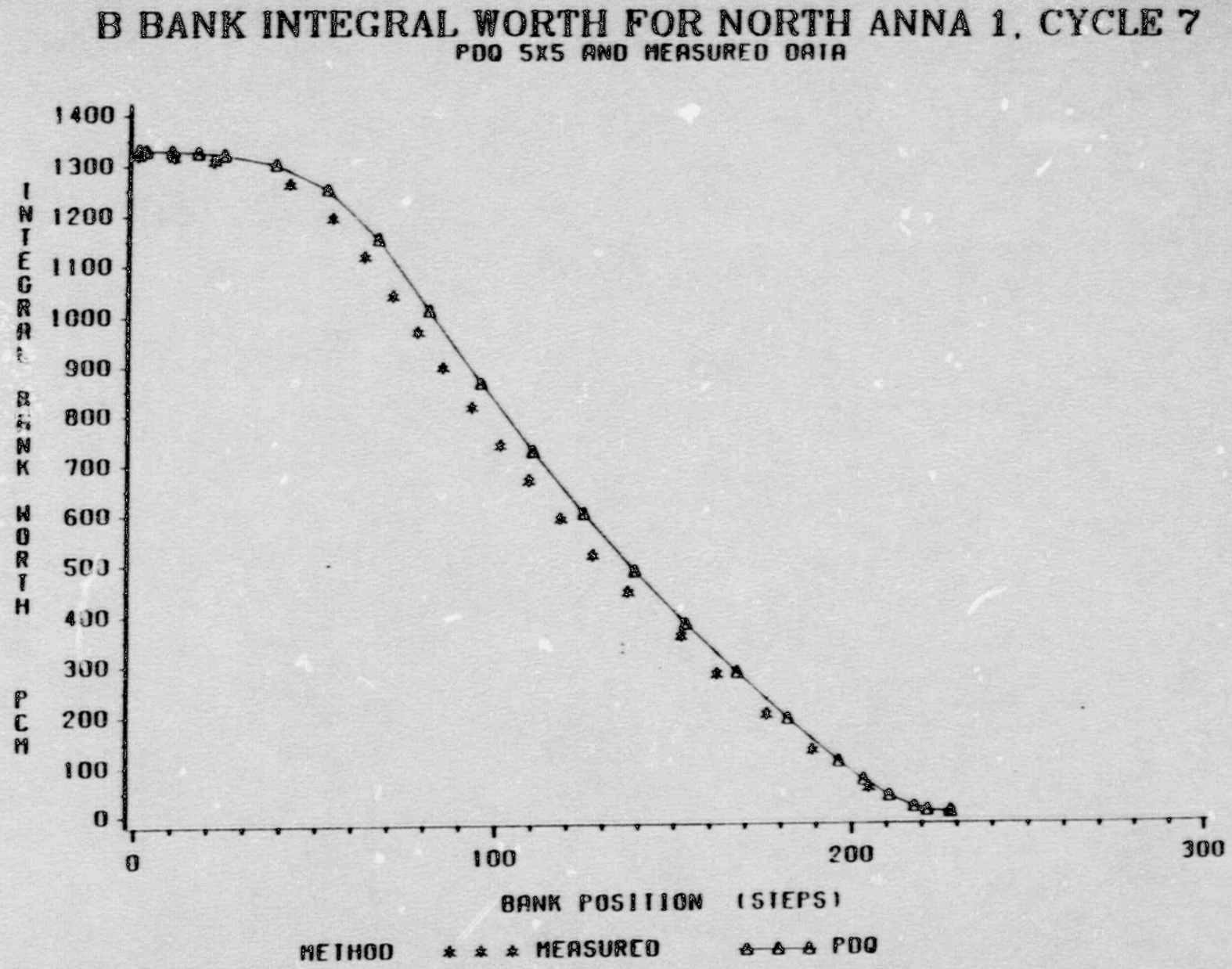
B BANK INTEGRAL WORTH FOR NORTH ANNA 1, CYCLE 7
PDQ 5X5 AND MEASURED DATA
INTEGRAL BANK WORTH PCM
1400
1300
1200
1100
1000
900
800
700
600
500
400
300
200
100
0
0
100
200
300
BANK POSITION (STEPS)
METHOD * * * MEASURED Δ—Δ—Δ PDQ

FIGURE 3-201

B BANK DIFFERENTIAL WORTH FOR NORTH ANNA 1, CYCLE 7

PDQ 5X5 AND MEASURED DATA

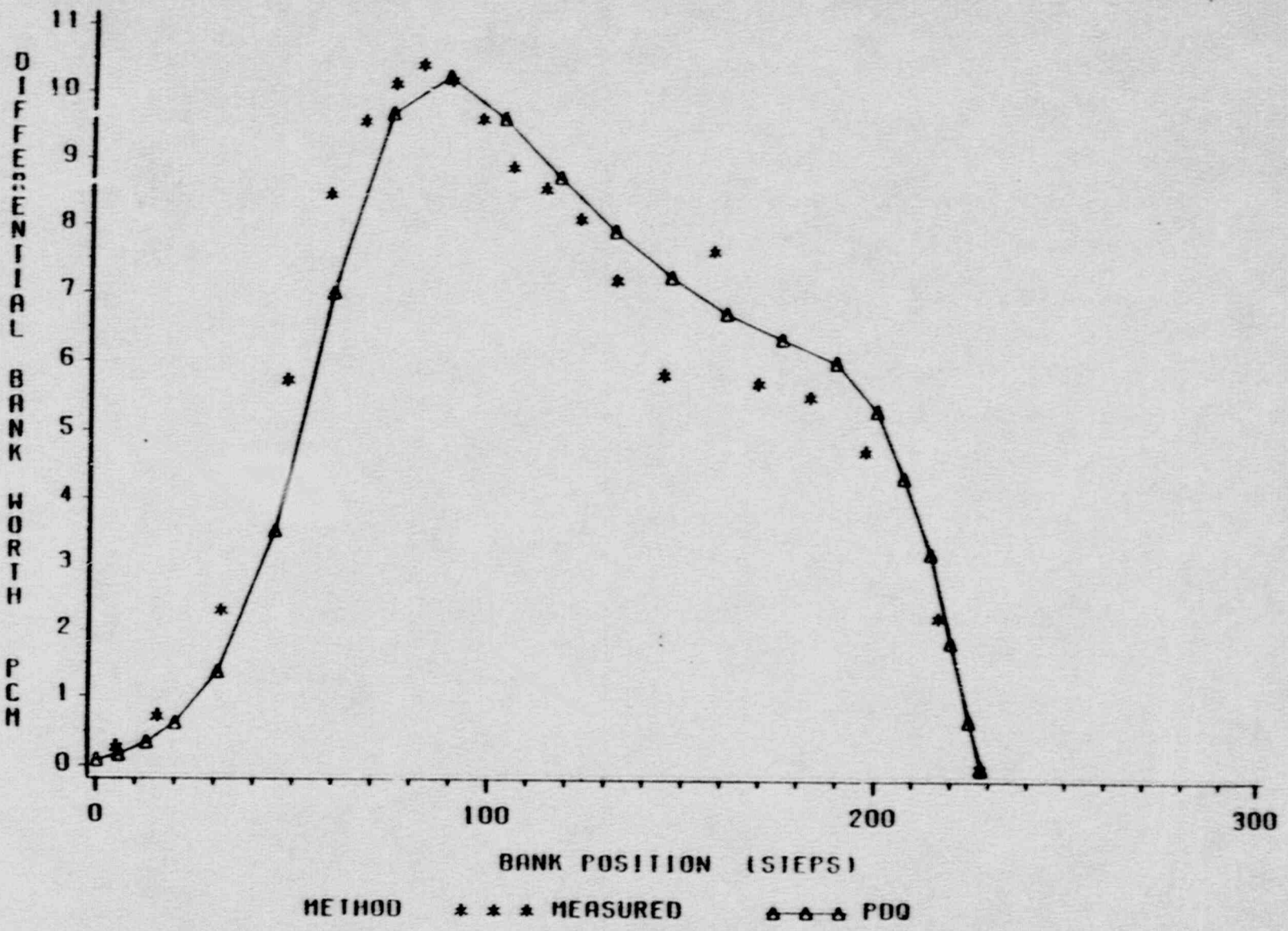

FIGURE 3-202

B BANK INTEGRAL WORTH FOR NORTH ANNA 2, CYCLE 2

PDQ 5X5 AND MEASURED DATA

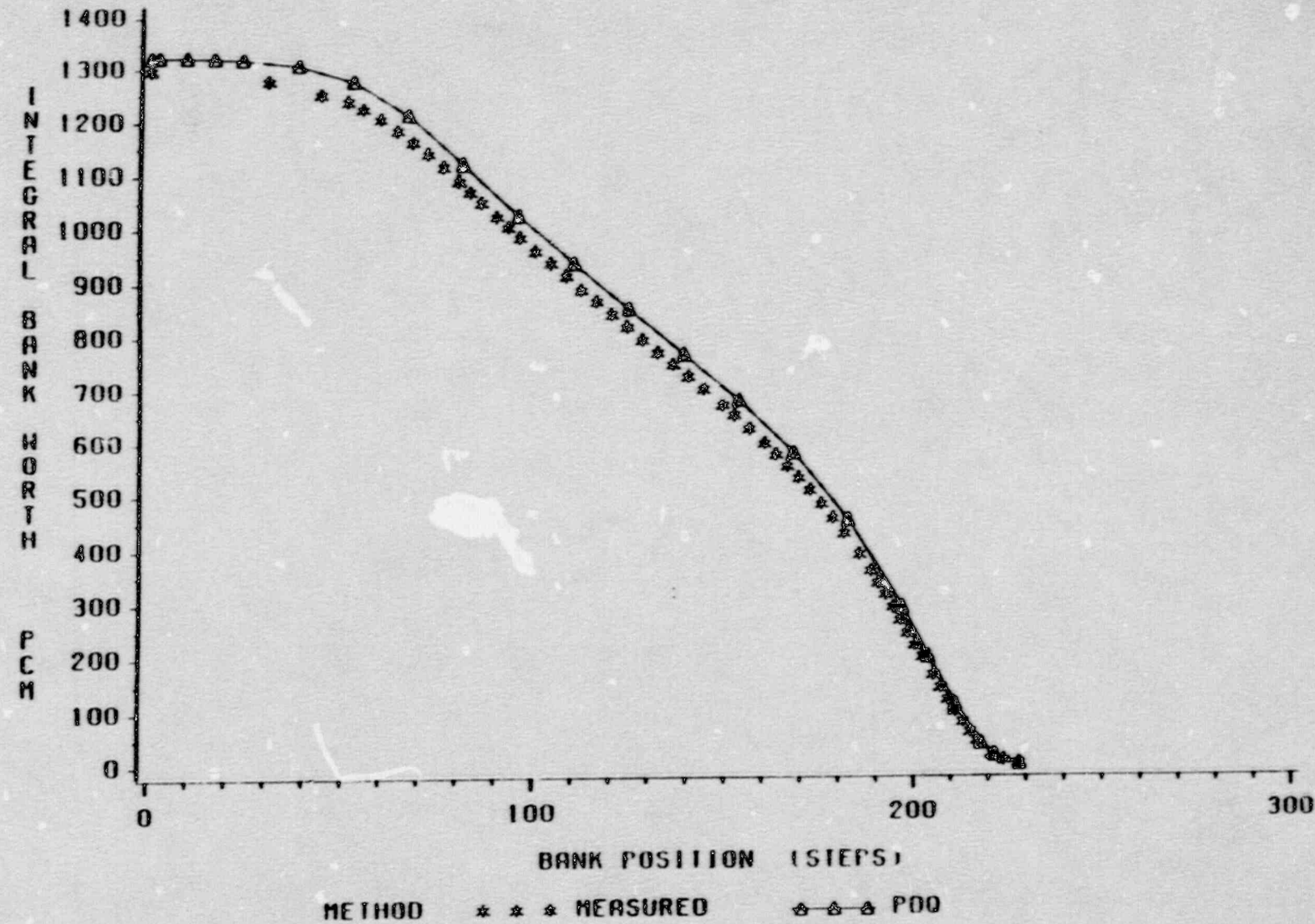

FIGURE 3-203

B BANK DIFFERENTIAL WORTH FOR NORTH ANNA 2, CYCLE 2

PDQ 5X5 AND MEASURED DATA

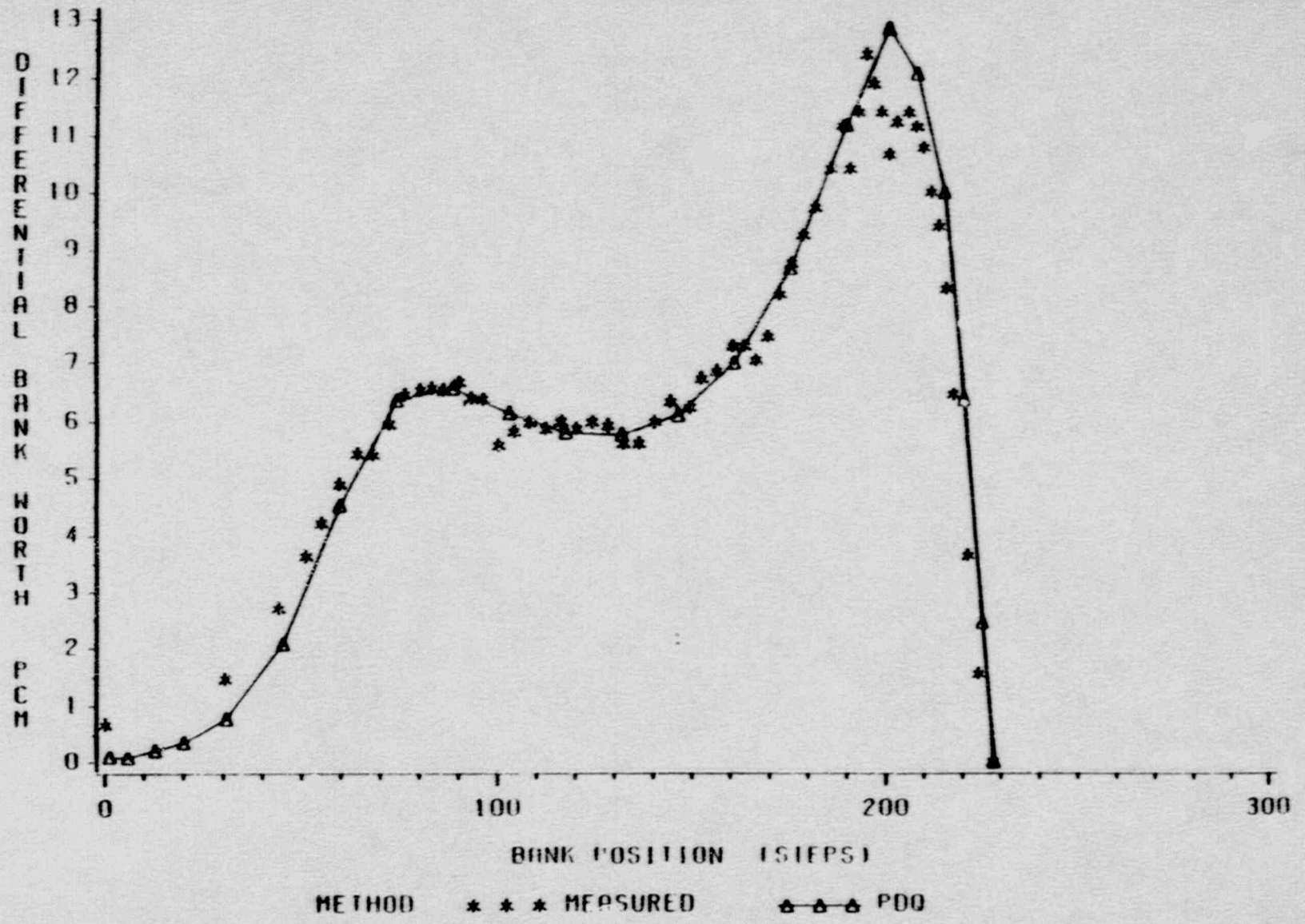

FIGURE 3-204

B BANK INTEGRAL W[illegible]TH FOR NORTH ANNA 2, CYCLE 5

PC[illegible].5 AND MEASURED DATA

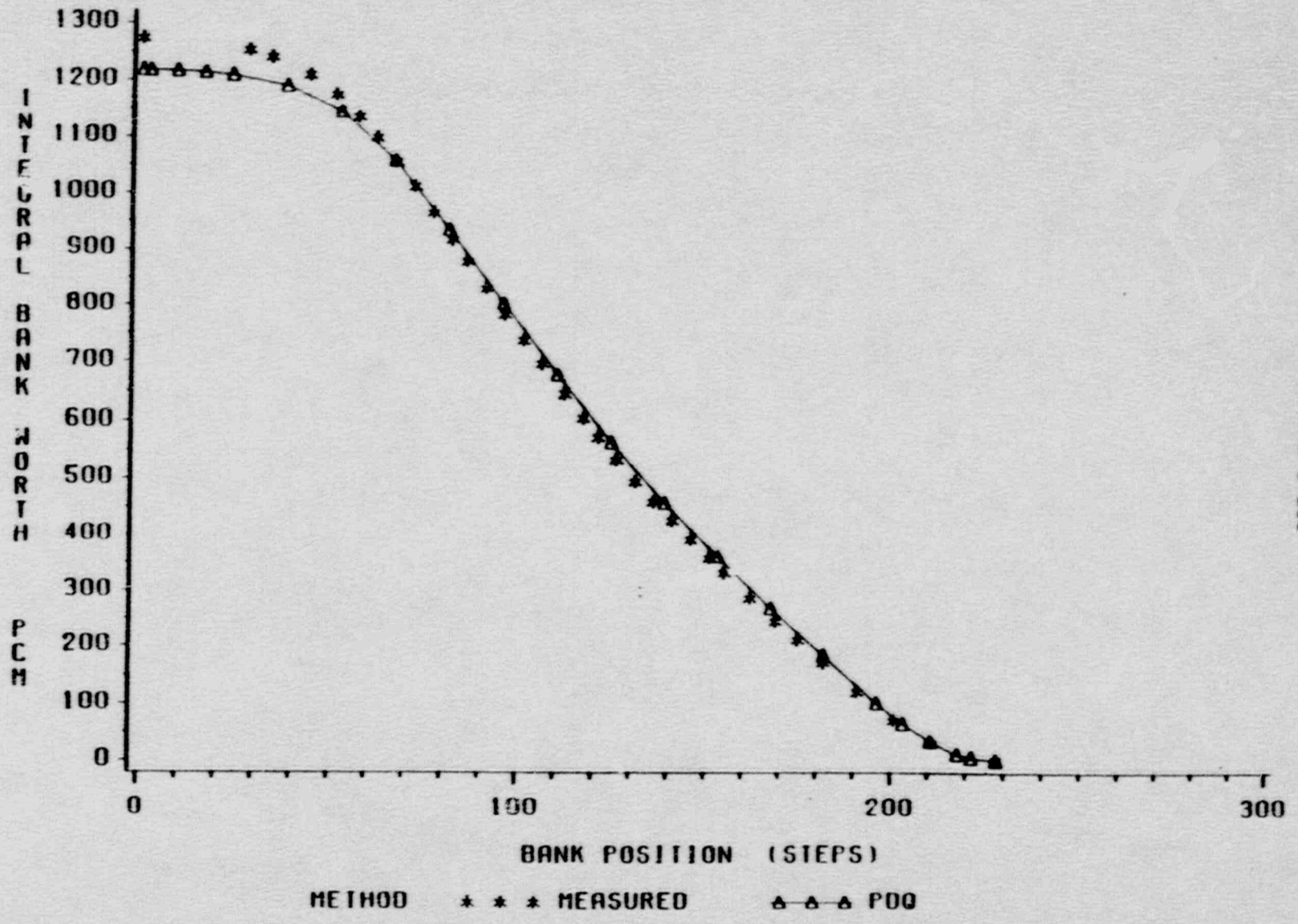

FIGURE 3-205

B BANK DIFFERENTIAL WORTH FOR NORTH ANNA 2, CYCLE 5

PDQ 5X5 AND MEASURED DATA

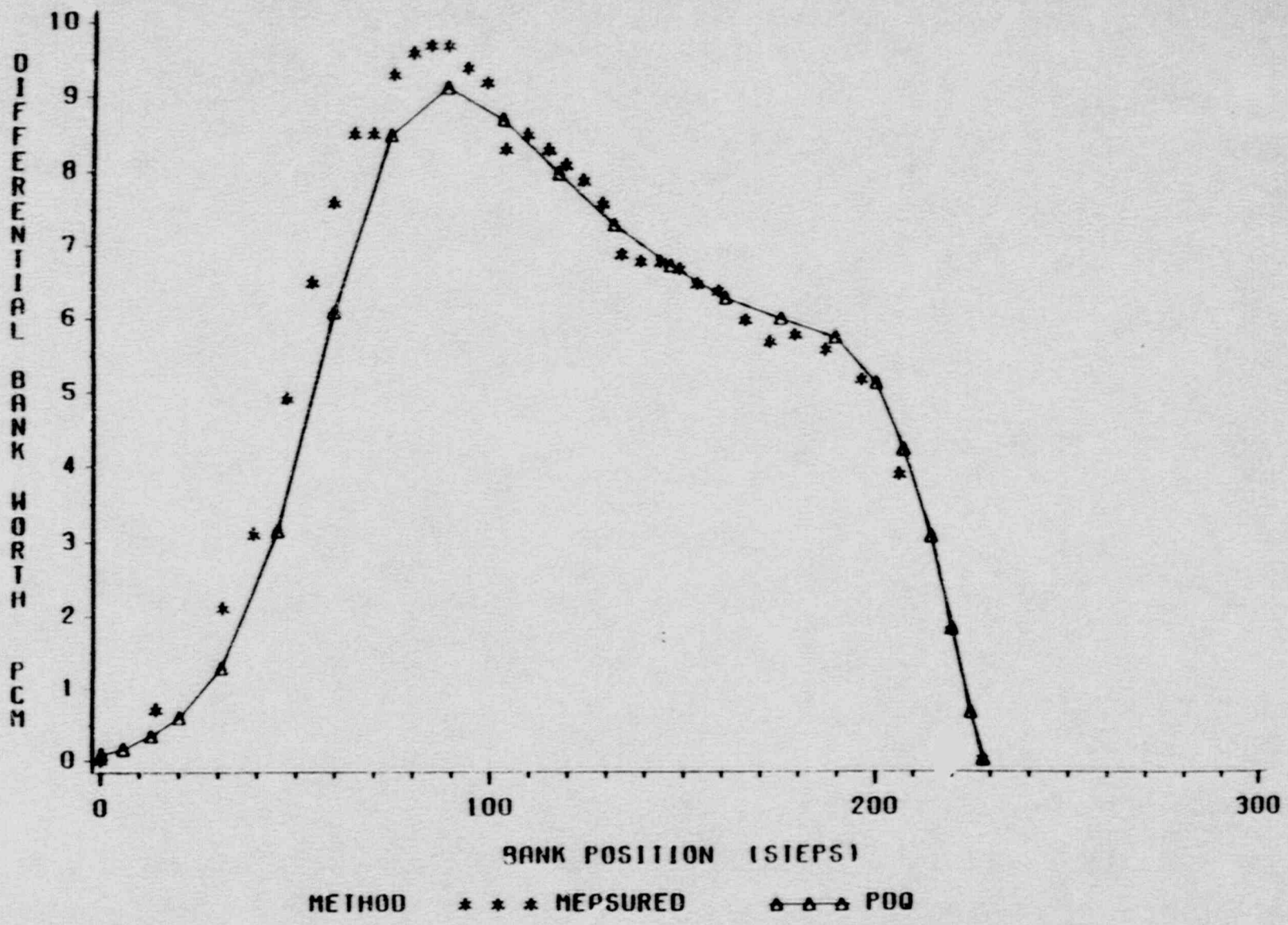

FIGURE 3-206

B BANK INTEGRAL WORTH FOR NORTH ANNA 2, CYCLE 6

PDQ 5X5 AND MEASURED DATA

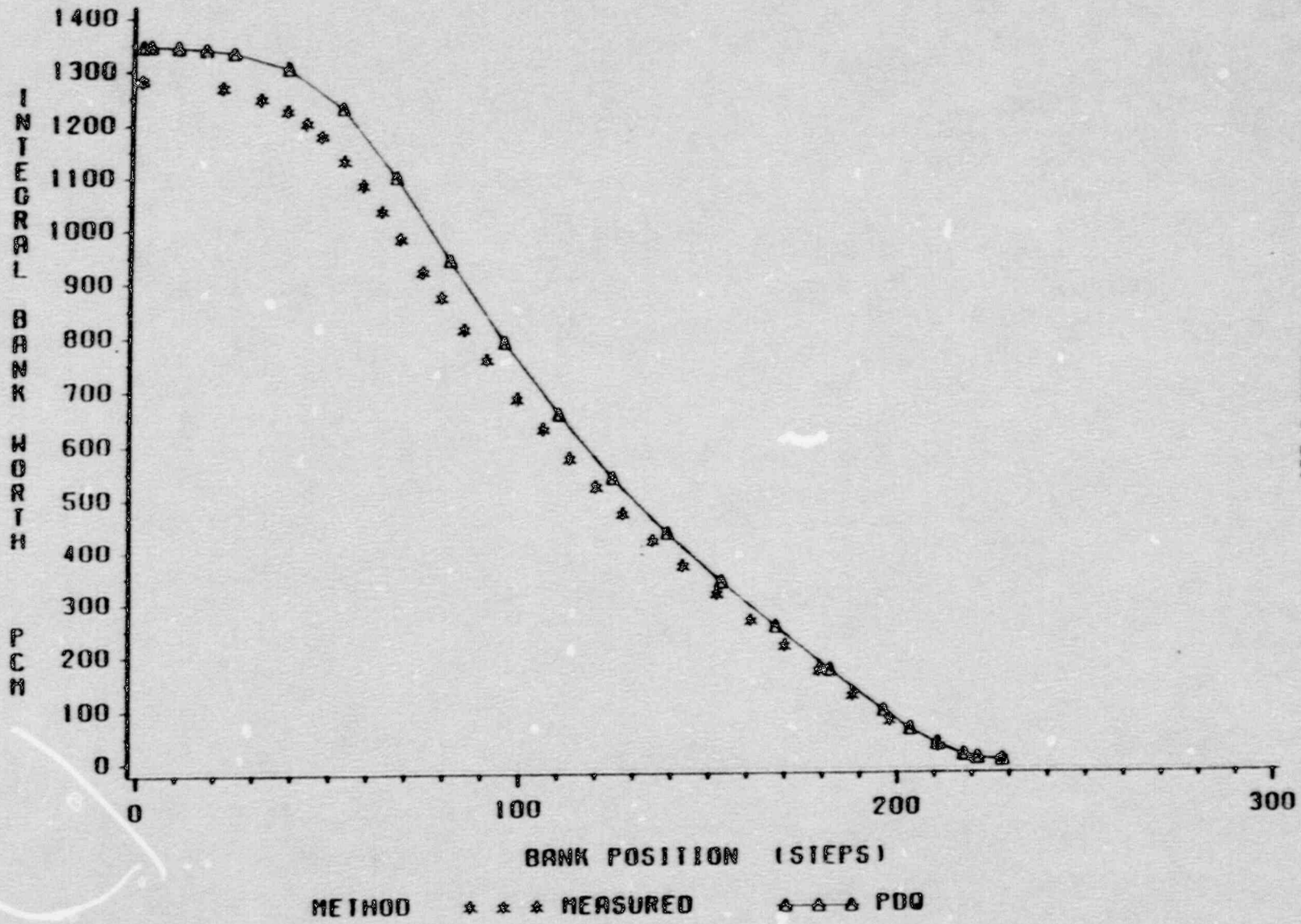

FIGURE 3-207

B BANK DIFFERENTIAL WORTH FOR NORTH ANNA 2, CYCLE 6

PDQ 5X5 AND MEASURED DATA

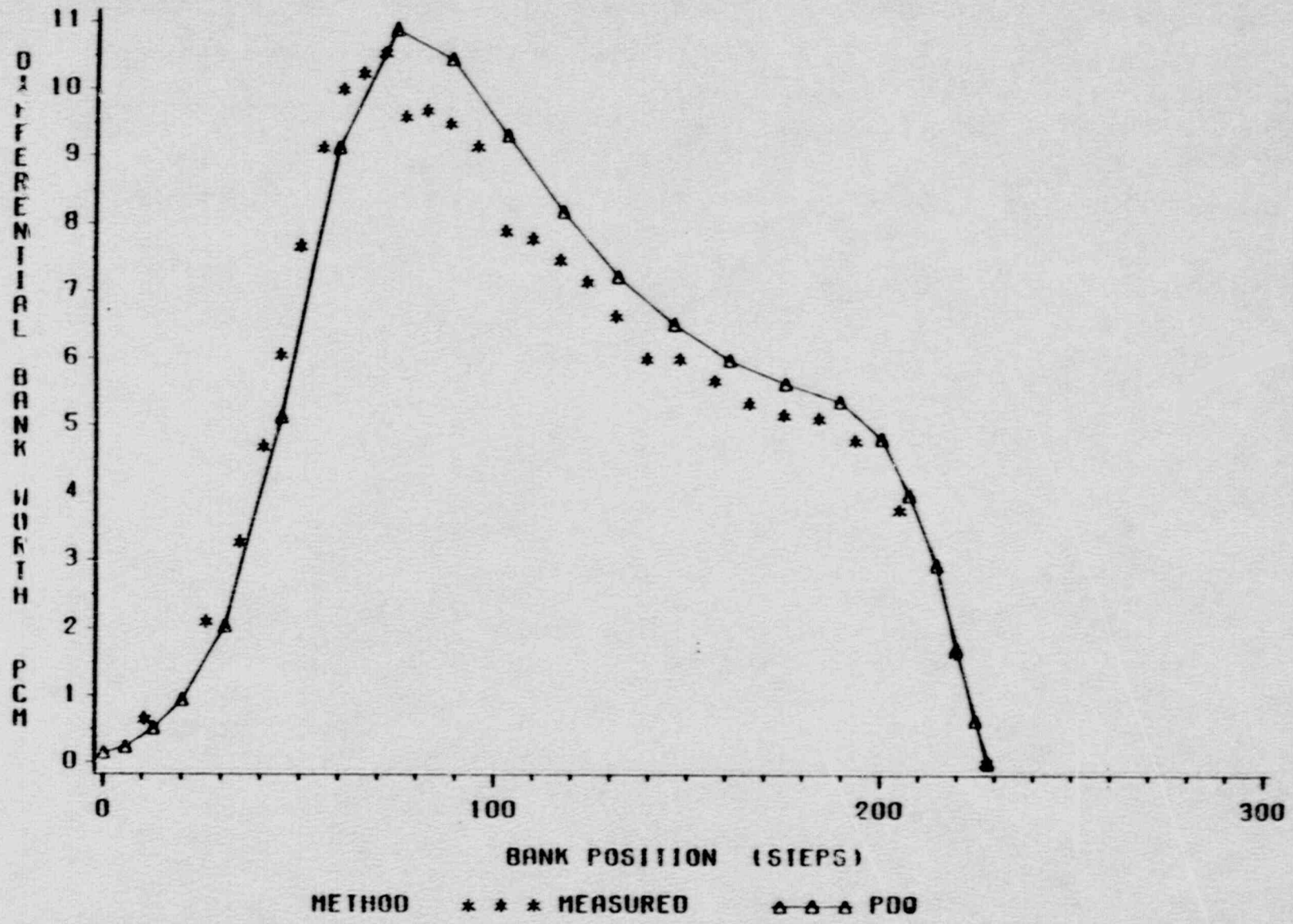

FIGURE 3-208

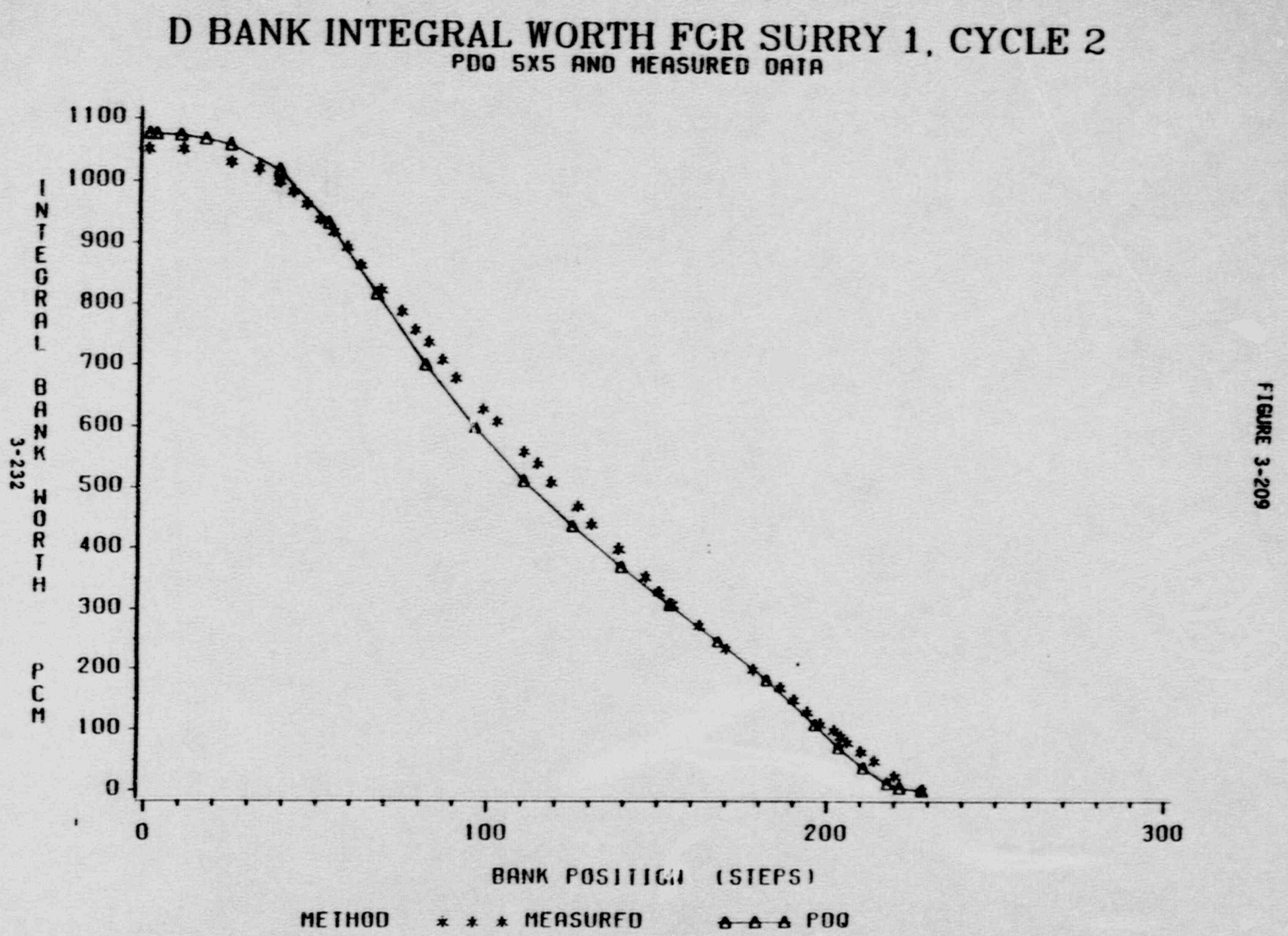
D BANK INTEGRAL WORTH FOR SURRY 1, CYCLE 2
PDQ 5X5 AND MEASURED DATA
INTEGRAL BANK WORTH PCM
1100
1000
900
800
700
600
500
400
300
200
100
0
0
100
200
300
BANK POSITION (STEPS)
METHOD * * * MEASURED △ △ △ PDQ

FIGURE 3-209

D BANK DIFFERENTIAL WORTH FOR SURRY 1, CYCLE 2

PDQ 5X5 AND MEASURED DATA

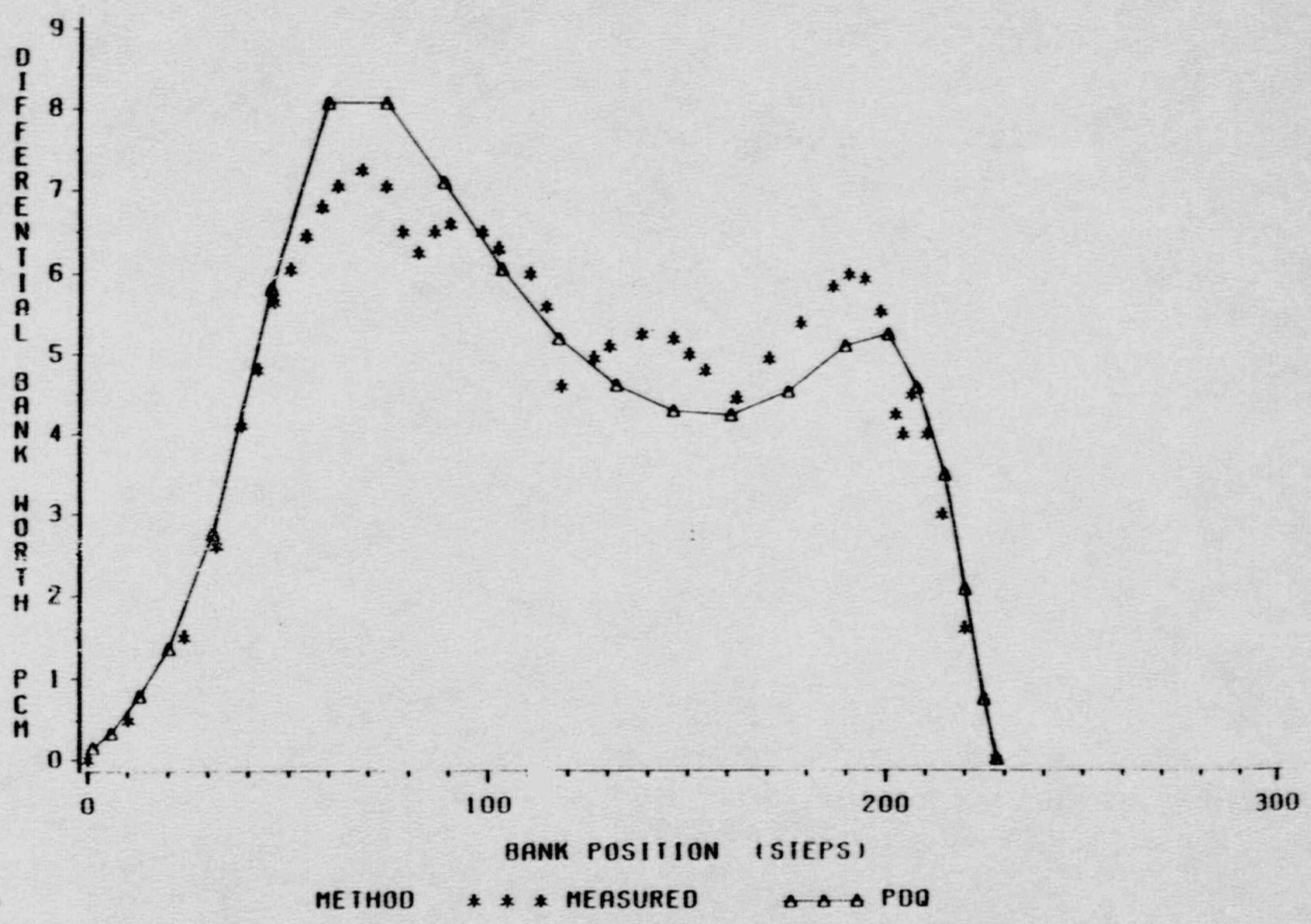

FIGURE 3-210

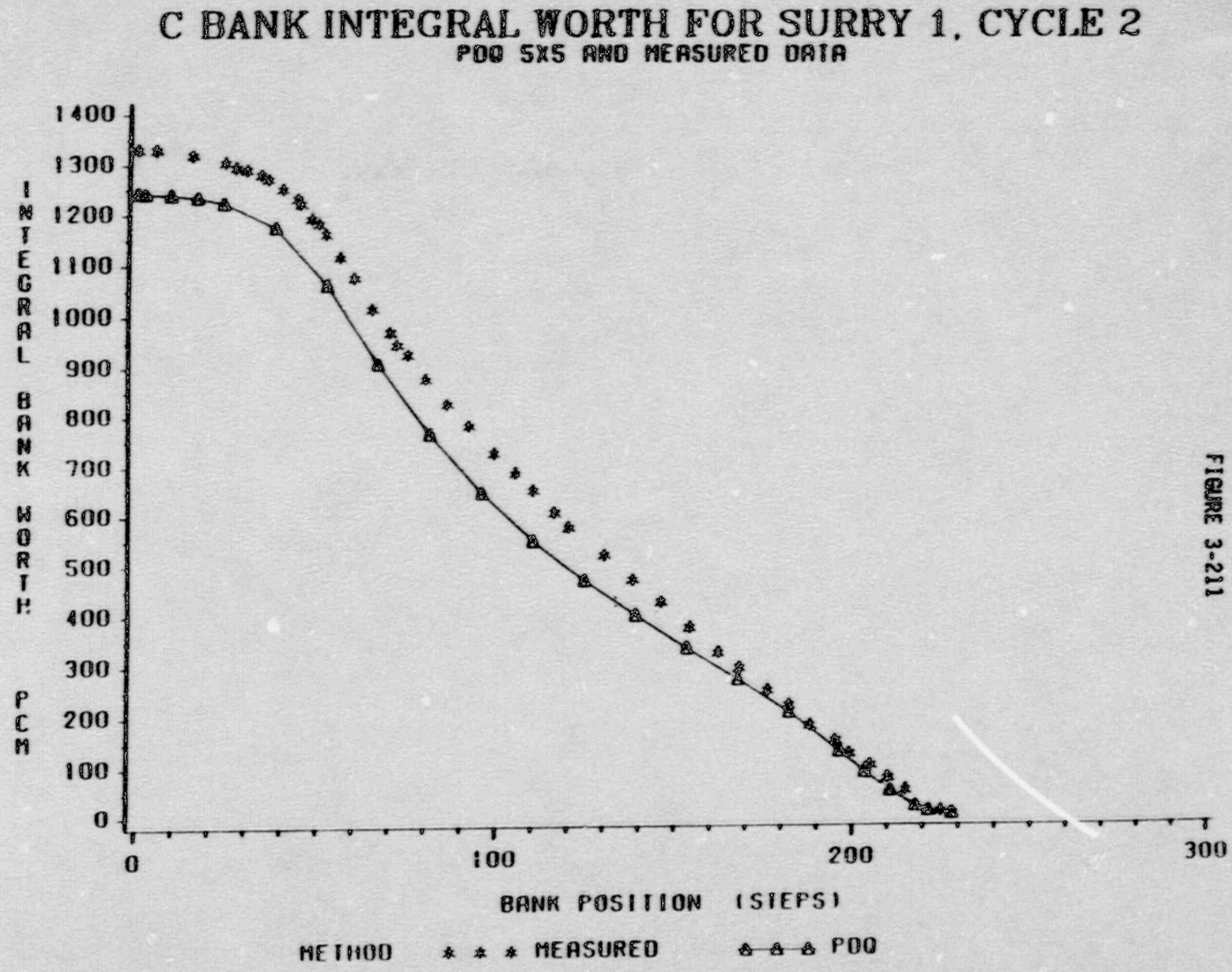
C BANK INTEGRAL WORTH FOR SURRY 1, CYCLE 2
PDQ 5X5 AND MEASURED DATA
INTEGRAL BANK WORTH PCM
1400
1300
1200
1100
1000
900
800
700
600
500
400
300
200
100
0
0
100
200
300
BANK POSITION (STEPS)
METHOD * * * MEASURED △ △ △ PDQ

FIGURE 3-211

C BANK DIFFERENTIAL WORTH FOR SURRY 1, CYCLE 2

PDQ 5X5 AND MEASURED DATA

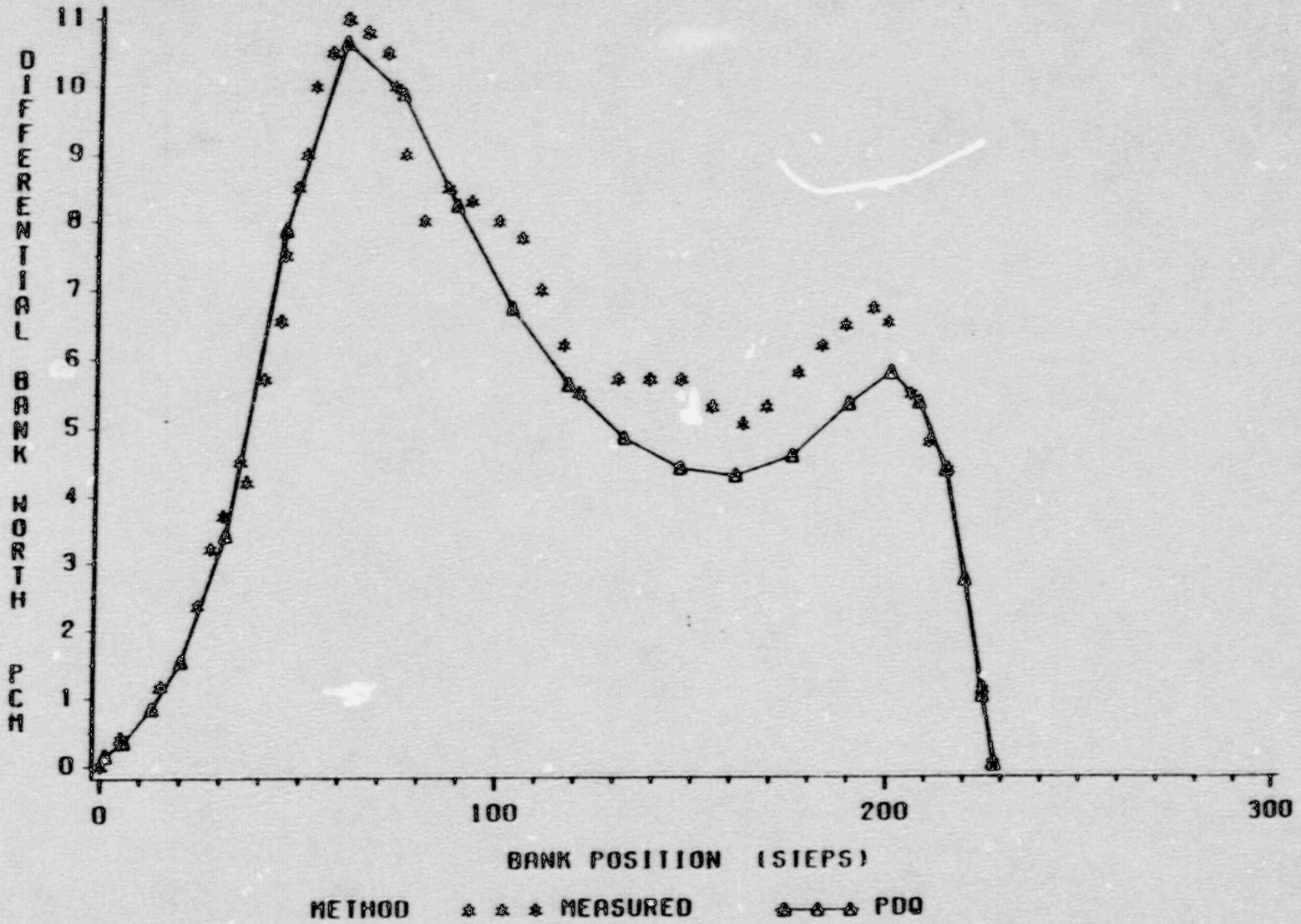

FIGURE 3-212

D BANK INTEGRAL WORTH FOR SURRY 1, CYCLE 3

PDQ 5X5 AND MEASURED DATA

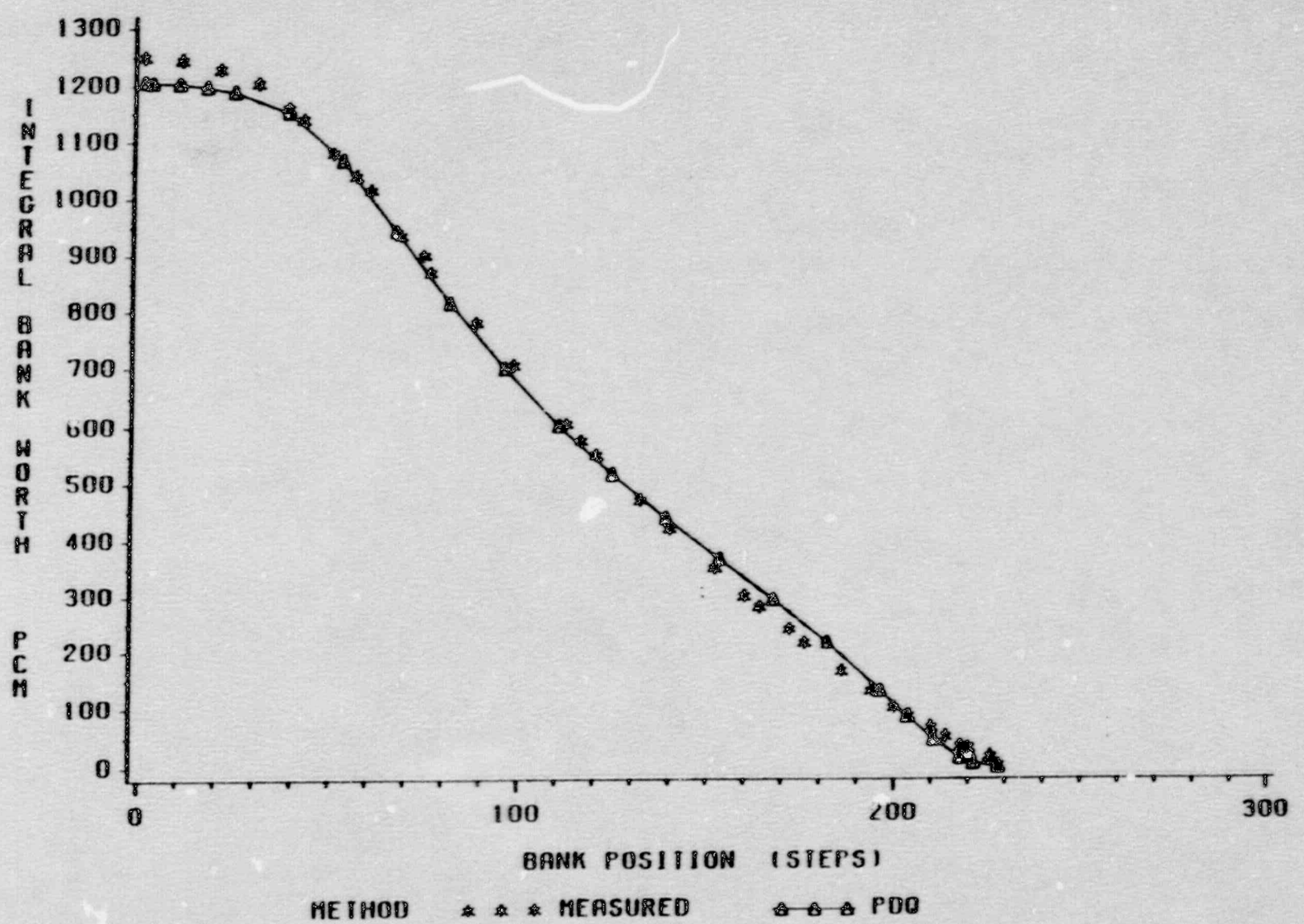

FIGURE 3-213

D BANK DIFFERENTIAL WORTH FOR SURRY 1, CYCLE 3

PDQ 5X5 AND MEASURED DATA

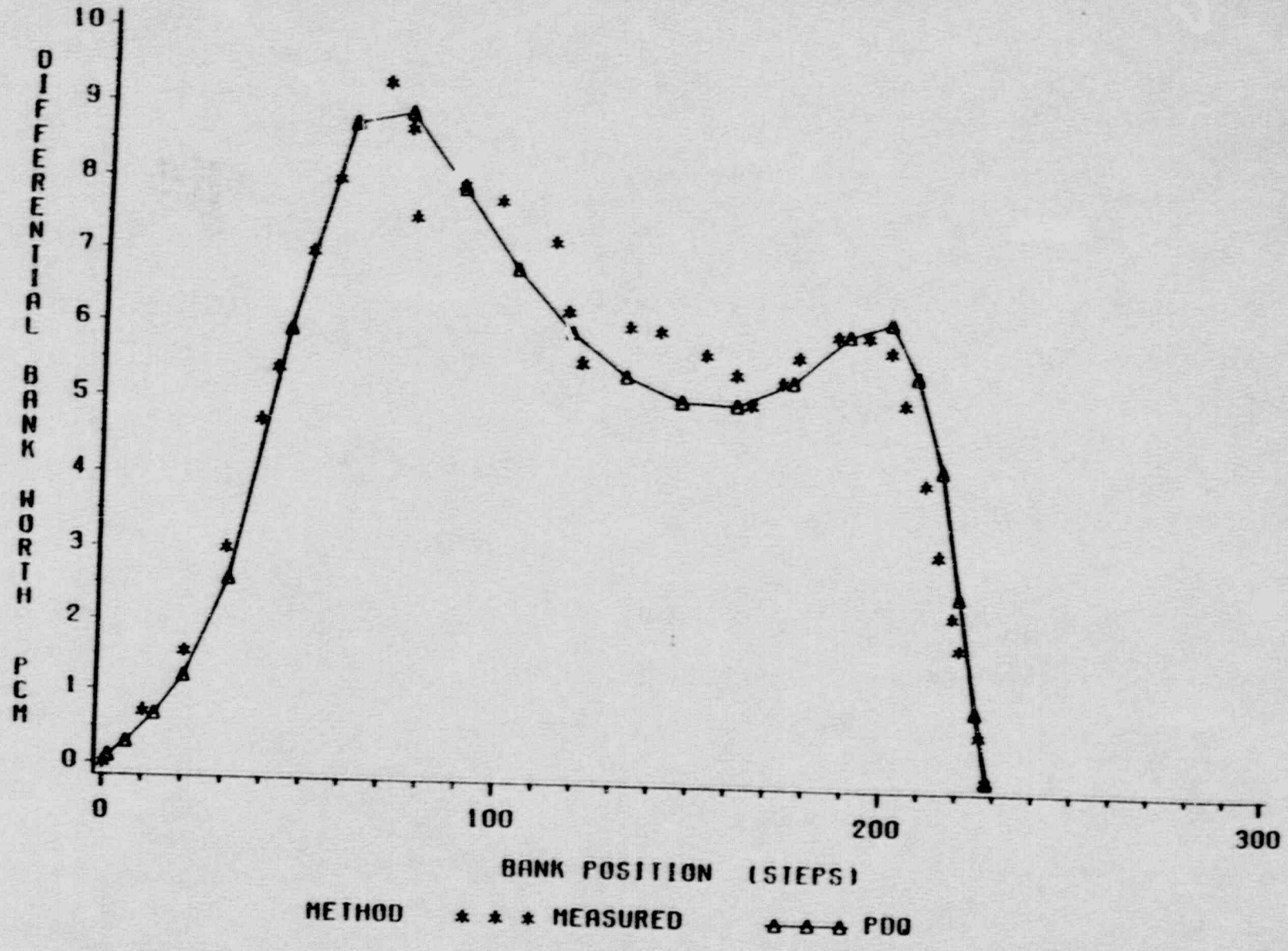

FIGURE 3-214

C BANK INTEGRAL WORTH FOR SURRY 1, CYCLE 3

PDQ 5X5 AND MEASURED DATA

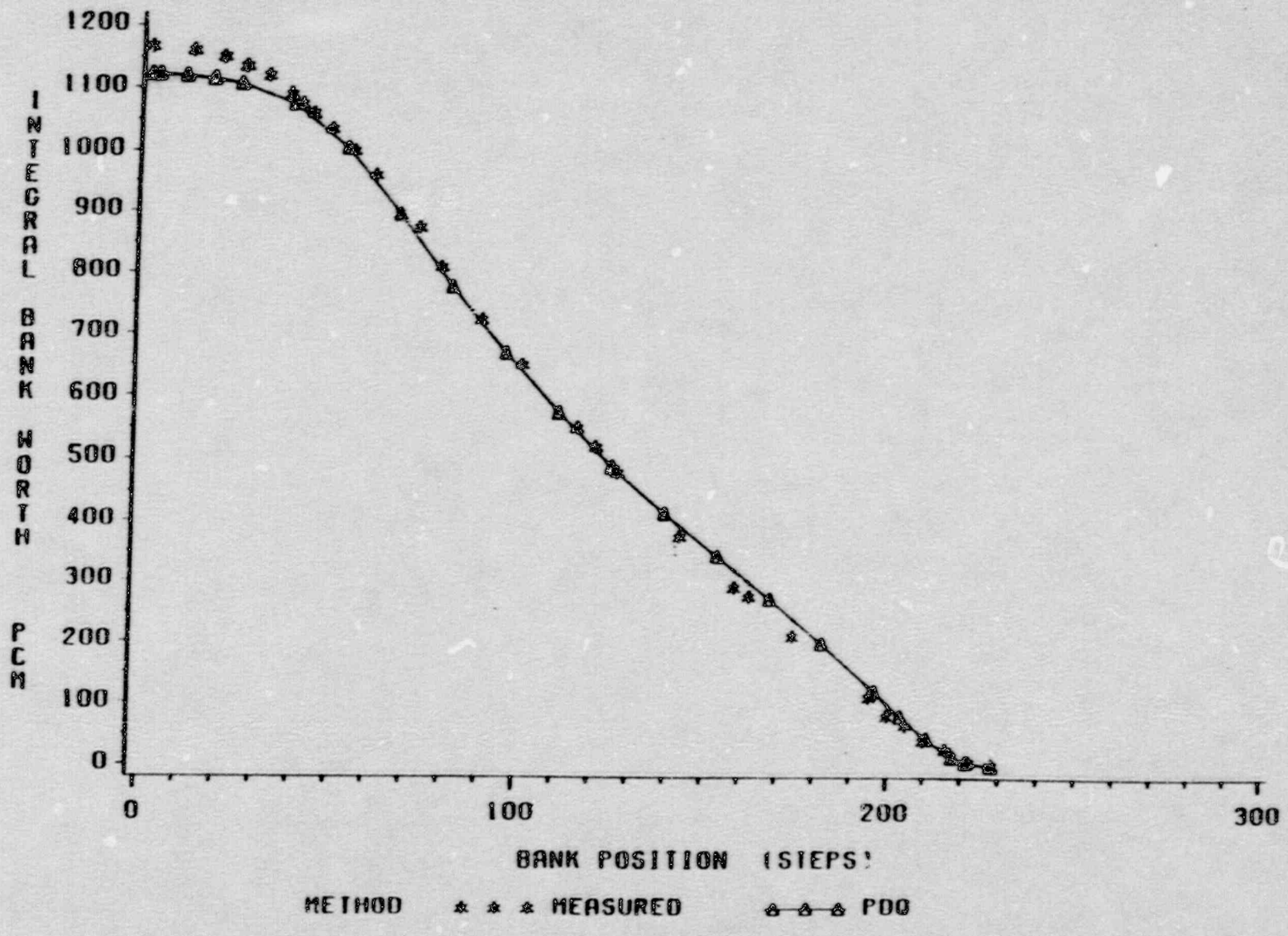

FIGURE 3-215

C BANK DIFFERENTIAL WORTH FOR SURRY 1, CYCLE 3

PDC 5X5 AND MEASURED DATA

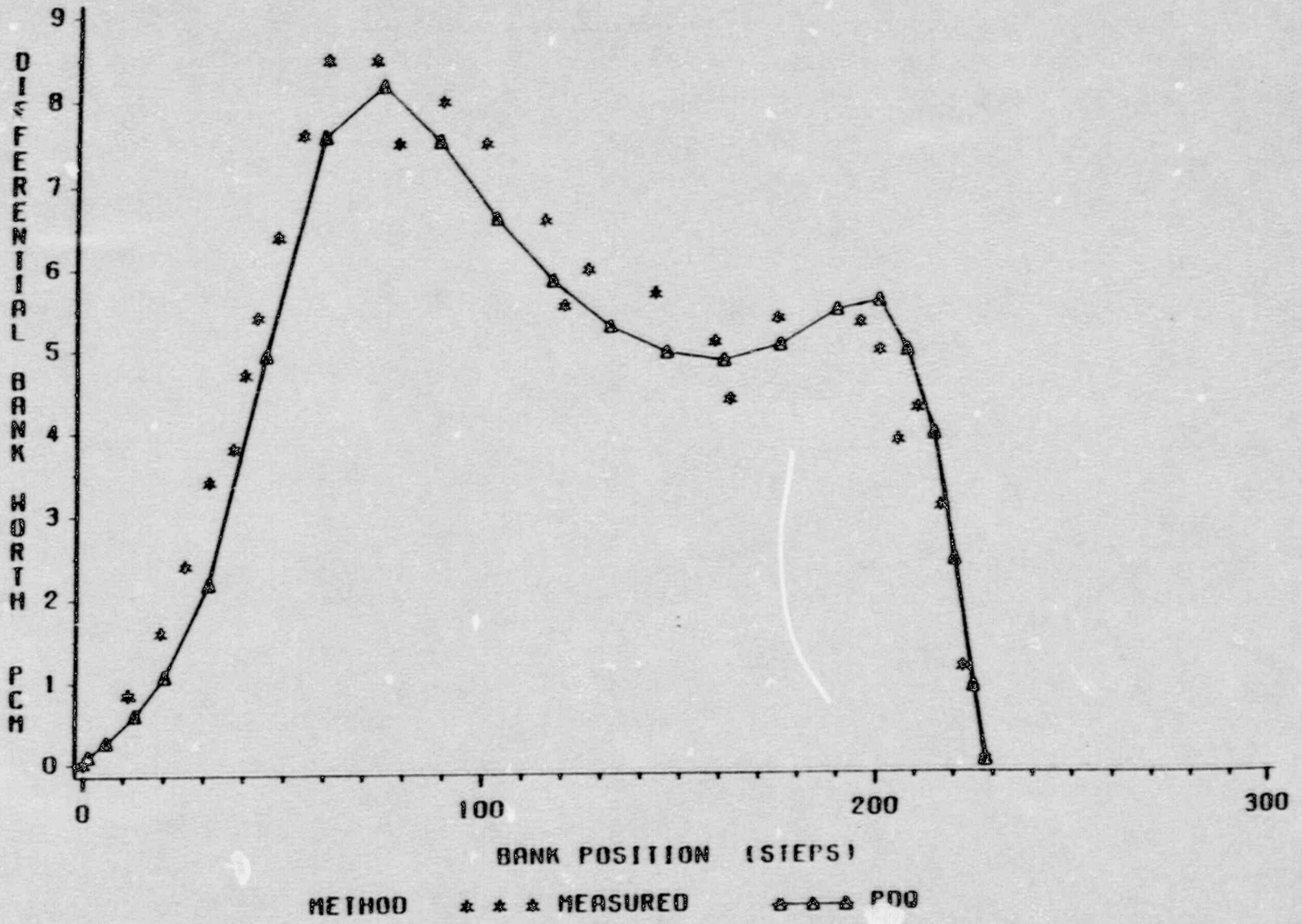

FIGURE 3-216

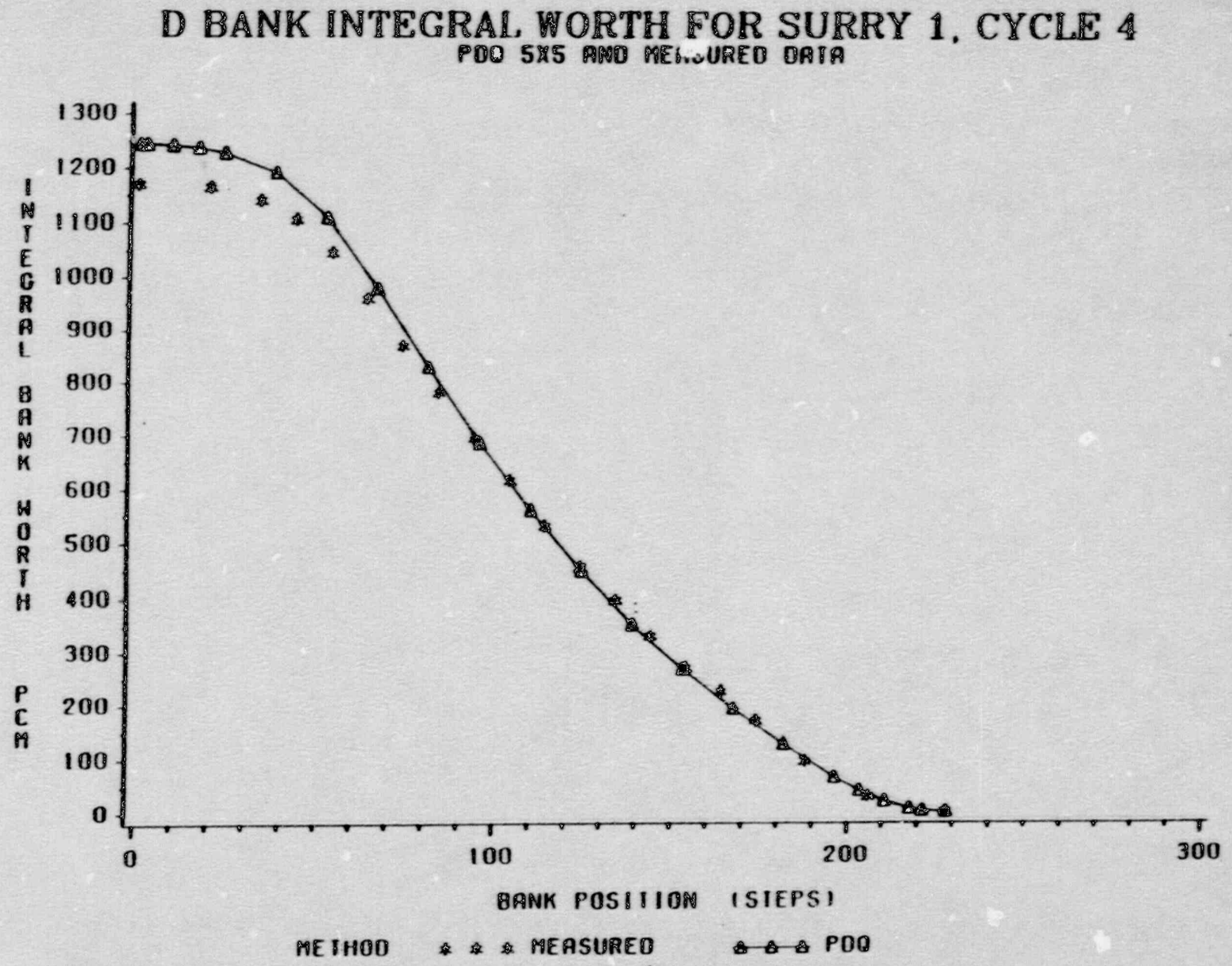
D BANK INTEGRAL WORTH FOR SURRY 1, CYCLE 4
PDQ 5X5 AND MEASURED DATA
INTEGRAL BANK WORTH PCM
1300
1200
1100
1000
900
800
700
600
500
400
300
200
100
0
0
100
200
300
BANK POSITION (STEPS)
METHOD
MEASURED
PDQ

FIGURE 3-217

D BANK DIFFERENTIAL WORTH FOR SURRY 1, CYCLE 4

PDQ 5X5 AND MEASURED DATA

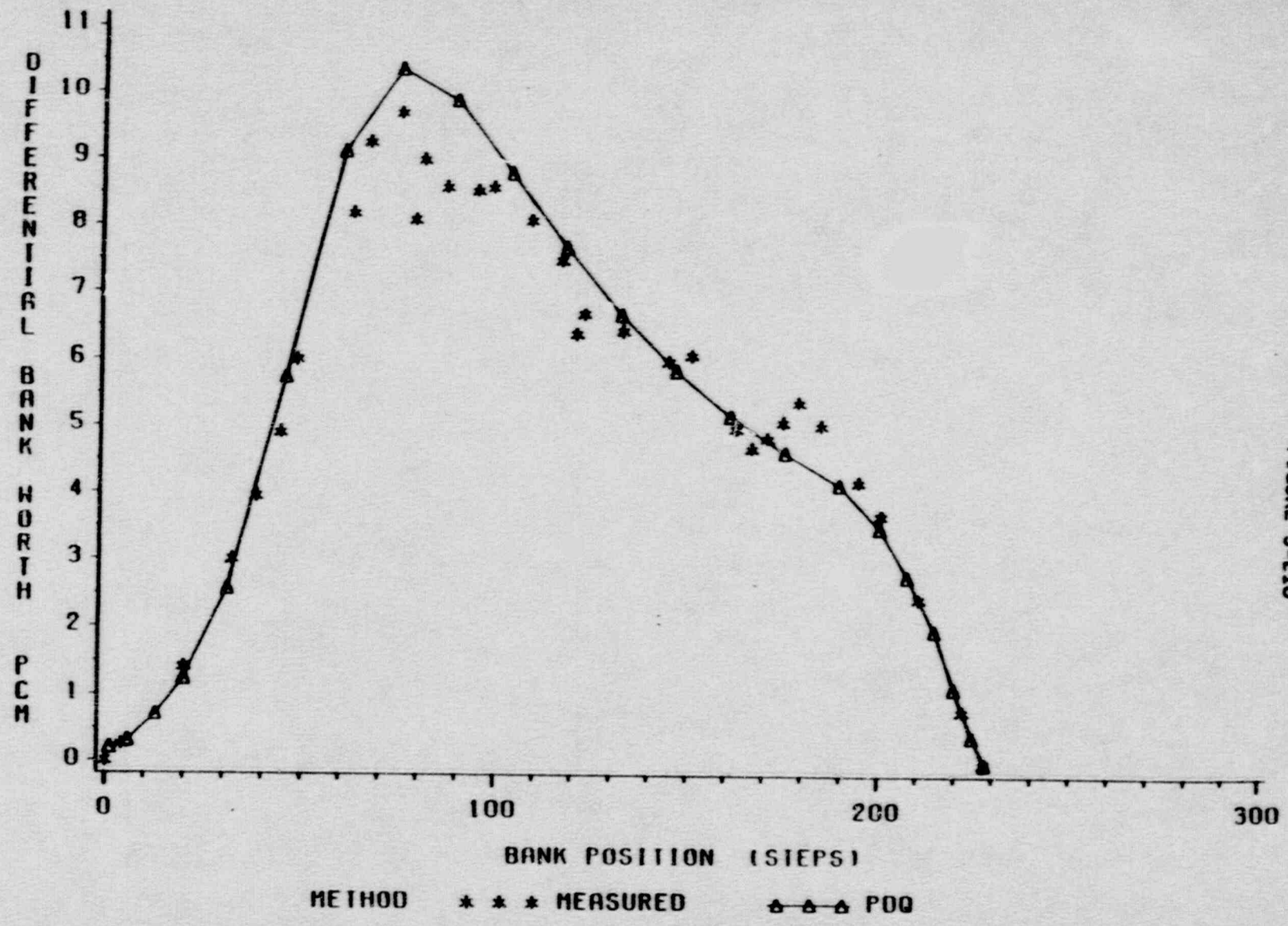

FIGURE 3-218

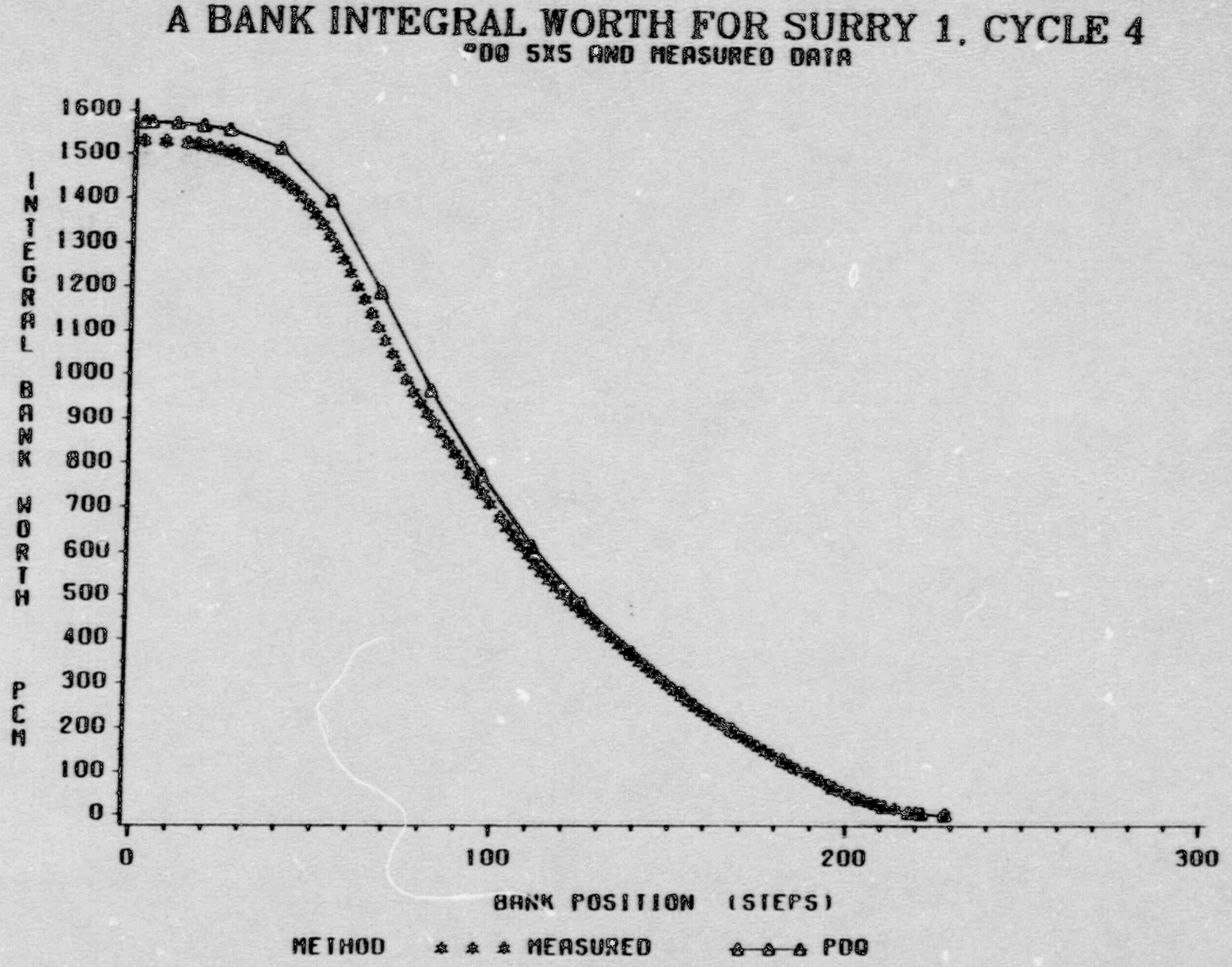
A BANK INTEGRAL WORTH FOR SURRY 1, CYCLE 4
PDQ 5XS AND MEASURED DATA
INTEGRAL BANK WORTH PCM
1600
1500
1400
1300
1200
1100
1000
900
800
700
600
500
400
300
200
100
0
0
100
200
300
BANK POSITION (STEPS)
METHOD * * * MEASURED Δ—Δ—Δ PDQ

FIGURE 3-219

A BANK DIFFERENTIAL WORTH FOR SURRY 1, CYCLE 4

PDQ 5X5 AND MEASURED DATA

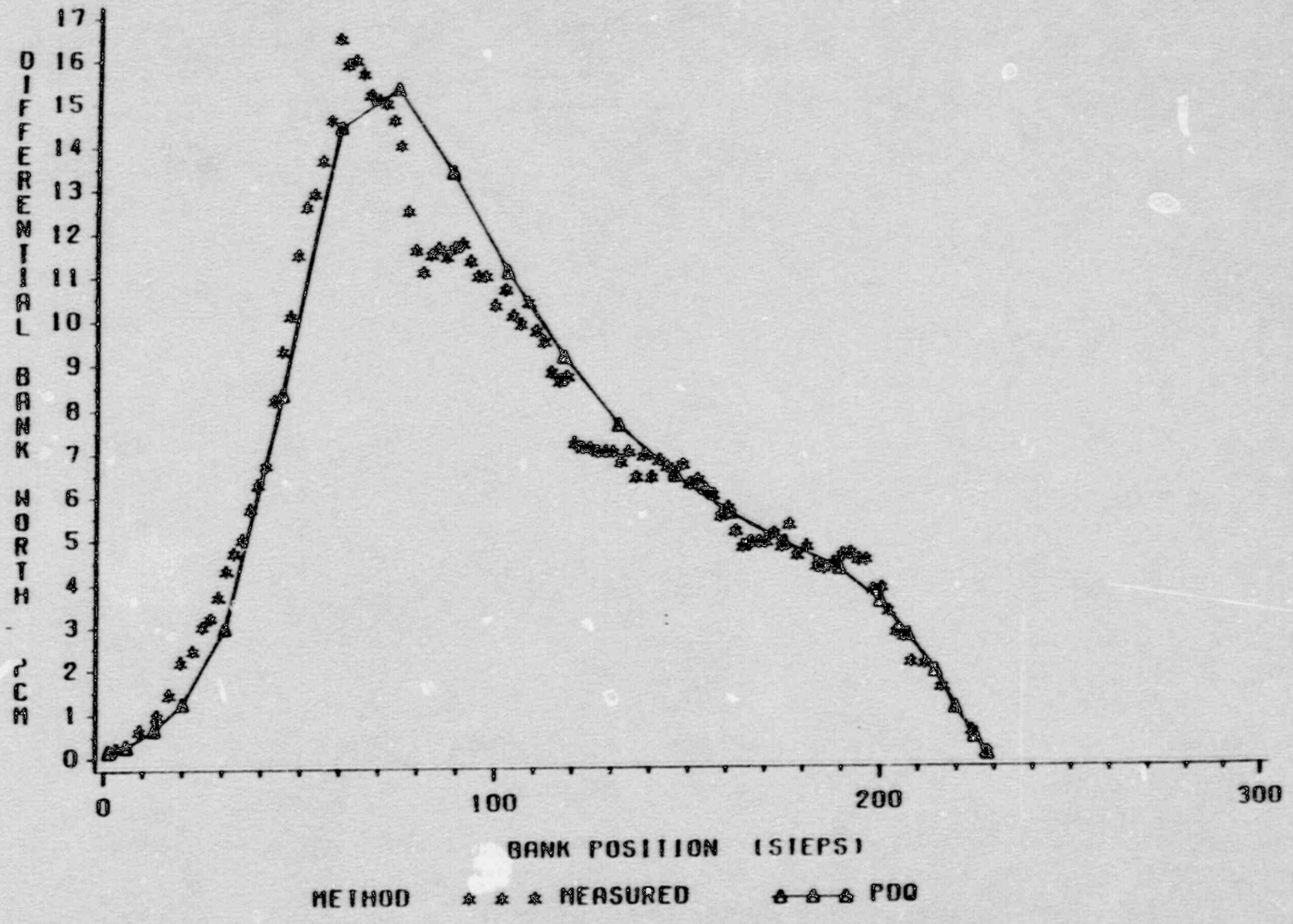

FIGURE 3-220

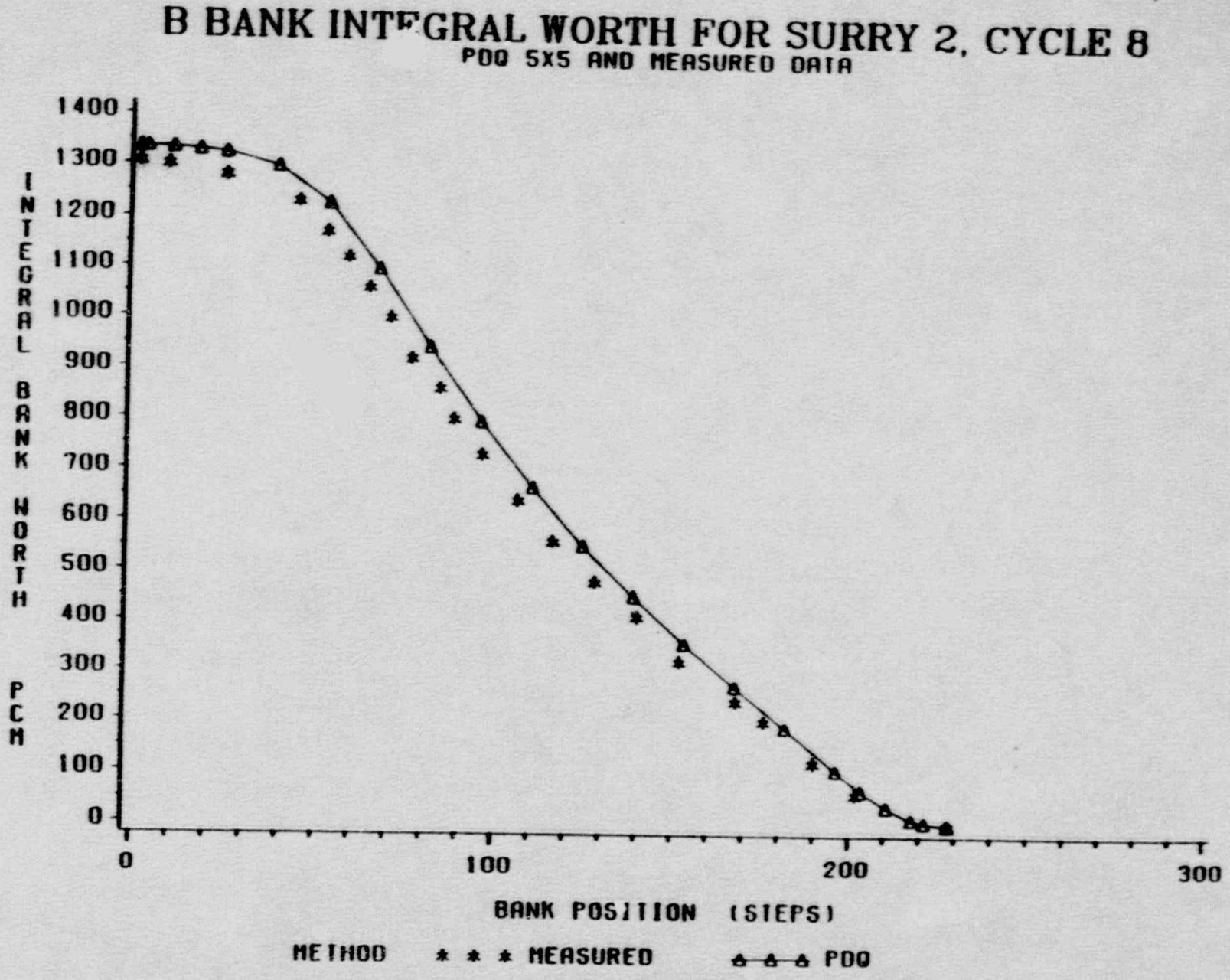
B BANK INTEGRAL WORTH FOR SURRY 2, CYCLE 8
PDQ 5X5 AND MEASURED DATA
INTEGRAL BANK WORTH PCM
1400
1300
1200
1100
1000
900
800
700
600
500
400
300
200
100
0
0
100
200
300
BANK POSITION (STEPS)
METHOD * * * MEASURED △ △ △ PDQ

FIGURE 3-221

B BANK DIFFERENTIAL WORTH FOR SURRY 2, CYCLE 8

PDQ 5X5 AND MEASURED DATA

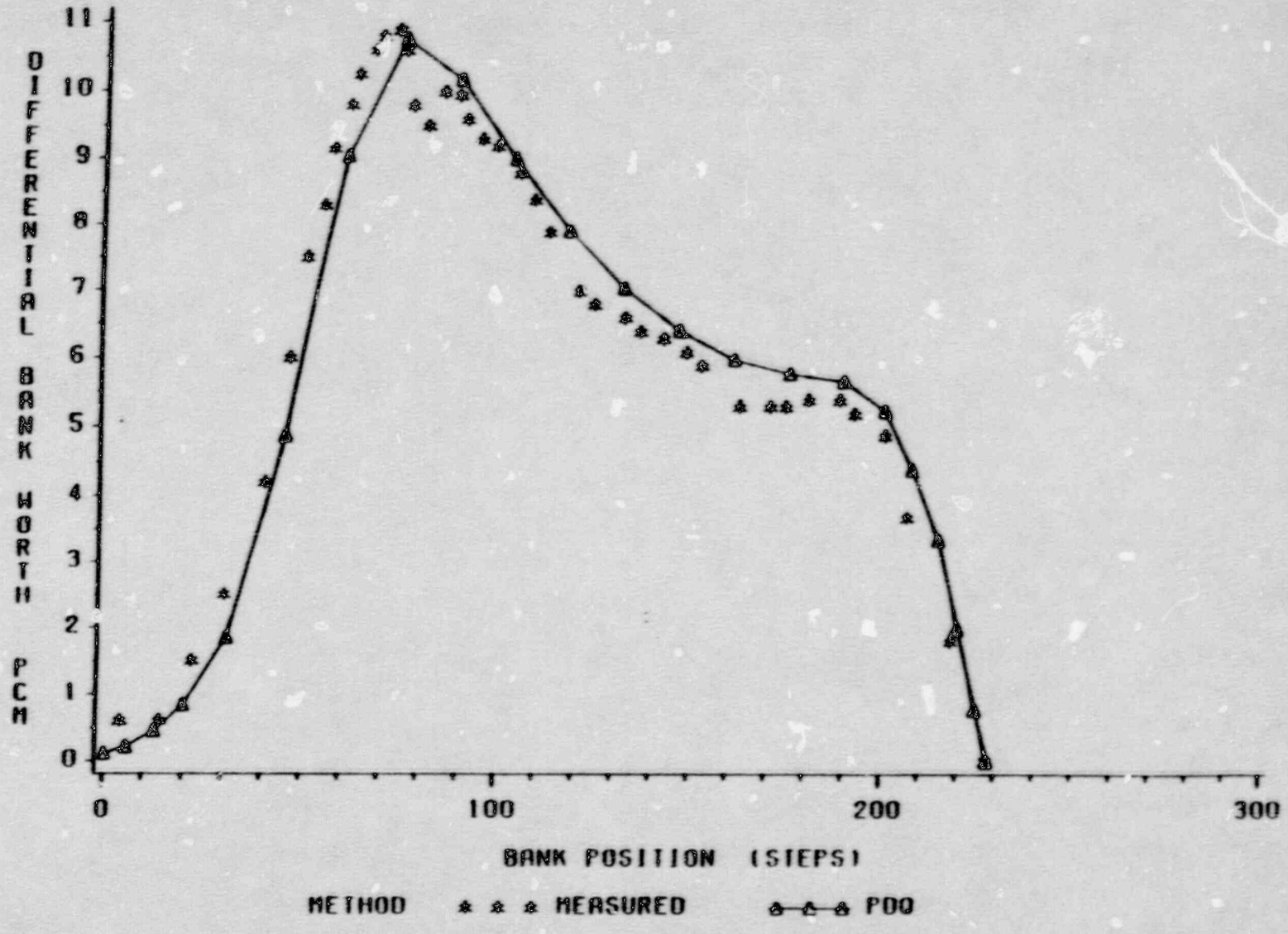

FIGURE 3-222

B BANK INTEGRAL WORTH FOR SURRY 2, CYCLE 9

PDQ 5X5 AND MEASURED DATA

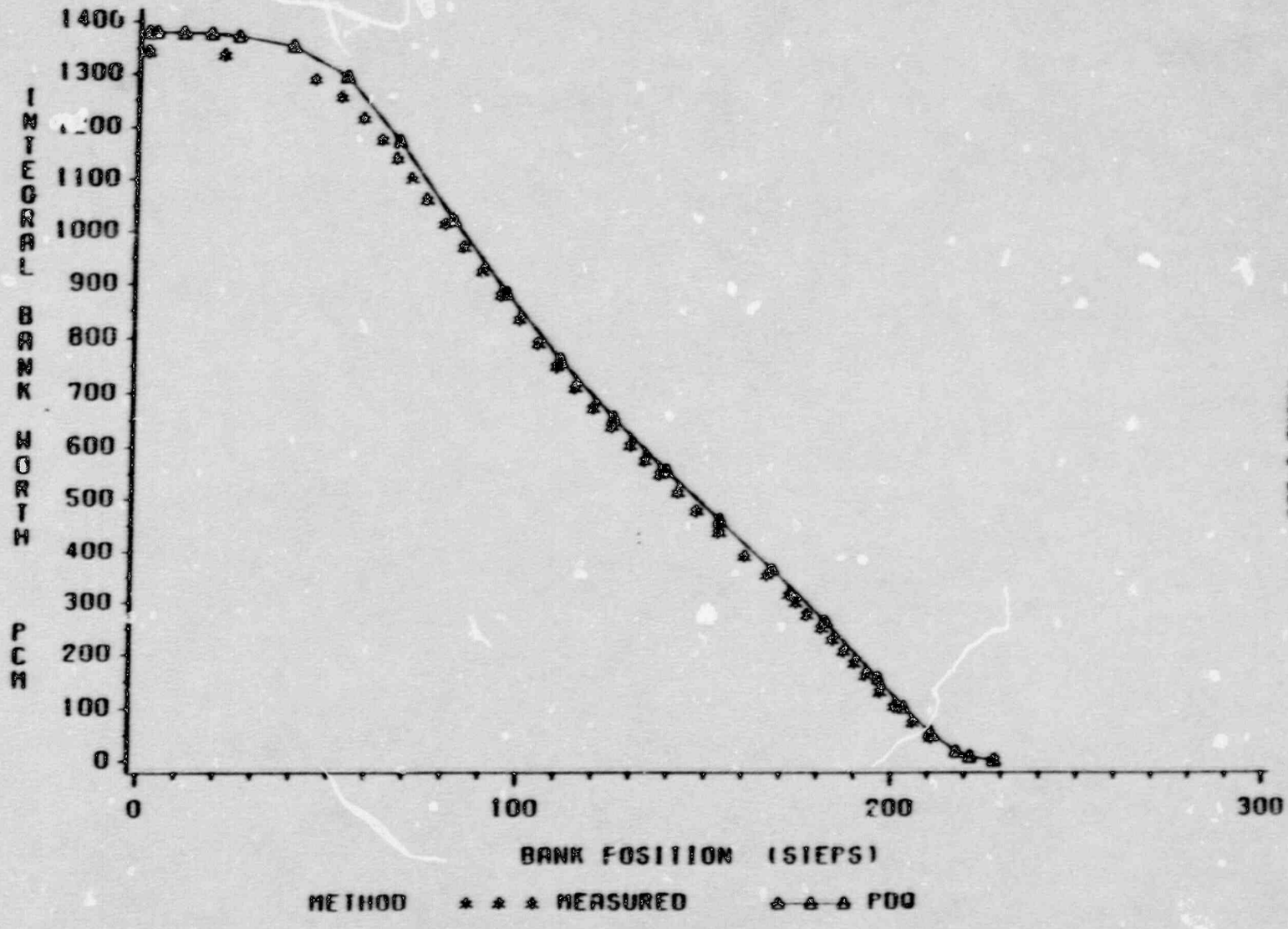

FIGURE 3-223

B BANK DIFFERENTIAL WORTH FOR SURRY 2, CYCLE 9

PDQ 5X5 AND MEASURED DATA

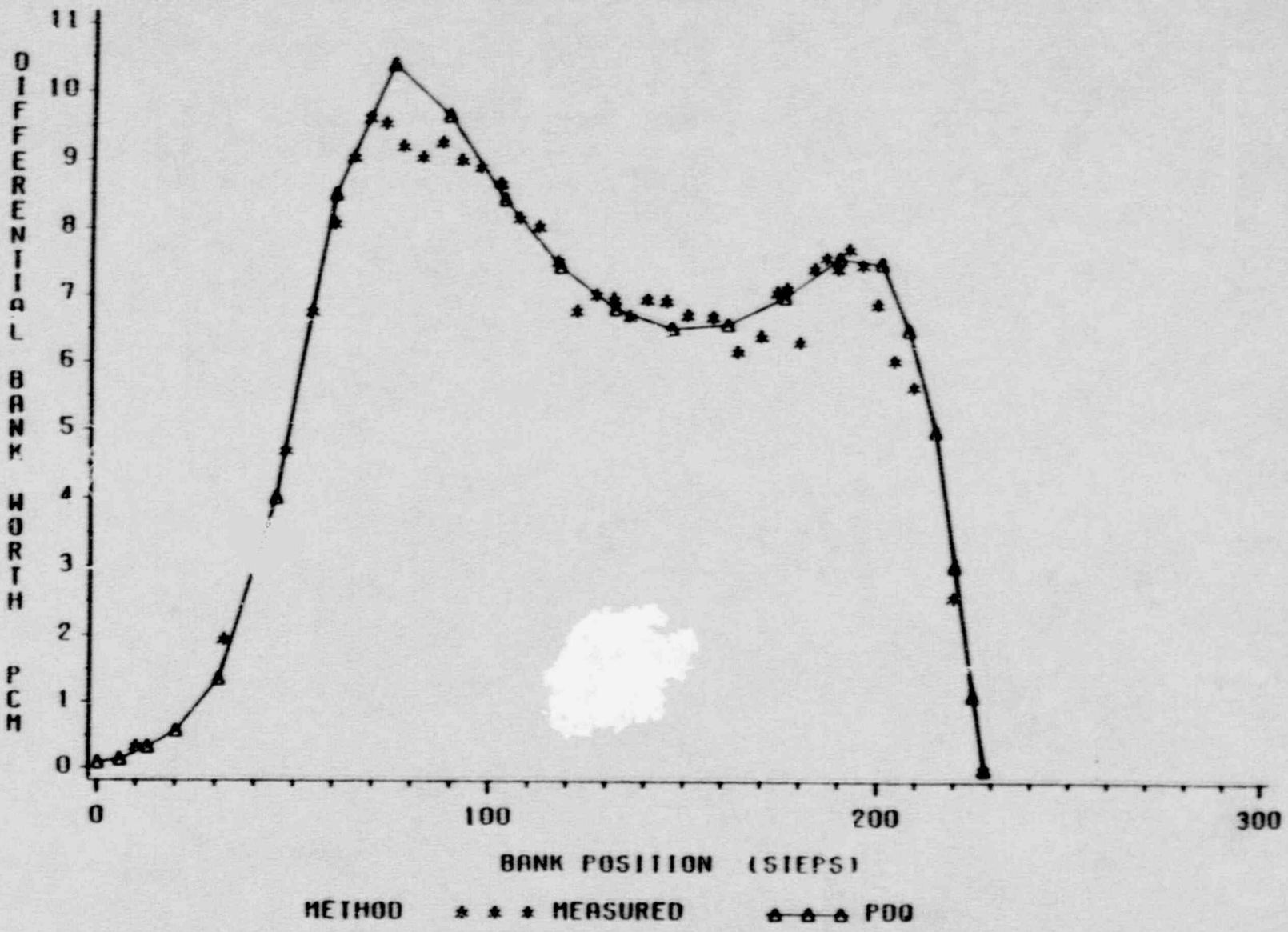

FIGURE 3-224

SURRY AND NORTH ANNA DIFFERENTIAL BORON WORTH: MEASURED VERSUS PREDICTED

STARTUP ACCEPTANCE CRITERIA: +/- 10%

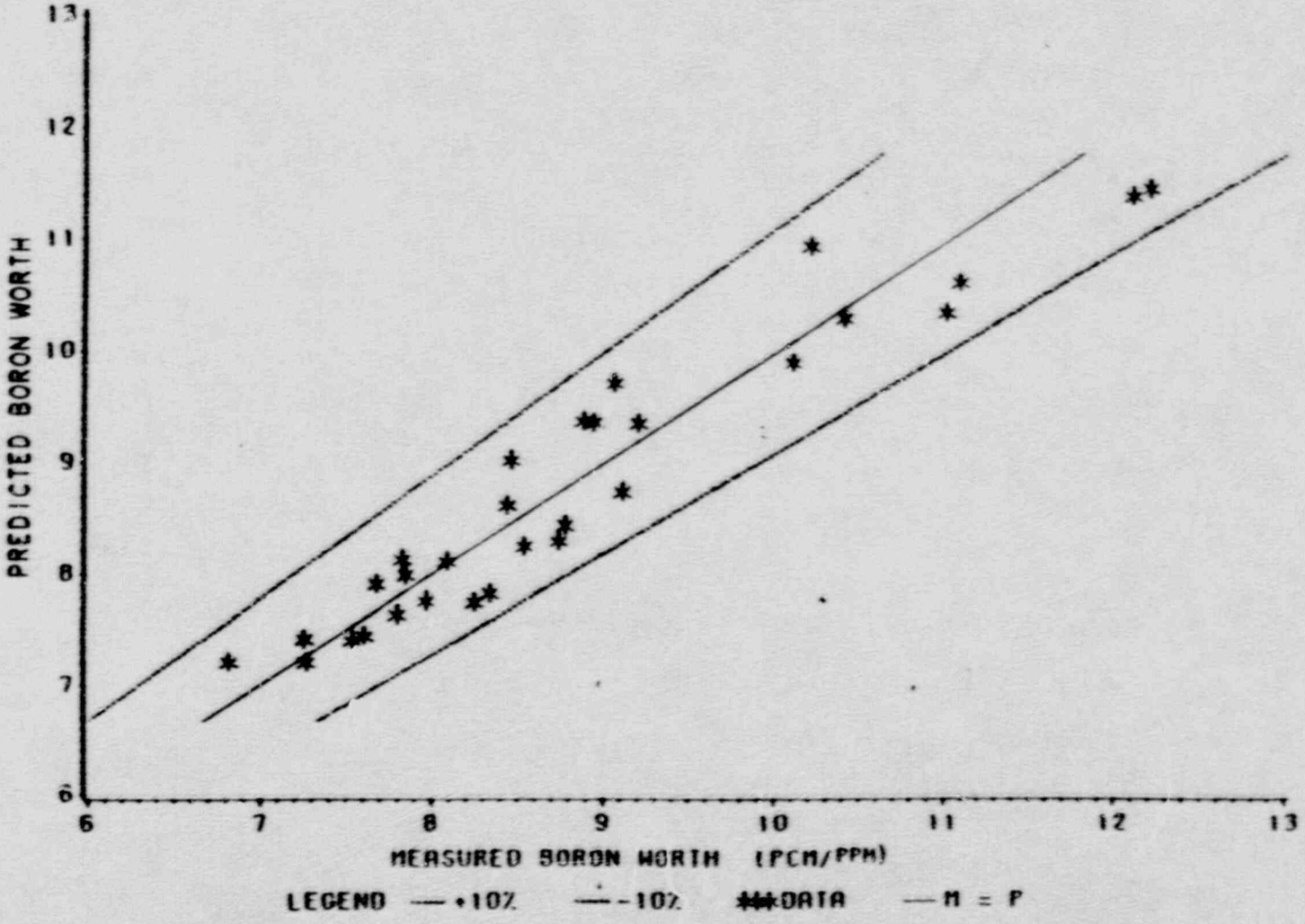

FIGURE 3-225

BORON LETDOWN CURVES FOR N1C1 AND N2C1

PDQ 3-D AND MEASURED

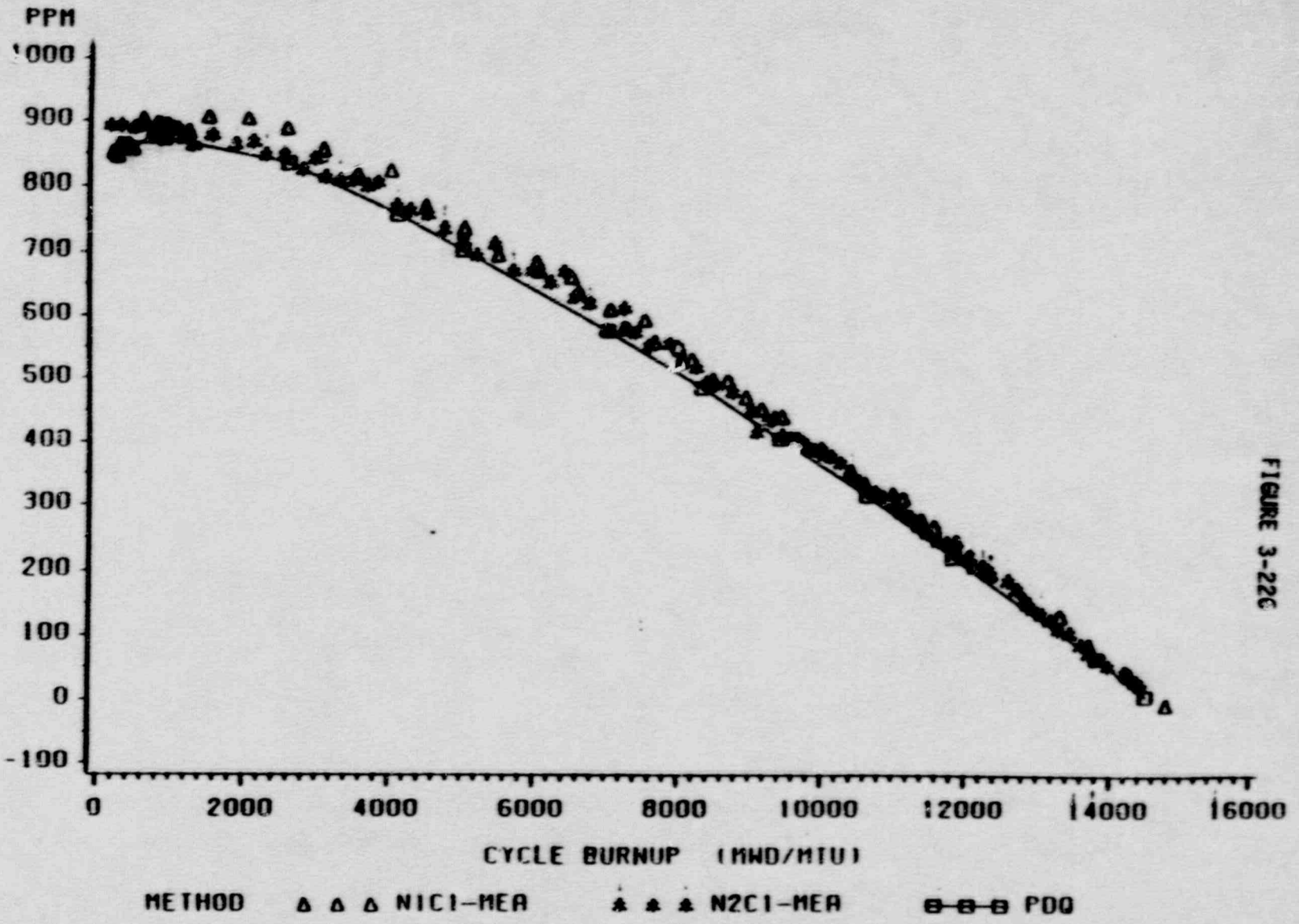

FIGURE 3-22C

BORON LETDOWN CURVES FOR N1C2

PDQ 3-D AND MEASURED

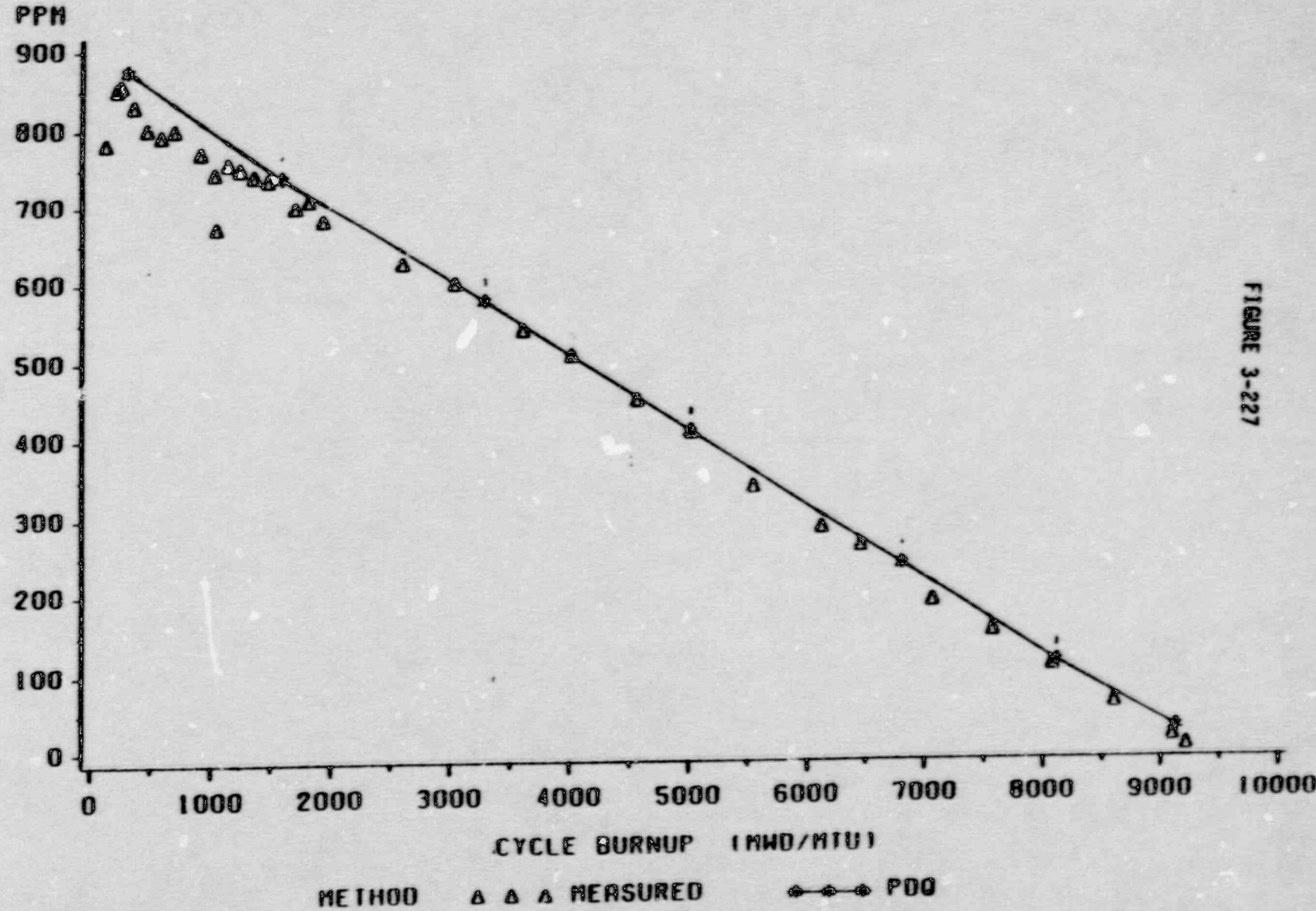

FIGURE 3-227

BORON LETDOWN CURVES FOR N1C3

PDQ 3-D AND MEASURED

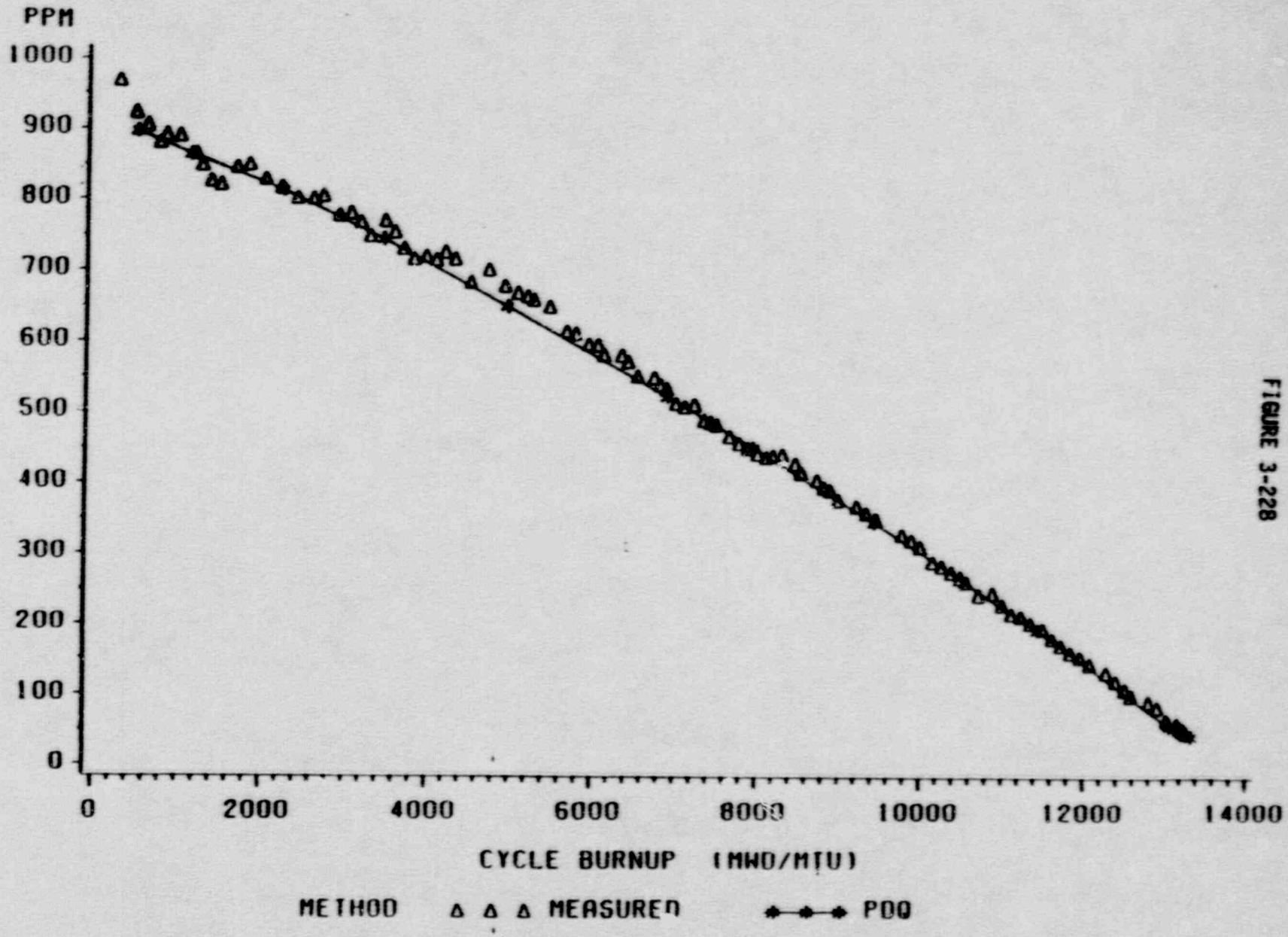

FIGURE 3-228

BORON LETDOWN CURVES FOR N1C4

PDQ 3-D AND MEASURED

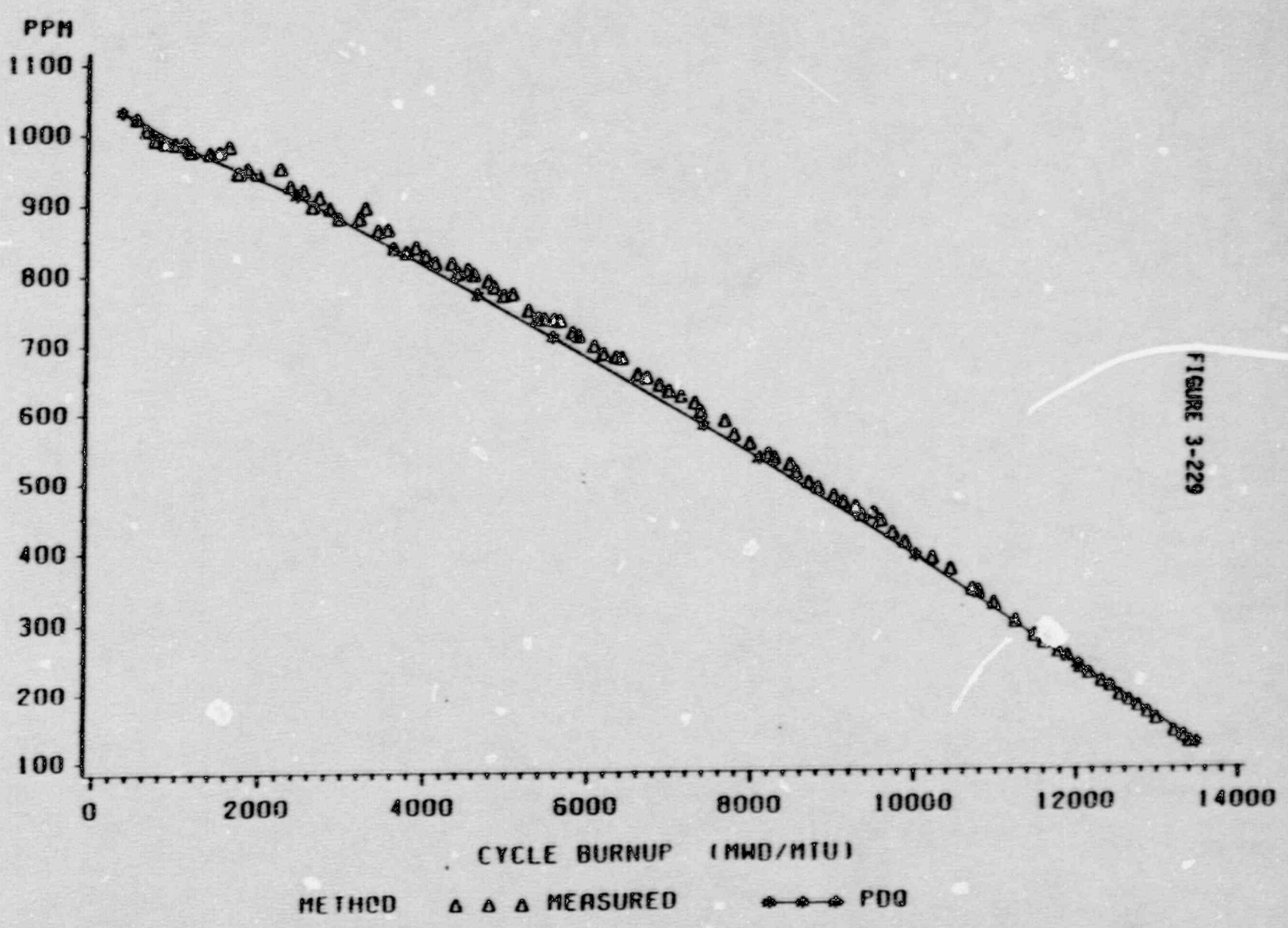

FIGURE 3-229

BORON LETDOWN CURVES FOR N1C5

PDQ 3-D AND MEASURED

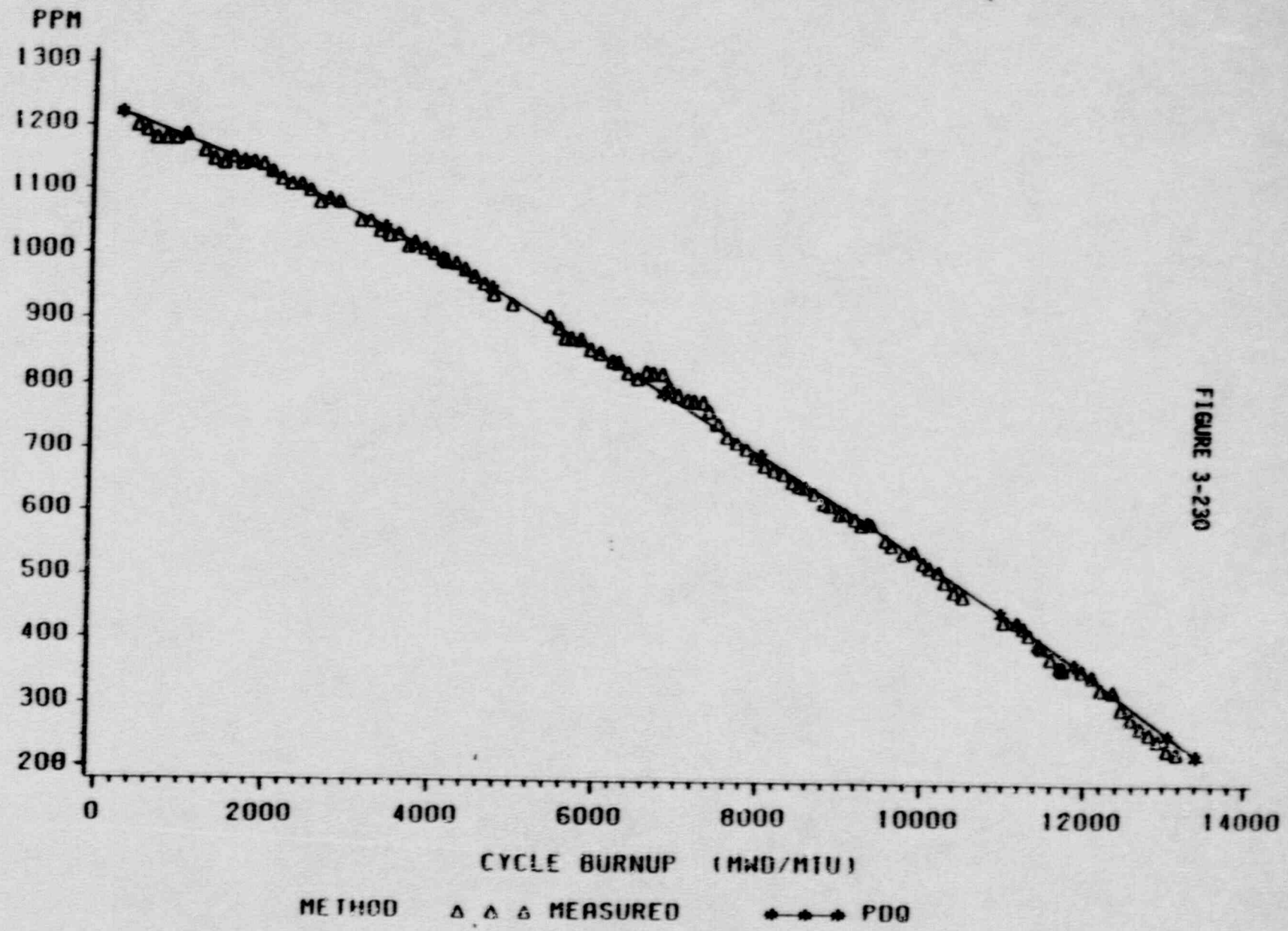

FIGURE 3-230

BORON LETDOWN CURVES FOR N1C6

PDQ 3-G AND MEASURED

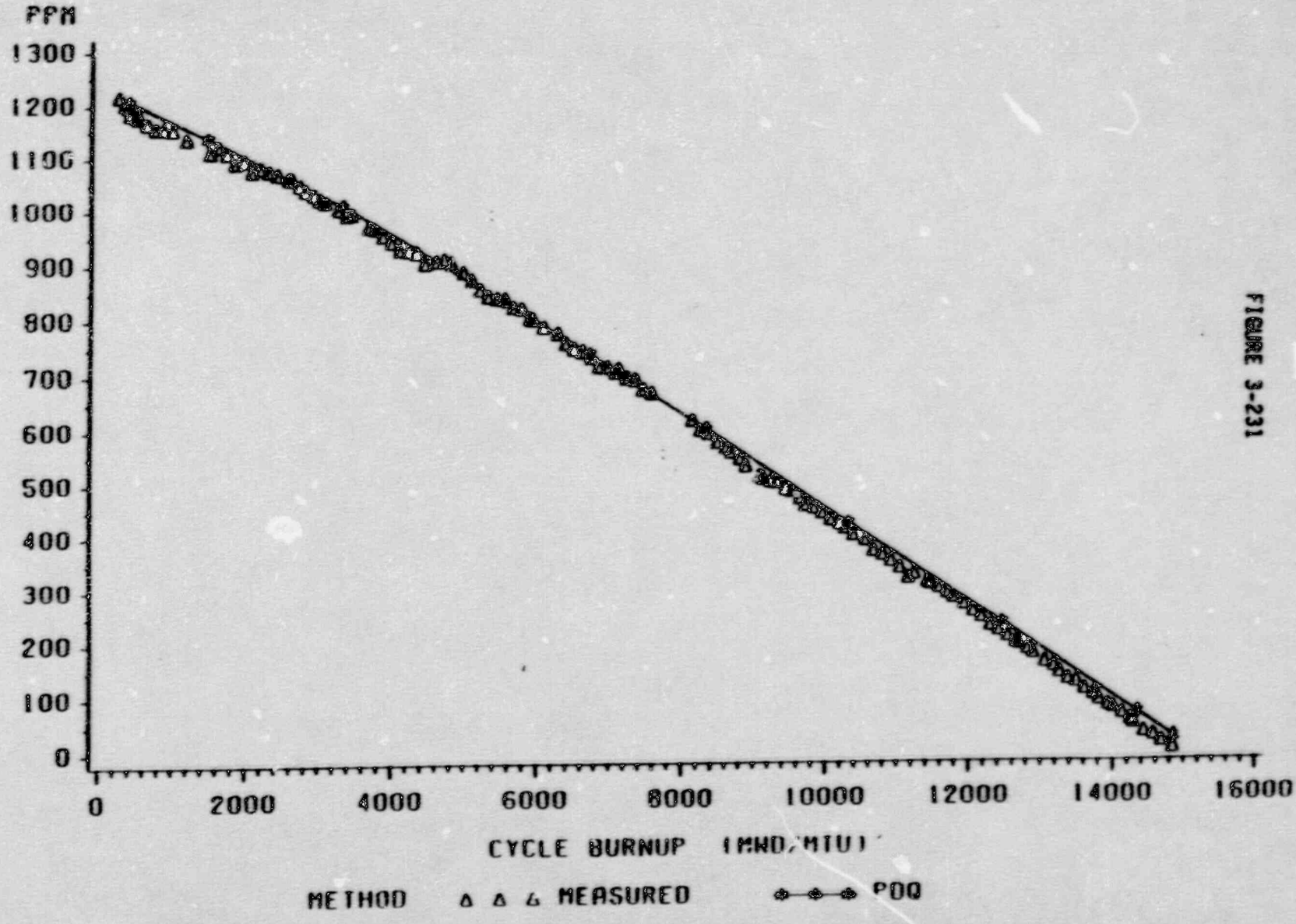

FIGURE 3-231

BORON LETDOWN CURVES FOR N1C7

POQ 3-D AND MEASURED

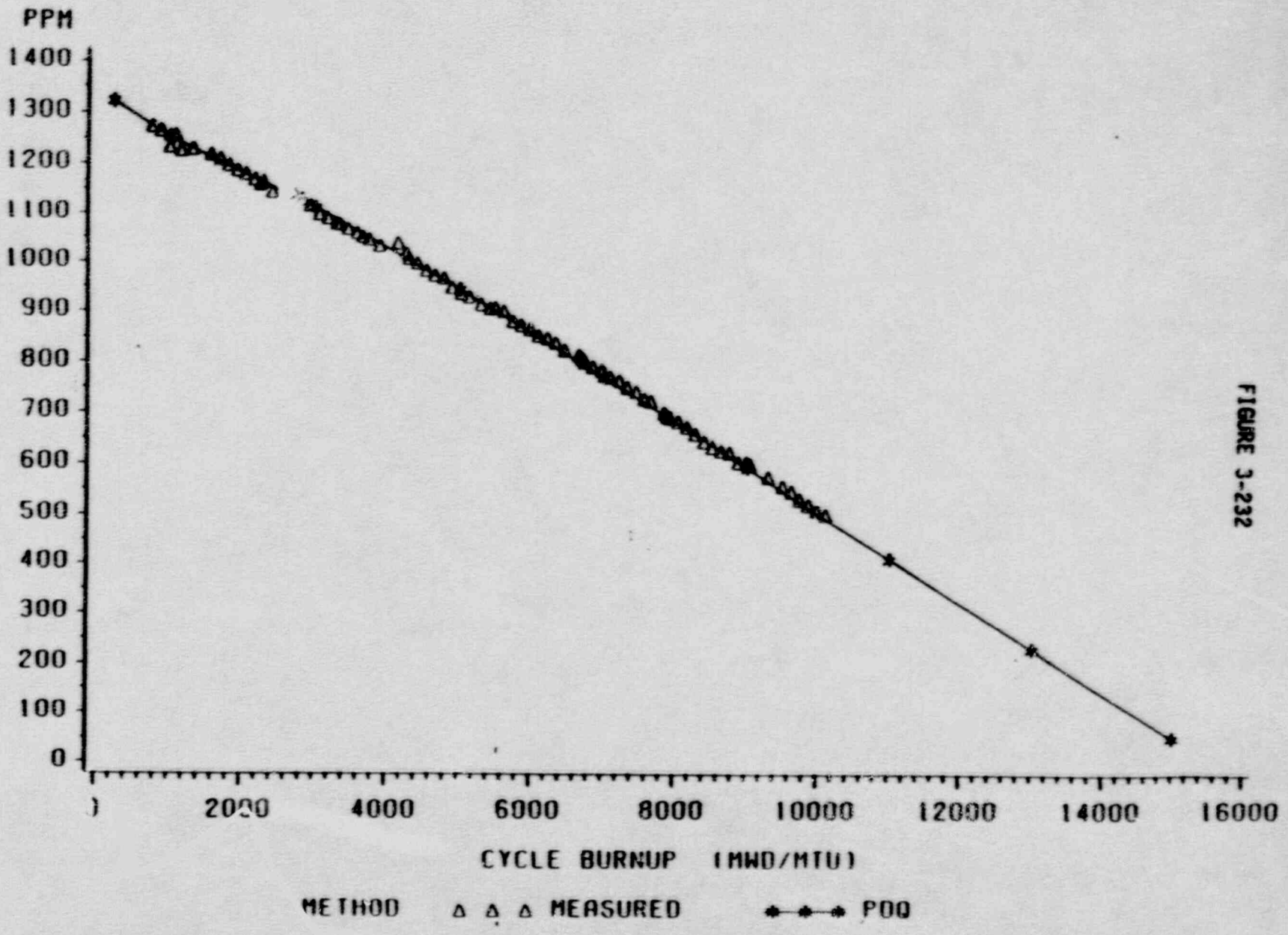

FIGURE 3-232

BORON LETDOWN CURVES FOR N2C2

PDQ 3-D AND MEASURED

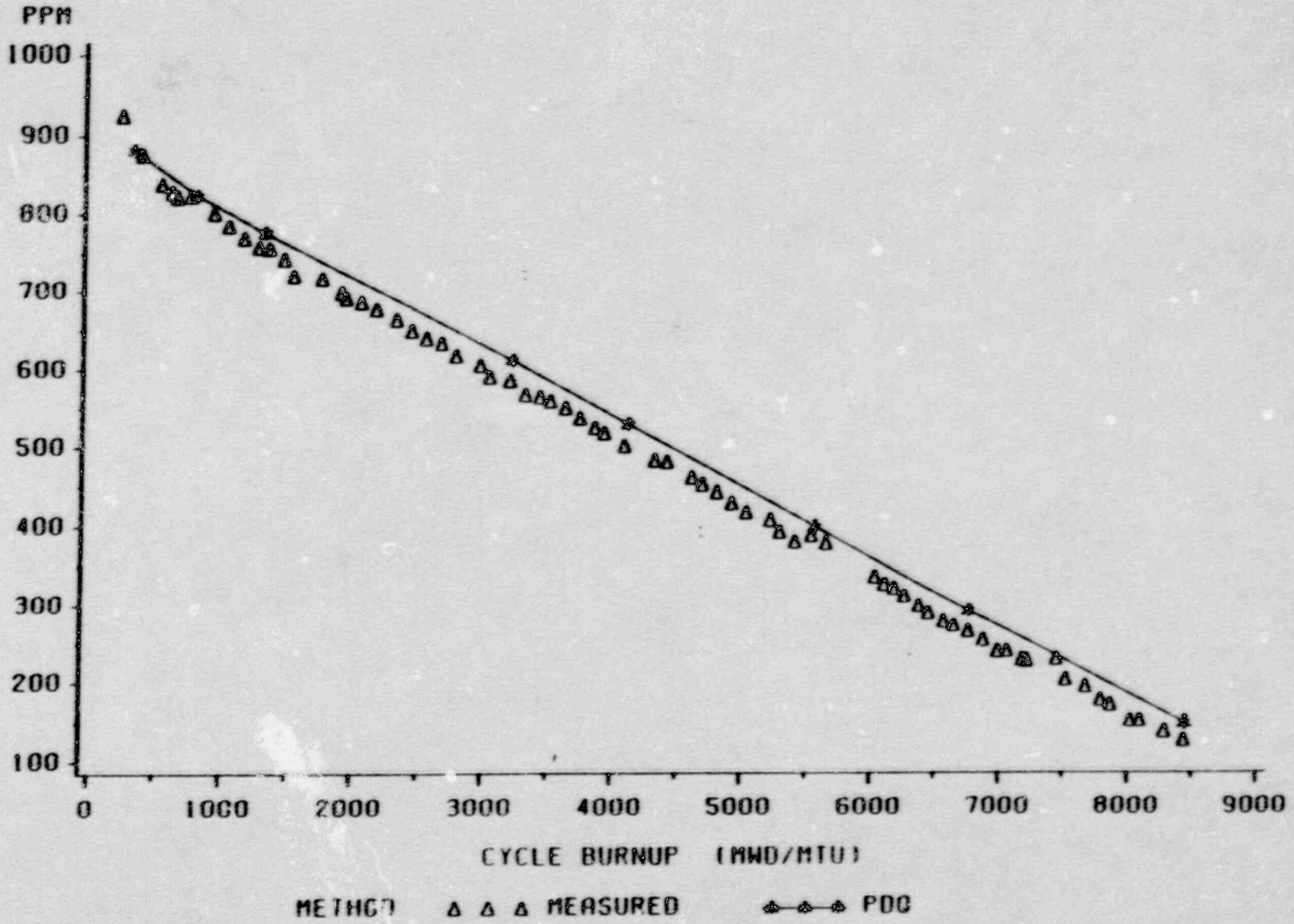

FIGURE 3-233

BORON LETDOWN CURVES FOR N2C3

PDQ 3-D AND MEASURED

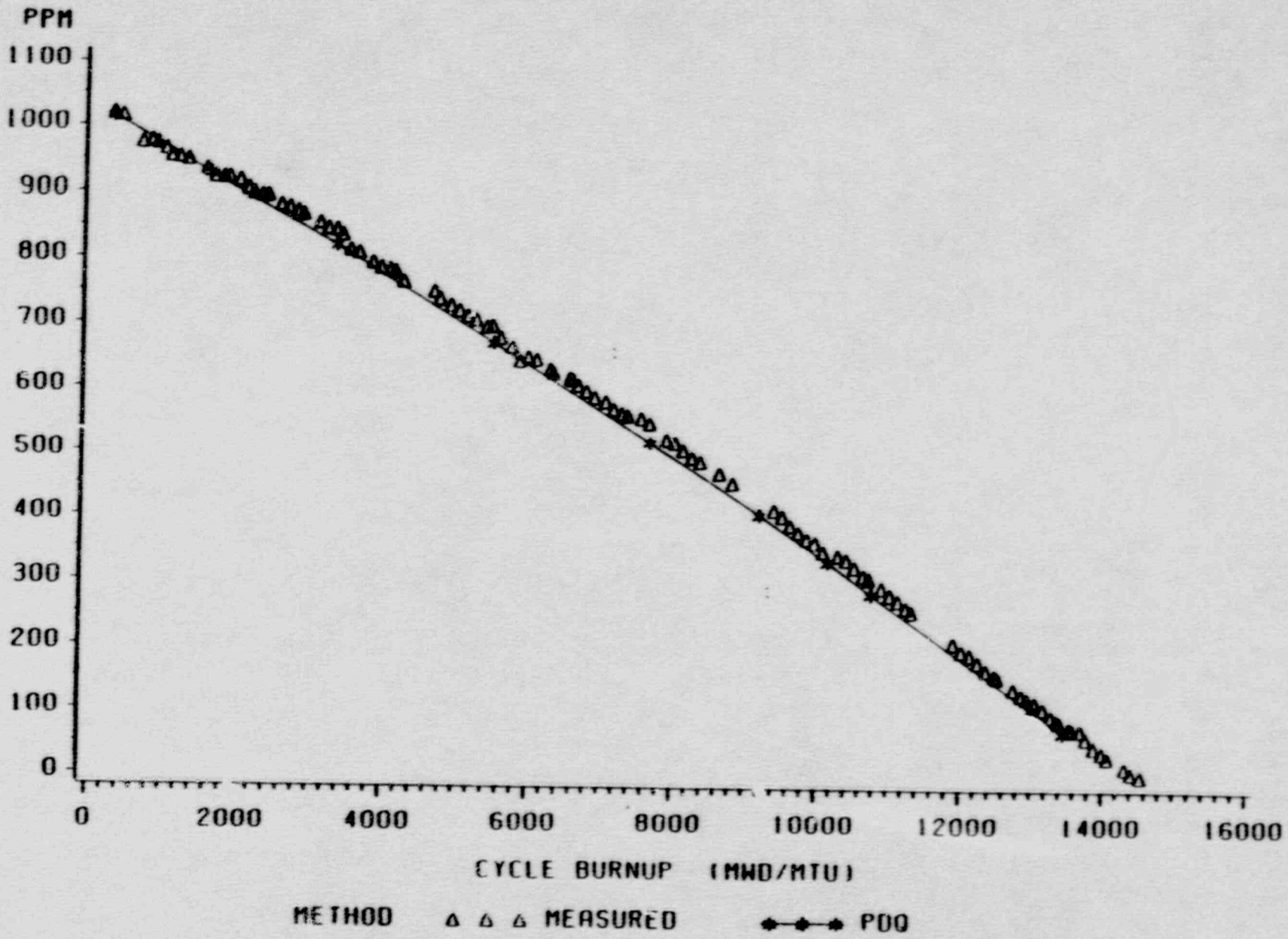

FIGURE 3-234

BORON LETDOWN CURVES FOR N2C4

PDQ 3-D AND MEASURED

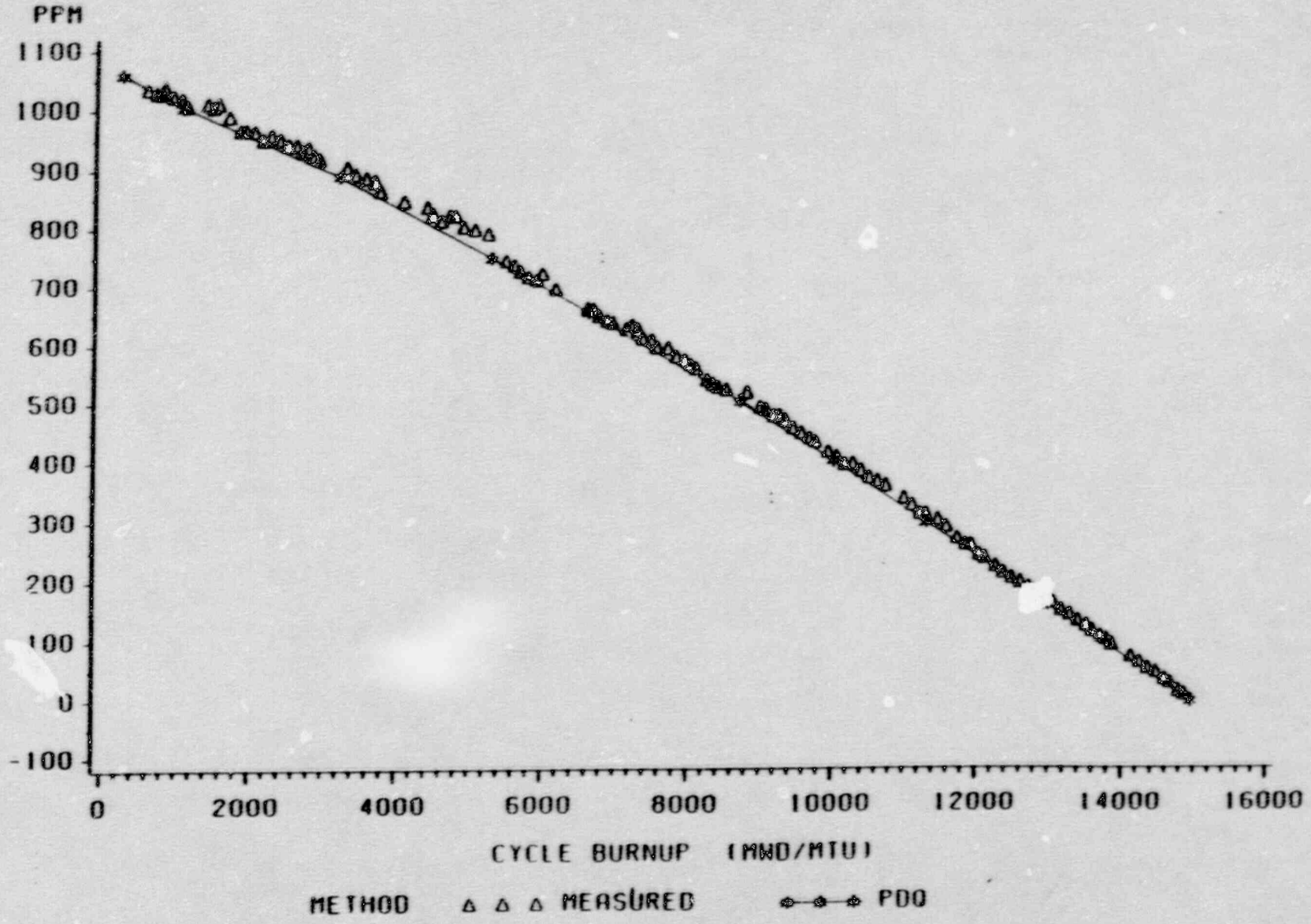

FIGURE 3-235

BORON LETDOWN CURVES FOR N2C5

PDQ 3-D AND MEASURED

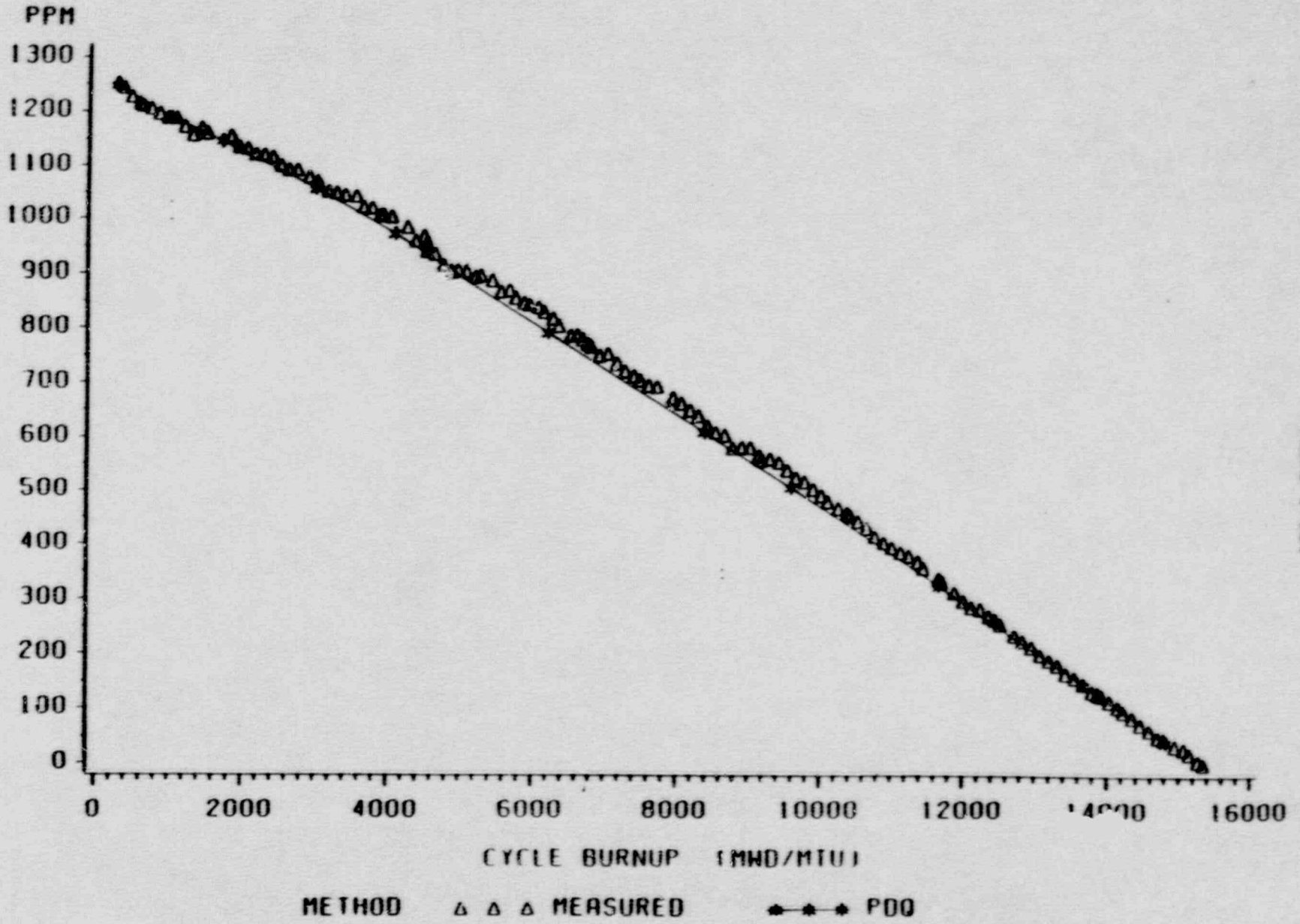

FIGURE 3-236

BORON LETDOWN CURVES FOR N2C6

PDQ 3-D AND MEASURED

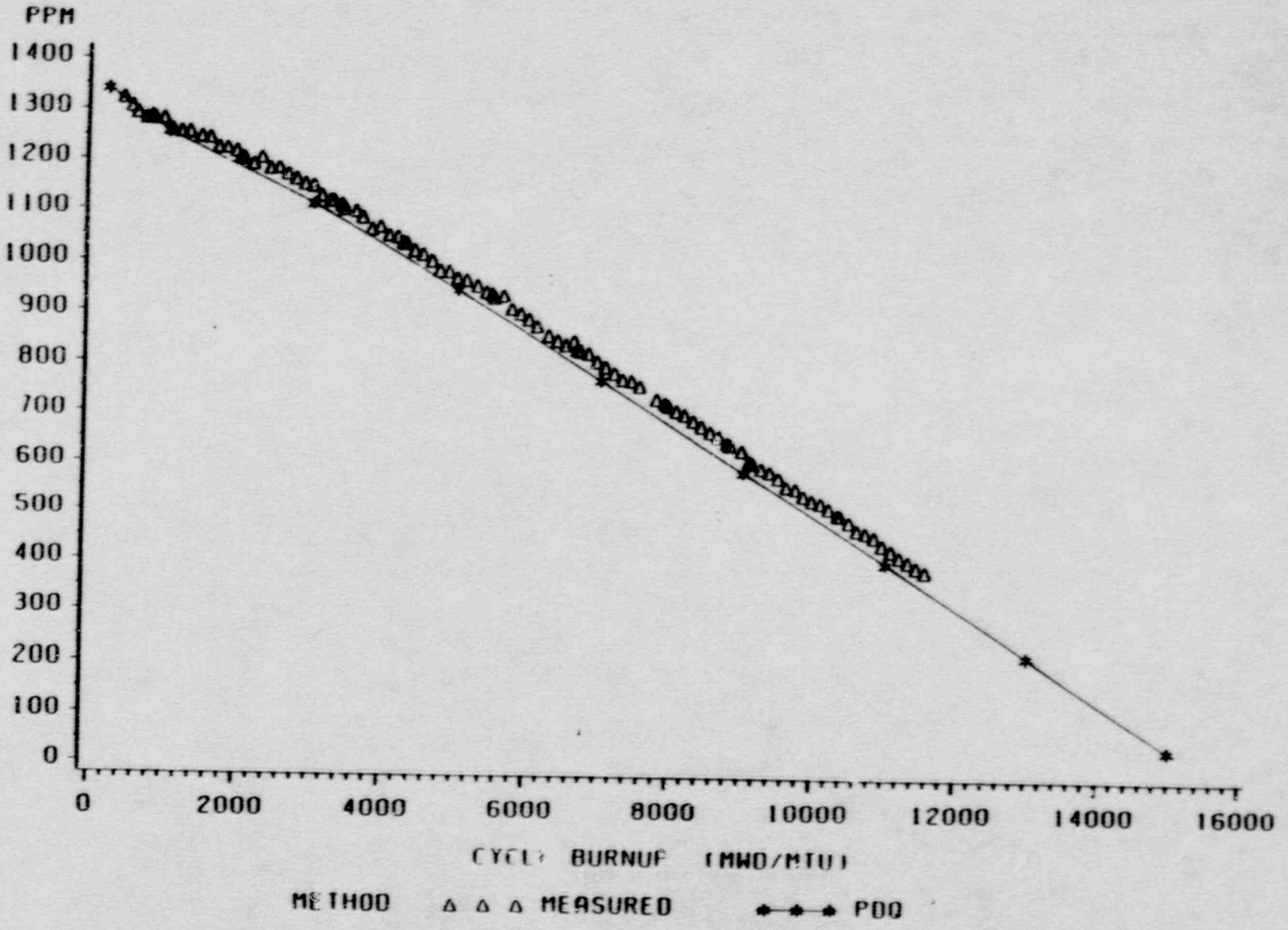

FIGURE 3-237

BORON LETDOWN CURVES FOR S1C2

PDQ 3-D AND MEASURED

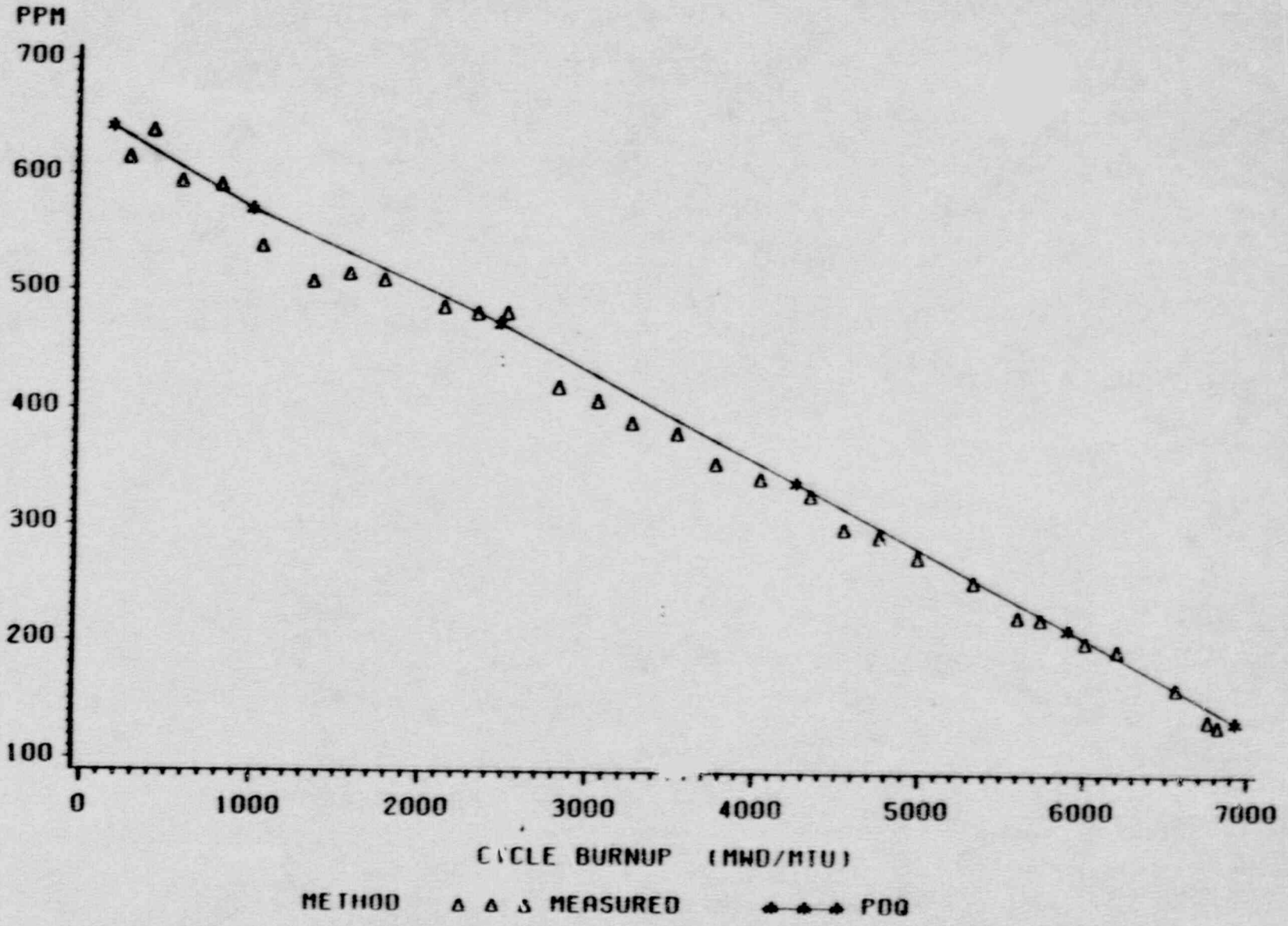

FIGURE 3-23a

BORON LETDOWN CURVES FOR S1C3

PDQ 3-D AND MEASURED

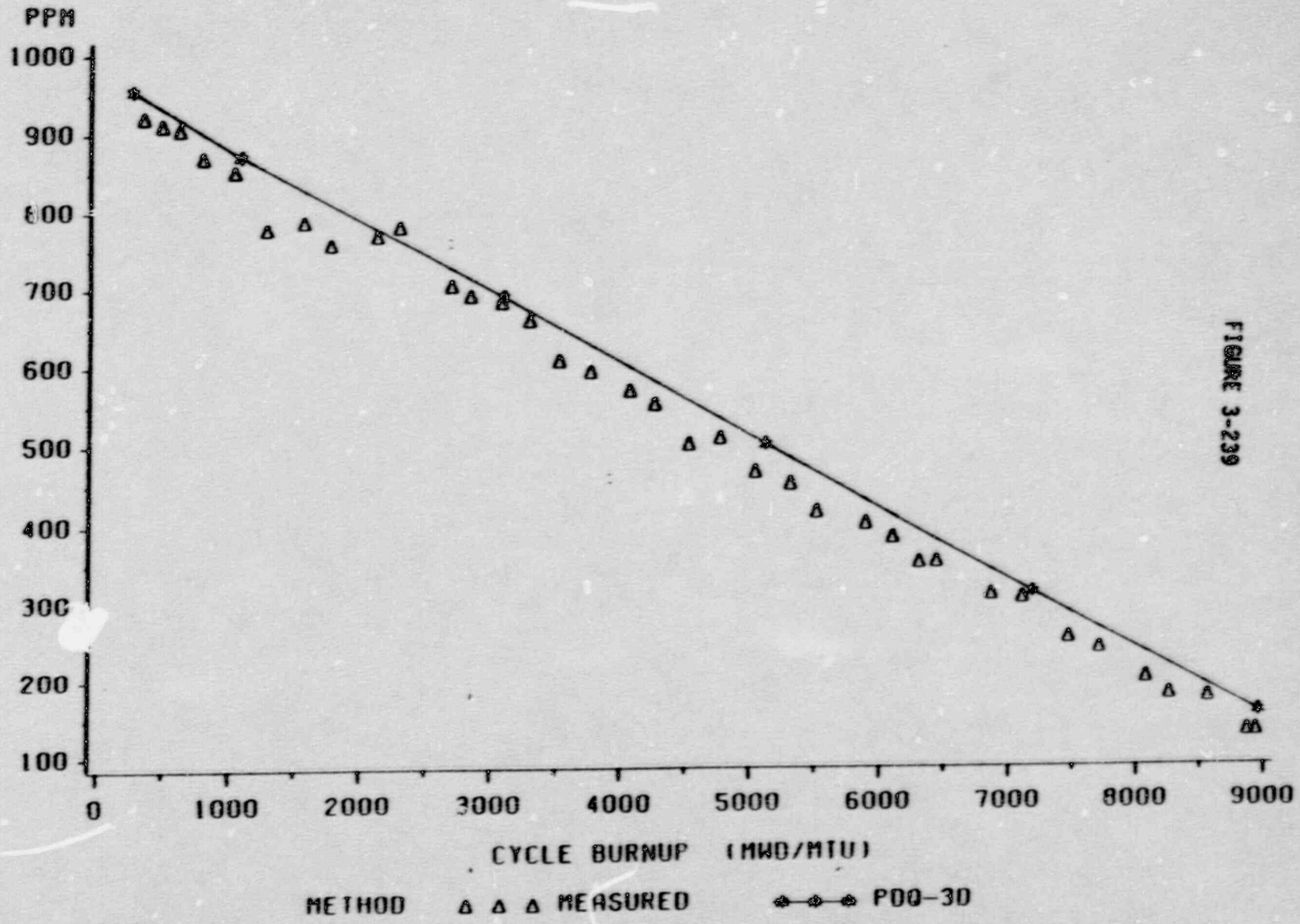

FIGURE 3-239

BORON LETDOWN CURVES FOR S1C4

PDQ 3-D AND MEASURED

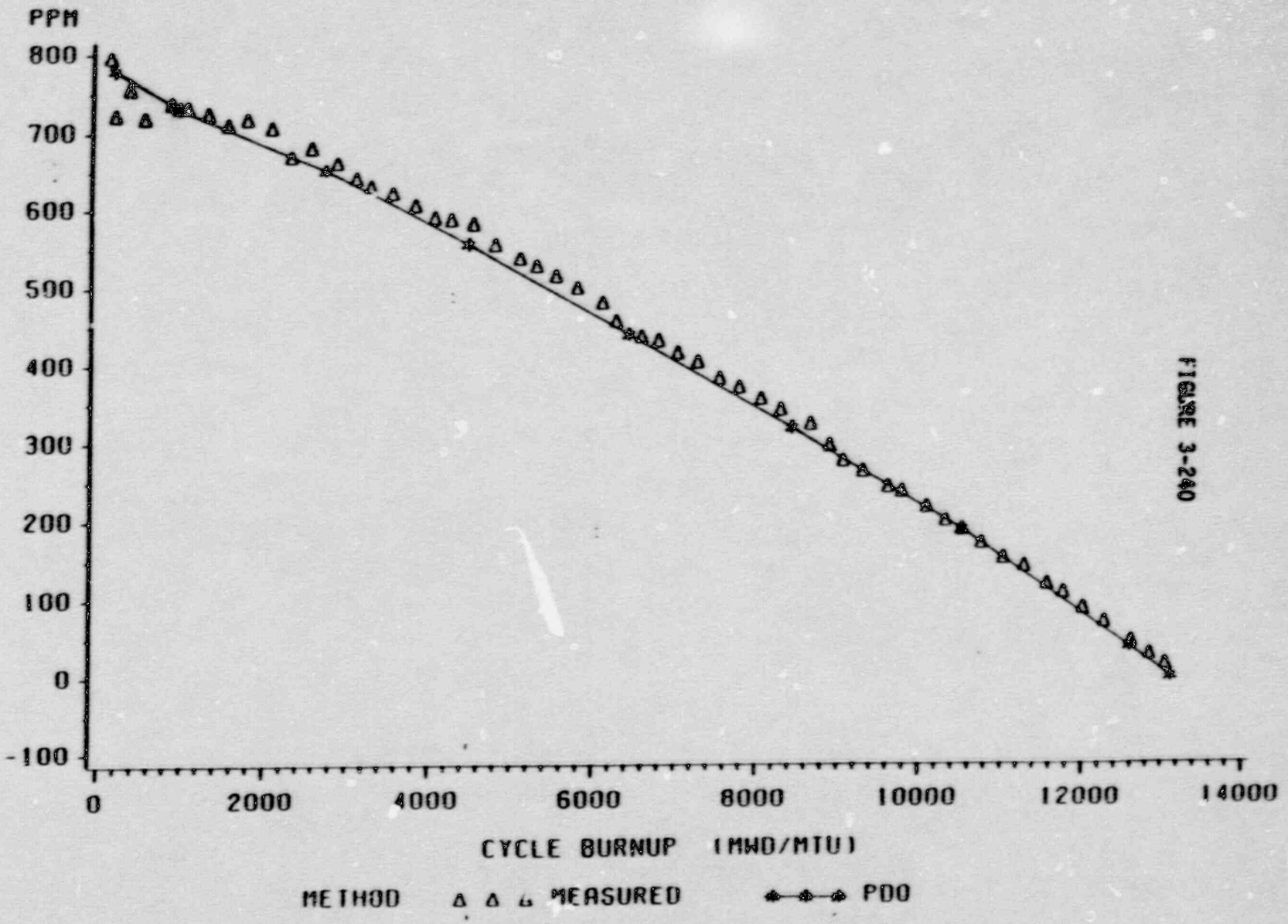

FIGURE 3-240

BORON LETDOWN CURVES FOR S1C5

PDQ 3-D AND MEASURED

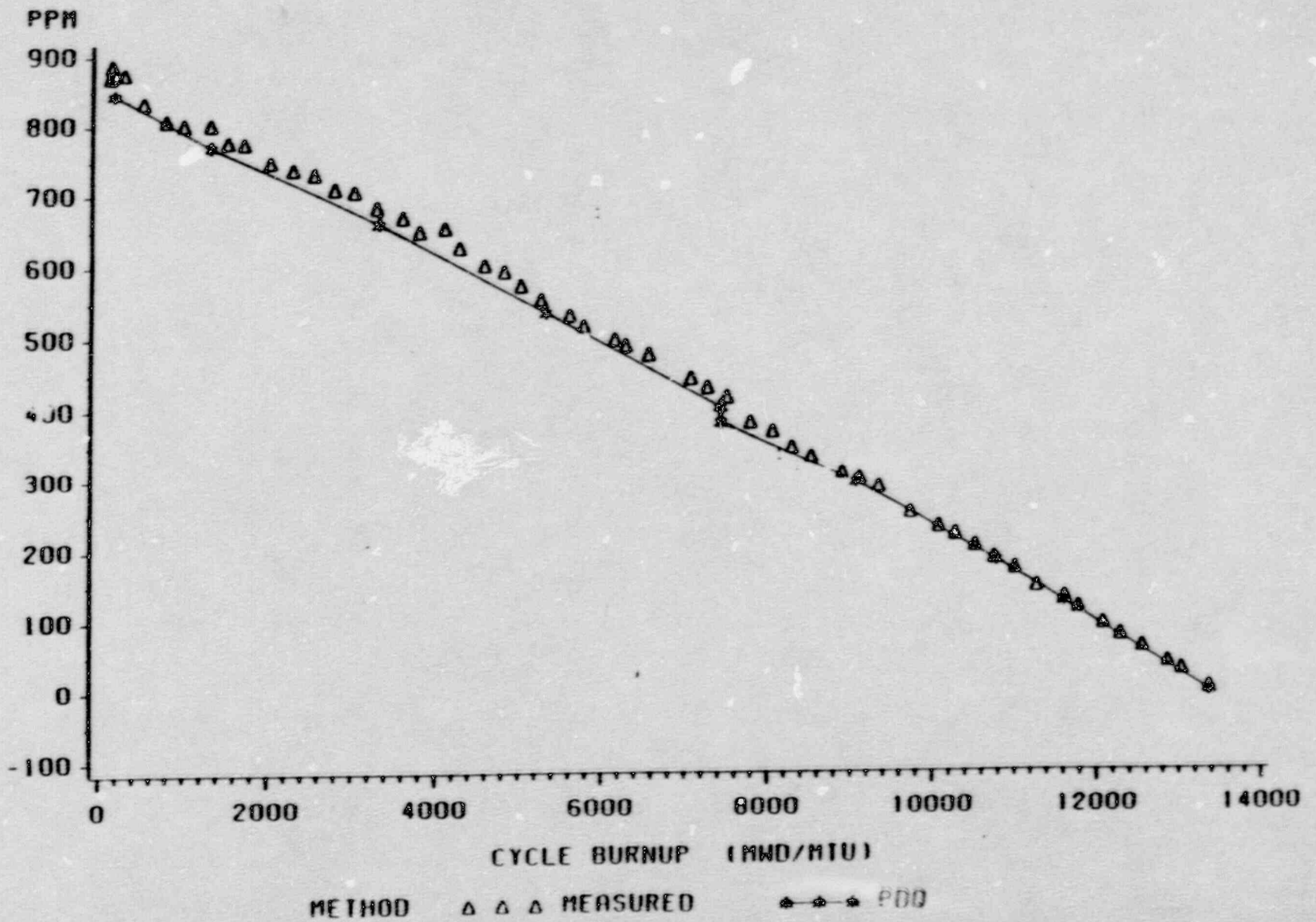

FIGURE 3-241

BORON LETDOWN CURVES FOR S1C6

PDQ 3-D AND MEASURED

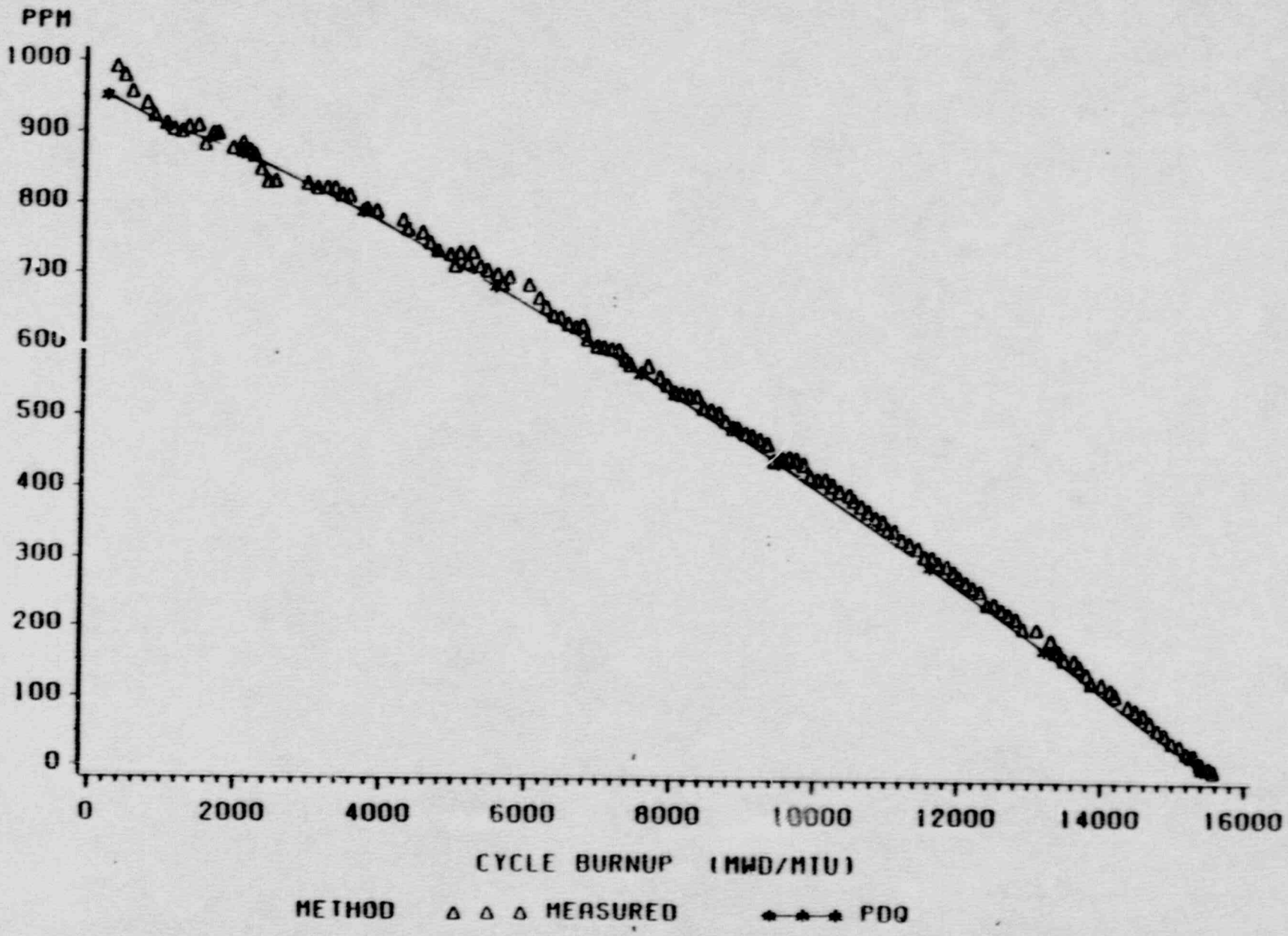

FIGURE 3-242

BORON LETDOWN CURVES FOR 31C7

PDQ 3-D AND MEASURED

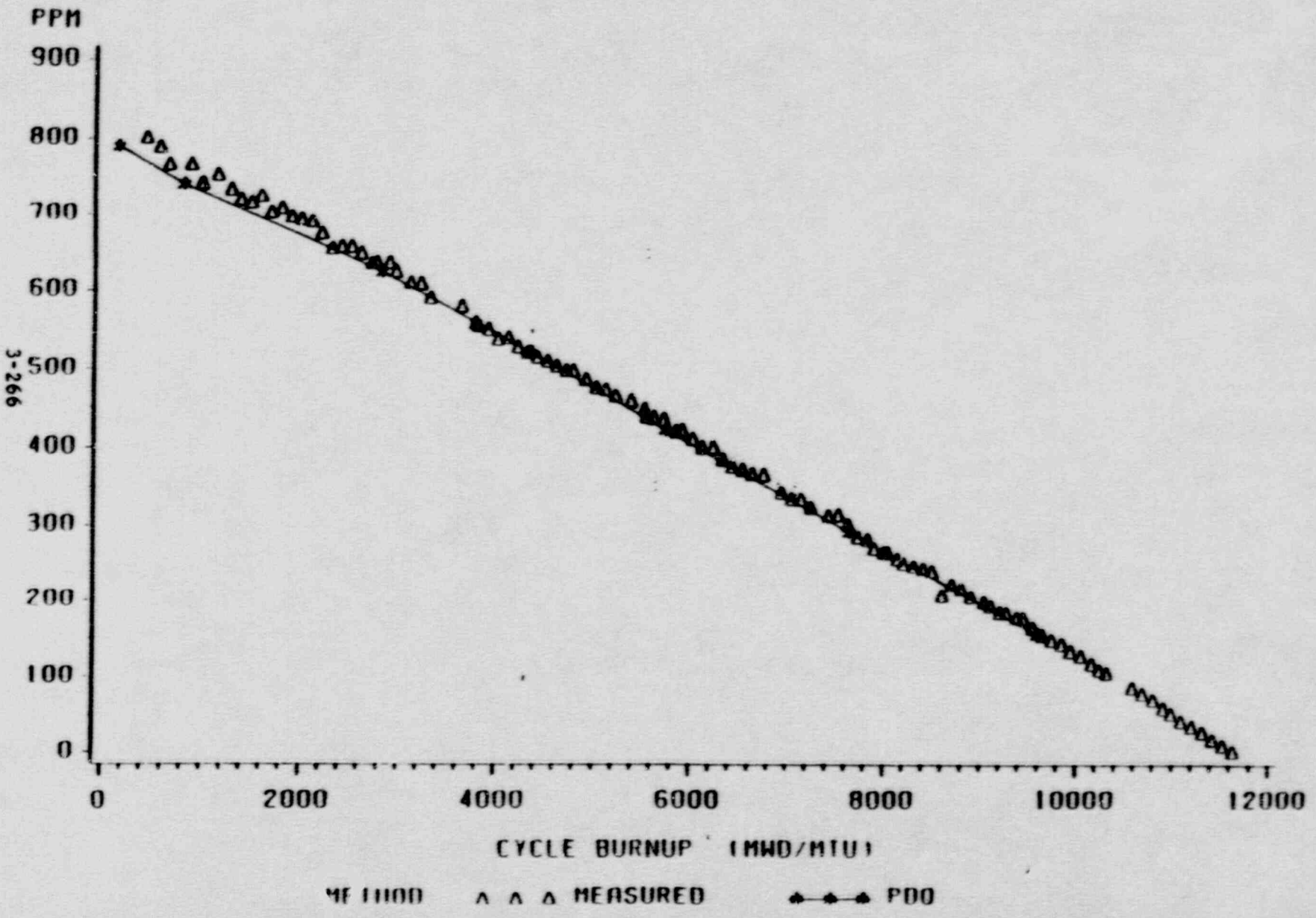

FIGURE 3-243

BORON LETDOWN CURVES FOR S1C8

PDQ 3-D AND MEASURED

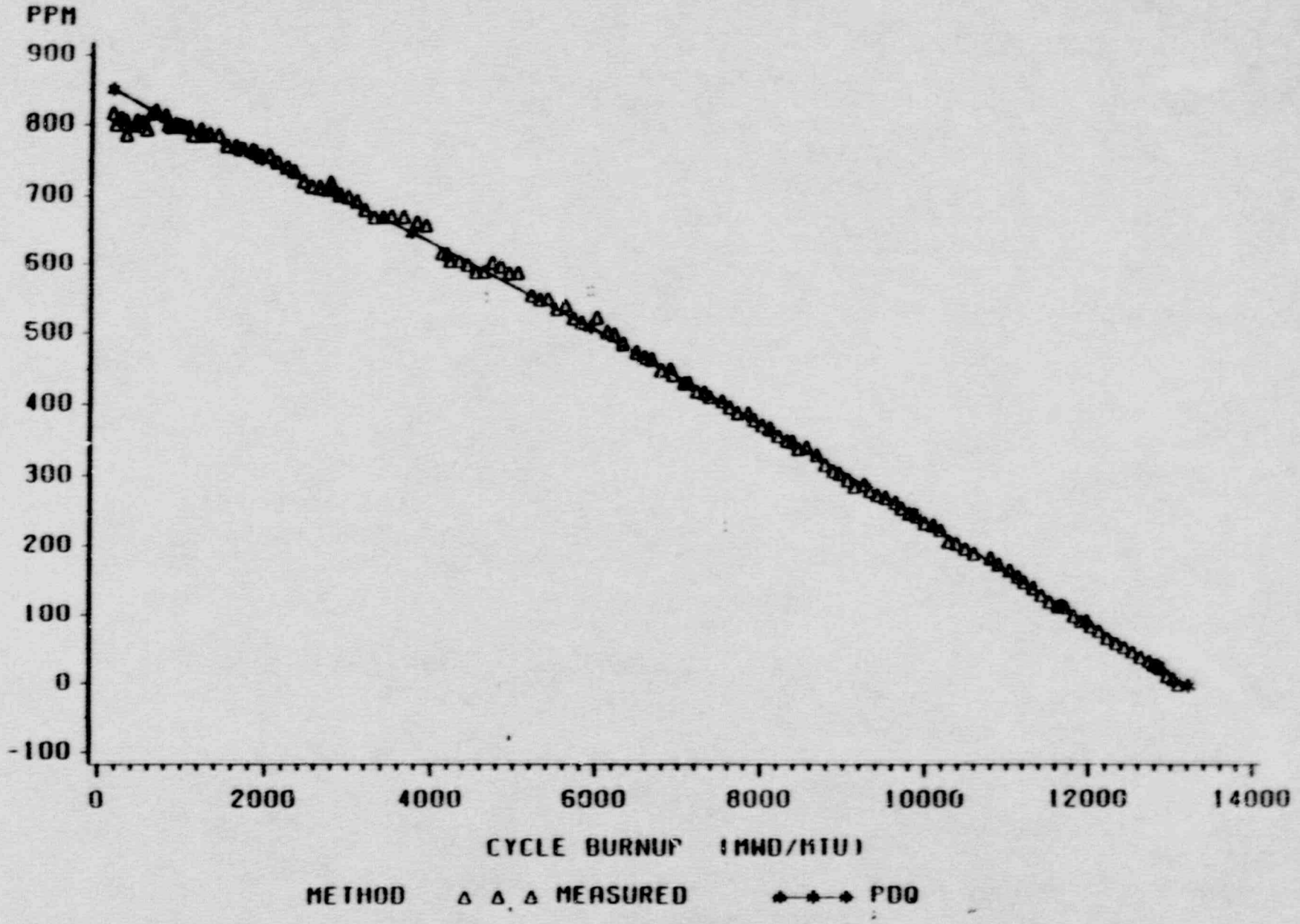

FIGURE 3-244

BORON LETDOWN CURVES FOR S1C9

PDQ 3-D AND MEASURED

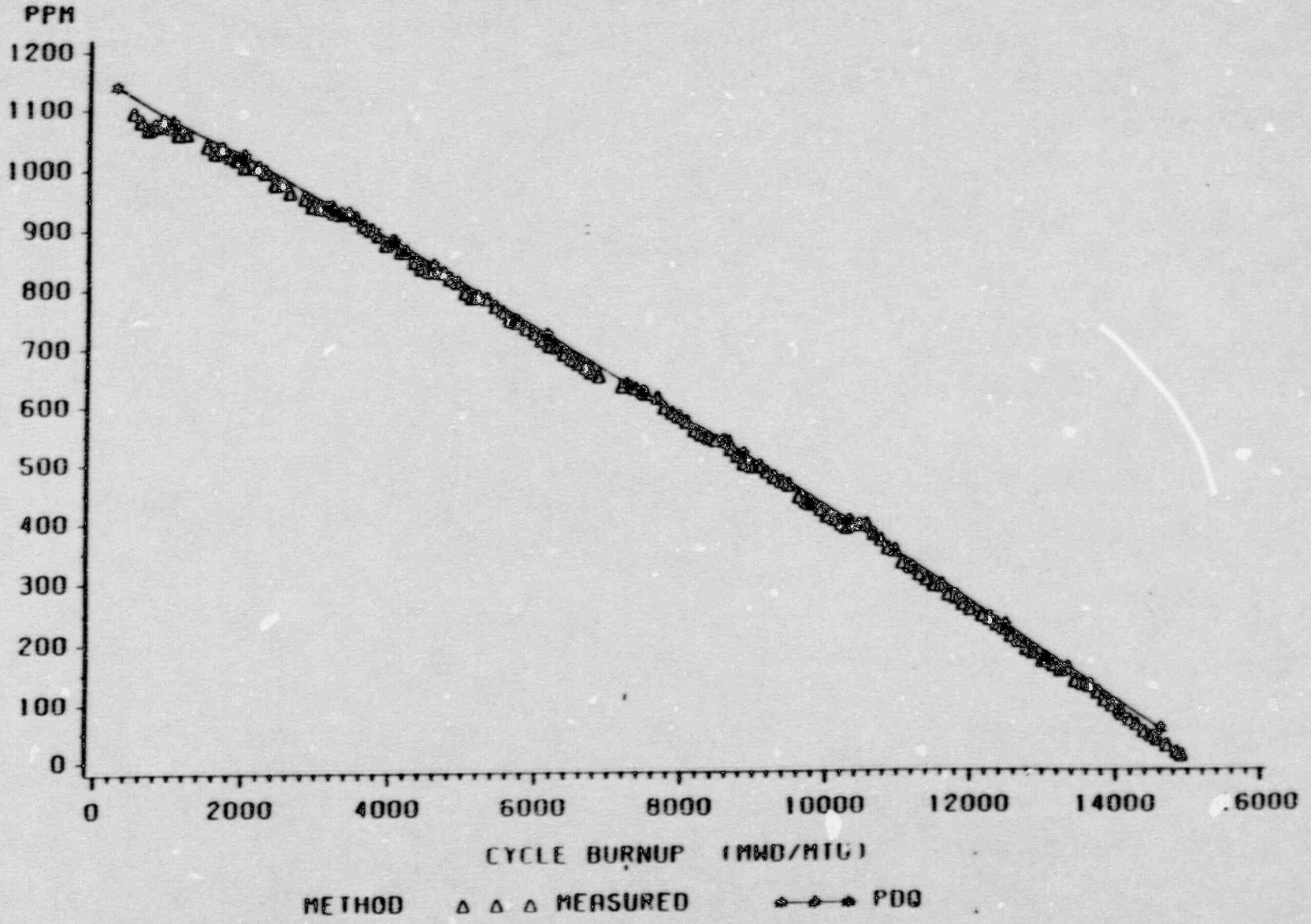

FIGURE 3-245

BORON LETDOWN CURVES FOR S2C2

PDQ 3-D AND MEASURED

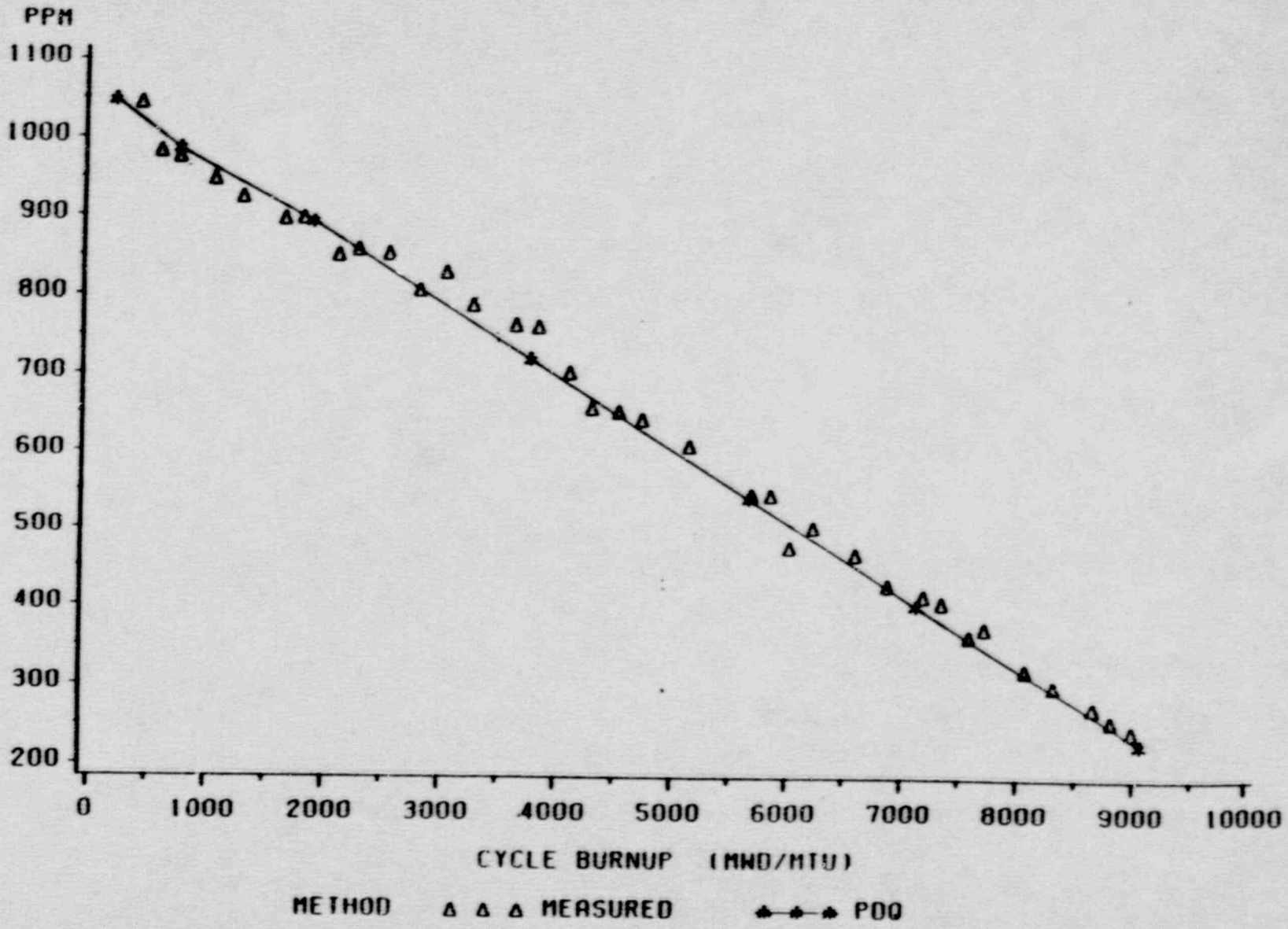

FIGURE 3-246

BORON LETDOWN CURVES FOR S2C3

PDQ 3-D AND MEASURED

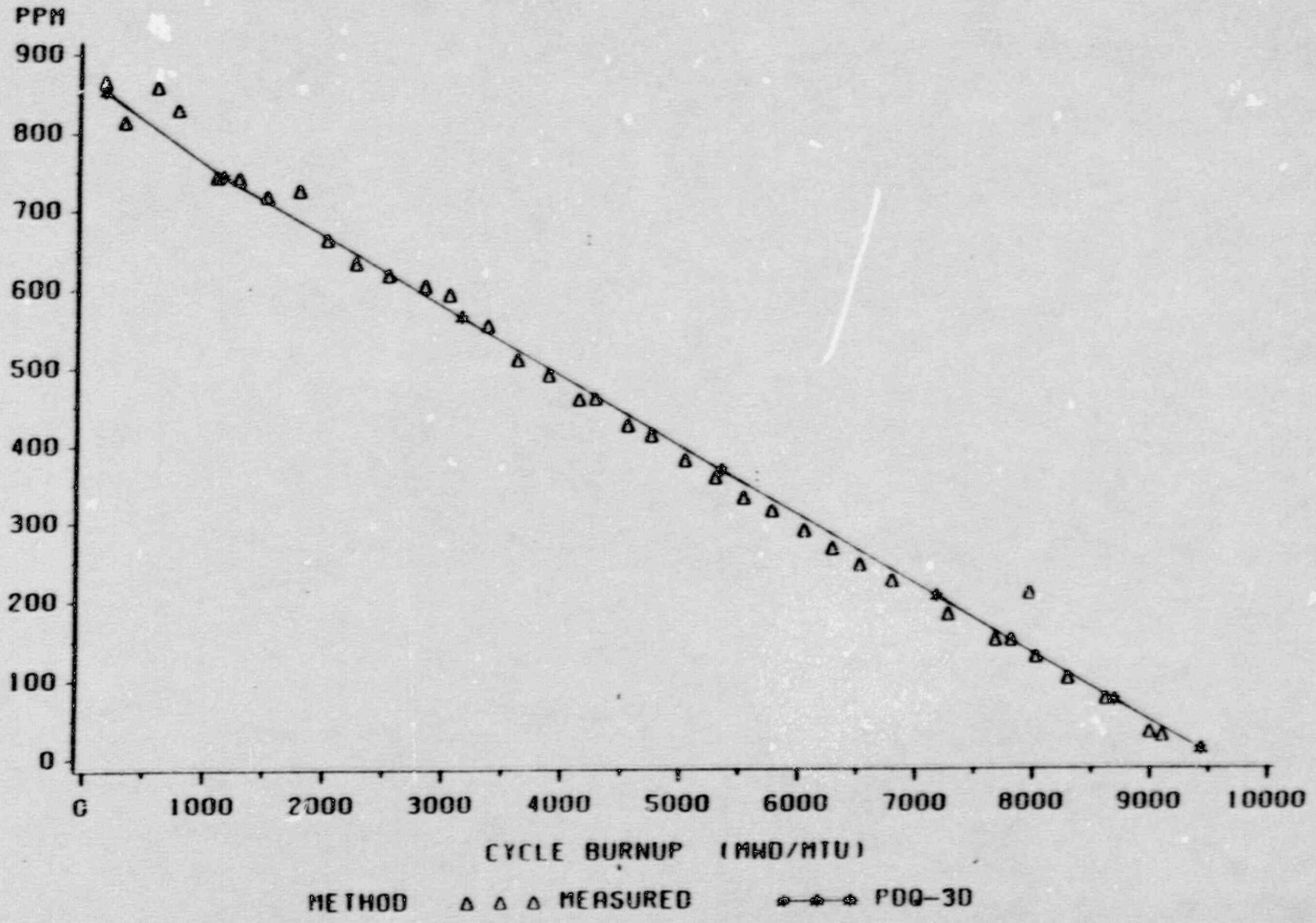

FIGURE 3-247

BORON LETDOWN CURVES FOR S2C4

PDQ 3-D AND MEASURED

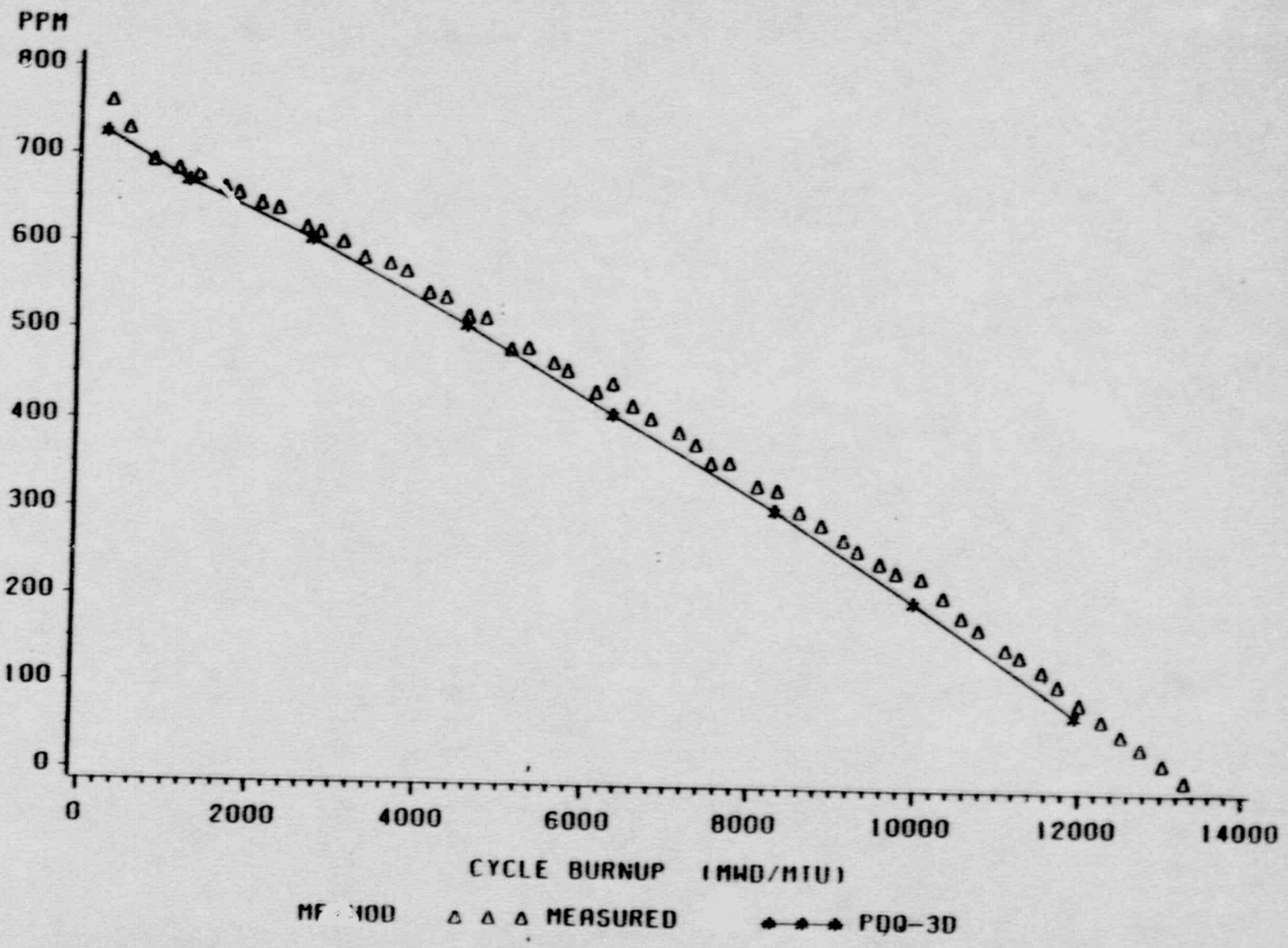

FIGURE 3-248

BORON LETDOWN CURVES FOR S2C5

PDQ 3-D AND MEASURED

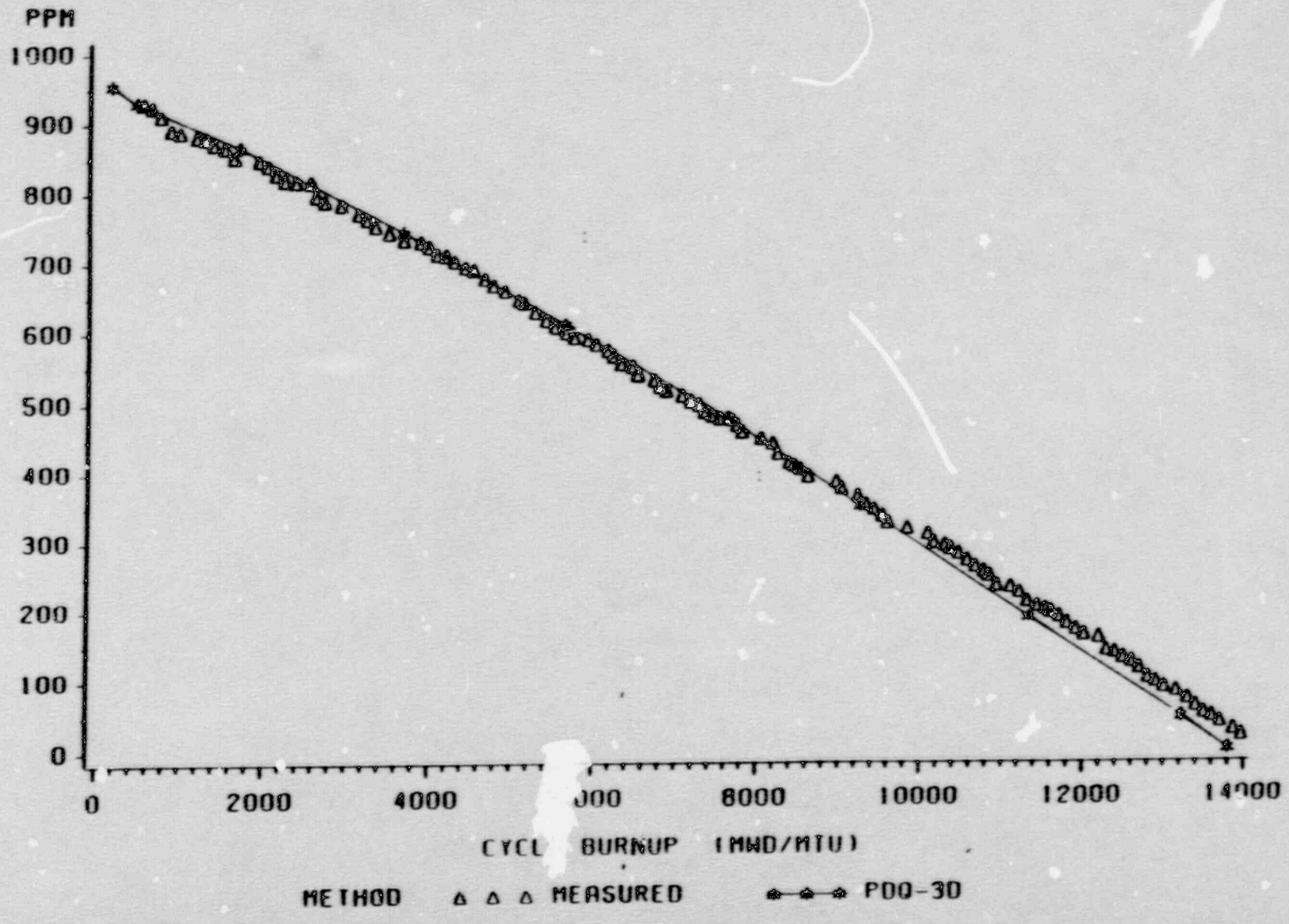

FIGURE 3-249

BORON LETDOWN CURVES FOR S2C6

PDQ 3-D AND MEASURED

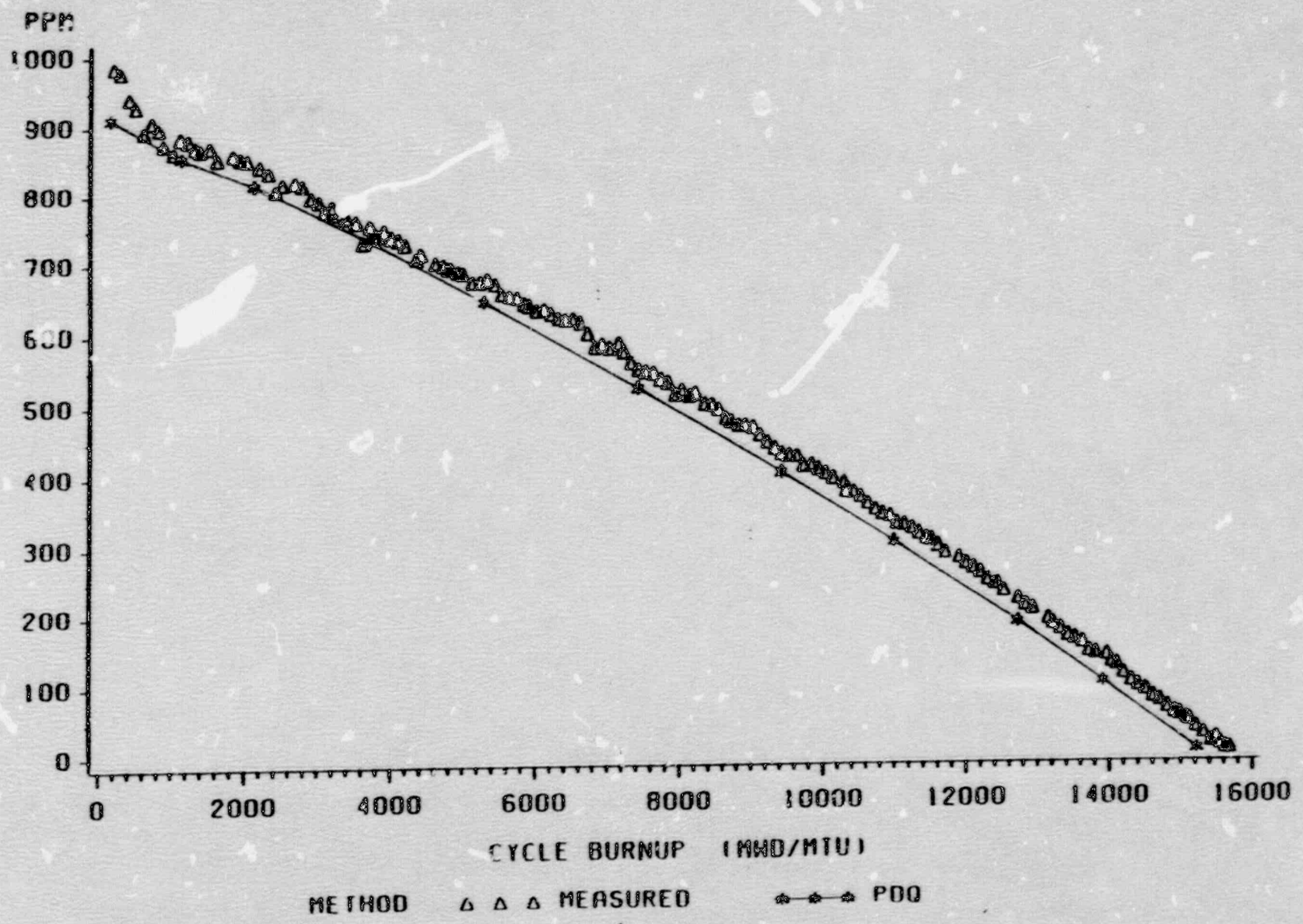

FIGURE 3-250

BORON LETDOWN CURVES FOR S2C7

PDQ 3-D AND MEASURED

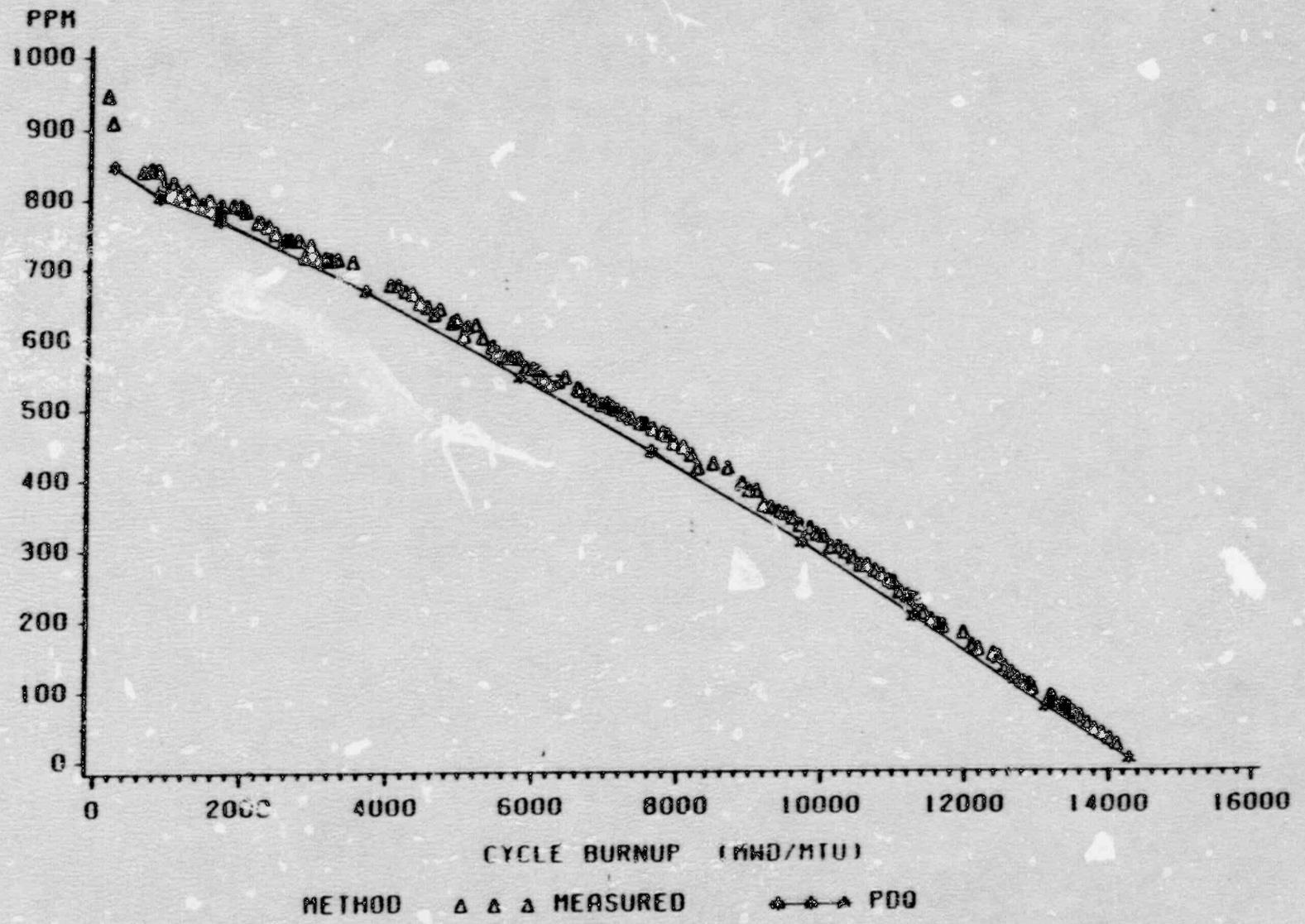

FIGURE 3-251

BORON LETDOWN CURVES FOR S2C8

PDQ 3-D AND MEASURED

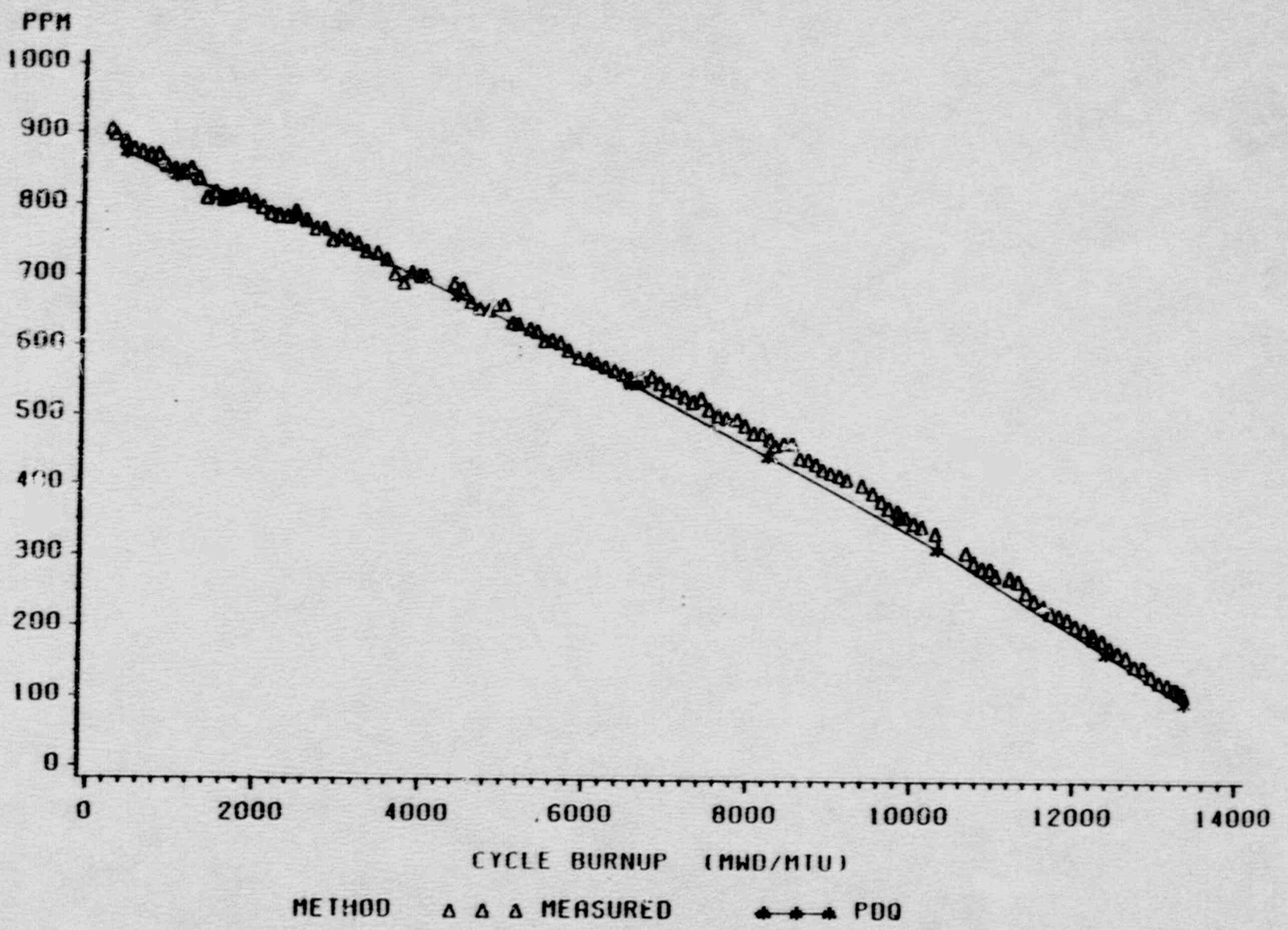

FIGURE 3-252

BORON LETDOWN CURVES FOR S2C9

PDQ 3-D AND MEASURED

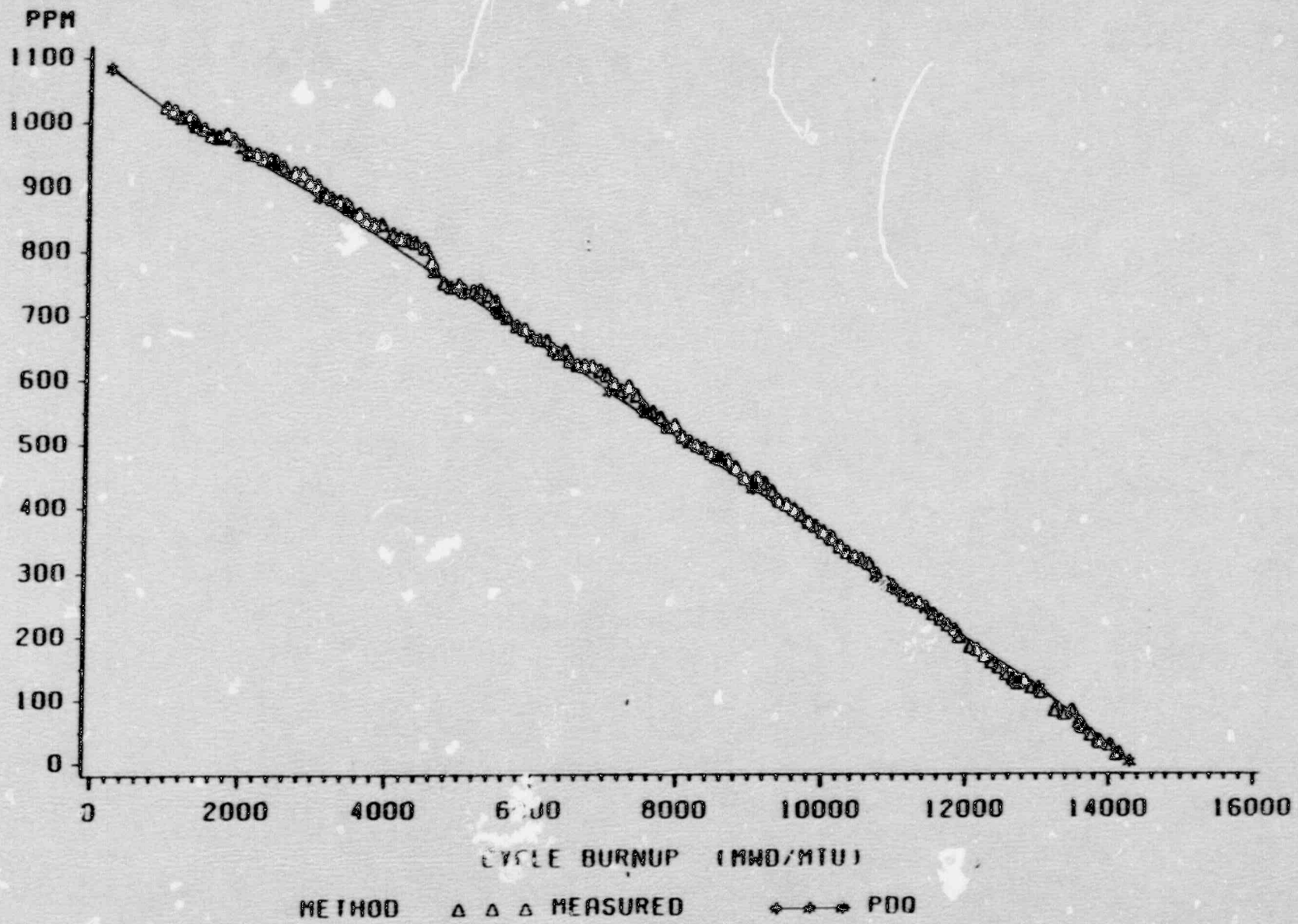

FIGURE 3-253

SURRY AND NORTH ANNA HZP BOC ITC RESULTS: MEASURED VERSUS PREDICTED

STARTUP ACCEPTANCE CRITERIA: +/- 3 PCM/ F

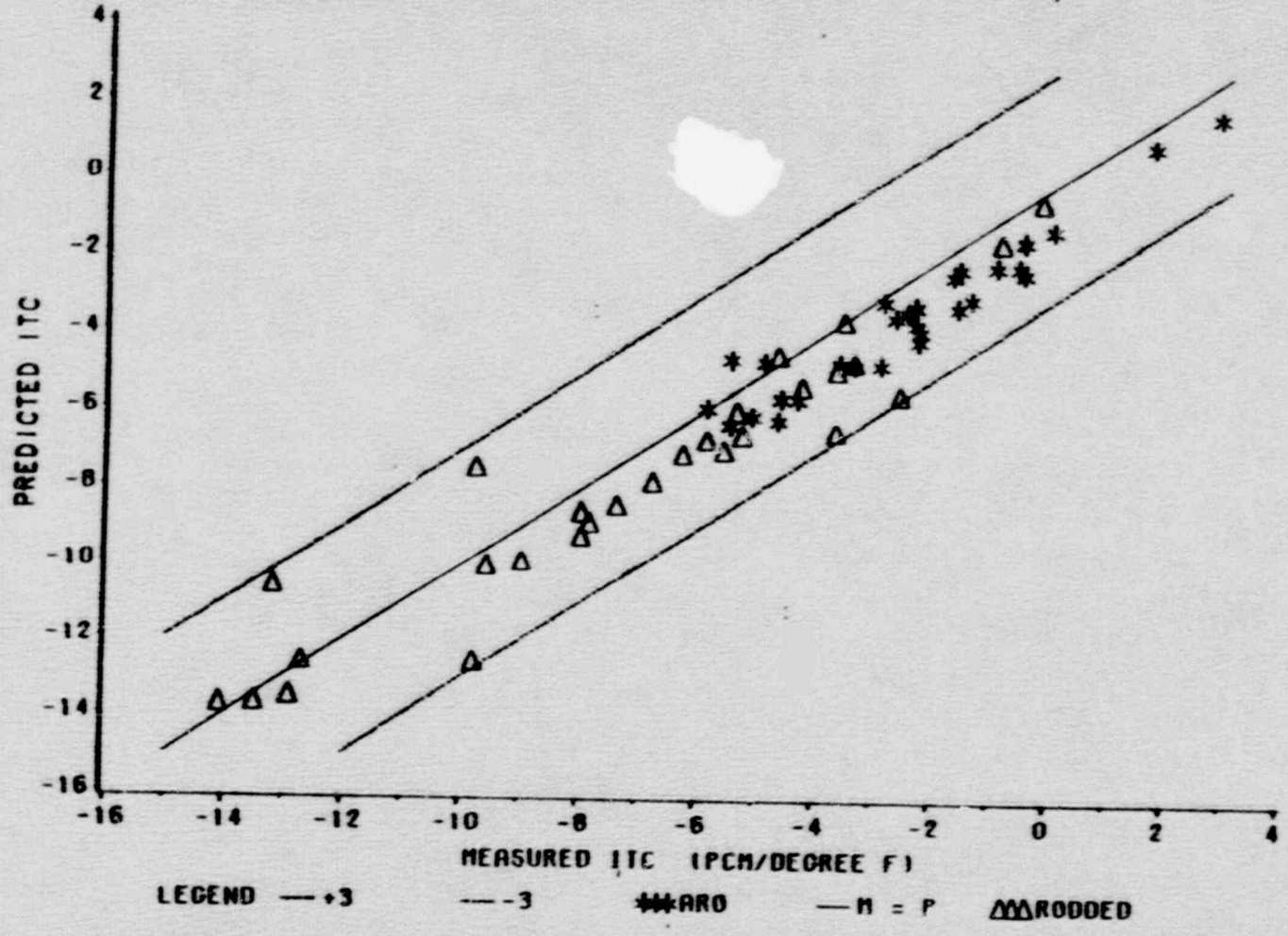

FIGUE 3-254

SECTION 4 - SUMMARY AND CONCLUSIONS

The Virginia Power PDQ two zone model has been developed for the purpose of performing three dimensional reactor physics calculations. The coarse mesh representation allows calculations to be performed both faster and with smaller computer memory requirements than would a discrete pin model, because fewer mesh lines are required to represent the geometry of the reactor core. The non-uniform radial and axial mesh makes best use of the computer resources by providing a better representation of the actual power distribution than would be provided by a uniform mesh model with the same number of mesh lines. The two zone feature (the segregation of control rods or burnable poison rods into the zone in the assembly where they exert the most influence) also aids in accurately determining the distribution of power between assemblies with and without control poisons. The 3-D two zone model is intended to predict power distributions in three dimensions for local vessel fluence calculations, to serve as a scoping tool for new fuel products requiring three dimensions, to serve as a benchmarking tool for the 3-D FLAME nodal model and a 2 D version of the PDQ two zone model (which will replace the PDQ one zone model), to serve as a single source cross section generation tool for the 1-D NOMAD model, and for calculations currently performed with the PDQ discrete pin model when 3-D detail is desirable. This includes calculation of critical boron concentrations, control rod bank worths (integral and differential), assemblywise power distributions (both axial and radial), peaking factors (both axial and radial) and reactivity coefficients for final production calculations to support reactor operations or safety analysis.

The accuracy of the two zone model has been demonstrated for each of the above production calculations through comparisons with measurements taken at Surry Units No. 1 and 2 and North Anna units No. 1 and 2. The results of these comparisons are:

1. Assembly average power distributions based on 14 HZP INCORE flux maps, 2 maps near 30% power, 2 maps near 50% power, and 76 HFP flux maps indicate a 95%/95% one sided tolerance limit of 1.028 for North Anna cycles and 1.027 for Surry cycles. The root mean square of the power distribution differences for rodded HZP maps compare favorably to the root mean square of the differences in the corresponding unrodded maps. In the rodded assemblies, differences between measured and predicted powers are typical of all assemblies in the map indicating no loss of accuracy in power distribution due to control rod insertion. The uncertainty factor compares favorably with the nuclear reliability factor of 1.05 for $F_{\Delta H}$ set forth in Reference 23.

2. Assembly $F_{\Delta H}$ comparisons to measurements from 14 HZP maps, 4 at 28 - 51% power, and 76 HFP maps resulted in a 95%/95% one sided tolerance limit of 1.034 for North Anna cycles and 1.031 for Surry cycles. Only monitored assemblies with both measured and predicted $F_{\Delta H} > 1.0$ were used. These results compare well to the current nuclear reliability factor of 1.05. Assembly $F_Q(Z)$ comparisons from the same maps for F_Q values > 1.0 yield tolerance limits of 1.067 for North Anna and 1.072 for Surry. These factors are within the existing nuclear reliability factor of 1.075. PDQ 3-D two zone model pin power reconstruction provides accuracy comparable to 2-D discrete PDQ pin powers and instrument thimble fluxes.

3. Control rod bank worths predicted by the two zone model are 1.0% above the measured worths on average with a standard deviation of 4.5%. The uncertainty factor of 1.10 derived statistically from the 157 data points is the same as the nuclear reliability factor for integral worths. If the uncertainty introduced by the reactivity computer is accounted for, the uncertainty factor drops to less than 1.06. Comparison of measured and predicted differential rod worth curves indicates generally good agreement typically within 1 pcm/step with the exception of localized dips at spacer grid locations. The current nuclear reliability factor of 2 pcm/step appears to be bounding.

4. Critical boron concentrations at startup are within 40 ppm of the measured value with only one exception. On average, startup critical boron is overpredicted by 6 ppm with a standard deviation of 20 ppm. Full power boron letdown curve comparisons show good agreement of predicted and measured shape and slope versus core burnup with absolute differences typically within about 30 ppm. The current nuclear reliability factor of 50 ppm is appropriate for this PDQ model. Results are acceptable for both startup and core follow applications. The differential boron worth uncertainty factor of 1.05 is consistent with measurents if the uncertainty introduced by the reactivity computer is considered.

5. Isothermal temperature coefficients are predicted within an average of 1.0 pcm/°F with a maximum difference of 2.9 pcm/°F relative to the measured values. There is a tendency to predict more negative than measured values by about 0.8 pcm/°F. The differences found are within the nuclear reliability factor of 3 pcm/°F.

Verification and model improvements will continue to be made as more experience is gained through continued application of the Virginia Power PDQ two zone model to the Surry and North Anna reactors.

SECTION 5 - REFERENCES

1. G. R. Poetschat, et al., "EPRI-PRESS, Volume 2: User's Manual," Part II, Chapter 5, ARMP-02, EPRI NP-4574, (August 1986).

2. R. E. MacFarlane et al., "Description of the CELL-2 Fast and Thermal Cross Section Libraries", Part II, Chapter 2, ARMP-02, EPRI NP-4574, (October 1987).

3. ARMP-02 (Advanced Recycle Methodology Program, [illegible]m Documentation, EPRI-NP-4574-CCM, (August, 1988).

4. R. B. Fancher, et al., "ESCORE - the EPRI Steady-State Core Reload Evaluator Code: General Description", EPRI-NP-5100, (February 1987)

5. "SCALE: A Modular Code System for Performing Standardized Computer Analyses for Licensing Evaluation", ORNL-NUREG-CSD-VI-R3, (December, 1984).

6. "KENO V.a - An Improved Monte Carlo Criticality Program with Supergrouping", Oak Ridge National Laboratory, ORNL-NUREG-CSD-2-VI-R2, (December, 1984).

7. H. A. Hassan, "SHUFFLE - Program to Perform Fuel Shuffle in Nuclear Reactor Core", BAW-422 Rev. 1, (July 1975).

8. C. J. Pfeifer, "PDQ-7 Reference Manual II", Bettis Atomic Power Laboratory, WAPD-TM-947(L), (February 1971).

9. W. A. Peterson, "The Virginia Power PCF Code", VEP-NE-739, Virginia Power, (March, 1990).

10. R. A. Hall, "The Virginia Power RECON Code Manual", VEP-NE-788, Virginia Power, (June, 1990).

11. W. C. Beck, "The Vepco FLAME Model", VEP-FRD-24A, Virginia Power, (July 1981).

12. M. L. Smith, "The PDQ07 Discrete Model", VEP-FRD-19A, Virginia Power, (July 1981).

13. S. M. Bowman, "The Vepco NOMAD Code and Model", VEP-NFE-1A, Virginia Power, (May 1985).

14. J. R. Rodes, "The PDQ07 One Zone Model", VEP-FRD-20A, Virginia Power, (July 1981).

15. S. A. Ahmed, "PDQDK Code Verification", VEP-NE-171, Virginia Power, (November 1980).

16. W. D. Leggett III and L. D. Eisenhart, "The INCORE Code", WCAP-7149 December, 1967.

17. Argonne Code Center; Benchmark Problem Book, Argonne National Laboratory, ANL-7416, Supplement to 277--282 (1977).

18. B. M. Rothleder, et al., "PWR Procedures for Core Model Development and Operational Analysis", Part III, Chapter 1, ARMP-02, EPRI NP-4574, (October 1988).

19. "XSDRNPM-S: A One Dimensional Discrete Ordinates Code for Transport Analysis", ORNL-NUREG-CSD-2-V2-R1, (June, 1983).

20. "NITAWL-S: Resonance Self-Shielding by the Nordheim Method", ORNL-NUREG-CSD-2-V2, (October, 1981).

21. T. R. England, et al., "Summary of ENDF/B-V Data for Fission Products and Actinides", EPRI-NP-3787, (December 1984).

22. T. K. Ross, et al., "Control Rod Reactivity Worth Determination by the Rod Swap Technique", VEP-FRD-36A, Virginia Power, (December 1980).

23. J. C. Miller, "Vepco Nuclear Design Reliability Factors", VEP-FRD-45A, Virginia Power, (October 1982).